

AD-764 123

ANALYSIS OF UNDERGROUND OPENINGS IN  
ROCK BY FINITE ELEMENT METHODS

Fred H. Kulhawy

Syracuse University

Prepared for:

Advanced Research Projects Agency  
Bureau of Mines

April 1973

DISTRIBUTED BY:

**NTIS**

National Technical Information Service  
U. S. DEPARTMENT OF COMMERCE  
5285 Port Royal Road, Springfield Va. 22151

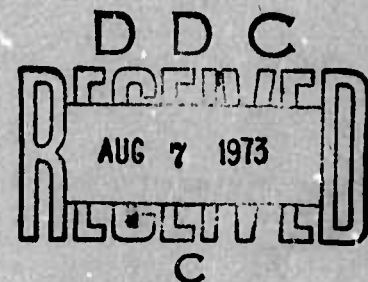
AD 764123

# ANALYSIS OF UNDERGROUND OPENINGS IN ROCK BY FINITE ELEMENT METHODS

FINAL REPORT  
APRIL, 1973

U.S. BUREAU OF MINES  
CONTRACT NUMBER H0210029

SPONSORED BY  
ADVANCED RESEARCH PROJECTS AGENCY  
ARPA ORDER No. 1579, AMEND. 2  
PROGRAM CODE 1F10



The views and conclusions contained in this document are those of the author and should not be interpreted as necessarily representing the official policies, either expressed or implied, of the Advanced Research Projects Agency or the U. S. Government.

Reproduced by  
NATIONAL TECHNICAL  
INFORMATION SERVICE  
U S Department of Commerce  
Springfield VA 22151

DISTRIBUTION STATEMENT A  
Approved for public release;  
Distribution Unlimited



Fred H. Kulhawy  
Principal Investigator

DEPARTMENT OF CIVIL ENGINEERING  
SYRACUSE UNIVERSITY

UNCLASSIFIED

AD-764123

3200.8 (Att 1 to Encl 1)

Mar 7, 66

DOCUMENT CONTROL DATA - R & D		
(Security classification of title, body of abstract and indexing annotation must be entered when the overall report is classified)		
1. ORIGINATING ACTIVITY (Corporate author)		2a. REPORT SECURITY CLASSIFICATION
Syracuse University		Unclassified
		2b. GROUP
3. REPORT TITLE		
ANALYSIS OF UNDERGROUND OPENINGS IN ROCK BY FINITE ELEMENT METHODS		
4. DESCRIPTIVE NOTES (Type of report and inclusive dates)		
Final Technical Report - March 11, 1971 - July 31, 1972		
5. AUTHOR(S) (First name, middle initial, last name)		
Fred H. Kulhawy		
6. REPORT DATE	7a. TOTAL NO. OF PAGES	7b. NO. OF REFS
April 1972	287 310	76
8a. CONTRACT OR GRANT NO.	9a. ORIGINATOR'S REPORT NUMBER(S)	
H0210020	None	
b. PROJECT NO.		
c.	9b. OTHER REPORT NO(S) (Any other numbers that may be assigned this report)	
d.	None	
10. DISTRIBUTION STATEMENT		
Distribution of this document is unlimited.		
11. SUPPLEMENTARY NOTES		12. SPONSORING MILITARY ACTIVITY
		Advanced Research Projects Agency Washington, D.C. 20301
13. ABSTRACT		
<p>Finite element modeling techniques for underground openings in rock were discussed and a generalized method for excavation simulation was presented and its applicability was demonstrated. Analyses were conducted to establish the physical modeling criteria and minimum criteria were established for these models. Simple, practical, nonlinear and stress-dependent relationships were presented for the rock modulus and Poisson's ratio and for the discontinuity stiffness. An extensive literature survey was conducted to evaluate the parameters required for these relationships. Generalized analyses were conducted to evaluate the effect of opening shape, excavation sequence, initial stress, magnitude, variation and orientation, rock and discontinuity properties, and discontinuity orientation on the resulting behavior of underground openings in rock. A case history example of Edward Hyatt Powerplant demonstrated the general applicability of these techniques as an effective design and evaluation approach.</p>		

DD FORM 1 NOV 65 1473

UNCLASSIFIED

Security Classification

UNCLASSIFIED

Security Classification

3200.8 (Att 1 to Encl 1)  
Mar 7, 66

14. KEY WORDS	LINK A		LINK B		LINK C	
	ROLE	WT	ROLE	WT	ROLE	WT
Underground Openings						
Finite Element Method						
Excavation Simulation						
Finite Element Mesh Design						
Nonlinear Stress-Strain Relationships						
Nonlinear Rock Properties						
Nonlinear Discontinuity Properties						
Openings in Homogeneous Rock						
Openings in Rock with a Planar Discontinuity						
Edward Hyatt Powerplant						

UNCLASSIFIED

Security Classification

- i a



FINAL TECHNICAL REPORT

MARCH 11, 1971 - JULY 31, 1972

ARPA Order Number: 1579, Amend. 2

Contract Number: H0210029

Program Code Number: 1F10

Principal Investigator:

Fred H. Kulhawy

Name of Contractor:

Telephone Number: (315) 476-5541  
Ext. 2311

Syracuse University

Effective Date of Contract:

Project Scientist or Engineer:

March 11, 1971

Fred H. Kulhawy

Telephone Number: (315) 476-5541  
Ext. 2311

Contract Expiration Date:

Short Title of Work:

July 31, 1972

Analysis of Underground Openings  
in Rock by Finite Element Methods

Amount of Contract:

\$32,738

This research was supported by the Advanced Research Projects Agency  
of the Department of Defense and was monitored by Bureau of Mines under Contract  
Number H0210029.

16

## TECHNICAL REPORT SUMMARY

### Contract Objective

The objective of this research program is to investigate the practical application of the finite element method to predicting the behavior of underground openings in discontinuous rock, simply and realistically. The scope of the program includes: (1) literature surveys to evaluate the nonlinear, stress-dependent and anisotropic properties of rock types and discontinuities, (2) the establishment of modeling criteria for arbitrary excavation sequences, finite element meshes, rock behavior and discontinuity behavior, (3) analyses of underground openings to evaluate the effects of opening shape, excavation sequence, initial stress values and orientations, material properties and discontinuity orientation and properties, (4) analyses of the relative importance of the parameters investigated, and (5) a case history example to demonstrate the applicability of the techniques presented.

### General Approach and Technical Results

The initial studies were oriented mainly toward establishing finite element modeling criteria and parameters for use in subsequent analyses. In Chapter 2, the modeling techniques for finite element analyses of underground openings are presented. In this chapter, the salient features and advantages of the finite element method are briefly discussed and a generalized procedure for incremental excavation analysis is presented and its general applicability is demonstrated. A number of analyses were conducted to establish minimum criteria for the design of finite element meshes for underground openings and the results of these analyses are presented in the form of several typical meshes for use in subsequent analyses.

An extensive literature survey was conducted to evaluate the properties of rock types for use in analyses and to examine the applicability for rock of simple, practical stress-strain relationships recently proposed for soil. The results of this study show that these relationships simulate the nonlinear, stress-dependent behavior of rock quite well. The results of the literature survey, which included 163 values under uniaxial test conditions and 115 values

under triaxial test conditions, were tabulated and analyzed. It was found that for certain classes of rock, material properties varied little and that nonlinearity and/or stress-dependency was sometimes a minor factor in the behavior. Furthermore, this survey showed the degree and importance of anisotropy of the material properties. Details of the above are included in Chapter 3.

Chapter 4 presents the results of analyses which were conducted to investigate the importance of material properties, initial stresses, excavation operations and opening shapes on the final stresses and displacements around underground openings in homogeneous rock masses. The results of these analyses show that opening shape, initial stress magnitude, initial stress orientation and gravity initial stresses, when shallow, effect the resulting stresses and displacements considerably, while the modulus, in a linear analysis, or the initial tangent stiffness and stress-dependency in a nonlinear analysis, greatly effect the displacements. Poisson's ratio variations cause relatively small effects on the stresses and displacements and all other parameters cause minor, if any, variations. It should be noted that in all of these analyses, representative strength parameters were used. The mobilized shear stresses which resulted were small and subsequently no shear failures occurred. Furthermore, tension zones were allowed to develop and no analysis modifications were made to account for tension failure.

In Chapter 5 generalized analytical results are presented which evaluate the significance of discontinuity stiffness and orientation on the resulting stresses and displacements around underground openings in rock containing a single, prominent, planar discontinuity. The results of these analyses show that the stress changes, i.e., load transfer, become more substantial, tension zones increase, normal and shear stresses on the discontinuity decrease and displacements increase as the discontinuity becomes softer. These changes are very significant when  $M$  (discontinuity modulus/rock modulus) goes from 1 to 10, are fairly important when  $M$  goes from 10 to 100 and are small when  $M$  goes from 100 to 1000.

When the planes of the discontinuity and the minimum principal stress coincide, a substantial reduction occurs in the dimensionless  $\sigma_1$  values, the dimensionless normal stresses on the discontinuity are greatest, the discontinuity compression is greatest and the inward displacements are least. When the planes of the discontinuity and the maximum principal stress coincide, a substantial increase occurs in the dimensionless  $\sigma_1$  values in the discontinuity with a decrease adjacent to the discontinuity, the dimensionless shear stresses on the discontinuity are greatest, the discontinuity compression is least and the inward displacements are greatest. When the discontinuity is at  $45^\circ$  to the initial principal stresses and as the discontinuity becomes softer, the dimensionless  $\sigma_1$  values in the discontinuity become equal to one and the dimensionless  $\sigma_3$  values in the discontinuity become equal to K, the ratio of initial minor to major principal stresses. All other changes are minor.

An extensive literature survey was conducted to evaluate the properties of discontinuities which may be treated as thin (or one-dimensional) linear features and to examine the applicability of a simple, practical stress-deformation relationship for rock discontinuities. The results of this study show that these relationships simulate the behavior quite well. The results of the literature survey, including 32 different types of discontinuities were tabulated and analyzed and representative values of the parameters were noted in Chapter 6. It was found that many of the parameters do not vary over a very wide range.

Chapter 7 presents the results of analyses which were conducted to evaluate the effect of variations in the normal and shear stiffnesses of a one-dimensional discontinuity on the resulting stresses and displacements around underground openings in rock containing a single prominent discontinuity. The results of these analyses are similar to those obtained when a two-dimensional discontinuity was analyzed. These results show that, as the discontinuity becomes softer, the stress changes (or load transfer) become more substantial, tension zones increase, normal and shear stresses on the discontinuity decrease and displacements of the opening increase.



These conclusions can be further amplified since the stiffness of the one-dimensional discontinuity is based upon independent normal and shear stiffnesses. These studies show that the resulting stresses and displacements are affected more by the normal stiffness than by the shear stiffness, indicating that the stiffness component acting in the same direction as the initial maximum principal stress is the most important in determining the resulting behavior of the opening. These studies further showed that the nonlinearity of the shear stiffness is of minor importance but that the initial stiffness and stress-dependency is significant in determining the stresses and displacements of the opening.

To demonstrate the general applicability of the finite element techniques discussed in the report, four types of finite element analyses (1 step linear, 3 step linear, 3 step nonlinear and 3 step jointed) were conducted for the Edward Hyatt Powerplant beneath Oroville Dam. Based upon the results of these analyses and comparisons with the measured displacements of the powerplant opening, as shown in Chapter 8, it can be said that all of the analyses can provide reasonable representations of the observed behavior if the material properties can be adequately defined. The 1 step linear analysis is limited because it cannot follow the excavation sequence. Both of the linear analyses are limited because the selection of material properties hinges to a large degree on the availability of a large body of field data and a broad generalization of these results. The nonlinear analysis appears to yield displacements somewhat lower than those measured but the values for analysis are easily and inexpensively obtained. The jointed analysis appears to yield the best overall method of evaluating the performance of the opening. The rock properties can be determined as easily as for the nonlinear analysis, but field data is required to define the prominent discontinuities and their properties. However, if this data is available, the resulting deformations, stresses and stability of the rock mass may be evaluated with a reasonable degree of accuracy.

In summary it may be said that the analyses presented during the course of this investigation show that the finite element method, coupled with the analytical techniques for simulating the excavation sequence and the nonlinear, stress-dependent behavior of the rock and the discontinuities, can predict the behavior of underground openings in rock quite well. This approach is well-suited for practical use because the material properties can be evaluated relatively easily and the field excavation sequence can be followed directly.

For preliminary design and evaluation, the generalized results presented may be used very effectively to evaluate the probable range of behavior for a proposed opening. For final design and evaluation, the techniques presented may be used to:

- (1) predict stresses and displacements around openings in rock,
- (2) assess zones of potential instability,
- (3) aid in the selection of instrument locations, and
- (4) interpret the results obtained from field instrumentation.

#### DoD Implications

The behavior of hardened facilities sited in the earth's crust depends to a large extent on the physical properties of the site media and their behavior. Survivability/Vulnerability studies for these facilities, employing finite element analyses, require values for the physical properties as input data. This report contains tabulations of these properties for both linear and nonlinear rock and discontinuity behavior and also contains guidelines which may be followed for modeling these facilities in finite element analyses. This report also contains the results of a wide range of generalized analyses for openings in homogeneous rock and in rock containing a single, prominent, planar discontinuity. Since these analyses cover the most probable range of stresses and material properties which may be encountered, they can provide an effective reference for preliminary evaluation of an underground facility. The applicability of the techniques and results presented are demonstrated through a detailed case history analysis which show that these data would be very useful in the design of underground facilities.

## TABLE OF CONTENTS

	<u>Page</u>
TECHNICAL REPORT SUMMARY	ii
LIST OF FIGURES	ix
LIST OF TABLES	xix
LIST OF SYMBOLS	xxi
 CHAPTER 1. INTRODUCTION	 1
Geologic Factors	2
Construction Factors	3
Need for Simple, Practical and Analytical Methods and Results	3
 CHAPTER 2. FINITE ELEMENT MODELING TECHNIQUES	 5
Characteristics of the Finite Element Method	5
Nonlinear Material Behavior	6
Incremental Excavation	7
Incremental Excavation Simulation	8
Finite Element Mesh Design	14
 CHAPTER 3. STRESS-STRAIN BEHAVIOR OF ROCK	 32
Uniaxial Modulus and Poisson's Ratio Values	32
Nonlinear Stress-Dependent Modulus Relationship	33
Nonlinear Modulus Parameters Under Triaxial Conditions	47
Nonlinear Stress-Dependent Poisson's Ratio Relationship	53
Nonlinear Poisson's Ratio Parameters Under Triaxial Conditions	58
 CHAPTER 4. ANALYSIS OF OPENINGS IN HOMOGENEOUS ROCK MASSES	 61
Finite Element Idealization	61
Linear Material Properties	65
Gravity Stresses	69
Varying Initial Stresses and Orientations	78
Opening Shape	84
Nonlinear Material Properties	105
Excavation Step and Sequence Variation	114
Summary	114

(Continued)

	<u>Page</u>
CHAPTER 5. ANALYSIS OF OPENINGS IN ROCK CONTAINING A SINGLE PLANAR TWO-DIMENSIONAL DISCONTINUITY	115
Finite Element Idealization	115
Stresses Around Opening	118
Discontinuity Stresses	146
Opening Displacements	157
Summary	167
CHAPTER 6. STRESS-DEFORMATION BEHAVIOR OF PLANAR DISCONTINUITIES	168
One-Dimensional Element	168
Properties of Discontinuities	171
Equivalence of One-Dimensional and Two-Dimensional Element Properties	173
CHAPTER 7. ANALYSIS OF OPENINGS IN ROCK CONTAINING A SINGLE PLANAR ONE-DIMENSIONAL DISCONTINUITY	176
Finite Element Idealization	176
Stresses Around Opening	178
Discontinuity Stresses	185
Opening Displacements	185
Summary	188
CHAPTER 8. ANALYSIS OF THE BEHAVIOR OF EDWARD HYATT POWERPLANT	190
General Description of Edward Hyatt Powerplant	190
Site Geology	194
Engineering Investigations	198
Finite Element Idealization	200
Displacements	210
Stresses	224
Summary	235
CHAPTER 9. SUMMARY AND CONCLUSIONS	237
ACKNOWLEDGMENTS	242
REFERENCES	243
APPENDIX A. SELECTED UNITS CONVERSION FACTORS	250
APPENDIX B. COMPUTER PROGRAM USER'S GUIDE	251
APPENDIX C. COMPUTER PROGRAM LISTING	262
DD FORM 1473	286



## LIST OF FIGURES

<u>Figure</u>	<u>Title</u>	<u>Page</u>
2-1	Arbitrary Quadrilateral Element and Boundary Stress Distribution	10
2-2	Comparison of FEM Stresses with Correct Stresses for Laterally Restrained Column	13
2-3	Comparison of Final Stresses Around Example Rectangular Opening for 1 and 2 Step Excavation Sequence	15
2-4	Sequences Employed in Example Excavation of Rectangular Opening	16
2-5	Coarse Finite Element Mesh for Rectangular Opening	18
2-6	Fine Finite Element Mesh for Rectangular Opening	19
2-7	Fine Irregular Finite Element Mesh for Rectangular Opening	20
2-8	Contours of $\sigma_y$ Around Example Rectangular Opening	21
2-9	Contours of $\sigma_x$ Around Example Rectangular Opening	22
2-10	Contours of $\tau_{xy}$ Around Example Rectangular Opening	23
2-11	Finite Element Mesh for Investigation of Boundary Effect	25
2-12	Comparison of Theoretical and FEM Displacements Along, and Stresses Near, the Face of a Circular Opening	26
2-13	Effect of External Boundary Location on Accuracy of FEM Solution	27
2-14	Finite Element Mesh for Circular Opening in Homogeneous Rock	29
2-15	Finite Element Mesh for Horseshoe Opening in Homogeneous Rock	30
2-16	Finite Element Mesh for Power Station Opening in Homogeneous Rock	31
3-1	Typical Hyperbolic Stress-Strain Curve and Transformed Linear Hyperbolic Plot	41
3-2	Experimental and Hyperbolic Stress-Strain Curves for Cedar City Tonalite	43
3-3	Variations of Initial Tangent Modulus with Confining Pressure	45
3-4	Experimental and Hyperbolic Axial Strain-Radial Strain Curves for Cedar City Tonalite	55
3-5	Variations of Initial Tangent Poisson's Ratio with Confining Pressure	57

(Continued)

<u>Figure</u>	<u>Title</u>	<u>Page</u>
4-1	Finite Element Mesh for Circular Opening in Homogeneous Rock - Quarter Mesh	62
4-2	Finite Element Mesh for Circular Opening in Homogeneous Rock - Full Mesh	63
4-3	Excavation Sequences Employed for Analyses of Circular Opening	64
4-4	Contours of $\sigma_1/\sigma_{1i}$ for Circular Opening in Homogeneous Linear Rock, $K=1/3$ , $\theta=0^\circ$ (Variable Poisson's Ratio)	66
4-5	Contours of $\sigma_3/\sigma_{1i}$ for Circular Opening in Homogeneous Linear Rock, $K=1/3$ , $\theta=0^\circ$ (Variable Poisson's Ratio)	67
4-6	Displacements of Circular Opening in Homogeneous Linear Rock, $K=1/3$ , $\theta=0^\circ$ (Variable Poisson's Ratio)	68
4-7	Contours of $\sigma_1/\sigma_{1i}$ for Circular Opening in Homogeneous Linear Rock, $K=0$ , $\theta=0^\circ$ (Gravity Stresses, 100 Foot Deep)	70
4-8	Contours of $\sigma_1/\sigma_{1i}$ for Circular Openings in Homogeneous Linear Rock, $K=0$ , $\theta=0^\circ$ (Gravity Stresses, 300 Foot Deep)	71
4-9	Contours of $\sigma_1/\sigma_{1i}$ for Circular Openings in Homogeneous Linear Rock, $K=0$ , $\theta=0^\circ$ (Gravity Stresses, 500 Foot Deep)	72
4-10	Contours of $\sigma_1/\sigma_{1i}$ for Circular Openings in Homogeneous Linear Rock, $K=0$ , $\theta=0^\circ$ (Gravity Stresses, 1000 Foot Deep)	73
4-11	Contours of $\sigma_1/\sigma_{1i}$ for Circular Openings in Homogeneous Linear Rock, $K=0$ , $\theta=0^\circ$	74
4-12	Contours of $\sigma_3/\sigma_{1i}$ for Circular Openings in Homogeneous Linear Rock, $K=0$ , $\theta=0^\circ$ (Gravity Stresses, 500 Foot Deep)	75
4-13	Contours of $\sigma_3/\sigma_{1i}$ for Circular Openings in Homogeneous Linear Rock, $K=0$ , $\theta=0^\circ$	76
4-14	Displacements of Circular Opening in Homogeneous Linear Rock, $K=0$ , $\theta=0^\circ$ (Gravity and Constant Initial Stresses)	77
4-15	Stress Contours for Circular Opening in Homogeneous Linear Rock, $K=0$ , $\theta=0^\circ$	79

(Continued)

<u>Figure</u>	<u>Title</u>	<u>Page</u>
4-16	Stress Contours for Circular Opening in Homogeneous Linear Rock, $K=1/3$ , $\theta=0^\circ$	80
4-17	Stress Contours for Circular Opening in Homogeneous Linear Rock, $K=1$ , $\theta=0^\circ$	81
4-18	Stress Contours for Circular Opening in Homogeneous Linear Rock, $K=1/2$ , $\theta=90^\circ$	82
4-19	Displacements of Circular Opening in Homogeneous Linear Rock (Variable Initial Stresses)	83
4-20	Contours of $\sigma_1/\sigma_{1i}$ for Circular Opening in Homogeneous Linear Rock, $K=1/3$ , $\theta=45^\circ$	85
4-21	Contours of $\sigma_3/\sigma_{1i}$ for Circular Opening in Homogeneous Linear Rock, $K=1/3$ , $\theta=45^\circ$	86
4-22	Contours of $\sigma_1/\sigma_{1i}$ for Circular Opening in Homogeneous Linear Rock, $K=1/3$ , $\theta=45^\circ$ , (Gravity Stresses, 500 Foot Deep)	87
4-23	Contours of $\sigma_3/\sigma_{1i}$ for Circular Opening in Homogeneous Linear Rock, $K=1/3$ , $\theta=45^\circ$ (Gravity Stresses, 500 Foot Deep)	88
4-24	Contours of $\sigma_1/\sigma_{1i}$ for Horseshoe in Homogeneous Linear Rock, $K=1/3$ , $\theta=0^\circ$	89
4-25	Contours of $\sigma_1/\sigma_{1i}$ for Horseshoe in Homogeneous Linear Rock, $K=1$ , $\theta=0^\circ$	90
4-26	Contours of $\sigma_1/\sigma_{1i}$ for Horseshoe in Homogeneous Linear Rock, $K=1/2$ , $\theta=90^\circ$	91
4-27	Contours of $\sigma_3/\sigma_{1i}$ for Horseshoe in Homogeneous Linear Rock, $K=1/3$ , $\theta=0^\circ$	93
4-28	Contours of $\sigma_3/\sigma_{1i}$ for Horseshoe in Homogeneous Linear Rock, $K=1$ , $\theta=0^\circ$	94
4-29	Contours of $\sigma_3/\sigma_{1i}$ for Horseshoe in Homogeneous Linear Rock, $K=1/2$ , $\theta=90^\circ$	95

(Continued)

<u>Figure</u>	<u>Title</u>	<u>Page</u>
4-30	Displacements of Horseshoe in Homogeneous Linear Rock	96
4-31	Contours of $\sigma_1/\sigma_{1i}$ for Power Station in Homogeneous Linear Rock, $K=1/3$ , $\theta=0^\circ$	97
4-32	Contours of $\sigma_1/\sigma_{1i}$ for Power Station in Homogeneous Linear Rock, $K=1$ , $\theta=0^\circ$	98
4-33	Contours of $\sigma_1/\sigma_{1i}$ for Power Station in Homogeneous Linear Rock, $K=1/2$ , $\theta=90^\circ$	99
4-34	Contours of $\sigma_3/\sigma_{1i}$ for Power Station in Homogeneous Linear Rock, $K=1/3$ , $\theta=0^\circ$	101
4-35	Contours of $\sigma_3/\sigma_{1i}$ for Power Station in Homogeneous Linear Rock, $K=1$ , $\theta=0^\circ$	102
4-36	Contours of $\sigma_3/\sigma_{1i}$ for Power Station in Homogeneous Linear Rock, $K=1/2$ , $\theta=90^\circ$	103
4-37	Displacements of Power Station in Homogeneous Linear Rock	104
4-38	Contours of $\sigma_1/\sigma_{1i}$ for Circular Opening in Nonlinear Rock, $K=1/3$ , $\theta=0^\circ$ (Nonlinear Modulus)	106
4-39	Contours of $\sigma_3/\sigma_{1i}$ for Circular Opening in Nonlinear Rock, $K=1/3$ , $\theta=0^\circ$ (Nonlinear Modulus)	108
4-40	Contours of $\sigma_3/\sigma_{1i}$ for Circular Opening in Homogeneous Linear Rock, $K=1/3$ , $\theta=0^\circ$	109
4-41	Displacements of Circular Opening in Nonlinear Rock, $K=1/3$ , $\theta=0^\circ$ (Nonlinear Modulus)	110
4-42	Contours of $\sigma_3/\sigma_{1i}$ for Circular Opening in Nonlinear Rock, $K=1/3$ , $\theta=0^\circ$ (Nonlinear Modulus and Poisson's Ratio)	111
4-43	Contours of $\sigma_3/\sigma_{1i}$ for Circular Opening in Nonlinear Rock, $K=1/3$ , $\theta=0^\circ$ (Nonlinear Modulus and Poisson's Ratio)	112



(Continued)

<u>Figure</u>	<u>Title</u>	<u>Page</u>
4-44	Displacements of Circular Opening in Nonlinear Rock, $K=1/3$ , $\theta=0^\circ$ (Nonlinear Modulus and Poisson's Ratio)	113
5-1	Finite Element Mesh for Circular Opening in Rock with a Planar Discontinuity	116
5-2	Finite Element Mesh for Circular Opening in Rock with a Planar Discontinuity at $45^\circ$	117
5-3	Stress Contours for Circular Opening in Rock with a Planar Discontinuity, $K=1/3$ , $\theta=0^\circ$ , $\alpha=0^\circ$ , $M=10$	119
5-4	Stress Contours for Circular Opening in Rock with a Planar Discontinuity, $K=1/3$ , $\theta=0^\circ$ , $\alpha=0^\circ$ , $M=100$	120
5-5	Stress Contours for Circular Opening in Rock with a Planar Discontinuity, $K=1/3$ , $\theta=0^\circ$ , $\alpha=0^\circ$ , $M=1000$	121
5-6	Stress Contours for Circular Opening in Rock with a Planar Discontinuity, $K=1/3$ , $\theta=0^\circ$ , $\alpha=90^\circ$ , $M=10$	122
5-7	Stress Contours for Circular Opening in Rock with a Planar Discontinuity, $K=1/3$ , $\theta=0^\circ$ , $\alpha=90^\circ$ , $M=100$	123
5-8	Stress Contours for Circular Opening in Rock with a Planar Discontinuity, $K=1/3$ , $\theta=0^\circ$ , $\alpha=90^\circ$ , $M=1000$	124
5-9	Contours of $\sigma_1/\sigma_{1i}$ for Circular Opening in Rock with a Planar Discontinuity, $K=1/3$ , $\theta=0^\circ$ , $\alpha=45^\circ$ , $M=10$	125
5-10	Contours of $\sigma_3/\sigma_{1i}$ for Circular Opening in Rock with a Planar Discontinuity, $K=1/3$ , $\theta=0^\circ$ , $\alpha=45^\circ$ , $M=10$	126
5-11	Contours of $\sigma_1/\sigma_{1i}$ for Circular Opening in Rock with a Planar Discontinuity, $K=1/3$ , $\theta=0^\circ$ , $\alpha=45^\circ$ , $M=1000$	127
5-12	Contours of $\sigma_3/\sigma_{1i}$ for Circular Opening in Rock with a Planar Discontinuity, $K=1/3$ , $\theta=0^\circ$ , $\alpha=45^\circ$ , $M=1000$	128
5-13	Stress Contours for Circular Opening in Rock with a Planar Discontinuity, $K=1$ , $\theta=0^\circ$ , $\alpha=0^\circ$ , $M=10$	130

(Continued)

<u>Figure</u>	<u>Title</u>	<u>Page</u>
5-14	Stress Contours for Circular Opening in Rock with a Planar Discontinuity, $K=1$ , $\theta=0^\circ$ , $\alpha=0^\circ$ , $M=100$	131
5-15	Stress Contours for Circular Opening in Rock with a Planar Discontinuity, $K=1$ , $\theta=0^\circ$ , $\alpha=0^\circ$ , $M=1000$	132
5-16	Stress Contours for Circular Opening in Rock with a Planar Discontinuity, $K=1$ , $\theta=0^\circ$ , $\alpha=90^\circ$ , $M=10$	133
5-17	Stress Contours for Circular Opening in Rock with a Planar Discontinuity, $K=1$ , $\theta=0^\circ$ , $\alpha=90^\circ$ , $M=100$	134
5-18	Stress Contours for Circular Opening in Rock with a Planar Discontinuity, $K=1$ , $\theta=0^\circ$ , $\alpha=90^\circ$ , $M=1000$	135
5-19	Contours of $\sigma_1/\sigma_{1i}$ for Circular Opening in Rock with a Planar Discontinuity, $K=1$ , $\theta=0^\circ$ , $\alpha=45^\circ$ , $M=10$	136
5-20	Contours of $\sigma_3/\sigma_{1i}$ for Circular Opening in Rock with a Planar Discontinuity, $K=1$ , $\theta=0^\circ$ , $\alpha=45^\circ$ , $M=10$	137
5-21	Contours of $\sigma_1/\sigma_{1i}$ for Circular Opening in Rock with a Planar Discontinuity, $K=1$ , $\theta=0^\circ$ , $\alpha=45^\circ$ , $M=1000$	138
5-22	Contours of $\sigma_3/\sigma_{1i}$ for Circular Opening in Rock with a Planar Discontinuity, $K=1$ , $\theta=0^\circ$ , $\alpha=45^\circ$ , $M=1000$	139
5-23	Stress Contours for Circular Opening in Rock with a Planar Discontinuity, $K=1/2$ , $\theta=90^\circ$ , $\alpha=0^\circ$ , $M=10$	140
5-24	Stress Contours for Circular Opening in Rock with a Planar Discontinuity, $K=1/2$ , $\theta=90^\circ$ , $\alpha=0^\circ$ , $M=100$	141
5-25	Stress Contours for Circular Opening in Rock with a Planar Discontinuity, $K=1/2$ , $\theta=90^\circ$ , $\alpha=0^\circ$ , $M=1000$	142
5-26	Stress Contours for Circular Opening in Rock with a Planar Discontinuity, $K=1/2$ , $\theta=90^\circ$ , $\alpha=90^\circ$ , $M=10$	143

(Continued)

<u>Figure</u>	<u>Title</u>	<u>Page</u>
5-27	Stress Contours for Circular Opening in Rock with a Planar Discontinuity, $K=1/2$ , $\theta=90^\circ$ , $\alpha=90^\circ$ , $M=100$	144
5-28	Stress Contours for Circular Opening in Rock with a Planar Discontinuity, $K=1/2$ , $\theta=90^\circ$ , $\alpha=90^\circ$ , $M=1000$	145
5-29	Contours of $\sigma_1/\sigma_{1i}$ for Circular Opening in Rock with a Planar Discontinuity, $K=1/2$ , $\theta=90^\circ$ , $\alpha=45^\circ$ , $M=10$	147
5-30	Contours of $\sigma_3/\sigma_{1i}$ for Circular Opening in Rock with a Planar Discontinuity, $K=1/2$ , $\theta=90^\circ$ , $\alpha=45^\circ$ , $M=10$	148
5-31	Contours of $\sigma_1/\sigma_{1i}$ for Circular Opening in Rock with a Planar Discontinuity, $K=1/2$ , $\theta=90^\circ$ , $\alpha=45^\circ$ , $M=1000$	149
5-32	Contours of $\sigma_3/\sigma_{1i}$ for Circular Opening in Rock with a Planar Discontinuity, $K=1/2$ , $\theta=90^\circ$ , $\alpha=45^\circ$ , $M=1000$	150
5-33	Normal Stresses on Horizontal Discontinuity	151
5-34	Normal Stresses on Vertical Discontinuity	152
5-35	Normal Stresses on $45^\circ$ Discontinuity	153
5-36	Shear Stresses Along Horizontal Discontinuity	154
5-37	Shear Stresses Along Vertical Discontinuity	155
5-38	Shear Stresses Along $45^\circ$ Discontinuity	156
5-39	Displacements of Circular Opening in Rock with a Planar Discontinuity, $K=1/3$ , $\theta=0^\circ$ , $\alpha=0^\circ$	158
5-40	Displacements of Circular Opening in Rock with a Planar Discontinuity, $K=1$ , $\theta=0^\circ$ , $\alpha=0^\circ$	159
5-41	Displacements of Circular Opening in Rock with a Planar Discontinuity, $K=1/2$ , $\theta=90^\circ$ , $\alpha=0^\circ$	160
5-42	Displacements of Circular Opening in Rock with a Planar Discontinuity, $K=1/3$ , $\theta=0^\circ$ , $\alpha=90^\circ$	161

(Continued)

<u>Figure</u>	<u>Title</u>	<u>Page</u>
5-43	Displacements of Circular Opening in Rock with a Planar Discontinuity, $K=1$ , $\theta=0^\circ$ , $\alpha=90^\circ$	162
5-44	Displacements of Circular Opening in Rock with a Planar Discontinuity, $K=1/2$ , $\theta=90^\circ$ , $\alpha=90^\circ$	163
5-45	Displacements of Circular Opening in Rock with a Planar Discontinuity, $K=1/3$ , $\theta=0^\circ$ , $\alpha=45^\circ$	164
5-46	Displacements of Circular Opening in Rock with a Planar Discontinuity, $K=1$ , $\theta=0^\circ$ , $\alpha=45^\circ$	165
5-47	Displacements of Circular Opening in Rock with a Planar Discontinuity, $K=1/2$ , $\theta=90^\circ$ , $\alpha=45^\circ$	166
6-1	Modes of Behavior of Discontinuity Element	169
6-2	Typical Stress-Deformation Behavior of Discontinuities	172
7-1	Finite Element Mesh for Circular Opening in Rock with a One-Dimensional Planar Discontinuity	177
7-2	Contours of $\sigma_1/\sigma_{1i}$ for Circular Opening in Rock with a 1-D Discontinuity, $K=1/3$ , $\theta=0^\circ$ , $\alpha=0^\circ$ , $M_j=20$	179
7-3	Contours of $\sigma_3/\sigma_{1i}$ for Circular Opening in Rock with a 1-D Discontinuity, $K=1/3$ , $\theta=0^\circ$ , $\alpha=0^\circ$ , $M_j=20$	180
7-4	Contours of $\sigma_1/\sigma_{1i}$ for Circular Opening in Rock with a 1-D Discontinuity, $K=1/3$ , $\theta=0^\circ$ , $\alpha=0^\circ$ , $M_j=2$	181
7-5	Contours of $\sigma_3/\sigma_{1i}$ for Circular Opening in Rock with a 1-D Discontinuity, $K=1/3$ , $\theta=0^\circ$ , $\alpha=0^\circ$ , $M_j=2$	182
7-6	Contours of $\sigma_1/\sigma_{1i}$ for Circular Opening in Rock with a 1-D Discontinuity, $K=1/3$ , $\theta=0^\circ$ , $\alpha=0^\circ$ , $M_j=200$	183
7-7	Contours of $\sigma_3/\sigma_{1i}$ for Circular Opening in Rock with a 1-D Discontinuity, $K=1/3$ , $\theta=0^\circ$ , $\alpha=0^\circ$ , $M_j=200$	184



(Continued)

<u>Figure</u>	<u>Title</u>	<u>Page</u>
7-8	Normal and Shear Stresses on Horizontal 1-D Discontinuity	186
7-9	Displacements of Circular Opening in Rock with a 1-D Discontinuity, $K=1/3$ , $\theta=0^\circ$ , $\alpha=0^\circ$ , $K_t$ Variable	187
7-10	Displacements of Circular Opening in Rock with a 1-D Discontinuity, $K=1/3$ , $\theta=0^\circ$ , $\alpha=0^\circ$ , $K_n$ Variable	189
8-1	Edward Hyatt Powerplant Near Completion of Excavation	191
8-2	Plan View of Oroville Dam and Edward Hyatt Powerplant	192
8-3	Location of Edward Hyatt Powerplant Beneath Oroville Dam	193
8-4	Model of Edward Hyatt Powerplant, Left Wall	195
8-5	Model of Edward Hyatt Powerplant, Right Wall	196
8-6	Isometric View of Edward Hyatt Powerplant Geology	197
8-7	Excavation Sequence for Crown Opening, Edward Hyatt Powerplant	201
8-8	Unit One Excavation Sequence, Edward Hyatt Powerplant	202
8-9	Mesh for Homogeneous Analyses of Edward Hyatt Powerplant	203
8-10	Discontinuities Through Unit One, Edward Hyatt Powerplant	205
8-11	Modeled Discontinuities Through Unit One, Edward Hyatt Powerplant	206
8-12	Mesh for Jointed Analysis of Edward Hyatt Powerplant	207
8-13	Typical Installation of Borehole Extensometers, Edward Hyatt Powerplant	211
8-14	Displacements of Opening Face, Edward Hyatt Powerplant - 1 Step Linear Analysis	217
8-15	Displacements of Opening Face, Edward Hyatt Powerplant - 3 Step Linear Analysis	218
8-16	Displacements of Opening Face, Edward Hyatt Powerplant - Nonlinear Analysis	219
8-17	Displacements of Opening Face, Unit One, Edward Hyatt Powerplant - Jointed Analysis	220
8-18	Movement of Rock Blocks Around Edward Hyatt Powerplant - Step 1	221
8-19	Movement of Rock Blocks Around Edward Hyatt Powerplant - Step 2	222
8-20	Movement of Rock Blocks Around Edward Hyatt Powerplant - Step 3	223

(Continued)

<u>Figure</u>	<u>Title</u>	<u>Page</u>
8-21	Contours of $\sigma_1/\sigma_{1i}$ for Unit One, Edward Hyatt Power-plant, Nonlinear Analysis - Steps 1 and 2	225
8-22	Contours of $\sigma_1/\sigma_{1i}$ for Unit One, Edward Hyatt Power-plant, Nonlinear Analysis - Step 3	226
8-23	Contours of $\sigma_3/\sigma_{1i}$ for Unit One, Edward Hyatt Power-plant, Nonlinear Analysis - Steps 1 and 2	227
8-24	Contours of $\sigma_3/\sigma_{1i}$ for Unit One, Edward Hyatt Power-plant, Nonlinear Analysis - Step 3	228
8-25	Contours of $\sigma_1$ for Unit One, Edward Hyatt Powerplant, Jointed Analysis - Step 1	229
8-26	Contours of $\sigma_1$ for Unit One, Edward Hyatt Powerplant, Jointed Analysis - Step 2	230
8-27	Contours of $\sigma_1$ for Unit One, Edward Hyatt Powerplant, Jointed Analysis - Step 3	231
8-28	Contours of $\sigma_3$ for Unit One, Edward Hyatt Powerplant, Jointed Analysis - Step 1	232
8-29	Contours of $\sigma_3$ for Unit One, Edward Hyatt Powerplant, Jointed Analysis - Step 2	233
8-30	Contours of $\sigma_3$ for Unit One, Edward Hyatt Powerplant, Jointed Analysis - Step 3	234
8-31	Mobilized Strength Along Discontinuities Around Edward Hyatt Powerplant	236

# LIST OF TABLES

<u>Table</u>	<u>Title</u>	<u>Page</u>
3-1	Uniaxial Stress-Strain Parameters for Igneous (Plutonic) Rock Types	34
3-2	Uniaxial Stress-Strain Parameters for Igneous (Volcanic) Rock Types and for Metamorphic (Non-Foliated) Rock Types	35
3-3	Uniaxial Stress-Strain Parameters for Metamorphic (Foliated) Rock Types	36
3-4	Uniaxial Stress-Strain Parameters for Sedimentary (Clastic) Rock Types	37
3-5	Uniaxial Stress-Strain Parameters for Sedimentary (Chemical) Rock Types	38
3-6	Summary of Uniaxial Stress-Strain Parameters	39
3-7	Triaxial Stress-Strain Parameters for Igneous (Plutonic and Volcanic) Rock Types	48
3-8	Triaxial Stress-Strain Parameters for Metamorphic (Foliated and Non-Foliated) Rock Types	49
3-9	Triaxial Stress-Strain Parameters for Sedimentary (Clastic) Rock Types	50
3-10	Triaxial Stress-Strain Parameters for Sedimentary (Chemical) Rock Types	51
3-11	Summary of Triaxial Stress-Strain Parameters	52
3-12	Triaxial Poisson's Ratio Parameters for Various Rock Types	59
3-13	Summary of Nonlinear Triaxial Poisson's Ratio Parameters	60
6-1	Properties of Discontinuities under Direct Shear Conditions	174
8-1	Summary of Rock Moduli, Edward Hyatt Powerplant	199
8-2	Description of Modeled Discontinuities, Edward Hyatt Powerplant	208
8-3	Summary of Properties Used in Analyses of Edward Hyatt Powerplant	209

(Continued)

<u>Table</u>	<u>Title</u>	<u>Page</u>
8-4	Measured and Computed Vertical Displacements for 20 Foot Centerline Crown Extensometers, Edward Hyatt Powerplant	212
8-5	Measured Relative Displacements for 40 Foot Extensometers, Edward Hyatt Powerplant	213
8-6	Measured and Computed Displacements for 40 Foot Extensometers, Edward Hyatt Powerplant	215

## LIST OF SYMBOLS

### English Letters

#### a) upper case

E	elastic modulus
$E_i, E_t$	initial tangent, tangent modulus
F	force; parameter relating variation of $v_i$ with $\sigma_3$
{F}	nodal force matrix
G	shear modulus; $v_i$ at one atmosphere
[H]	boundary geometry matrix
K	modulus number (always $\gg 1$ ); ratio of $\sigma_{3i}/\sigma_{1i}$ (always $\leq 1$ )
$K_j$	stiffness number
$K_n, K_s$	normal, shear stiffness
$K_{si}, K_{st}$	initial tangent, tangent shear stiffness
M	ratio of rock modulus/discontinuity modulus
$M_j$	ratio of rock modulus/unit normal stiffness
[Q]	matrix relating nodal forces and element stresses
R	radius
$R_f, R_{fj}$	failure ratio, discontinuity failure ratio
T	discontinuity thickness

#### b) lower case

a	reciprocal of initial tangent modulus
{a}	interpolation coefficient matrix
b	reciprocal of asymptote to stress-strain curve
c	cohesion
$c_j$	discontinuity cohesion
d	tangent Poisson's ratio parameter
f	tangent Poisson's ratio parameter
[m]	coordinate matrix for stresses
n	modulus exponent
$n_j$	stiffness exponent



(Continued)

$[n]$	nodal point coordinate matrix
$p_a$	atmospheric pressure
$x$	horizontal coordinate
$y$	vertical coordinate

Greek Letters

$\alpha$	orientation of discontinuity counterclockwise from horizontal
$\gamma$	unit weight
$\gamma_w$	unit weight of water
$\delta$	displacement
$\delta_n, \delta_s$	normal, shear displacement of discontinuity
$\epsilon$	strain
$\epsilon_a, \epsilon_r$	axial, radial strain
$\theta$	orientation of $\sigma_{3i}$ counterclockwise from horizontal
$\nu$	Poisson's ratio
$\nu_i, \nu_t$	initial tangent, tangent Poisson's ratio
$\sigma$	stress
$\sigma_x, \sigma_y$	horizontal, vertical stress
$\sigma_1, \sigma_3$	maximum, minimum principal stress
$\sigma_{1i}, \sigma_{3i}$	initial maximum, minimum principal stress
$\sigma_H, \sigma_V$	horizontal, vertical stress
$\sigma_{ni}, \sigma_n$	initial normal, normal stress
$\sigma_j$	discontinuity normal stress
$(\sigma_1 - \sigma_3)_f$	deviator stress at failure
$(\sigma_1 - \sigma_3)_{ult}$	ultimate deviator stress
$\tau$	shear stress
$\tau_j$	discontinuity shear stress
$\tau_{xy}$	shear stress on xy plane
$\phi$	angle of friction
$\phi_j$	discontinuity angle of friction

CHAPTER 1  
INTRODUCTION

Widespread use of instrumentation in many large underground openings in rock during recent years has shown that substantial movements may occur even in the most carefully analyzed and designed openings. Even though methods of construction and instrumentation and techniques for predicting geologic conditions are rapidly improving, the recent literature contains numerous case histories of well-engineered underground openings in which substantial movement and breakage occurred. This movement and breakage becomes of special significance when there is a loss of human life or of equipment, or when it is found that redesign of the support system is necessary to accommodate the rock mass behavior.

Sufficiently general theoretical methods for predicting the behavior of underground openings in rock are virtually non-existent. For this reason, engineers must rely upon experience and upon case histories when they design and attempt to predict the behavior of a proposed opening. Therefore it is desirable to develop a rational and practical procedure for predicting the behavior of underground openings in rock. Such a procedure could be used to: (1) predict the stresses and movements in underground openings prior to construction, (2) isolate potentially troublesome zones around a proposed opening, (3) study the effects of various construction sequences on the behavior of an opening, (4) help in selecting the types and locations of proposed instruments and (5) aid in the interpretation of the results of instrumentation studies.

The rapid development of large capacity, high speed, digital computers in the last decade, coupled with powerful new methods of analysis such as the finite element method, has made it feasible to investigate the complex behavior of underground openings. Since the finite element method can be applied, at least in principle, to any continuous system and to many classes of discontinuous systems, it possesses the flexibility and generality needed to analyze the behavior of underground openings.

Therefore this study was initiated to investigate the practical application of the finite element method to predicting opening behavior, simply and realistically. Approaches will be presented for simulating actual field construction sequences and nonlinear material behavior within the basic context of the finite element

method. Furthermore, guidelines and results will be presented for realistically modeling and treating the numerous interacting factors influencing the resulting behavior of underground openings during construction.

### Geologic Factors

Rock masses are complex media composed of three distinct, yet interacting, components which could be described as the rock types, rock structures and discontinuities. Rock types are numerous and range from sedimentary types, formed by induration of sediments or chemical precipitation, to igneous types, formed by cooling of the magma at or beneath the surface of the earth, to metamorphic types, formed by alteration of the sedimentary or igneous rocks by heat, pressure or chemical action. Although genetically different, many rock types perform similarly under load and therefore, from an engineering standpoint, the physical behavior of the rock must be considered. Under these conditions, it is found that rock types range in behavior under load from linear, elastic and brittle to nonlinear, inelastic and ductile, and from isotropic to anisotropic. Any method of analysis which models rock properties should have the capabilities to model this range of properties in a relatively straightforward manner and should be based upon parameters which can be obtained relatively easily in the laboratory. Elastic, elastic-plastic, rheological, and other types of models have shortcomings in this sense because they are based upon limited ranges of rock behavior and/or upon parameters not readily obtainable in the laboratory.

Rock structural features are of two main types: bedding and folding. Features of this type are mainly geometric and could readily be treated in finite element analyses by introducing the appropriate geometry and material properties of the units involved. However, there are substantial problems involved in modeling these features because the behavior of the bedding plane contacts must be considered and the initial stress field must be known in the beds as well as in the folded structures. Assuming that these problems can be surmounted, realistic models can be established to treat these structures in analyses.

Discontinuities play a major role in the behavior of rock masses. These features may range from random minute joints to large planar features such as faults, any of which may have nearly any orientation within the rock mass. Modeling these discontinuities is a complex problem from both engineering and geologic standpoints. Geologically, the attitude, continuity, uniformity, thickness and

repetitiveness of the discontinuities must be known. From an engineering standpoint, the physical behavior must be known. Recent studies (e.g., Goodman, 1969) along these lines indicate that discontinuities also have a wide range in behavior under load. Analytical methods should be able to incorporate these discontinuities and their physical properties to provide realistic evaluations of the behavior of the rock masses.

Stress systems existing in rock masses further complicate any analytical analyses because the stresses may be isotropic, transversely isotropic or highly anisotropic. Furthermore the major principal stress may range from horizontal to vertical and may or may not coincide with the orientation of the discontinuities. In any case, it is imperative that the initial stresses be known and that analyses be capable of modeling the initial stress conditions in the rock masses.

#### Construction Factors

When an underground opening is made in a rock mass, stress changes occur which cause movements around the opening. The type and magnitude of stress changes and movements which occur are not only a function of the geologic conditions cited above, but are also a function of the sequence of construction operations employed to make the opening. For example, a multiple drift sequence may cause undesirable roof movements along a discontinuity in an opening while a full face sequence might not because of an arching mechanism maintaining the integrity of the roof. If behavior such as this occurs, the support system required will be substantially different and the extent of overbreak may differ greatly. Because of these effects, it is important to be able to predict beforehand the stresses and movements which may occur around an underground opening and to correlate these with construction sequences to be employed in the field.

#### Need For Simple, Practical Analytical Methods and Results

The various factors briefly discussed above indicate some of the more important points to be considered in analyses of underground openings in rock. Numerous research studies have been conducted during recent years along these lines, but a large number of these studies have been "technique oriented" rather than "result oriented". Many questions remain to be answered. Among those are: (1) How nonlinear and/or anisotropic are rocks and how important is this in analyses? (2) How can the

nonlinearity be treated in a relatively straightforward manner? (3) How important are discontinuities in the behavior of rock masses around underground openings? (4) What are the properties of discontinuities? (5) How important are the initial stress conditions in rock masses? and (6) How important are construction sequences and opening shapes upon the resulting behavior of an opening?

Advances have been made into many of these areas, but few guidelines have been established. Realistic models, literature surveys and finite element analyses can be employed to provide further guidelines. It is hoped that through this study, guidelines may be provided in an effort to help to resolve these questions.



## CHAPTER 2

### FINITE ELEMENT MODELING TECHNIQUES

A number of procedures have been employed to perform analyses of stresses and/or movements around underground openings in rock. These have included closed-form elasticity solutions, finite difference numerical analyses, photoelastic analyses and finite element analyses. Examples of the first three can be referred to in basic Rock Mechanics texts (e.g., Obert and Duvall, 1967), while examples of the fourth can be found in both the International Rock Mechanics Congresses and in geo-technical journals.

Although many interesting and useful results have been obtained using each of these procedures, the finite element method of analysis is the most general and useful. It may be used for analyses of stresses and movements around underground openings in nonhomogeneous, discontinuous and anisotropic rock and, with suitable techniques, may be used to obtain approximate solutions for problems involving nonlinear material properties. Furthermore, the method may be used for problems in which the initial stress conditions and construction operations should be considered. The important characteristics of the finite element method as applied to analyses of underground openings in rock and procedures for its use are described in subsequent sections of this chapter.

#### Characteristics of the Finite Element Method

Since its introduction by Turner et al. (1956), the finite element method has been shown to be a very powerful procedure for stress analyses and has been used for many different purposes. A number of excellent papers have been published on this method (notably Clough, 1960, 1965, and Wilson, 1963) as well as two textbooks (Zienkiewicz and Cheung, 1967 and Desai and Abel, 1971).

For analysis by the finite element method, the continuous body is represented by a set of elements which are connected at their joints or nodal points. On the basis of an assumed variation of strains within elements together with the stress-strain characteristics of the element material, the stiffness of each nodal point of each element is computed. For each nodal point in the system, two equilibrium equations may be written expressing the nodal point forces in

terms of the nodal point displacements and stiffnesses. These equations are solved to determine the unknown displacements. With the displacements of all nodal points known, strains and stresses within each element may be computed. Analyses of realistic systems commonly requires formulation and solution of several hundred simultaneous equations, and the technique is only practical when formulated for high-speed digital computers.

Various types of elements have been developed; these elements differ in shape, number of nodal points, and assumed mode of strain variation within elements. The element used in this study is a quadrilateral consisting of two linear strain triangles (Felippa, 1966). Within this element strains are assumed to vary linearly, but to insure compatibility between elements, the strains on the outside boundaries of the quadrilateral are assumed to be constant. Studies by Felippa (1966) have shown that this element provides a good combination of efficiency and accuracy over a wide range of loading conditions.

The analyses performed in this study are plane strain analyses of sections normal to the axis of the underground opening. This type of analysis represents a close approximation of the actual strain conditions within essentially homogeneous rock masses and within rock masses containing beds and discontinuities whose strike and dip are reasonably coincident with the trend and plunge of the axis of the opening. For other cases, this type of analysis often will provide useful and reasonably accurate approximations of the true behavior.

#### Nonlinear Material Behavior

Two types of stress-strain behavior, linear and nonlinear, have been employed in the analyses to be conducted for this study. In the linear analyses, constant and equal values of modulus and Poisson's ratio are assigned to all of the finite elements modeling the rock mass. In the nonlinear analyses, the nonlinearity is approximated by assigning modulus and Poisson's ratio values to each element which are consistent with the stress values in the element. The analyses are performed using a step-by-step or incremental analysis procedure in which successive stages in the excavation of an opening are simulated. During each step or increment the relationship between stress and strain is assumed to be linear; nonlinearity is approximated in the analyses by appropriate changes in the values of modulus and Poisson's ratio during successive stages of the analyses. The procedures

for determining the modulus and Poisson's ratio parameters required for use in these analyses are described in a subsequent chapter of this report.

#### Incremental Excavation

Underground openings are excavated by a number of different procedures. Small openings with simple shapes such as circles are commonly excavated in one step either by tunnelling machines or by a single full face blast. Large openings or openings with complex shapes such as a power station opening are commonly excavated in several or more steps by multiple drift or head and bench procedures. To realistically model these variable excavation procedures, techniques must be employed in the analytical simulation which are capable of following arbitrary construction sequences. Several procedures for analytically simulating excavation operations have been proposed in recent years (Goodman and Brown, 1963; Brown and King, 1966; Dunlop et al, 1968; Duncan and Goodman, 1968; Chang and Duncan, 1970; and Clough and Duncan, 1969). All of these procedures have been developed primarily for surface excavations in soil, but they have shown that excavation operations can be realistically simulated in finite element analyses. The most general of these procedures, that of Clough and Duncan (1969), can be readily adapted for any type of excavation operation.

The basic premise in these procedures is that the soil or rock is in equilibrium and at rest in an initially stressed state. The excavation is simulated by evaluating the stresses along the potential excavation surface, computing the equivalent forces at the nodes of the finite elements along the excavation surface, reversing the signs of the forces and then applying these forces to the finite element mesh while reducing the modulus of the "removed" elements to an insignificant value. The computed stresses, strains and displacements are then added to the original values to obtain the stresses, strains and displacements at the end of the excavation step. This procedure can then be continued for any number of excavation steps such that an excavation can be followed readily on a step-by-step basis.

This approach is in contrast to those commonly employed in finite element analyses of underground openings in which "gravity turn-on" or relaxation approaches are used. In the "gravity turn-on" approach, two analyses must be conducted. These two analyses are conducted by first applying gravity to a finite

element mesh without the opening and secondly applying gravity to a finite element mesh with the opening. The differences between the two analyses are the stresses, strains and displacements caused by making the opening. This approach suffers from several drawbacks. First, Goodman and Brown (1963), among others cited previously, have shown that the resulting stresses are independent of construction sequence only in homogeneous, isotropic, linear elastic materials. Second, Dunlop et al (1968) have shown that the step-by-step and "gravity turn-on" analyses are equivalent only when the initial stresses are directly related by Poisson's ratio,  $\nu$ , or  $\sigma_3 = (\frac{\nu}{1-\nu})\sigma_1$ , in which  $\sigma_3$  and  $\sigma_1$  are the minimum and maximum principal stresses, respectively, and  $\sigma_1$  is the vertical stress. Third, the "gravity turn-on" analysis cannot model a construction sequence.

In the relaxation approach, also known as the residual stress approach, the final geometry of the opening is usually established in the initial finite element mesh. The elements representing the surrounding rock mass are initially stressed to some desired values which are subsequently relaxed to provide a final equilibrium stress state around the opening. With this approach it is difficult to follow a construction sequence simply and therefore to follow the incremental changes of the rock properties as the opening is made. In addition, the relaxation is controlled exclusively by the stresses existing in the elements which are part of the rock mass remaining after the opening is excavated. The stresses existing in the elements removed during excavation are usually not considered.

On the other hand, the stress reversal approach considers the stresses existing in the elements on both sides of a proposed excavation boundary at any stage of excavation, and based upon these stresses evaluates the equivalent nodal forces to be applied along the boundary to release the stresses actually occurring along the boundary. Furthermore by following the stress changes at each stage of excavation and subsequently changing the values of modulus and Poisson's ratio in accordance with the changing stress values in the elements, the actual nonlinear behavior of the rock mass can be followed on a more rational basis. Details of this approach are given below.

#### Incremental Excavation Simulation

In the finite element method, stresses are commonly determined at either the center of the elements or midway between two opposing nodal points, depending

upon the type of elements used, but excavation boundaries pass between elements. Therefore a technique must be employed to interpolate from the center stresses to the nodal or boundary stresses before the nodal point forces are evaluated. The approach outlined below is essentially the one used by Clough and Duncan (1969), with only slight modification, and is repeated here because the details of the method are not readily available in the general literature.

To express the relationship between the known stresses at the element centers and the unknown stresses at the nodal points, a polynomial interpolation formula of the form given below may be used:

$$\sigma = a_1 + a_2 x + a_3 y + a_4 xy \quad (2-1)$$

in which  $\sigma$  is the interpolated nodal stress,  $x$  and  $y$  are the nodal point coordinates and  $a_1, a_2, a_3$  and  $a_4$  are the interpolation coefficients. In its most general form, the excavation of a quadrilateral element creates four excavation boundaries and Equation 2-1 is used to determine the stresses at the four element nodes. By assuming a linear stress variation between the nodal stress values, the complete stress distribution is obtained around the element, as shown in Figure 2-1. Equivalent nodal point forces can then be established from the boundary stress distribution.

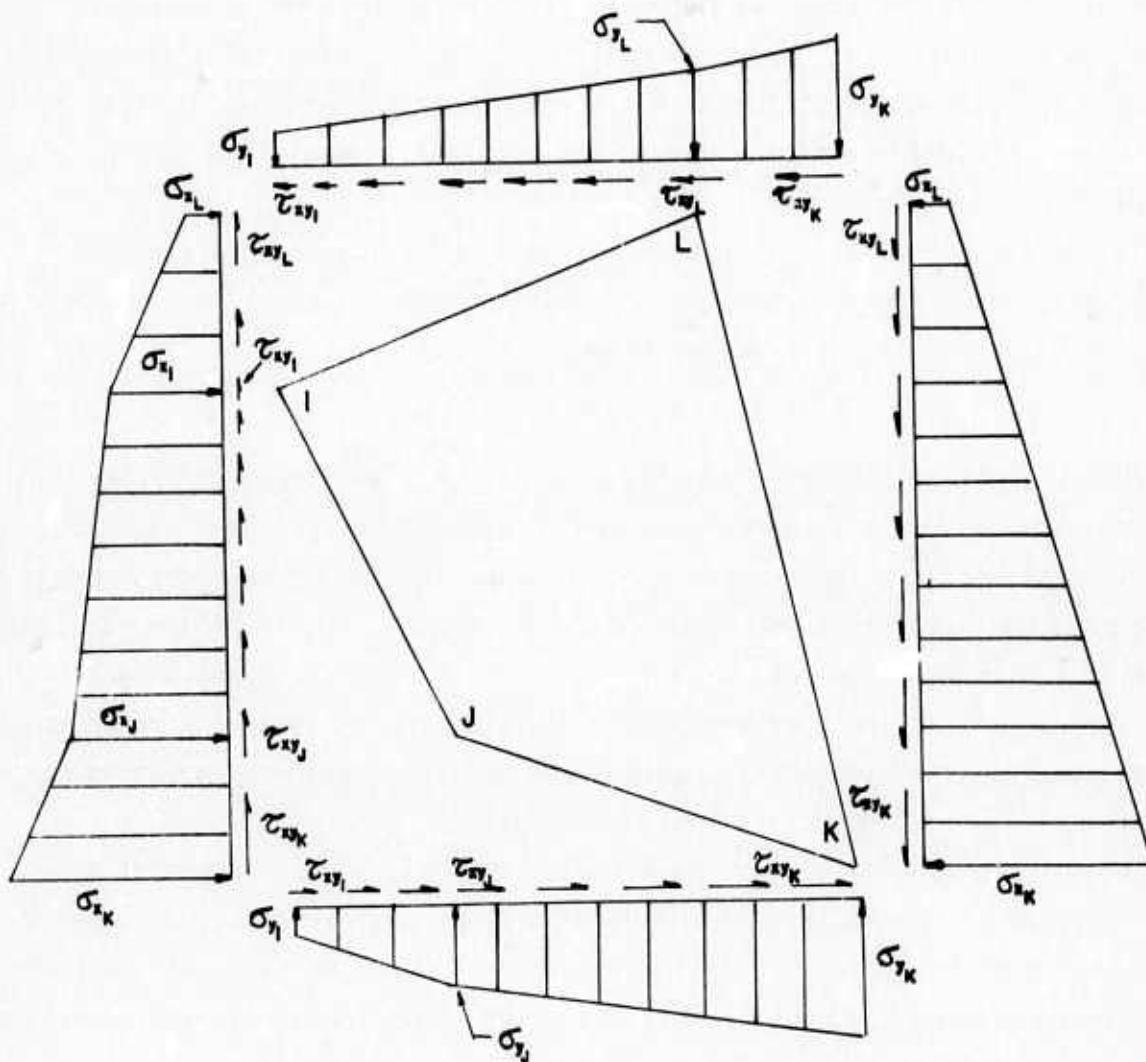
To use Equation 2-1 to determine the stresses at a nodal point of an excavated element, three sets of the interpolation coefficients are computed (one each for the  $x$ ,  $y$  and  $xy$  stresses) using the known stresses in the four elements surrounding the nodal point, one of which is the element to be excavated. For a given stress  $\sigma$ , these relationships can be expressed as:

$$\begin{Bmatrix} \sigma(1) \\ \sigma(2) \\ \sigma(3) \\ \sigma(4) \end{Bmatrix} = \begin{bmatrix} 1 & x_1 & y_1 & x_1 y_1 \\ 1 & x_2 & y_2 & x_2 y_2 \\ 1 & x_3 & y_3 & x_3 y_3 \\ 1 & x_4 & y_4 & x_4 y_4 \end{bmatrix} \begin{Bmatrix} a_1 \\ a_2 \\ a_3 \\ a_4 \end{Bmatrix} \quad (2-2)$$

in which  $\sigma(i)$  is the stress in element  $i$ . Equations 2-2 can be expressed in symbolic form as follows:

$$\{\sigma_e\} = [m] \{a\} \quad (2-3)$$





$$YIJ = y_I - y_J$$

$$YJK = y_J - y_K$$

$$YKL = y_K - y_L$$

$$YLI = y_L - y_I$$

$$XJI = x_J - x_I$$

$$XKJ = x_K - x_J$$

$$XLK = x_L - x_K$$

$$XIL = x_I - x_L$$

NOTE: ALL STRESSES AND GRADIENTS ASSUMED POSITIVE AS SHOWN

FIG.2-1 ARBITRARY QUADRILATERAL ELEMENT  
AND BOUNDARY STRESS DISTRIBUTION

in which  $\{\sigma_e\}$  is the known element stress matrix,  $[m]$  is the known coordinate matrix for the stress points and  $\{a\}$  is the unknown interpolation coefficient matrix, which can be solved for as below:

$$\{a\} = [m]^{-1} \{\sigma_e\} \quad (2-4)$$

The interpolation coefficients can then be used to evaluate the nodal point stresses,  $\{\sigma_n\}$ , of the element to be excavated, as shown below:

$$\{\sigma_n\} = [n] \{a\} \quad (2-5)$$

or

$$\{\sigma_n\} = [n] [m]^{-1} \{\sigma_e\} \quad (2-6)$$

in which  $[n]$  is the coordinate matrix for the I, J, K, L nodal points. Equation 2-6 therefore expresses the nodal point stresses in terms of the center stresses of four adjacent elements.

Using the principle of virtual work and the stress distribution shown in Figure 2-1, the equivalent horizontal and vertical nodal point forces can be established for each nodal point. For example, the vertical force at J can be expressed as:

$$F_y^J = \frac{1}{6} [ (XJI) \sigma_{yI} + 2 (XJI + XKJ) \sigma_{yJ} + (XKJ) \sigma_{yK} + (YIJ) \tau_{xyI} + 2 (YIJ + YJK) \tau_{xyJ} + (YJK) \tau_{xyK} ] \quad (2-7)$$

This operation can then be repeated for all eight nodal point forces, resulting in the following equations:

$$\{F_n\} = [H] \{\sigma_n\} \quad (2-8)$$

or

$$\{F_n\} = [H] [n] [m]^{-1} \{\sigma_e\} \quad (2-9)$$

or

$$\{F_n\} = [Q] \{\sigma_e\} \quad (2-10)$$

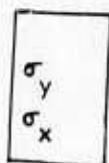
in which  $\{F_n\}$  is the  $8 \times 1$  nodal force matrix,  $[H]$  is the  $8 \times 12$  boundary geometry matrix,  $\{\sigma_n\}$  is the  $12 \times 1$  nodal stress matrix and  $[Q]$  is the  $8 \times 12$  resultant matrix relating the unknown nodal forces and the known element center stresses.

The manner in which this approach is implemented is to specify the nodal points along an excavation boundary and, for each nodal point, to specify the four elements surrounding the nodal point. Usually two of these elements are to be excavated and two are to remain as a portion of the rock mass. However, situations arise where four elements do not surround a nodal point. In this case, one should select the four closest elements, as long as no three of the four elements have centers which lie on a horizontal or vertical line because then the matrix  $[m]$  becomes singular (zero determinant) and no solution is possible.

To test the validity of this approach and to check whether modifications were necessary, a simple excavation problem was considered of a laterally restrained column, fixed at the base, in which the top layer was excavated. This problem is shown in Figure 2-2. At the left of this figure is shown the initial stress distribution. First the top ten elements were excavated in one step and the results were compared with the closed form solution. The results were identical, as indicated to the right of the initial stress distribution. Secondly a two step excavation sequence was conducted with five elements being removed at each step. The resulting  $\sigma_x$  and  $\sigma_y$  values are shown in the respective elements and the values of  $\tau_{xy}$  were in the range of  $10^{-3}$  to  $10^{-4}$ . The correct values of  $\sigma_x$  and  $\sigma_y$  are shown on the left of the mesh and the correct values of  $\tau_{xy}$  should be zero. It can be seen that, except for the  $\sigma_y$  values of the two central elements in the top layer, the difference between the finite element (FEM) solution and the correct closed-form solution are about 2% or less. The other two elements have errors of approximately 12%. In practice, a much finer finite element mesh would be used in this central portion where there is a stress concentration after the first step, and subsequently the error would be reduced to a few percent or less. All other values are well within an acceptable error range, even though such a coarse mesh was employed.

In an effort to determine whether the accuracy of the results could be improved, even with this coarse mesh, an analysis was conducted using double

KEY:



FINAL STRESSES FOR  
2 STEP FEM SOLUTION

NOTE:  $\tau_{xy}$  IS IN THE RANGE  
OF  $10^{-3}$  TO  $10^{-4}$

$$\nu = 0.25$$

$$\delta = 0.1$$

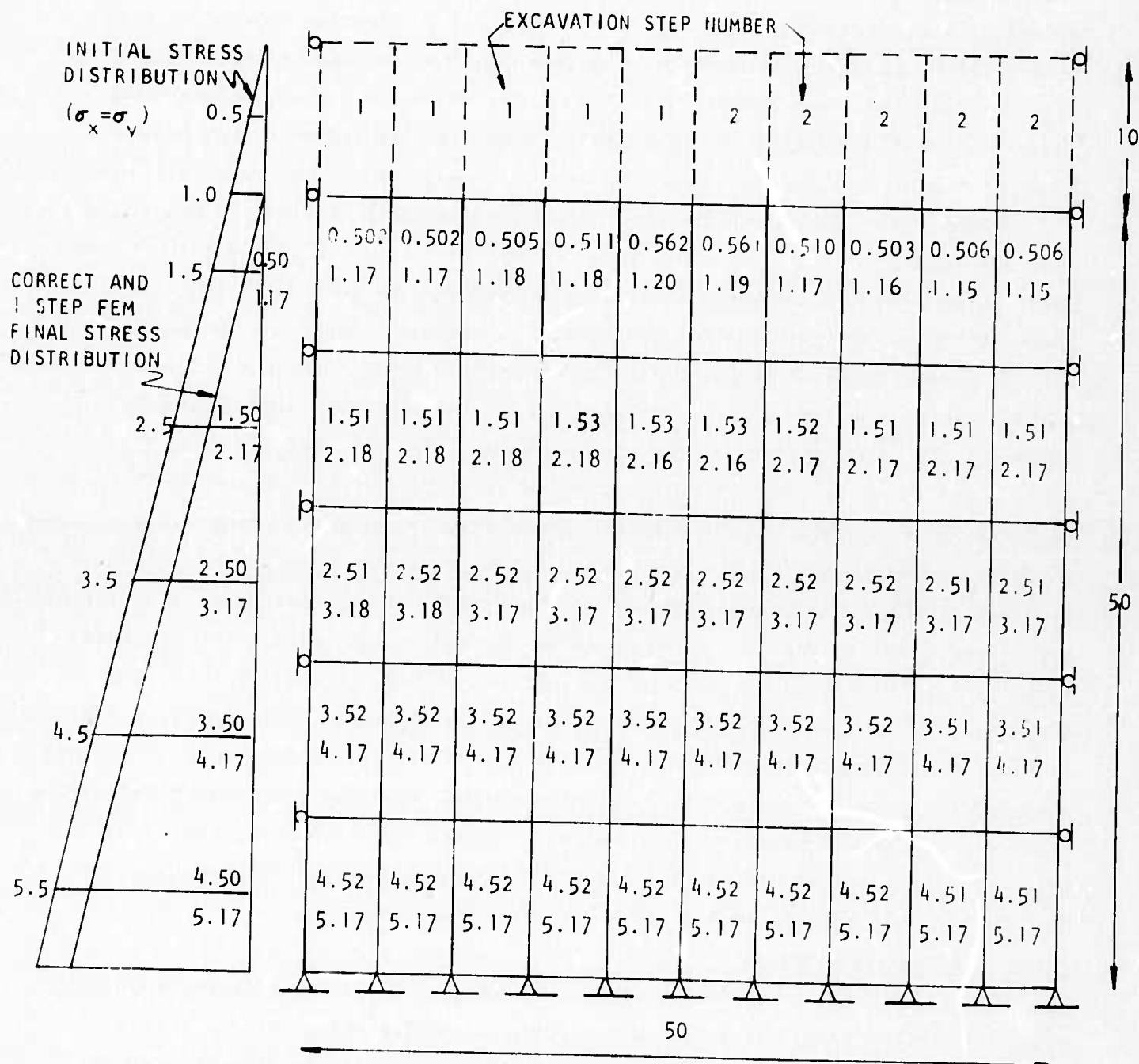


FIG.2-2 COMPARISON OF FEM STRESSES WITH CORRECT STRESSES FOR LATERALLY RESTRAINED COLUMN

precision calculations. The results of this analysis were virtually identical, although substantially more computer time, storage and accuracy was involved. To see whether an improved interpolation function would improve the accuracy of the results, Equation 2-1, the interpolation function, was expanded to six terms. An analysis conducted with the improved interpolation function showed, at best, a very slight increase in accuracy. Considering the increase in input data required for a six term interpolation function, it was felt that the improved interpolation function was not warranted. These results indicate that only a finer mesh around zones of stress concentration will lead to more accurate results.

Furthermore, during the course of investigating this problem, it was found that the modulus of the excavated elements must be reduced to at least  $10^{-6}$  times their value prior to excavation. If they are reduced by substantially lesser amounts, the values computed for the remaining elements change for the worse.

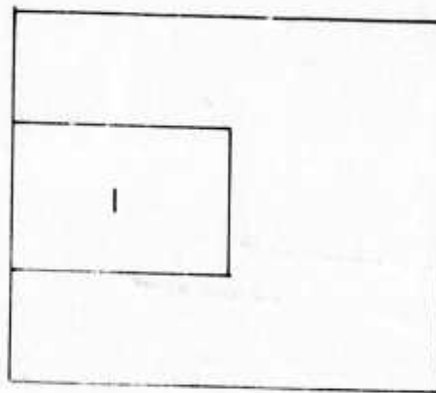
As a more general example of the applicability of this approach, the problem shown in Figure 2-3 was analyzed. One, two and three step excavation sequences, as shown in Figure 2-4, were employed. The computed values of  $\sigma_x$ ,  $\sigma_y$  and  $\tau_{xy}$  are shown for the elements resulting from the one and two step construction sequence analyses; the results from the three step sequence are essentially the same as these values. This example was selected because it has a horizontal plane of symmetry, sharp stress concentrations in the corners of the excavation and external boundaries close to the excavation which will significantly affect the computed stress values during a multiple step excavation sequence. As can be seen, the computed stress values compare very closely in all respects. The largest differences occur in the elements near the horizontal faces of the excavation where the stress changes are large and the computed values are small and near the excavation corners where the stress concentration is greatest. Ordinarily, in solving practical problems, more elements of smaller size would be used and the corresponding inaccuracies would be even smaller than in this example problem.

#### Finite Element Mesh Design

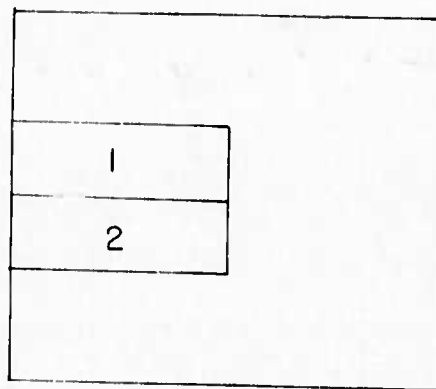
Solutions obtained by finite element analyses are only approximate solutions since the method itself is based upon a physical approximation of the actual system. Because of this, care must be exercised when a finite element mesh is designed to ensure that the results are not being significantly altered because



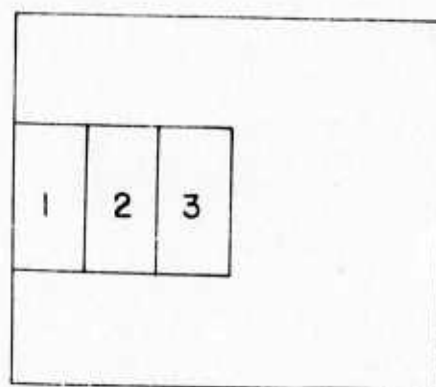




1 STEP  
EXCAVATION



2 STEP  
EXCAVATION



3 STEP  
EXCAVATION

FIG. 2-4 SEQUENCES EMPLOYED IN EXAMPLE  
EXCAVATION OF RECTANGULAR OPENING

the mesh is not fine enough or the boundaries are not far enough away from the opening. If only one or two problems are to be investigated, perhaps five hundred or more elements may be used to ensure an accurate idealization. But when numerous problems are to be investigated, the number of elements must be minimized because of the large cost of computer time and plotting and interpreting the results obtained from the solution.

a) Mesh Configuration and Size Effects

To investigate the effects of mesh configuration and number of elements in the mesh, a sample problem was analyzed of a rectangular opening with a vertical plane of symmetry. This problem was selected because of the stress concentrations which will occur in the corners. Three meshes were used: the first, shown in Figure 2-5, was a coarse mesh containing 60 rectangular elements of equal size; the second, shown in Figure 2-6, was a fine mesh containing 120 square elements of equal size; and the third, shown in Figure 2-7, was a fine mesh containing 156 rectangular elements of unequal size with the element size increasing away from the opening. In each case, excavation was conducted in a one step sequence. The initial values of  $\sigma_x$  and  $\sigma_y$  were equal to 1.0, the modulus was equal to 1000 and Poisson's ratio was equal to 0.25 for all of the elements in the three different meshes. Any consistent units can be applied to these values.

The results obtained from these three analyses are shown in Figures 2-8, 2-9 and 2-10. Contours of the vertical stress,  $\sigma_y$ , are shown in Figure 2-8. They show that the coarse mesh indicates tensile stresses existing in the roof of the opening and only a minor stress concentration near the corner of the opening. On the other hand, the contours resulting from the fine and the fine irregular meshes do not show the roof tensile zones and do show larger stress concentrations near the corner of the opening. Furthermore the contours are very consistent with each other, the only difference being that the fine irregular mesh indicates somewhat better the magnitude of the stress concentration near the corner of the opening and the magnitude of the stress reduction mid-height of the opening wall. Similar results are indicated for the horizontal stresses,  $\sigma_x$ , in Figure 2-9 and for the shear stresses,  $\tau_{xy}$ , in Figure 2-10. It is felt that the results obtained from a finer mesh would exhibit stress contours nearly the same as those from the fine and fine irregular meshes, but would probably define the

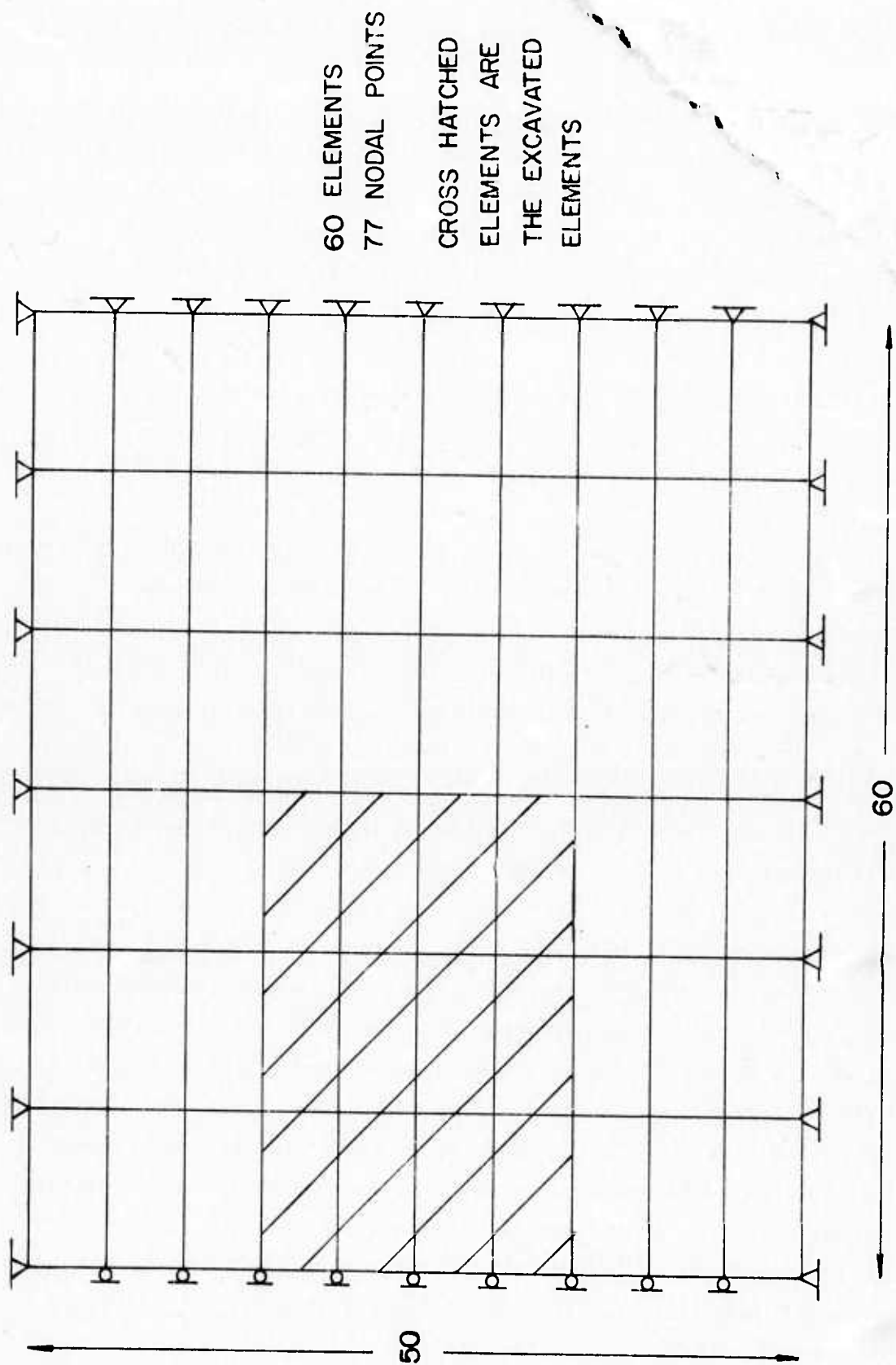


FIG.2-5 COARSE FINITE ELEMENT MESH FOR RECTANGULAR  
OPENING.

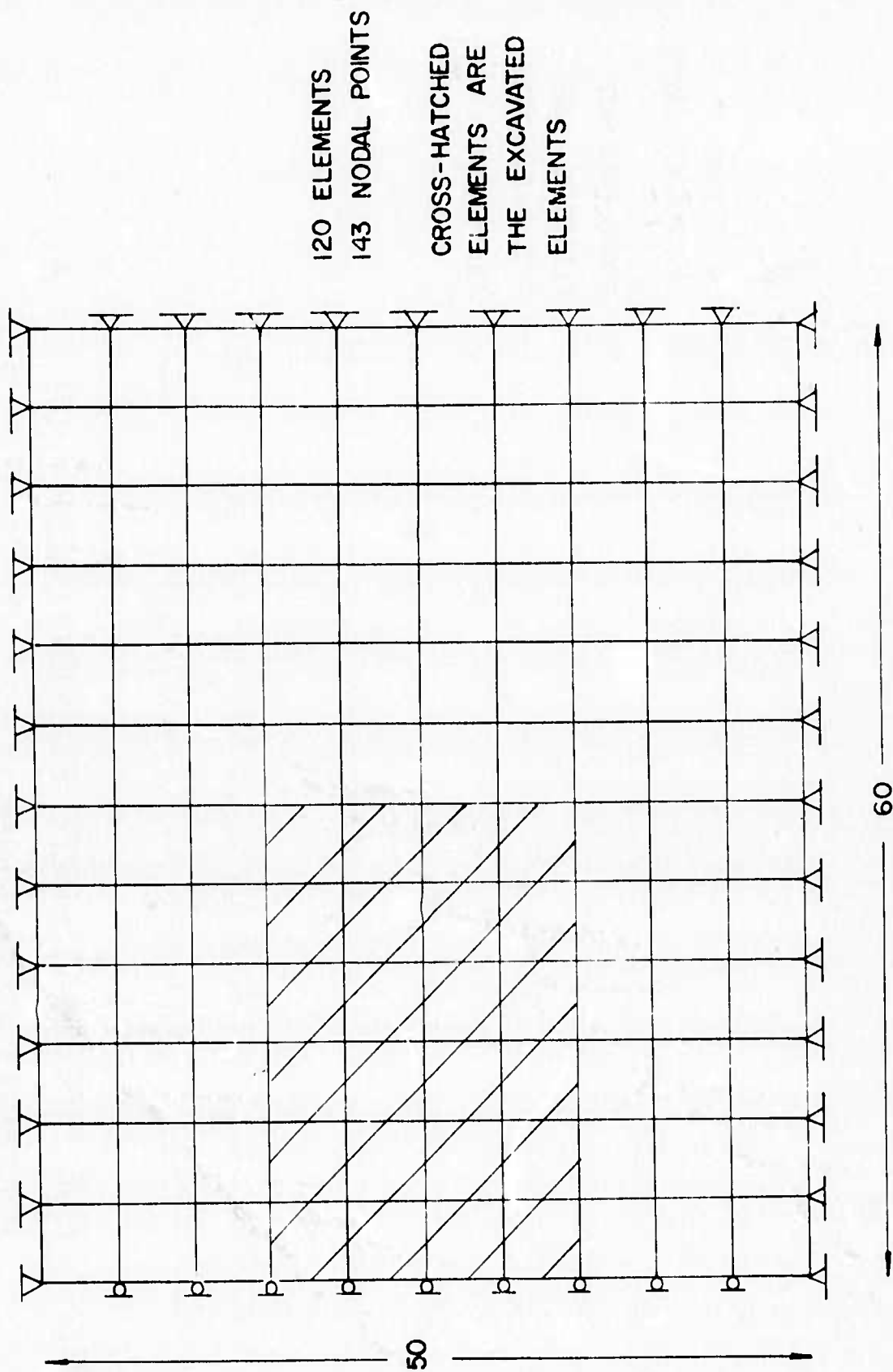


FIG.2-6 FINE FINITE ELEMENT MESH FOR RECTANGULAR  
OPENING.



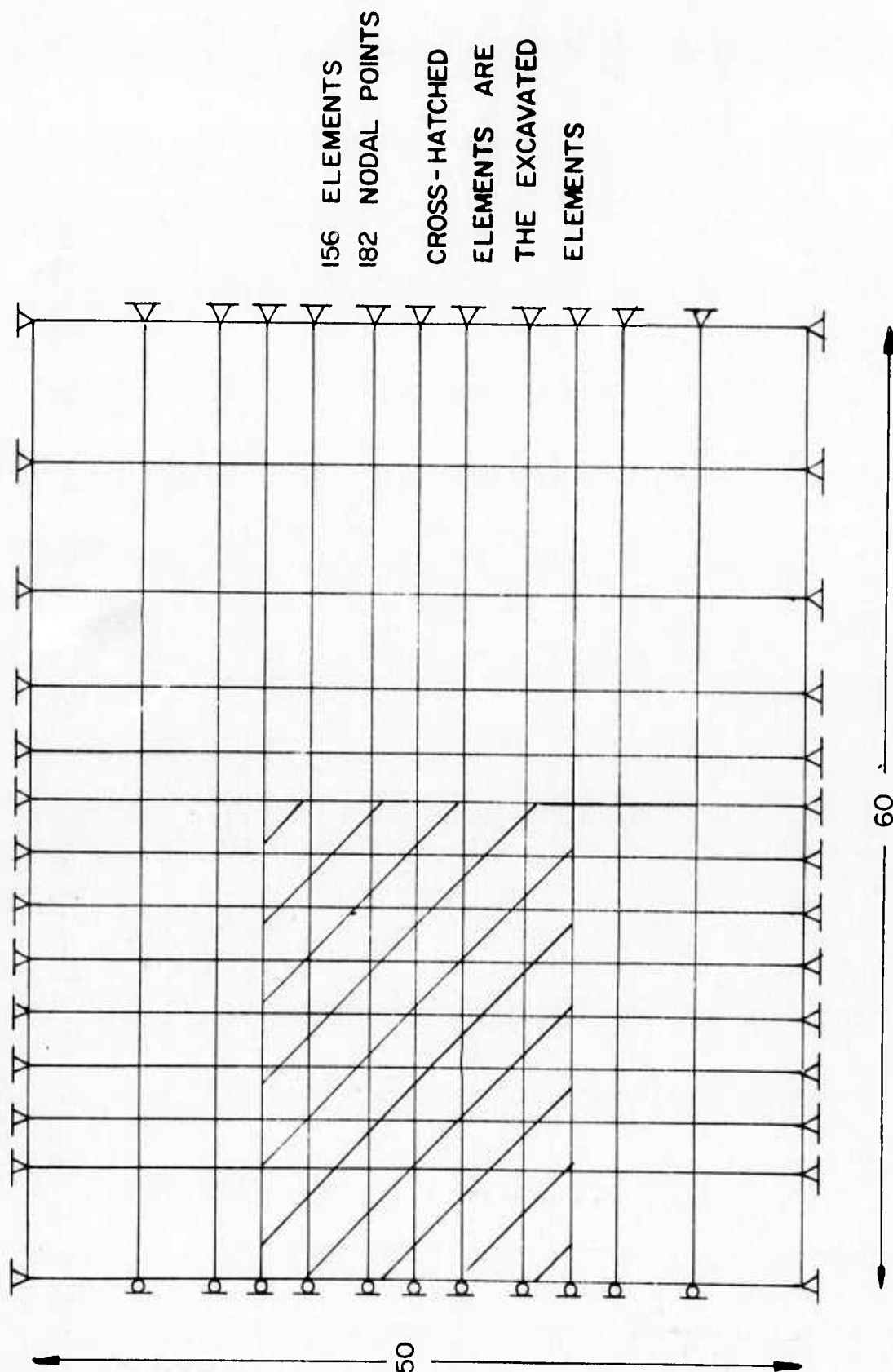
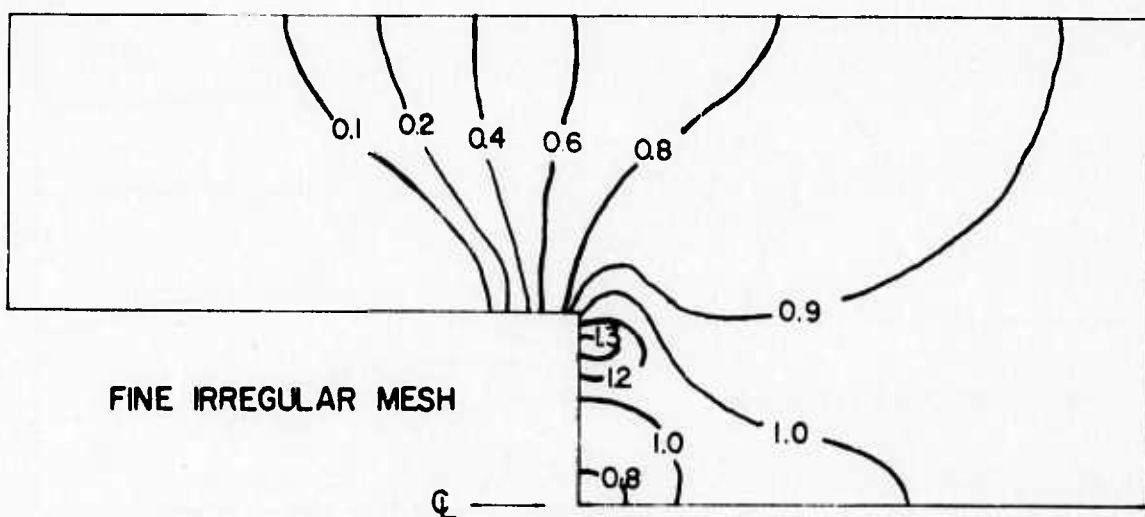
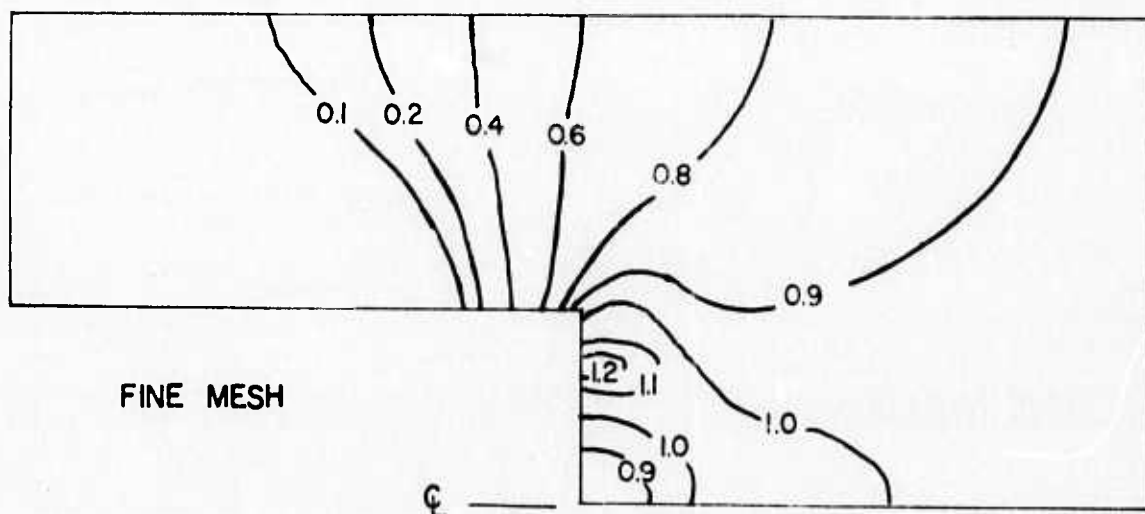
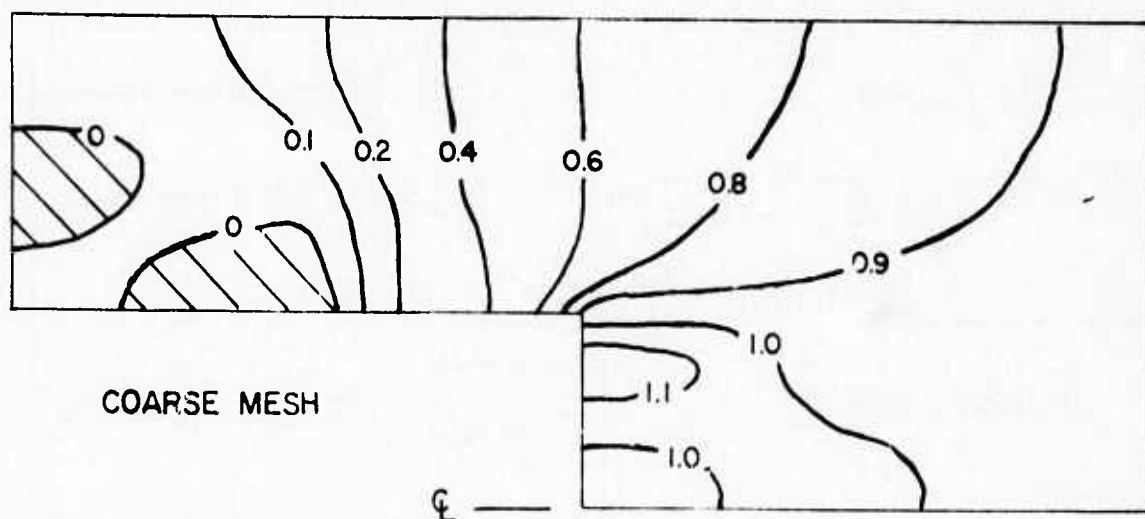
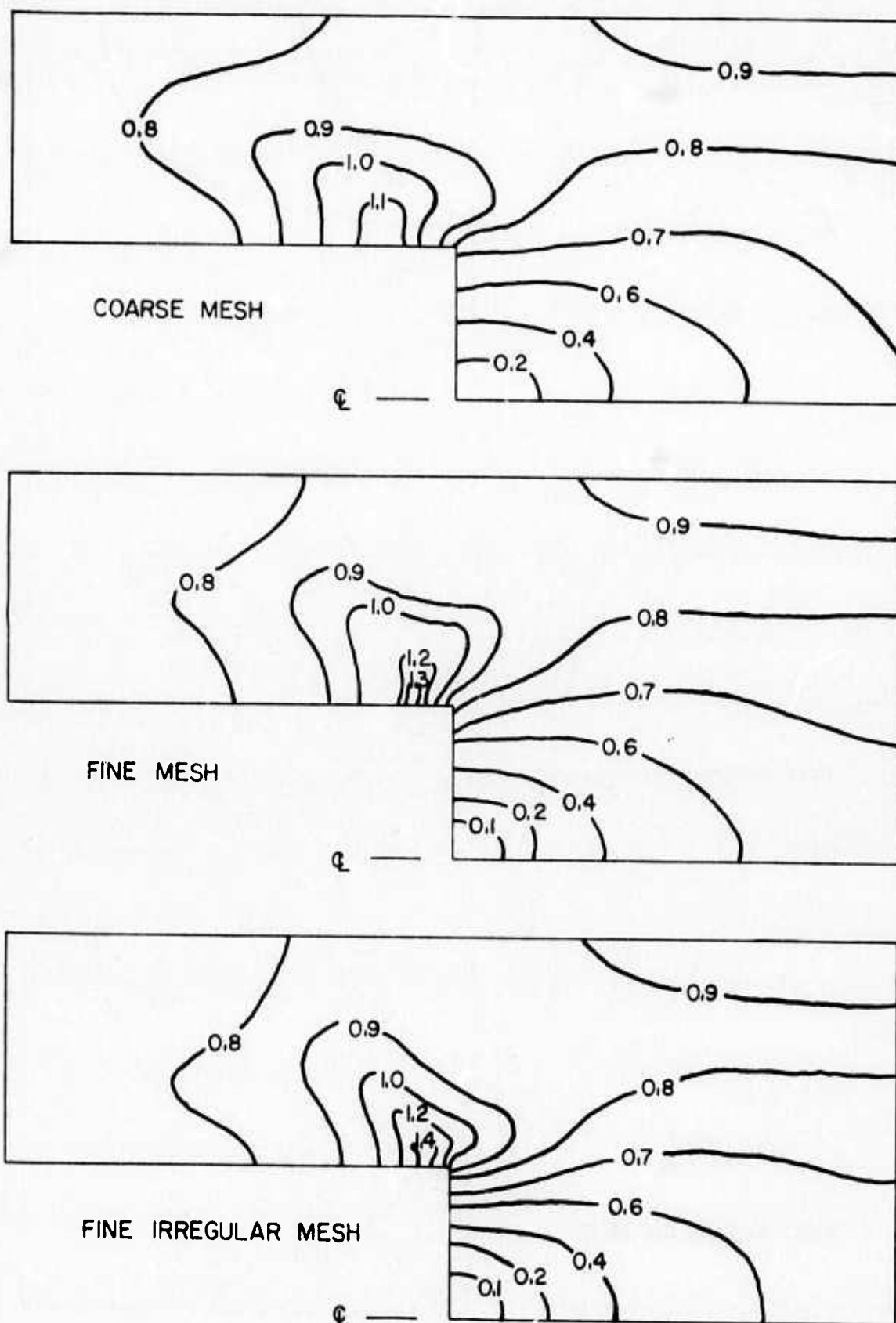


FIG.2-7 FINE IRREGULAR FINITE ELEMENT MESH FOR  
RECTANGULAR OPENING.



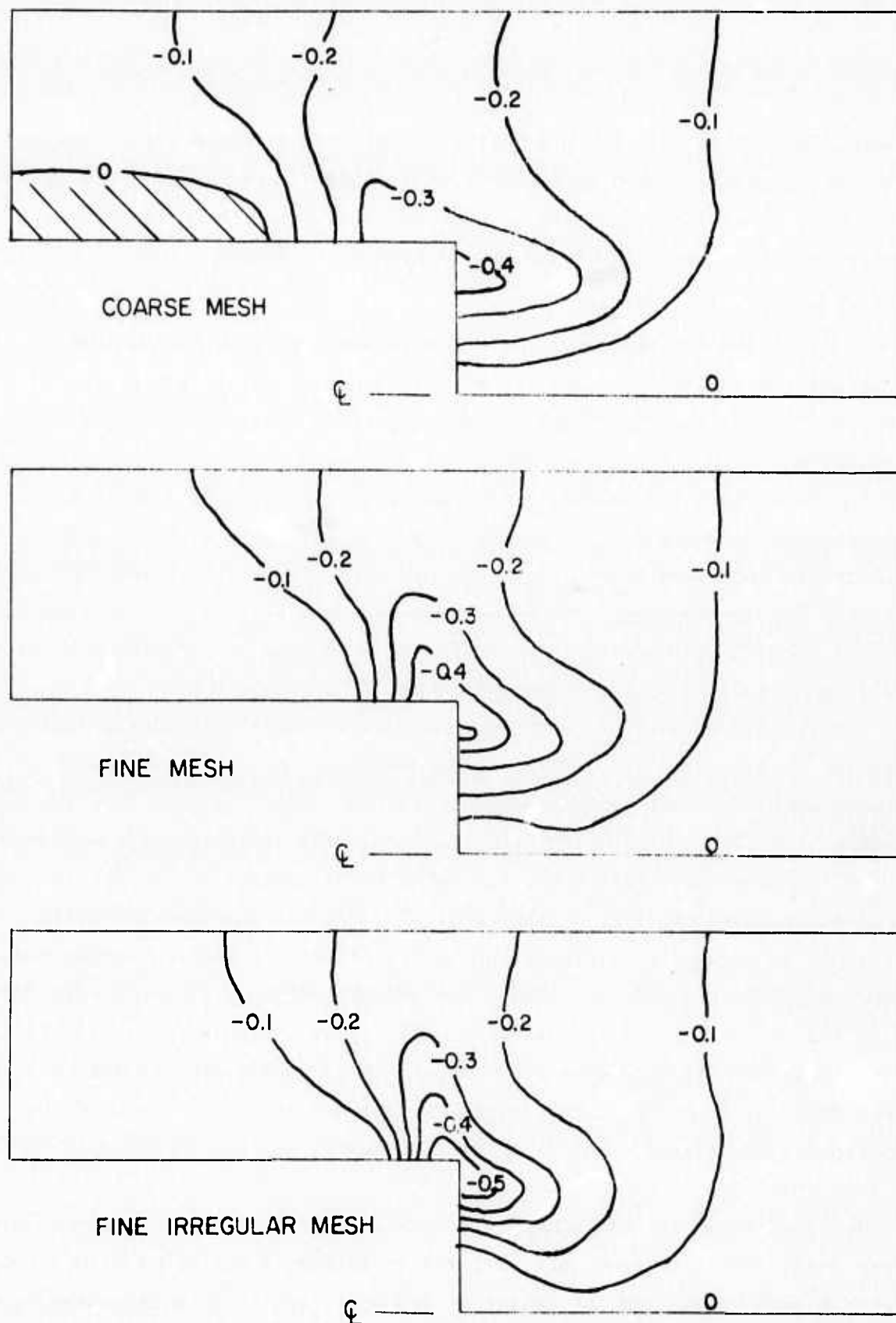
ALL RESULTS ARE SYMMETRICAL ABOUT THE CENTERLINE

FIG.2-8 CONTOURS OF  $\sigma_y$  AROUND EXAMPLE RECTANGULAR OPENING , 1 STEP EXCAVATION



ALL RESULTS ARE SYMMETRICAL ABOUT THE CENTERLINE

FIG.2-9 CONTOURS OF  $\sigma_x$  AROUND EXAMPLE  
RECTANGULAR OPENING , 1 STEP EXCAVATION  
- 22 -



ALL RESULTS ARE SYMMETRICAL ABOUT THE CENTERLINE

FIG.2-10 CONTOURS OF  $\tau_{xy}$  AROUND EXAMPLE  
RECTANGULAR OPENING , 1 STEP EXCAVATION

maximum and minimum values a bit better. Therefore a reasonable criterion for meshes would be that a minimum of 125 to 150 elements should suffice for analyses of simple structures in homogeneous rock where there is a plane of symmetry and only one-half of the system need be analyzed.

b) Boundary Location Effects

Since the finite element method involves a physical approximation of the actual system, the location of the finite boundaries from the area of interest will influence the results obtained in an analysis. This effect must be minimized to ensure realistic results

To investigate the magnitude of the boundary effects, a number of analyses were conducted with a circular opening in meshes with different distances to the fixed boundary. The basic mesh employed is shown in Figure 2-11. Different systems were obtained by varying the boundary location in this basic mesh. A total of five systems were analyzed with boundary locations varying from 3 radii to 9 radii away from the center of the opening.

The results obtained from these analyses are shown in Figure 2-12 for the nodal points along the face of the opening and for the innermost row of elements along the face of the opening. It can readily be seen that the boundary location is quite significant and that the greatest differences occur between the vertical displacements at nodal point A (also equivalent to horizontal displacements at B), the vertical stresses in element D (also equivalent to horizontal stresses in element C) and the shear stresses midway between elements C and D. To have a perfect comparison with the closed-form theoretical solution, the boundaries of the finite element mesh would have to be at infinity. Since this perfect comparison is impossible, it was felt that a mesh would be adequate if the largest difference between any one of the computed or theoretical stresses or displacements, on or near the opening face, was less than 10%.

By re-plotting the maximum points in Figure 2-12 in the form shown in Figure 2-13, it can be seen that this 10% criterion is satisfied with a boundary located 6 radii away from the center of the opening. It is interesting to note that, for boundaries located closer to the opening, the largest percent difference increases rapidly while, for boundaries located further from the opening, the largest percent difference decreased slowly. Therefore the 6 radii



150 ELEMENTS  
176 NODAL POINTS  
 $E = 1000$   
 $\nu = 0.25$

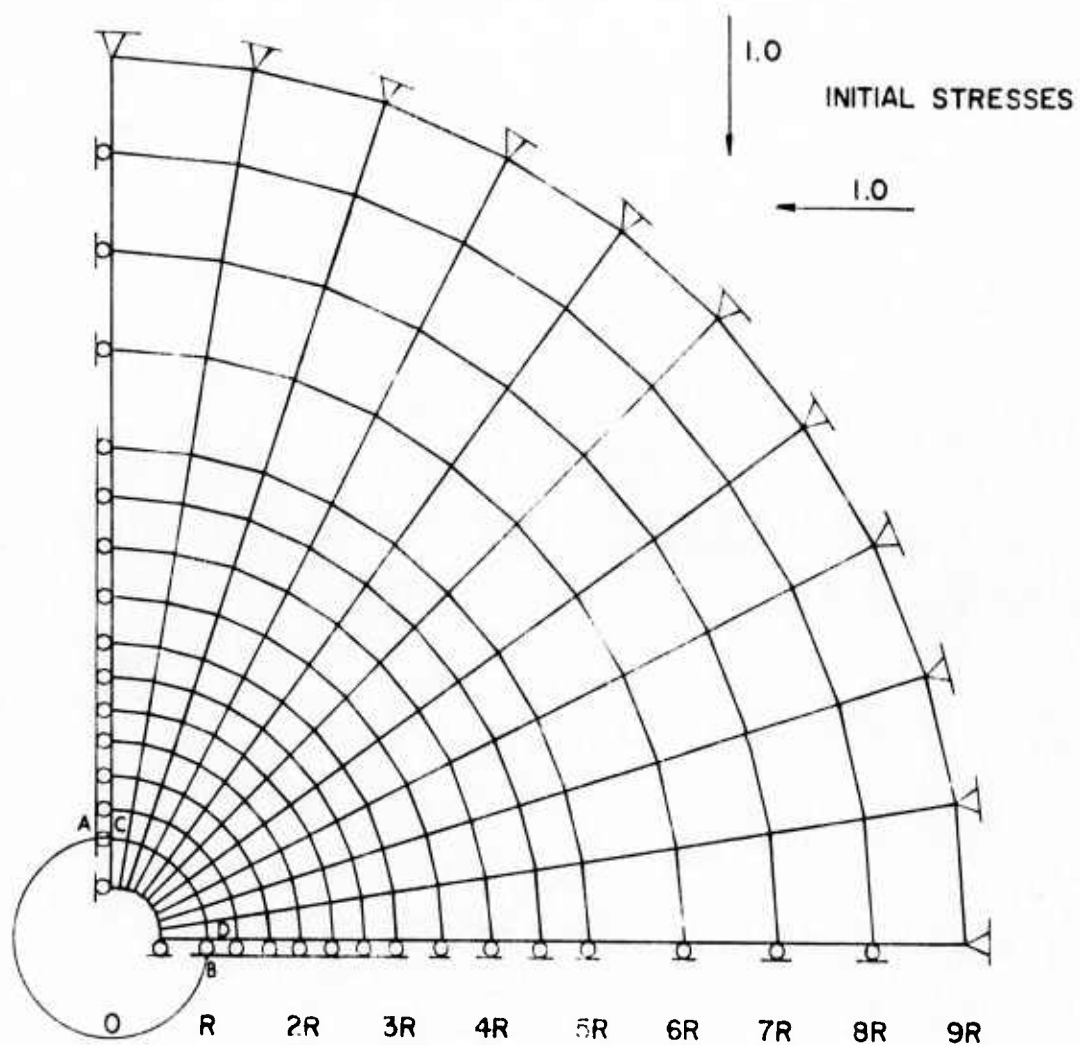


FIG.2-II FINITE ELEMENT MESH FOR INVESTIGATION  
OF BOUNDARY EFFECT

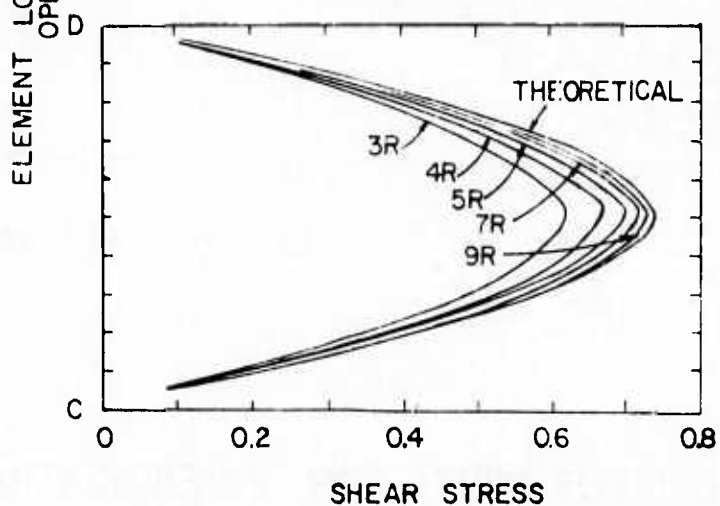
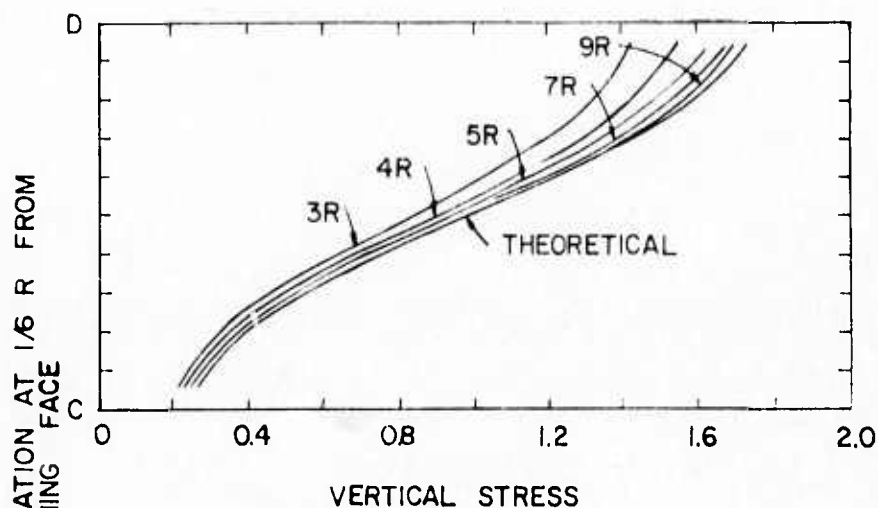
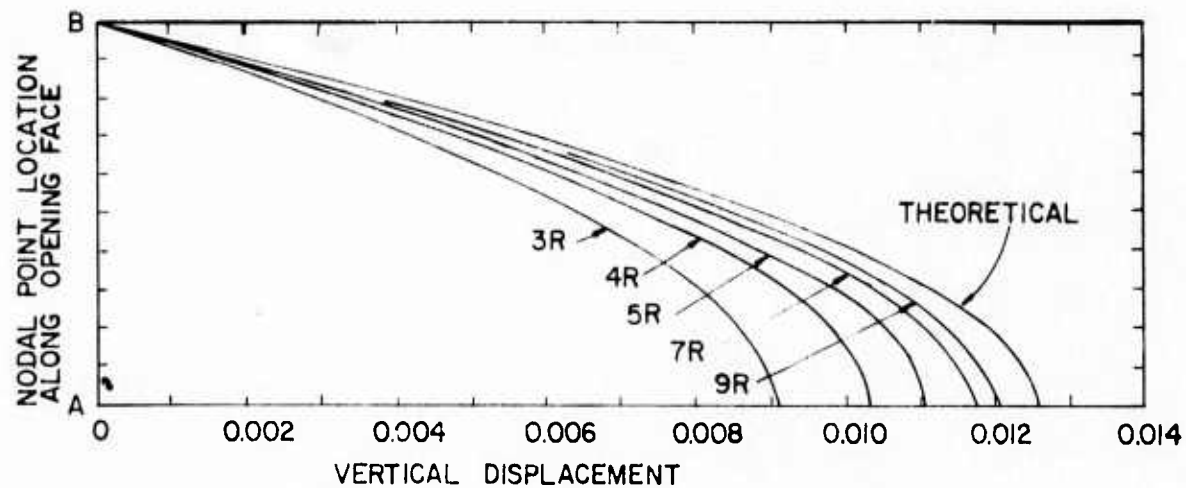


FIG.2-12 COMPARISON OF THEORETICAL AND FEM DISPLACEMENTS ALONG, AND STRESSES NEAR, THE FACE OF A CIRCULAR OPENING

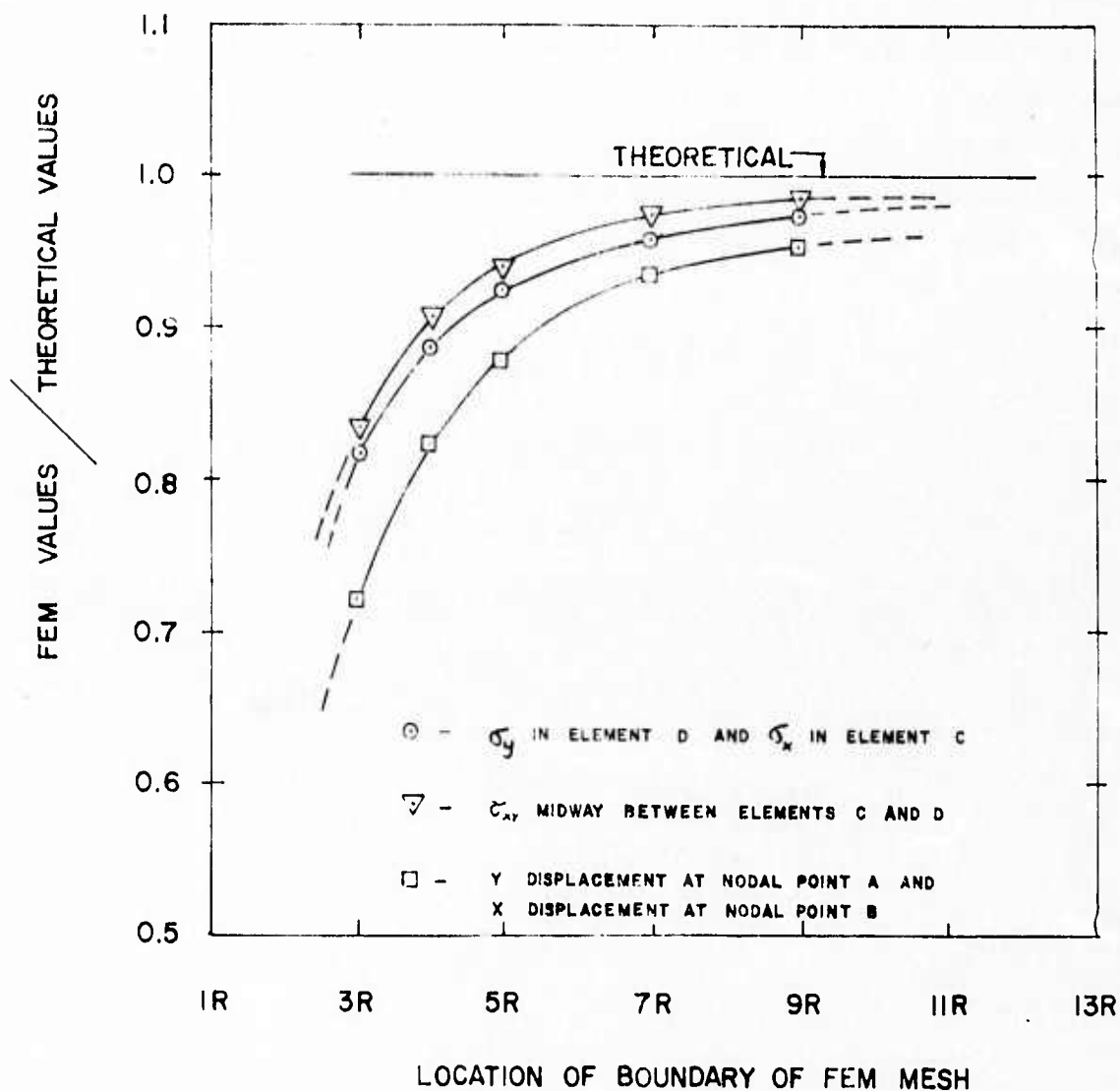
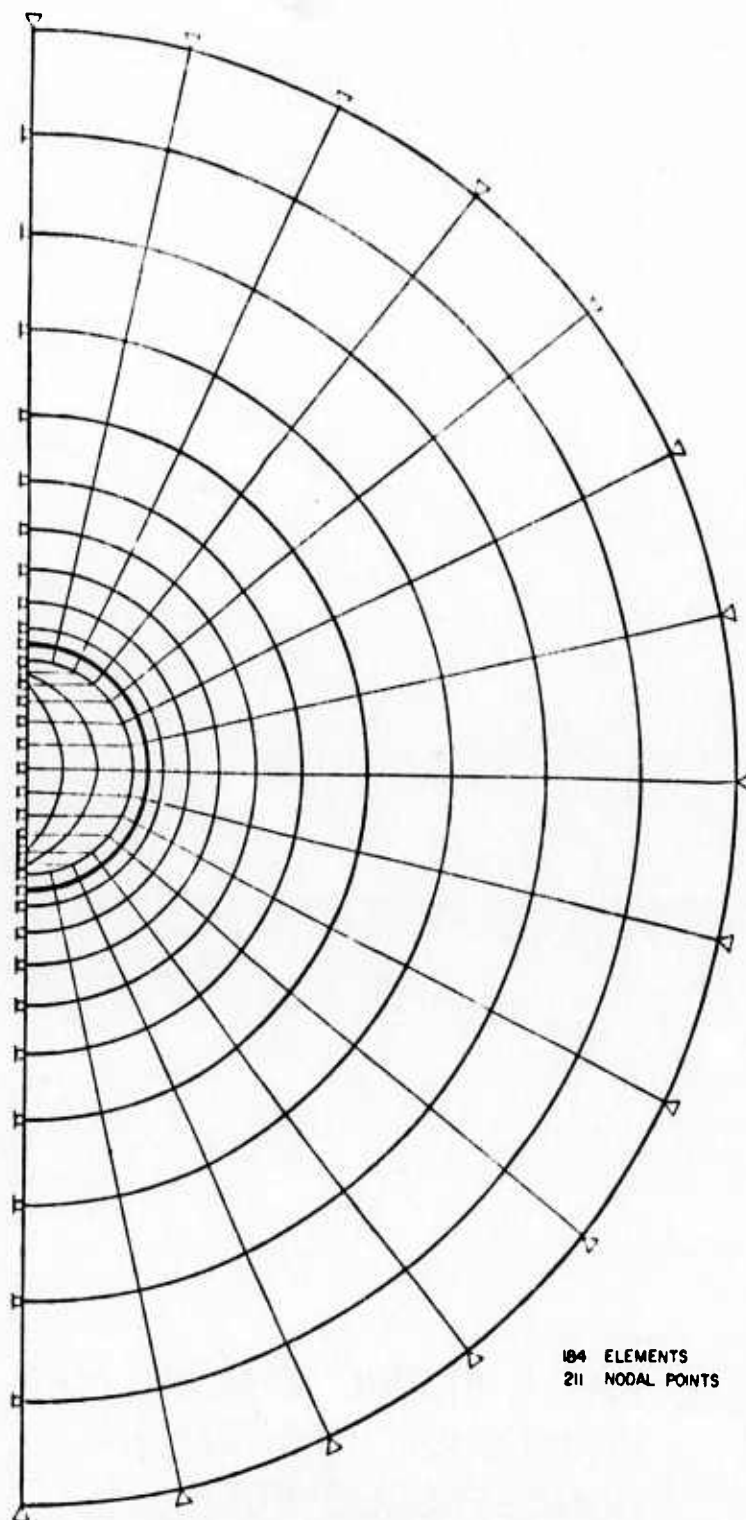


FIG.2-13 EFFECT OF EXTERNAL BOUNDARY LOCATION ON ACCURACY OF FEM SOLUTION

criterion was adopted for all meshes to be employed in this investigation.

c) Representative Finite Element Meshes

In accordance with the criteria established above, three finite element meshes were designed for use during the course of this investigation. These three meshes are shown in Figures 2-14, 2-15 and 2-16 and they satisfy both the element and boundary criteria. These meshes are for a circular opening, 6 meters in diameter, a horseshoe opening, 5.5 meters high with a base width of 5.5 meters (yielding an area similar to that of the circular opening) and a power station opening, 30 meters high, 20 meters base width and 25 meters wide at the base of the crown arch. These openings and their dimensions were selected because they are both common and representative.



**FIG.2-11 FINITE ELEMENT MESH FOR  
CIRCULAR OPENING IN  
HOMOGENEOUS ROCK.**



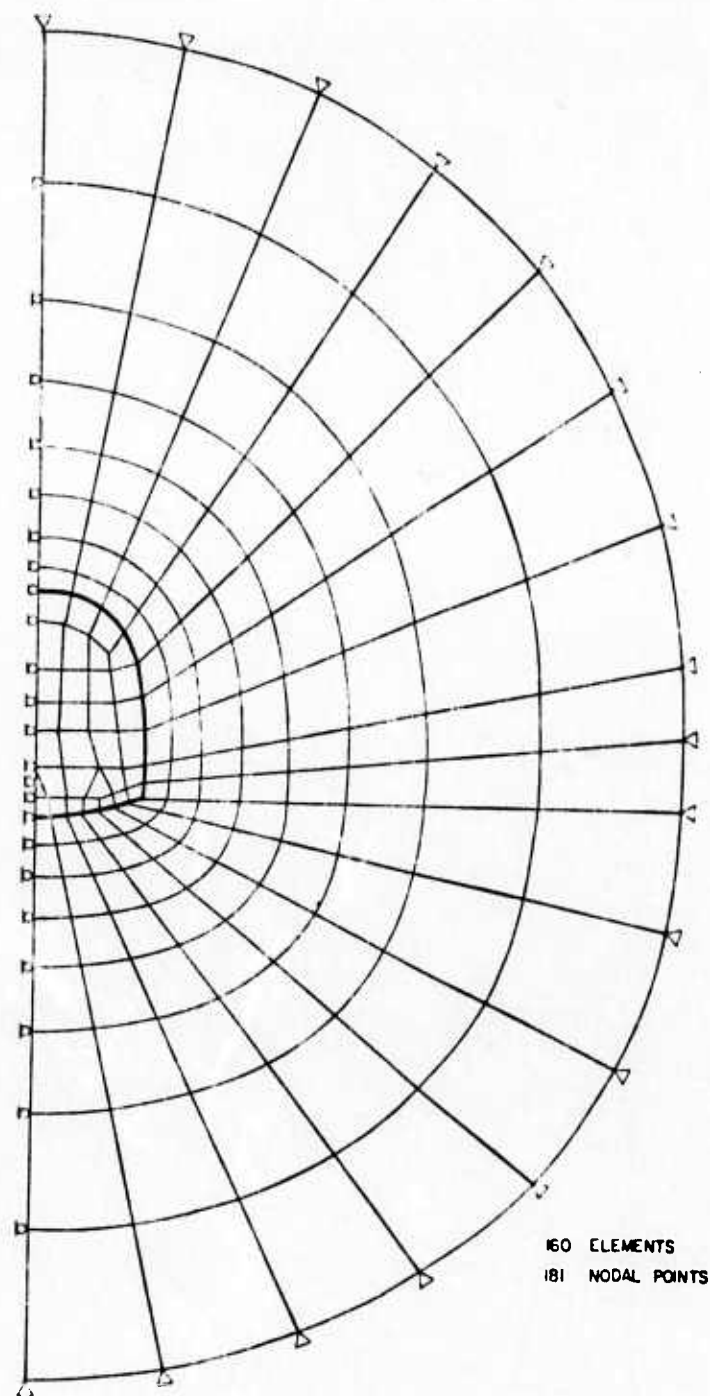


**FIG.2-15 FINITE ELEMENT MESH FOR  
HORSESHOE OPENING IN  
HOMOGENEOUS ROCK.**

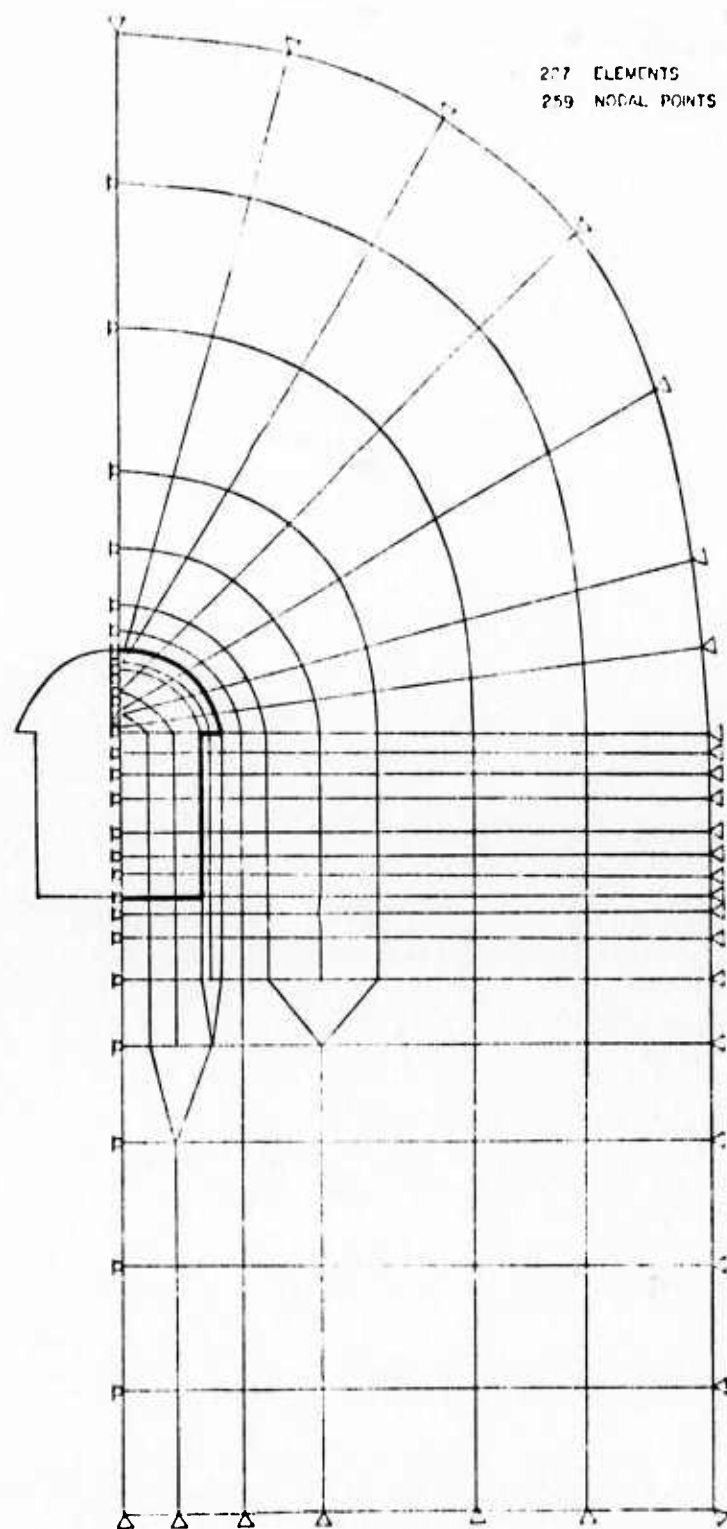


**FIG.2-16 FINITE ELEMENT MESH FOR  
POWER STATION OPENING IN  
HOMOGENEOUS ROCK.**

### CHAPTER 3

#### STRESS-STRAIN BEHAVIOR OF ROCK

The stress-strain behavior of many types of rock depends upon a number of factors including density, porosity, structure, degree of weathering, type and quality of cementing agent, stress history, duration of loading, confining pressure, and shear stress. In many cases it may be possible to take account of these factors by selecting rock specimens and testing conditions which simulate the anticipated field conditions. But even when the rock specimens and test conditions are carefully selected to duplicate field conditions, it is commonly found that rock stress-strain behavior, over a wide range in stresses, is non-linear and dependent upon the magnitude of confining pressure.

More often than not, only uniaxial compression tests are conducted and the values of modulus and Poisson's ratio, for use in subsequent analyses, are based upon the uniaxial results alone. Therefore the studies described in this chapter were conducted: (1) to evaluate and summarize the available modulus and Poisson's ratio data for various rock types under uniaxial test conditions, (2) to examine the range of applicability, for rocks, of recently proposed methods of representing the nonlinear and stress-dependent values of modulus and Poisson's ratio of soils, (3) to evaluate and summarize the available nonlinear modulus and Poisson's ratio parameter values for various rock types under triaxial test conditions, and (4) to provide guidelines for inter-relating these parameters and using them in analyses.

#### Uniaxial Modulus and Poisson's Ratio Values

In an effort to evaluate the modulus and Poisson's ratio values for rock types under uniaxial test conditions, an extensive literature survey was conducted to isolate these data. The literature searched included the major rock mechanics journals, the international rock mechanics congresses, the U.S. and Canadian rock mechanics symposia, major Ph.D. dissertations and the reports of U.S. government agencies involved in rock mechanics work. While this survey cannot be expected to be all-inclusive, it is felt that a very substantial percentage of the available data are included. Furthermore, since data of this type are rarely presented in graphical form, it is unknown in most cases whether the modulus and Poisson's ratio values are initial tangent values, secant values or "best-fit" values.

Fortunately, many types of rocks exhibit nearly linear behavior under uniaxial conditions to greater than 50% of failure, in which case the initial tangent, secant and "best-fit" values are identical.

In all, data for uniaxial conditions alone were available for 154 different types of rocks; inclusion of several conditions for a given rock type yielded a total of 163 values. These data were grouped together genetically and were tabulated as shown in Tables 3-1 through 3-5. Whenever sufficient data were available, the full description, density, specific gravity, porosity, modulus, Poisson's ratio, compressive strength and tensile strength were included. As can be seen, all of these data were not available for all of the rock types. On first impression it appears that there is a very wide scatter in the values of modulus and Poisson's ratio for these rock types. Yet as shown in the summary in Table 3-6, the range is not that great. Typically the maximum modulus values are in the range of  $80 \times 10^6 \text{ KN/m}^2$  ( $11.6 \times 10^6 \text{ psi}$ ) to  $100 \times 10^6 \text{ KN/m}^2$  ( $14.5 \times 10^6 \text{ psi}$ ) while the minimum modulus values are in the range of  $1 \times 10^6 \text{ KN/m}^2$  ( $0.14 \times 10^6 \text{ psi}$ ) to  $10 \times 10^6 \text{ KN/m}^2$  ( $1.45 \times 10^6 \text{ psi}$ ). The average values are in the range of  $20 \times 10^6 \text{ KN/m}^2$  ( $2.9 \times 10^6 \text{ psi}$ ) to  $60 \times 10^6 \text{ KN/m}^2$  ( $8.7 \times 10^6 \text{ psi}$ ) while the overall average for the 163 tests is  $43.4 \times 10^6 \text{ KN/m}^2$  ( $6.3 \times 10^6 \text{ psi}$ ). Similarly, the maximum values of Poisson's ratio vary from 0.32 to 0.73 (0.46 if the one dilatant value is excluded) while the minimum values vary from 0.02 to 0.09. The average values range only from 0.15 to 0.26 while the overall average for the 141 tests is 0.20.

Little data were available on anisotropic properties under uniaxial conditions. The available data on two sandstones (SCU-7 and SCU-8) and one shale (SCU-24), however, indicate that anisotropy is relatively unimportant. In fact, these values are close enough so that they are well within the range of material variation and test scatter.

#### Nonlinear Stress-Dependent Modulus Relationship

Recently, Duncan and Chang (1970) proposed a simple, practical stress-strain relationship for soils and demonstrated its applicability in use for a deep excavation in soil (Chang and Duncan, 1970). This relationship was formulated from empirical nonlinear and stress-dependent relationships proposed previously and only includes parameters readily obtainable from conventional laboratory shear tests. It is interesting to note that work presently near completion at

ROCK NUMBER	DESCRIPTION	DENSITY (GM/CM <sup>3</sup> )	SPECIFIC GRAVITY	POROSITY (%)	ELASTIC MODULUS (KN/M <sup>2</sup> × 10 <sup>-6</sup> )	POISSON'S RATIO	COMPRESSIVE STRENGTH (KN/M <sup>2</sup> × 10 <sup>-3</sup> )	TENSILE STRENGTH (KN/M <sup>2</sup> × 10 <sup>-3</sup> )	REFERENCE
IPU-1	GRANITE	2.63	2.67	1.6	52.1	0.16	161.3	-	JUDD (1969)
IPU-2	GUADARRAMA GRANITE	2.60	-	-	24.4	-	62.8	-	SALAS (1968)
IPU-3	FREMONT CANYON GRANITE (HOMOGENEOUS, COARSE-GRAINED)	-	2.62	0.8	64.1	0.14	-	8.62	NESBITT (1960)
IPU-4	FREMONT CANYON GRANITE (COARSE-GRAINED, SLIGHTLY WEATHERED)	-	2.61	1.7	45.1	0.10	-	2.62	NESBITT (1960)
IPU-5	FREMONT CANYON GRANITE (COARSE-GRAINED)	-	2.63	1.0	73.8	0.15	-	-	NESBITT (1960)
IPU-6	SALIDA GRANITE	2.64	-	-	70.7	0.18	324.0	-	HOSKINS & HORINO (1969)
IPU-7	MITIDIERI QUARRY PORPHYRIC GRANITE	2.68	2.74	3.6	69.6	0.24	91.7	-	RUI2 (1966)
IPU-8	VALINHOS QUARRY GRANITE	2.56	2.72	3.2	65.8	0.18	107.2	-	RUI2 (1966)
IPU-9	CANTAREIRA QUARRY GRANITE	2.75	2.81	2.2	64.1	0.25	111.3	-	RUI2 (1966)
IPU-10	PICCIACCO QUARRY TOURMALINE GRANITE	2.62	2.65	1.2	75.5	0.16	127.1	-	RUI2 (1966)
IPU-11	GRANITE	-	-	-	70.3	0.30	-	-	GEYER & MYUNG (1970)
IPU-12	GRANITE	-	-	-	58.6	0.20	-	-	GEYER & MYUNG (1970)
IPU-13	GRANITE	-	-	-	71.0	0.25	-	-	GEYER & MYUNG (1970)
IPU-14	ALC NEVADA TEST SITE GRANITE (DENSE, COARSE-GRAINED, UNWEATHERED)	2.69	2.69	0.3	73.8 <sup>A</sup>	0.22 <sup>A</sup>	141.1	11.7	STOWE (1969)
IPU-15	GRAND COULEE GRANITE (MASSIVE, MEDIUM-GRAINED)	-	2.63	1.6	32.5	0.14	148.8	-	BALMER (1953)
IPU-16	POLE HILL POWER PLANT GRANITE (COARSE-GRAINED)	-	2.63	1.0	26.2	0.12	72.2	-	BALMER (1953)
IPU-17	GRAND COULEE GRANITE (MEDIUM-GRAINED, SLIGHTLY ALTERED)	-	2.61	2.4	8.96	0.11	64.8	-	BALMER (1953)
IPU-18	GRAND COULEE GRANITE (MEDIUM-GRAINED, SLIGHTLY ALTERED)	-	2.61	2.4	7.79	0.13	56.9	-	BALMER (1953)
IPU-19	POLE HILL PEGMATITE GRANITE (VERY COARSE-GRAINED)	-	2.62	1.0	19.0	0.09	48.8	-	BALMER (1953)
IPU-20	PIKES PEAK GRANITE (COARSE-GRAINED, WEATHERED)	2.67	-	-	33.4 <sup>A</sup>	0.37 <sup>A</sup>	88.9	3.93	MILLER (1965)
IPU-21	PIKES PEAK GRANITE (DENSE, MEDIUM TO FINE-GRAINED)	2.64	-	-	70.6 <sup>A</sup>	0.18 <sup>A</sup>	226.0	11.9	MILLER (1965)
IPU-22	BARRE GRANITE (DENSE, MEDIUM-GRAINED)	2.64	-	-	61.4 <sup>A</sup>	0.39 <sup>A</sup>	194.4	10.7	MILLER (1965)
IPU-23	AEC NEVADA SITE QUARTZ MONZONITE (UNWEATHERED, UNCRACKED)	2.68	-	-	71.7	-	183.3	-	CORRING (1967)
IPU-24	AEC NEVADA SITE QUARTZ MONZONITE (UNWEATHERED, SLIGHTLY CRACKED)	2.68	-	-	74.4	-	100.6	-	CORRING (1967)
IPU-25	AEC NEVADA SITE QUARTZ MONZONITE (SLIGHTLY ALTERED)	2.66	-	-	46.9	-	71.0	-	CORRING (1967)
IPU-26	GARDEN VALLEY DAM QUARTZ DIORITE (COARSE-GRAINED, SLIGHTLY FRACTURED)	-	2.50	2.7	25.5	0.10	87.4	-	BALMER (1953)
IPU-27	GABBRO	-	-	-	75.8	0.16	-	-	GEYER & MYUNG (1970)
IPU-28	GABBRO	-	-	-	67.6	0.17	-	-	GEYER & MYUNG (1970)
IPU-29	GABBRO	-	-	-	84.1	0.20	-	-	GEYER & MYUNG (1970)
IPU-30	MORROW POINT DAM PEGMATITE (MASSIVE, HARD, COARSE-GRAINED)	-	2.64	0.9	18.5	0.05	122.0	-	USBR (1965)
IPU-31	PORPHYRY	2.35	2.57	9.6	31.2	0.21	126.8	-	JUDD (1969)
IPU-32	GRAND COULEE MONZONITE PORPHYRY (DENSE, MASSIVE)	-	2.58	2.4	41.6	0.18	147.8	-	BALMER (1953)
IPU-33	GRAND COULEE MONZONITE PORPHYRY (DENSE, MASSIVE, VERY HARD)	-	-	-	42.9	0.16	170.5	-	BALMER (1953)
IPU-34	CEDAR CITY TONALITE (FRIABLE, MEDIUM TO FINE-GRAINED)	-	2.60	4.9	19.2	0.17	101.5	6.40	SAUCIER (1969)
IPU-35	CASCATA QUARRY DIABASE	2.79	2.94	6.0	69.0	0.20	155.8	-	RUI2 (1966)
IPU-36	CHAPADAO QUARRY DIABASE	2.96	3.04	3.0	91.2	0.24	152.3	-	RUI2 (1966)
IPU-37	DIABASE	-	2.91	0.6	74.8	0.27	228.0	-	JUDD (1969)
IPU-38	PALISADES DIABASE (DENSE, MASSIVE, MEDIUM-GRAINED)	2.92	-	-	81.8 <sup>A</sup>	0.28 <sup>A</sup>	-	11.4	MILLER (1965)
IPU-39	COGGINS DIABASE (DENSE, MASSIVE, MEDIUM-GRAINED)	3.06	-	-	97.4 <sup>A</sup>	0.38 <sup>A</sup>	321.0	11.9	MILLER (1965)
IPU-40	FRENCH CREEK DIABASE (DENSE, MASSIVE, MEDIUM-GRAINED)	3.06	-	-	99.4 <sup>A</sup>	0.35 <sup>A</sup>	301.0	12.2	MILLER (1965)

Note: 1KN/M<sup>2</sup> = 1/100 BAR; 1/100 ATMOSPHERE; 1/100 TON/FT<sup>2</sup>; 1/100 KG/CM<sup>2</sup>; 1/7 PSI

A - Test Results at 50% of Failure

TABLE 3-1 UNIAxIAL STRESS-STRAIN PARAMETERS FOR  
IGNEOUS (PLUTONIC) ROCK TYPES



ROCK NUMBER	DESCRIPTION	DENSITY (GM/CM <sup>3</sup> )	SPECIFIC GRAVITY	POROSITY (%)	ELASTIC MODULUS (KN/M <sup>2</sup> × 10 <sup>-6</sup> )	POISSON'S RATIO	COMPRESSIVE STRENGTH (KN/M <sup>2</sup> × 10 <sup>-3</sup> )	TENSILE STRENGTH (KN/M <sup>2</sup> × 10 <sup>-3</sup> )	REFERENCE
IVU-1	JHPA DAM BASALT (DENSE)	2.92	3.00	2.7	73.0	0.21	104.8	-	RUIZ (1966)
IVU-2	BARRA BONITA DAM BASALT (DENSE)	2.82	2.97	5.0	61.0	0.19	137.4	-	RUIZ (1966)
IVU-3	JURUMIRIM DAM BASALT (DENSE)	2.52	2.71	6.7	42.8	0.16	133.0	-	RUIZ (1966)
IVU-4	MUSSA QUARRY BASALT (DENSE)	2.50	2.68	6.9	44.0	0.19	126.8	-	RUIZ (1966)
IVU-5	AEC NEVADA SITE BASALT (DENSE, FINE-GRAINED, UNWEATHERED)	2.70	2.83	4.6	34.9 <sup>A</sup>	0.32 <sup>A</sup>	148.0	13.1	STOWE (1969)
IVU-6	HOWARD PRAIRIE DAM BASALT (VERY DENSE, FINE-GRAINED)	-	2.73	3.1	61.8	0.23	194.0	-	BALMER (1953)
IVU-7	LOWER GRANITE BASALT (MASSIVE, COMPACT)	2.73	-	-	50.2 <sup>A</sup>	0.24 <sup>A</sup>	228.0	12.9	MILLER (1965)
IVU-8	LITTLE GOOSE BASALT (MASSIVE, COMPACT)	2.82	-	-	77.5 <sup>A</sup>	0.27 <sup>A</sup>	296.0	11.1	MILLER (1965)
IVU-9	JOHN DAY BASALT (MASSIVE, COMPACT TO VESICULAR)	2.87	-	-	83.8 <sup>A</sup>	0.29 <sup>A</sup>	355.0	14.5	MILLER (1965)
IVU-10	BASALT	2.66	2.86	10.2	38.8	0.16	146.1	-	JUDD (1969)
IVU-11	PALISADES DAM HYPERSTHENE ANDESITE (FINE-GRAINED, VERY HARD)	-	2.57	4.2	44.3	0.16	130.6	-	BALMER (1953)
IVU-12	AEC NEVADA SITE TUFF (RED TO RED-YELLOW, W=19.3%)	1.92	-	-	3.45 <sup>A</sup>	0.24 <sup>A</sup>	9.65	-	CORRING (1967)
IVU-13	AEC NEVADA SITE TUFF (YELLOW, W=17.5%)	2.00	-	-	15.6 <sup>A</sup>	0.09 <sup>A</sup>	35.3	-	CORRING (1967)
IVU-14	AEC NEVADA SITE TUFF (RED AND YELLOW, W=4.6%)	1.60	-	-	6.34 <sup>A</sup>	0.15 <sup>A</sup>	22.3	-	CORRING (1967)
IVU-15	AEC NEVADA SITE TUFF (FAIRLY WELOED ASH, W=21.1%)	1.92	2.39	19.8	3.65 <sup>A</sup>	0.19 <sup>A</sup>	11.3	1.17	STOWE (1969)
IVU-16	HOWARD PRAIRIE DAM LITHIC TUFF (HIGHLY POROUS, FINE TO MEDIUM-GRAINED)	-	1.45	42.5	1.25	0.05	3.65	-	BALMER (1953)
IVU-17	NTS-E TUNNEL TUFF (POROUS, CEMENTED)	1.61	-	-	5.03 <sup>A</sup>	0.21 <sup>A</sup>	24.1	1.45	MILLER (1965)
MNFU-1	GASPAR QUARRY GRANULITE	2.58	2.63	1.9	41.7	0.31	110.0	-	RUIZ (1966)
MNFU-2	QUARTZITE	2.70	2.82	1.1	62.9	0.16	292.0	-	JUDD (1969)
MNFU-3	JARAGUA HILL QUARTZITE	2.63	2.67	1.2	54.8	0.08	226.0	-	RUIZ (1966)
MNFU-4	QUARTZITE (FRACTURED)	-	-	-	76.4	0.10	-	-	GEYER & MYUNG (1970)
MNFU-5	QUARTZITE (FRACTURED)	-	-	-	64.4	0.22	-	-	GEYER & MYUNG (1970)
MNFU-6	QUARTZITE (FINE-GRAINED)	-	-	-	79.3	0.17	-	-	LEEMAN (1966)
MNFU-7	BARABOO QUARTZITE (MASSIVE, BRITTLE, FINE-GRAINED)	2.62	-	-	88.4 <sup>A</sup>	0.11 <sup>A</sup>	320.0	11.0	MILLER (1965)
MNFU-8	MARBLE	2.69	2.75	0.9	35.9	0.24	102.3	11.8	JUDD (1969)
MNFU-9	CARTHAGE MARBLE	2.64	-	-	47.9	0.17	106.0	-	HOSKINS & MORINO (1969)
MNFU-10	TACONIC WHITE MARBLE (MASSIVE, FINE-GRAINED)	2.71	-	-	47.9 <sup>A</sup>	0.40 <sup>A</sup>	62.0	1.17	MILLER (1965)
MNFU-11	CHEROKEE MARBLE (MEDIUM TO COARSE-GRAINED)	2.71	-	-	55.8 <sup>A</sup>	0.25 <sup>A</sup>	66.9	1.79	MILLER (1965)
MNFU-12	IMPERIAL OANBY MARBLE (MASSIVE, MEDIUM-GRAINED)	2.71	-	-	60.4 <sup>A</sup>	0.34 <sup>A</sup>	64.8	2.21	MILLER (1965)

Note: 1KN/M<sup>2</sup> = 1/100 BAR; 1/100 ATMOSPHERE; 1/100 TON/FT<sup>2</sup>; 1/100 KG/CM<sup>2</sup>; 1/7 PSI

A - Test Results at 50% of Failure

**TABLE 3-2 UNIAXIAL STRESS-STRAIN PARAMETERS FOR  
IGNEOUS (VOLCANIC) ROCK TYPES AND FOR  
METAMORPHIC (NON-FOLIATED) ROCK TYPES**

ROCK NUMBER	DESCRIPTION	DENSITY (GM/CM <sup>3</sup> )	SPECIFIC GRAVITY	POROSITY (%)	ELASTIC MODULUS (KN/M <sup>2</sup> × 10 <sup>-6</sup> )	POISSON'S RATIO	COMPRESSIVE STRENGTH (KN/M <sup>2</sup> × 10 <sup>-3</sup> )	TENSILE STRENGTH (KN/M <sup>2</sup> × 10 <sup>-3</sup> )	REFERENCE
MFU-1	EUCALDES DA CUNHA DAM GNEISS	2.75	2.79	1.4	78.4	0.22	132.4	-	RUIZ (1966)
MFU-2	GRAMINHA DAM GNEISS	2.63	2.73	3.7	76.3	0.27	165.0	-	RUIZ (1966)
MFU-3	C.T.A. QUARRY GNEISS	2.62	2.70	3.1	52.7	0.19	105.6	-	RUIZ (1966)
MFU-4	JAGUARE QUARRY GNEISS	2.70	2.73	1.1	78.3	0.24	137.1	-	RUIZ (1966)
MFU-5	CAMARUEIRO QUARRY GNEISS	2.60	2.63	1.4	48.8	0.40	93.6	-	RUIZ (1966)
MFU-6	GNEISS	-	-	-	64.1	0.19	-	-	GEYER & MYUNG (1970)
MFU-7	GNEISS	-	-	-	72.4	0.19	-	-	GEYER & MYUNG (1970)
MFU-8	OWORSHAK GNEISS (MEDIUM TO FINE-GRAINED) (FOLIATION AT 45° TO CORE AXIS)	2.79	-	-	53.6 <sup>A</sup>	0.34 <sup>A</sup>	162.0	6.89	MILLER (1965)
MFU-9	O.E.R. QUARRY GRANITIC GNEISS	2.68	2.74	2.2	46.6	0.23	88.8	-	RUIZ (1966)
MFU-10	EUCALDES DA CUNHA DAM GRANITIC GNEISS	2.65	2.68	1.1	81.7	-	151.0	-	RUIZ (1966)
MFU-11	MONTEZUMA TUNNEL DIORITE GNEISS (HARD, MEDIUM TO COARSE-GRAINED)	-	2.86	0.4	68.4	0.09	84.5	-	BALMER (1953)
MFU-12	MIGMATITE	-	-	-	80.0	0.22	-	-	GEYER & MYUNG (1970)
MFU-13	MIGMATITE	-	-	-	80.0	0.17	-	-	GEYER & MYUNG (1970)
MFU-14	SCHIST	2.74	2.80	3.7	34.9	0.11	50.3	-	JUOD (1969)
MFU-15	FREMONT CANYON SCHIST (DENSE, VERY FINE-GRAINED)	-	-	-	69.0	0.19	-	17.4	NESBITT (1960)
MFU-16	LUTHER FALLS SCHIST (MICACEOUS FOLIATION) (FOLIATION ⊥ TO CORE AXIS)	2.81	-	-	20.7 <sup>A</sup>	0.31 <sup>A</sup>	55.2	0.55	MILLER (1965)
-16a	(FOLIATION // TO CORE AXIS)	2.82	-	-	58.1 <sup>A</sup>	0.18 <sup>A</sup>	82.7	5.24	
MFU-17	MORROW POINT DAM QUARTZ MICA AUGEN SCHIST (HARD, MEDIUM-GRAINED)	-	2.72	0.7	28.5	0.06	107.5	-	USBR (1965)
MFU-18	MORROW POINT DAM QUARTZ MICA SCHIST (MEDIUM TO COARSE-GRAINED)	-	2.74	2.0	8.20	0.04	44.0	-	USBR (1965)
MFU-19	MORROW POINT DAM MUSCOVITE BIOTITE SCHIST (COARSE-GRAINED)	-	2.83	1.7	5.93	0.02	24.9	-	USBR (1965)
MFU-20	MONTEZUMA TUNNEL BIOTITE SCHIST (HARD, MIXTURE OF SCHIST & PEGMATITE)	-	2.70	0.8	39.8	0.05	68.1	-	BALMER (1953)
MFU-21	MONTEZUMA TUNNEL BIOTITE-CHLORITE SCHIST (HARD, FINE-GRAINED)	-	2.71	0.8	66.9	0.18	78.3	-	BALMER (1953)
MFU-22	MONTEZUMA TUNNEL BIOTITE-SILLIMANITE SCHIST (MODERATELY HARD, MEDIUM TO FINE-GRAINED, SLIGHTLY ALTERED)	-	2.72	1.0	21.2	-	21.0	-	BALMER (1953)
MFU-23	MONTEZUMA TUNNEL BIOTITE-SILLIMANITE SCHIST (SOFT TO MODERATELY HARD, QUARTZ INJECTIONS)	-	2.71	2.8	23.3	0.09	19.9	-	BALMER (1953)
MFU-24	SLY PARK DAM QUARTZOSE SERICITE SCHIST (POROUS, MEDIUM-GRAINED)	-	2.47	11.4	8.62	0.06	15.0	-	BALMER (1953)
MFU-25	MORROW POINT DAM HORNBLENDE SCHIST (MEDIUM-GRAINED)	-	2.74	0.4	61.0	0.14	198.7	-	USBR (1965)
MFU-26	SLY PARK DAM GRAPHITIC PHYLLITE (POROUS, FINE-GRAINED, SLIGHTLY TO MODERATELY WEATHERED)	-	2.35	15.3	9.45	-	6.69	-	BALMER (1953)
MFU-27	SLY PARK DAM QUARTZOSE PHYLLITE (POROUS, FINE-GRAINED, SLIGHTLY WEATHERED)	-	2.18	22.4	8.62	0.02	9.38	-	BALMER (1953)
MFU-28	SLY PARK DAM SERICITE PHYLLITE (POROUS, FINE-GRAINED, MODERATELY WEATHERED) (FOLIATION AT 30° TO CORE AXIS)	-	2.34	17.4	17.3	-	9.80	-	BALMER (1953)

Note: 1KN/M<sup>2</sup> = 1/100 BAR; 1/100 ATMOSPHERE; 1/100 TON/FT<sup>2</sup>; 1/100 KG/CM<sup>2</sup>; 1/7 PSI

A - Test Results at 50% of Failure

TABLE 3-3 UNIAXIAL STRESS-STRAIN PARAMETERS FOR  
METAMORPHIC (FOLIATED) ROCK TYPES

ROCK NUMBER	DESCRIPTION	DENSITY (GM/CM <sup>3</sup> )	SPECIFIC GRAVITY	POROSITY (%)	ELASTIC MODULUS (KN/M <sup>2</sup> × 10 <sup>-6</sup> )	POISSON'S RATIO	COMPRESSIVE STRENGTH (KN/M <sup>2</sup> × 10 <sup>-3</sup> )	TENSILE STRENGTH (KN/M <sup>2</sup> × 10 <sup>-3</sup> )	REFERENCE
SCU-1	BRECCIA	2.66	2.71	14.2	14.7	-	110.3	-	JUDD (1969)
SCU-2	CONGLOMERATE	-	2.72	-	13.0	0.15	226.0	-	JUDD (1969)
SCU-3	SANDSTONE	2.22	2.32	21.4	5.0	0.14	62.7	1.93	JUDD (1969)
SCU-4	LONGMONT SANDSTONE	2.35	-	-	31.2	0.08	169.8	-	HOSKINS & HORINO (1969)
SCU-5	BOULCATU SANDSTONE	2.32	2.44	5.0	22.8	0.11	76.1	-	RUIZ (1966)
SCU-6a	BUNTER SANDSTONE	-	-	-	16.6	0.20	-	-	MORGENSTERN & PHUKAN (1966)
-6b	-	-	-	-	12.0	0.21	-	-	
-6c	-	-	-	-	10.0	0.15	-	-	
-6d	-	-	-	-	15.3	0.18	-	-	
SCU-7	W.A.C. BENNETT N4 SANDSTONE (HARD, CHERTY)	-	-	-	17.9	-	136.5	-	IMRIE & JORY (1968)
-7a	(ALONG STRIKE)	-	-	-	16.5	-	133.0	-	
-7b	(ALONG DIP)	-	-	-	15.9	-	122.0	-	
-7c	(NORMAL TO BEDDING)	-	-	-	-	-	-	-	
SCU-8	W.A.C. BENNETT N5 SANDSTONE (HARD, CHERTY)	-	-	-	17.2	-	113.0	-	IMRIE & JORY (1968)
-8a	(ALONG STRIKE)	-	-	-	15.2	-	129.6	-	
-8b	(ALONG DIP)	-	-	-	17.9	-	140.0	-	
-8c	(NORMAL TO BEDDING)	-	-	-	-	-	-	-	
SCU-9	BEREA SANDSTONE (MASSIVE, FINE-GRAINED, SLIGHTLY POROUS)	2.18	-	-	19.3 <sup>A</sup>	0.38 <sup>A</sup>	73.8	1.17	MILLER (1965)
SCU-10	CRAB ORCHARD SANDSTONE (DENSE, FINE-GRAINED)	2.53	-	-	39.2 <sup>A</sup>	0.46 <sup>A</sup>	214.0	8.14	MILLER (1965)
SCU-11	NAVAJO SANDSTONE (POROUS, MEDIUM TO FINE-GRAINED)	2.02	-	-	15.3 <sup>A</sup>	0.31 <sup>A</sup>	42.4	1.24	MILLER (1965)
SCU-12	ALCOVA POWER PLANT TENSLEEP SANDSTONE (POROUS, FINE-GRAINED)	-	2.33	13.8	19.1	0.11	72.4	-	BALMER (1953)
SCU-13	SILTSTONE	2.15	2.67	16.6	32.8	0.23	108.2	-	JUDD (1969)
SCU-14	HACKENSACK SILTSTONE (DENSE, MASSIVE, CLAYEY, CEMENTED)	2.59	-	-	26.2 <sup>A</sup>	0.22 <sup>A</sup>	122.7	2.96	MILLER (1965)
SCU-15	MONTICELLO DAM SILTSTONE (POROUS, FINE-GRAINED)	-	2.50	10.3	13.1	0.09	24.1	-	BALMER (1953)
SCU-16	GRAYWACKE	-	2.46	9.2	20.1	0.08	79.3	-	JUDD (1969)
SCU-17	SUBGRAYWACKE	-	2.66	3.3	33.1	0.08	80.0	-	JUDD (1969)
SCU-18	MONTICELLO DAM SUBGRAYWACKE (POROUS, MASSIVE, COARSE-GRAINED)	-	2.46	10.3	11.4	0.05	54.5	-	BALMER (1953)
SCU-19	MONTICELLO DAM SUBGRAYWACKE (POROUS, COARSE-GRAINED, SLIGHTLY WEATHERED)	-	2.49	9.7	9.52	0.08	30.6	-	BALMER (1953)
SCU-20	MONTICELLO DAM SUBGRAYWACKE (POROUS, MASSIVE, FINE-GRAINED)	-	2.41	12.0	11.4	0.07	48.3	-	BALMER (1953)
SCU-21	MONTICELLO DAM SUBGRAYWACKE (POROUS, MASSIVE, MEDIUM-GRAINED)	-	2.44	11.5	12.3	0.06	48.8	-	BALMER (1953)
SCU-22	MONTICELLO DAM SUBGRAYWACKE (POROUS, MASSIVE, MEDIUM TO COARSE-GRAINED)	-	2.49	9.7	9.93	0.05	50.7	-	BALMER (1953)
SCU-23	SHALE	2.21	2.59	16.2	21.9	0.18	67.6	2.41	JUDD (1969)
SCU-24	W.A.C. BENNETT N5 SHALE (SILTY, RELATIVELY SOFT)	-	-	-	38.6	-	94.4	-	IMRIE & JORY (1968)
-24a	(ALONG STRIKE)	-	-	-	30.4	-	81.3	-	
-24b	(ALONG DIP)	-	-	-	36.5	-	112.3	-	
-24c	(NORMAL TO BEDDING)	-	-	-	-	-	-	-	
SCU-25	MARBLE CANYON DAM CALCAREOUS SHALE (HARD, FINE-GRAINED)	-	2.67	1.8	13.7	0.03	36.0	-	BALMER (1953)
SCU-26	MARBLE CANYON DAM QUARTZOSE SHALE (HARD, LAMINATED)	-	2.69	6.6	15.0	0.07	122.5	-	BALMER (1953)

Note: 1KN/M<sup>2</sup> = 1/100 BAR; 1/100 ATMOSPHERE; 1/100 TON/FT<sup>2</sup>; 1/100 KG/CM<sup>2</sup>; 1/7 PSI

A - Test Results at 50% of Failure

TABLE 3-4 UNIAXIAL STRESS-STRAIN PARAMETERS FOR  
SEDIMENTARY (CLASTIC) ROCK TYPES

ROCK NUMBER	DESCRIPTION	DENSITY (GM/CM <sup>3</sup> )	SPECIFIC GRAVITY	POROSITY (%)	ELASTIC MODULUS (KN/M <sup>2</sup> X 10 <sup>-6</sup> )	POISSON'S RATIO	COMPRESSIVE STRENGTH (KN/M <sup>2</sup> X 10 <sup>-3</sup> )	TENSILE STRENGTH (KN/M <sup>2</sup> X 10 <sup>-3</sup> )	REFERENCE
SCHU-1	SOLENHOFEN LIMESTONE (MASSIVE, VERY FINE-GRAINED)	2.62	-	-	63.8 <sup>A</sup>	0.29 <sup>A</sup>	245.0	4.00	MILLER (1965)
SCHU-2	LIMESTONE	2.67	2.90	11.5	34.7	0.22	75.1	-	JUDD (1969)
SCHU-3	KANSAS LIMESTONE	2.10	-	-	25.7	0.20	50.6	-	MOSKINS & MORINO (1969)
SCHU-4	TAQUARUSSU QUARRY LIMESTONE	2.74	2.79	2.0	82.4	0.33	90.7	-	RUIZ (1966)
SCHU-5	PERUS QUARRY LIMESTONE	2.72	2.75	1.2	64.4	0.23	62.9	-	RUIZ (1969)
SCHU-6	PIRAPORINHA QUARRY LIMESTONE	2.71	2.73	0.4	90.0	0.28	67.6	-	RUIZ (1969)
SCHU-7	AEC NEVADA SITE LIMESTONE (DENSE, FINE-GRAINED, STYLOLITE SEAMS)	2.70	2.72	0.5	77.4 <sup>A</sup>	0.26 <sup>A</sup>	77.1	8.34	STOWE (1969)
SCHU-8	BEDFORD LIMESTONE (POROUS, OOLITIC)	2.21	-	-	28.5 <sup>A</sup>	0.29 <sup>A</sup>	51.0	1.58	MILLER (1965)
SCHU-9	OZARK TAVERNALL LIMESTONE (DENSE, FINE-GRAINED)	2.65	-	-	55.6 <sup>A</sup>	0.30 <sup>A</sup>	97.9	3.92	MILLER (1965)
SCHU-10	MARBLE CANYON DAM LIMESTONE (FINE-GRAINED, SLIGHTLY POROUS)	-	2.71	3.4	67.5	0.25	80.4	-	BALMER (1953)
SCHU-11	MARBLE CANYON DAM LIMESTONE (MEDIUM-GRAINED, MODERATELY POROUS)	-	2.68	4.7	34.3	0.20	127.4	-	BALMER (1953)
SCHU-12	MARBLE CANYON DAM LIMESTONE (HIGHLY POROUS)	-	2.44	13.9	18.7	0.19	133.2	-	BALMER (1953)
SCHU-13	MARBLE CANYON DAM CHALCEDONIC LIMESTONE (HARD, FINE-GRAINED)	-	2.60	5.4	57.9	0.21	107.4	-	BALMER (1953)
SCHU-14	MARBLE CANYON DAM OOLITIC LIMESTONE (HARD, MEDIUM TO FINE-GRAINED)	-	2.67	1.6	47.3	0.18	99.4	-	BALMER (1953)
SCHU-15	MARBLE CANYON DAM STYLOLITIC LIMESTONE (MEDIUM TO FINE-GRAINED)	-	2.73	3.9	41.6	0.16	79.6	-	BALMER (1953)
SCHU-16	ENIWETOK REEF BRECCIA LIMESTONE (HARD, VERY POROUS, FINE-GRAINED)	-	2.30	15.3	37.8	0.16	34.2	-	BALMER (1953)
SCHU-17	ENIWETOK REEF BRECCIA LIMESTONE (VERY POROUS, FRIABLE)	-	1.82	32.7	7.72	0.12	5.93	-	BALMER (1953)
SCHU-18	ENIWETOK REEF HEAD LIMESTONE (VERY POROUS, FRIABLE)	-	1.79	36.0	20.2	0.24	21.2	-	BALMER (1953)
SCHU-19	MARLSTONE	-	2.22	2.9	19.3	0.04	114.4	-	JUDD (1969)
SCHU-20	DOLOMITE	-	2.62	5.8	46.3	-	96.5	-	JUDD (1969)
SCHU-21	CACUPE QUARRY DOLOMITE	2.83	2.84	0.3	67.2	0.14	102.9	-	RUIZ (1966)
SCHU-22	DOLOMITE	-	-	-	78.5	0.30	-	-	GEYER & MYUNG (1970)
SCHU-23	ONEOTA DOLOMITE (POROUS, MASSIVE, FINE-GRAINED)	2.45	-	-	43.9 <sup>A</sup>	0.34 <sup>A</sup>	86.9	4.41	MILLER (1965)
SCHU-24	LOCKPORT DOLOMITE (POROUS, MASSIVE, GRANULAR, VERY FINE-GRAINED)	2.58	-	-	51.0 <sup>A</sup>	0.34 <sup>A</sup>	90.3	3.03	MILLER (1965)
SCHU-25	BONNE TERRE DOLOMITE (DENSE, FINE-GRAINED)	2.64	-	-	66.2 <sup>A</sup>	0.35 <sup>A</sup>	151.7	5.03	MILLER (1965)
SCHU-26	ANHYDRITE	-	-	-	75.8	0.27	-	-	GEYER & MYUNG (1970)
SCHU-27	DOMINION ROCK SALT	-	2.20	-	4.65	-	35.6	-	MUIR & COCHRANE (1966)
SCHU-28	DOMINION ROCK SALT	-	2.90	-	51.5	-	157.0	-	MUIR & COCHRANE (1966)
SCHU-29	DOMINION ROCK SALT	-	2.71	-	44.3	-	103.7	-	MUIR & COCHRANE (1966)
SCHU-30	DIAMOND CRYSTAL ROCK SALT (MASSIVE, COARSE-GRAINED)	2.16	-	-	4.89 <sup>A</sup>	0.73 <sup>A</sup>	21.4	0.83	MILLER (1965)

Note: 1KN/M<sup>2</sup> = 1/100 BAR; 1/100 ATMOSPHERE; 1/100 TON/FT<sup>2</sup>; 1/100 KG/CM<sup>2</sup>; 1/7 PSI

A - Test Results at 50% of Failure

TABLE 3-5 UNIAXIAL STRESS-STRAIN PARAMETERS FOR  
SEDIMENTARY (CHEMICAL) ROCK TYPES

ROCK TYPE PARAMETER		IGNEOUS		METAMORPHIC		SEDIMENTARY		ALL
		PLUTONIC	VOLCANIC	NON-FOLIATED	FOLIATED	CLASTIC	CHEMICAL	
DENSITY (GM/CM <sup>3</sup> )	NO. VALUES	20	14	9	11	10	14	78
	MAXIMUM	3.06	2.92	2.71	2.82	2.66	2.83	3.06
	MINIMUM	2.35	1.60	2.58	2.60	2.02	2.10	1.60
	AVERAGE	2.71	2.40	2.67	2.71	2.32	2.56	2.57
SPECIFIC GRAVITY	NO. VALUES	22	10	4	21	17	20	94
	MAXIMUM	3.04	3.00	2.82	2.86	2.72	2.90	3.04
	MINIMUM	2.50	1.45	2.63	2.18	2.32	1.79	1.45
	AVERAGE	2.68	2.61	2.72	2.66	2.53	2.56	2.62
POROSITY	NO. VALUES	22	10	4	21	20	17	94
	MAXIMUM	9.6	42.5	1.9	22.4	21.4	36.0	42.5
	MINIMUM	0.3	2.7	0.9	0.4	1.8	0.3	0.3
	AVERAGE	2.3	10.6	1.3	4.5	11.3	8.3	6.6
COMPRESSIVE STRENGTH (KN/M <sup>2</sup> × 10 <sup>-3</sup> )	NO. VALUES	31	17	9	24	31	28	140
	MAXIMUM	324.0	355.0	320.0	198.7	226.0	245.0	355.0
	MINIMUM	48.8	3.65	62.0	6.69	24.1	5.93	3.65
	AVERAGE	146.4	123.9	150.0	79.6	96.3	88.1	109.7
TENSILE STRENGTH (KN/M <sup>2</sup> × 10 <sup>-3</sup> )	NO. VALUES	10	6	5	4	6	8	39
	MAXIMUM	12.2	14.5	11.8	17.4	8.14	9.34	17.4
	MINIMUM	2.6	1.17	1.17	0.55	1.17	0.83	0.55
	AVERAGE	9.1	9.0	5.6	7.5	3.0	3.9	6.5
ELASTIC MODULUS, E (KN/M <sup>2</sup> × 10 <sup>-6</sup> )	NO. VALUES	40	17	12	29	35	30	163
	MAXIMUM	99.4	83.8	88.4	81.7	39.2	90.0	99.4
	MINIMUM	7.8	1.2	35.9	5.9	5.0	4.6	1.2
	AVERAGE	56.6	38.1	59.6	47.0	19.3	47.0	43.4
POISSON'S RATIO, ν	NO. VALUES	36	17	12	25	25	26	141
	MAXIMUM	0.39	0.32	0.40	0.40	0.46	0.73	0.73
	MINIMUM	0.05	0.09	0.08	0.02	0.03	0.04	0.02
	AVERAGE	0.20	0.20	0.21	0.17	0.15	0.26	0.20

Note: 1 KN/M<sup>2</sup> = 1/100 BAR; 1/100 ATMOSPHERE; 1/100 TON/FT<sup>2</sup>; 1/100 KG/CM<sup>2</sup>; 1/7 PSI

TABLE 3-6 SUMMARY OF UNIAXIAL STRESS-STRAIN PARAMETERS

Duke University (Clough, 1971) has shown that this relationship very well models the stress-strain behavior of soils over virtually all stress and strain conditions to at least about 75% of failure. On the other hand, this same study showed that many other stress-strain relationships (i.e., non-linear elastic, elasto-plastic, empirical, etc.) had limited range of applicability. Justification for these conclusions was obtained from controlled triaxial and plane strain shear tests, numerical analyses and X-ray observations of actual material behavior during shear. Since soil and rock usually has similar stress-strain characteristics, it is expected that the same conclusions would hold for rock as well as for soil. In the following sections, this stress-strain relationship is reviewed and its applicability to rock is discussed.

#### a) Nonlinearity

The nonlinearity of the stress-strain curves was simulated using a hyperbolic relationship proposed by Kondner and his co-workers (Kondner, 1963; Kondner and Zelasko, 1963a and 1963b; Kondner and Horner, 1965). In their approach, a nonlinear stress-strain curve is represented by a hyperbola of the form:

$$(\sigma_1 - \sigma_3) = \frac{\epsilon_a}{a + b\epsilon_a} \quad (3-1)$$

in which  $(\sigma_1 - \sigma_3)$  is the deviator stress,  $\epsilon_a$  is the axial strain, and  $a$  and  $b$  are parameters whose values are determined empirically. As shown in Figure 3-1, these parameters are the reciprocals of the initial slope (initial tangent modulus) and the asymptote to the stress-strain curve.

For purposes of determining the values of the parameters  $a$  and  $b$  it is convenient to transform Equation 3-1 into the following linear form:

$$\frac{\epsilon_a}{(\sigma_1 - \sigma_3)} = a + b\epsilon_a \quad (3-2)$$

As shown in Figure 3-1, when the relationship is represented in this transformed manner, the parameters  $a$  and  $b$  are, respectively, the intercept and the slope of the straight line.

The value of the asymptotic deviator stress,  $(\sigma_1 - \sigma_3)_{ult}$ , is always somewhat larger than the compressive strength or deviator stress at failure,  $(\sigma_1 - \sigma_3)_f$ .



# TYPICAL HYPERBOLIC STRESS-STRAIN CURVE

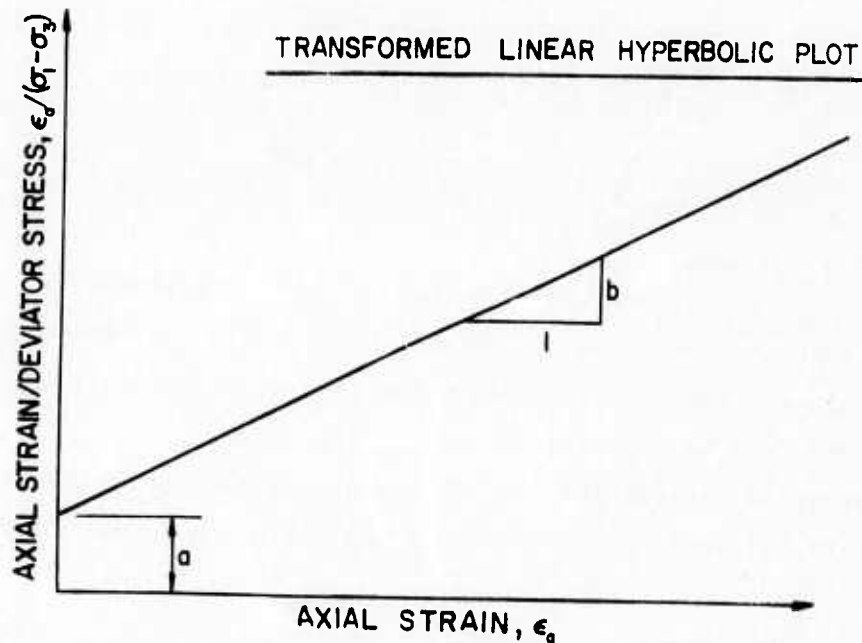
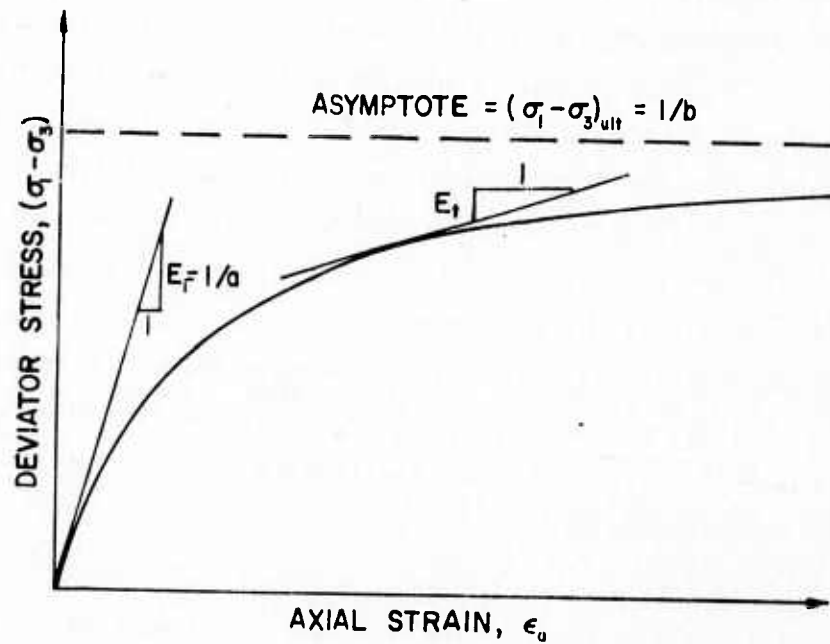


**FIG. 3-1 TYPICAL HYPERBOLIC STRESS-STRAIN CURVE AND TRANSFORMED LINEAR HYPERBOLIC PLOT.**

These two values may be related as follows:

$$(\sigma_1 - \sigma_3)_f = R_f (\sigma_1 - \sigma_3)_{ult} \quad (3-3)$$

in which  $R_f$  is a correlation factor called the "failure ratio", which always has a value less than unity. The value of  $R_f$ , which is determined empirically by comparing the values of  $(\sigma_1 - \sigma_3)_f$  and  $(\sigma_1 - \sigma_3)_{ult}$ , is a measure of how nearly the shape of the stress-strain curve may be approximated by a hyperbola. Values of  $R_f$  equal to unity correspond to stress-strain curves of precisely hyperbolic shape, and smaller values to stress-strain curves of other shapes. Values of  $R_f$  for a variety of different rocks have been found to be essentially independent of confining pressure.

The curves shown in Figure 3-2 demonstrate the usefulness of this simple hyperbolic representation for Cedar City Tonalite. The average value of the failure ratio for this rock is very low (0.32) indicating that the actual stress-strain curves are not close to hyperbolic in shape. The hyperbolic curves, shown as dotted lines in Figure 3-2, would continue to much greater values of deviator stress than the actual compressive strength. As further shown in Figure 3-2, the hyperbolic representation is not employed for values of deviator stress exceeding the compressive strength; at larger strains, the curves are represented by nearly horizontal straight lines. Because of numerical difficulties it is not possible at the present time to simulate a reduction in deviator stress beyond the peak in incremental finite element analyses of the type described herein. However, it may be noted that the hyperbolae and straight lines provide a reasonable approximation of the stress-strain curves for the tonalite even though the failure ratio is very low. Studies of the stress-strain curves for 115 different rock types and test orientations described in subsequent sections have demonstrated the suitability of this relationship for a wide range of rock types.

#### b) Stress-Dependency

The stress-strain characteristics of rock commonly depends on the confining pressure. As shown in Figure 3-2, the steepness of the initial portion of the stress-strain curves and the strength values both increase with increasing magnitude of the confining pressure employed in the tests. The influence of confining pressure on the stress-strain characteristics may be incorporated in the stress-strain relationship by relating the values of the

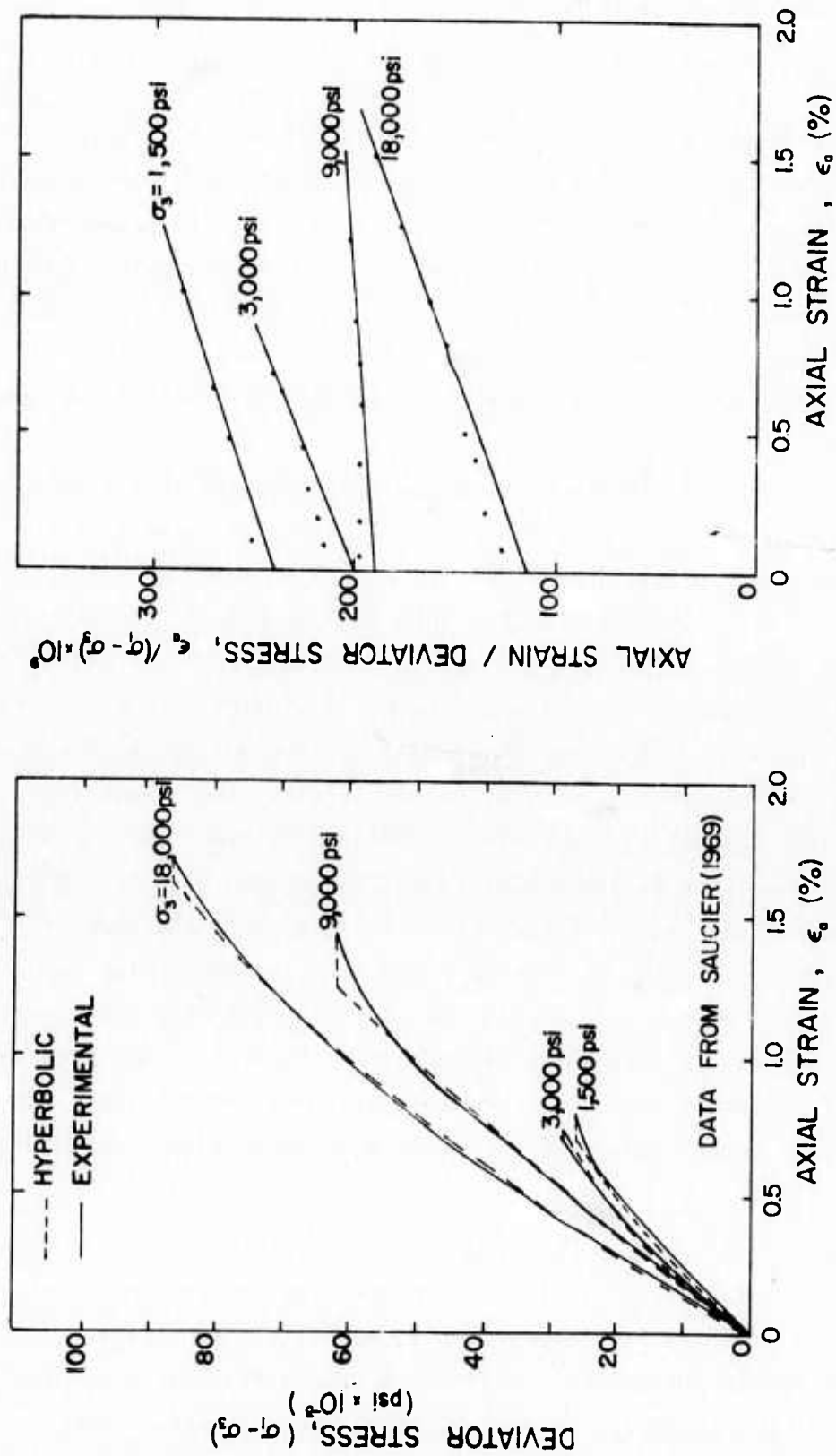


FIG.3-2 EXPERIMENTAL AND HYPERBOLIC STRESS-STRAIN CURVES FOR CEDAR CITY TONALITE

initial tangent modulus and strength with confining pressure.

The variation of initial tangent modulus with confining pressure may be expressed very conveniently in the following form, suggested by Janbu (1963):

$$E_i = K p_a \left( \frac{\sigma_3}{p_a} \right)^n \quad (3-4)$$

in which  $E_i$  is the initial tangent modulus,  $\sigma_3$  is the minimum principal stress,  $p_a$  is atmospheric pressure expressed in the same units as  $E_i$  and  $\sigma_3$ ,  $K$  is the modulus number, and  $n$  is the exponent determining the rate of variation of  $E_i$  with  $\sigma_3$ ; both  $K$  and  $n$  are pure numbers. Values of the parameters  $K$  and  $n$  may be determined readily from the results of a series of tests by plotting the values of  $E_i$  against  $\sigma_3$  on log-log scales and fitting a straight line to the data, as shown in Figure 3-3. The data shown in Figure 3-3 represent tests conducted on three different types of rock and in each case these data can be represented to a reasonable degree of accuracy by a straight line on a log-log plot.

The relationship between compressive strength and confining pressure may be expressed in terms of the Mohr-Coulomb failure criterion as follows:

$$(\sigma_1 - \sigma_3)_f = \frac{2c \cos \phi + 2\sigma_3 \sin \phi}{1 - \sin \phi} \quad (3-5)$$

in which  $c$  and  $\phi$  are the Mohr-Coulomb strength parameters.

Equations 3-4 and 3-5, in combination with the previously described hyperbolic relationship, provide a means for relating stress to strain by means of the 5 parameters,  $K$ ,  $n$ ,  $c$ ,  $\phi$ , and  $R_f$ .

#### c) Tangent Modulus

The nonlinear, stress-dependent stress-strain relationship discussed previously may be used very conveniently in incremental stress analyses, because it is possible to determine from this relationship the value of tangent modulus corresponding to any point on the stress-strain curve. If the value of  $\sigma_3$  is assumed to be constant, the tangent modulus may be expressed in the form:

$$E_t = \frac{\partial (\sigma_1 - \sigma_3)}{\partial \epsilon} \quad (3-6)$$

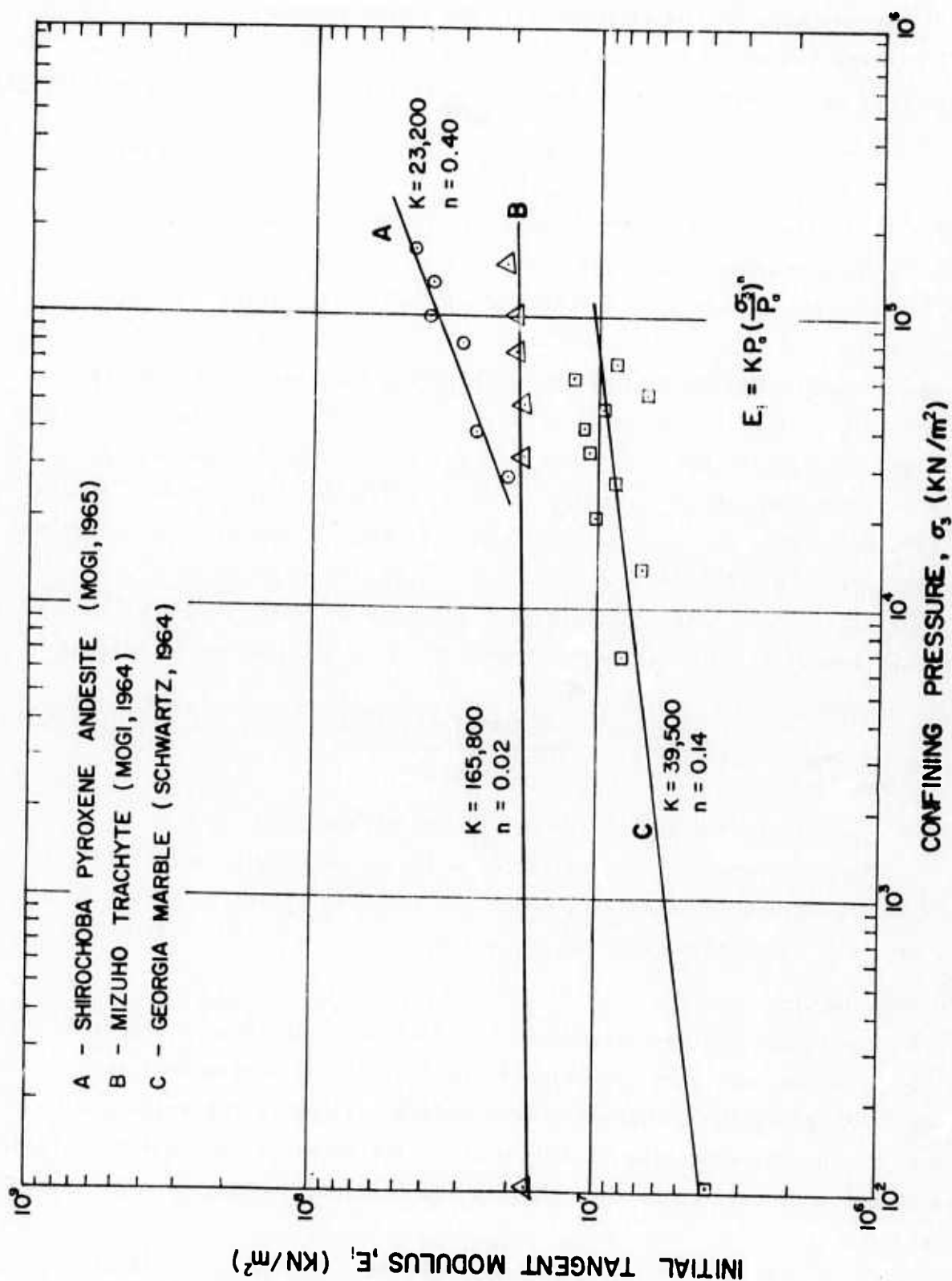


FIG.3-3 VARIATIONS OF INITIAL TANGENT MODULUS WITH CONFINING PRESSURE

Performing the indicated differentiation on Equation 3-1 and substituting the parameters discussed previously, the tangent modulus may be expressed as:

$$E_t = \frac{\frac{1}{E_i}}{\left[ \frac{1}{E_i} + \frac{R_f \epsilon}{(\sigma_1 - \sigma_3)_f} \right]^2} \quad (3-7)$$

Although this expression for the tangent modulus value could be employed in incremental stress analyses, it has one significant shortcoming: the value of tangent modulus,  $E_t$ , is related to the strain, which has a completely arbitrary reference state. Because the reference state for strain is arbitrary, and because stresses may be calculated more accurately than strains in many rock mechanics problems, it seems logical to eliminate strain and express the tangent modulus in terms of the deviator stress. The resulting equation for the tangent modulus is:

$$E_t = K p_a \left( \frac{\sigma_3}{p_a} \right)^n \left[ 1 - \frac{R_f (1 - \sin \phi) (\sigma_1 - \sigma_3)}{2 c \cos \phi + 2 \sigma_3 \sin \phi} \right]^2 \quad (3-8)$$

The usefulness of Equation 3-8 results from its simplicity with regard to two factors:

- (1) Because the tangent modulus is expressed in terms of stresses only, and not strains, it may be employed for analyses of problems involving arbitrary initial stress conditions without any complications.
- (2) The parameters involved in this relationship may be determined readily from the results of conventional laboratory tests. The amount of effort required to determine values of the parameters  $K$ ,  $n$ , and  $R_f$  is not much greater than that required to determine values of  $c$  and  $\phi$ .

To study the applicability of this stress-strain relationship to various types of rock, and to determine values of the required parameters for these materials, a review of published stress-strain information has been made. The



results of this review are summarized in the following sections.

#### Nonlinear Modulus Parameters Under Triaxial Conditions

In a manner similar to that discussed previously, an extensive literature survey was conducted to locate data on rock properties under triaxial test conditions. In all, data were available for 87 different types of rocks; consideration of the data available for one rock type tested at several orientations yielded a total of 115 modulus values. Since several stress-strain curves were analyzed to obtain each set of nonlinear modulus parameters, it can be seen that at least several hundred stress-strain curves were analyzed; in all cases, the empirical fit was good. It should be noted that a least squares fit was employed in obtaining these values.

These data were grouped together genetically and were tabulated as shown in Tables 3-7 through 3-10. Whenever sufficient data were available, the full description, density, specific gravity, porosity, modulus number ( $K$ ), exponent ( $n$ ), failure ratio ( $R_f$ ), cohesion ( $c$ ), angle of friction ( $\phi$ ) and range of confining pressure were included. As can be seen, all of these data were not available for all of the rock types.

Examination of these data, a summary of which is shown in Table 3-11, indicates a number of general trends for the modulus parameters  $K$ ,  $n$  and  $R_f$ :

- (1) Hard, crystalline or homogeneous rocks of low porosity tend to have high values of  $K$  and low values of  $n$  and  $R_f$ . The low  $n$  value indicates that the modulus is little affected by confining pressure while the low  $R_f$  value indicates stress-strain curves which are close to being linear.
- (2) Porous, clastic or closely jointed rocks tend to have relatively low values of  $K$  and relatively high values of  $n$  and  $R_f$ , indicating substantial stress-dependency and nonlinearity.
- (3) Anisotropic properties tend to be governed primarily by the value of  $K$  while, for the most part, the values of  $n$ ,  $R_f$ ,  $c$  and  $\phi$  tend to be quite consistent.
- (4) Based upon the average values shown in Table 3-11, it can be seen that the average values of  $n$  and  $R_f$  are fairly consistent with each other, while there is substantial variation in the  $K$  values.

ROCK NUMBER	DESCRIPTION	DENSITY (GM/CM <sup>3</sup> )	SPECIFIC GRAVITY	POROSITY (%)	MODULUS NUMBER K (x10 <sup>-3</sup> )	EXPONENT N	FAILURE RATIO, R <sub>f</sub>	COHESION, C (KN/M <sup>2</sup> x10 <sup>-3</sup> )	ANGLE OF FRICTION, φ	RANGE OF CONFINING PRESSURE (KN/M <sup>2</sup> x10 <sup>-3</sup> )	REFERENCE
IPT-1	INADA BIOTITE GRANITE (MEDIUM-GRAINED)	2.61	-	0.4	988.	0	0.72	55.2	47.7	0.1-98	MOGI (1964)
IPT-2	WESTERLY GRANITE	-	2.61	-	544.	0.03	-	55.2	-	0.1-100.	BIRCH (1966)
IPT-3	STONE MT. GRANITE (MEDIUM-GRAINED)	2.61	2.66	0.2	63.2	0.19	0.18	55.1	51.0	0-68.9	SCHWARTZ (1964)
IPT-4	AEC NEVADA SITE GRANITE (DENSE, COARSE-GRAINED, UNWEATHERED)	2.69	2.69	0.3	694.	0.01	0.19	22.1	52.0	0-27.6	STOWE (1969)
IPT-5	QUARTZ MONZONITE (MEDIUM-GRAINED, PORPHYRITIC)	-	-	-	-	-	-	-	-	-	-
-5a	(MUTUALLY PERPENDICULAR AXES)	2.68	2.70	0.2	789.	0.01	0.26	36.9	53.0	0-20.7	DEKLOTZ & HECK (1965)
-5b		2.69	2.69	0.2	884.	0.01	0.29	40.3	53.0	0-20.7	
-5c		2.68	2.68	0.2	878.	0.01	0.27	36.2	56.0	0-27.7	
IPT-6	AEC NEVADA SITE QUARTZ MONZONITE	2.66	-	0.2	822.	-0.01	-	27.6	56.0	1.0-9.3	CORDING (1967)
IPT-7	UKIGANE DIORITE (VERY DENSE, MEDIUM-GRAINED)	3.09	-	0.2	1101.	0	0.70	56.2	41.5	0.1-98.	MOGI (1964)
IPT-8	ORIKABE QUARTZ DIORITE (FINE-GRAINED)	2.78	-	0.4	168.7	0.14	0.62	176.0	23.8	18.-250.	MOGI (1965)
IPT-9	HABE-ISHI HORNBLENDE PERIDOTITE (MEDIUM-GRAINED)	3.16	-	0.02	690.	0	0.48	63.0	37.6	18.-250.	MOGI (1965)
IPT-10	CEGAR CITY TONALITE (FRIABLE, MEDIUM TO FINE-GRAINED)	-	2.60	4.9	242.	0.03	0.32	16.5	45.0	0-69.	SAUCIER (1969)
IPT-11	OMEGA DIABASE	-	3.04	-	1027.	0.01	-	88.2	31.0	69.-248	BIRCH (1966)
IVT-1	HOWARD PRAIRIE DAM BASALT	-	2.82	-	756.	0.01	-	-	-	0.1-100.	BIRCH (1966)
IVT-2	AEC NEVADA SITE BASALT (DENSE, FINE-GRAINED, UNWEATHERED)	2.70	2.83	4.6	286.	0.05	0.39	27.6	64.0	0-3.4	STOWE (1969)
IVT-3	PANGUNA ANDESITE (CLOSELY JOINTED)	-	-	-	1.7	1.15	0.68	66.2	31.0	3.4-34.5	JAEGER (1969)
IVT-4	HONKOMATSU AUGITE ANDESITE (DENSE, COARSE TO FINE-GRAINED)	2.23	-	9.9	154.0	0	0.80	0	36.6	0-6.5	
IVT-5	SHIROCHOBA PYROXENE ANDESITE	2.08	-	5.1	269.	0.03	0.65	3.72	33.4	6.5-41.4	
IVT-6	SHIROCHOBA PYROXENE ANDESITE	2.45	-	5.1	23.2	0.40	0.27	20.6	28.2	0.1-145.	MOGI (1964)
IVT-7	SHIMOMATSU PYROXENE ANDESITE (VERY POROUS)	2.17	-	12.6	388.	0	0.59	36.1	35.3	0.1-147.	MOGI (1964)
IVT-8	MIZUHO TRACHYTE (MASSIVE, HOLOCYSTALLINE)	2.24	-	8.5	43.0	0.26	0.55	35.0	39.5	28.-130.	MOGI (1965)
IVT-9	MIZUHO TRACHYTE (MASSIVE, HOLOCYSTALLINE)	2.24	-	8.7	165.8	0.02	0.79	72.4	0	13.-100.	MOGI (1965)
IVT-10	SAKU-ISHI ANDESITIC WELDED TUFF (POROUS)	1.95	-	21.6	100.4	0	0.23	56.0	18.4	15.-200.	MOGI (1965)
IVT-11	AO-ISHI DACITE PUMICE TUFF (DENSE, FINELY LAMINATED)	2.00	-	24.0	33.5	0	0.54	27.4	27.7	0.1-147.	MOGI (1964)
IVT-12	TATSUYAMA DACITE PUMICE TUFF (DENSE)	2.23	-	11.2	241.	0	0.62	25.0	0	10.-50.	MOGI (1965)
IVT-13	OJOYA-ISHI DACITE PUMICE TUFF (MASSIVE, SLIGHTLY ALTERED)	1.45	-	30.0	20.2	-0.08	0.57	17.6	19.4	0.1-147.	MOGI (1964)
IVT-14	TATSUYAMA DACITE PUMICE TUFF (DENSE, LAMINATED)	2.26	-	10.2	274.	0	0.42	38.7	28.5	0.1-147.	MOGI (1964)
IVT-15	AO-ISHI TUFF (MASSIVE, FINELY LAMINATED)	2.01	-	17.3	110.6	0.07	0.51	2.6	15.5	0.1-147.	MOGI (1964)
IVT-16	AEC NEVADA SITE TUFF (FAIRLY WELDED ASH, W=21.1%)	1.92	2.39	19.8	36.0	0.08	0.26	38.0	0.0	6.5-200.	MOGI (1965)
								3.75	22.5	0-10.3	STOWE (1969)

Note: 1 KN/M<sup>2</sup> = 1/100 BAR; 1/100 ATMOSPHERE; 1/100 TON/FT<sup>2</sup>; 1/100 KG/CM<sup>2</sup>; 1/7 PSI

TABLE 3-7 TRIAXIAL STRESS-STRAIN PARAMETERS FOR  
IGNEOUS (PLUTONIC AND VOLCANIC) ROCK TYPES

ROCK NUMBER	DESCRIPTION	DENSITY (GM/CM <sup>3</sup> )	SPECIFIC GRAVITY	POROSITY (%)	MODULUS NUMBER K (10 <sup>-3</sup> )	EXPONENT N	FAILURE RATIO, R <sub>f</sub>	COHESION, C (KN/M <sup>2</sup> × 10 <sup>-3</sup> )	ANGLE OF FRICTION, φ	RANGE OF CONFINING PRESSURE (KN/M <sup>2</sup> × 10 <sup>-3</sup> )	REFERENCE
MFT-1	SCHISTOSE GNEISS (FINE-GRAINED) (⊥ TO FOLIATION)	2.79	2.80	0.5	434.	0.04	0.47	20.7	43.0	0-20.7	DEKLOTZ ET AL (1965)
MFT-2	SCHISTOSE GNEISS (30° TO FOLIATION)	-	2.75	1.9	281.	0.02	0.40	46.9	28.0	20.7-70.	
MFT-3	METTAWEE SLATE (FINE-GRAINED) (⊥ TO FOLIATION)	-	-	-	32.7	0.17	0.55	14.8	27.6	0-69.	DEKLOTZ ET AL (1966a)
MFT-4	TEXAS SLATE (FINE-GRAINED) (// TO FOLIATION)	-	-	-	166.2	0.17	0.18	46.6	47.6	0-203.	HANDIN & HAGER (1957)
-4c	(10° TO FOLIATION)	-	-	-	258.0	0.09	0.33	60.7	33.5	34.5-276.	McLAMORE (1966)
-4b	(20° TO FOLIATION)	-	-	-	25.7	0.34	0.35	51.7	28.5	34.5-276.	
-4c	(30° TO FOLIATION)	-	-	-	98.6	0.18	0.66	29.0	25.0	34.5-276.	
-4d	(40° TO FOLIATION)	-	-	-	116.6	0.14	0.52	26.2	21.0	34.5-276.	
-4e	(50° TO FOLIATION)	-	-	-	95.8	0.18	0.8	35.2	19.0	34.5-276.	
-4f	(60° TO FOLIATION)	-	-	-	50.5	0.26	0.59	52.4	15.0	34.5-276.	
-4g	(70° TO FOLIATION)	-	-	-	23.8	0.36	0.50	53.8	20.0	34.5-276.	
-4h	(80° TO FOLIATION)	-	-	-	50.6	0.27	0.46	64.1	22.5	34.5-276.	
-4i	(⊥ TO FOLIATION)	-	-	-	70.2	0.28	0.61	67.0	24.7	34.5-276.	
-4j	(⊥ TO FOLIATION)	-	-	-	-	-	-	70.3	26.9	34.5-276.	
MNFT-1	SIoux QUARTZITE (FINE-GRAINED)	-	-	-	360.	0.06	0.57	70.6	48.0	0-203.	HANDIN & HAGER (1957)
MNFT-2	YAMAGUCHI MARBLE (PURE, FINE-GRAINED)	2.62	-	0.3	538.	0	0.91	30.4	29.2	0.1-147.	MOGI (1964)
MNFT-3	MITO MARBLE (LITTLE QUARTZ, MEDIUM-GRAINED)	2.69	-	0.2	730.	0	0.84	22.8	30.6	0.1-147.	MOGI (1964)
MNFT-4	YAMAGUCHI MARBLE (PURE, COARSE-GRAINED)	2.48	-	0.1	272.	0	0.83	22.2	27.8	0.1-147.	MOGI (1964)
MNFT-5	WOMBEEYAN MARBLE (COARSE-GRAINED)	-	-	-	348.	0	-	-	-	0-100.	PATERSON (1958)
MNFT-6	CARRARA MARBLE	-	-	-	473.	0	-	-	-	0-320.	HEARO (1967)
MNFT-7	GEOGIA MARBLE (CALCITIC, VERY DENSE)	2.69	2.76	0.3	39.5	0.14	0.43	0	60.0	0-5.6	SCHWARTZ (1964)
MNFT-8	YULE MARBLE (MEDIUM-GRAINED)	-	-	-	240.	0	-	21.2	25.3	5.6-68.9	GRIGGS (1936)
MNFT-9	YULE MARBLE (MEDIUM-GRAINED)	-	-	-	512.	0	0.67	1.12	35.3	0-101.	
-9a	(⊥ TO FOLIATION)	-	-	-	287.	0	0.92	14.6	36.4	0-203.	
MNFT-10	CABRAMURRA SERPENTINE	-	-	-	585.	0	-	-	-	100.-500.	RALEIGH & PATERSON (1965)

Notes: 1 KN/M<sup>2</sup> = 1/100 BAR; 1/100 ATMOSPHERE; 1/100 TON/FT<sup>2</sup>; 1/100 KG/CM<sup>2</sup>; 1/7 PSI

TABLE 3-8 TRIAXIAL STRESS-STRAIN PARAMETERS FOR  
METAMORPHIC (FOLIATED AND NON-FOLIATED)  
ROCK TYPES

ROCK NUMBER	DESCRIPTION	DENSITY (GM/CM <sup>3</sup> )	SPECIFIC GRAVITY	POROSITY (%)	$\nu$ ( $\times 10^{-3}$ )	MODULUS NUMBER	EXPONENT N	FAILURE RATIO, $R_f$	COHESION, C (KN/M <sup>2</sup> $\times 10^{-3}$ )	ANGLE OF FRICTION, $\phi$	RANGE OF CONFINING PRESSURE (KN/M <sup>2</sup> $\times 10^{-3}$ )	REFERENCE
SCT-1	STOCKTON SHALE BRECCIA (WAXY TO EARTHY)	2.48	-	-	19.4	0.26	-	1.45	36-50	D.1-12.4	DEKLOTZ ET AL (1966b)	
SCT-2	BEREA SANDSTONE (MEDIUM-GRAINED, WELL-CEMENTED)	-	2.66	18.2	43.6	0.25	0.73	27.2	27.8	0-200.	HANDIN ET AL (1963)	
SCT-3	WEEK'S ISLAND SANDSTONE (MASSIVE, HARD, FRIABLE, FINE- GRAINED, WELL-CEMENTED)	-	-	-	5.96	0.39	0.66	55.2	27.5	0-203.	HANDIN & HAGER (1957)	
SCT-4	DILL CREEK SANDSTONE (MASSIVE, VERY HARD, VERY FINE- GRAINED, WELL-CEMENTED)	-	-	-	161.8	0.07	0.42	22.1	44.5	0-203.	HANDIN & HAGER (1957)	
SCT-5	BARTLESVILLE SANDSTONE (MASSIVE, FINE-GRAINED, WELL-CEMENTED)	-	-	-	58.6	0.27	0.64	8.0	37.2	0-203.	HANDIN & HAGER (1957)	
SCT-6	POTTSVILLE SANDSTONE (UNWEATHERED, ALMOST PURE SILICA)	2.28	2.64	14.0	106.0	0.07	0.25	14.9	45.2	0-68.9	SCHWARTZ (1964)	
SCT-7	HOISE SANDSTONE (WELL-CEMENTED)	1.90	-	27.0	73.6	0.12	-	-	-	1.4-34.4	KING (1968)	
SCT-8	MASE SANDSTONE (UNIFORM, MEDIUM-GRAINED)	2.69	-	0.9	135.4	0.08	0.62	41.9	41.5	0.1-150.	HOSHINO & KOLDE (1970)	
SCT-10	BARNES SANDSTONE (MASSIVE, FINE-GRAINED, WELL-CEMENTED)	-	-	-	127.0	0.07	-	-	-	0-243.	HEARD (1967)	
-10a	(// TO BEDDING)	-	-	-	48.0	0.07	0.60	8.6	34.0	0-203.	HANDIN & HAGER (1957)	
-10b	( $\perp$ TO BEDDING)	-	-	-	62.4	0.10	0.52	8.2	34.0	0-203.		
SCT-11	REPETTO SILTSTONE (HARD, FISSILE, DRY)	-	2.58	5.6	76.8	0	0.55	34.7	32.1	51.-203.	HANDIN & HAGER (1957)	
SCT-12	REPETTO SILTSTONE (HARD, FISSILE, SATURATED)	-	2.58	5.6	25.8	0.16	0.72	34.7	32.1	0-200.	HANDIN ET AL (1963)	
SCT-13	STOCKTON NORTHVIEW SHALE (DENSE, SILTY, FINE-GRAINED)	2.47	-	-	2.07	0.23	-	0.69	21.0	0.8-4.1	DEKLOTZ ET AL (1966b)	
SCT-14	STOCKTON SHALE (SOFT, WAXY)	2.38	-	-	4.06	0.08	-	0.34	22.0	0.8-4.1	DEKLOTZ ET AL (1966b)	
SCT-15	MUDDY SHALE (HARD, FINE-GRAINED, DRY)	-	2.67	4.7	3.57	0.43	0.36	35.4	55.5	0-203.	HANDIN & HAGER (1957)	
SCT-16	MUDDY SHALE (HARD, FINE-GRAINED, SATURATED)	-	2.67	4.7	85.6	0.01	0.36	38.4	14.4	0-200.	HANDIN ET AL (1963)	
SCT-17	"5900 FOOT SANDS FORMATION" SHALE (HARD, FISSILE)	-	-	-	94.6	0.12	0.78	24.7	23.8	0-203.	HANDIN & HAGER (1957)	
SCT-18	EDMONTON CLAY SHALE (W=20%)	-	-	-	0.18	0.80	0.55	0.1	28.0	0.1-0.8	SINCLAIR & BROOKER (1967)	
SCT-19	EDMONTON BENTONITIC SHALE (W=30%)	-	-	-	0.22	0.68	0.78	0.3	7.5	0.1-3.1	SINCLAIR & BROOKER (1967)	
SCT-20	GREEN RIVER SHALE (HARD, CALCAREOUS)	-	-	-	0.06	1.22	0.84	0	46.6	0-203.	HANDIN & HAGER (1957)	
-20a	(// TO BEDDING)	-	-	-	54.9	0.11	0.81	24.9	22.6	0-203.		
-20b	( $\perp$ TO BEDDING)	-	-	-	-	-	-	-	-	-		
SCT-21	GREEN RIVER SHALE-1 (FINE-GRAINED, BRITTLE, CALCITIC & DOLOMITIC, INTERBEDDED WITH KERGEN)	-	-	-	131.2	0.10	0.66	73.1	29.0	6.9-172.	McLAMBRE (1966)	
-21a	(// TO BEDDING)	-	-	-	97.5	0.15	0.64	62.0	30.0	6.9-172.		
-21b	(15° TO BEDDING)	-	-	-	115.6	0.08	0.46	53.8	30.0	6.9-172.		
-21c	(20° TO BEDDING)	-	-	-	85.0	0.14	0.50	44.1	30.5	6.9-172.		
-21d	(30° TO BEDDING)	-	-	-	97.9	0.12	0.57	55.8	30.5	6.9-172.		
-21e	(45° TO BEDDING)	-	-	-	117.0	0.11	0.49	59.3	30.0	6.9-172.		
-21f	(60° TO BEDDING)	-	-	-	61.8	0.21	0.45	59.3	30.5	6.9-172.		
-21g	(75° TO BEDDING)	-	-	-	85.6	0.13	0.38	62.7	30.5	6.9-172.		
-21h	( $\perp$ TO BEDDING)	-	-	-	-	-	-	-	-	-		
SCT-22	GREEN RIVER SHALE-2 (FINE-GRAINED, PLASTIC, CALCITIC & DOLOMITIC, INTERBEDDED WITH KERGEN)	-	-	-	50.3	0.13	0.64	44.5	21.0	6.9-172.	McLAMBRE (1966)	
-22a	(// TO BEDDING)	-	-	-	67.3	0.04	0.74	41.4	20.5	6.9-172.		
-22b	(10° TO BEDDING)	-	-	-	56.5	0.07	0.75	34.5	19.9	6.9-172.		
-22c	(20° TO BEDDING)	-	-	-	29.9	0.11	0.63	29.0	18.0	6.9-172.		
-22d	(30° TO BEDDING)	-	-	-	27.9	0.15	0.65	31.7	19.0	6.9-172.		
-22e	(40° TO BEDDING)	-	-	-	13.9	0.25	0.69	36.5	20.6	6.9-172.		
-22f	(60° TO BEDDING)	-	-	-	78.9	0.03	0.80	38.6	20.7	6.9-172.		
-22g	( $\perp$ TO BEDDING)	-	-	-	-	-	-	-	-	-		

Note: 1 KN/M<sup>2</sup> = 1/100 BAR; 1/100 ATMOSPHERE; 1/100 TON/FT<sup>2</sup>; 1/100 KG/CM<sup>2</sup>; 1/7 PSI

TABLE 3-9 TRIAXIAL STRESS-STRAIN PARAMETERS FOR  
SEDIMENTARY (CLASTIC) ROCK TYPES

ROCK NUMBER	DESCRIPTION	DENSITY (GM/CM <sup>3</sup> )	SPECIFIC GRAVITY	POROSITY (%)	MODULUS NUMBER K (X10 <sup>-3</sup> )	EXPONENT N	FAILURE RATIO, R <sub>f</sub>	COHESION, C (KN/M <sup>2</sup> X10 <sup>-3</sup> )	ANGLE OF FRICTION, φ	RANGE OF CONFINING PRESSURE (KN/M <sup>2</sup> X10 <sup>-3</sup> )	REFERENCE
SCHT-1	DEVONIAN LIMESTONE (HETEROGENEOUS, COARSE-GRAINED)	-	-	-	123.1	0.12	0.96	20.6	33.6	0-203.	HANDIN & HAGER (1957)
SCHT-2	FUSSELMAN LIMESTONE (HETEROGENEOUS, COARSE-GRAINED)	-	-	-	63.3	0.20	0.60	11.1	32.7	0-203.	HANDIN & HAGER (1957)
SCHT-3	WOLF CAMP LIMESTONE (HETEROGENEOUS, FINE-GRAINED)	-	-	-	77.8	0.28	0.63	23.6	34.8	0-203.	HANDIN & HAGER (1957)
SCHT-4	MARIANNA LIMESTONE (MASSIVE, FRIABLE, DRY)	-	2.70	13.0	107.5	0	0.34	26.8	26.4	0-203.	HANDIN & HAGER (1957)
SCHT-5	MARIANNA LIMESTONE (MASSIVE, FRIABLE, SATURATED)	-	2.70	13.0	59.9	0.09	0.80	12.6	37.6	0.3-4.4	HANDIN ET AL (1963)
SCHT-6	WELLS STATION LIMESTONE (HETEROGENEOUS, FINE-GRAINED)	-	-	-	455.	0	-	-	-	20.6-98.	PATERSON (1958)
SCHT-7	SOLEHOFEN LIMESTONE (HOMOGENEOUS)	-	-	-	594.	0	-	-	-	0.1-1013.	GRIGGS (1936)
SCHT-8	SOLEHOFEN LIMESTONE (HOMOGENEOUS, AT 25° C.)	-	-	-	315.	0.06	-	-	-	0-500.	HEARO (1960)
SCHT-9	LIMESTONE	-	2.64	-	544.	0.02	-	-	-	0.1-100.	BIRCH (1966)
SCHT-10	INDIANA LIMESTONE (OOLITIC)	2.20	2.70	19.4	44.5	0.18	0.54	6.72	42.0	0-9.6	SCHWARTZ (1964)
SCHT-11	CROWN POINT LIMESTONE	-	-	-	52.1	0.25	0.58	29.6	7.0	9.6-68.9	DONATH (1970)
SCHT-12	AEC NEVAOA SITE LIMESTONE (DENSE, FINE-GRAINED)	2.70	2.72	0.5	742.	0.0	0.33	86.0	21.3	20.-180.	
SCHT-13	BLAIR DOLOMITE (HOMOGENEOUS, FINE-GRAINED)	-	-	-	168.6	0.16	0.50	14.5	44.0	0-27.6	STOWE (1969)
SCHT-14	CLEAR FORK DOLOMITE (COARSE TO FINE-GRAINED)	-	-	-	196.5	0.22	0.39	35.9	39.0	0-203.	HANDIN & HAGER (1957)
SCHT-15	FUSSELMAN DOLOMITE (HETEROGENEOUS, FINE-GRAINED, CALCITIC)	-	-	-	86.9	0.26	0.60	73.1	35.0	0-203.	HANDIN & HAGER (1957)
SCHT-16	GLORIETA DOLOMITE (HETEROGENEOUS, MEDIUM-GRAINED, CALCITIC)	-	-	-	60.5	0.29	0.74	48.4	39.5	0-203.	HANDIN & HAGER (1957)
SCHT-17	LUNING DOLOMITE (FINE-GRAINED, CALCITIC)	-	-	-	101.3	0.21	0.88	25.8	35.0	0-203.	HANDIN & HAGER (1957)
SCHT-18	HASHMARK DOLOMITE (HOMOGENEOUS, DRY, COARSE-GRAINED)	-	-	-	176.2	0.11	0.86	23.7	34.0	0-203.	HANDIN & HAGER (1957)
18a	(// TO FOLIATION)	-	2.91	3.5	153.6	0.13	0.81	23.1	32.1	101.-203.	HANDIN & HAGER (1957)
18b	(⊥ TO FOLIATION)	-	2.91	3.5	88.0	0.17	0.61	45.6	30.6	0-203.	
SCHT-19	HASHMARK DOLOMITE (HOMOGENEOUS, COARSE-GRAINED, SATURATED)	-	2.91	3.5	231.0	0.02	-	22.8	35.5	0.8-5.9	HANDIN ET AL (1963)
SCHT-20	STOCKTON DOLOMITE & DOLOMITE BRECCIA (CALCAREOUS, MEDIUM TO FINE-GRAINED)	2.56	-	-	56.6	0.27	-	3.45	61.0	0.05-12.4	OEKLOTZ ET AL (1966b)
SCHT-21	STOCKTON DOLOMITE WITH SHALE SEAMS (LAMINATED)	2.56	-	-	68.9	0.32	-	0.69	51.0	0.4-12.4	OEKLOTZ ET AL (1966b)
SCHT-22	STOCKTON DOLOMITE WITH STYLOLITES (CLAY-FILLED)	2.56	-	-	68.9	0.32	-	0.76	56.0	0.8-4.1	OEKLOTZ ET AL (1966b)
SCHT-23	CHALK (95% CaCO <sub>3</sub> )	1.62	2.72	40.0	0.13	0.67	0.54	0	31.5	10.-50.	DAYRE ET AL (1970)
SCHT-24	BLAINE ANHYDRITE (FINE-GRAINED)	-	-	-	93.2	0.10	0.78	43.4	29.4	0-203.	HANDIN & HAGER (1957)

Note: 1 KN/M<sup>2</sup> = 1/100 BAR; 1/100 ATMOSPHERE; 1/100 TON/FT<sup>2</sup>; 1/100 KG/CM<sup>2</sup>; 1/7 PSI

TABLE 3-10 TRIAXIAL STRESS-STRAIN PARAMETERS FOR  
SEDIMENTARY (CHEMICAL) ROCK TYPES

ROCK TYPE PARAMETER		IGNEOUS		METAMORPHIC		SEDIMENTARY		ALL
		PLUTONIC	VOLCANIC	NON-FOLIATED	FOLIATED	CLASTIC	CHEMICAL	
DENSITY (GM/CM <sup>3</sup> )	NO. VALUES	10 (8)	14	4	1	6	6	41 (39)
	MAXIMUM	3.16	2.70	2.69	-	2.69	2.70	3.16
	MINIMUM	2.61	1.45	2.48	-	1.90	1.62	1.45
	AVERAGE	2.76	2.14	2.62	2.79	2.37	2.37	2.45
SPECIFIC GRAVITY	NO. VALUES	8 (6)	3	1	2	6	9 (8)	29 (26)
	MAXIMUM	3.04	2.83	-	2.80	2.67	2.91	3.04
	MINIMUM	2.60	2.39	-	2.75	2.58	2.64	2.39
	AVERAGE	2.71	2.68	2.76	2.78	2.63	2.77	2.72
POROSITY	NO. VALUES	11 (9)	14	4	2	8	8 (7)	47 (44)
	MAXIMUM	4.9	30.0	0.3	1.9	27.0	40.0	40.0
	MINIMUM	0.02	4.6	0.1	0.5	0.9	0.5	0.02
	AVERAGE	0.7	13.5	0.2	1.2	10.1	12.0	8.0
COHESION, c (KN/M <sup>2</sup> x 10 <sup>-3</sup> )	NO. VALUES	12 (9)	17 (15)	8 (6)	14 (4)	35 (20)	22 (20)	108 (74)
	MAXIMUM	176.0	77.4	70.6	70.3	73.1	86.0	176.0
	MINIMUM	16.5	0.0	0.0	14.8	0.0	0.0	0.0
	AVERAGE	56.1	32.2	22.9	45.7	31.7	26.3	34.5
ANGLE OF FRICTION, φ	NO. VALUES	12 (9)	17 (15)	8 (6)	14 (4)	35 (20)	22 (20)	108 (74)
	MAXIMUM	56.0	64.0	60.0	47.6	55.5	61.0	64.0
	MINIMUM	23.8	0.0	25.3	15.0	7.5	7.0	0.0
	AVERAGE	45.6	24.7	36.6	27.3	29.2	35.9	32.0
MODULUS NUMBER, K ( x 10 <sup>-3</sup> )	NO. VALUES	13 (11)	16	11 (10)	13 (4)	37 (22)	25 (24)	115 (87)
	MAXIMUM	1101.0	756.0	730.0	434.0	161.8	742.0	1101.0
	MINIMUM	63.2	1.4	39.5	23.8	0.1	1.0	0.1
	AVERAGE	683.9	181.4	398.6	134.9	62.2	186.4	216.5
EXPONENT, n	NO. VALUES	13 (11)	16	11 (10)	13 (4)	37 (22)	25 (24)	115 (87)
	MAXIMUM	0.19	1.15	0.14	0.36	1.22	0.67	1.22
	MINIMUM	-0.01	-0.08	0.00	0.02	0.00	0.00	-0.08
	AVERAGE	0.03	0.12	0.02	0.19	0.20	0.17	0.14
FAILURE RATIO, R <sub>f</sub>	NO. VALUES	10 (8)	15	7 (6)	13 (4)	32 (17)	18 (17)	95 (67)
	MAXIMUM	0.72	0.80	0.92	0.68	0.84	0.96	0.96
	MINIMUM	0.18	0.23	0.43	0.18	0.25	0.33	0.18
	AVERAGE	0.40	0.52	0.74	0.49	0.57	0.64	0.56

Note: 1 KN/M<sup>2</sup> = 1/100 BAR; 1/100 ATMOSPHERE; 1/100 TON/FT<sup>2</sup>; 1/100 KG/CM<sup>2</sup>; 1/7 PSI

Numbers in parentheses indicate number of different rock types.

TABLE 3-11 SUMMARY OF TRIAXIAL STRESS-STRAIN PARAMETERS



These general relationships and trends may provide a useful context for interpreting the results of tests on other types of rocks and the average values of the parameters may be useful for generalized studies or for studies of a preliminary nature. For example, since the average  $n$  and  $R_f$  values are fairly consistent, one could approximate the nonlinear, stress-dependent behavior of a given rock type for preliminary purposes with these values and the uniaxial modulus since the modulus at one atmosphere is equal to  $Kp_a$ . However, in view of the wide variation in the values of the stress-strain parameters, it may be concluded that values of these parameters for use in accurate analyses should be determined by conducting the appropriate tests on suitably selected and prepared rock specimens.

#### Nonlinear Stress-Dependent Poisson's Ratio Relationship

In a manner consistent with the definition of tangent modulus discussed previously, the tangent Poisson's ratio may be defined as the rate of variation of radial strain with axial strain under axial compression or:

$$v_t = \frac{\partial \epsilon_r}{\partial \epsilon_a} \quad (3-9)$$

in which  $v_t$  is the tangent Poisson's ratio,  $\epsilon_r$  is the radial strain and  $\epsilon_a$  is the axial strain. Commonly it is found that the value of the tangent Poisson's ratio is nonlinear as well as stress-dependent. Recently Kulhawy et al (1969) proposed a simple, practical Poisson's ratio relationship for soils and demonstrated its applicability in soil mechanics problems. This relationship was also formulated from empirical nonlinear and stress-dependent relationships and only includes parameters readily obtainable from conventional laboratory shear tests with either radial or volumetric strain measurements. In the following sections, this relationship is reviewed and its applicability to rock is discussed.

#### a) Nonlinearity

Nonlinear relationships between axial and radial strains may be approximated by an empirical hyperbolic equation of the form:

$$\epsilon_a = \frac{\epsilon_r}{f + d\epsilon_r} \quad (3-10)$$

in which  $f$  and  $d$  are parameters whose values are determined empirically. If Equation 3-10 is rewritten as:

$$\frac{\epsilon_r}{\epsilon_a} = f + d\epsilon_r \quad (3-11)$$

it may be noted that the parameter  $f$  is the value of the ratio  $\epsilon_r/\epsilon_a$  at zero strain. Thus the parameter  $f$  is equal to the value of tangent Poisson's ratio at zero strain, which herein is called the initial tangent Poisson's ratio,  $\nu_i$ . The parameter  $d$  is the slope of the line represented by Equation 3-11.

A study of the behavior of a variety of rock types conducted during the course of this investigation has shown that the volume change characteristics of rocks may be represented to a reasonable degree of accuracy by the empirical relationship shown above. For example, data derived from tests on Cedar City Tonalite are shown in Figure 3-4. It should be noted that all of the curves for the different confining pressures are not presented in this figure because many were close to each other and overlapped. Nevertheless, it can be seen that the hyperbolic and experimental curves are in good agreement.

Although the empirical hyperbolic relationship may be used for any values of Poisson's ratio, conventional finite element analyses may presently only be performed for materials having values of Poisson's ratio less than one-half. Therefore, if the value of Poisson's ratio determined from the laboratory test results is greater than or equal to one-half, it is necessary to assign a value slightly less than one-half for purposes of analysis.

#### b) Stress-Dependency

As shown in Figure 3-4, the variations of radial strain with axial strain depend on the value of confining pressure as well as the value of strain. Kulhawy et al (1969) found that the value of  $\nu_i$  (initial tangent Poisson's ratio) tended to decrease with increasing confining pressure, with the value of  $\nu_i$  being approximately linear with logarithm of confining pressure as shown below:

$$\nu_i = G - F \log \left( \frac{\sigma_3}{p_a} \right) \quad (3-12)$$

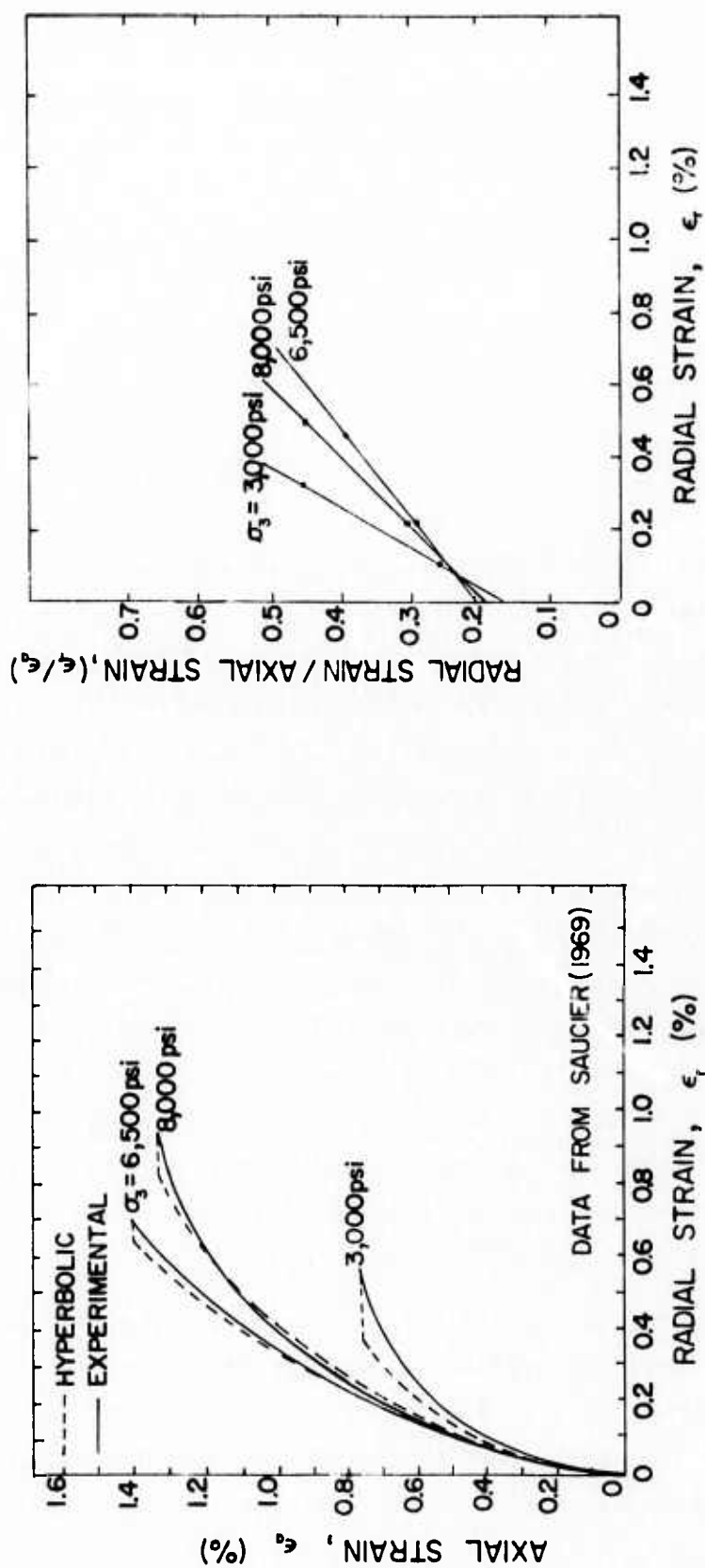


FIG.3-4 EXPERIMENTAL AND HYPERBOLIC AXIAL STRAIN-RADIAL STRAIN CURVES FOR CEDAR CITY TONALITE

in which  $G$  is the value of  $v_i$  at a confining pressure of one atmosphere,  $\sigma_3$  is the minimum principal stress or confining pressure,  $p_a$  is atmospheric pressure expressed in the same units as  $\sigma_3$ , and  $F$  is a parameter whose value is determined empirically and which represents the rate of change of  $v_i$  with increasing confining pressure. Figure 3-5 shows this variation for two types of rock, a sandstone and a basalt, from which it can be seen that these data can be represented to a reasonable degree of accuracy by a straight line.

c) Tangent Poisson's Ratio

The relationships expressing nonlinearity and stress-dependency may be used to define a value of tangent Poisson's ratio for any state of stress. According to Equation 3-9, which defines the tangent Poisson's ratio:

$$\frac{1}{v_t} = \frac{\partial \epsilon_a}{\partial \epsilon_r} \quad (3-13)$$

By performing the indicated differentiation on Equation 3-10, the tangent Poisson's ratio may be expressed as:

$$v_t = \frac{f}{(1 - d\epsilon_a)^2} \quad (3-14)$$

As shown previously, the parameter  $f$  is equal to  $v_i$ , the value of tangent Poisson's ratio at zero strain, which is related to confining pressure as shown by Equation 3-12. Substituting Equation 3-12 into Equation 3-14 results in the following expression:

$$v_t = \frac{G - F \log (\sigma_3/p_a)}{(1 - d\epsilon_a)^2} \quad (3-15)$$

The axial strain may be eliminated from Equation 3-15 by expressing this strain in terms of the stresses and stress-strain parameters, using Equation 3-1 as follows:

$$\epsilon_a = \frac{(\sigma_1 - \sigma_3)}{K p_a \left(\frac{\sigma_3}{p_a}\right)^n \left[ 1 - \frac{R_f (\sigma_1 - \sigma_3) (1 - \sin \phi)}{2c \cos \phi + 2\sigma_3 \sin \phi} \right]} \quad (3-16)$$



When this equation is substituted into Equation 3-15, the tangent Poisson's ratio may be expressed as:

$$v_t = \frac{G - F \log (\sigma_3/p_a)}{d(\sigma_1 - \sigma_3)} \left[ 1 - \frac{K p_a (\frac{\sigma_3}{p_a})^n \left\{ 1 - \frac{R_f (\sigma_1 - \sigma_3) (1 - \sin \phi)}{2c \cos \phi + 2\sigma_3 \sin \phi} \right\}}{d(\sigma_1 - \sigma_3)} \right]^2 \quad (3-17)$$

This expression contains eight parameters: The five modulus parameters  $K$ ,  $n$ ,  $c$ ,  $\phi$ , and  $R_f$ ; and three additional parameters  $G$ ,  $F$ , and  $d$ . The values of all of these parameters may be determined from the results of a series of triaxial or plane strain compression tests with volume change or radial strain measurements. Studies conducted to determine values of these parameters for various rock types are described in the following section.

#### Nonlinear Poisson's Ratio Parameters Under Triaxial Conditions

Very little data were available in the literature which could be employed to obtain the nonlinear and stress-dependent Poisson's ratio parameters discussed above. Table 3-12 shows these parameters for the eight rock types available. Since one of these rock types had data available for three test orientations, a total of 10 sets of parameters were obtained. Maximum, minimum and average values of these parameters are shown in Table 3-13. Analysis of these limited data shows that the variation in the values of  $d$  are relatively small, indicating that the rate of increase of Poisson's ratio with strain or stress level is similar for these rock types. The values of  $F$  range from -0.05 to 0.05 indicating that the initial tangent Poisson's ratio values may either decrease or increase 0.05 per log cycle of stress, a factor which may or may not be significant depending upon the magnitude of stress changes in a given field problem. However, six of the ten values showed that there is little, if any, change of Poisson's ratio with confining pressure. The largest and most significant variations occurred in the values of  $G$ , the initial tangent Poisson's ratio at one atmosphere. These values varied from 0.11 to 0.30, but it is interesting to note that the average of these values, 0.20, is the same average obtained for Poisson's ratio under uniaxial test conditions. Furthermore the data for the quartz monzonite indicates that, at least for this rock, anisotropy of the Poisson's ratio parameters is relatively insignificant.



ROCK NUMBER	DESCRIPTION	DENSITY (GM/CM <sup>3</sup> )	SPECIFIC GRAVITY	POROSITY (%)	POISSON'S RATIO PARAMETERS			RANGE OF CONFINING PRESSURE (KN/M <sup>2</sup> x 10 <sup>-3</sup> )	REFERENCE
					G	F	d		
IPT-4	AEC NEVADA SITE GRANITE (DENSE, COARSE-GRAINED, UNWEATHERED)	2.69	2.69	0.3	0.23	-0.01	115.	0-27.6	STOWE (1969)
IPT-5	QUARTZ MONZONITE (MEDIUM-GRAINED, PORPHYRITIC)	2.68	2.70	0.2	0.19	0	114.	0-20.7	DEKLOTZ & HECK (1965)
-5a		2.69	2.69	0.2	0.20	0.01	120.	0-20.7	
-5b		2.68	2.68	0.2	0.19	-0.01	128.	0-20.7	
-5c	(MUTUALLY PERPENDICULAR AXES)								
IPT-10	CEDAR CITY TONALITE (FRIABLE, MEDIUM TO FINE-GRAINED)	-	2.60	4.9	0.11	-0.05	62.	0-248.	SAUCIER (1969)
IVT-2	AEC NEVADA SITE BASALT	2.70	2.83	4.6	0.28	0.05	107.	0-34.5	STOWE (1969)
IVT-16	(DENSE, FINE-GRAINED, UNWEATHERED)	1.92	2.39	19.8	0.24	0.03	114.	0-10.3	STOWE (1969)
MFT-1	AEC NEVADA SITE TUFF (FAIRLY WELDED ASH, W=21.1%)								
	SCHISTOSE GNEISS	2.79	2.80	0.5	0.11	-0.04	194.	0-70.0	DEKLOTZ ET AL (1965)
	(FINE-GRAINED, GRANULAR)								
	( $\perp$ FOLIATION)								
SCT-7	BOISE SANDSTONE (WELL-CEMENTED)	1.90	-	27.0	0.13	-0.01	-	1.4-34.4	KING (1968)
SCHT-12	AEC NEVADA SITE LIMESTONE (DENSE, FINE-GRAINED, STYLOLITE SEAMS)	2.70	2.72	0.5	0.30	-0.01	77.	0-27.6	STOWE (1969)

Note: 1 KN/M<sup>2</sup> = 1/100 BAR; 1/100 ATMOSPHERE; 1/100 TON/FT<sup>2</sup>; 1/100 KG/CM<sup>2</sup>; 1/7 PSI

TABLE 3-12 TRIAXIAL POISSON'S RATIO PARAMETERS FOR VARIOUS ROCK TYPES

PARAMETER	NUMBER OF VALUES	MAXIMUM	MINIMUM	AVERAGE
G	10	0.30	0.11	0.20
F	10	0.05	-0.05	0.00
d	9	194.	62.	115.

TABLE 3-13 SUMMARY OF NONLINEAR TRIAXIAL  
POISSON'S RATIO PARAMETERS

## CHAPTER 4

### ANALYSIS OF OPENINGS IN HOMOGENEOUS ROCK MASSES

Some types of rock masses may be treated as homogeneous continua from the standpoint of analyzing the response of the mass caused by making an underground opening. The rock masses commonly in this category are those composed of massive, competent units in which prominent discontinuities are infrequent and do not intersect the opening or pass near it, and, on occasion, those masses which are intensely fractured to the extent that they may be statistically homogeneous. The response of rock masses falling into these categories may be adequately evaluated in many cases by using any of a number of closed form mathematical solutions covered in many textbooks. (For example, see Obert and Duvall, 1967). Virtually all of these solutions are based upon linear elasticity and, because of mathematical complexities, are for smooth opening shapes in which there are no corners and for initial stresses which are constant with depth. Because of these limitations, other opening shapes or in-situ conditions must be analyzed by methods such as photo-elastic experimental methods or finite element numerical methods.

Therefore, the studies presented in this chapter were conducted to evaluate the behavior of underground openings in homogeneous rock masses for conditions generally unavailable in closed form, to identify the significance of the key parameters controlling the behavior of an opening, and to provide a reference base for later comparison of the behavior of openings in homogeneous rock with those in rock containing a single planar discontinuity.

#### Finite Element Idealization

The finite element meshes employed in the studies conducted for this chapter are shown in Figures 4-1 and 4-2 and in Figures 2-14 through 2-16 shown previously. All of these meshes satisfy the criteria for mesh design discussed in Chapter 2. Quarter, half and full meshes were used for the circular opening analyses depending upon the symmetry of the cases analyzed. Somewhat more detailed results were subsequently obtained for the quarter mesh analyses than the half mesh analyses which in turn were more detailed than the full mesh analyses.

Excavations were mainly simulated in one step in these analyses although two forms of three step excavation, as shown in Figure 4-3, were simulated as well. Slight variations from straight lines were made in the three step excavation meshes to facilitate mesh design. Unless otherwise noted, the results to be discussed subsequently in this chapter are based upon one step excavation.

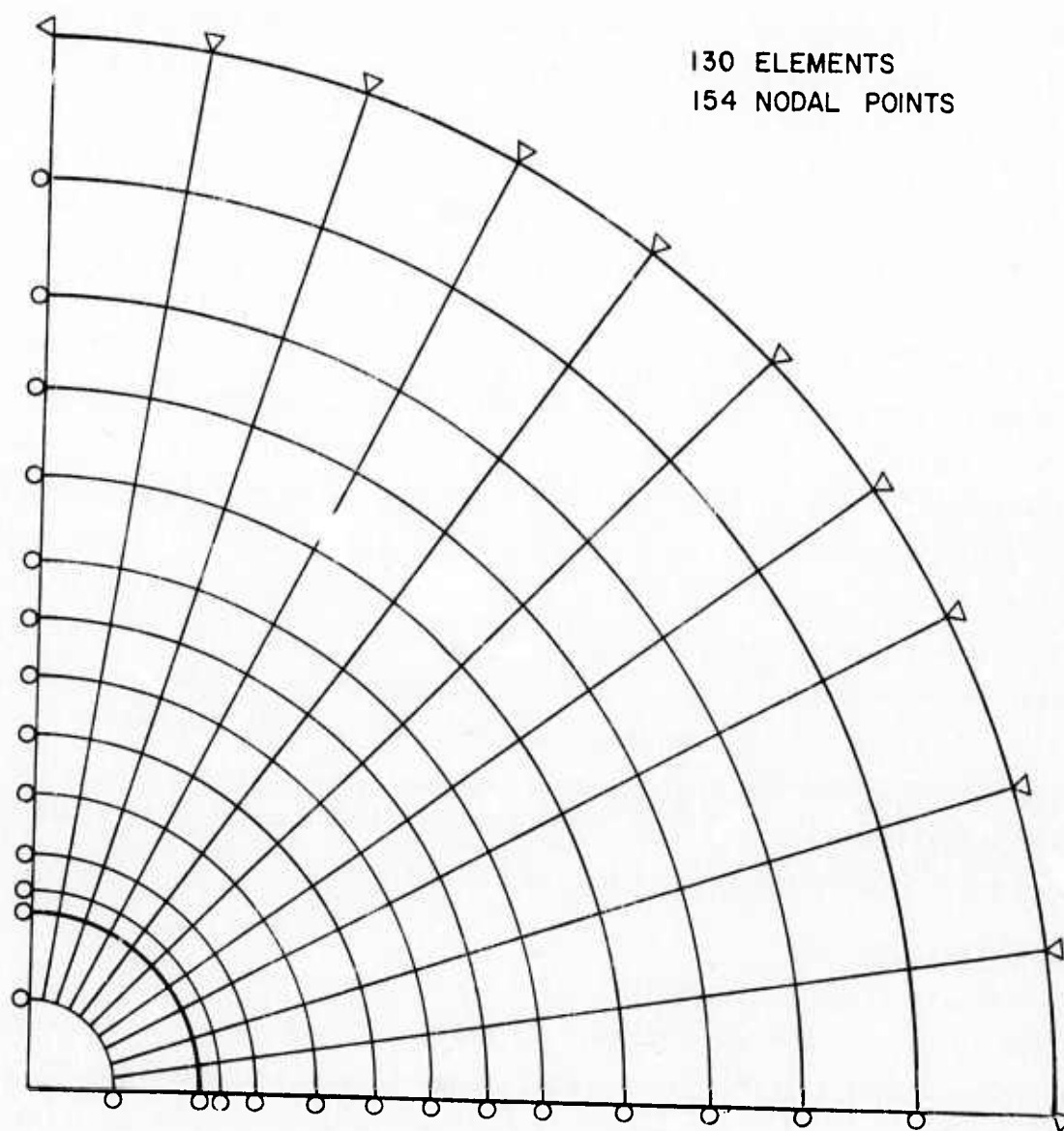


**FIG. 4-1 FINITE ELEMENT MESH FOR  
CIRCULAR OPENING IN  
HOMOGENEOUS ROCK - QUARTER MESH**

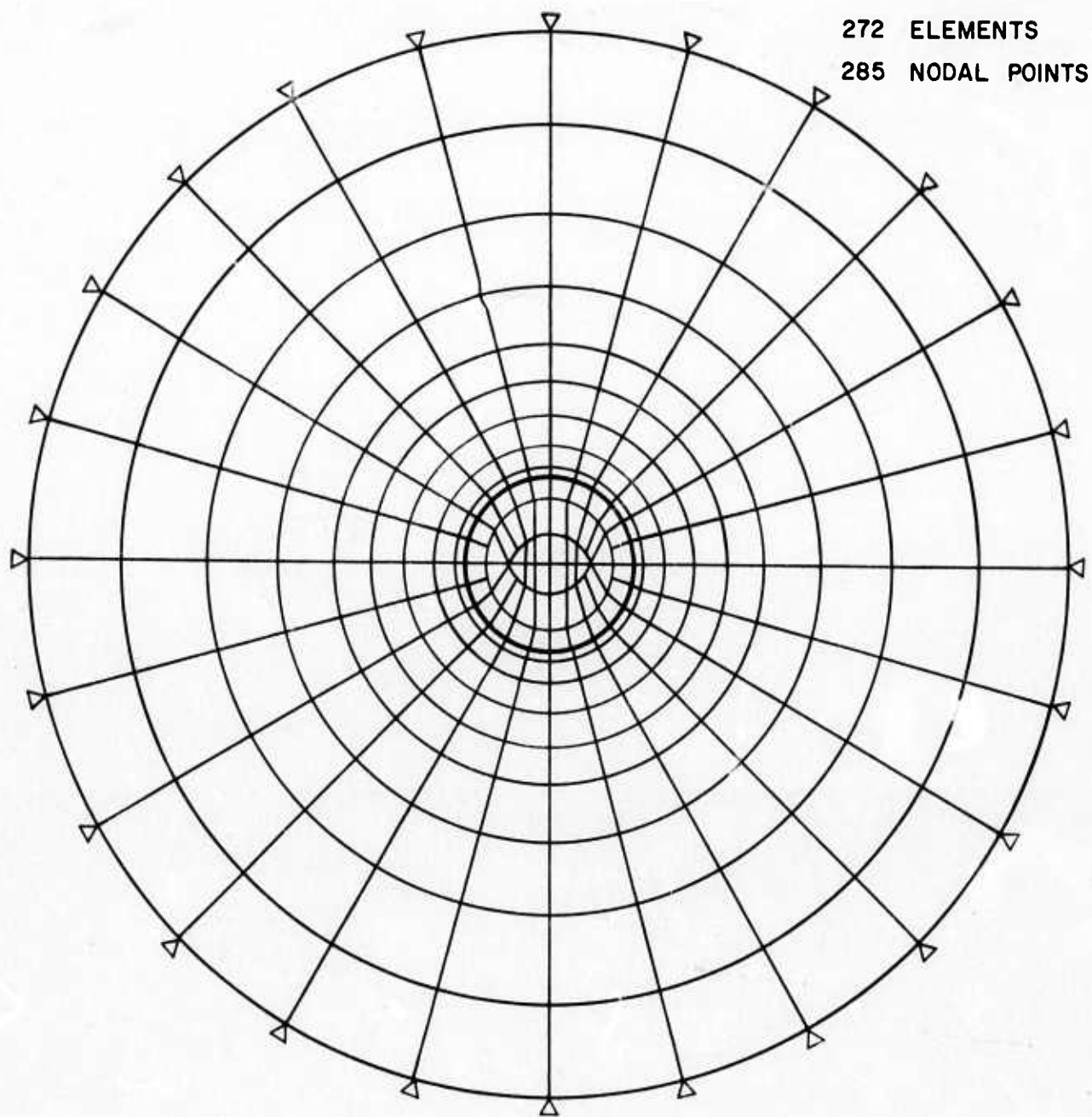
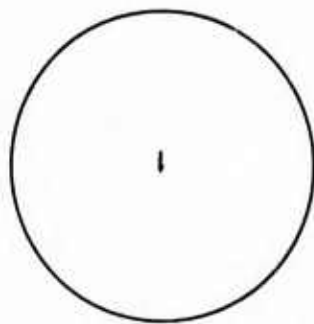
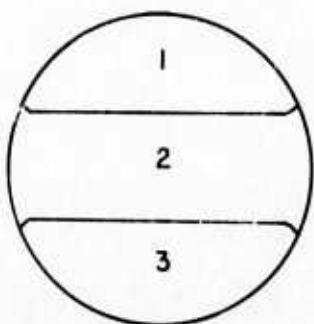


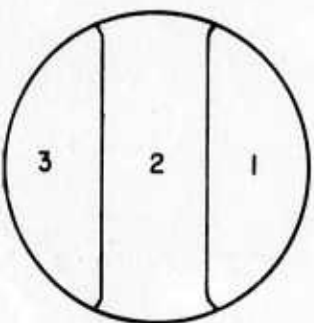
**FIG. 4-2 FINITE ELEMENT MESH FOR CIRCULAR OPENING  
IN HOMOGENEOUS ROCK - FULL MESH**



1 STEP  
EXCAVATION



3 STEP  
HORIZONTAL  
EXCAVATION



3 STEP  
VERTICAL  
EXCAVATION

**FIG. 4-3 EXCAVATION SEQUENCES EMPLOYED  
FOR ANALYSES OF CIRCULAR OPENING**



### Linear Material Properties

The theoretical solutions show that the stresses occurring around an opening are independent of Poisson's ratio, but in the finite element method, the stresses are dependent upon Poisson's ratio. To evaluate the magnitude of these effects, analyses were conducted with constant initial stresses and with Poisson's ratio varying from 0.10 to 0.40, the typical bounding values found in Chapter 3. No analyses were conducted to evaluate modulus effects because the displacements are inversely proportional to the modulus.

The stresses computed for these two bounding cases are shown in Figures 4-4 and 4-5, plotted on a dimensionless basis with respect to the initial maximum principal stress ( $\sigma_{1i}$ ). In these and subsequent figures,  $K^*$  represents the initial principal stress ratio,  $\frac{\sigma_{3i}}{\sigma_{1i}}$ , and  $\theta$  represents the orientation of the initial minimum principal stress,  $\sigma_3$ , measured counterclockwise from horizontal. Figure 4-4 shows that the maximum principal stresses which result are little affected by variations in Poisson's ratio. Around the opening, the stresses are virtually unaffected; at some depth beyond the opening the values with  $\nu = 0.1$  are 5% to 10% higher than those with  $\nu = 0.4$ . Figure 4-5 shows that the minimum principal stresses are consistently lower when a higher value of Poisson's ratio is used. These results occur because the changes in minimum principal stress caused by excavation are greater with a higher value of Poisson's ratio, resulting in lower final stress values. Although there are differences, it should be noted that in all cases the differences are relatively small, particularly around the opening.

The displacements of the opening face are shown in Figure 4-6 for these two cases along with those from an intermediate value of Poisson's ratio equal to 0.25. These values have been made dimensionless with respect to the modulus (E), opening radius (R), and initial maximum principal stress ( $\sigma_{1i}$ ) for ease in comparison. This figure shows that the largest crown and invert movements occur with the smallest value of Poisson's ratio, but that the differences in the three cases analyzed are quite small. Springline movements differ more and range from movement toward the opening center with a high value of Poisson's ratio to movement away from the opening center with a low value of Poisson's ratio. This form of movement occurs because there is more horizontal stress release from excavation for higher values of Poisson's ratio and subsequently the springline movements will be greater while the crown and invert movements will be less.

\* - K values representing the stress ratio are always  $\leq 1$ .

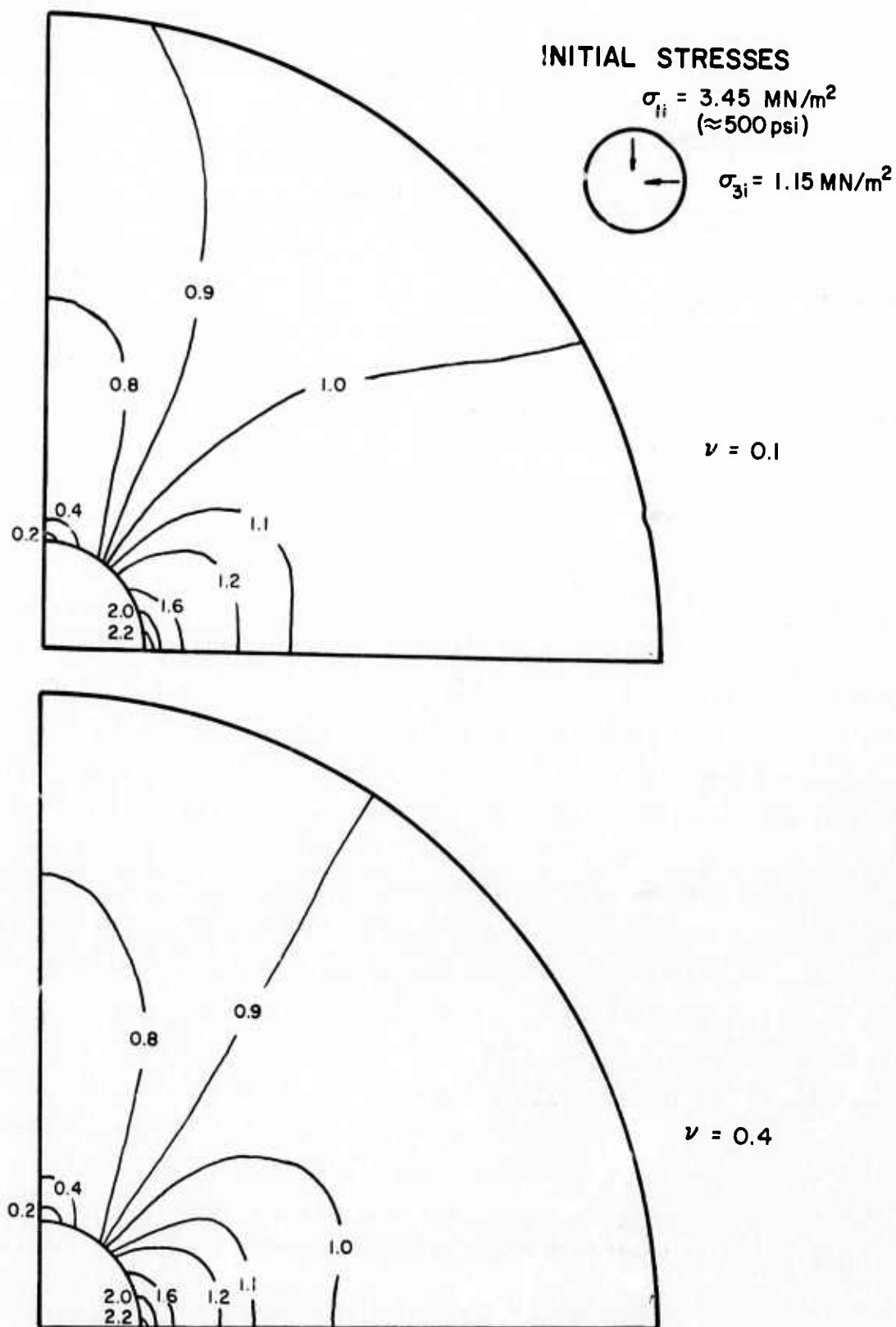


**FIG. 4-4 CONTOURS OF  $\sigma_1/\sigma_{1i}$  FOR CIRCULAR OPENING IN HOMOGENEOUS LINEAR ROCK,  $K=1/3$ ,  $\theta=0^\circ$  (VARIABLE POISSON'S RATIO)**

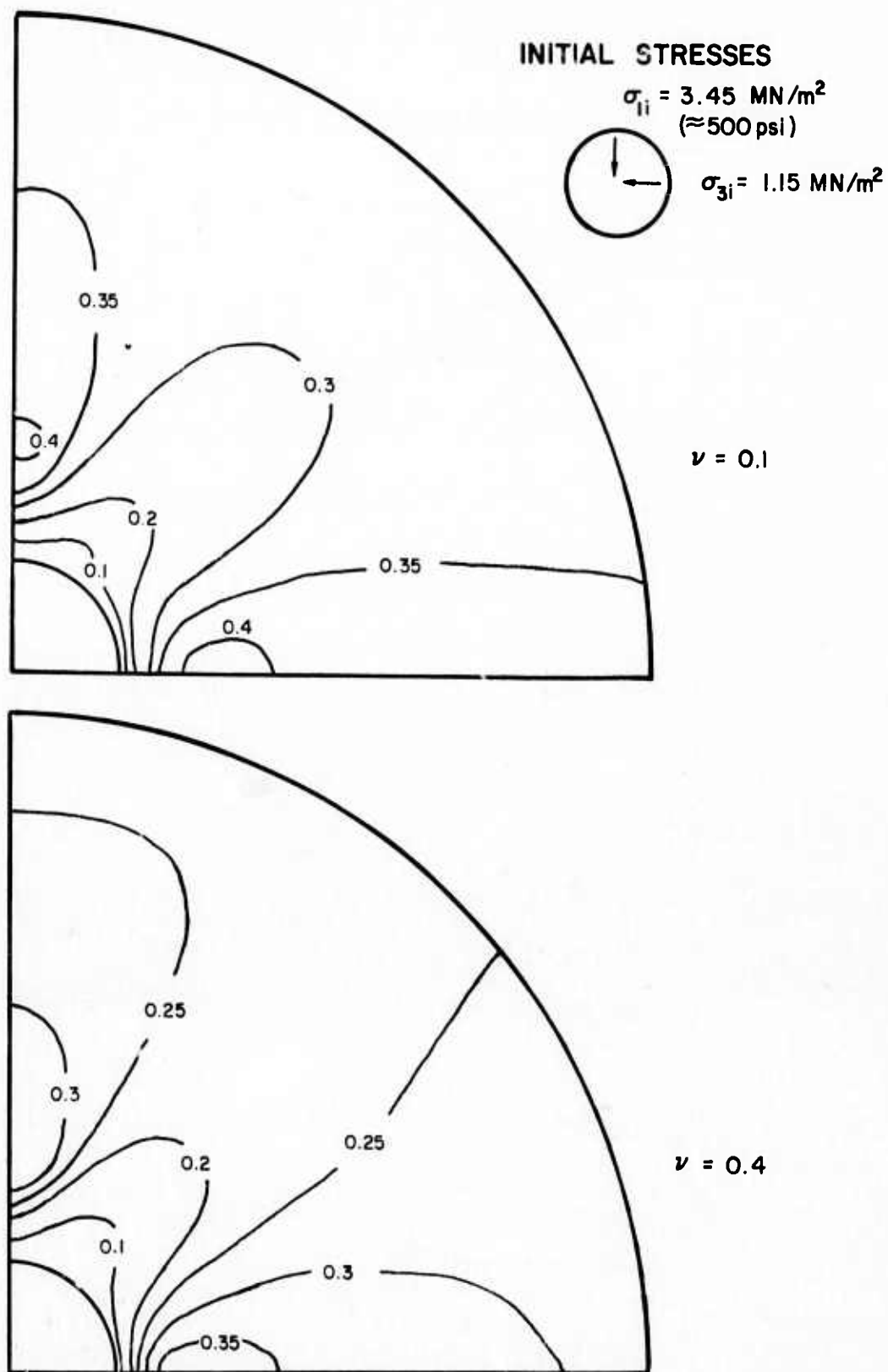


**FIG. 4-5 CONTOURS OF  $\sigma_3/\sigma_{ii}$  FOR CIRCULAR OPENING IN HOMOGENEOUS LINEAR ROCK,  $K=1/3$ ,  $\theta=0^\circ$  (VARIABLE POISSON'S RATIO)**

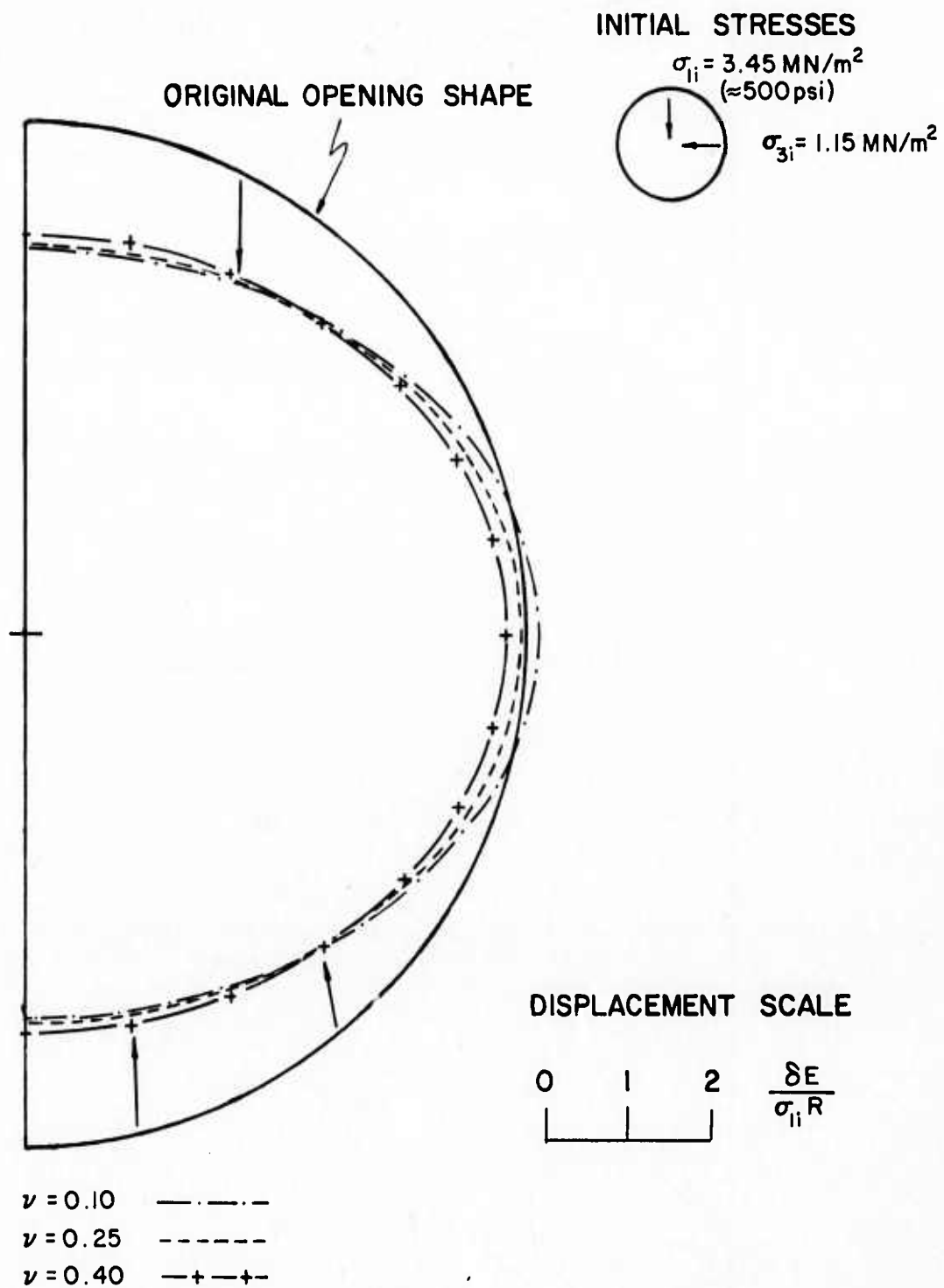


**FIG. 4-6 DISPLACEMENTS OF CIRCULAR OPENING  
IN HOMOGENEOUS LINEAR ROCK,  $K=1/3$ ,  $\theta=0^\circ$   
(VARIABLE POISSON'S RATIO)**

The results of these cases indicate that, although the Poisson effects are relatively small, any analyses should be conducted with representative values of Poisson's ratio; these values may be estimated from those presented in Chapter 3. For purposes of subsequent analyses, the intermediate value of  $\nu = 0.25$  was selected, but it should be remembered that the results are not independent of variations in Poisson's ratio.

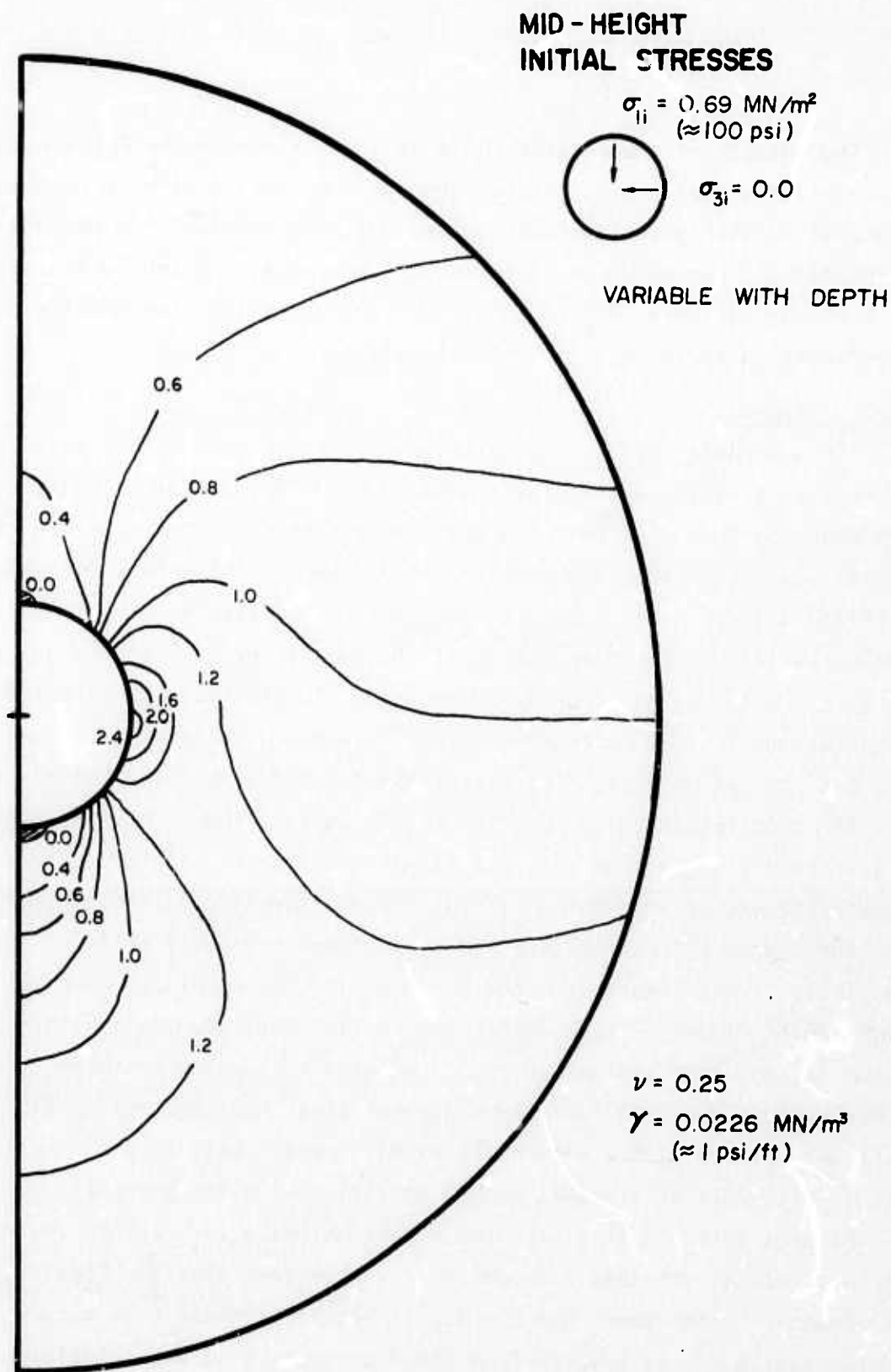
### Gravity Stresses

The available theoretical solutions are based upon a rock mass in which the initial stresses are constant with depth. This stress state is compatible with deep openings, but not with shallow openings. To evaluate the depth effect, several analyses were conducted simulating the initial stress conditions in the center of the opening for depths ranging from 100 feet to 1000 feet. Gravity loading vertically was taken to be at the equivalent rate of one psi per foot of depth and Poisson's ratio of 0.25 was used. To minimize the parameters to be compared, the initial minimum principal stresses were set equal to zero so that only the initial maximum principal stresses would vary significantly with depth.

The computed dimensionless  $\sigma_1/\sigma_{1i}$  values are shown in Figures 4-7 through 4-10. These figures show that the stresses along the opening boundary are little affected by variations in the initial gravity stress conditions. But at more than about one radius, the stress distribution is greatly affected with substantially higher stresses in the region below the opening. Comparing these figures with Figure 4-11, in which the initial stresses are constant with depth, it can be seen that the values of  $\sigma_1$  for gravity loading are very similar and differ by less than 10% for depths greater than about 500 feet. At depths shallower than this, the values differ by progressively larger amounts, indicating that gravity initial stresses should be included in the analysis.

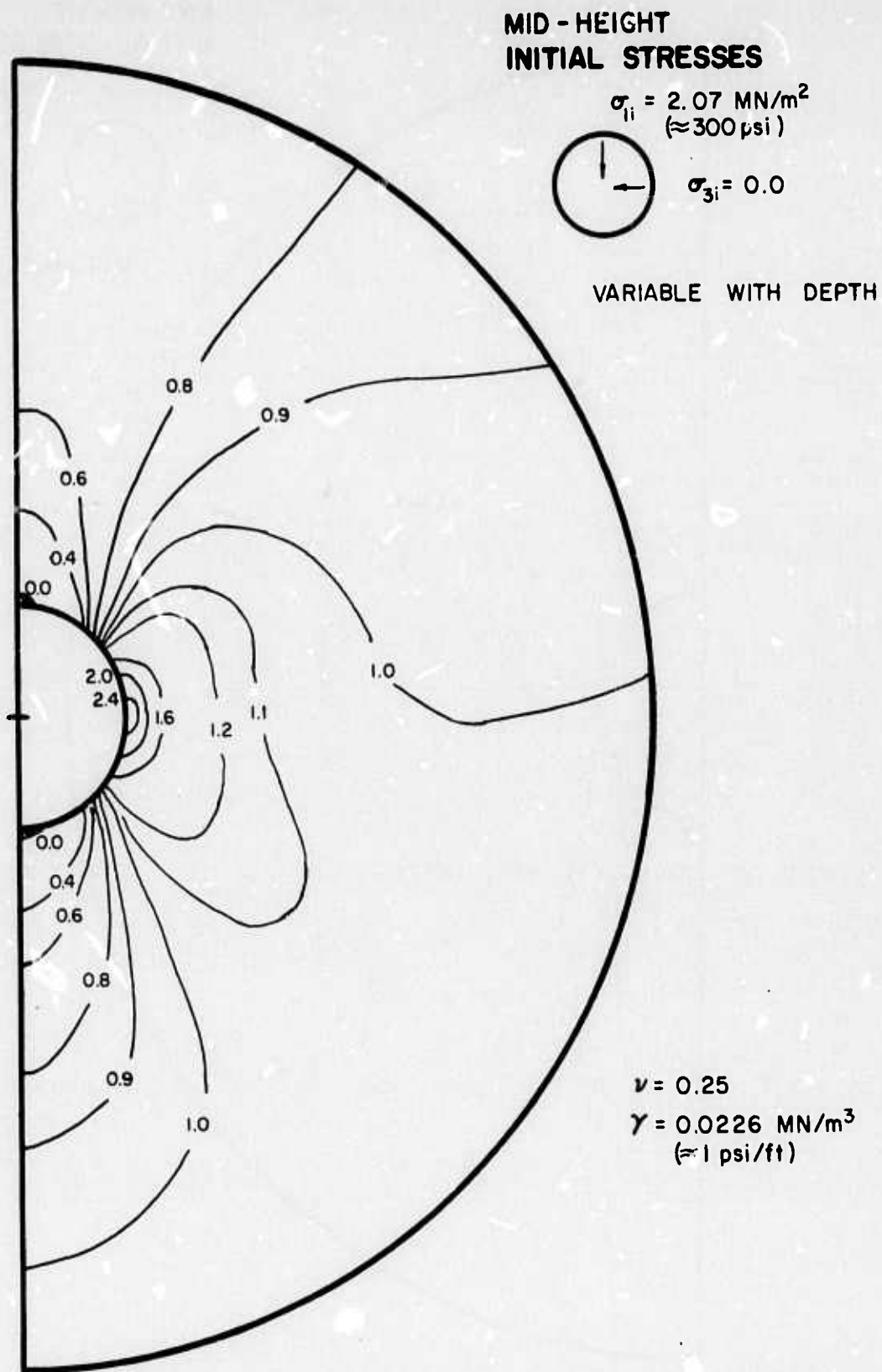
Figures 4-12 and 4-13 show the dimensionless  $\sigma_3/\sigma_{1i}$  values for gravity and constant initial stresses from which it can be seen that the final  $\sigma_3/\sigma_{1i}$  values are essentially the same when  $K = 0$ . It should be noted that Figure 4-12 is representative of the results from the four gravity stress solutions.

Figure 4-14 shows the dimensionless displacements for the gravity and constant initial stress solutions and it can be seen that the displacements are essentially the same at depths greater than about 500 feet.



**FIG. 4 - 7    CONTOURS OF  $\sigma_1 / \sigma_{1i}$  FOR CIRCULAR OPENING  
IN HOMOGENEOUS LINEAR ROCK ,  $K=0$  ,  $\theta=0^\circ$   
(GRAVITY STRESSES , 100 FOOT DEEP)**





**FIG. 4-8    CONTOURS OF  $\sigma_1 / \sigma_{1i}$  FOR CIRCULAR OPENING  
IN HOMOGENEOUS LINEAR ROCK ,  $K=0$  ,  $\theta=0^\circ$   
(GRAVITY STRESSES, 300 FOOT DEEP)**

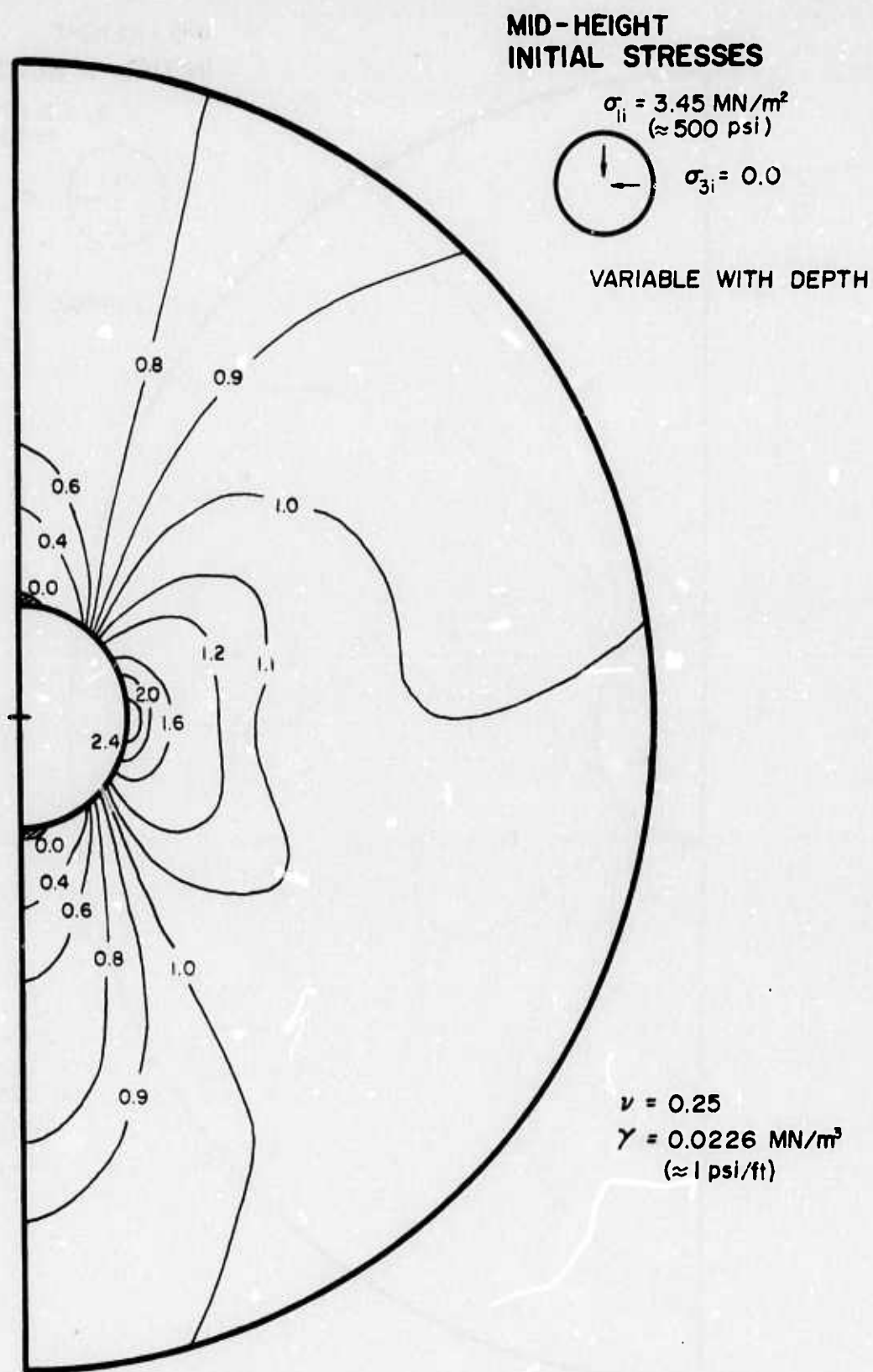


**FIG. 4-9    CONTOURS OF  $\sigma_1/\sigma_{1i}$  FOR CIRCULAR OPENING  
IN HOMOGENEOUS LINEAR ROCK,  $K=0$ ,  $\theta=0^\circ$   
(GRAVITY STRESSES, 500 FOOT DEEP)**

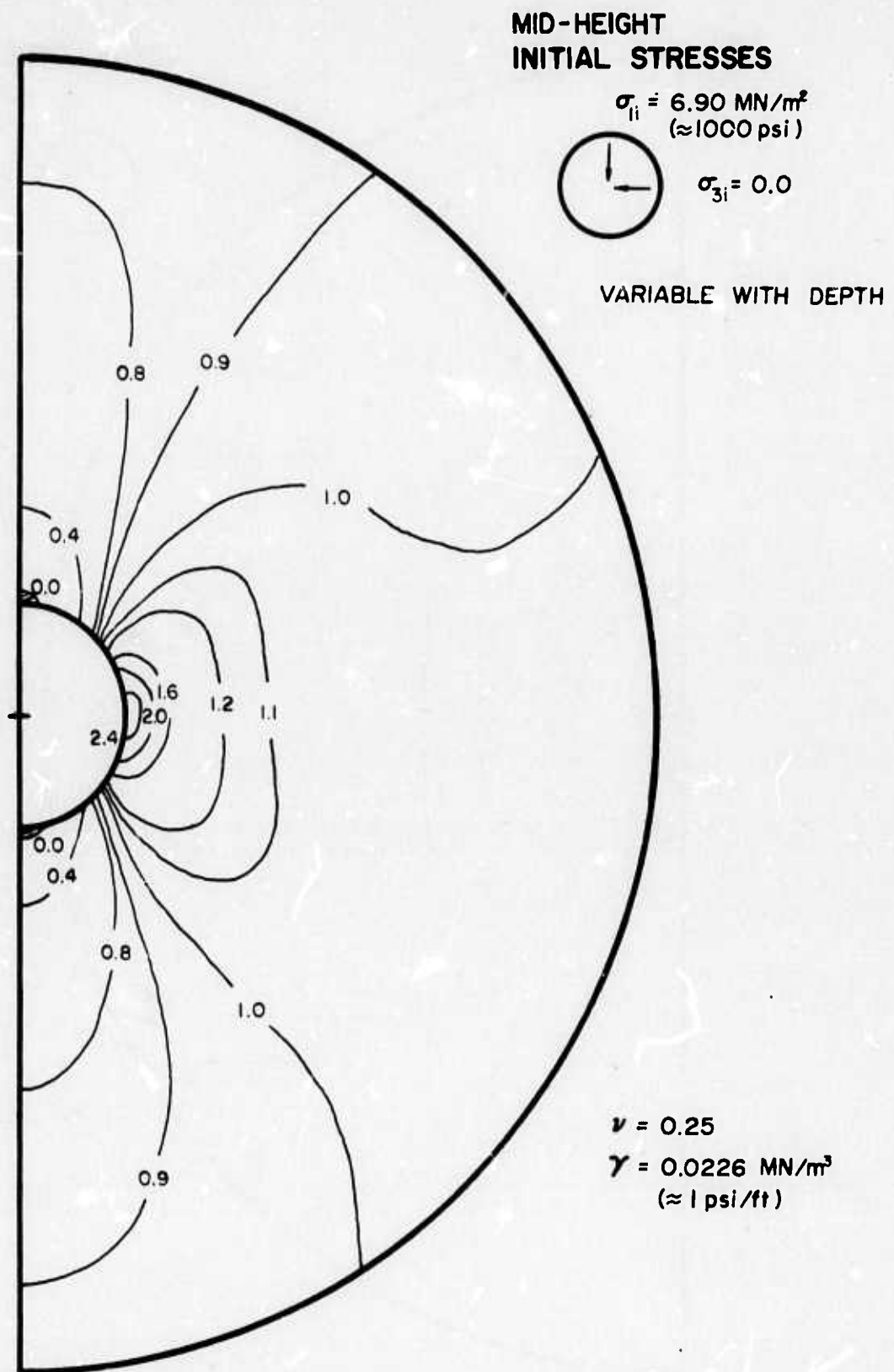


**FIG. 4-10 CONTOURS OF  $\sigma_1/\sigma_{1i}$  FOR CIRCULAR OPENING  
IN HOMOGENEOUS LINEAR ROCK,  $K=0$ ,  $\theta=0^\circ$   
(GRAVITY STRESSES, 1000 FOOT DEEP)**

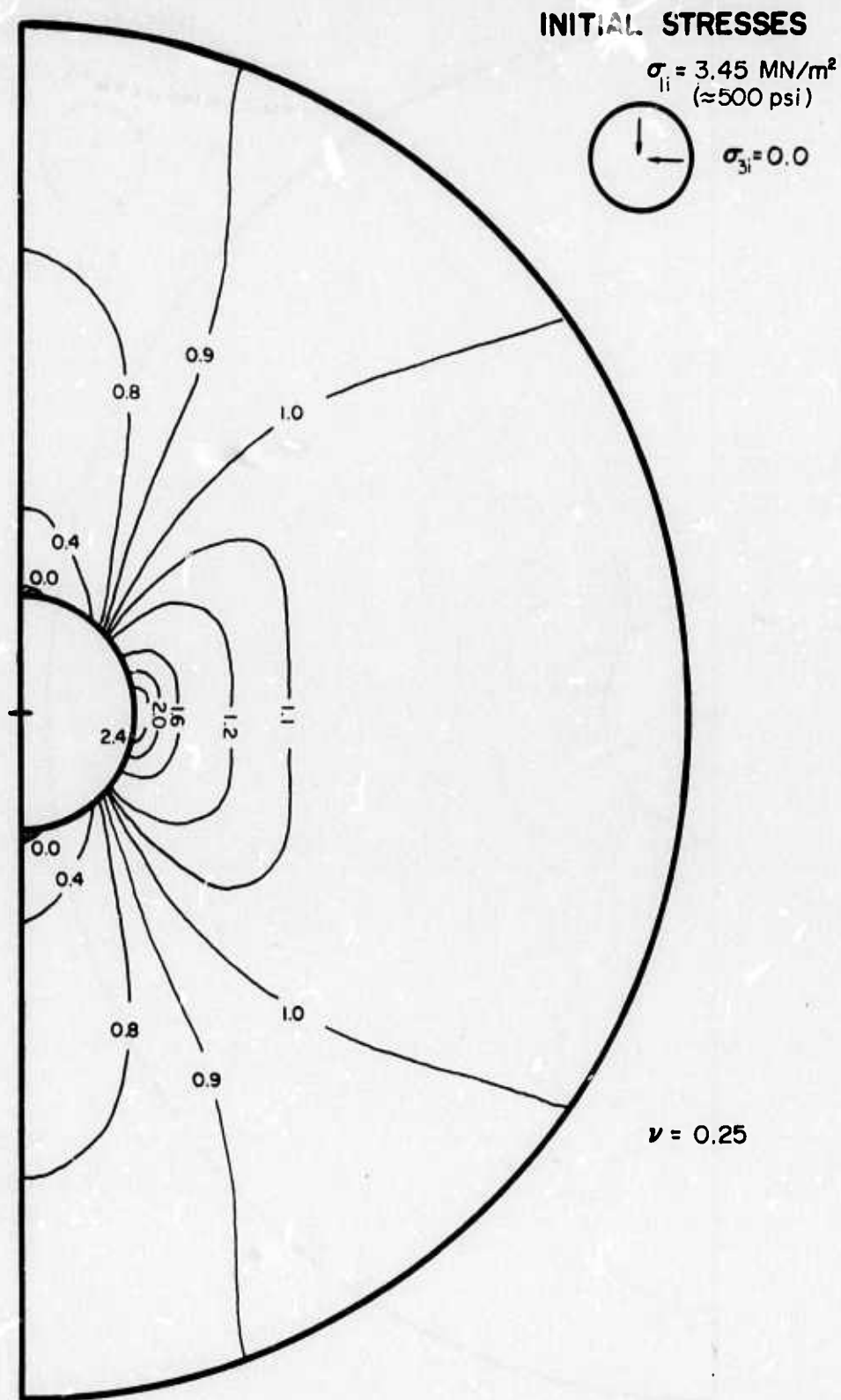


**FIG. 4-II    CONTOURS OF  $\sigma_1/\sigma_{li}$  FOR CIRCULAR OPENING  
IN HOMOGENEOUS LINEAR ROCK,  $K=0$ ,  $\theta=0^\circ$**

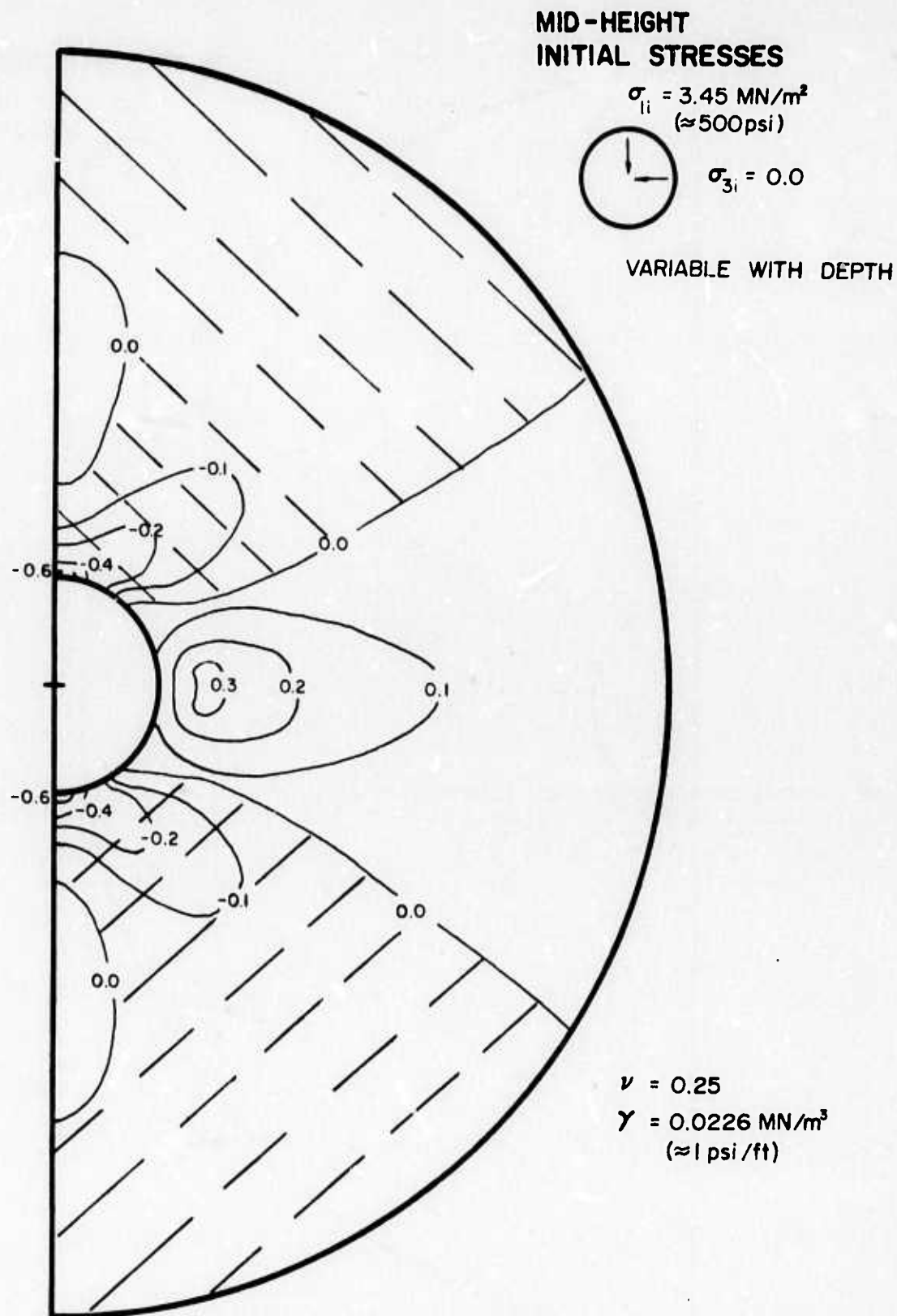


**FIG. 4-12    CONTOURS OF  $\sigma_3/\sigma_{li}$  FOR CIRCULAR OPENING  
IN HOMOGENEOUS LINEAR ROCK,  $K=0$ ,  $\theta=0^\circ$   
(GRAVITY STRESSES, 500 FOOT DEEP)**



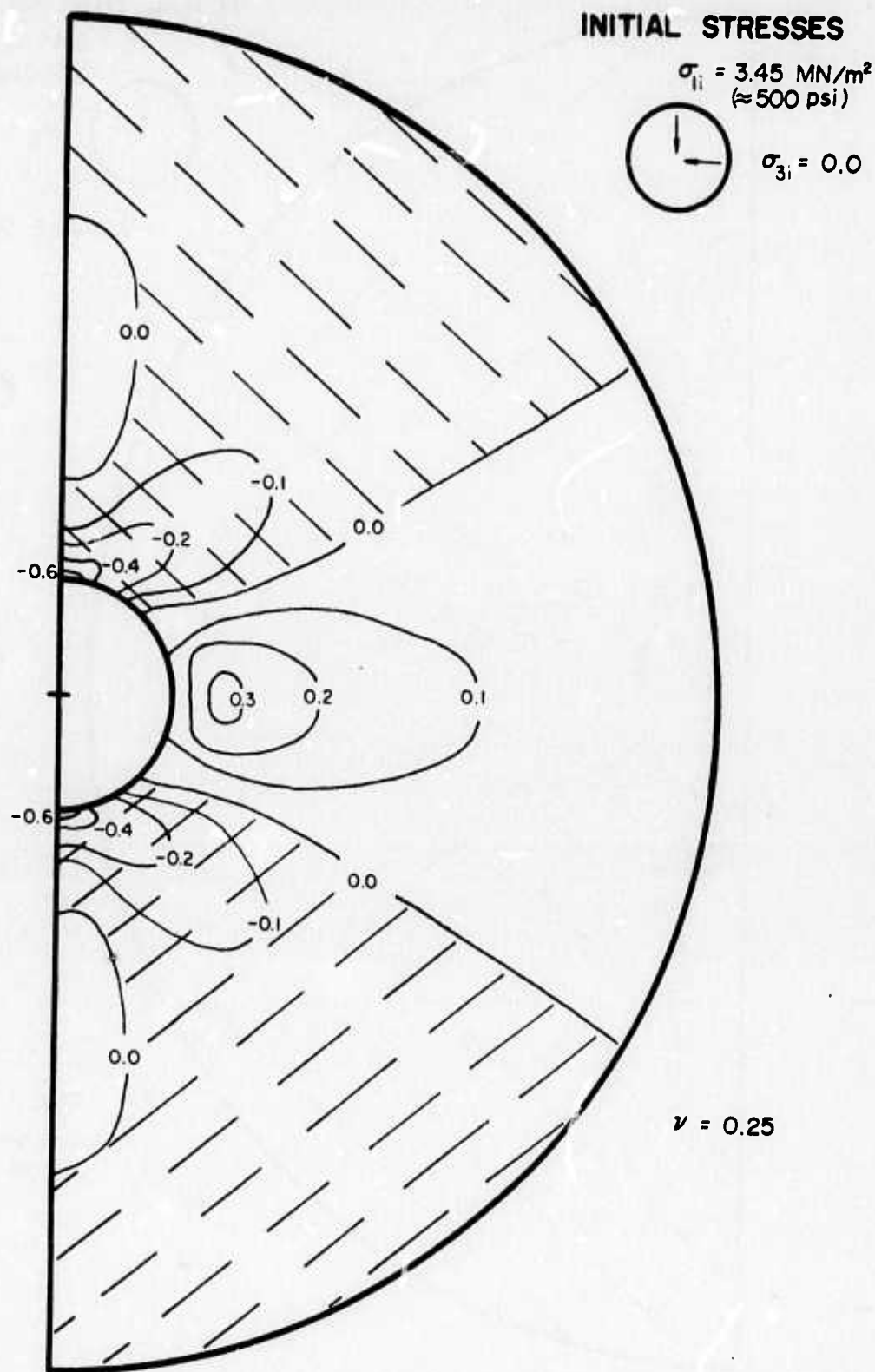
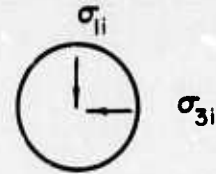


**FIG. 4-13**    **CONTOURS OF  $\sigma_3/\sigma_{1i}$  FOR CIRCULAR OPENING**  
**IN HOMOGENEOUS LINEAR ROCK,  $K=0$  ,  $\theta=0^\circ$**



MID-HEIGHT  
INITIAL STRESSES

ORIGINAL OPENING SHAPE

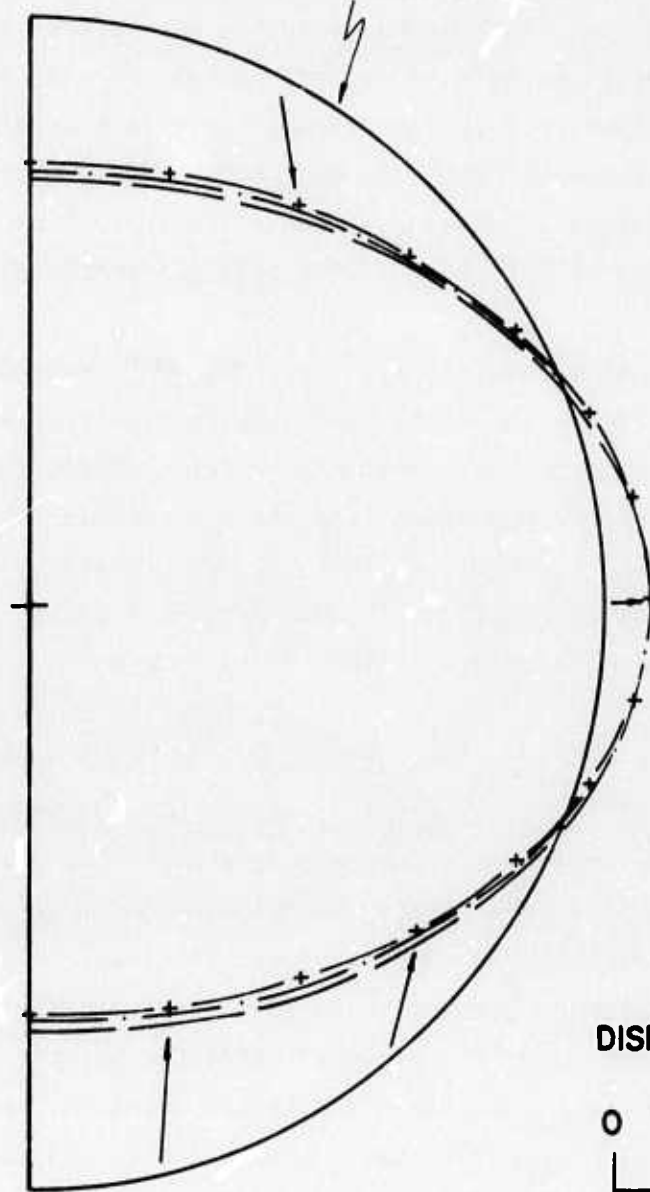


VARIES WITH DEPTH  
FOR CASES 2-5

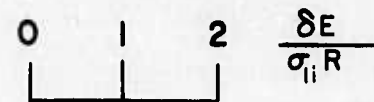
$$\gamma = 0.0226 \text{ MN/m}^3$$

$$(\approx 1 \text{ psi/ft})$$

$$\nu = 0.25$$



DISPLACEMENT SCALE



CASE	1	2	3	4	5
SYMBOL	— — — — —	- + - + -	- · - · -	APPROX. EQUAL TO 1	
DEPTH (FEET)	ALL	100	300	500	1000
$\sigma_{1i}$ (MN/m <sup>2</sup> )	ALL	0.69	2.07	3.45	6.90
$\sigma_{3i}$ (MN/m <sup>2</sup> )	0.0	0.0	0.0	0.0	0.0

**FIG. 4-14 DISPLACEMENTS OF CIRCULAR OPENING  
IN HOMOGENEOUS LINEAR ROCK,  $K=0$ ,  $\theta=0^\circ$   
(GRAVITY AND CONSTANT INITIAL STRESSES)**

### Varying Initial Stresses and Orientations

The magnitudes and orientations of the in-situ stresses found in rock masses vary over a wide range. In columnar basalts, the lateral stresses may approach zero while in major tectonic belts the lateral stresses may be two or more times the vertical stresses. To investigate the effect of these variable initial stress conditions, several analyses were conducted in which the ratio of horizontal to vertical initial stress varied from zero to two; the vertical stresses were held constant at  $3.45 \text{ MN/m}^2$  ( $\approx 500 \text{ psi}$ ) and a Poisson's ratio of 0.25 was used.

Figures 4-15 through 4-18 show the results of these solutions. Since the initial stresses are constant with depth, two symmetry planes develop and subsequently it is only necessary to show a quarter circle representation of the stresses. These figures show that, except for the isotropic case, the dimensionless  $\sigma_1$  contours are similar in form, but that the maximum stress concentration occurs in the same plane as the initial minimum principal stress,  $\sigma_{3i}$ . These figures also show that slightly greater stress concentrations occur with lower K values.

The variations in the dimensionless  $\sigma_3$  contours are much more pronounced. The resulting values range from large tension values to relatively high compression values, with the largest compression values occurring for the highest K values. It can be seen that tension only occurs when the K value is less than  $1/3$ , a value less than that which is normally found in-situ.

The dimensionless displacements for these four cases are shown on Figure 4-19 which shows that face movements are greatly affected by the initial stress values. The inward movements of the crown and invert increase proportionately as the ratio of horizontal to vertical stresses decreases. Wall movements vary in an inverse manner, with the greatest inward movement occurring when the horizontal stresses are greatest. Essentially no wall movement occurs when  $\sigma_H/\sigma_V = 1/3$  and outward movement occurs when  $\sigma_H/\sigma_V$  is less than  $1/3$ .

When the initial stresses are oriented at angles other than horizontal or vertical, the solutions just presented can be used by rotating the axes to correspond to the orientation of the oblique initial stresses. However, this procedure is only applicable when homogeneous, linear, elastic, isotropic materials are considered and when the initial stresses are constant with depth. For other conditions an appropriate analysis must be conducted. It should be

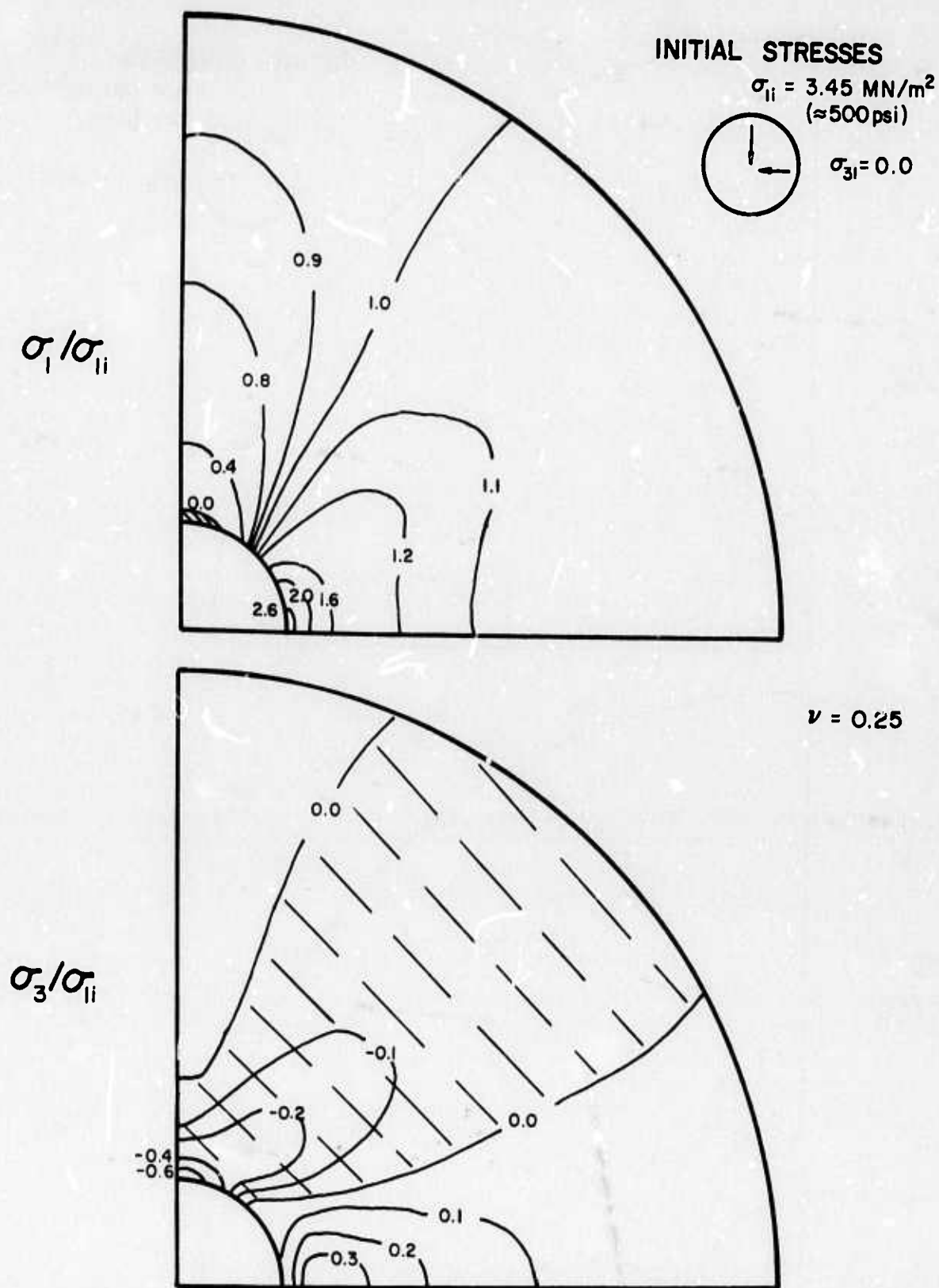


**FIG. 4-15 STRESS CONTOURS FOR CIRCULAR OPENING  
 IN HOMOGENEOUS LINEAR ROCK,  $K=0$ ,  $\theta=0^\circ$**

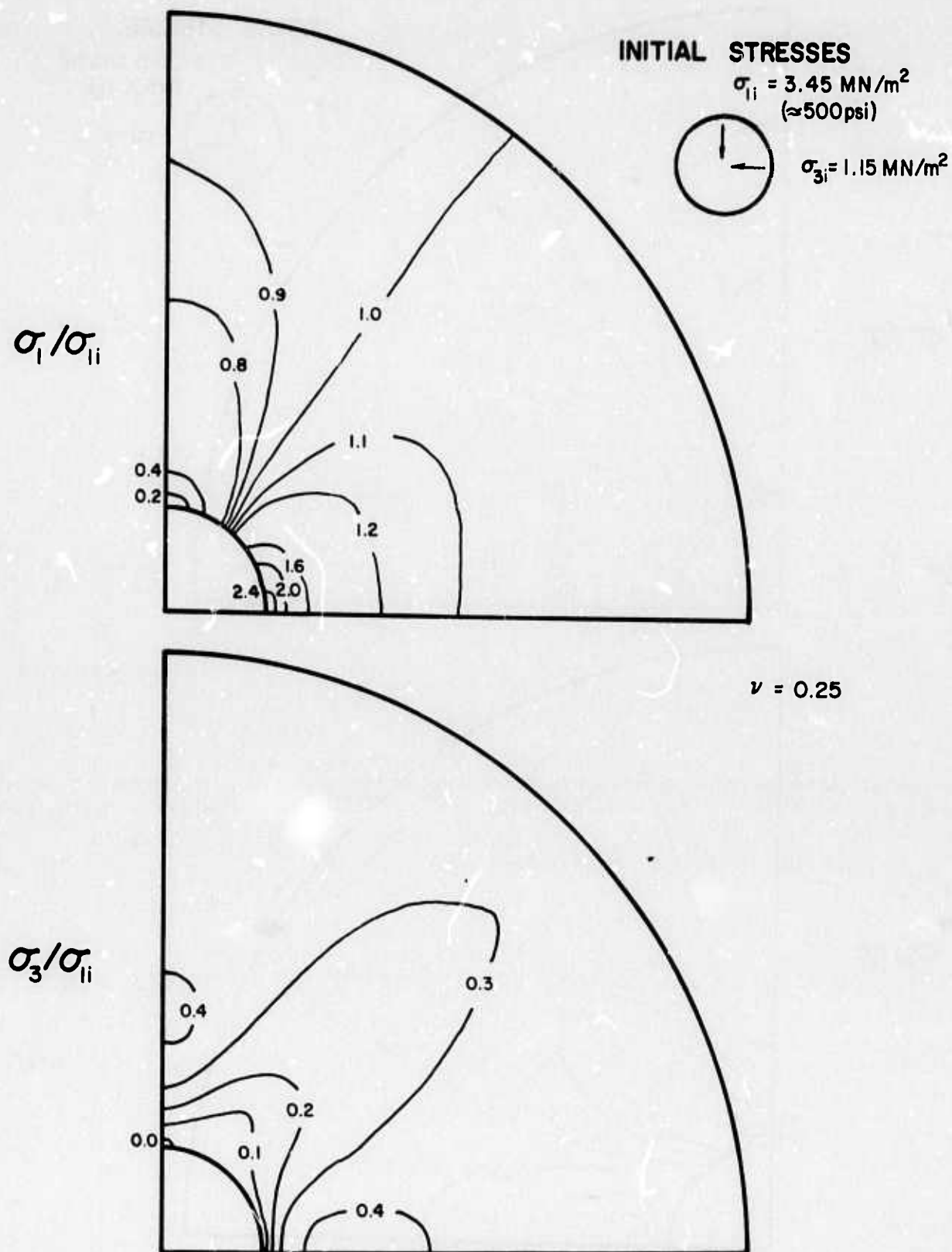


**FIG. 4-16 STRESS CONTOURS FOR CIRCULAR OPENING  
 IN HOMOGENEOUS LINEAR ROCK,  $K=1/3$ ,  $\theta=0^\circ$**

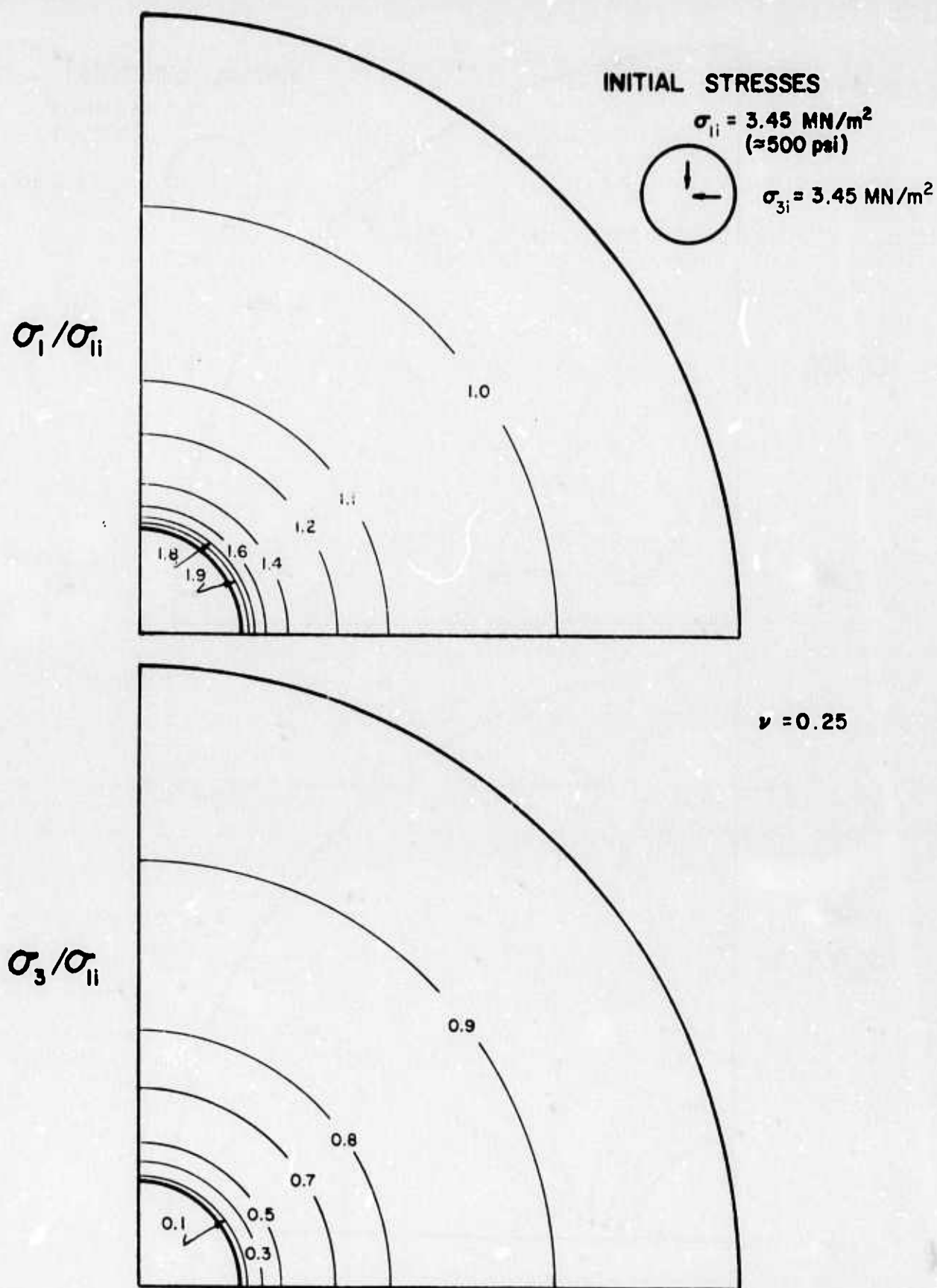


**FIG. 4-17 STRESS CONTOURS FOR CIRCULAR OPENING  
 IN HOMOGENEOUS LINEAR ROCK,  $K=1$ ,  $\theta=0^\circ$**



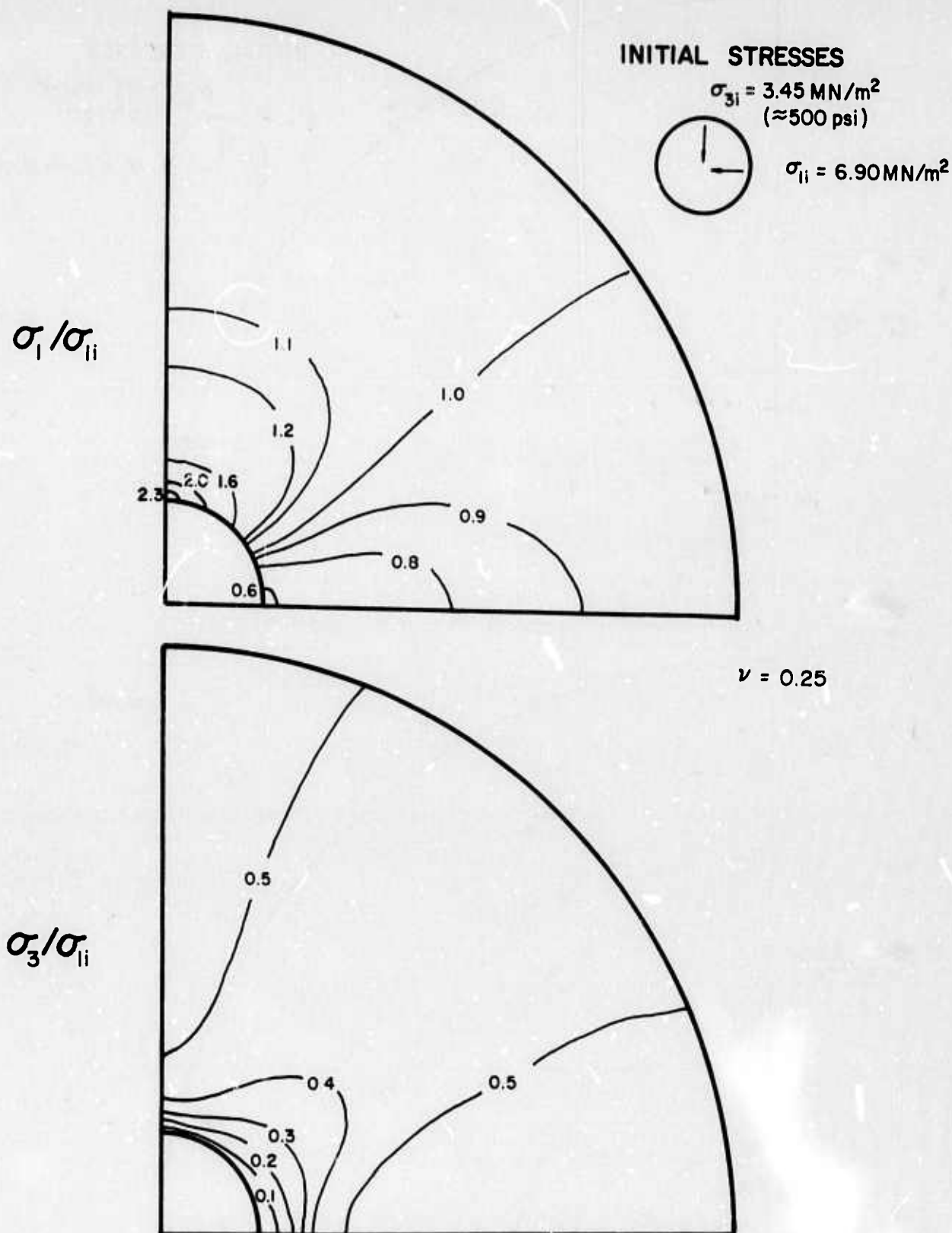


**FIG. 4-18 STRESS CONTOURS FOR CIRCULAR OPENING IN HOMOGENEOUS LINEAR ROCK,  $K=1/2$ ,  $\theta=90^\circ$**



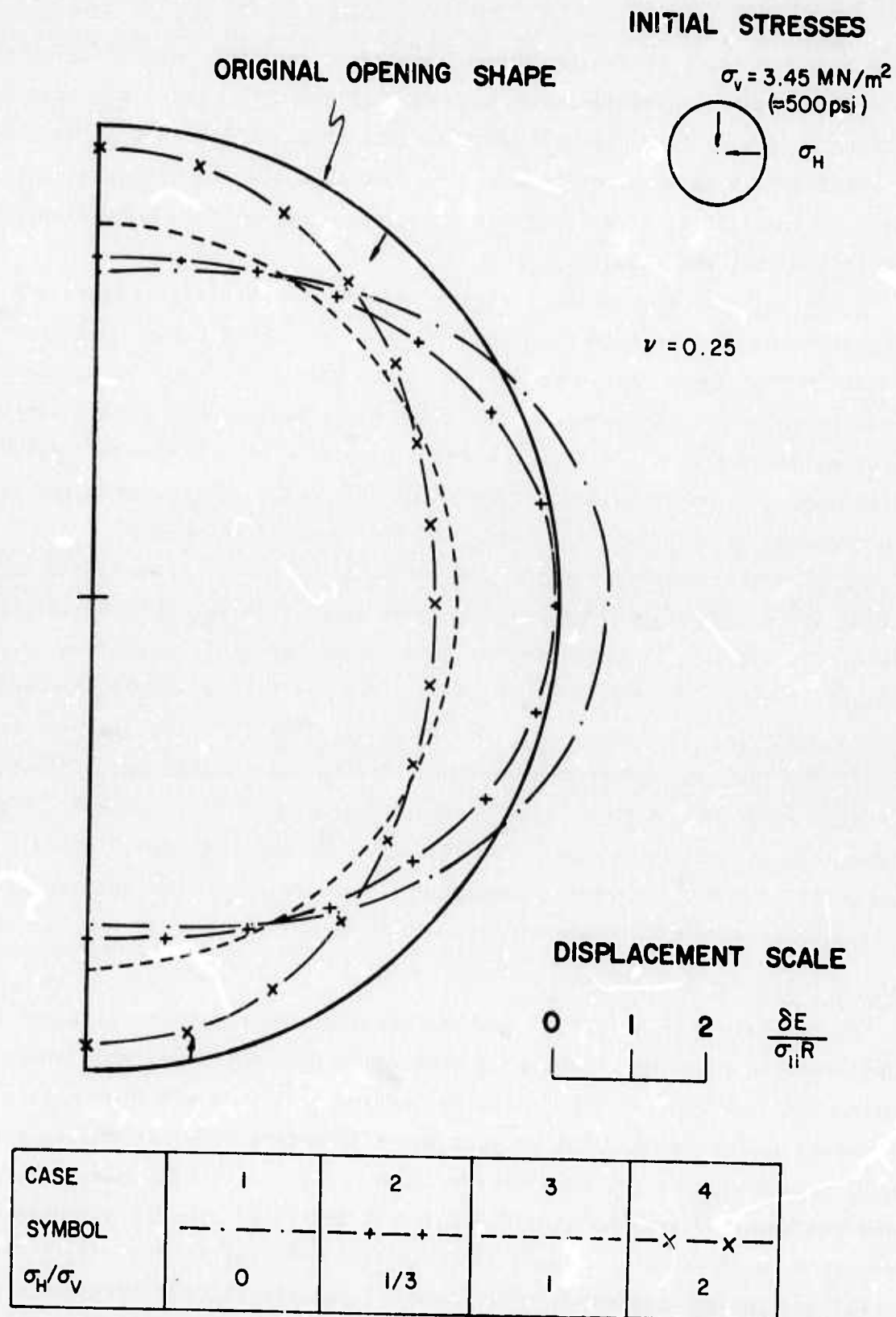


**FIG. 4-19 DISPLACEMENTS OF CIRCULAR OPENING  
IN HOMOGENEOUS LINEAR ROCK  
(VARIABLE INITIAL STRESSES)**

noted that, in terms of finite element analyses, when the initial stresses are oblique, a full circular mesh such as that shown in Figure 4-2 must be employed. If a half circle mesh such as that shown in Figure 2-14 is used, the results will be in error because the modeled system is unsymmetrical with regard to the initial stresses and subsequently the boundary conditions will adversely affect the results.

A typical example showing the results when the initial stresses are oriented at  $45^\circ$  is shown in Figures 4-20 and 4-21. This solution is comparable to that shown in Figure 4-16 with the only difference being the initial stress orientation. The contours obtained from the full mesh are slightly different because the full mesh has 272 elements while the quarter mesh has 130 elements, or an equivalent 520 element full mesh; subsequently the full mesh accuracy is slightly less than that for the quarter mesh.

To determine whether the 500 foot depth criteria for gravity and constant initial stress compatibility would still be applicable for oblique initial stress orientations, an analysis was conducted under gravity loading for the same case shown in Figures 4-20 and 4-21. Figures 4-22 and 4-23 show the results of this analysis. Comparison of the two cases shows that the stresses are essentially the same around the opening, but that there are small differences at more than about two to three radii from the opening center. However, these differences are generally less than 10% so it may be said that, from a practical standpoint, the 500 foot depth compatibility criteria is also applicable for oblique initial stress orientations.

#### Opening Shape

To determine the effect of opening shape on the resulting stresses and displacements, a series of analyses were conducted on typical horseshoe and power station opening shapes. The horseshoe opening is 5.5 meters high with a base of 5.5 meters and the power station opening is 30 meters high, 20 meters base width and 25 meters wide at the base of the crown arch. The finite element meshes for these two openings are shown in Figures 2-15 and 2-16. The values used in these analyses were: Poisson's ratio = 0.25, initial vertical stress =  $3.45 \text{ MN/m}^2$ , and initial horizontal stresses =  $1/3$ , 1 and 2 times the initial vertical stress.


##### a) Horseshoe Opening

Figures 4-24 through 4-26 show the dimensionless  $\sigma_1$  values for the horseshoe opening with the three initial stress conditions. These figures show that the

INITIAL STRESSES

$$\sigma_{ii} = 3.45 \text{ MN/m}^2$$

( $\approx 500 \text{ psi}$ )



$$\sigma_{3i} = 1.15 \text{ MN/m}^2$$

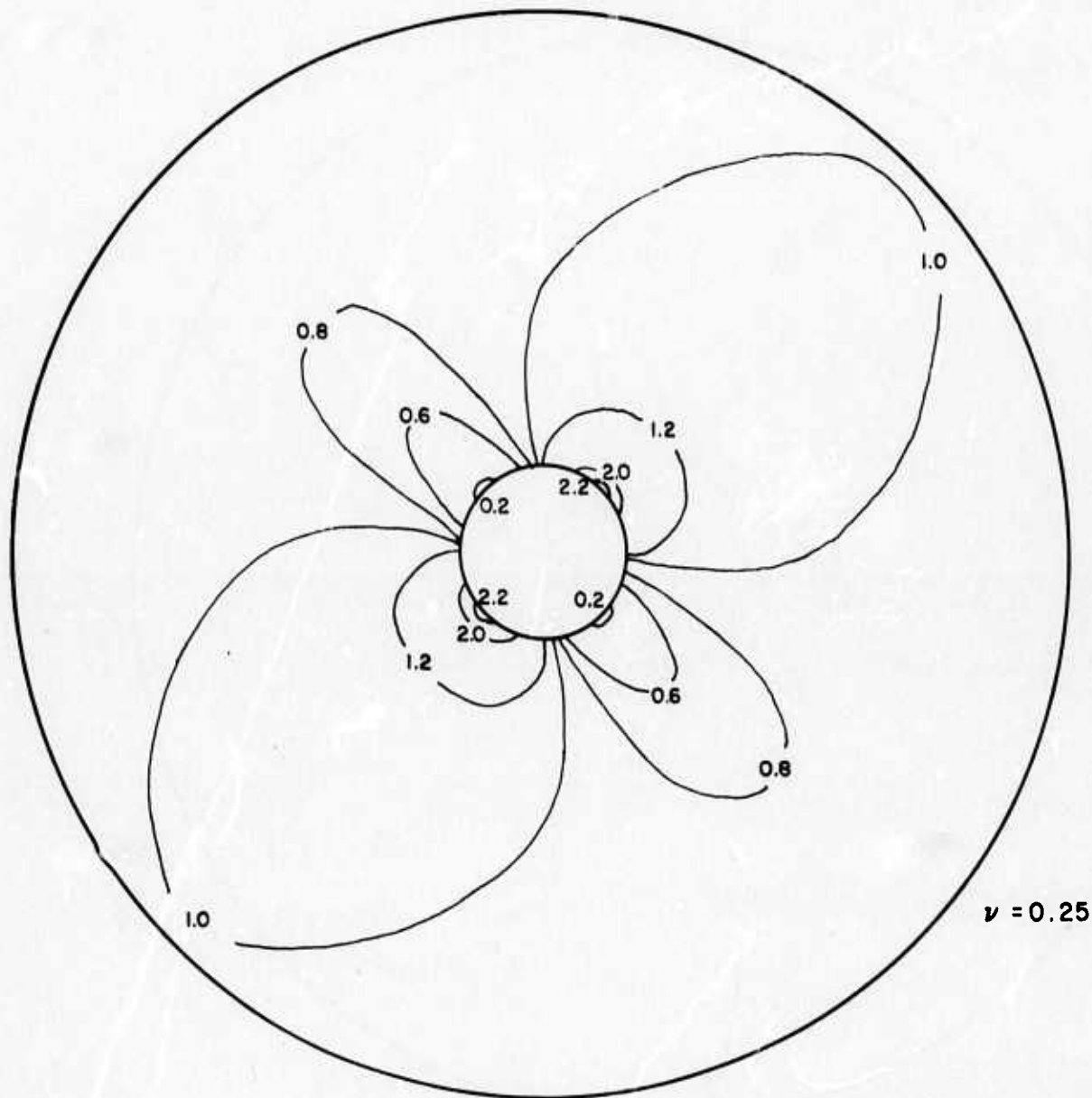



**FIG. 4-20 CONTOURS OF  $\sigma_1/\sigma_{ii}$  FOR CIRCULAR OPENING IN HOMOGENEOUS LINEAR ROCK,  $K=1/3$ ,  $\theta=45^\circ$**

INITIAL STRESSES

$$\sigma_{1i} = 3.45 \text{ MN/m}^2$$

( $\approx 500 \text{ psi}$ )



$$\sigma_{3i} = 1.15 \text{ MN/m}^2$$

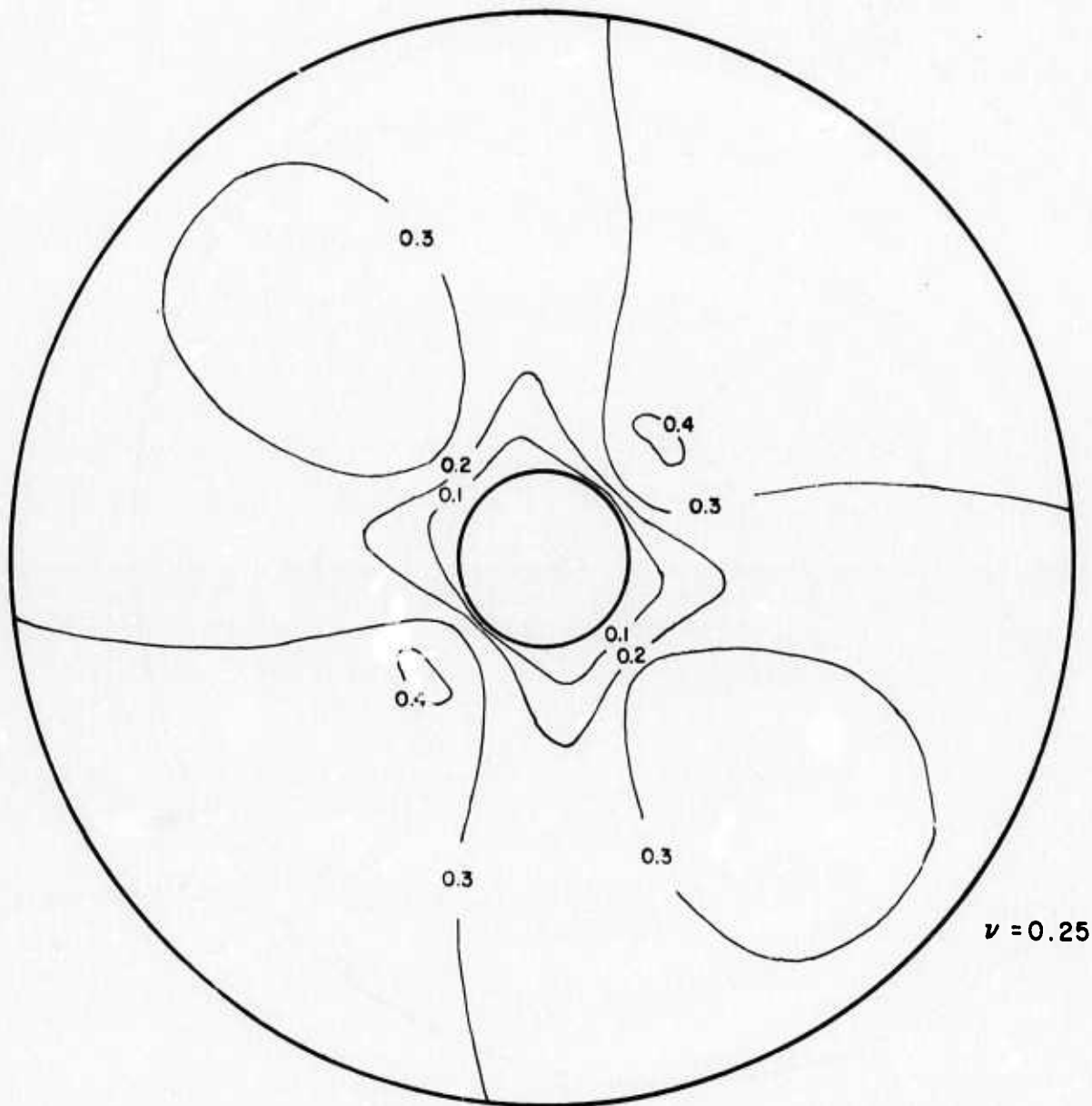


**FIG. 4-21 CONTOURS OF  $\sigma_3/\sigma_{1i}$  FOR CIRCULAR OPENING IN HOMOGENEOUS LINEAR ROCK,  $K=1/3$ ,  $\theta=45^\circ$**

MID-HEIGHT  
INITIAL STRESSES

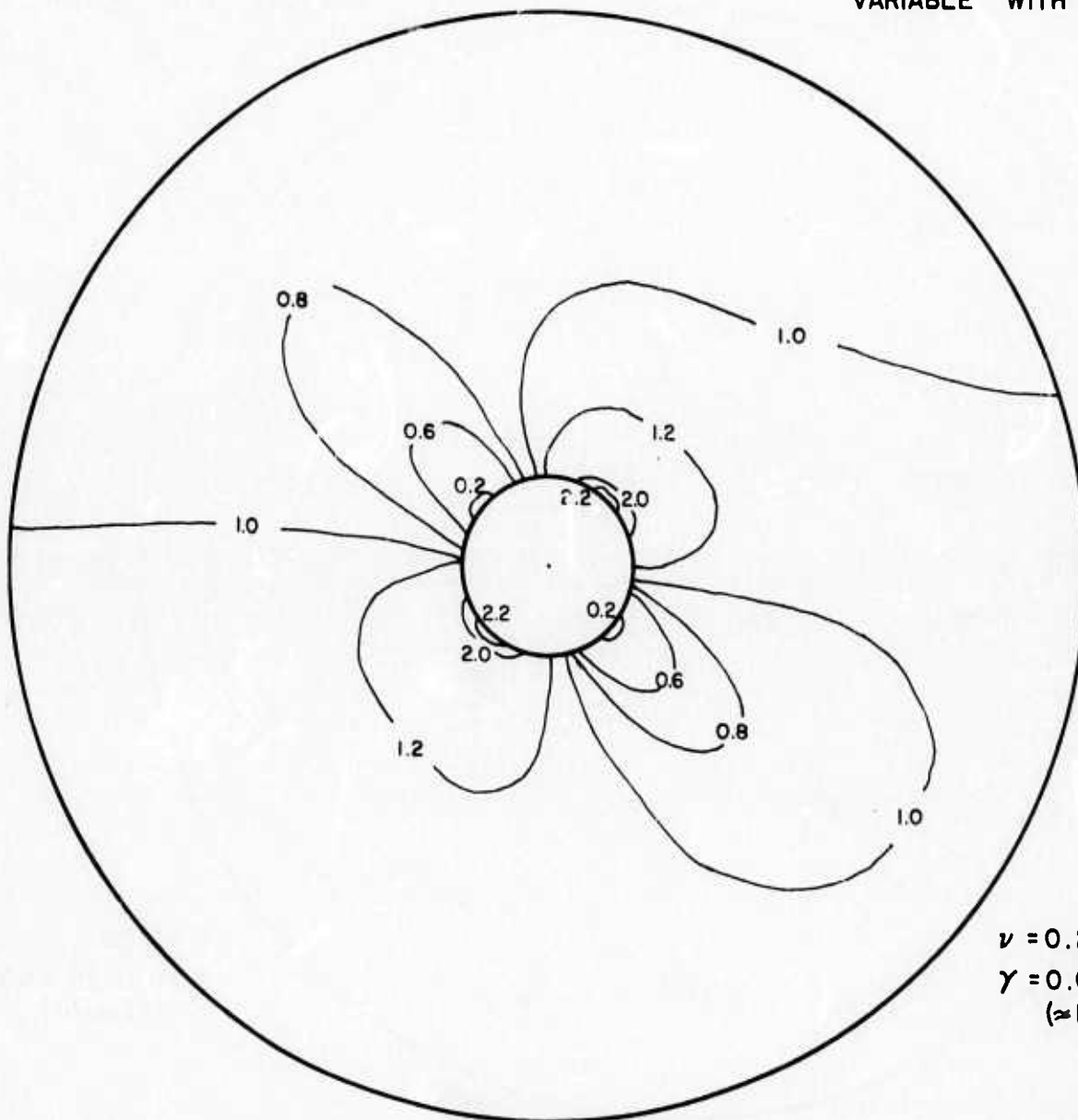
$$\sigma_{ii} = 3.45 \text{ MN/m}^2$$

( $\approx 500 \text{ psi}$ )



$$\sigma_{3i} = 1.15 \text{ MN/m}^2$$

VARIABLE WITH DEPTH



$$\nu = 0.25$$

$$\gamma = 0.0226 \text{ MN/m}^3$$

( $\approx 1 \text{ psi/ft}$ )

**FIG. 4-22 CONTOURS OF  $\sigma_1/\sigma_{ii}$  FOR CIRCULAR OPENING  
IN HOMOGENEOUS LINEAR ROCK,  $K=1/3$ ,  $\theta=45^\circ$   
(GRAVITY STRESSES, 500 FOOT DEEP)**

MID-HEIGHT  
INITIAL STRESSES

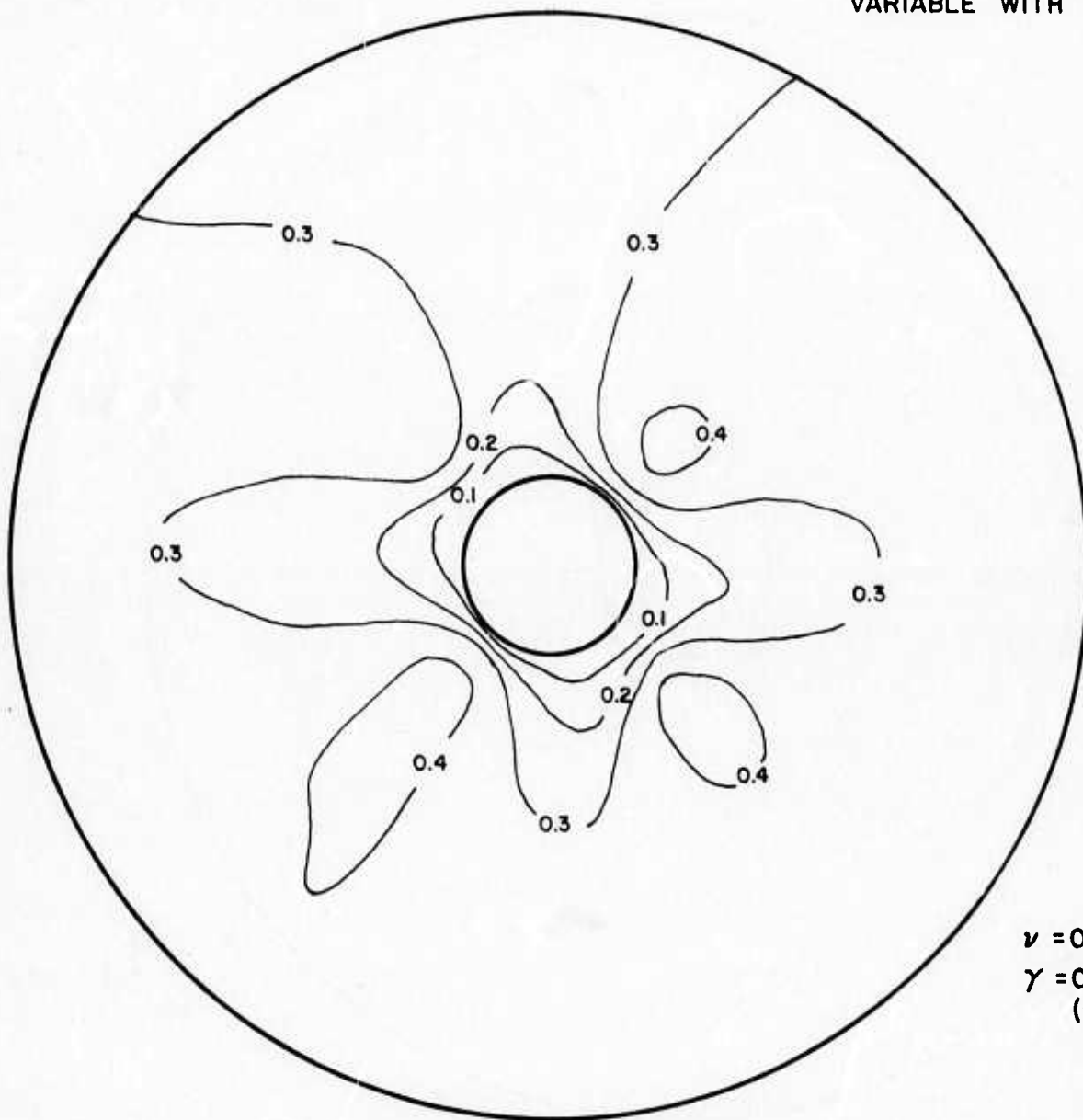
$$\sigma_{li} = 3.45 \text{ MN/m}^2$$

( $\approx 500 \text{ psi}$ )



$$\sigma_{3i} = 1.15 \text{ MN/m}^2$$

VARIABLE WITH DEPTH



$$\nu = 0.25$$

$$\gamma = 0.0226 \text{ MN/m}^3$$

( $\approx 1 \text{ psi/ft}$ )

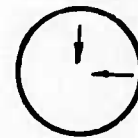
**FIG. 4-23 CONTOURS OF  $\sigma_3/\sigma_{li}$  FOR CIRCULAR OPENING  
IN HOMOGENEOUS LINEAR ROCK,  $K=1/3$ ,  $\theta=45^\circ$   
(GRAVITY STRESSES, 500 FOOT DEEP)**



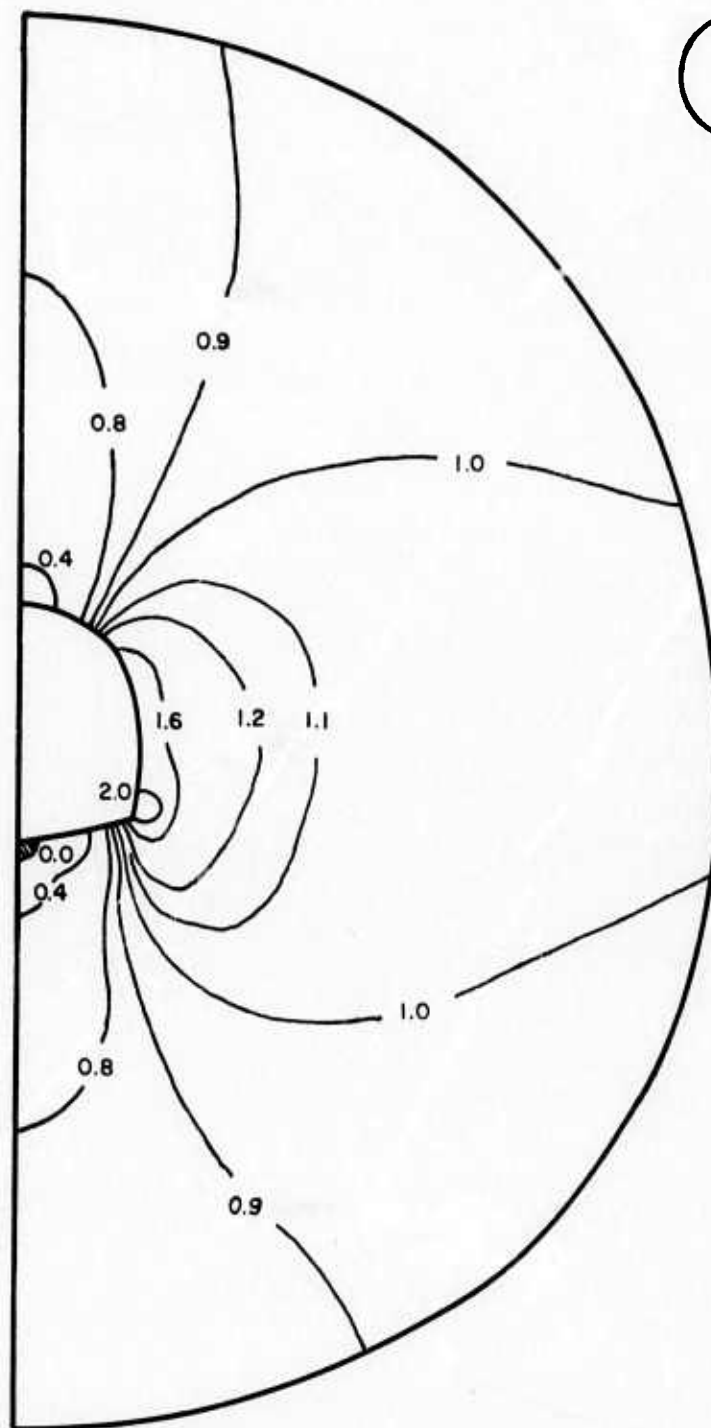
# INITIAL STRESSES

$$\sigma_{11} = 3.45 \text{ MN/m}^2$$

( $\approx 500 \text{ psi}$ )



$$\sigma_{33} = 1.15 \text{ MN/m}^2$$



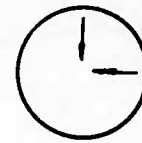
$$\nu = 0.25$$

**FIG. 4-24 CONTOURS OF  $\sigma_1/\sigma_3$  FOR HORSESHOE  
IN HOMOGENEOUS LINEAR ROCK,  $K=1/3$ ,  $\theta=0^\circ$**

# INITIAL STRESSES

$$\sigma_{1i} = 3.45 \text{ MN/m}^2$$

( $\approx 500 \text{ psi}$ )



$$\sigma_{3i} = 3.45 \text{ MN/m}^2$$

$$\nu = 0.25$$

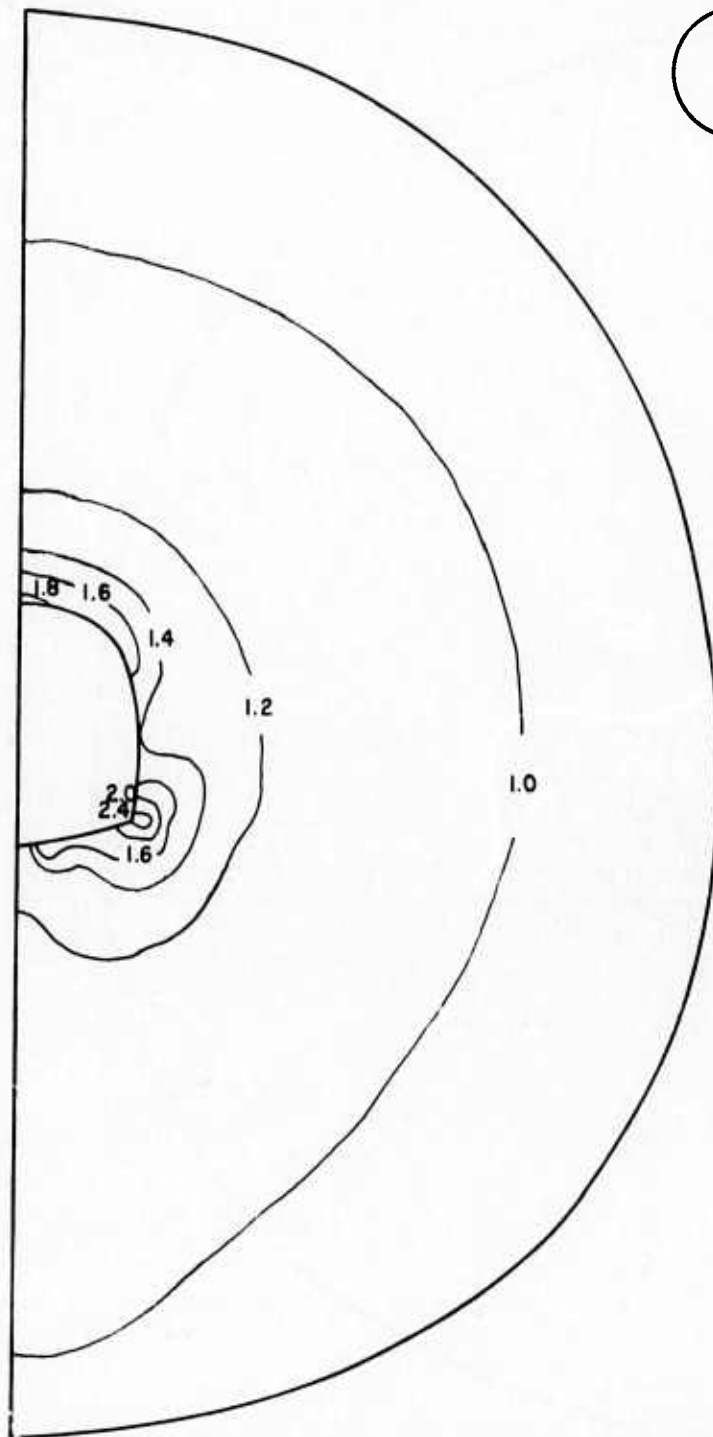


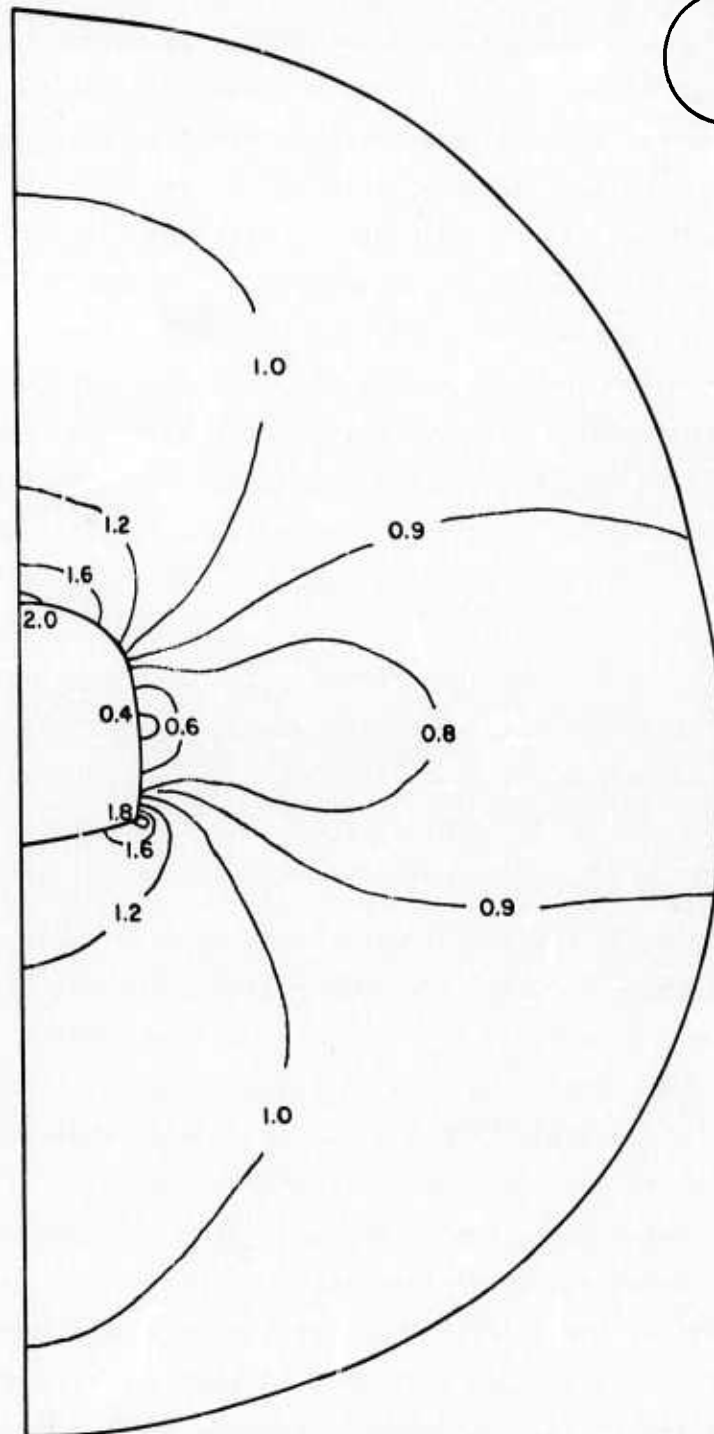
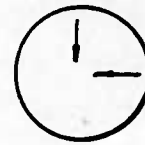
**FIG. 4-25 CONTOURS OF  $\sigma_1 / \sigma_{1i}$  FOR HORSESHOE IN HOMOGENEOUS LINEAR ROCK,  $K=1$ ,  $\theta=0^\circ$**

# INITIAL STRESSES

$$\sigma_{3i} = 3.45 \text{ MN/m}^2$$

( $\approx 500 \text{ psi}$ )

$$\sigma_{1i} = 6.90 \text{ MN/m}^2$$



$$\nu = 0.25$$

**FIG. 4-26 CONTOURS OF  $\sigma_1/\sigma_{ii}$  FOR HORSESHOE IN HOMOGENEOUS LINEAR ROCK,  $K=1/2, \theta=90^\circ$**

resulting stresses are very similar to those for the circular opening, except within about one equivalent "radius" of the opening face. Within this zone, a stress concentration is developed at the lower horseshoe corner, with the largest value occurring under isotropic initial stresses and the lowest value occurring when the horizontal stresses are twice as great as the vertical. The crown stresses follow the same pattern as those for the circular opening, i.e., the stresses increase as the initial lateral stresses increase.

Figures 4-27 through 4-29 show the dimensionless  $\sigma_3$  values for the same three cases. The resulting stresses are again very similar to those for the circular opening, except within about one equivalent "radius" of the opening face. A stress concentration is developed at the lower horseshoe corner, with the values increasing as the initial horizontal stresses decrease. It is interesting to note that, regardless of initial stress values, a small tension zone develops at the invert, indicating that this shape causes substantial load transfer to occur.

The horseshoe displacements, shown in Figure 4-30, also display patterns similar to the circular opening. The inward movements of the crown and invert increase as the initial horizontal stresses decrease, while the inward wall movements increase as the initial horizontal stresses increase.

#### b) Power Station Opening

Figures 4-31 through 4-33 show the dimensionless  $\sigma_1$  values for the power station opening with the three initial stress conditions. Comparing these figures with the comparable figures for the circular and horseshoe openings, it can be seen that the same general pattern of stress contours develops, except for immediately around the opening. Within this area the stresses are markedly affected because of the three geometric corners defining the opening, i.e., those at the base of the crown arch, top of the wall and bottom of the wall.

The highest stress concentration always occurs at the intersection of the wall and floor, regardless of the initial stresses. As with the horseshoe opening, the highest value occurs under isotropic initial stresses while the lowest value occurs when the initial horizontal stresses are twice the vertical stresses. Furthermore, the stress concentrations are greater than those at the base of the horseshoe opening, for the same stress condition.

At the base of the crown arch, another stress concentration develops which is of minor importance when the initial horizontal stresses are large but becomes very important as the initial horizontal stresses decrease until when  $K = 1/3$ , it

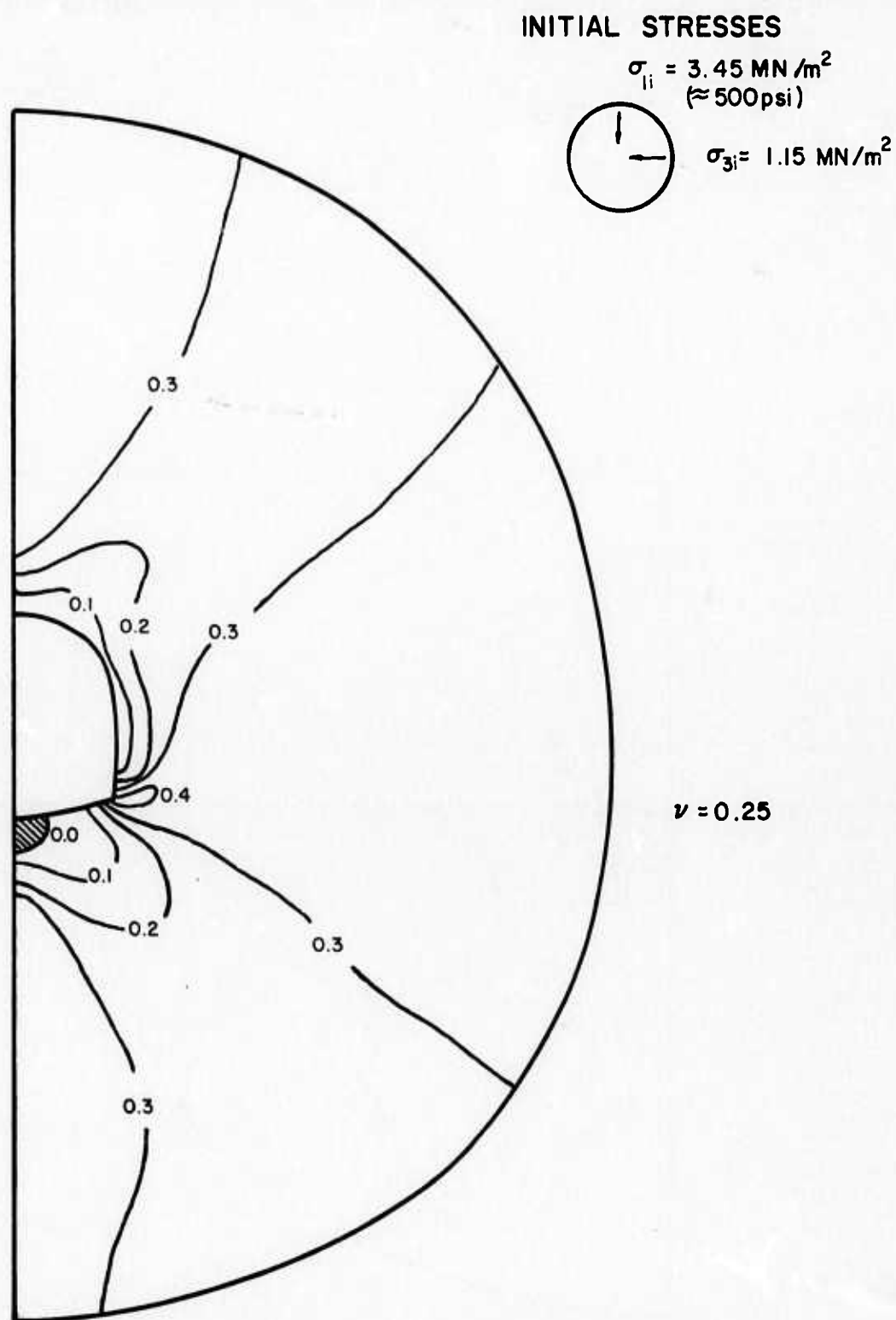
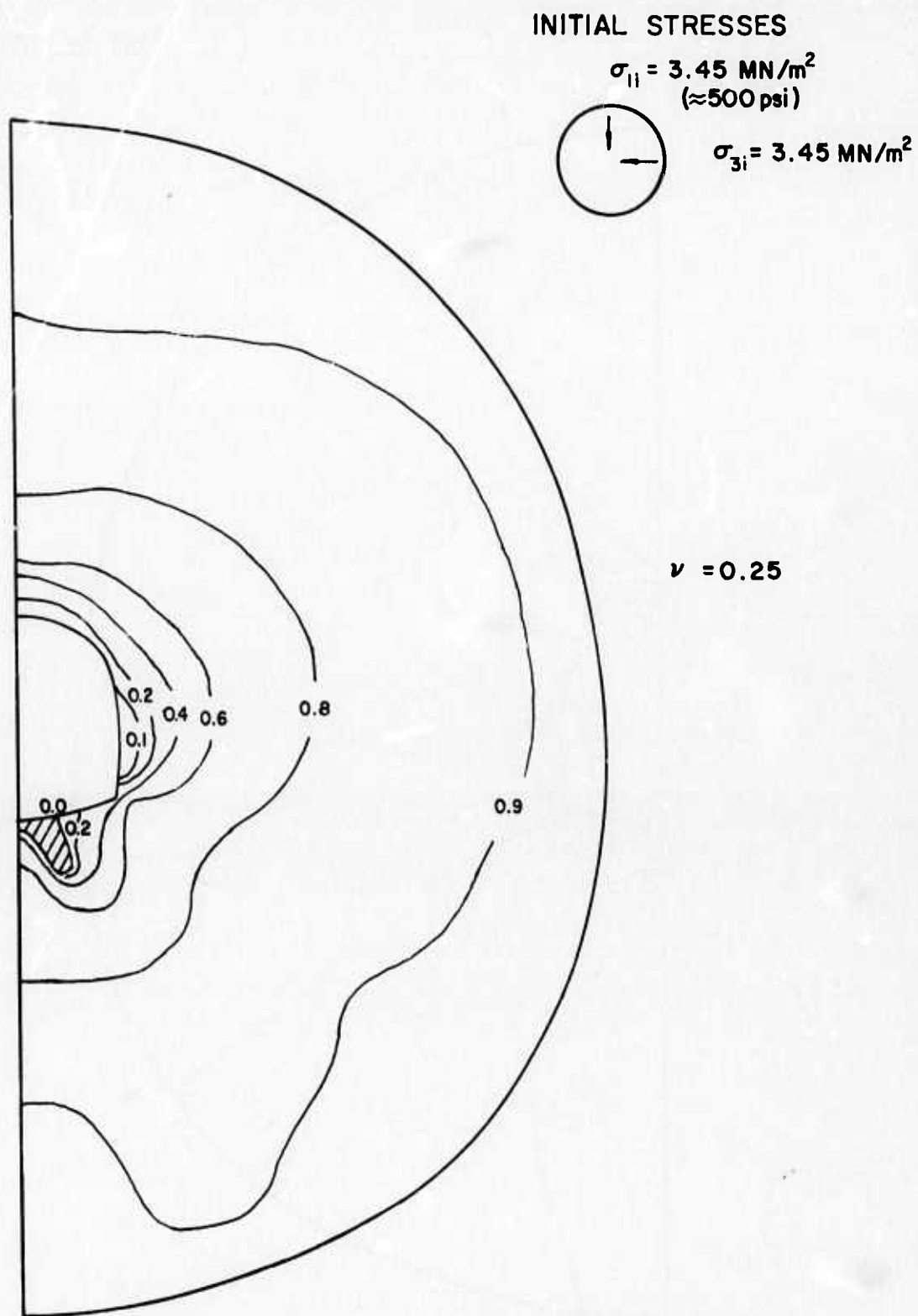


FIG. 4-27 CONTOURS OF  $\sigma_3 / \sigma_{li}$  FOR HORSESHOE  
 IN HOMOGENEOUS LINEAR ROCK,  $K=1/3$ ,  $\theta=0^\circ$



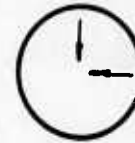
**FIG. 4-28 CONTOURS OF  $\sigma_3/\sigma_{1i}$  FOR HORSESHOE  
IN HOMOGENEOUS LINEAR ROCK,  $K=1$ ,  $\theta=0^\circ$**



# INITIAL STRESSES

$$\sigma_{3i} = 3.45 \text{ MN/m}^2$$

( $\approx 500 \text{ psi}$ )



$$\sigma_{1i} = 6.90 \text{ MN/m}^2$$

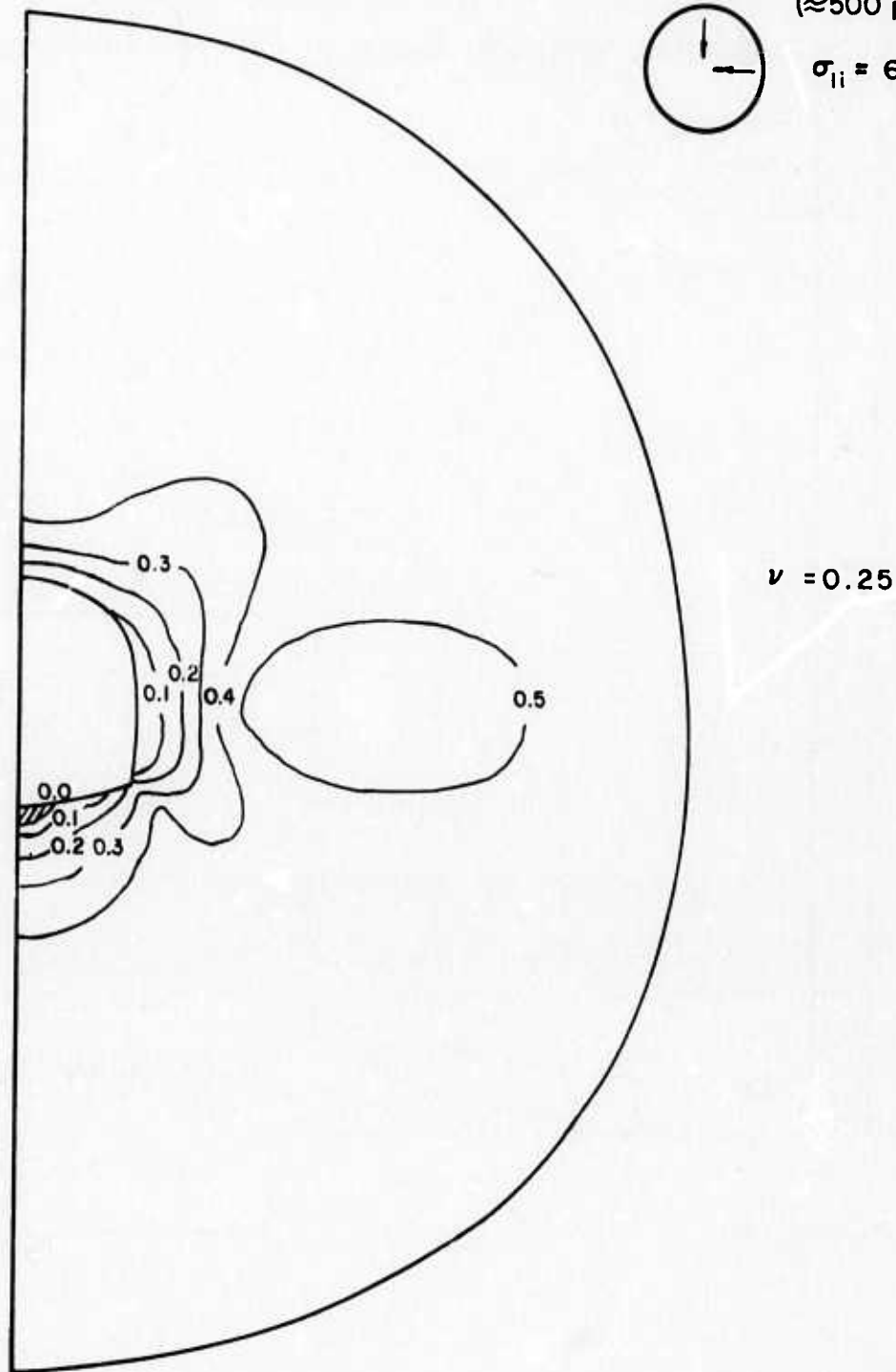


**FIG. 4-29 CONTOURS OF  $\sigma_3/\sigma_{1i}$  FOR HORSESHOE  
IN HOMOGENEOUS LINEAR ROCK,  $K=1/2, \theta=90^\circ$**

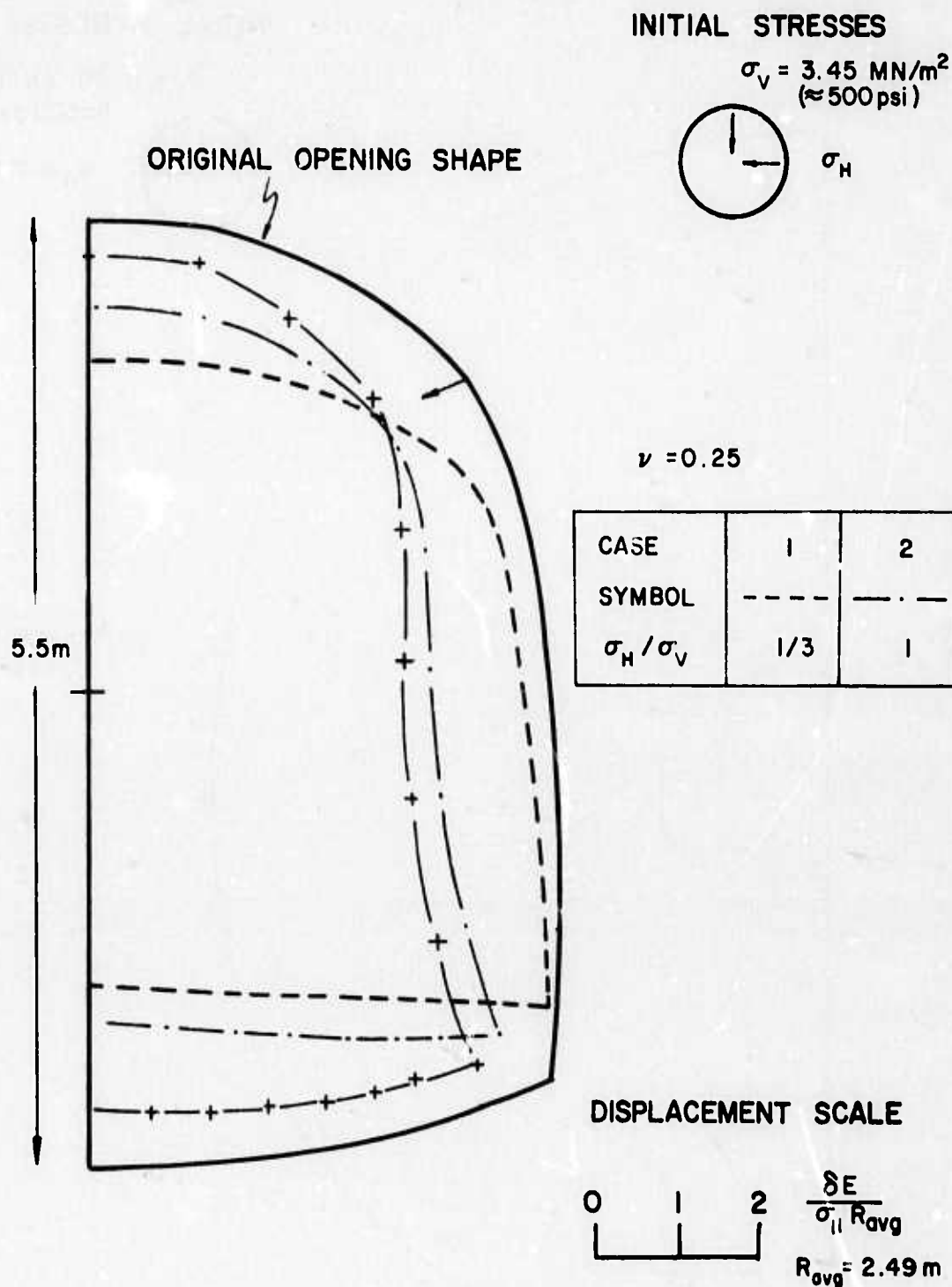


**FIG. 4-30 DISPLACEMENTS OF HORSESHOE  
IN HOMOGENEOUS LINEAR ROCK**

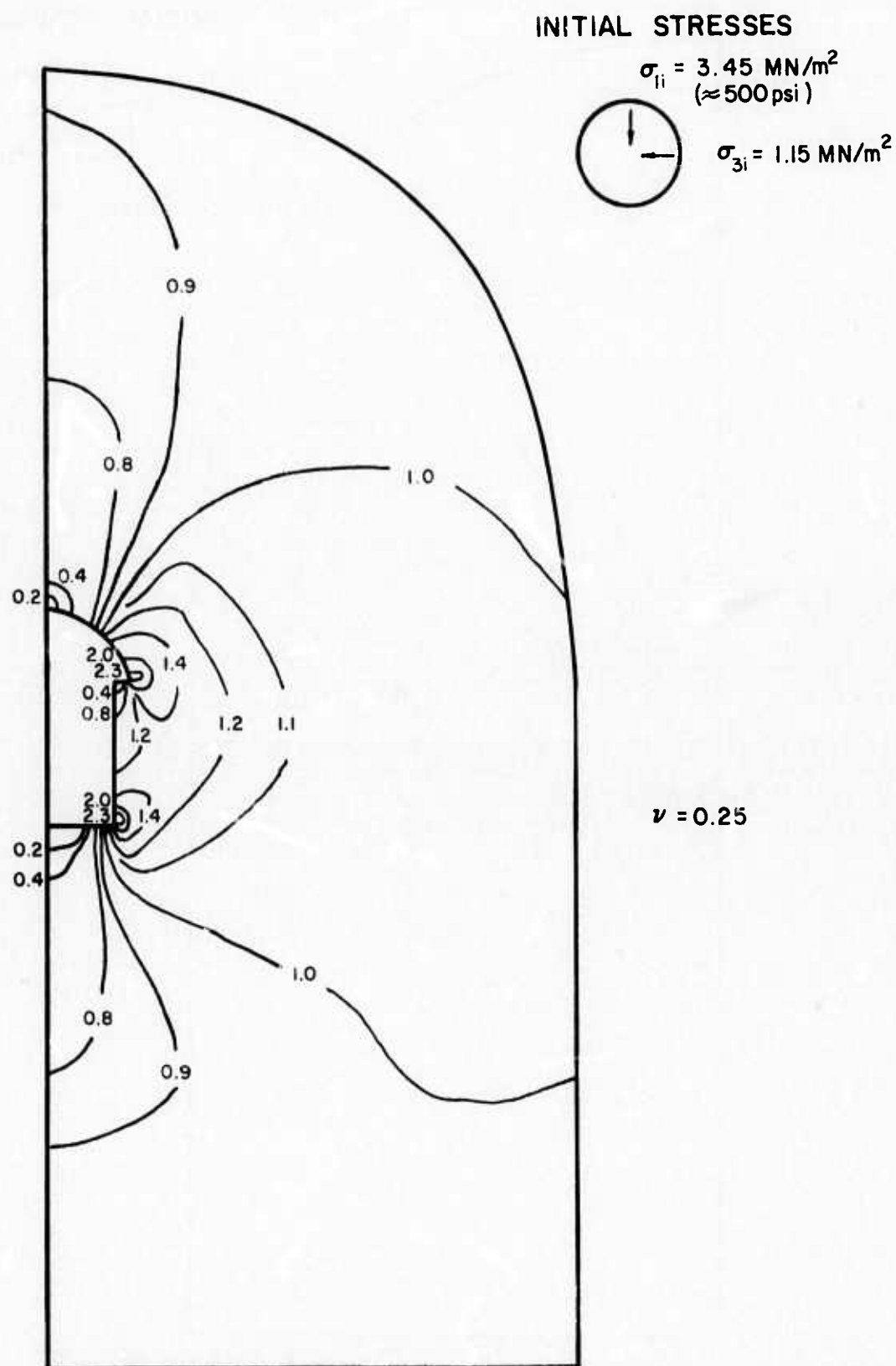


**FIG. 4-31 CONTOURS OF  $\sigma_1 / \sigma_{1i}$  FOR POWER STATION  
IN HOMOGENEOUS LINEAR ROCK,  $K=1/3$ ,  $\theta=0^\circ$**

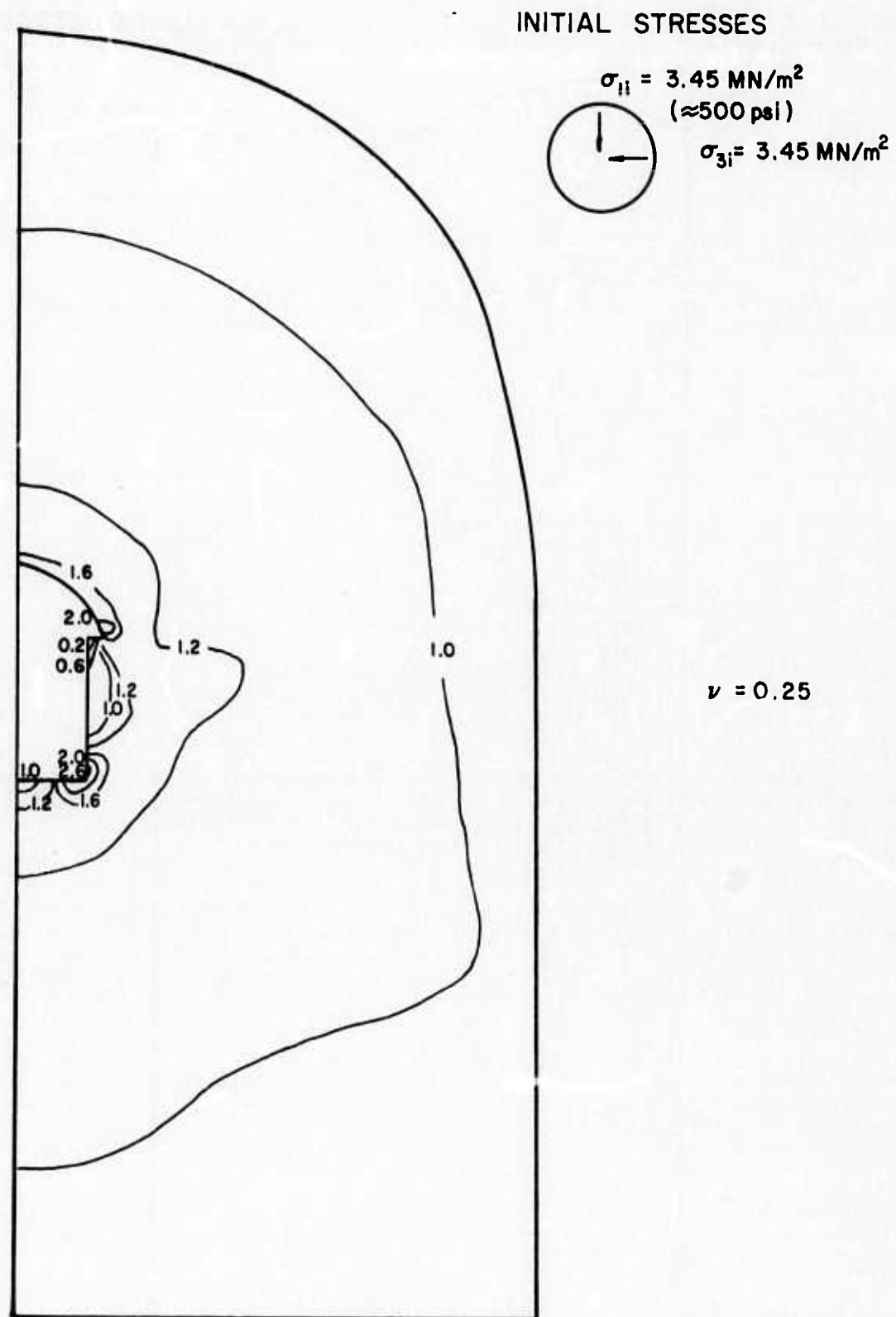


**FIG. 4-32 CONTOURS OF  $\sigma_1/\sigma_{1i}$  FOR POWER STATION  
IN HOMOGENEOUS LINEAR ROCK,  $K=1$ ,  $\theta=0^\circ$**

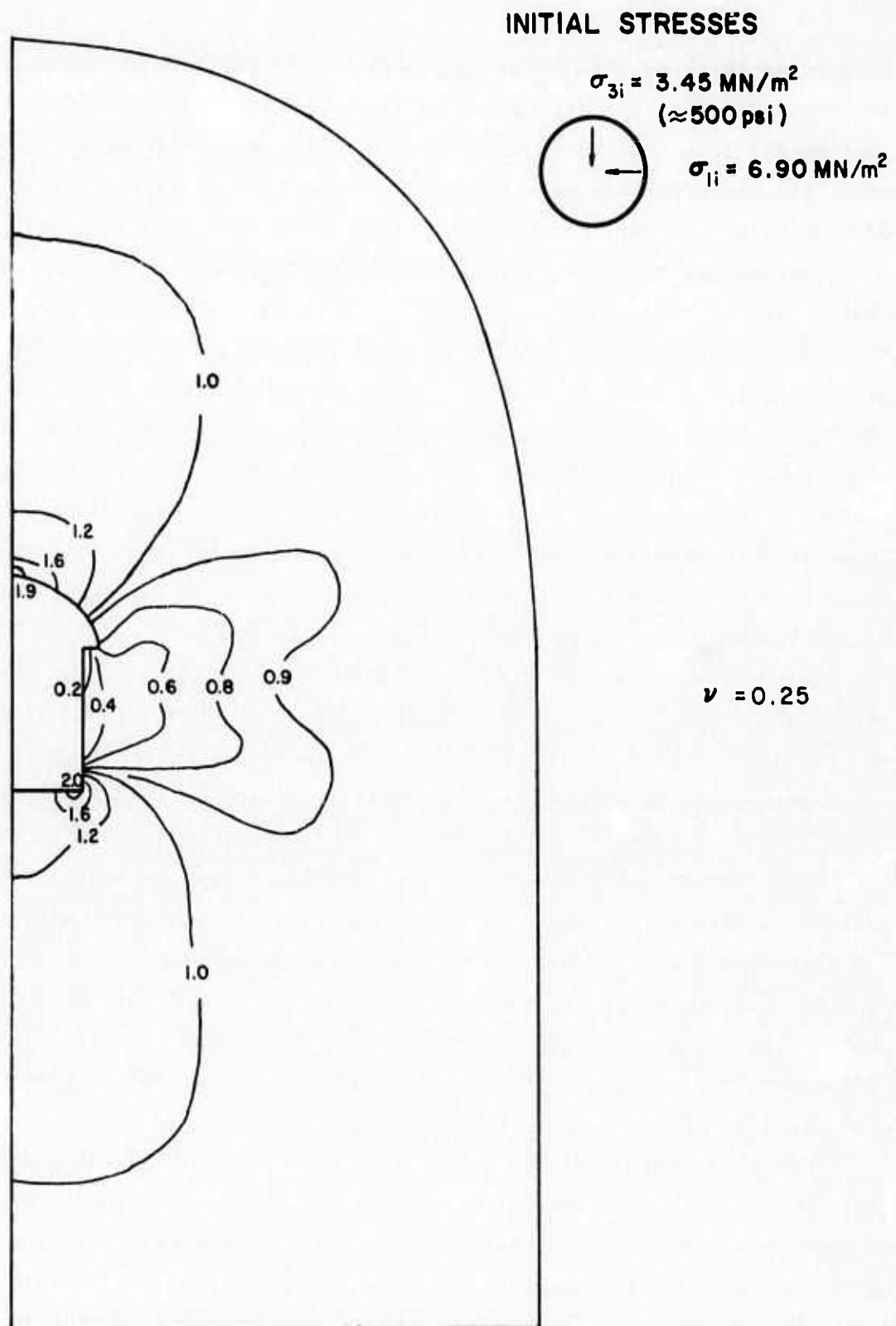


**FIG. 4-33 CONTOURS OF  $\sigma_1/\sigma_{1i}$  FOR POWER STATION  
IN HOMOGENEOUS LINEAR ROCK,  $K=1/2, \theta=90^\circ$**

becomes as large as the stress concentration at the base of the wall. The mid-crown stresses are also affected by shape with the values from the power station all less than those developing with the horseshoe opening. Furthermore, the mid-crown stresses vary with the initial stresses, with larger values developing as the horizontal stresses increase.

Perhaps the most significant effect of the power station opening shape is that of stress relief in the wall. In all three cases the stresses are reduced to small values, especially at the top of the wall, and the smallest values occur when the initial horizontal stresses are highest. In addition the wall stresses are all less than those developing in the wall of the horseshoe opening.

Figures 4-34 through 4-36 show the dimensionless  $\sigma_3$  values for the power station opening with the three initial stress conditions. Patterns similar to those of the horseshoe opening also develop. Stress concentrations develop at the intersection of the wall and floor, with the largest occurring under isotropic initial stresses and the smallest occurring with  $K = 1/3$ . Comparing these values to those from the horseshoe opening, it can be seen that the values are slightly less for the power station when  $K = 1/3$ , but are greater for the other two cases. Stress concentrations also occur at the base of the crown arch and become larger as the initial horizontal stresses decrease.

However, the most important aspect of the power station shape is the large amount of tension which develops. In all three cases, a large portion of the wall is in tension. Furthermore, with low initial horizontal stresses, both the mid-crown and mid-floor are in tension; with isotropic initial stresses, a portion of the floor is in tension; and with high initial horizontal stresses, neither the floor nor crown is in tension. This large variation in tensile zone development clearly demonstrates the importance of initial stresses in evaluating the stability of power station openings.

The power station displacements, shown in Figure 4-37, also display patterns similar to those of the circular and horseshoe openings. The inward movements of the crown and invert increase as the initial horizontal stresses decrease, while the inward wall movements increase as the initial horizontal stresses increase. While most of the dimensionless displacements for the three opening shapes are of the same order of magnitude, it should be noted that when  $K = 1/3$ , the dimensionless inward movements of the power station opening are substantially greater than those of the horseshoe opening which in turn are substantially greater than those of the circular opening.



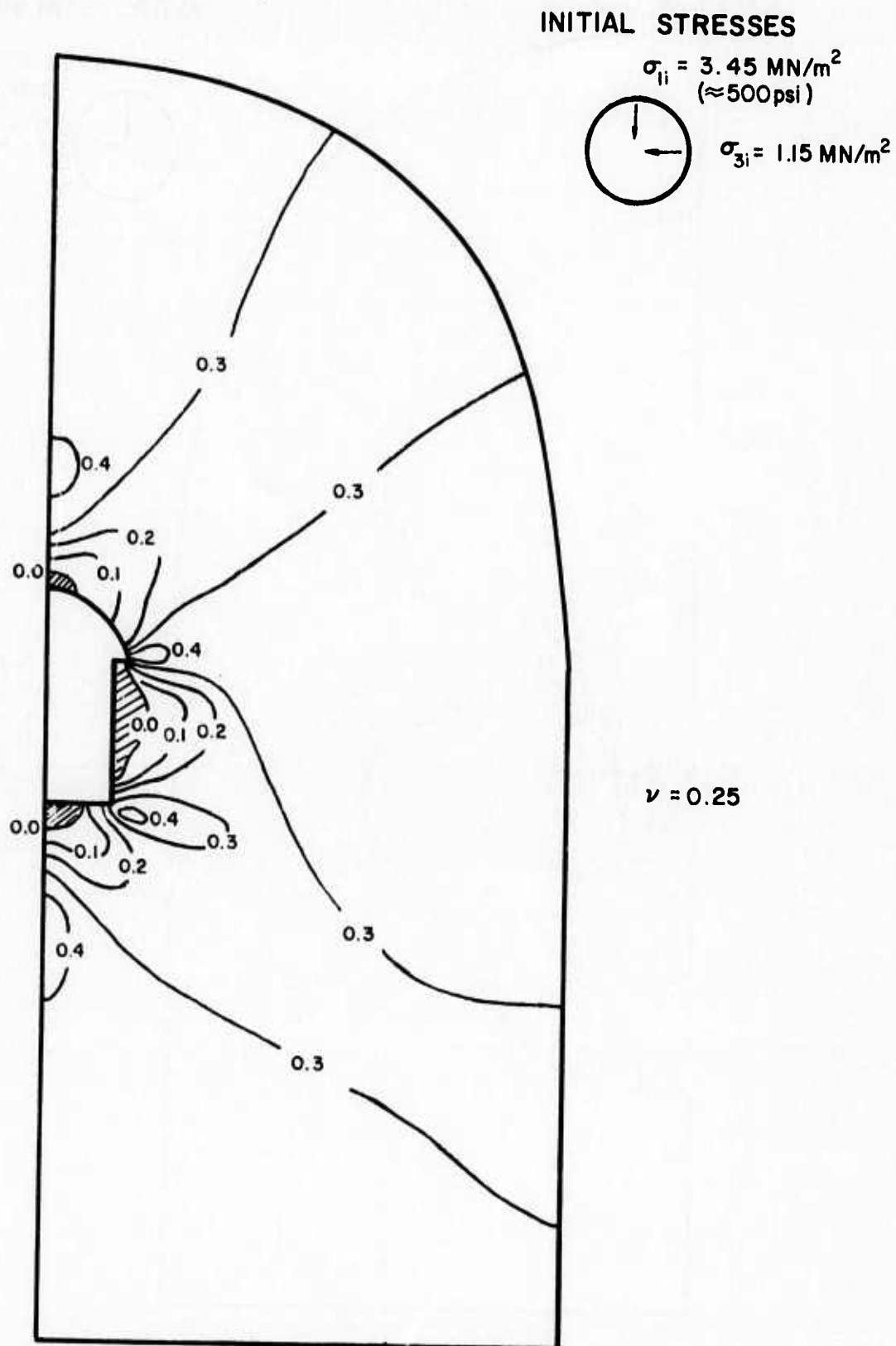


**FIG. 4-34 CONTOURS OF  $\sigma_3 / \sigma_{1i}$  FOR POWER STATION  
IN HOMOGENEOUS LINEAR ROCK,  $K=1/3$ ,  $\theta=0^\circ$**

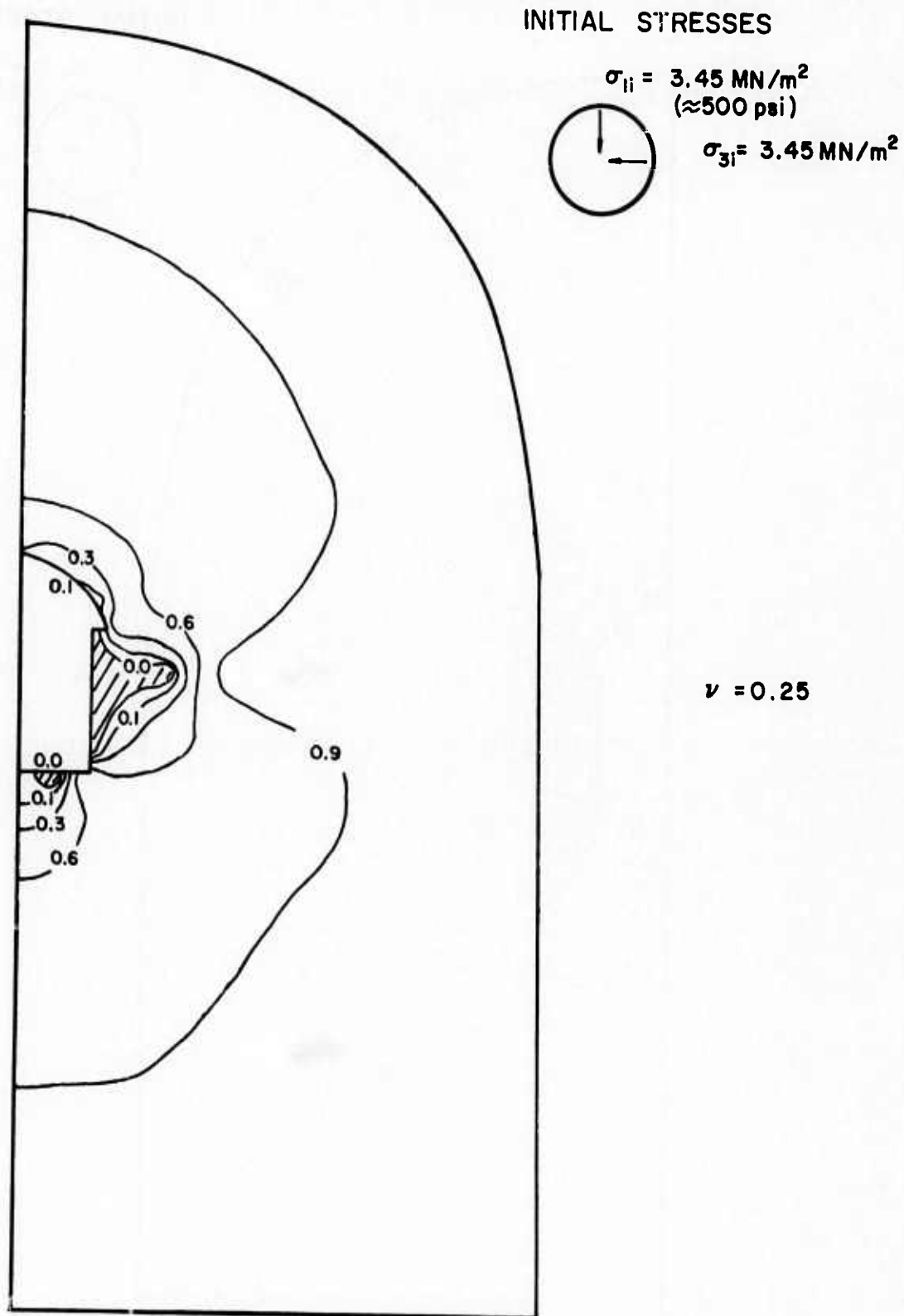
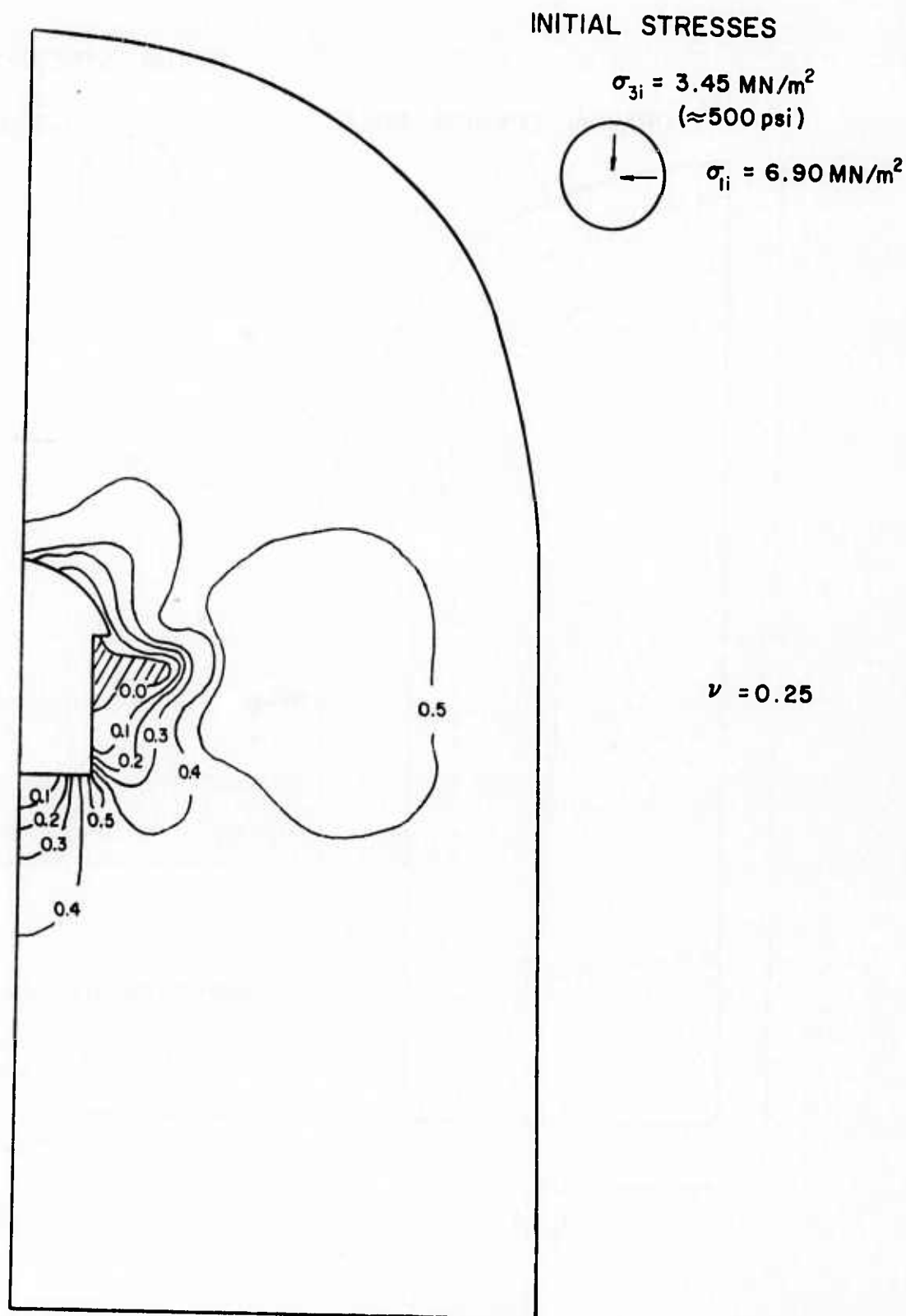
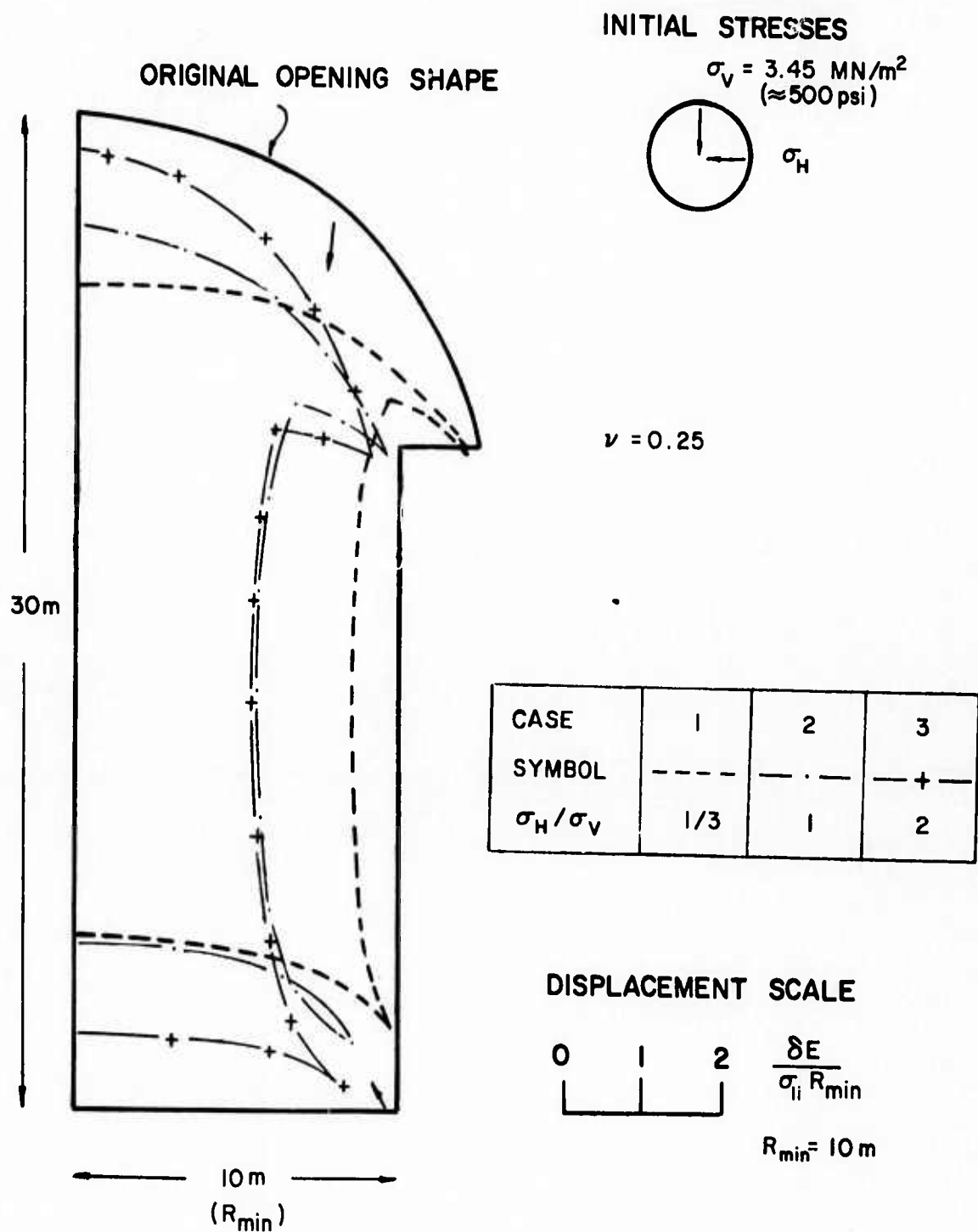


FIG. 4-35 CONTOURS OF  $\sigma_3/\sigma_{ii}$  FOR POWER STATION  
IN HOMOGENEOUS LINEAR ROCK,  $K=1$ ,  $\theta=0^\circ$



**FIG. 4-36 CONTOURS OF  $\sigma_3/\sigma_{1i}$  FOR POWER STATION  
 IN HOMOGENEOUS LINEAR ROCK,  $K=1/2, \theta=90^\circ$**



**FIG. 4-37 DISPLACEMENTS OF POWER STATION  
IN HOMOGENEOUS LINEAR ROCK**

### Nonlinear Material Properties

The studies presented in Chapter 3 have shown that many rock types are nonlinear and stress-dependent with respect to both the modulus and Poisson's ratio and that most rock types can be reasonably well represented by empirical equations in which the nonlinearity is represented by a hyperbolic equation and the stress-dependency is represented by a straight line variation with the confining pressure on a log-log plot for the modulus and on a semi-log plot for the Poisson's ratio. In addition to the strength parameters,  $c$  and  $\phi$ , the modulus variations are defined with three additional parameters. The modulus parameters are: modulus number,  $K$ , defining the initial tangent modulus; exponent,  $n$ , defining the modulus variation with confining pressure; and failure ratio,  $R_f$ , defining the nonlinearity of the stress-strain curve (See Equation 3-8.). The Poisson's ratio parameters are:  $G$ , defining the initial tangent Poisson's ratio;  $F$ , defining the Poisson's ratio variation with confining pressure; and  $d$ , defining the nonlinearity of the axial strain-radial strain curve (See Equation 3-17.).

To investigate the effects of these variations in material properties on the resulting stresses and displacements and, because of these variations, to investigate the effects of number of excavation steps as well as excavation sequence, a number of analyses were conducted. To limit the number of variables, the following analysis parameters were maintained constant: circular opening, initial vertical stress ( $\sigma_{1i}$ ) =  $3.45 \text{ MN/m}^2$ , initial horizontal stress ( $\sigma_{3i}$ ) =  $1.15 \text{ MN/m}^2$ , cohesion ( $c$ ) =  $15 \text{ MN/m}^2$  and angle of friction ( $\phi$ ) =  $35^\circ$ . It should be noted that in all of the following analyses, the developed shear stresses were small and the rock mass was not stressed even close to failure.

#### a) Modulus Parameter Variations

Several analyses were conducted to investigate the effect of modulus parameter variations. In these analyses, a three step horizontal excavation sequence was employed (See Figure 4-3.), a constant Poisson's ratio = 0.25 was used and the modulus number,  $K$ , was taken as 100,000 since it was found that  $K$  doesn't effect the stresses and can be included as a factor when defining the dimensionless displacements. The values of  $n$  were varied from 0.0 to 0.4 and the values of  $R_f$  were varied from 0.25 to 0.75. The values were selected to cover the range of these parameters found for most of the rock types discussed in Chapter 3.

Figure 4-38 shows the dimensionless  $\sigma_1$  values obtained for  $n = 0.0$  and  $R_f = 0.25$ . This figure is representative of all values of  $n$  and  $R_f$  investigated since virtually no differences were found for the analyses conducted. Comparing this

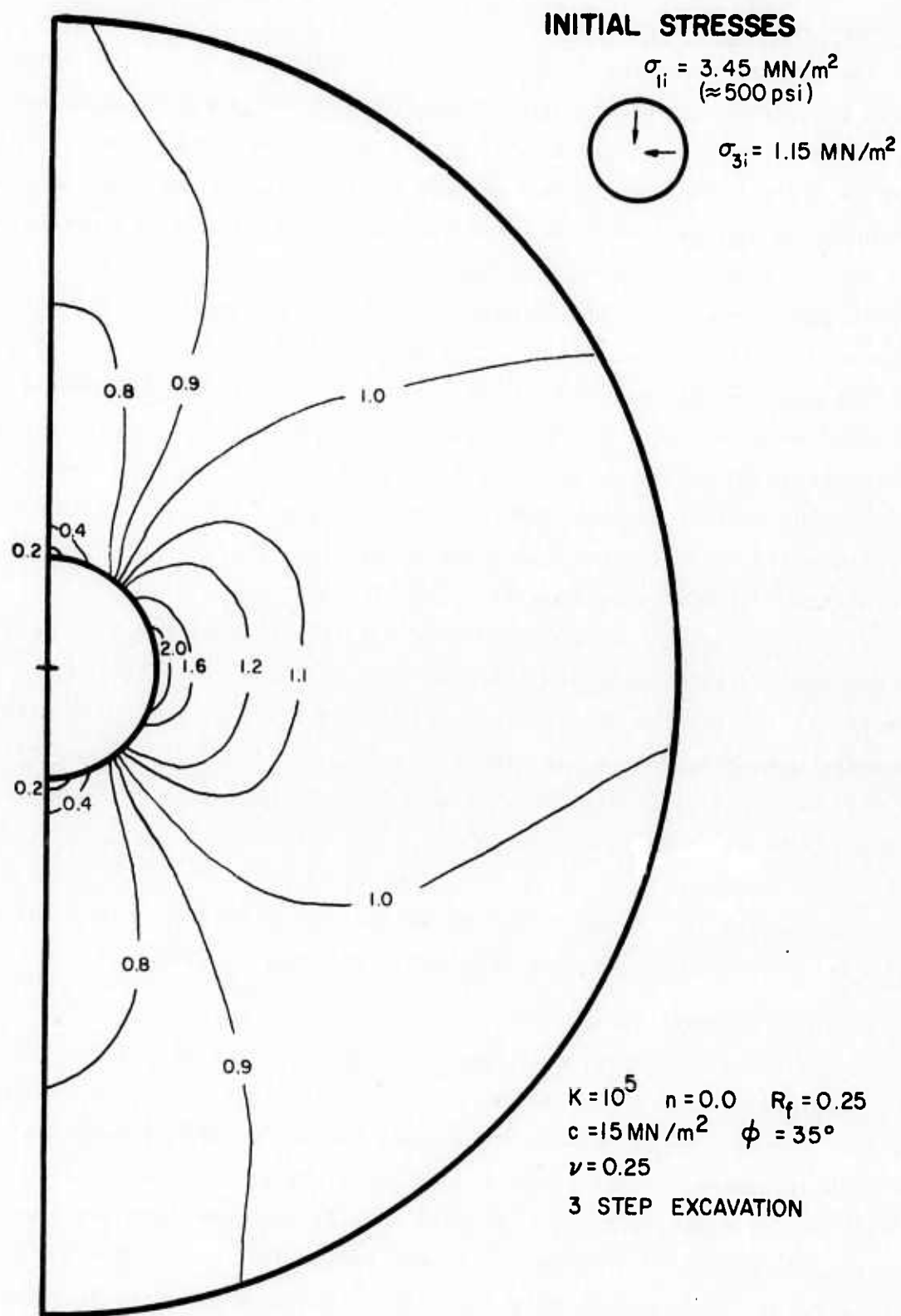


**FIG. 4-38   CONTOURS OF  $\sigma_1/\sigma_{1i}$  FOR CIRCULAR OPENING  
IN NONLINEAR ROCK,  $K=1/3$ ,  $e=0^\circ$   
(NONLINEAR MODULUS)**



figure with Figure 4-16, it can be seen that for all practical purposes the  $\sigma_1$  values are the same regardless of whether the modulus is linear or is non-linear and stress-dependent.

Figure 4-39 shows the dimensionless  $\sigma_3$  values obtained for  $n = 0.0$  and  $R_f = 0.25$ , which is also representative of all  $n$  and  $R_f$  values investigated. Comparing this figure with Figure 4-40, the linear analysis, it can be seen that small variations occur in the stress contours, but these variations occur at excavation levels and are very small so it is felt that these variations are insignificant and are a function of variations caused by the relatively coarse mesh employed in these analyses.

The displacements for the cases investigated are shown in Figure 4-41. This figure shows that variations in displacements caused by nonlinearity, represented by  $R_f$ , are very small but that variations in displacements caused by stress-dependency, represented by  $n$ , are significant and should be included in analyses of underground openings because larger  $n$  values, or greater stress-dependencies, cause less displacements to occur.

#### b) Poisson's Ratio Parameter Variations

Several analyses were conducted to investigate the effect of Poisson's ratio parameter variations. In these analyses, a three step horizontal excavation sequence was also employed and the modulus parameters were held constant at  $K = 100,00$ ,  $n = 0.2$  and  $R_f = 0.5$ . The value of  $d$  was held constant at 100.0 since the results shown in Chapter 3 indicated that  $d$  variations were small and also because analysis of the data presented in Chapter 3 showed that nonlinearity of Poisson's ratio is less than that of the modulus, the effect of which has already been shown to be very small. The values of  $G$  were varied from 0.1 to 0.3 and the values of  $F$  were varied from -0.05 to +0.05. These values were selected to cover the range of these parameters found for most of the rock types discussed in Chapter 3.

The dimensionless  $\sigma_1$  values obtained from these analyses were essentially the same as each other as well as those obtained for the modulus variations shown in Figure 4-38. The dimensionless  $\sigma_3$  contours varied to a small degree and the bounding variations are shown in Figures 4-42 and 4-43, which show that the variations are small and do not differ by more than 10% or so.

The bounding displacements for these cases of Poisson's ratio parameter variations are shown in Figure 4-44. This figure shows that, regardless of variations

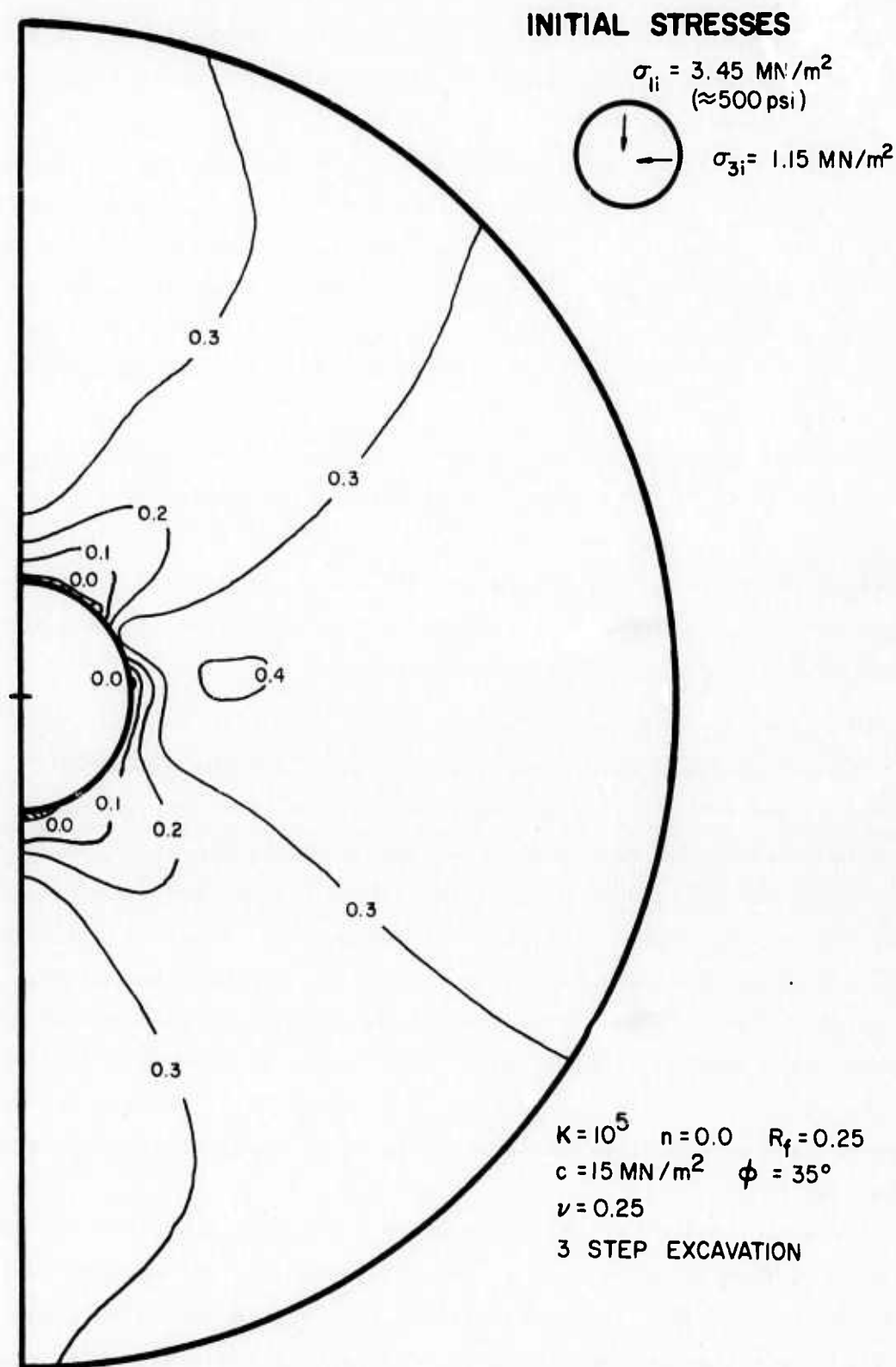


**FIG. 4-39   CONTOURS OF  $\sigma_3/\sigma_{li}$  FOR CIRCULAR OPENING  
IN NONLINEAR ROCK,  $K = 1/3$ ,  $\theta = 0^\circ$   
(NONLINEAR MODULUS)**

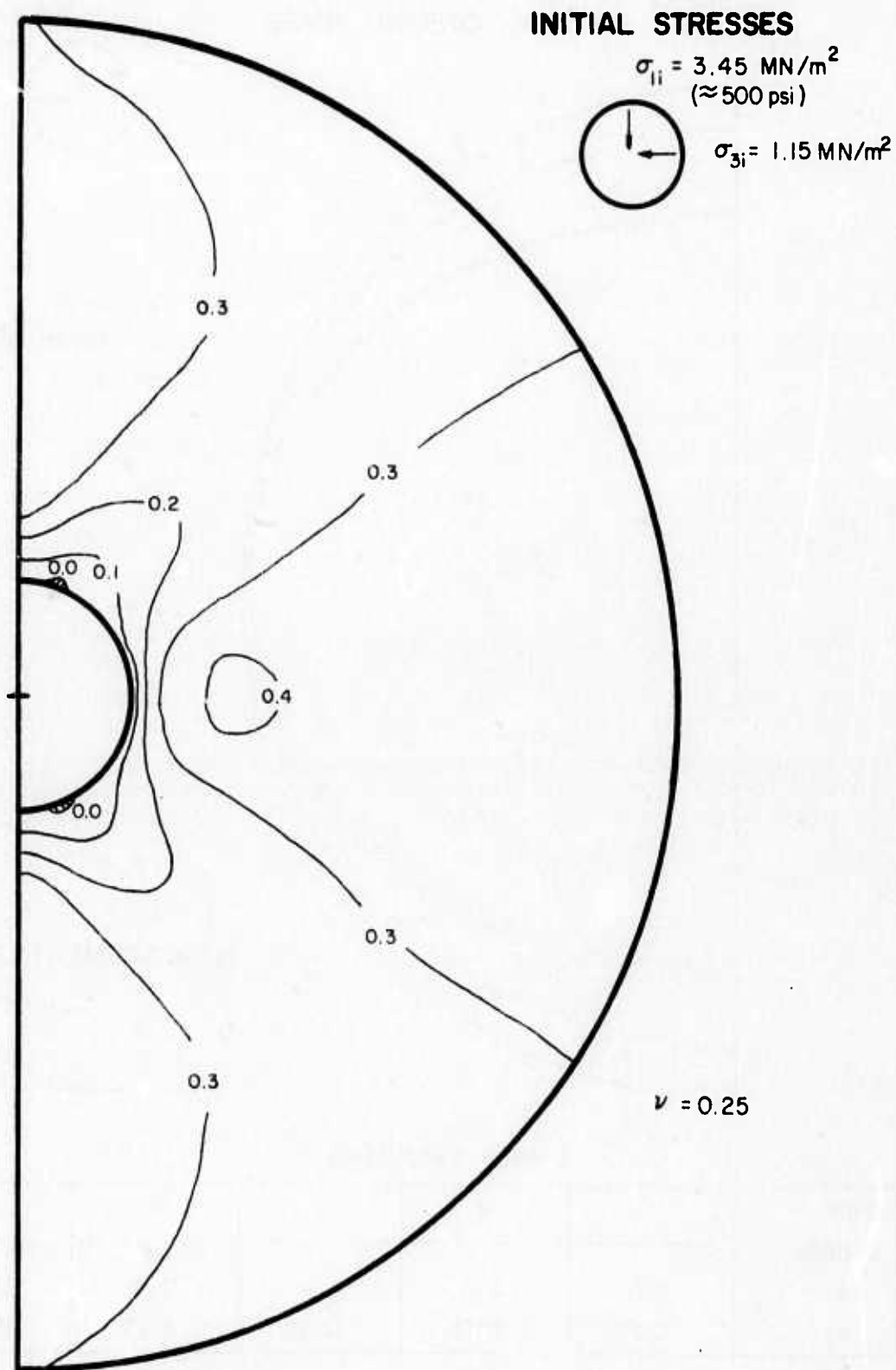
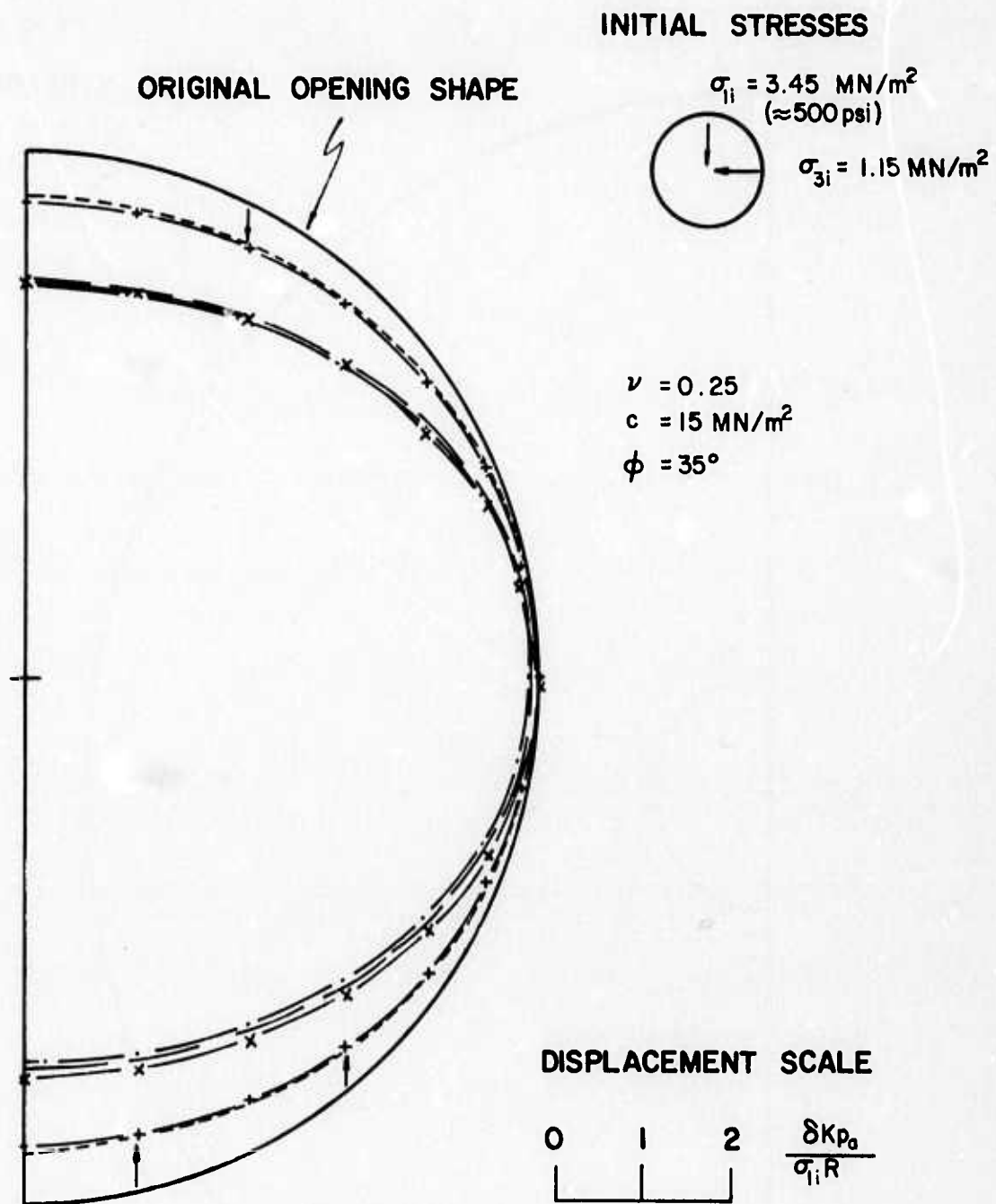


**FIG. 4-40 CONTOURS OF  $\sigma_3/\sigma_{11}$  FOR CIRCULAR OPENING IN HOMOGENEOUS LINEAR ROCK,  $K=1/3$ ,  $\theta=0^\circ$**



**3 STEP EXCAVATION**

CASE SYMBOL	1	2	3	4	5
n	0.0	0.0	0.4	0.4	0.0
R <sub>f</sub>	0.25	0.75	0.25	0.75	LINEAR

**FIG. 4-41 DISPLACEMENTS OF CIRCULAR OPENING IN NONLINEAR ROCK,  $K=1/3$ ,  $\theta=0^\circ$  (NONLINEAR MODULUS)**

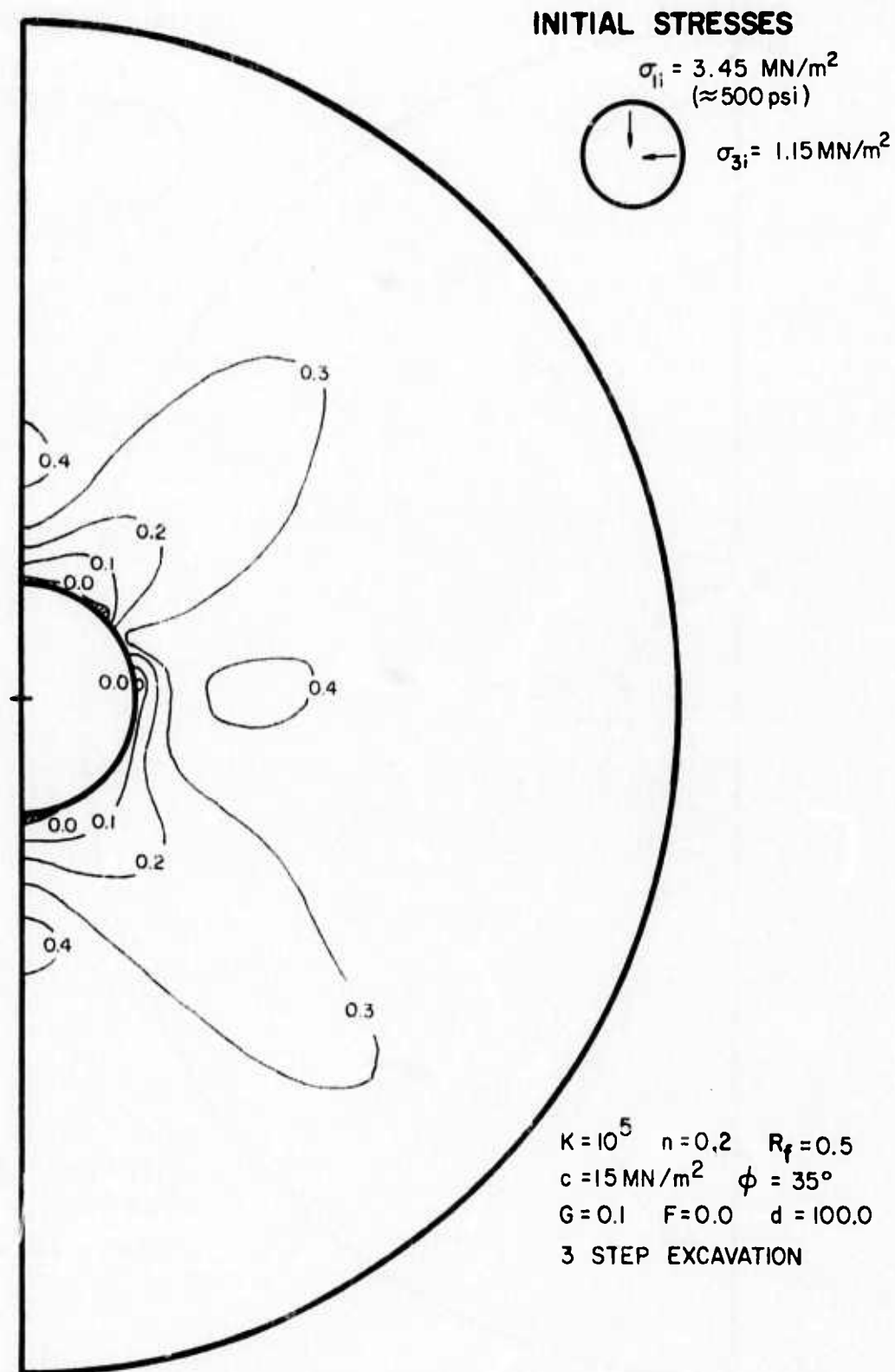


**FIG. 4-42 CONTOURS OF  $\sigma_3/\sigma_{1i}$  FOR CIRCULAR OPENING  
IN NONLINEAR ROCK,  $K=1/3$ ,  $\theta=0^\circ$   
(NONLINEAR MODULUS AND POISSON'S RATIO)**

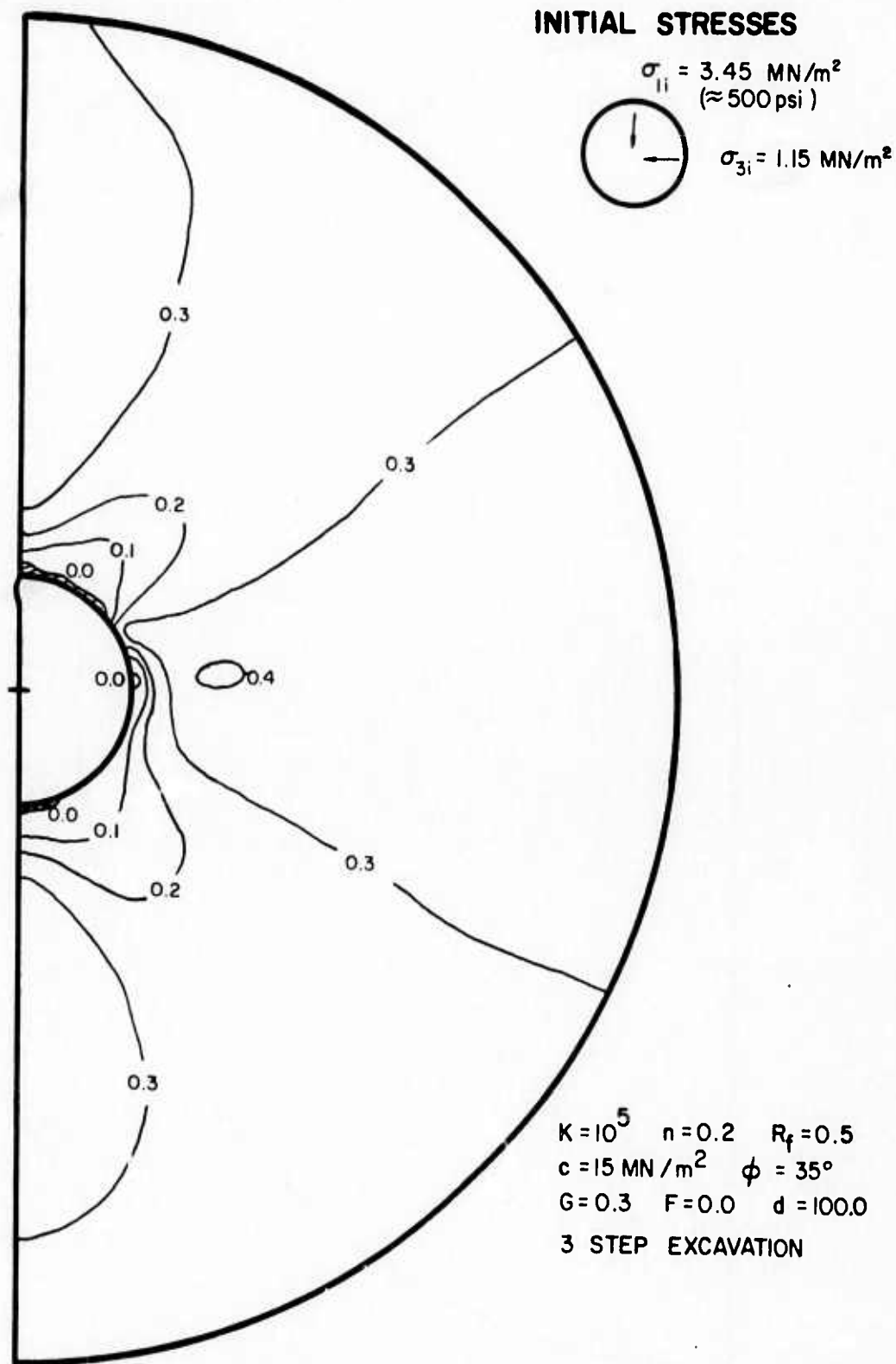


**FIG. 4-43 CONTOURS OF  $\sigma_3/\sigma_{11}$  FOR CIRCULAR OPENING IN NONLINEAR ROCK,  $K = 1/3$ ,  $\theta = 0^\circ$  (NONLINEAR MODULUS AND POISSON'S RATIO)**



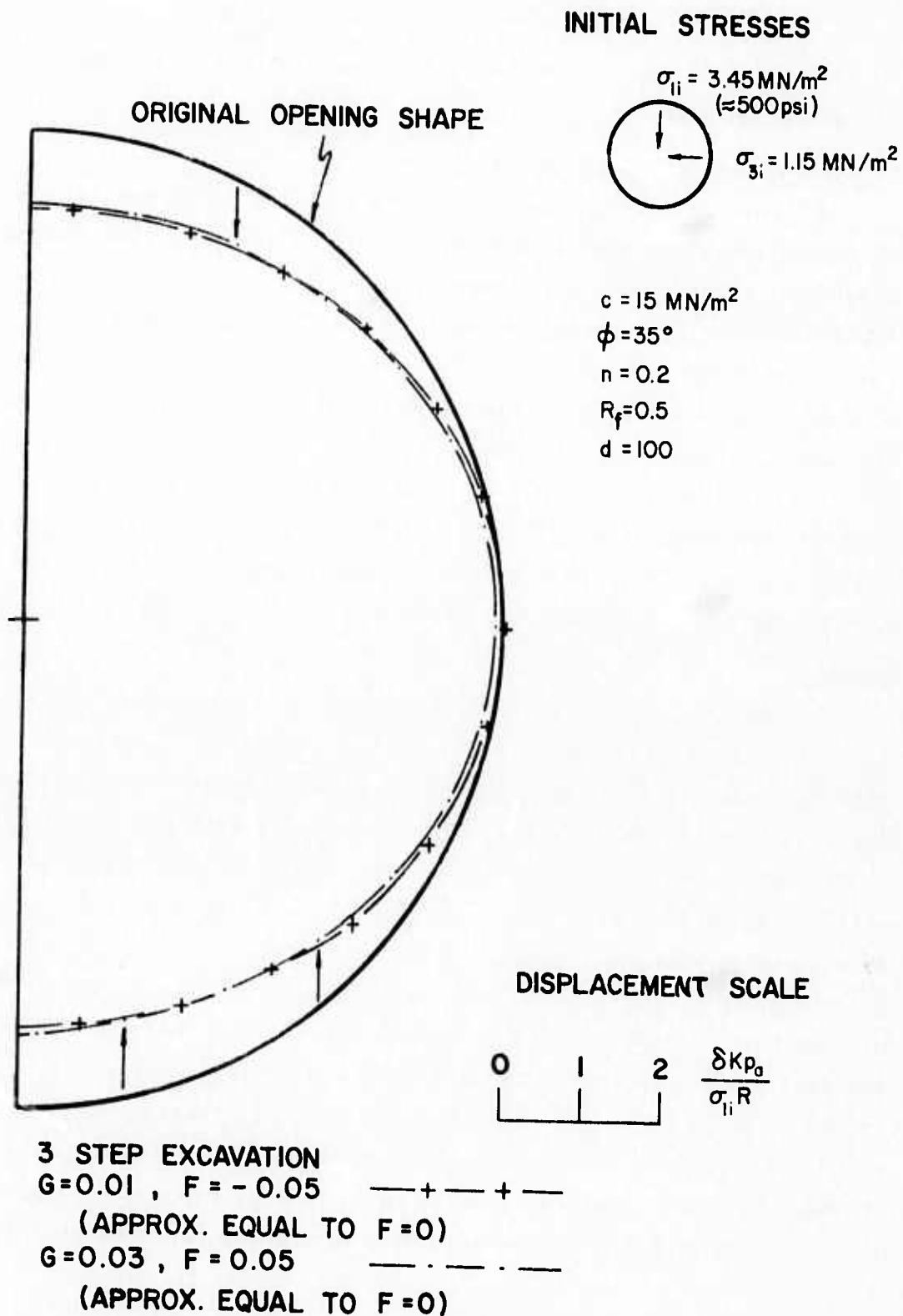


**FIG. 4-44 DISPLACEMENTS OF CIRCULAR OPENING  
IN NONLINEAR ROCK,  $K=1/3, \theta=0^\circ$   
(NONLINEAR MODULUS AND POISSON'S RATIO)**

in the Poisson's ratio parameters, the dimensionless displacements will be virtually the same.

#### Excavation Step and Sequence Variation

A number of analyses were conducted to investigate the effects of number of excavation steps and excavation sequence on the resulting stresses and displacements of an underground opening. One step, three step horizontal and three step vertical excavation sequences were employed (See Figure 4-3.). The results of these studies showed that, regardless of excavation sequence, number of excavation steps or material property variations, the results were essentially the same as those presented previously. Furthermore, it should be noted that, in all of the cases analyzed, no shear failure occurred anywhere within the modeled rock mass, leading to the conclusion that excavation operations have little, if any, significant effect on the resulting stresses and displacements around underground openings in homogeneous isotropic rock.

#### Summary

The analyses presented in this chapter were conducted to investigate the importance of material properties, initial stresses, excavation operations and opening shapes on the final stresses and displacements around underground openings in homogeneous rock masses. The results of these analyses showed that opening shape, initial stress magnitude, initial stress orientation and gravity initial stresses, when shallow, effect the resulting stresses and displacements considerably, while the modulus, in a linear analysis, or the initial tangent stiffness and stress-dependency in a nonlinear analysis, greatly effect the displacements. Poisson's ratio variations cause relatively small effects on the stresses and displacements and all other parameters cause minor, if any, variations. It should be noted that in all of these analyses, representative strength parameters were used. The mobilized shear stresses which resulted were small and subsequently no shear failures occurred. Furthermore, tension zones were allowed to develop and no analysis modifications were made to account for tension failure.

## CHAPTER 5

### ANALYSIS OF OPENINGS IN ROCK CONTAINING A SINGLE PLANAR TWO-DIMENSIONAL DISCONTINUITY

Many types of rock masses cannot be treated as homogeneous continua because of natural discontinuities which pervade the mass. Foremost among these are faults, seams, sheared zones and crushed zones which are all nearly linear features of finite width composed of material substantially different in physical properties from the parent rock mainly because of alteration or weathering. The discontinuity is in effect a weakness plane which may substantially alter the stress and displacement pattern around an underground opening in rock. Therefore the studies presented in this chapter were conducted to evaluate the effect of a single prominent discontinuity on the resulting stress and displacement around underground openings in rock.

#### Finite Element Idealization

In this Chapter, all of the analyses were conducted using a circular opening with a three meter radius and a discontinuity with a width of 2/3 meter. This was the minimum width which could be used in the mesh selected so that the length to width ratio of the elements would not exceed five. Discontinuity orientations analyzed were horizontal, vertical and at  $45^{\circ}$  counterclockwise from horizontal. The term  $\alpha$  was used to denote the orientation on the figures. The finite element meshes used are shown in Figures 5-1 and 5-2; Figure 5-1 is also representative of the vertical discontinuity mesh by rotating the axes  $90^{\circ}$ . All analyses were conducted using a one step excavation sequence.

The initial stresses were constant with depth and in all cases the initial vertical stresses were equal to  $3.45 \text{ MN/m}^2$  ( $\approx 500 \text{ psi}$ ) while the initial horizontal stresses were varied at 1/3, 1 and 2 times the vertical. A Poisson's ratio value of 0.25 was used for both the intact rock and the discontinuity. Different discontinuity stiffnesses were modeled by varying the ratio of rock

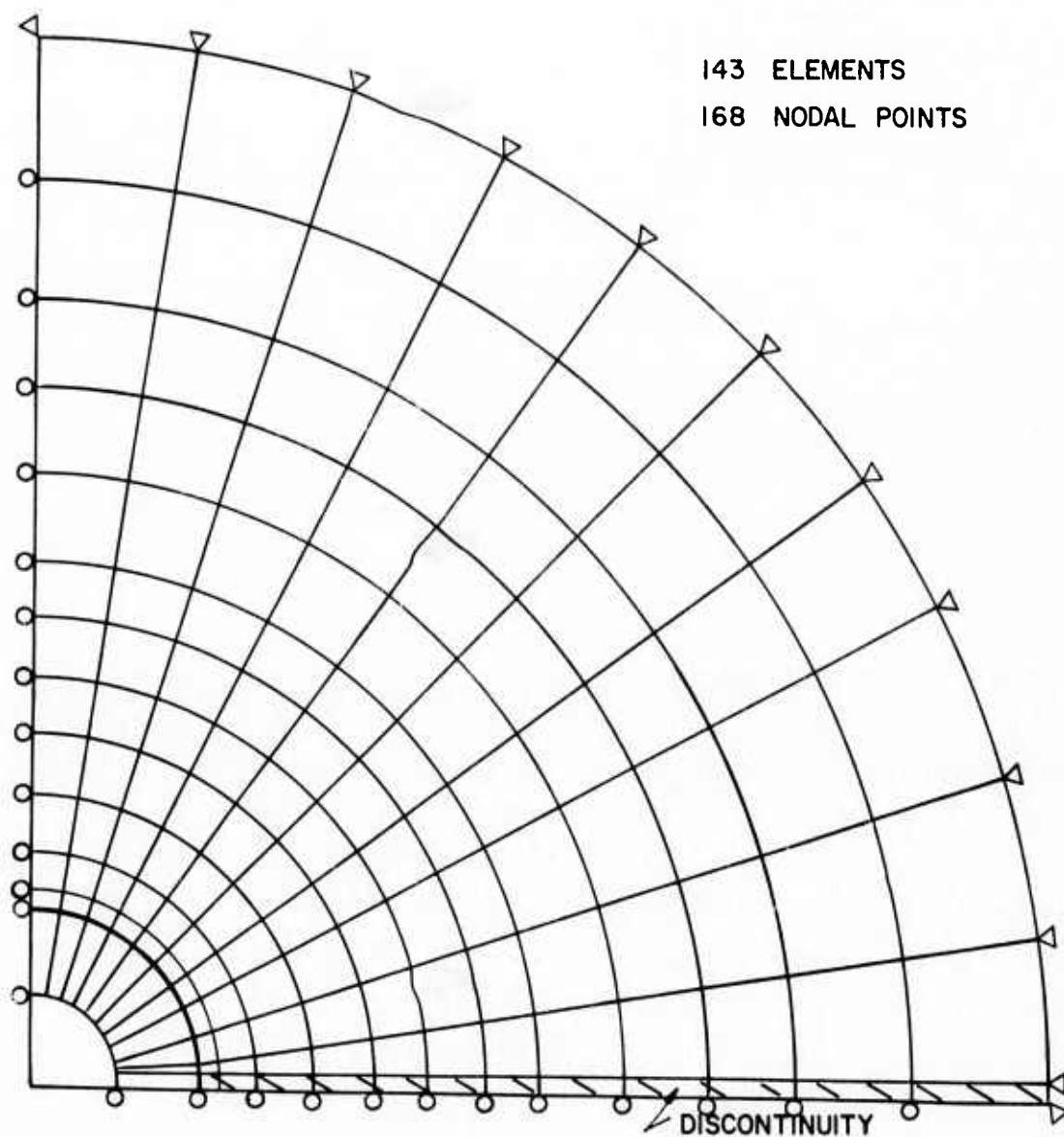


**FIG. 5-1 FINITE ELEMENT MESH FOR  
CIRCULAR OPENING IN ROCK  
WITH A PLANAR DISCONTINUITY**

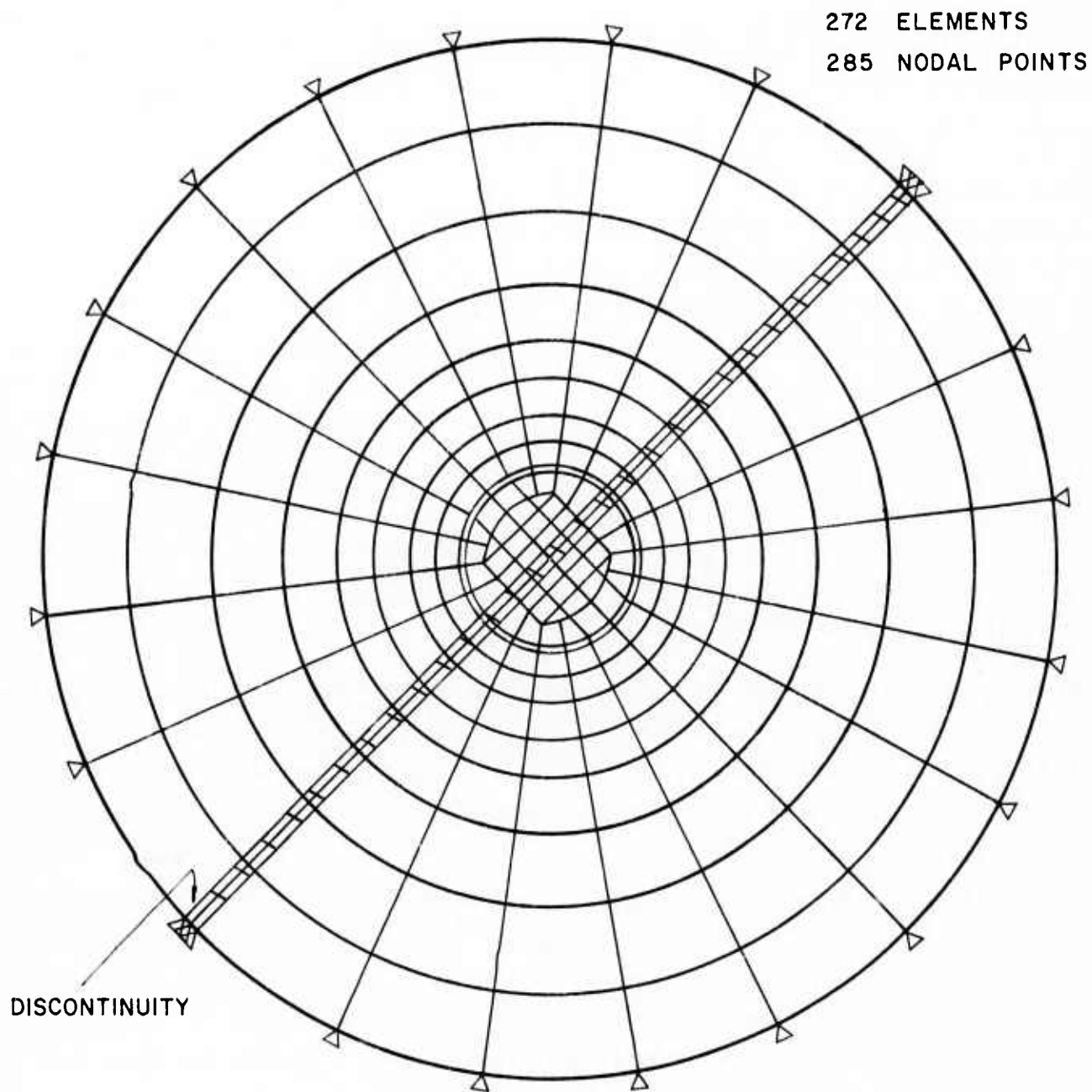


**FIG. 5-2 FINITE ELEMENT MESH FOR CIRCULAR OPENING  
IN ROCK WITH A PLANAR DISCONTINUITY AT 45°**

modulus to discontinuity *modulus*, denoted by  $M$  on the figures. The values of  $M$  were used 10, 100 and 1000 such that a low  $M$  would indicate a relatively stiff discontinuity, while a high  $M$  value would indicate a relatively soft discontinuity. The cases comparable to  $M = 1$  (no discontinuity) were discussed in Chapter 4 and were shown in Figures 4-16 through 4-18.

#### Stresses Around Opening

Analysis of the 27 cases in which the initial stresses, discontinuity orientations and modulus ratios were varied, and the three comparable cases with no discontinuities ( $M = 1$ ) showed that several points were common in all comparisons. These were: (1) as the discontinuity becomes softer, i.e., larger  $M$  values, the stresses change markedly with the largest changes occurring near and along the discontinuities, (2) the stress changes are substantial when  $M$  goes from 1 to 10, are fairly important when  $M$  goes from 10 to 100 and are minor when  $M$  goes from 100 to 1000, and (3) tension zones develop around the intersection of the discontinuity and the opening face as  $M$  increases. Individual comparisons, discussed below, vary depending upon the case but the above effects were noted in all cases.

##### a) Initial Horizontal Stresses Equal to One-Third the Vertical Stresses

Figures 5-3 through 5-5 show the stress contours for the horizontal discontinuity. It can be seen that a substantial reduction occurs in the springline stress concentration factor, from more than 2.4 when  $M = 1$  to less than 1.0 when  $M = 1000$ , and also occurs in the dimensionless  $\sigma_1$  values near and in the discontinuity. Changes in the dimensionless  $\sigma_3$  contours are small with a general tendency toward a reduction in values as  $M$  increases.

Figures 5-6 through 5-8 show the stress contours for the vertical discontinuity. The resulting pattern with the dimensionless  $\sigma_1$  contours is different because the springline stress concentration factors do not vary significantly, but the  $\sigma_1$  values increase substantially within the discontinuity while a decrease occurs adjacent to the discontinuity near the opening face. The general pattern with the  $\sigma_3$  contours is of the same form as for the horizontal discontinuity, i.e., a small reduction as  $M$  increases.

Figures 5-9 through 5-12 show the stress contours for the  $45^\circ$  discontinuity. The  $M = 100$  contours are not shown because the  $M = 10$  and  $M = 1000$  contours are not materially different. The same pattern develops for the other initial stress



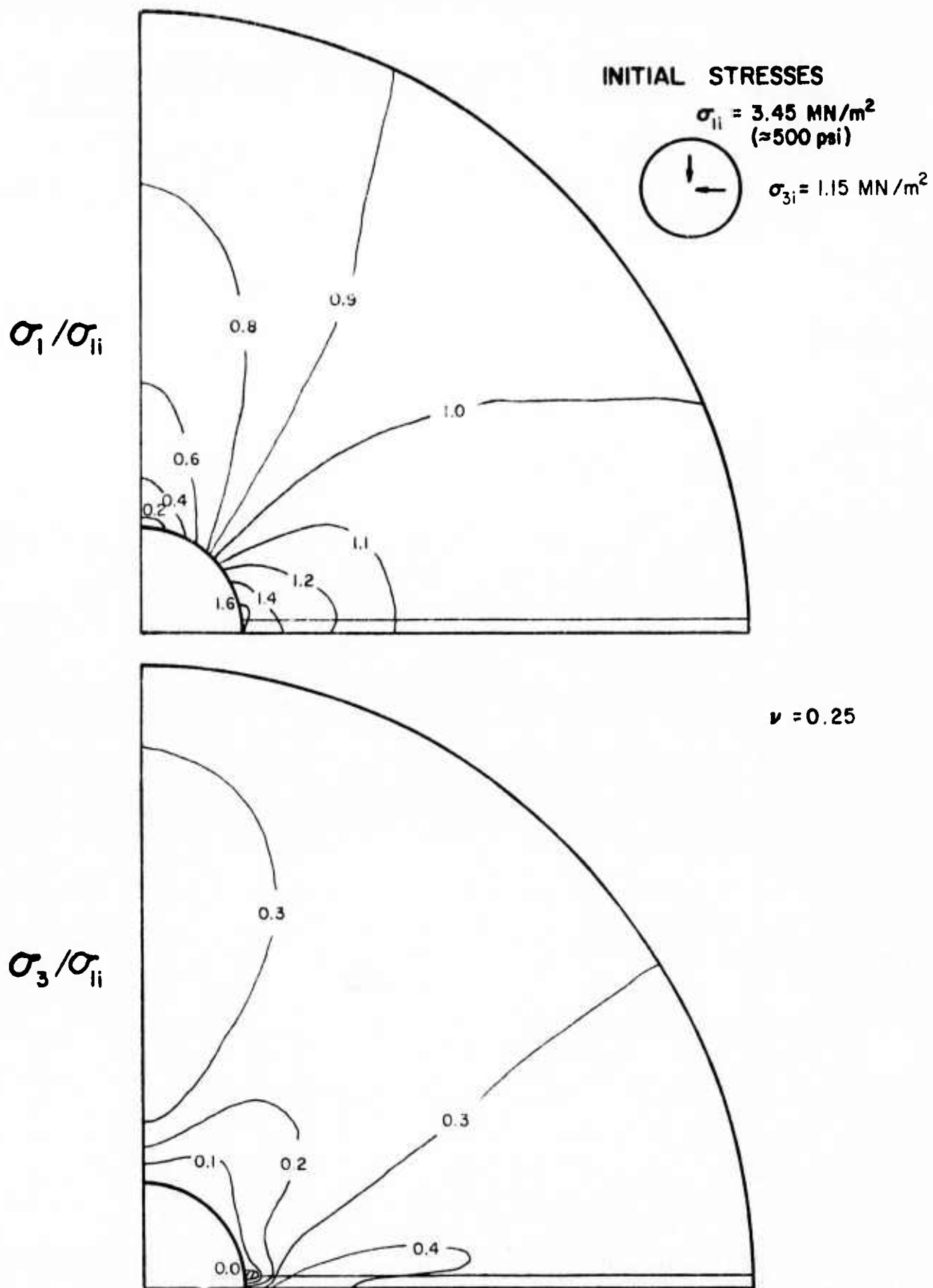


**FIG. 5-3 STRESS CONTOURS FOR CIRCULAR OPENING  
 IN ROCK WITH A PLANAR DISCONTINUITY  
 $K = 1/3$ ,  $\theta = 0^\circ$ ,  $\alpha = 0^\circ$ ,  $M = 10$**

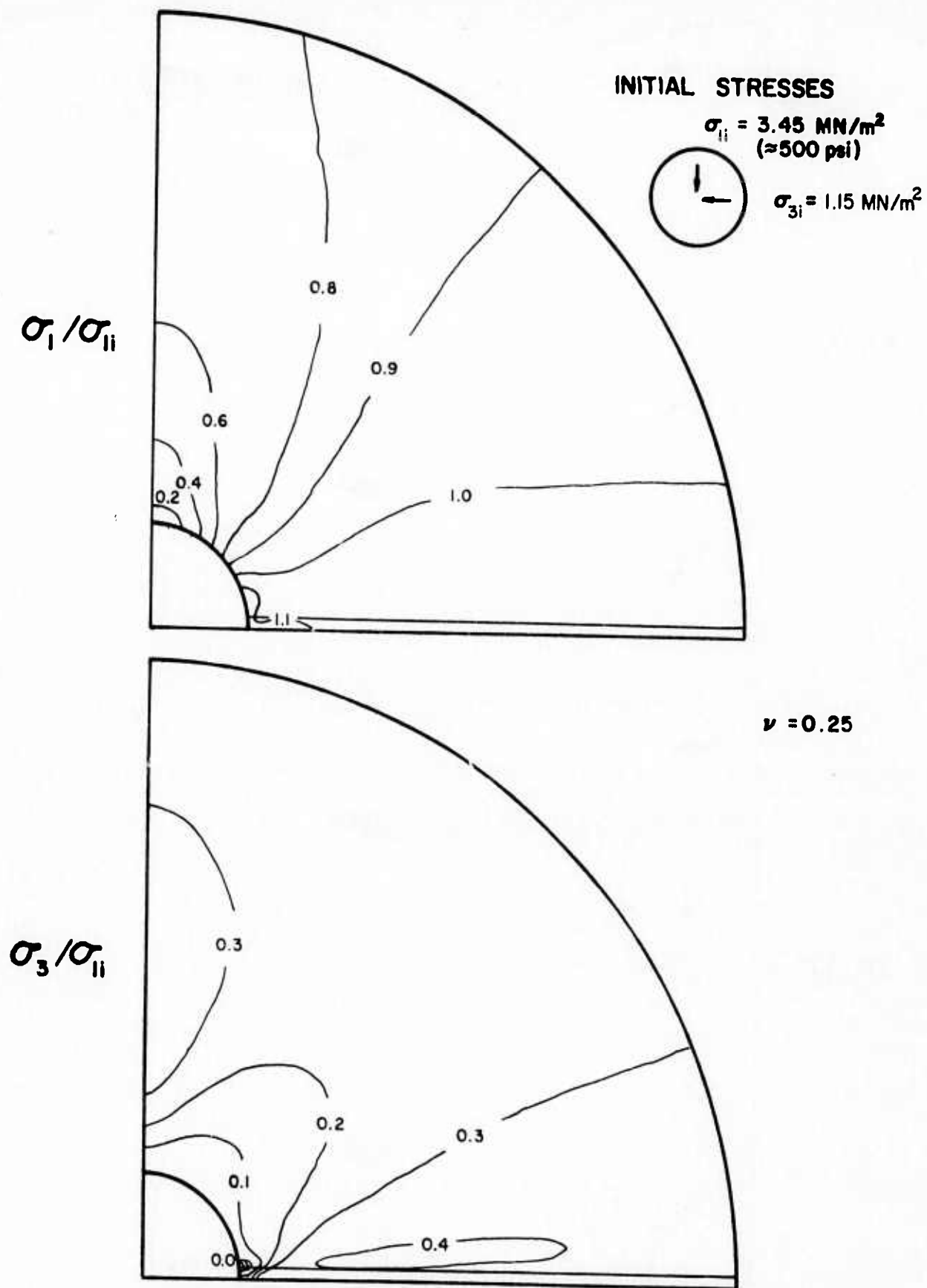


**FIG. 5-4 STRESS CONTOURS FOR CIRCULAR OPENING  
 IN ROCK WITH A PLANAR DISCONTINUITY  
 $K = 1/3$ ,  $\theta = 0^\circ$ ,  $\alpha = 0^\circ$ ,  $M = 100$**

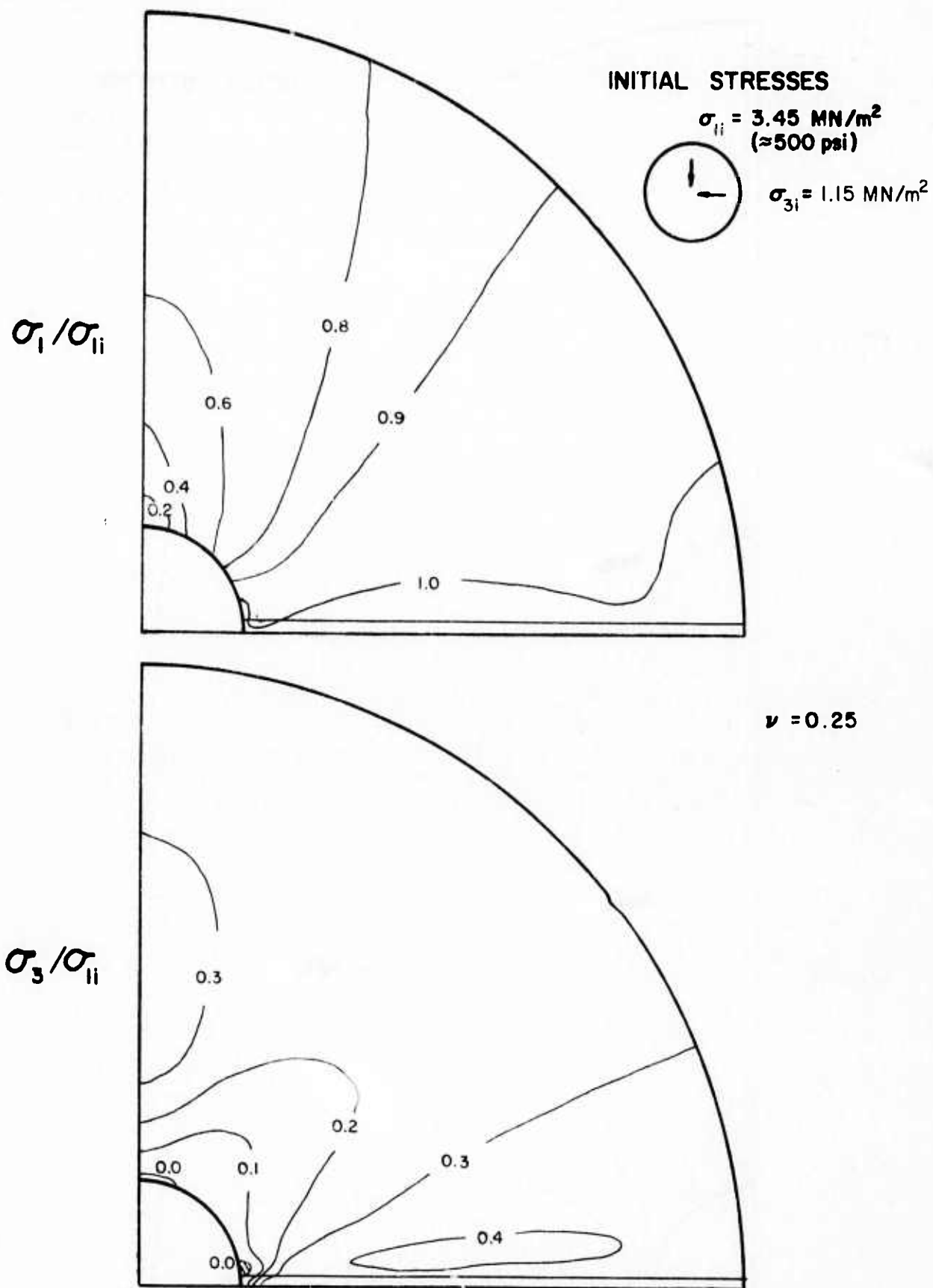


**FIG. 5-5 STRESS CONTOURS FOR CIRCULAR OPENING  
 IN ROCK WITH A PLANAR DISCONTINUITY  
 $K=1/3$ ,  $\theta=0^\circ$ ,  $\alpha=0^\circ$ ,  $M=1000$**

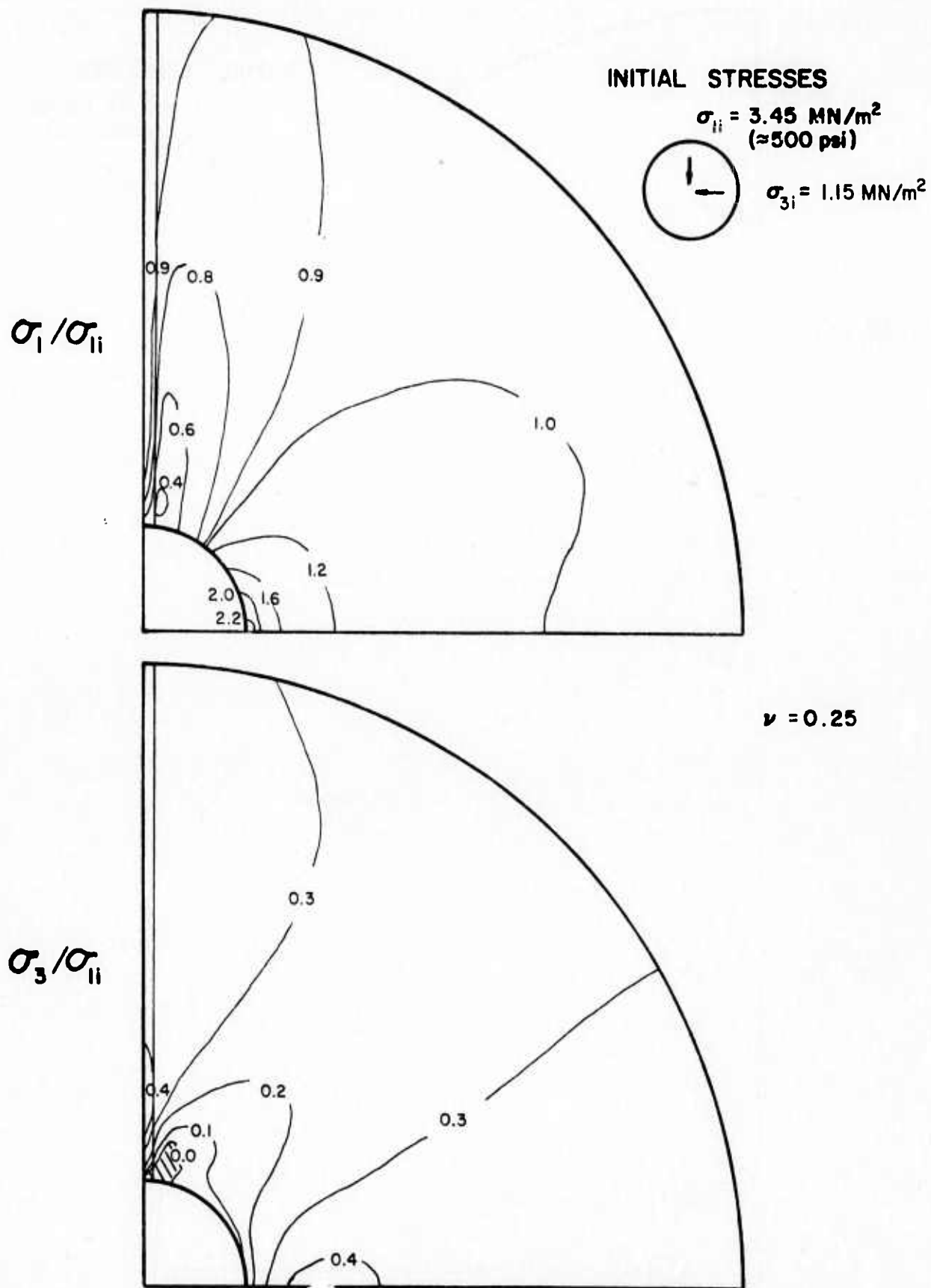


**FIG. 5-6 STRESS CONTOURS FOR CIRCULAR OPENING  
 IN ROCK WITH A PLANAR DISCONTINUITY  
 $K = 1/3$ ,  $\theta = 0^\circ$ ,  $\alpha = 90^\circ$ ,  $M = 10$**

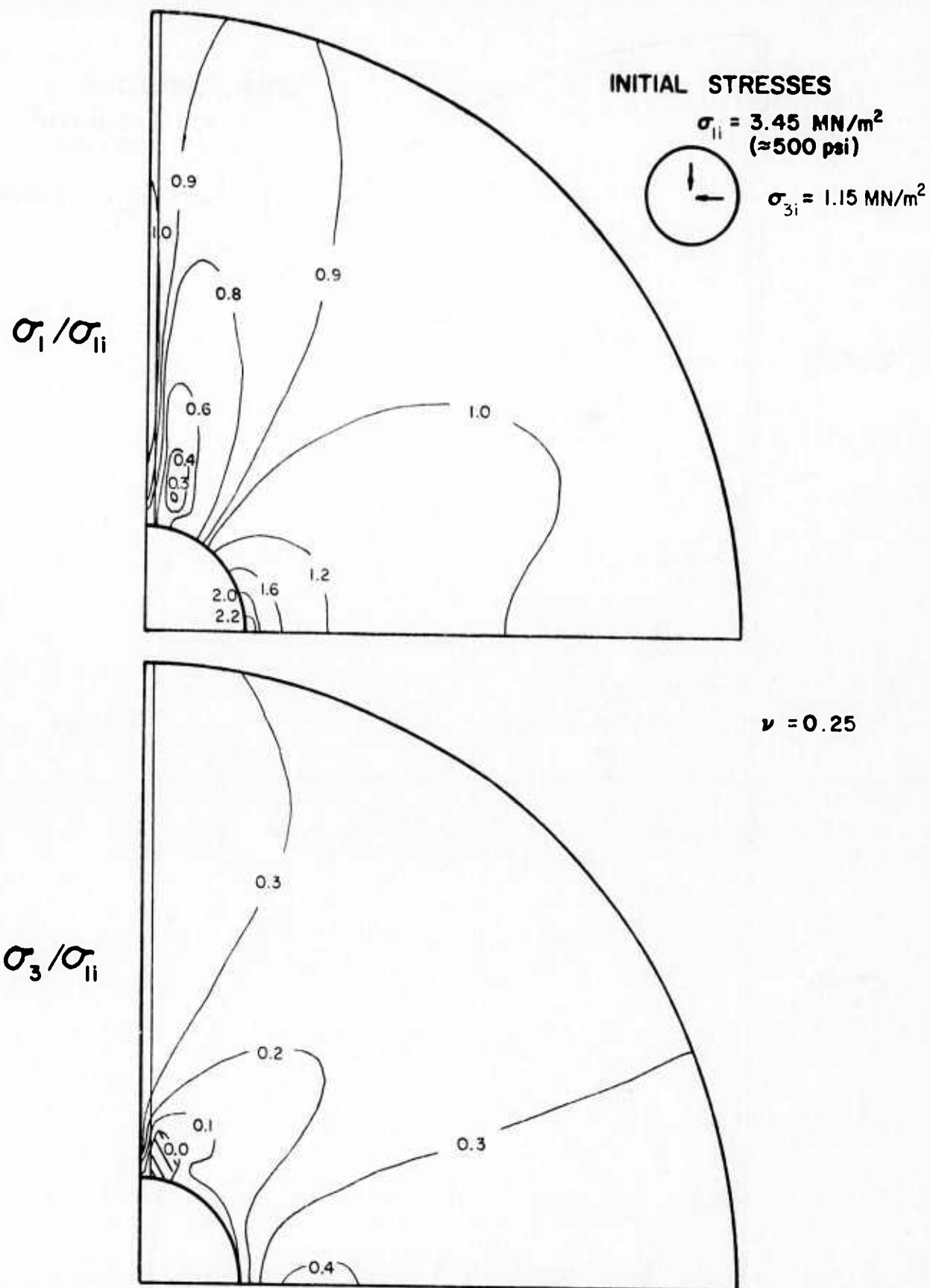


**FIG. 5-7 STRESS CONTOURS FOR CIRCULAR OPENING  
 IN ROCK WITH A PLANAR DISCONTINUITY  
 $K = 1/3$ ,  $\theta = 0^\circ$ ,  $\alpha = 90^\circ$ ,  $M = 100$**

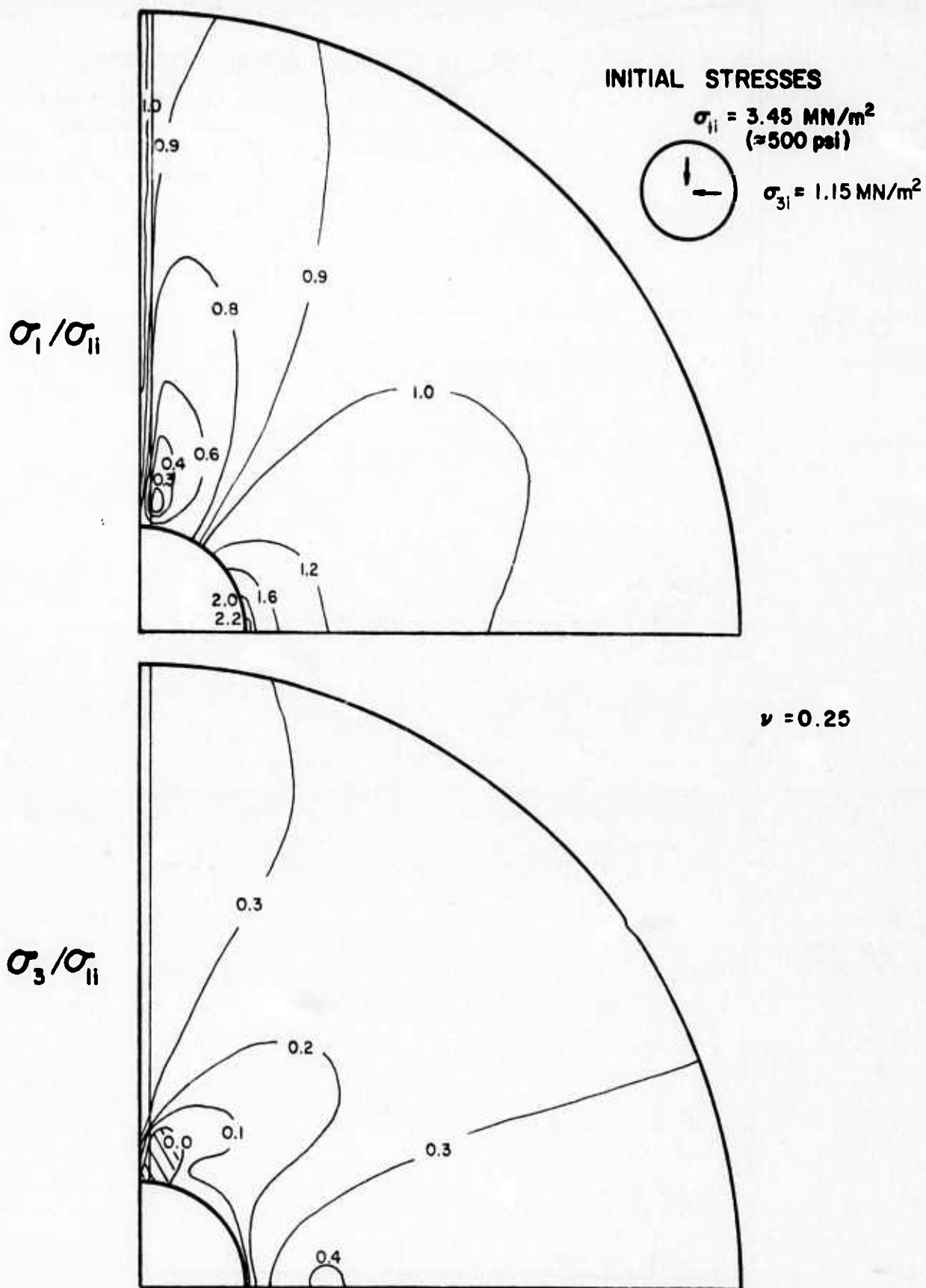


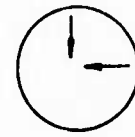
**FIG. 5-8 STRESS CONTOURS FOR CIRCULAR OPENING  
IN ROCK WITH A PLANAR DISCONTINUITY  
 $K = 1/3$ ,  $\theta = 0^\circ$ ,  $\alpha = 90^\circ$ ,  $M = 1000$**



INITIAL STRESSES

$$\sigma_{1i} = 3.45 \text{ MN/m}^2$$

( $\approx 500 \text{ psi}$ )



$$\sigma_{3i} = 1.15 \text{ MN/m}^2$$

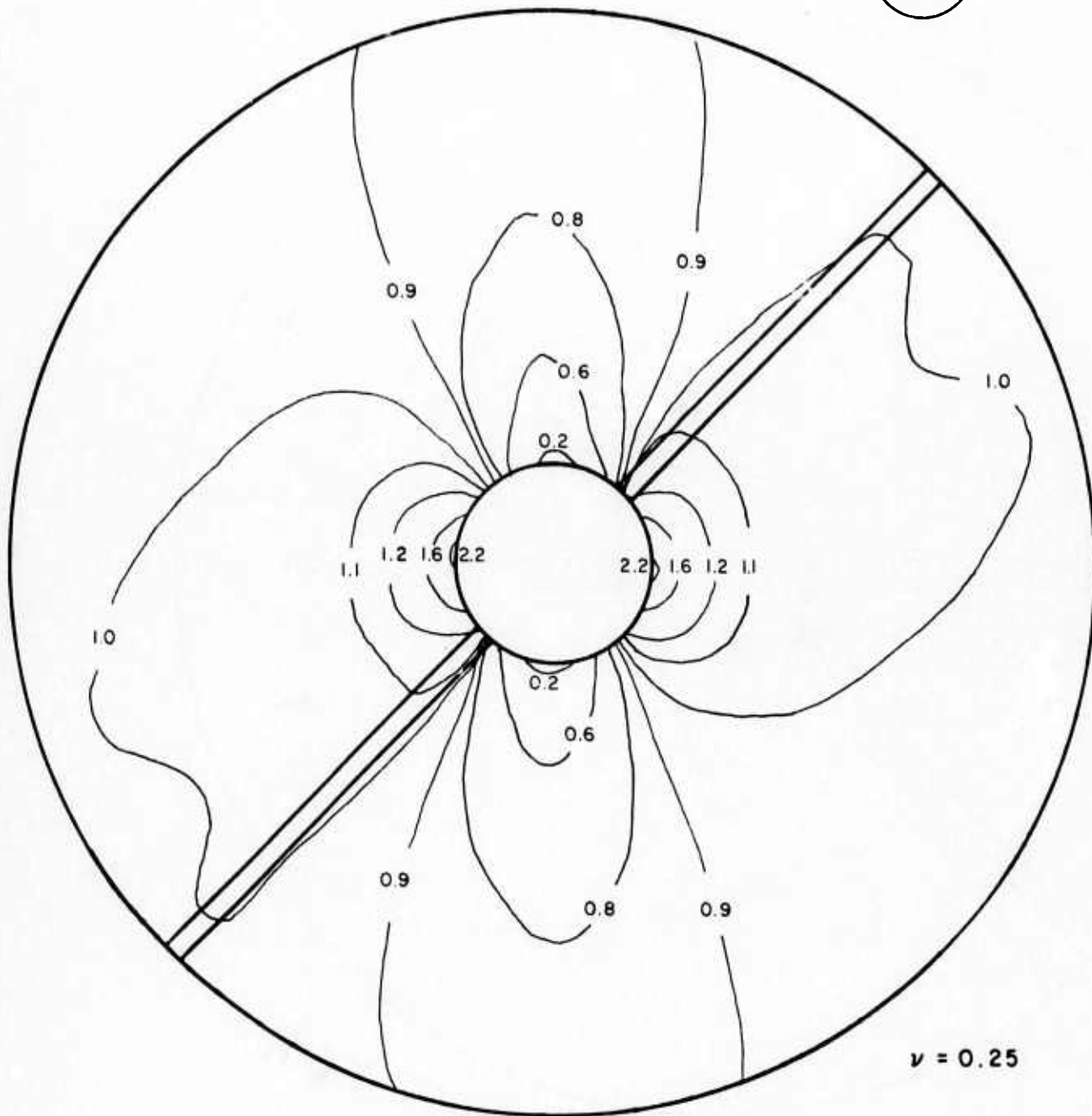
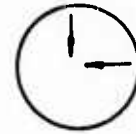


**FIG. 5-9 CONTOURS OF  $\sigma_t/\sigma_{1i}$  FOR CIRCULAR OPENING  
IN ROCK WITH A PLANAR DISCONTINUITY  
 $K=1/3$ ,  $\theta=0^\circ$ ,  $\alpha=45^\circ$ ,  $M=10$**

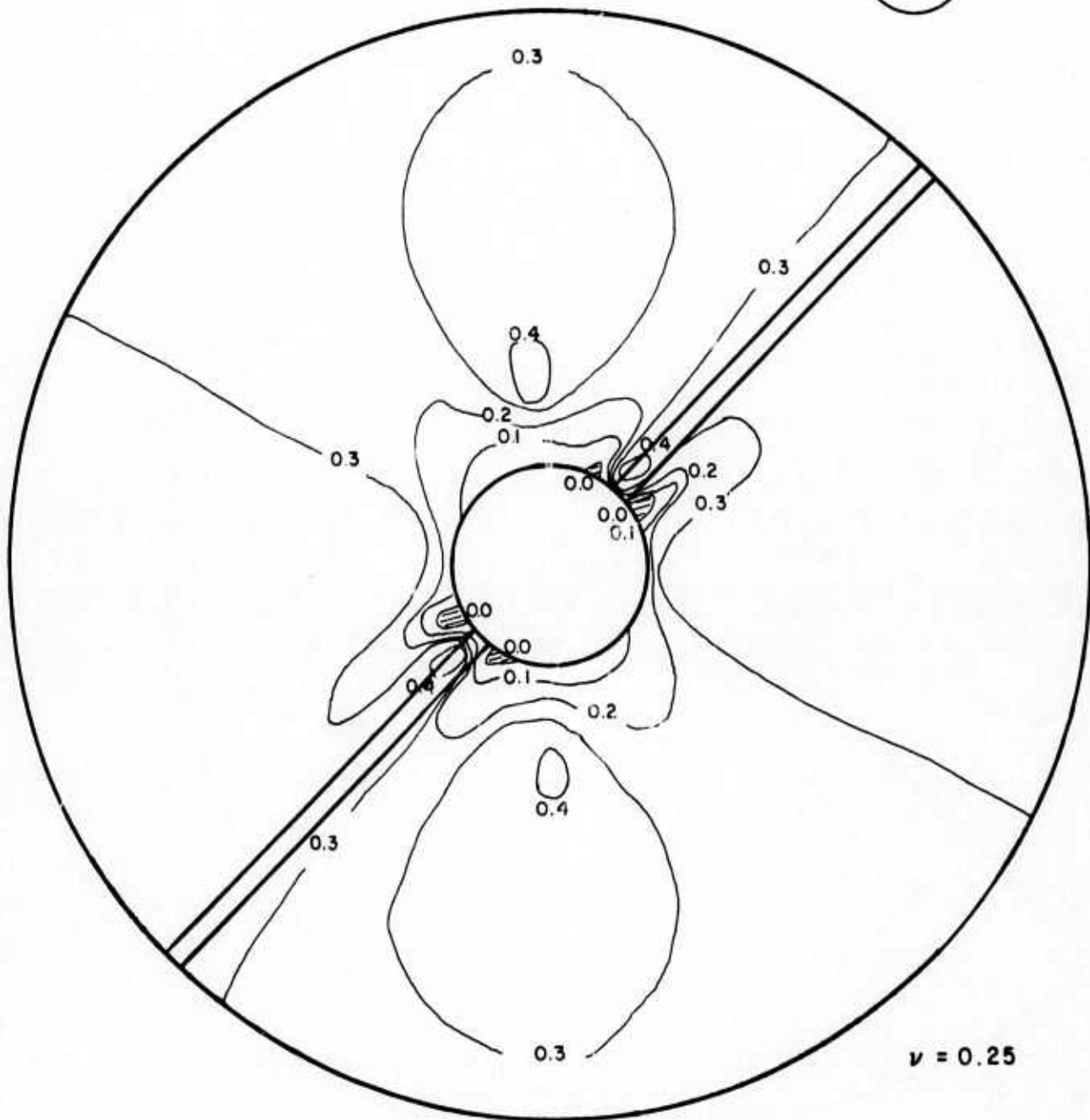
INITIAL STRESSES

$$\sigma_{ii} = 3.45 \text{ MN/m}^2$$

( $\approx 500 \text{ psi}$ )



$$\sigma_{3i} = 1.15 \text{ MN/m}^2$$



$$\nu = 0.25$$

**FIG. 5-10 CONTOURS OF  $\sigma_3/\sigma_{ii}$  FOR CIRCULAR OPENING  
IN ROCK WITH A PLANAR DISCONTINUITY  
 $K=1/3$ ,  $\theta=0^\circ$ ,  $\alpha=45^\circ$ ,  $M=10$**

INITIAL STRESSES

$$\sigma_{1i} = 3.45 \text{ MN/m}^2$$

( $\approx 500 \text{ psi}$ )



$$\sigma_{3i} = 1.15 \text{ MN/m}^2$$

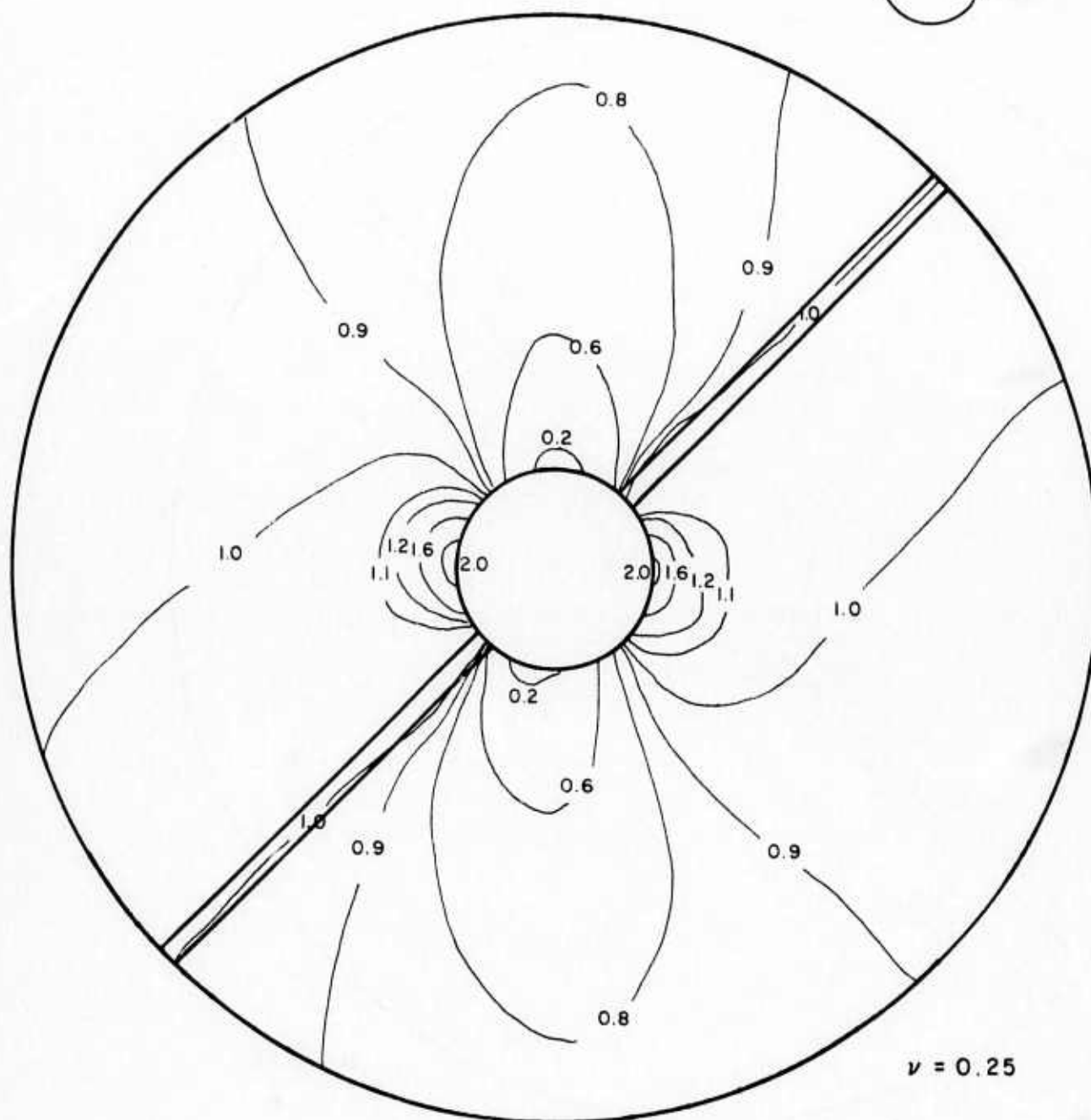
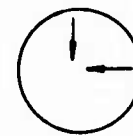


**FIG. 5-II CONTOURS OF  $\sigma_1/\sigma_{1i}$  FOR CIRCULAR OPENING  
IN ROCK WITH A PLANAR DISCONTINUITY  
 $K=1/3$ ,  $\theta=0^\circ$ ,  $\alpha=45^\circ$ ,  $M=1000$**

INITIAL STRESSES

$$\sigma_{1i} = 3.45 \text{ MN/m}^2$$

( $\approx 500 \text{ psi}$ )



$$\sigma_{3i} = 1.15 \text{ MN/m}^2$$

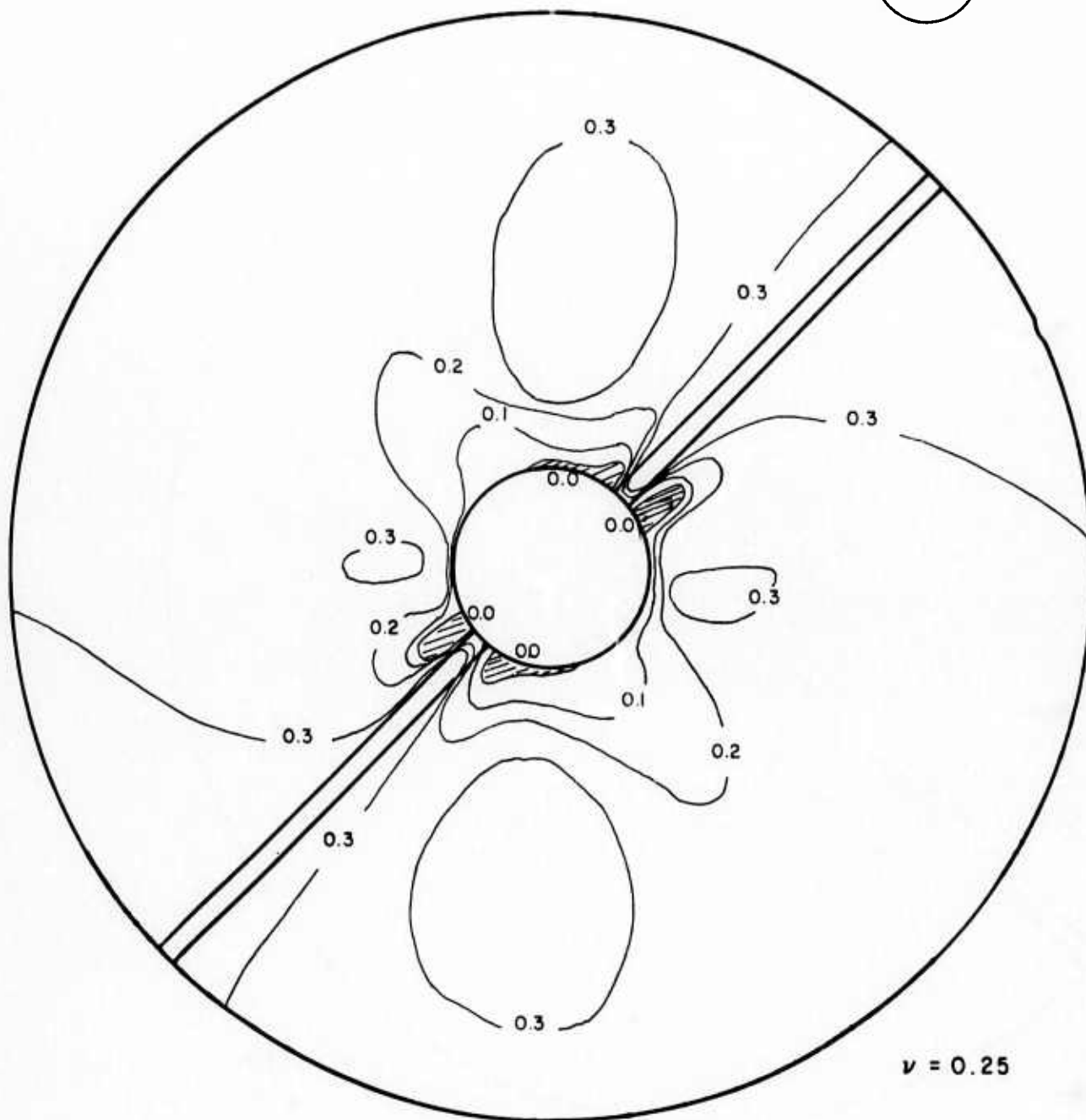


**FIG. 5-12 CONTOURS OF  $\sigma_3/\sigma_{1i}$  FOR CIRCULAR OPENING  
IN ROCK WITH A PLANAR DISCONTINUITY  
 $K=1/3$ ,  $\theta=0^\circ$ ,  $\alpha=45^\circ$ ,  $M=1000$**

conditions as well, so the  $M = 100$  contours have not been included for any of the solutions with a  $45^\circ$  discontinuity. For both the dimensionless  $\sigma_1$  and  $\sigma_3$  contours, the changes are generally small, with a decrease in the crown and springline stresses as  $M$  increases. The stresses within the discontinuity show a decrease in  $\sigma_1$  and  $\sigma_3$  as  $M$  increases.

b) Initial Horizontal Stresses Equal to the Vertical Stresses

The stress contours for the horizontal discontinuity are shown in Figures 5-13 through 5-15. These figures show that for  $\sigma_1$ , the crown stresses decrease slightly while the discontinuity stresses decrease greatly as  $M$  increases. For  $\sigma_3$  the crown stresses decrease slightly while the discontinuity stresses increase greatly as  $M$  increases. When the discontinuity is vertical, as shown in Figures 5-16 through 5-18, the results are the same as the horizontal with the axes shifted by  $90^\circ$ .

When the discontinuity is oriented at  $45^\circ$ , as shown in Figures 5-19 through 5-22, the dimensionless  $\sigma_1$  values decrease in general with large decreases in the discontinuity. The maximum stress concentration decreases slightly as well. The  $\sigma_3$  values decrease in most areas but increase substantially within the discontinuity. It is interesting to note that, in these cases, the maximum stress concentration is located perpendicular to the discontinuity where normally it would be located at either the crown or springline depending upon the initial stress magnitude.

c) Initial Horizontal Stresses Equal to Twice the Vertical Stresses

Figures 5-23 through 5-25 show the stress contours for the horizontal discontinuity. The resulting pattern with the dimensionless  $\sigma_1$  contours shows that the crown stress concentration does not vary significantly, but the  $\sigma_1$  values increase substantially within the discontinuity while a decrease occurs adjacent to the discontinuity near the opening face. Changes in the dimensionless  $\sigma_3$  contours are small with a general tendency toward a reduction in values as  $M$  increases.

The stress contours for the vertical discontinuity are shown in Figures 5-26 through 5-28. It can be seen that a substantial reduction occurs in the crown stress concentration factor, from more than 2.3 when  $M = 1$  to less than 1.0 when  $M = 1000$ , and in the dimensionless  $\sigma_1$  values near and in the discontinuity.

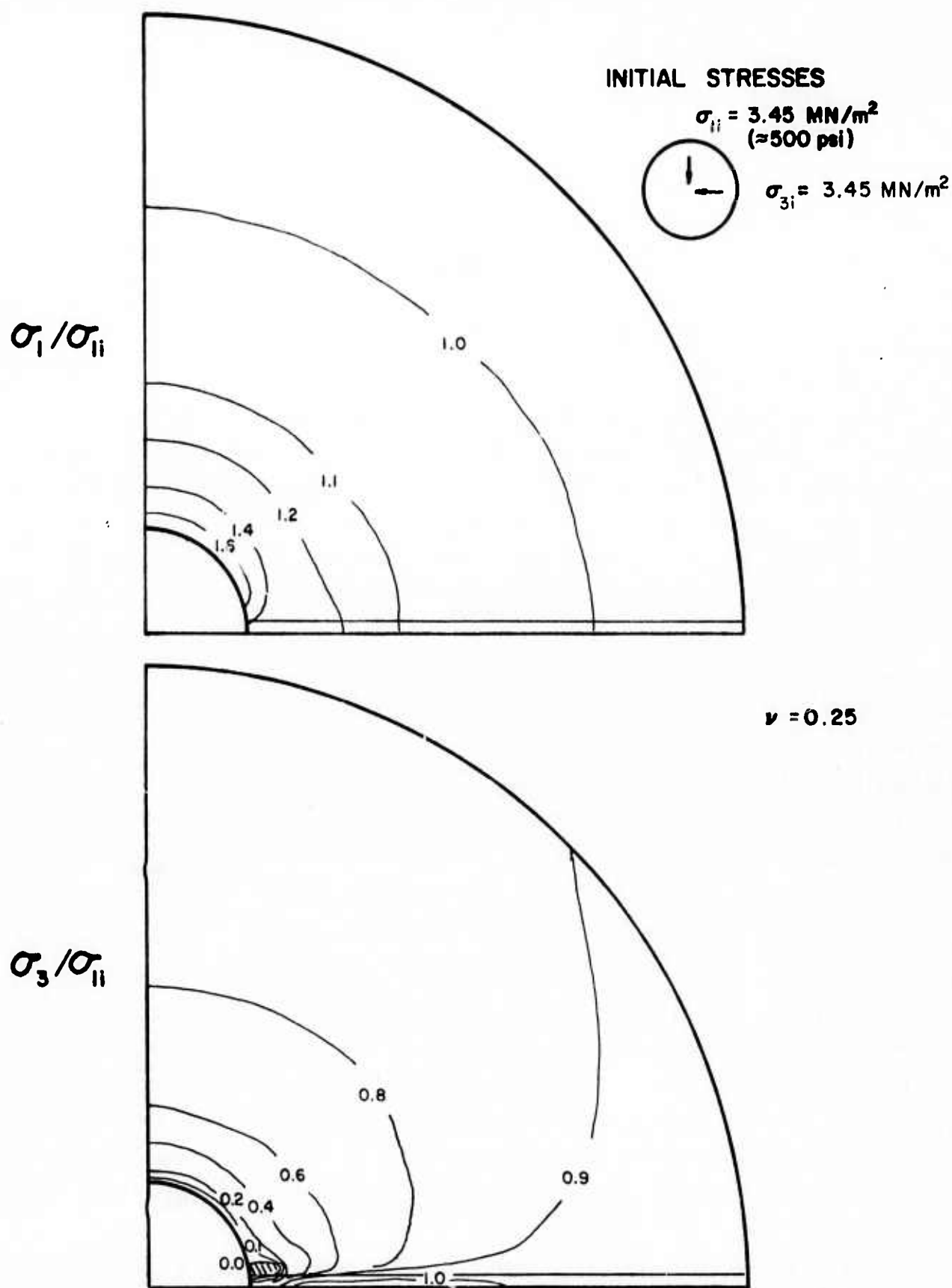


**FIG. 5-13 STRESS CONTOURS FOR CIRCULAR OPENING  
 IN ROCK WITH A PLANAR DISCONTINUITY  
 $K=1$  ,  $\theta=0^\circ$  ,  $\alpha=0^\circ$  ,  $M=10$**



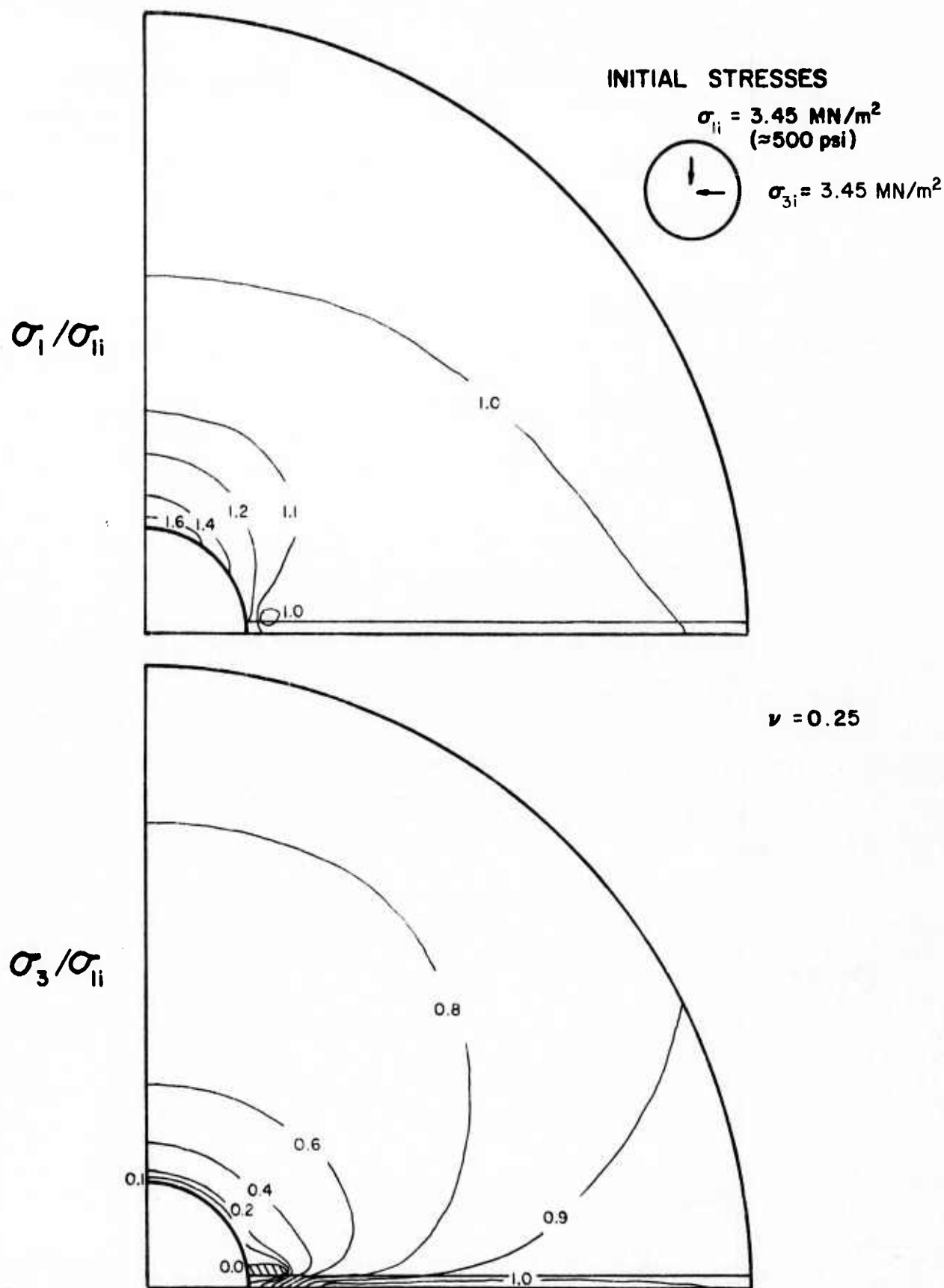


**FIG. 5-14 STRESS CONTOURS FOR CIRCULAR OPENING  
 IN ROCK WITH A PLANAR DISCONTINUITY  
 $K=1$  ,  $\theta=0^\circ$  ,  $\alpha=0^\circ$  ,  $M=100$**

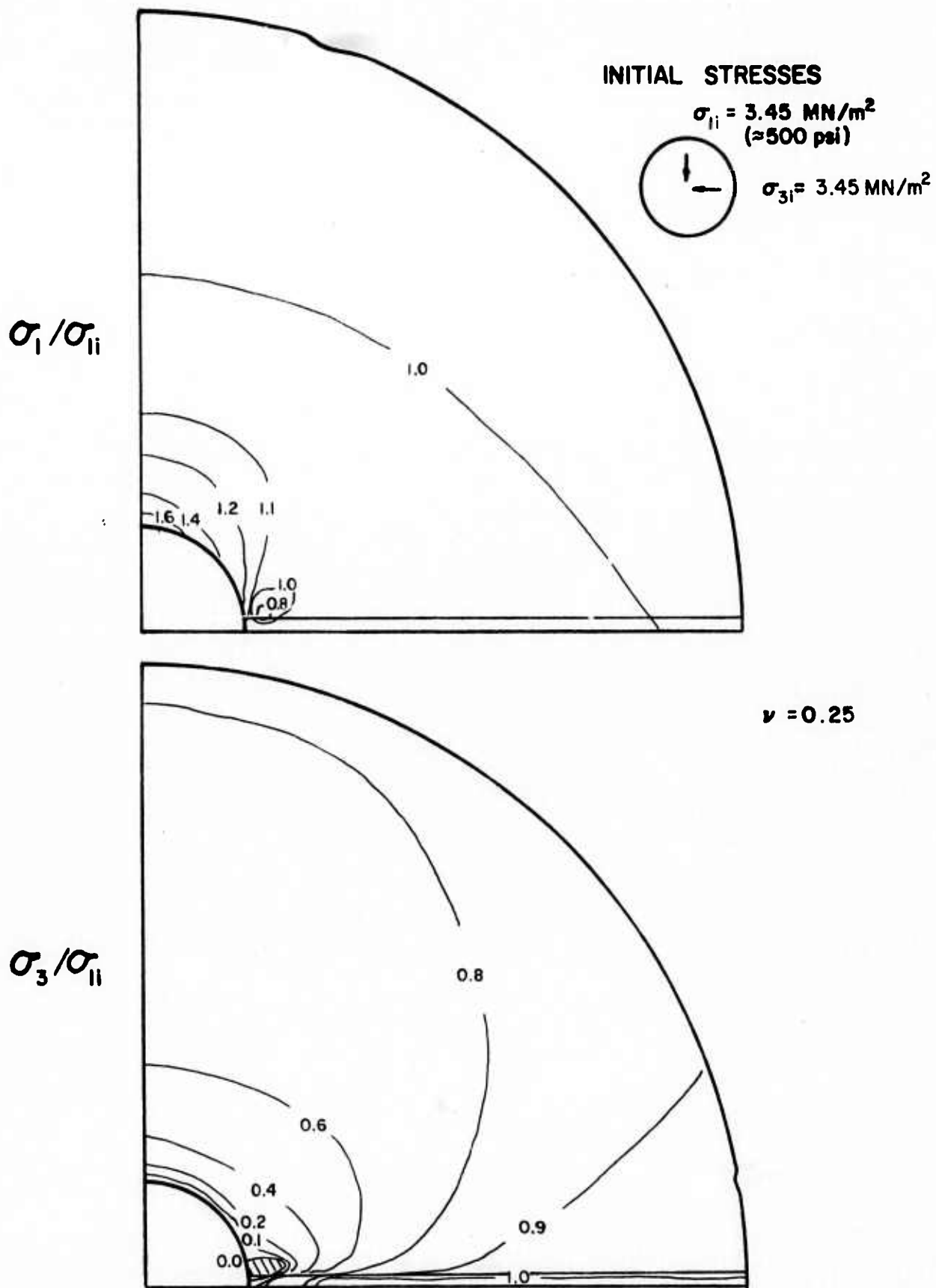


**FIG. 5-15 STRESS CONTOURS FOR CIRCULAR OPENING  
 IN ROCK WITH A PLANAR DISCONTINUITY  
 $K=1$  ,  $\theta=0^\circ$  ,  $\alpha=0^\circ$  ,  $M=1000$**

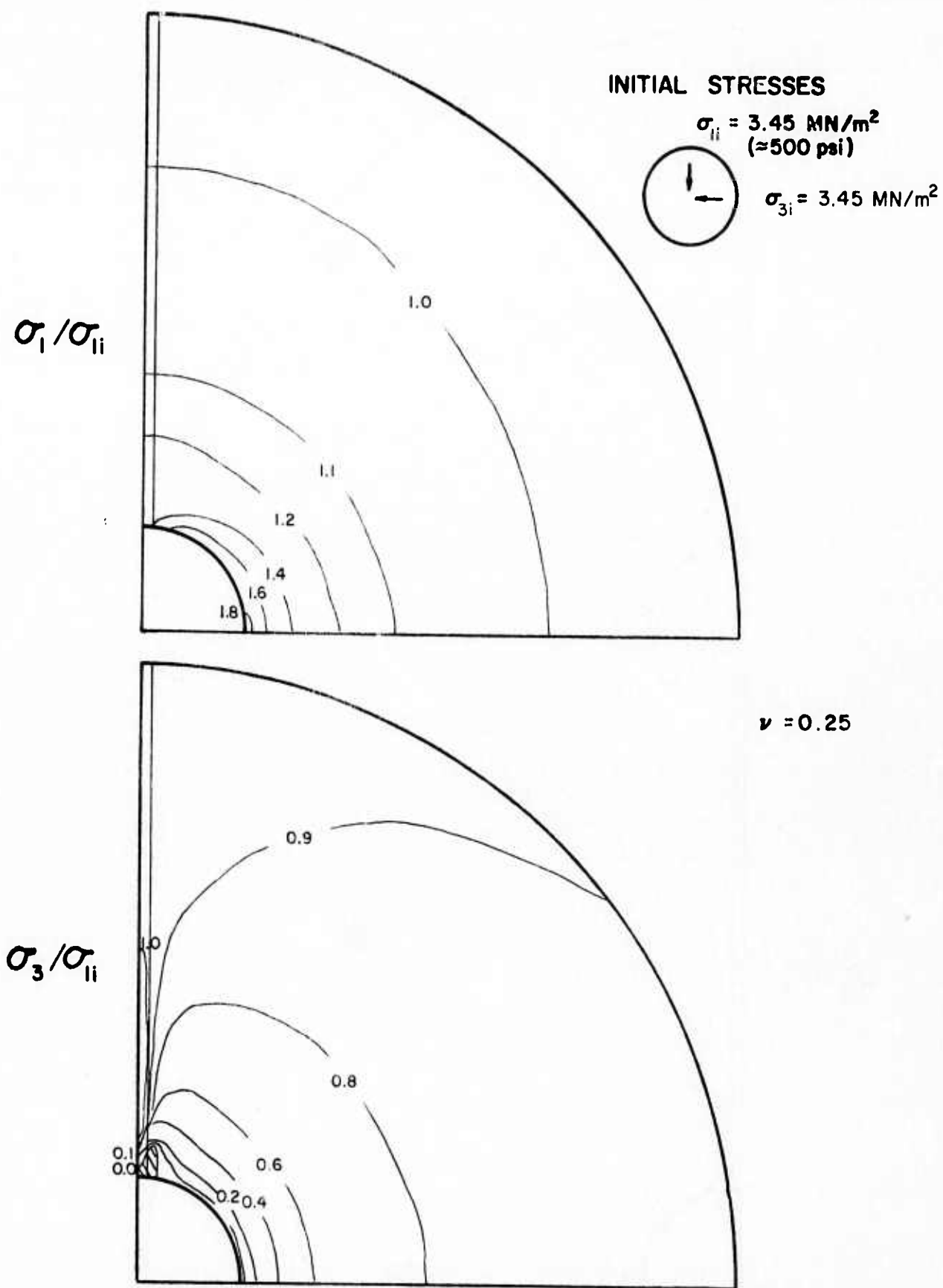


**FIG. 5-16 STRESS CONTOURS FOR CIRCULAR OPENING  
IN ROCK WITH A PLANAR DISCONTINUITY  
 $K=1$  ,  $\theta=0^\circ$  ,  $\alpha=90^\circ$  ,  $M=10$**

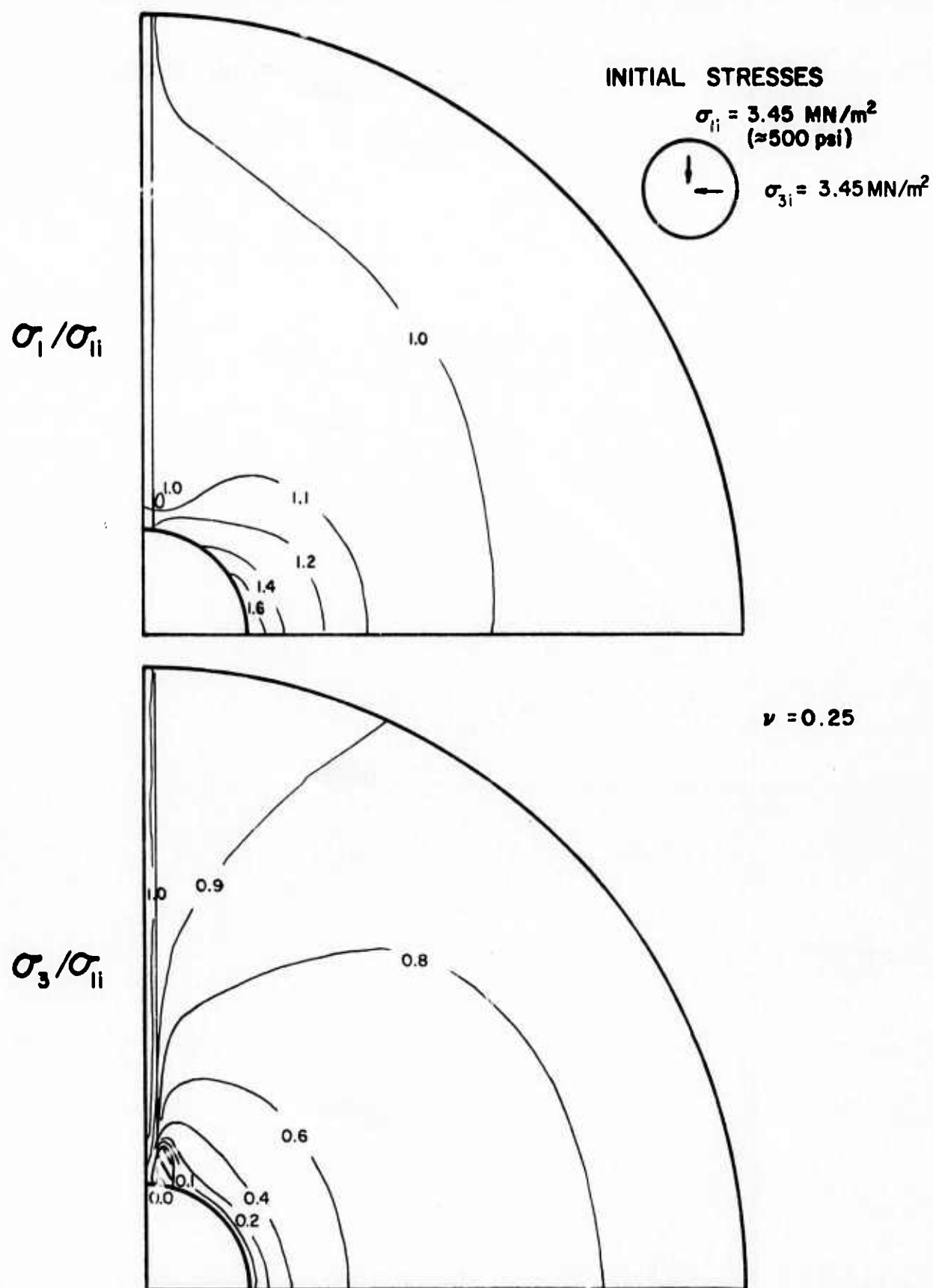


**FIG. 5-17 STRESS CONTOURS FOR CIRCULAR OPENING  
IN ROCK WITH A PLANAR DISCONTINUITY  
 $K=1$  ,  $\theta=0^\circ$  ,  $\alpha=90^\circ$  ,  $M=100$**

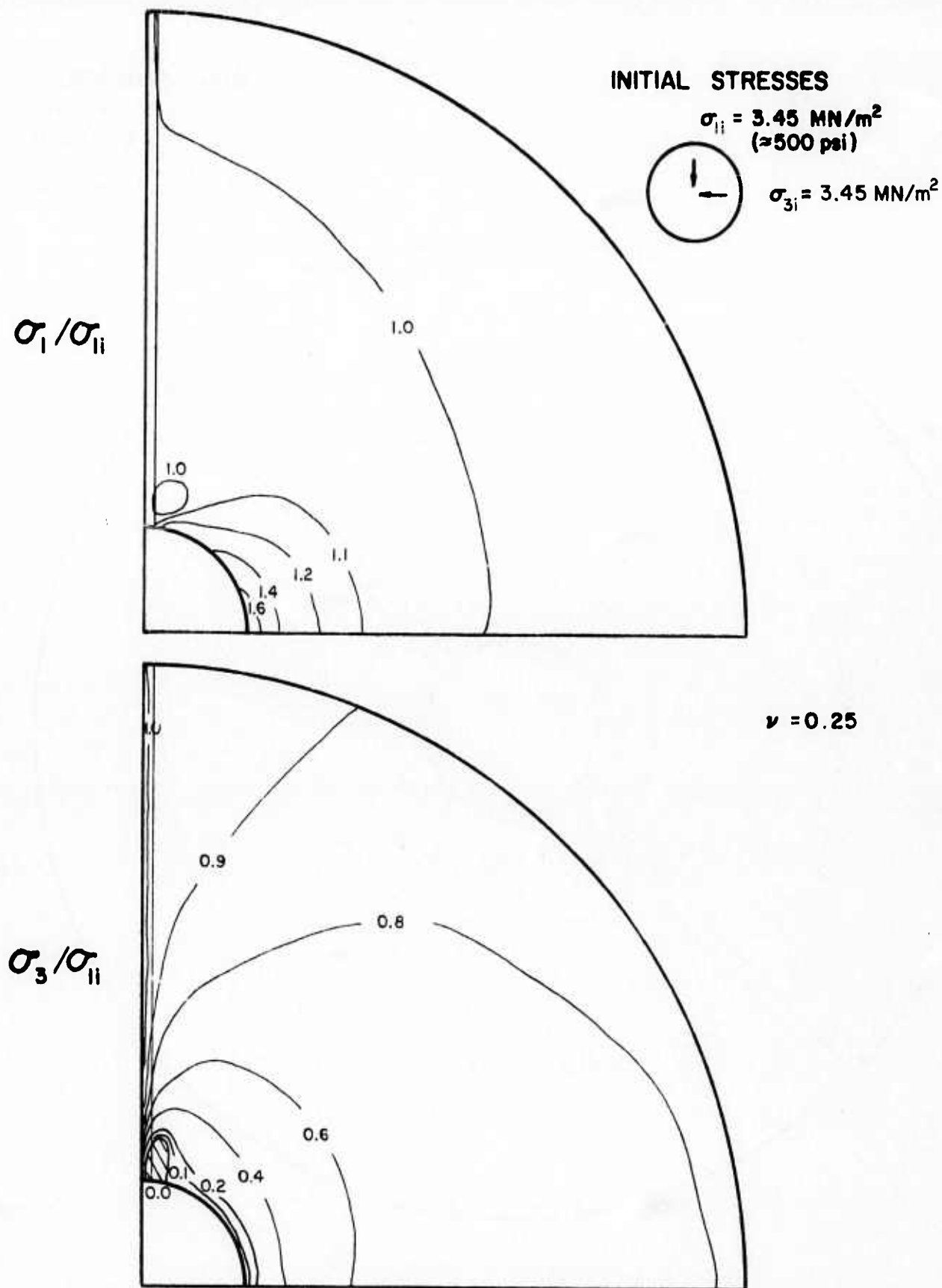
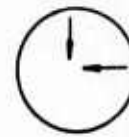


**FIG. 5-18 STRESS CONTOURS FOR CIRCULAR OPENING  
 IN ROCK WITH A PLANAR DISCONTINUITY  
 $K=1$  ,  $\theta=0^\circ$  ,  $\alpha=90^\circ$  ,  $M=1000$**

INITIAL STRESSES

$$\sigma_{1i} = 3.45 \text{ MN/m}^2$$

( $\approx 500 \text{ psi}$ )



$$\sigma_{3i} = 3.45 \text{ MN/m}^2$$

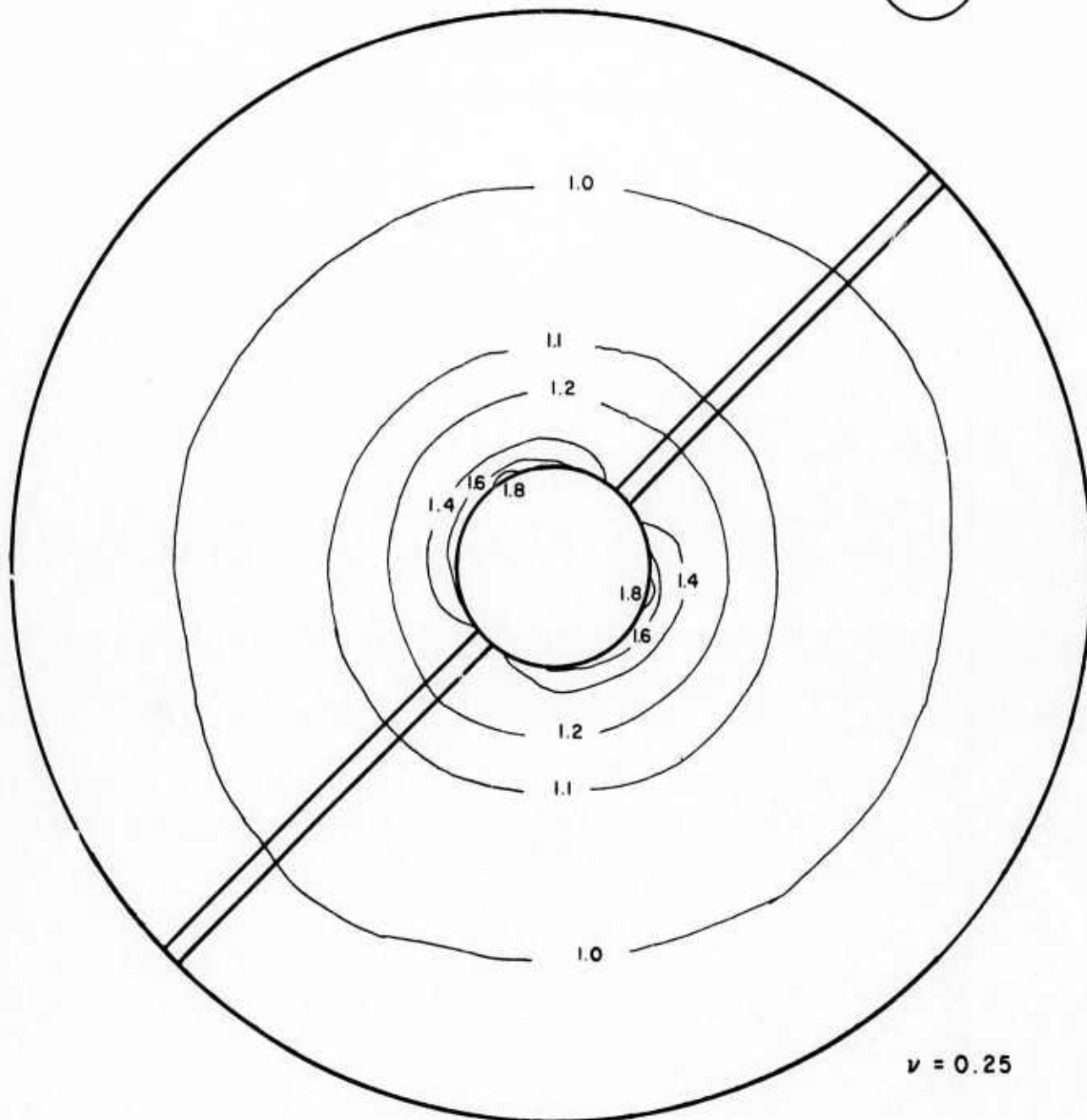


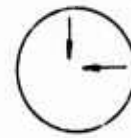
**FIG. 5-19 CONTOURS OF  $\sigma_1/\sigma_{ii}$  FOR CIRCULAR OPENING  
IN ROCK WITH A PLANAR DISCONTINUITY  
 $K=1$  ,  $\theta=0^\circ$  ,  $\alpha=45^\circ$  ,  $M=10$**



INITIAL STRESSES

$$\sigma_{1i} = 3.45 \text{ MN/m}^2$$

( $\approx 500 \text{ psi}$ )



$$\sigma_{3i} = 3.45 \text{ MN/m}^2$$

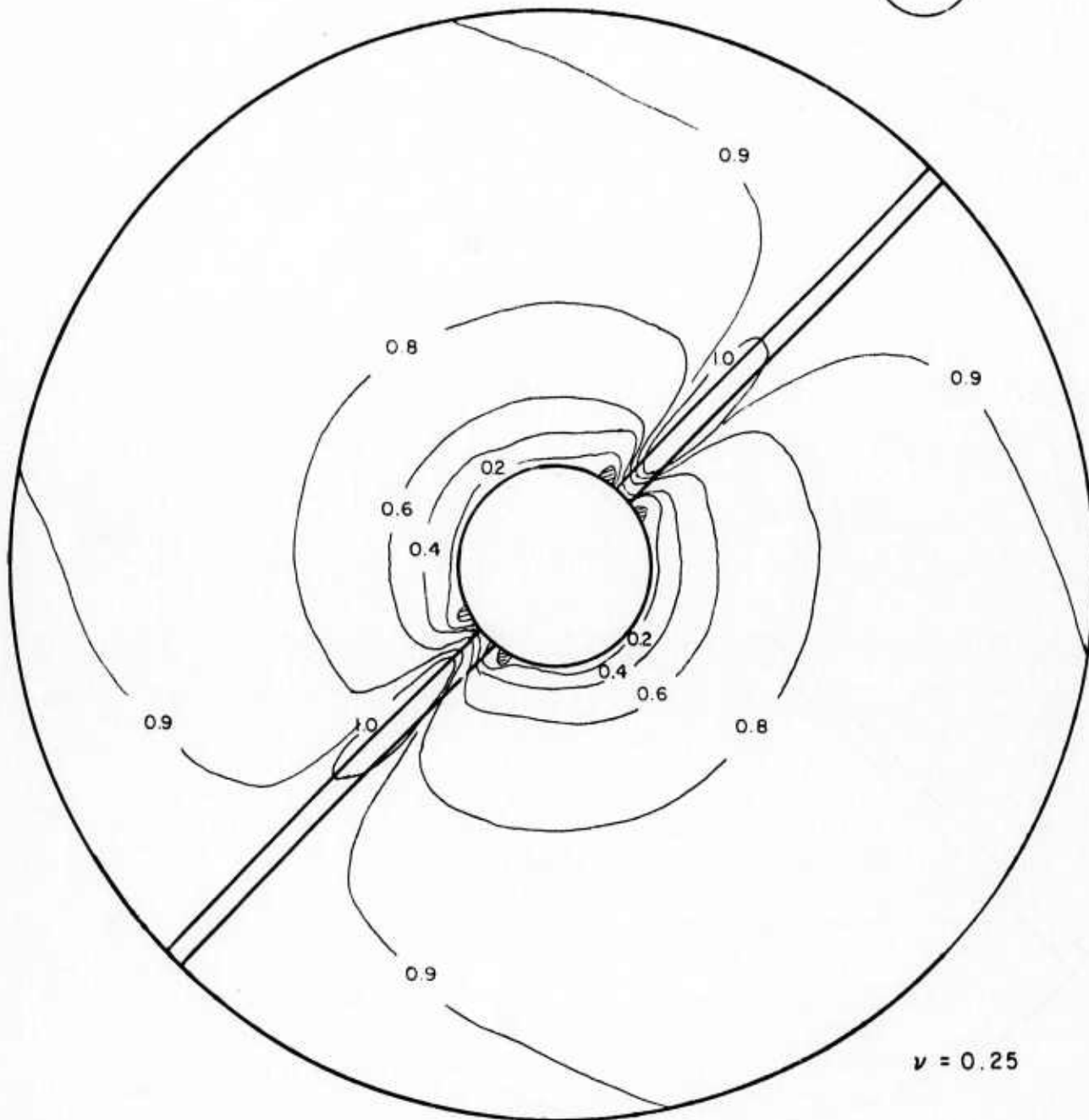
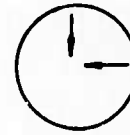


**FIG. 5-20 CONTOURS OF  $\sigma_3/\sigma_{1i}$  FOR CIRCULAR OPENING  
IN ROCK WITH A PLANAR DISCONTINUITY  
 $K=1$  ,  $\theta=0^\circ$  ,  $\alpha=45^\circ$  ,  $M=10$**

INITIAL STRESSES

$$\sigma_{11} = 3.45 \text{ MN/m}^2$$

( $\approx 500 \text{ psi}$ )



$$\sigma_{33} = 3.45 \text{ MN/m}^2$$

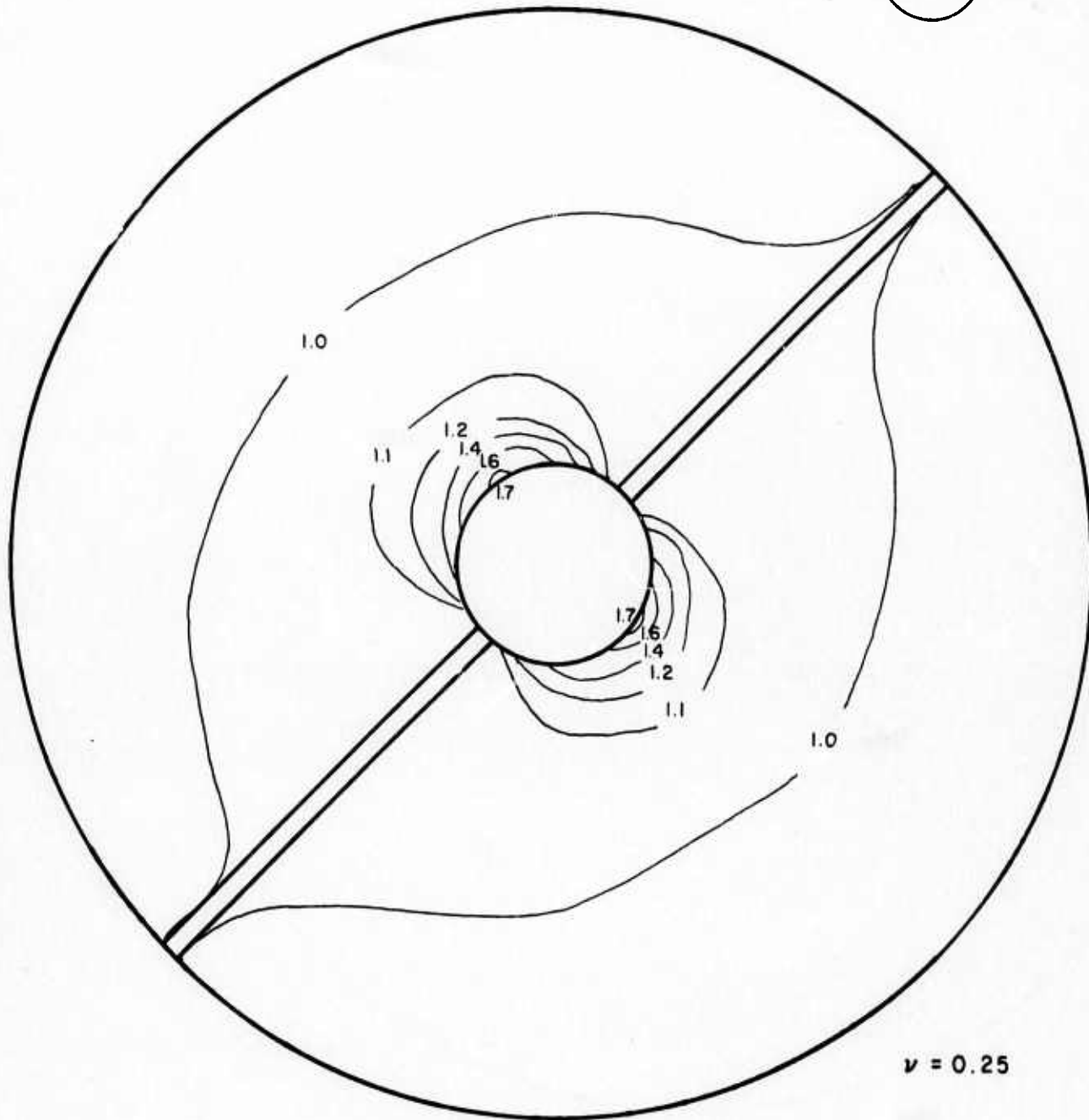


**FIG. 5-21 CONTOURS OF  $\sigma_1/\sigma_{11}$  FOR CIRCULAR OPENING  
IN ROCK WITH A PLANAR DISCONTINUITY  
 $K=1$  ,  $\theta=0^\circ$  ,  $\alpha=45^\circ$  ,  $M=1000$**

INITIAL STRESSES

$$\sigma_{li} = 3.45 \text{ MN/m}^2$$

( $\approx 500 \text{ psi}$ )



$$\sigma_{3i} = 3.45 \text{ MN/m}^2$$

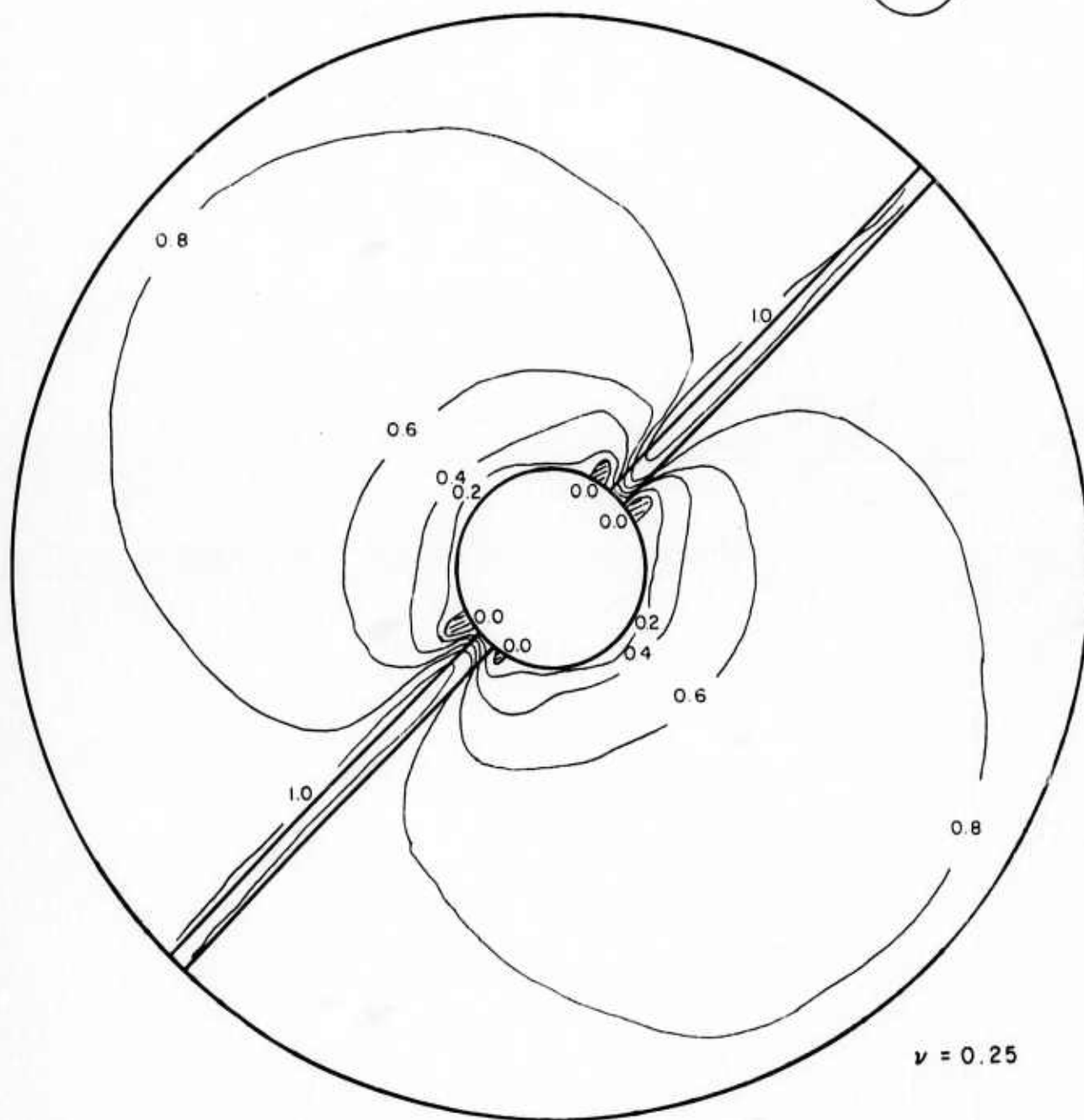


**FIG. 5-22 CONTOURS OF  $\sigma_3/\sigma_{li}$  FOR CIRCULAR OPENING  
IN ROCK WITH A PLANAR DISCONTINUITY  
 $K=1$  ,  $\theta=0^\circ$  ,  $\alpha=45^\circ$  ,  $M=1000$**

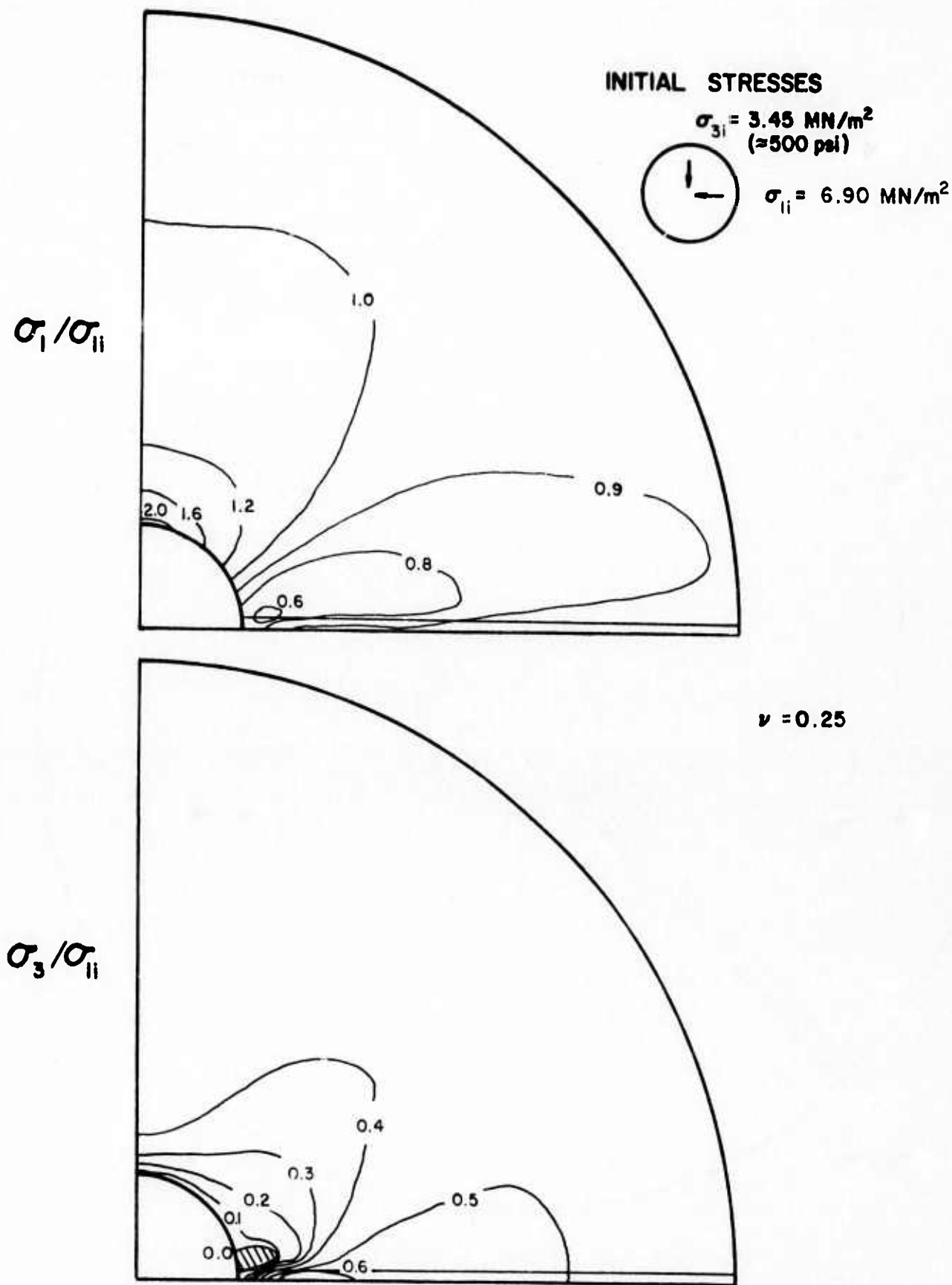


**FIG. 5-23 STRESS CONTOURS FOR CIRCULAR OPENING  
IN ROCK WITH A PLANAR DISCONTINUITY  
 $K = 1/2$ ,  $\theta = 90^\circ$ ,  $\alpha = 0^\circ$ ,  $M = 10$**

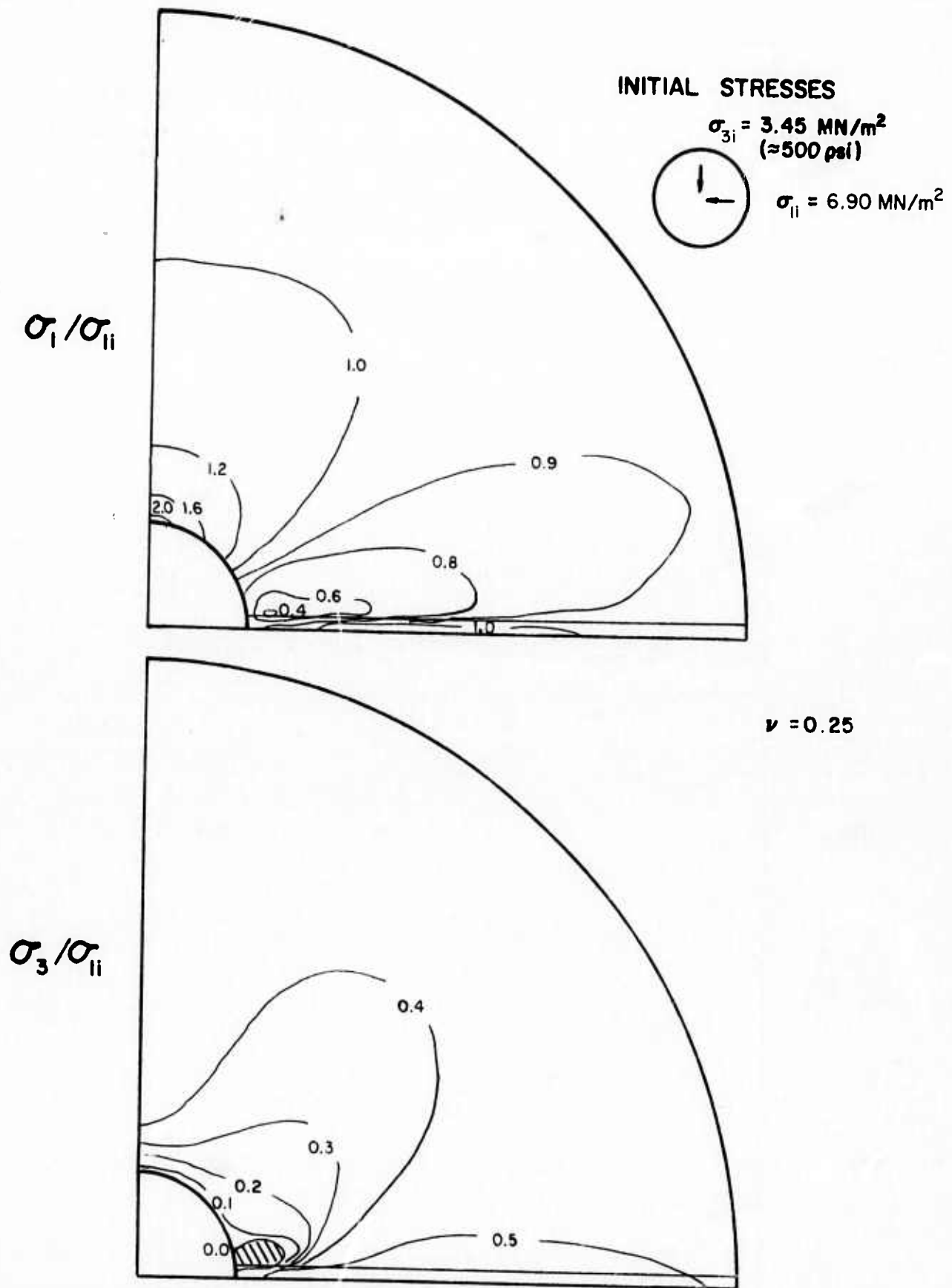


**FIG. 5-24 STRESS CONTOURS FOR CIRCULAR OPENING  
IN ROCK WITH A PLANAR DISCONTINUITY  
 $K=1/2$ ,  $\theta=90^\circ$ ,  $\alpha=0^\circ$ ,  $M=100$**

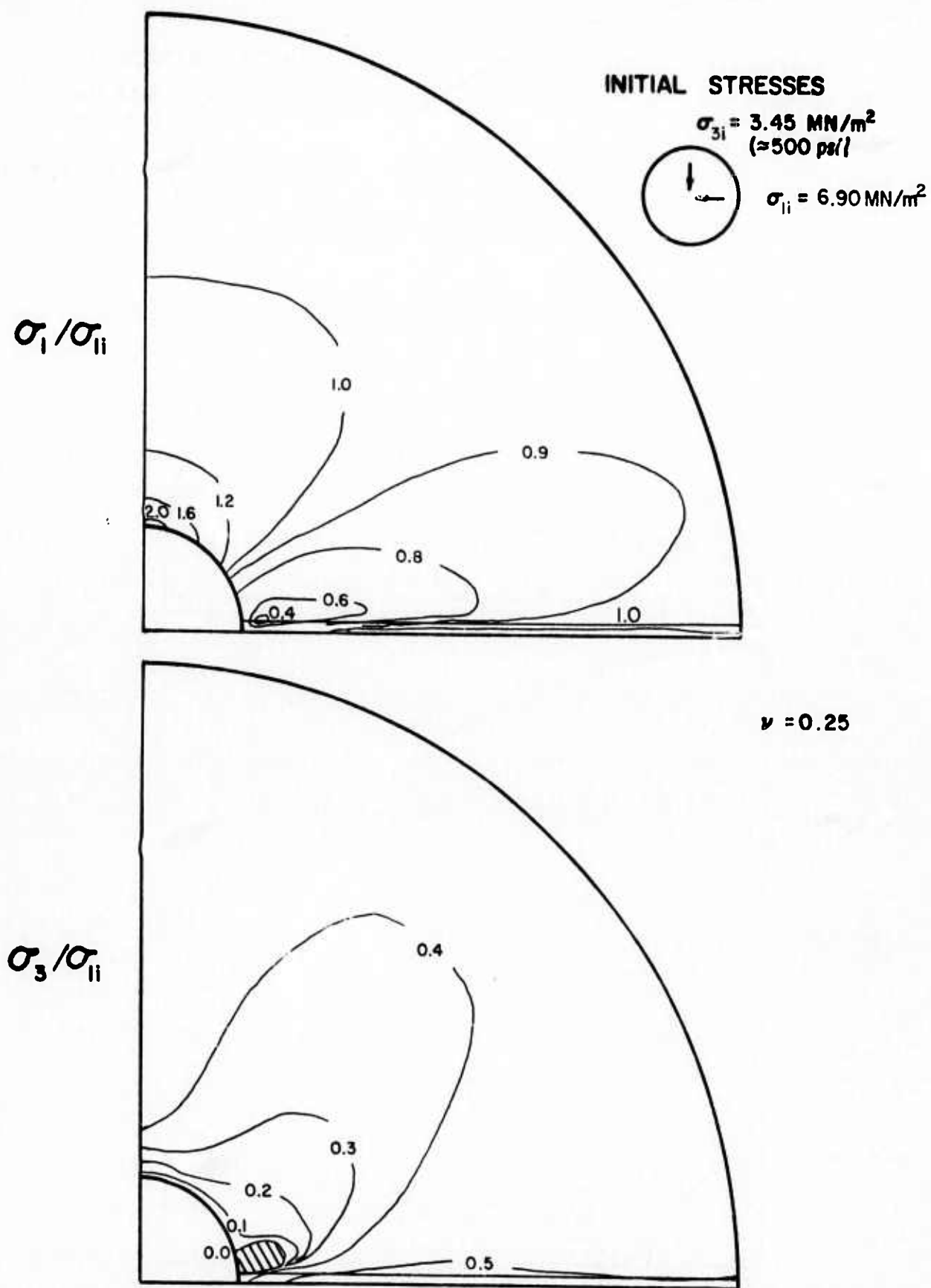


**FIG. 5-25 STRESS CONTOURS FOR CIRCULAR OPENING  
IN ROCK WITH A PLANAR DISCONTINUITY  
 $K=1/2$ ,  $\theta=90^\circ$ ,  $\alpha=0^\circ$ ,  $M=1000$**



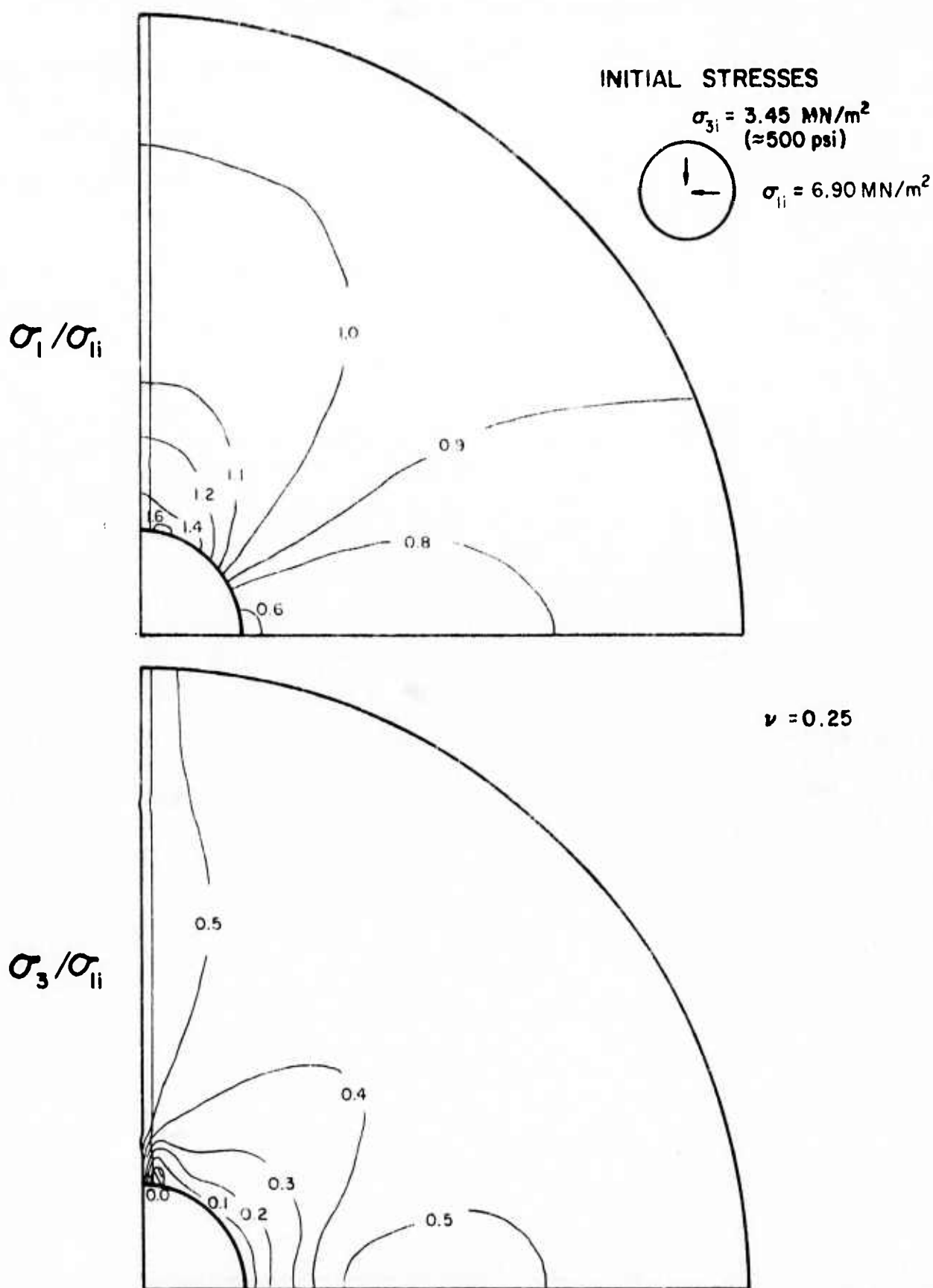


**FIG. 5-26 STRESS CONTOURS FOR CIRCULAR OPENING  
IN ROCK WITH A PLANAR DISCONTINUITY  
 $K = 1/2$ ,  $\theta = 90^\circ$ ,  $\alpha = 90^\circ$ ,  $M = 10$**

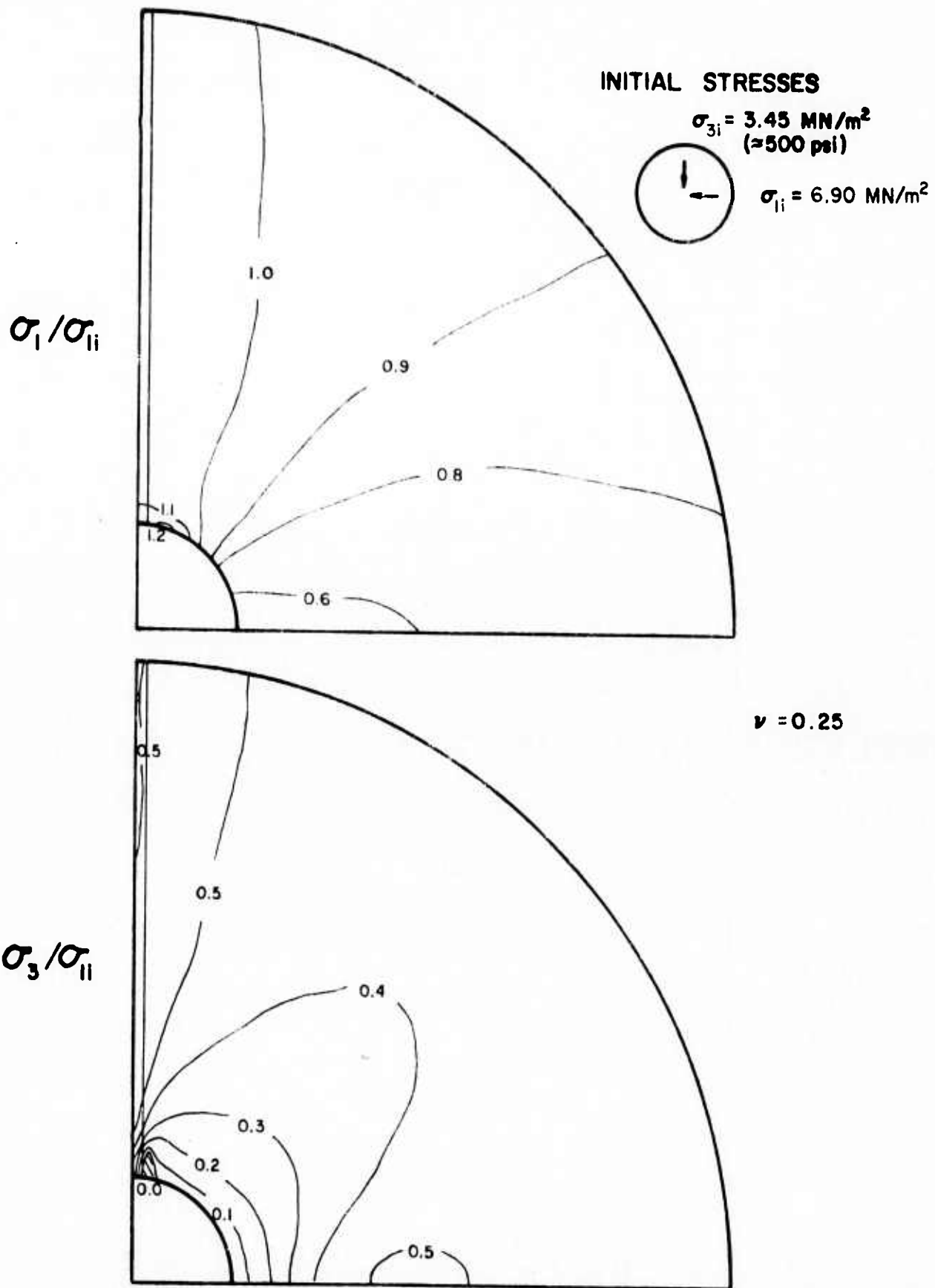


**FIG. 5-27 STRESS CONTOURS FOR CIRCULAR OPENING  
IN ROCK WITH A PLANAR DISCONTINUITY  
 $K=1/2$ ,  $\theta=90^\circ$ ,  $\alpha=90^\circ$ ,  $M=100$**

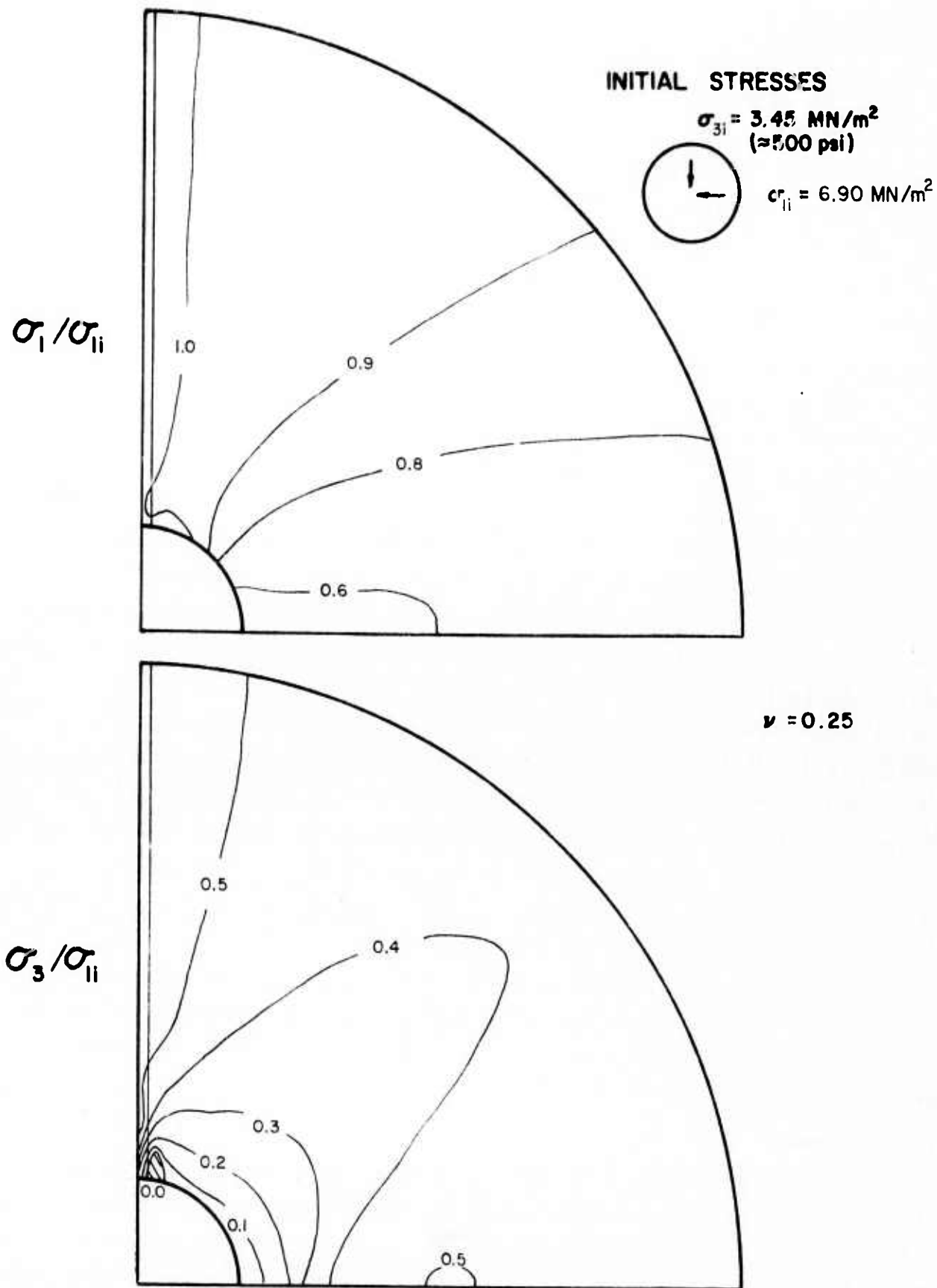


**FIG. 5-28 STRESS CONTOURS FOR CIRCULAR OPENING  
 IN ROCK WITH A PLANAR DISCONTINUITY  
 $K = 1/2$ ,  $\theta = 90^\circ$ ,  $\alpha = 90^\circ$ ,  $M = 1000$**

Changes in the dimensionless  $\sigma_3$  contours are small with a general tendency toward a reduction in values as M increases.

Figures 5-29 through 5-32 show the stress contours for the  $45^\circ$  discontinuity. For both the dimensionless  $\sigma_1$  and  $\sigma_3$  contours, the changes are generally small, with a decrease in the crown and springline stresses. The stresses within the discontinuity show a decrease in  $\sigma_1$  and in  $\sigma_3$  as M increases.

### Discontinuity Stresses

#### a) Normal Stresses

A further way of assessing the relative importance of discontinuities in rock masses is to evaluate the normal and shear stresses in the discontinuity as a result of excavation. The normal stresses on the discontinuity for the 27 cases analyzed are shown in Figures 5-33 through 5-35. These values were made dimensionless by dividing by the initial normal stress on the discontinuity.

In all of these cases it can be seen that the normal stresses are greater for stiffer discontinuities but that the normal stresses return to their original values within three radii of the opening face. When the initial minimum principal stress acts in the plane of the discontinuity, the normal stresses are greatest and generally increase toward the opening face. When the initial maximum principal stress acts in the plane of the discontinuity, the normal stresses are least and are very small at the opening face. Furthermore as the initial principal stress ratio increases, the normal stresses at the face either increase or decrease further depending on the orientation of the discontinuity. When the initial stresses are isotropic, intermediate values are obtained.

When the discontinuity is at  $45^\circ$  to the initial principal stresses, the resulting normal stresses do not vary significantly even though the values are slightly higher with lower M values. Furthermore in all cases the normal stresses are smallest at the opening face.

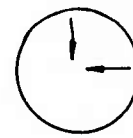
#### b) Shear Stresses

Figures 5-36 through 5-38 show the shear stresses along the discontinuity for the cases analyzed. These values were also made dimensionless by dividing by the initial normal stress on the discontinuity even though it would be better to use the initial shear stress but, because of obvious difficulties such as the initial shear stresses equal to zero in many cases, this could not be used. The results should be interpreted with this in mind.

INITIAL STRESSES

$$\sigma_{3i} = 3.45 \text{ MN/m}^2$$

( $\approx 500 \text{ psi}$ )



$$\sigma_{1i} = 6.90 \text{ MN/m}^2$$

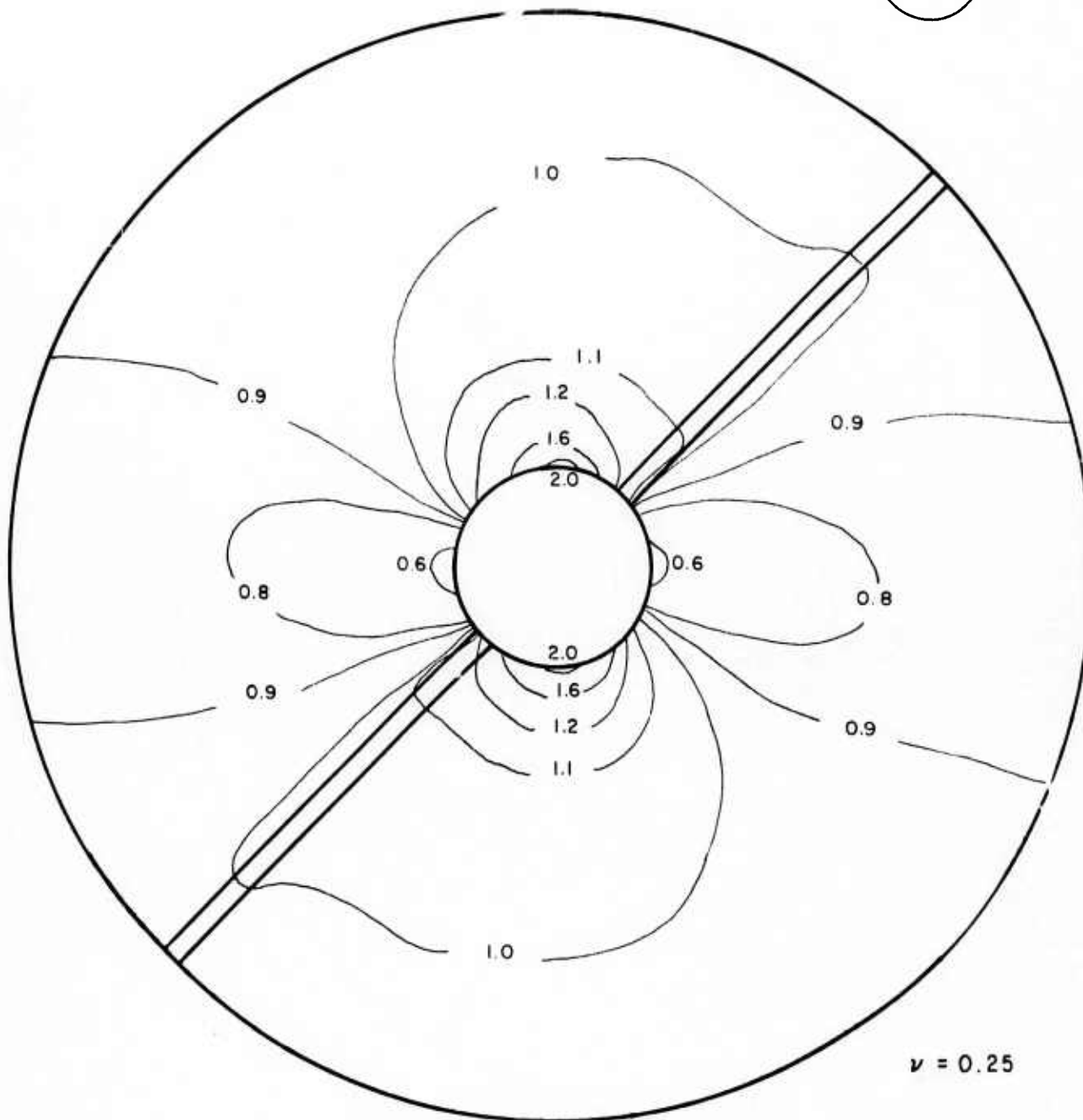
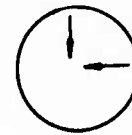


**FIG. 5-29 CONTOURS OF  $\sigma_i/\sigma_{ii}$  FOR CIRCULAR OPENING  
IN ROCK WITH A PLANAR DISCONTINUITY  
 $K=1/2$ ,  $\theta=90^\circ$ ,  $\alpha=45^\circ$ ,  $M=10$**

# INITIAL STRESSES

$$\sigma_{3i} = 3.45 \text{ MN/m}^2$$

( $\approx 500 \text{ psi}$ )



$$\sigma_{1i} = 6.90 \text{ MN/m}^2$$

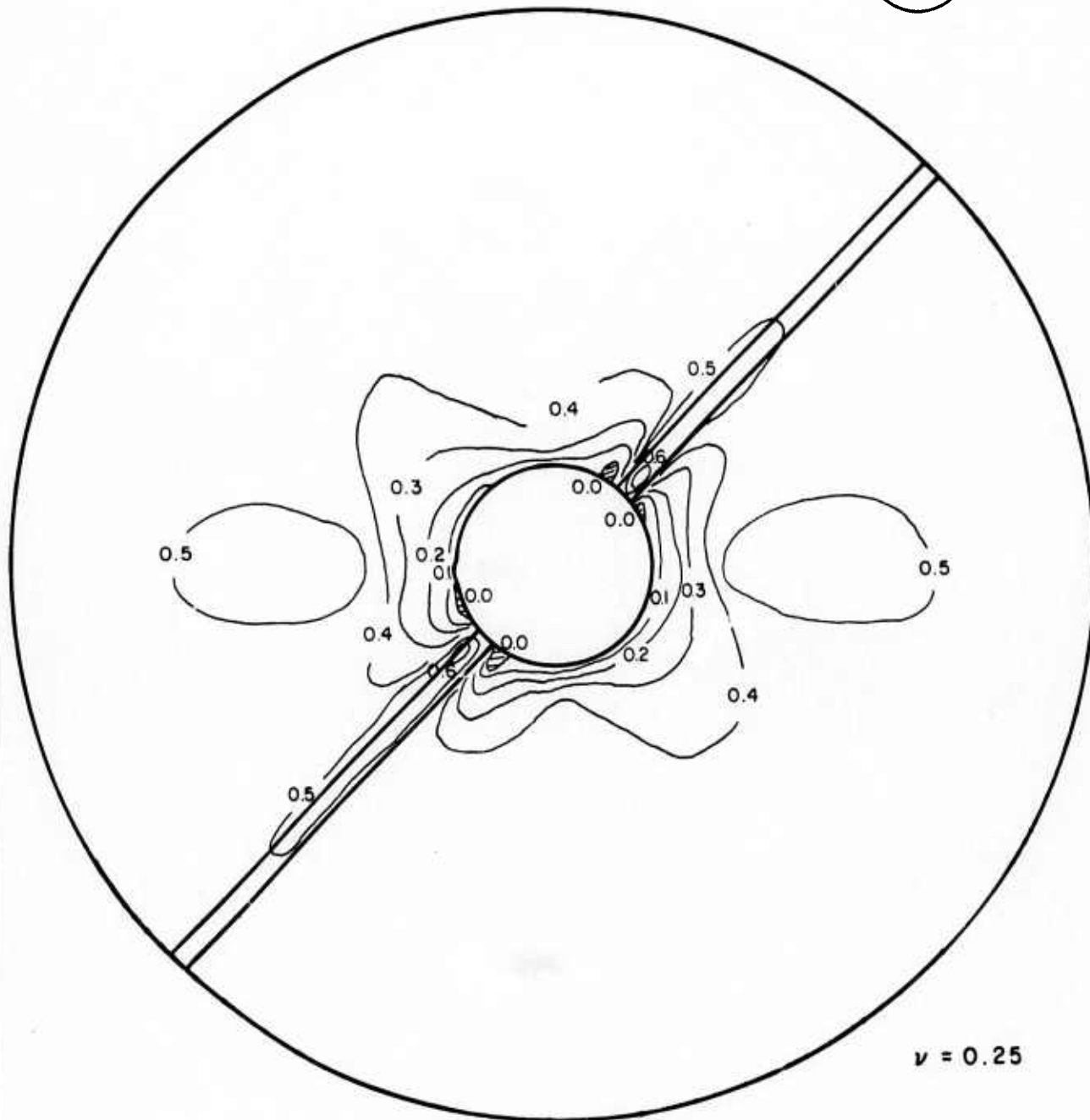


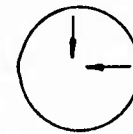
**FIG. 5-30 CONTOURS OF  $\sigma_3/\sigma_{1i}$  FOR CIRCULAR OPENING  
IN ROCK WITH A PLANAR DISCONTINUITY  
 $K=1/2$ ,  $\theta=90^\circ$ ,  $\alpha=45^\circ$ ,  $M=10$**



INITIAL STRESSES

$$\sigma_{3i} = 3.45 \text{ MN/m}^2$$

( $\approx 500 \text{ psi}$ )



$$\sigma_{1i} = 6.90 \text{ MN/m}^2$$

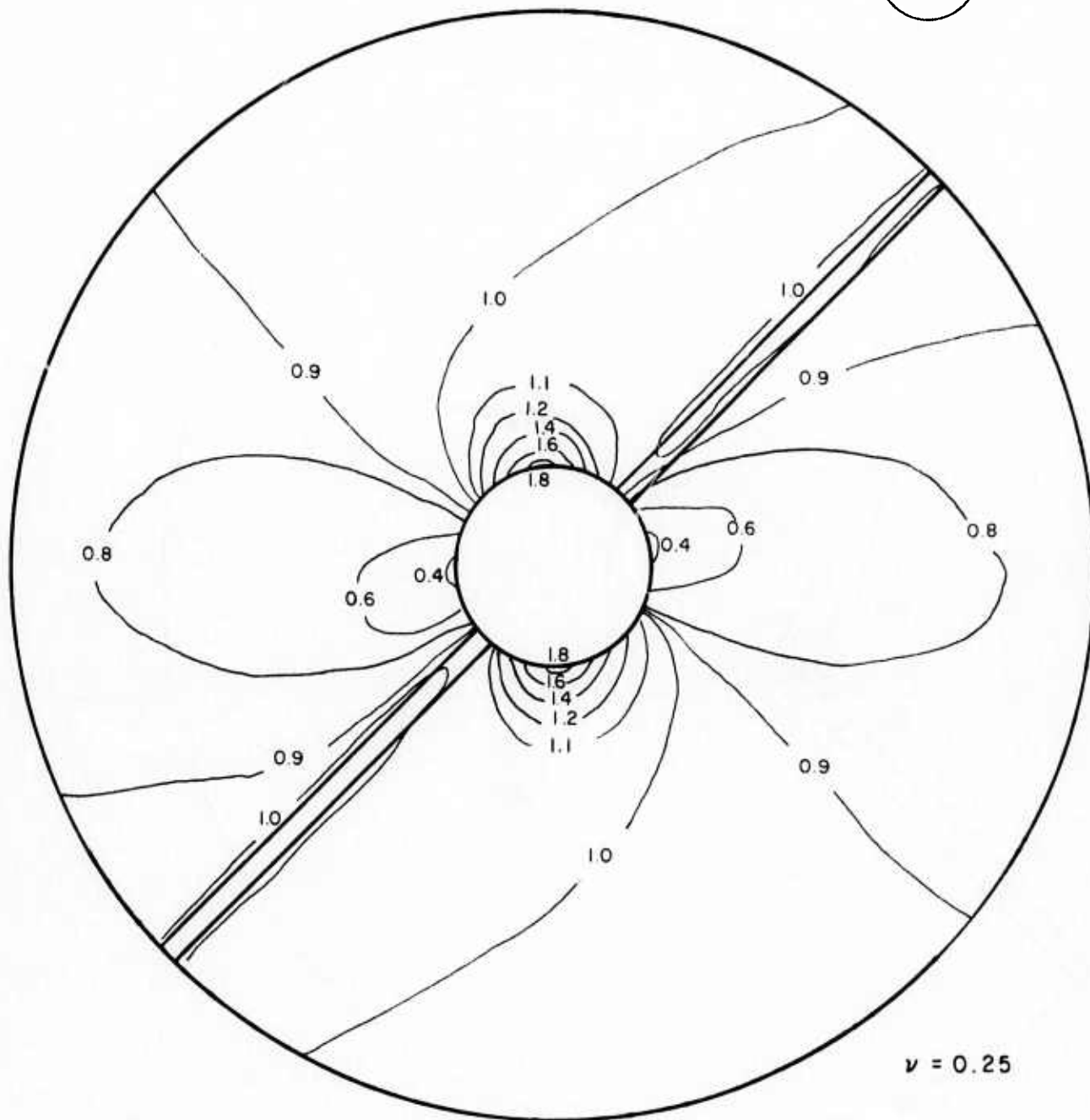
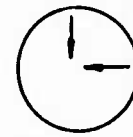


**FIG. 5-31 CONTOURS OF  $\sigma_i/\sigma_{ii}$  FOR CIRCULAR OPENING  
IN ROCK WITH A PLANAR DISCONTINUITY  
 $K=1/2$ ,  $\theta=90^\circ$ ,  $\alpha=45^\circ$ ,  $M=1000$**

INITIAL STRESSES

$$\sigma_{3i} = 3.45 \text{ MN/m}^2$$

( $\approx 500 \text{ psi}$ )



$$\sigma_{1i} = 6.90 \text{ MN/m}^2$$

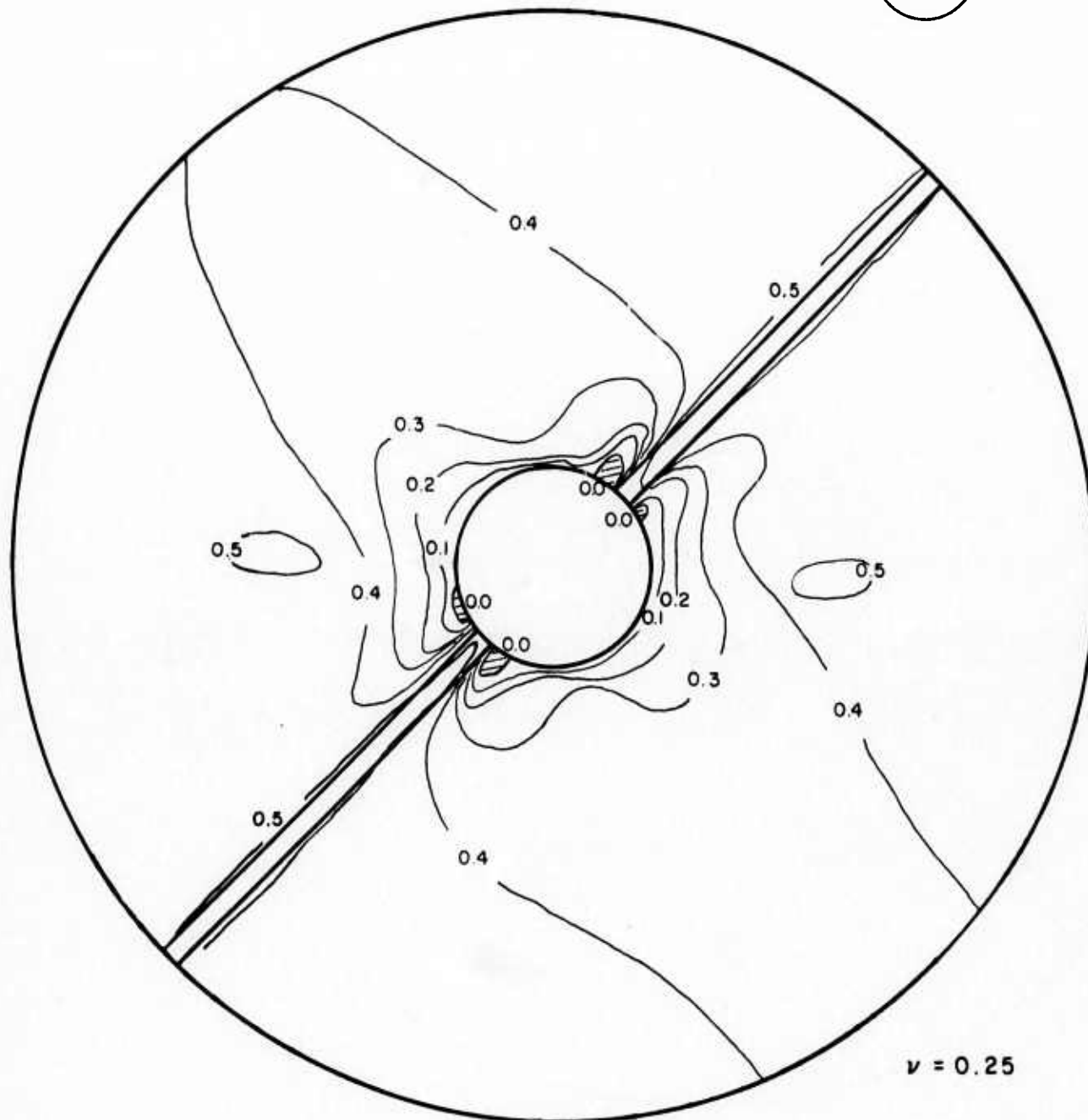


**FIG. 5-32 CONTOURS OF  $\sigma_3/\sigma_{1i}$  FOR CIRCULAR OPENING  
IN ROCK WITH A PLANAR DISCONTINUITY  
 $K=1/2$ ,  $\theta=90^\circ$ ,  $\alpha=45^\circ$ ,  $M=1000$**

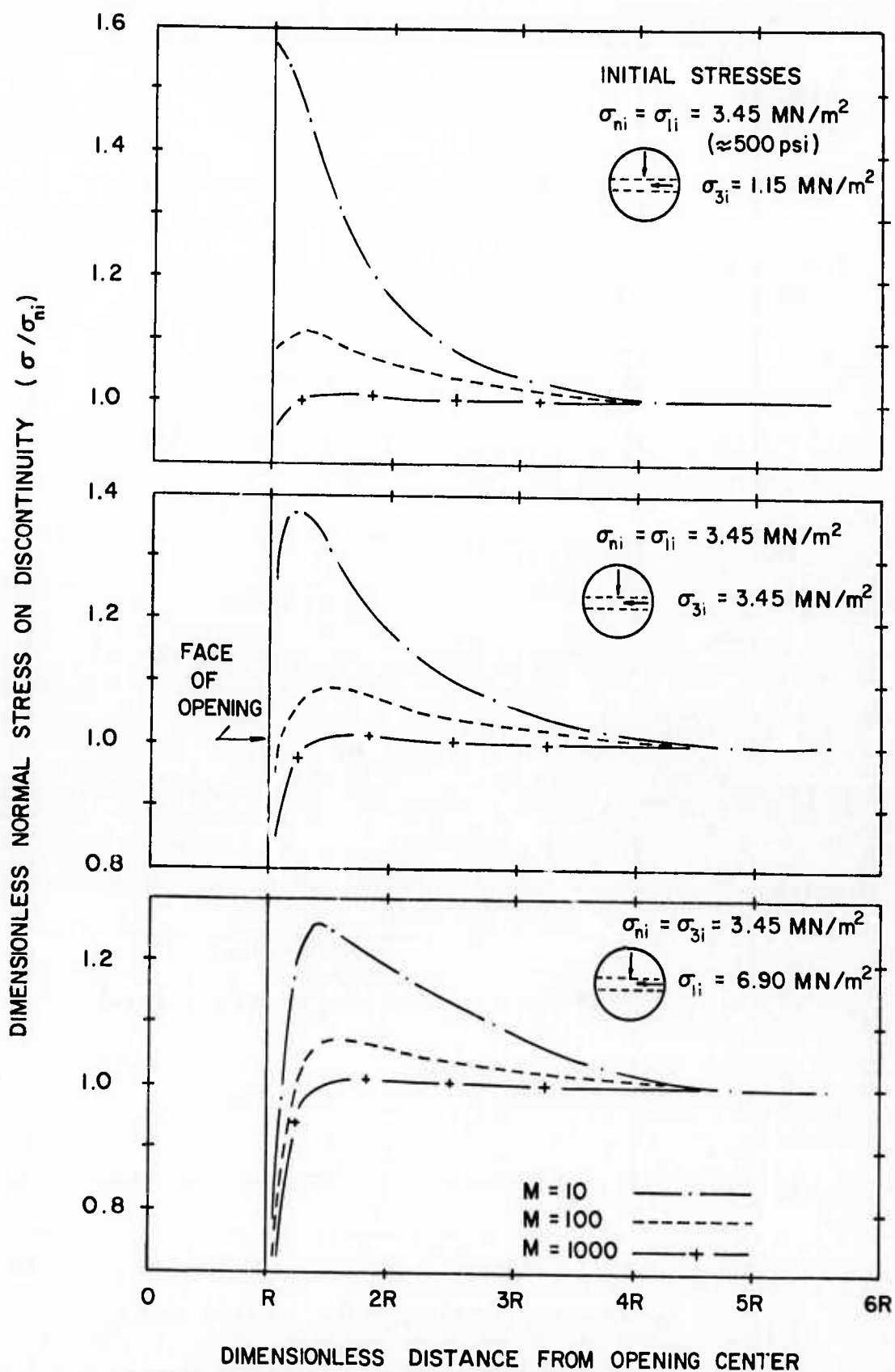


**FIG. 5-33 NORMAL STRESSES ON HORIZONTAL DISCONTINUITY**

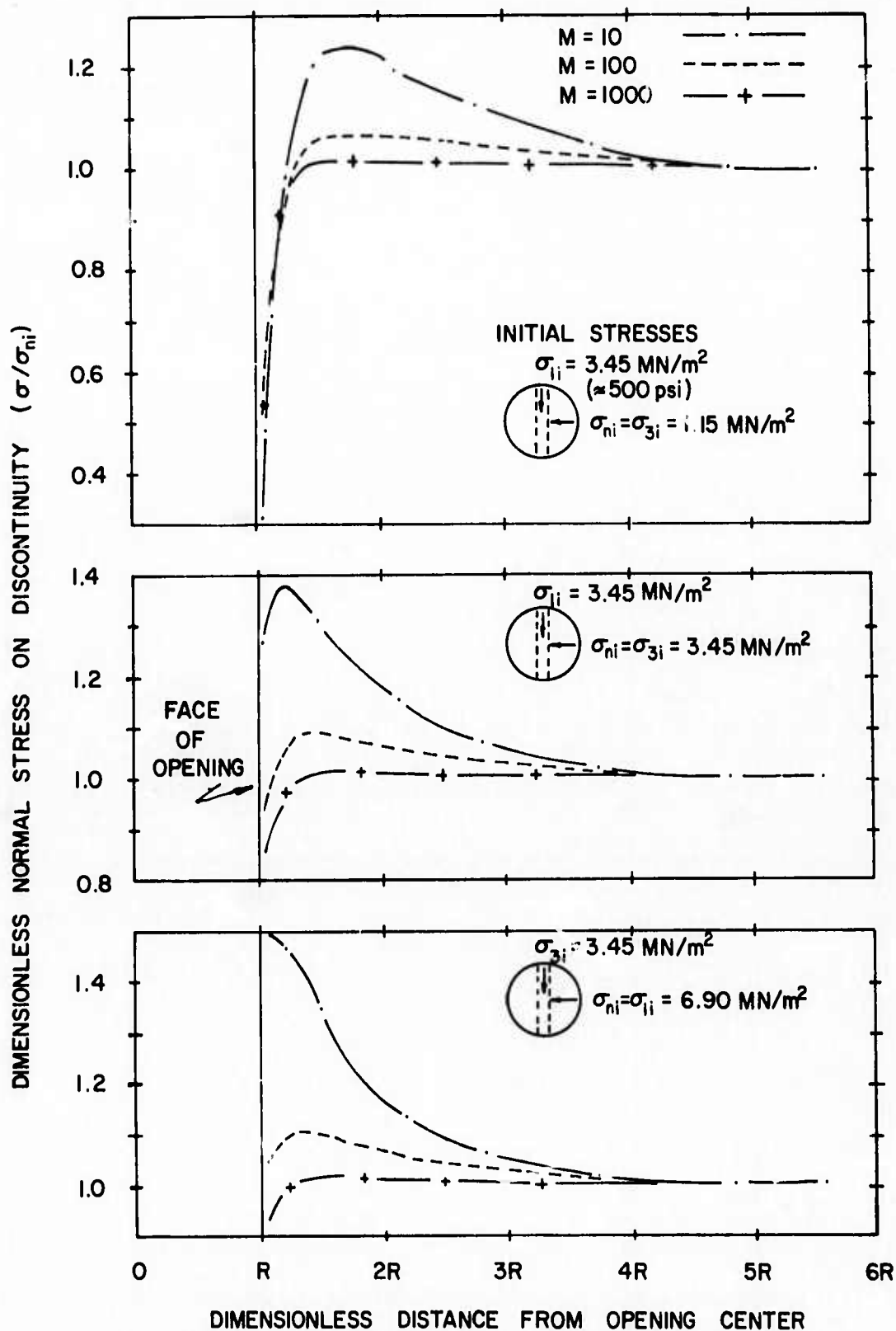


**FIG. 5-34 NORMAL STRESSES ON VERTICAL DISCONTINUITY**

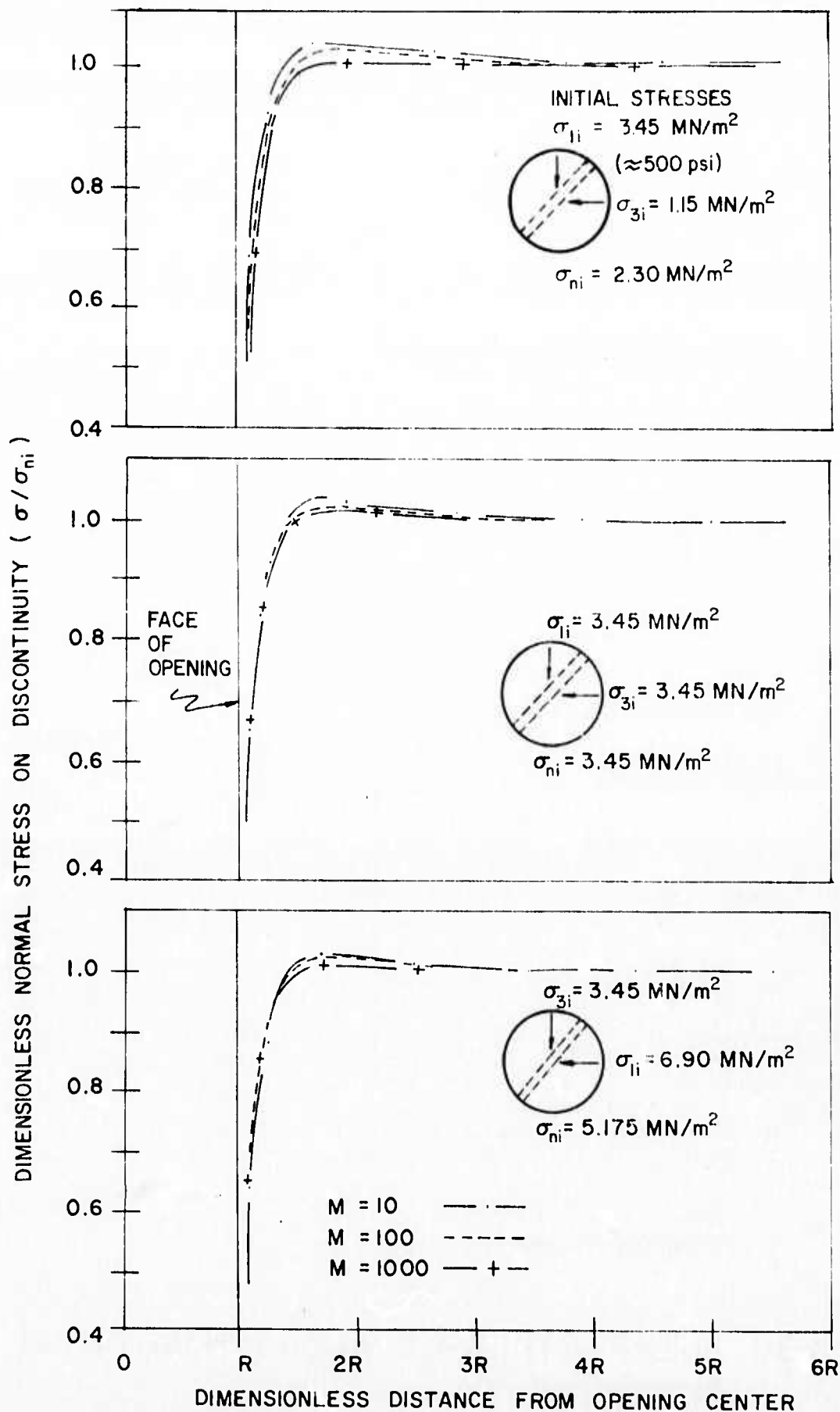


**FIG. 5-35 NORMAL STRESSES ON 45° DISCONTINUITY**

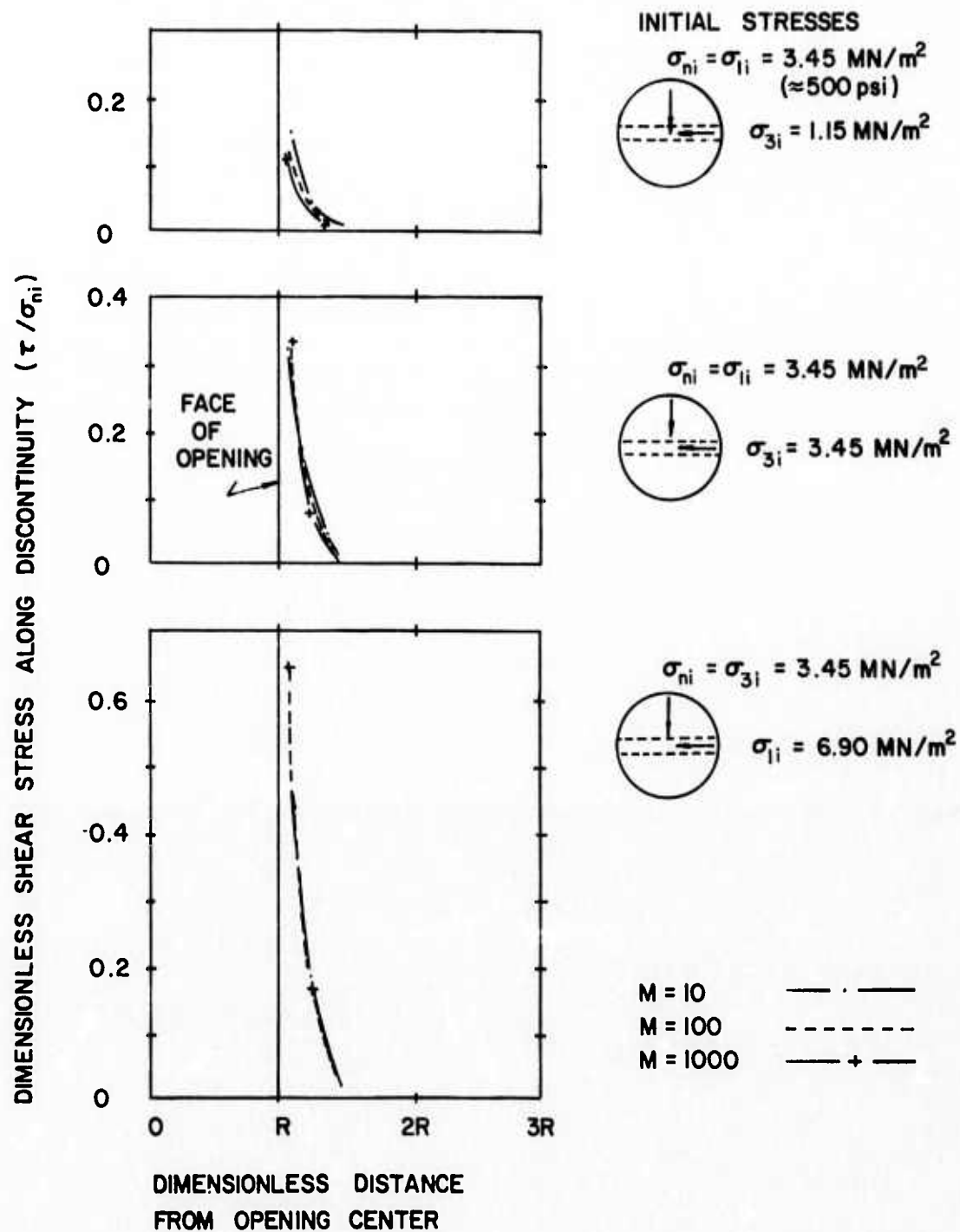


**FIG. 5-36 SHEAR STRESSES ALONG HORIZONTAL DISCONTINUITY**



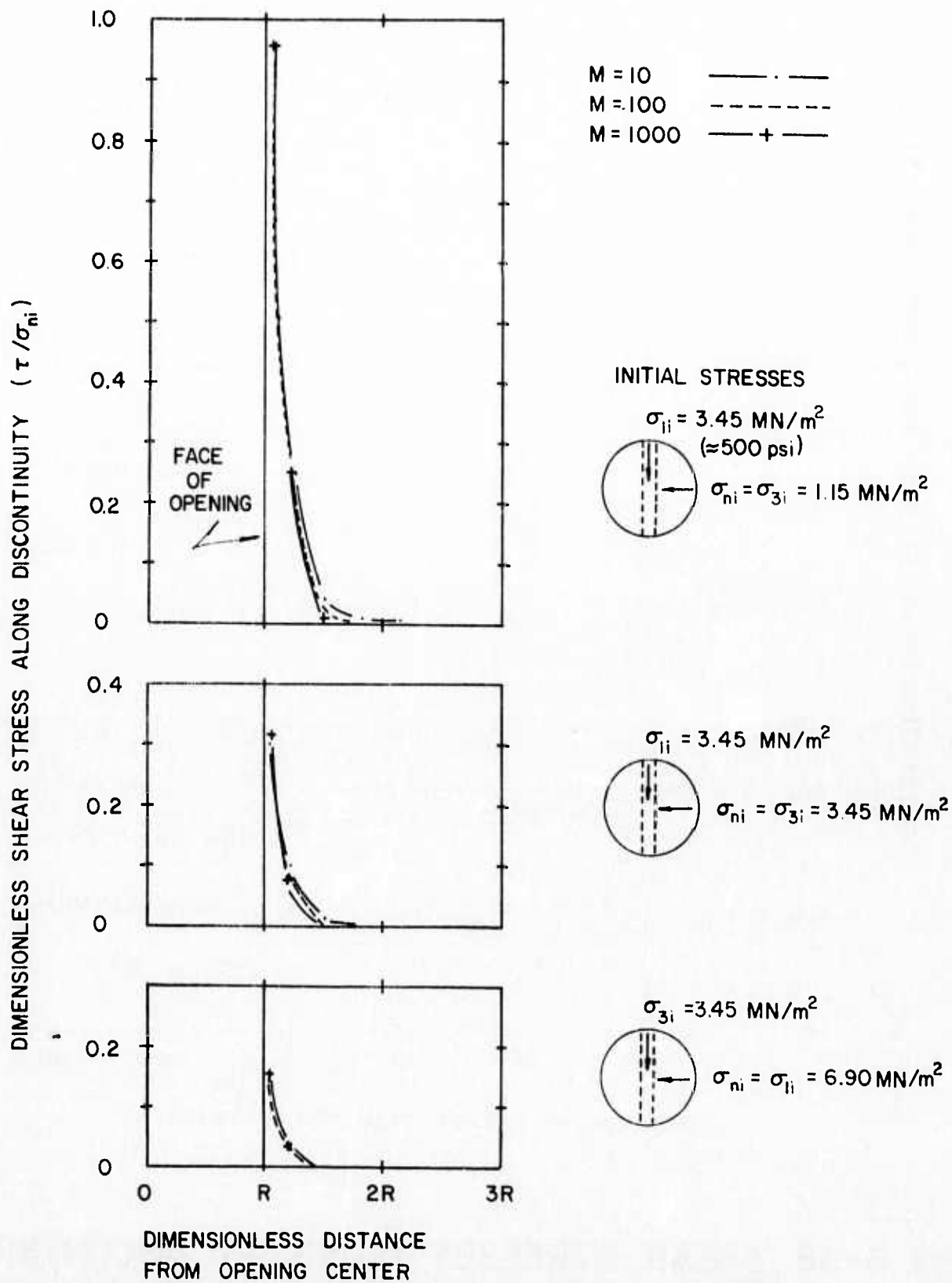


**FIG. 5-37 SHEAR STRESSES ALONG VERTICAL DISCONTINUITY**

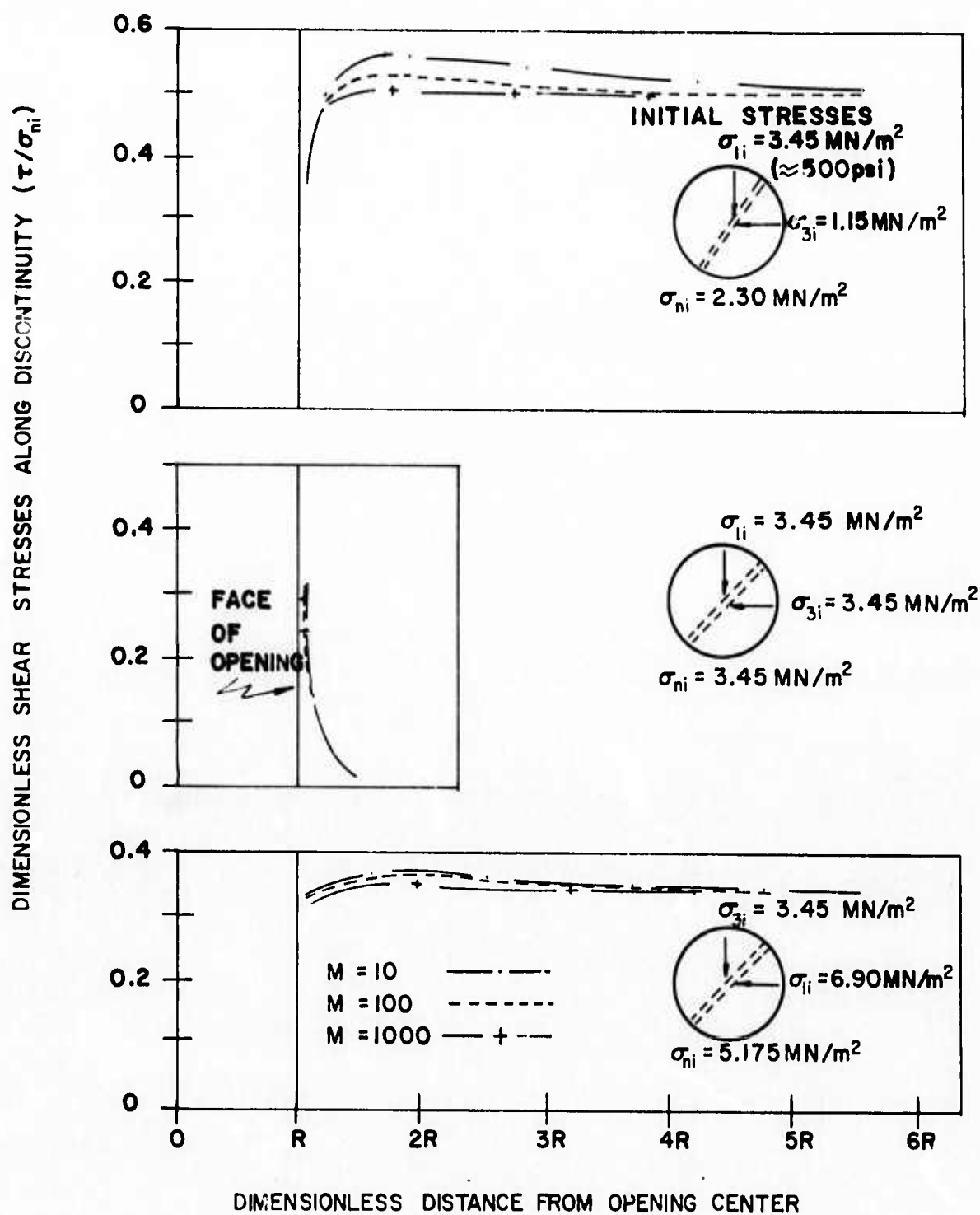


**FIG. 5-38 SHEAR STRESSES ALONG 45° DISCONTINUITY**

In all of these cases it can be seen that the shear stresses are slightly greater for stiffer discontinuities, but for all practical purposes, the shear stresses are about the same regardless of stiffness. It can also be seen that the shear stresses are only effective within a very short distance of the opening face, typically within one radius, at which point they return to their original values.

When the initial maximum principal stress acts in the plane of the discontinuity, the dimensionless shear stresses are greatest and increase with increasing principal stress ratio, while when the initial minimum principal stress acts in the plane of the discontinuity, the dimensionless shear stresses are least. Intermediate values are obtained when the initial stresses are isotropic. It is interesting to note that when the initial stresses are anisotropic for the  $45^\circ$  discontinuity, the resultant shear stresses are not very different from the initial shear stresses.

#### Opening Displacements

Figures 5-39 through 5-41 show the opening displacements for the horizontal discontinuity and Figures 5-42 through 5-44 show the opening displacements for the vertical discontinuity. In all of these figures it can be seen that the displacements increase as the  $M$  value increases, with the greatest increases occurring when the plane of the discontinuity and the initial minimum principal stress coincide.

When the plane of the discontinuity and the plane of the initial maximum principal stress coincide, the amount of compression is small but the movement inward toward the opening center is large. At an offset of  $90^\circ$ , the movement is inward and small and becomes smaller as the initial principal stress ratio increases. When the plane of the discontinuity and the plane of the initial minimum principal stress coincide, the amount of compression is large but the inward or outward movement is small. At an offset of  $90^\circ$ , the movement is inward and large and is larger when the initial principal stress ratio is smaller. When the initial stresses are isotropic, intermediate results are obtained.

When the discontinuity is at  $45^\circ$ , as shown in Figures 5-45 through 5-47, it is again found that the displacements increase as the  $M$  value increases and that the largest inward movements occur in the plane of the initial maximum principal stress while the smallest inward movements occur in the plane of the initial minimum principal stress. It can also be seen that when the initial maximum principal stress is vertical, the discontinuity movement is down and inward but when it is horizontal, the movement is up and inward.

# INITIAL STRESSES

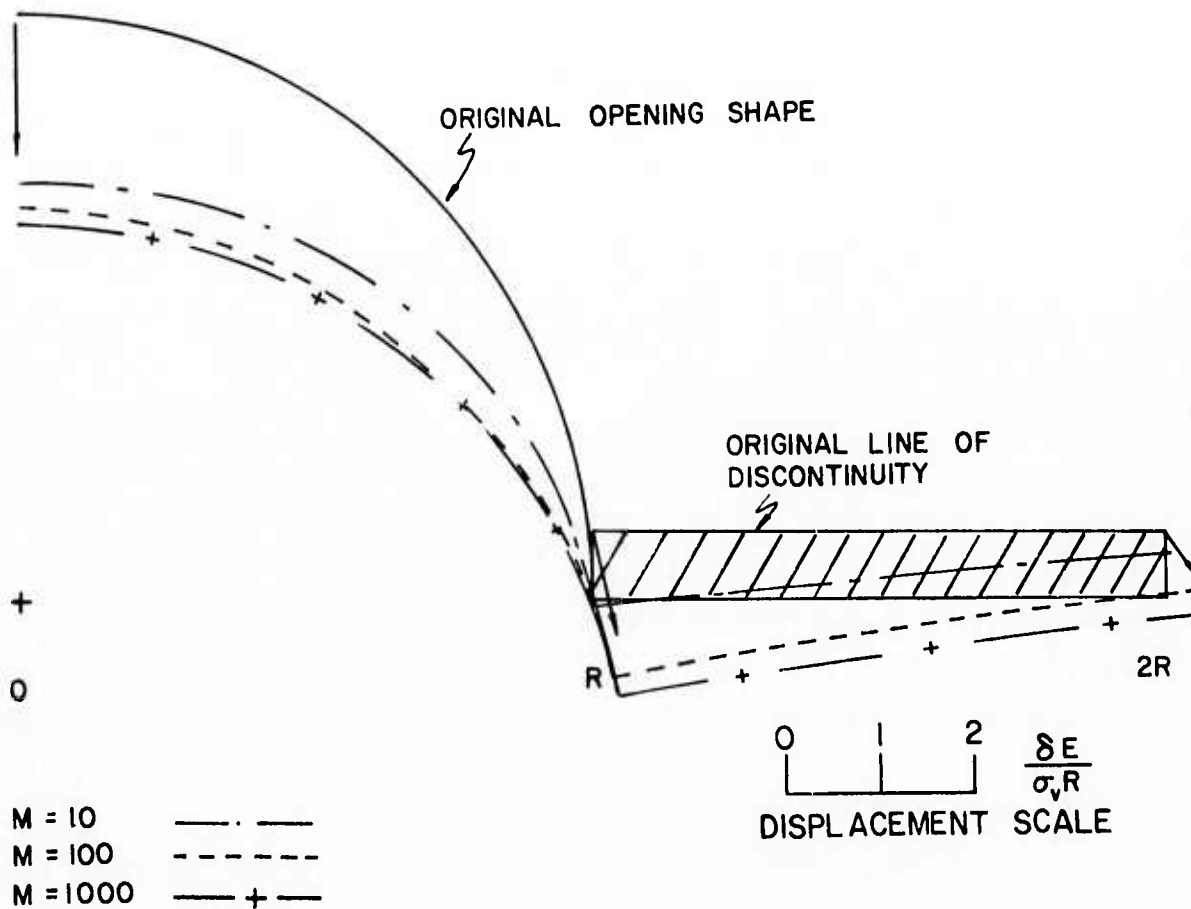
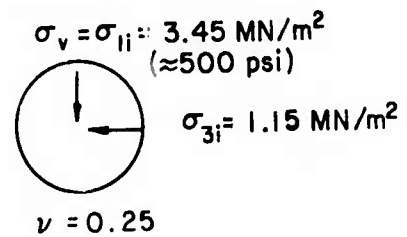


**FIG. 5-39 DISPLACEMENTS OF CIRCULAR OPENING  
 IN ROCK WITH A PLANAR DISCONTINUITY**  
 $K = 1/3$  ,  $\theta = 0^\circ$  ,  $\alpha = 0^\circ$

# INITIAL STRESSES

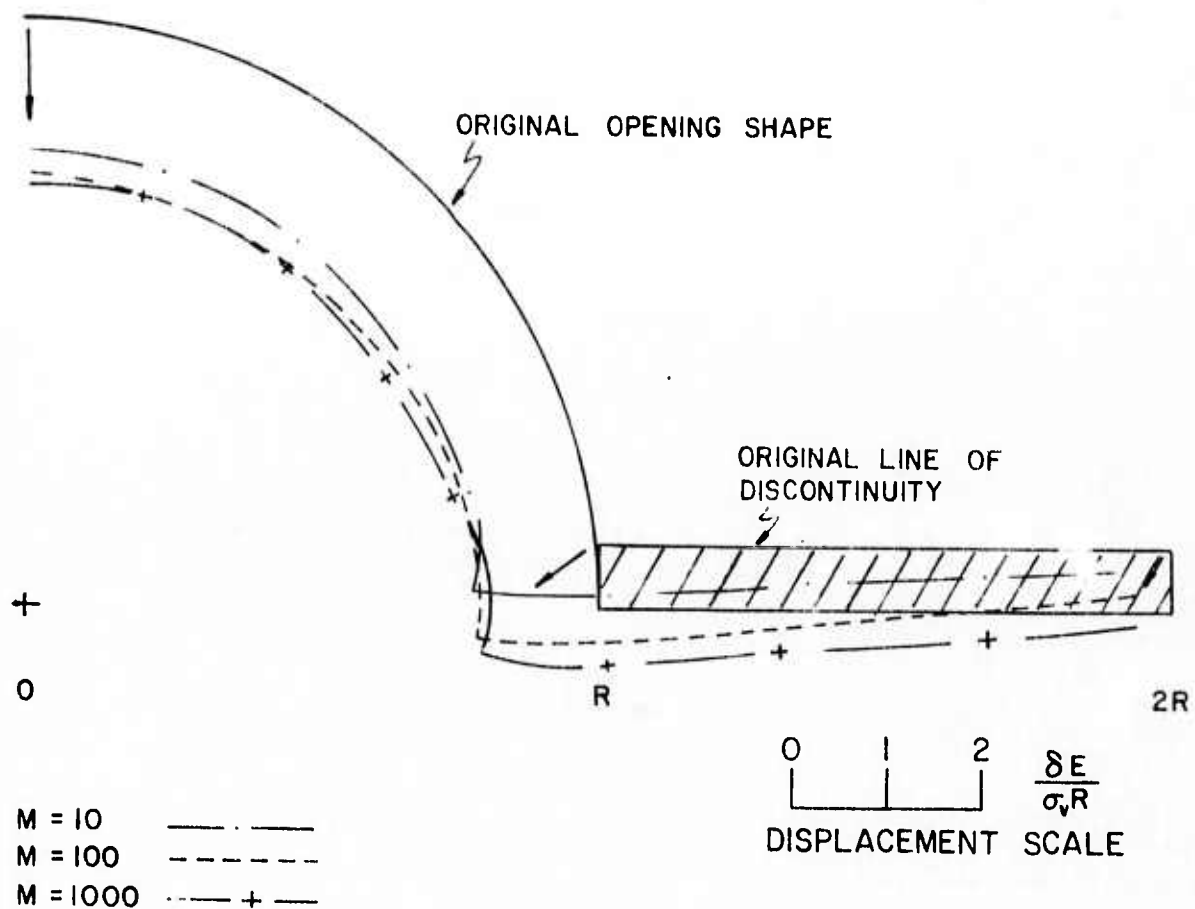
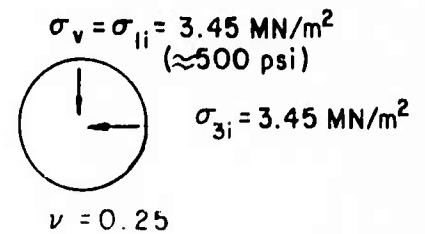


**FIG. 5-40 DISPLACEMENTS OF CIRCULAR OPENING  
 IN ROCK WITH A PLANAR DISCONTINUITY**  
 $K = 1$  ,  $\theta = 0^\circ$  ,  $\alpha = 0^\circ$

# INITIAL STRESSES

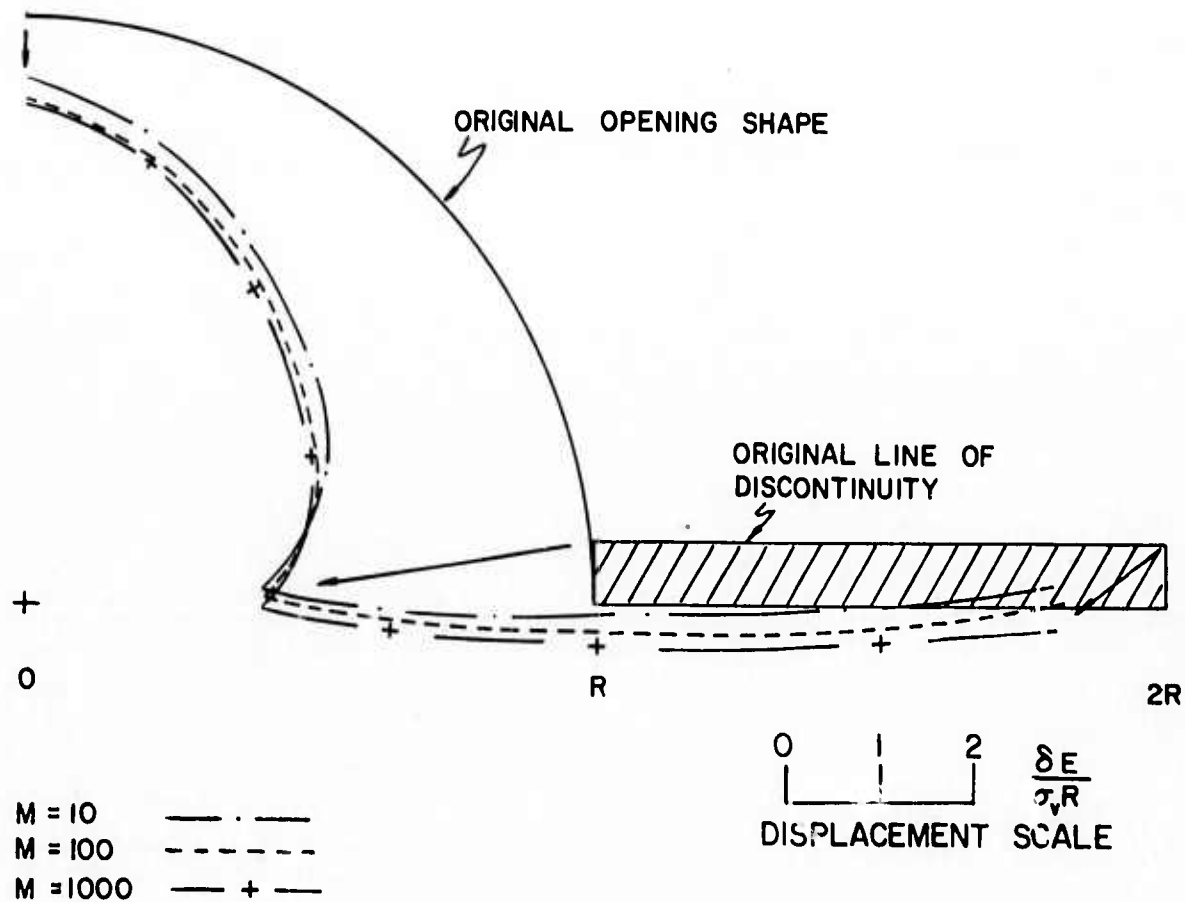
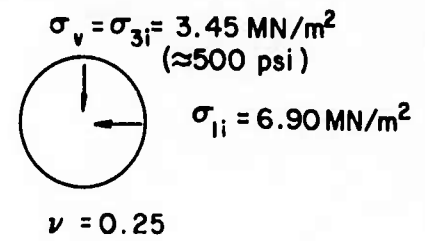


**FIG. 5-41 DISPLACEMENTS OF CIRCULAR OPENING  
 IN ROCK WITH A PLANAR DISCONTINUITY**  
 $K = 1/2$  ,  $\theta = 90^\circ$  ,  $\alpha = 0^\circ$



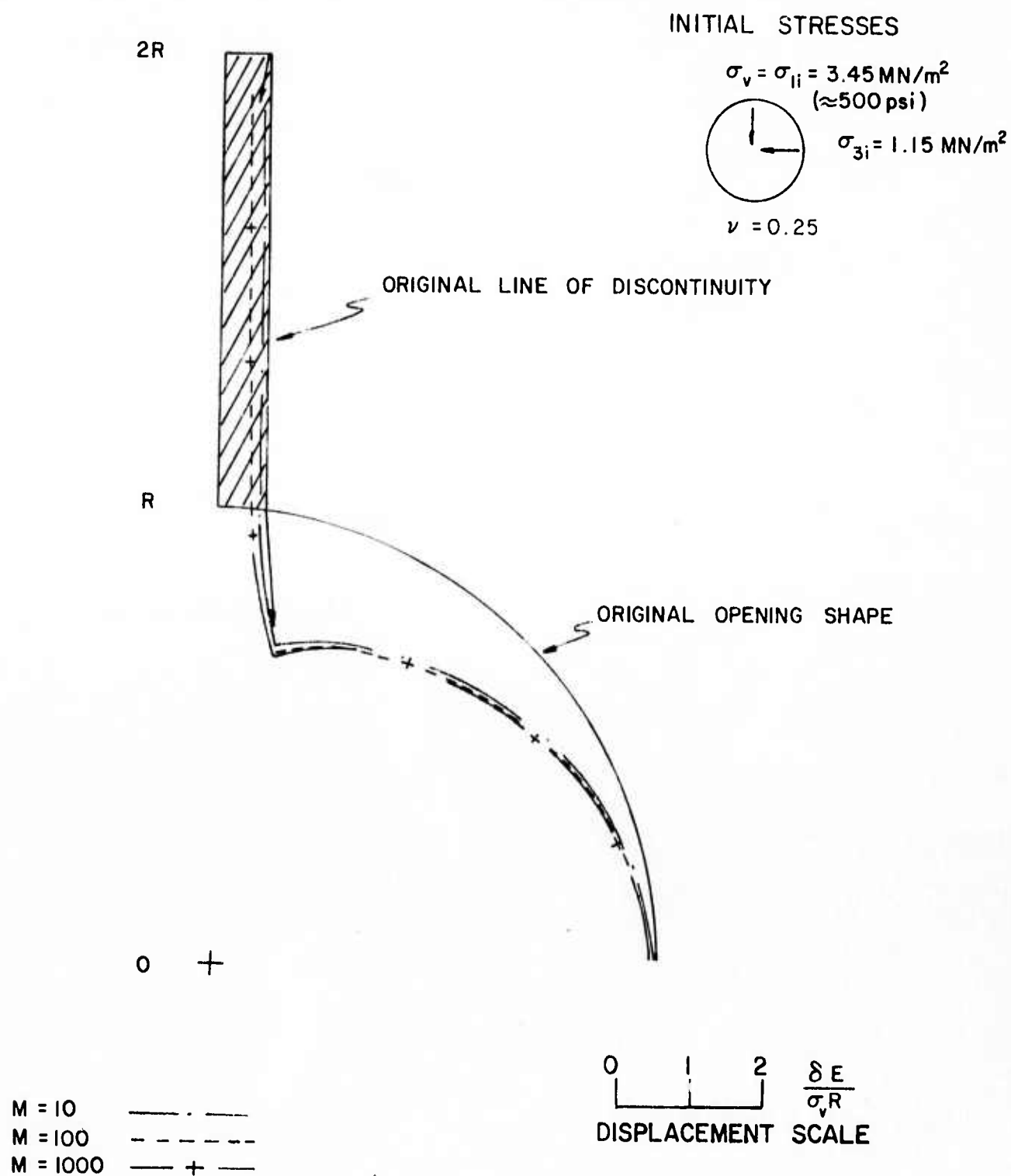


**FIG. 5-42 DISPLACEMENTS OF CIRCULAR OPENING  
IN ROCK WITH A PLANAR DISCONTINUITY  
 $K = 1/3$  ,  $\theta = 0^\circ$  ,  $\alpha = 90^\circ$**

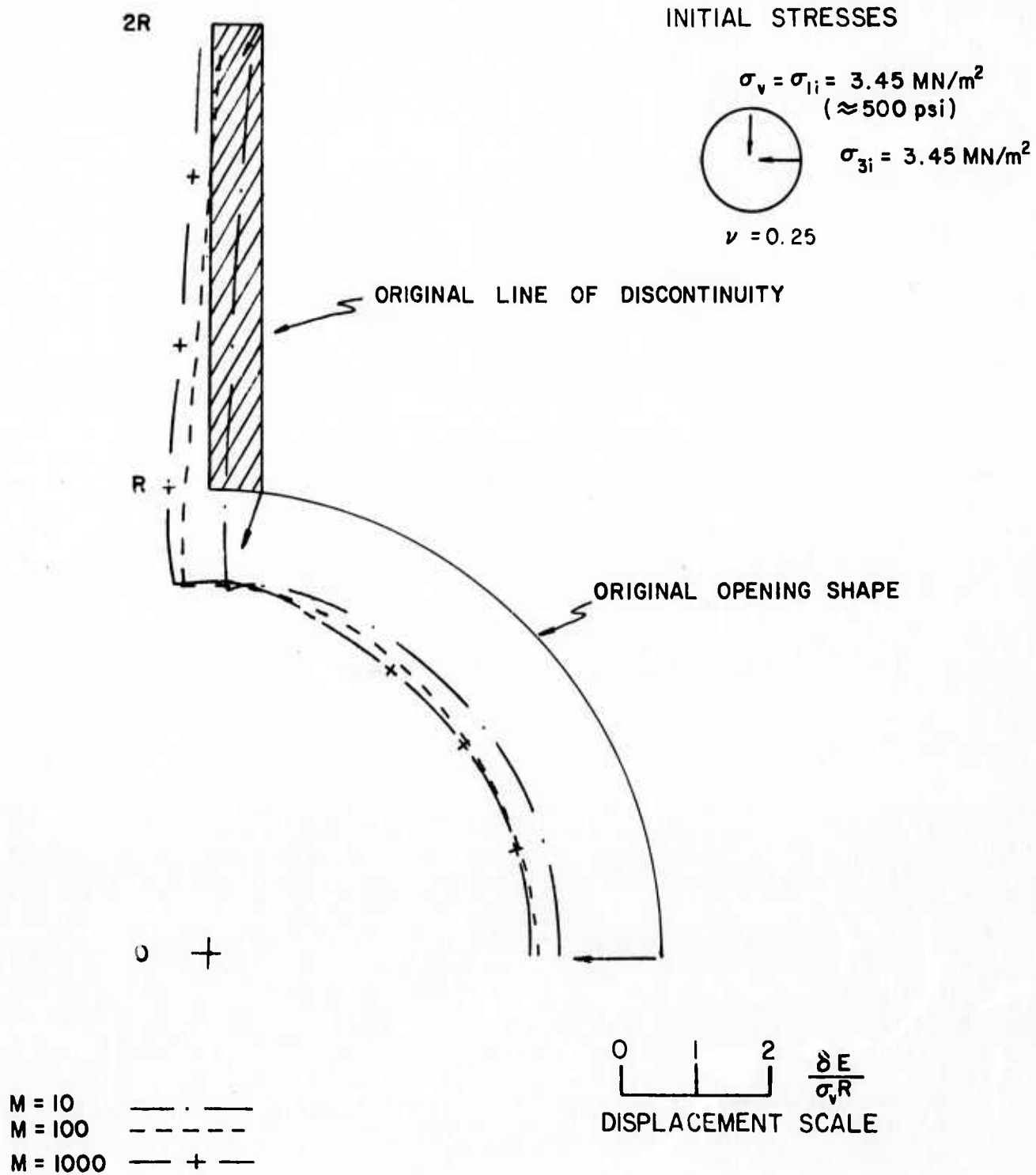


**FIG. 5-43 DISPLACEMENTS OF CIRCULAR OPENING  
 IN ROCK WITH A PLANAR DISCONTINUITY**  
 $K = 1$  ,  $\theta = 0^\circ$  ,  $\alpha = 90^\circ$

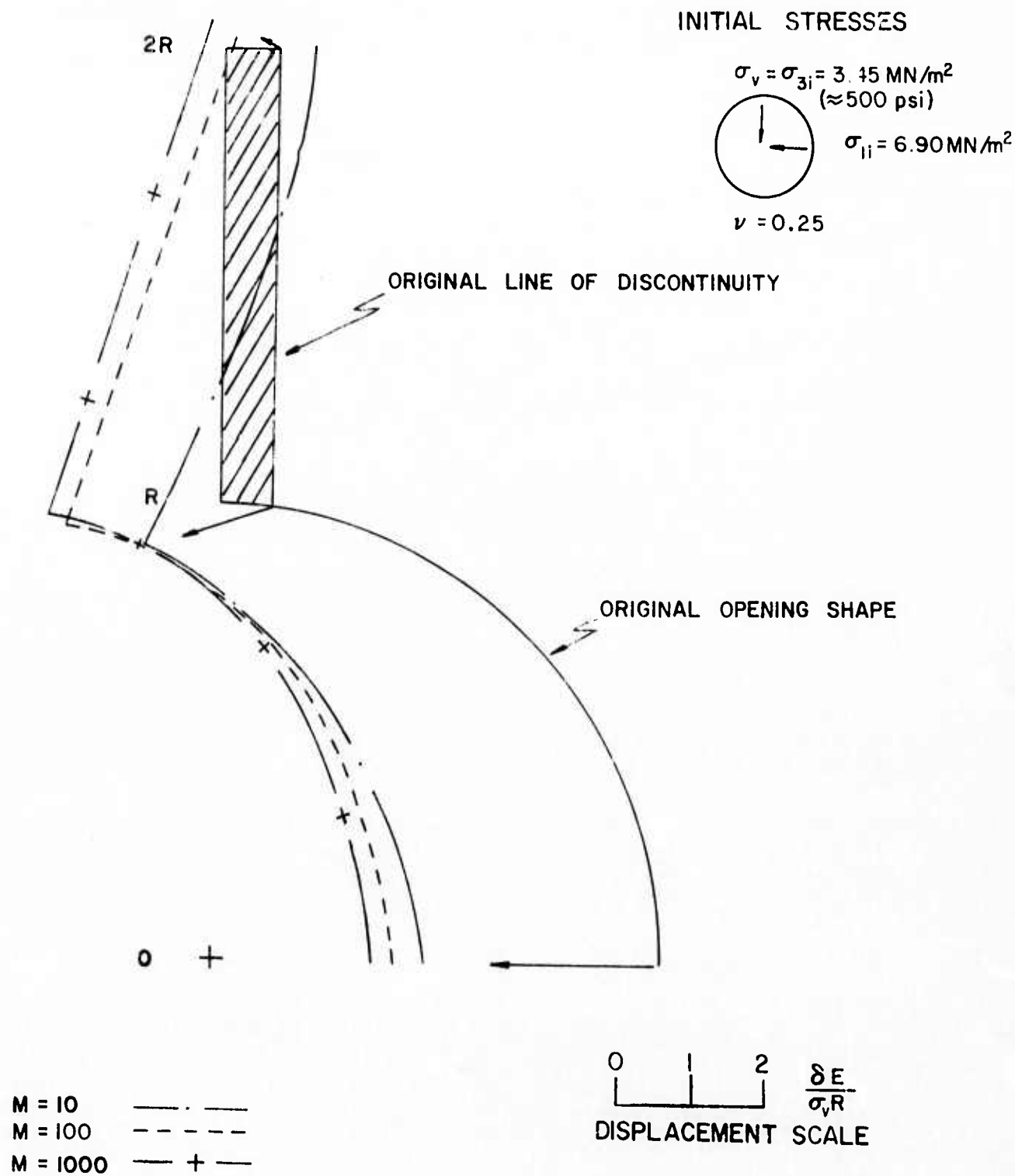


**FIG. 5-44 DISPLACEMENTS OF CIRCULAR OPENING  
IN ROCK WITH A PLANAR DISCONTINUITY  
 $K = 1/2$  ,  $\theta = 90^\circ$  ,  $\alpha = 90^\circ$**

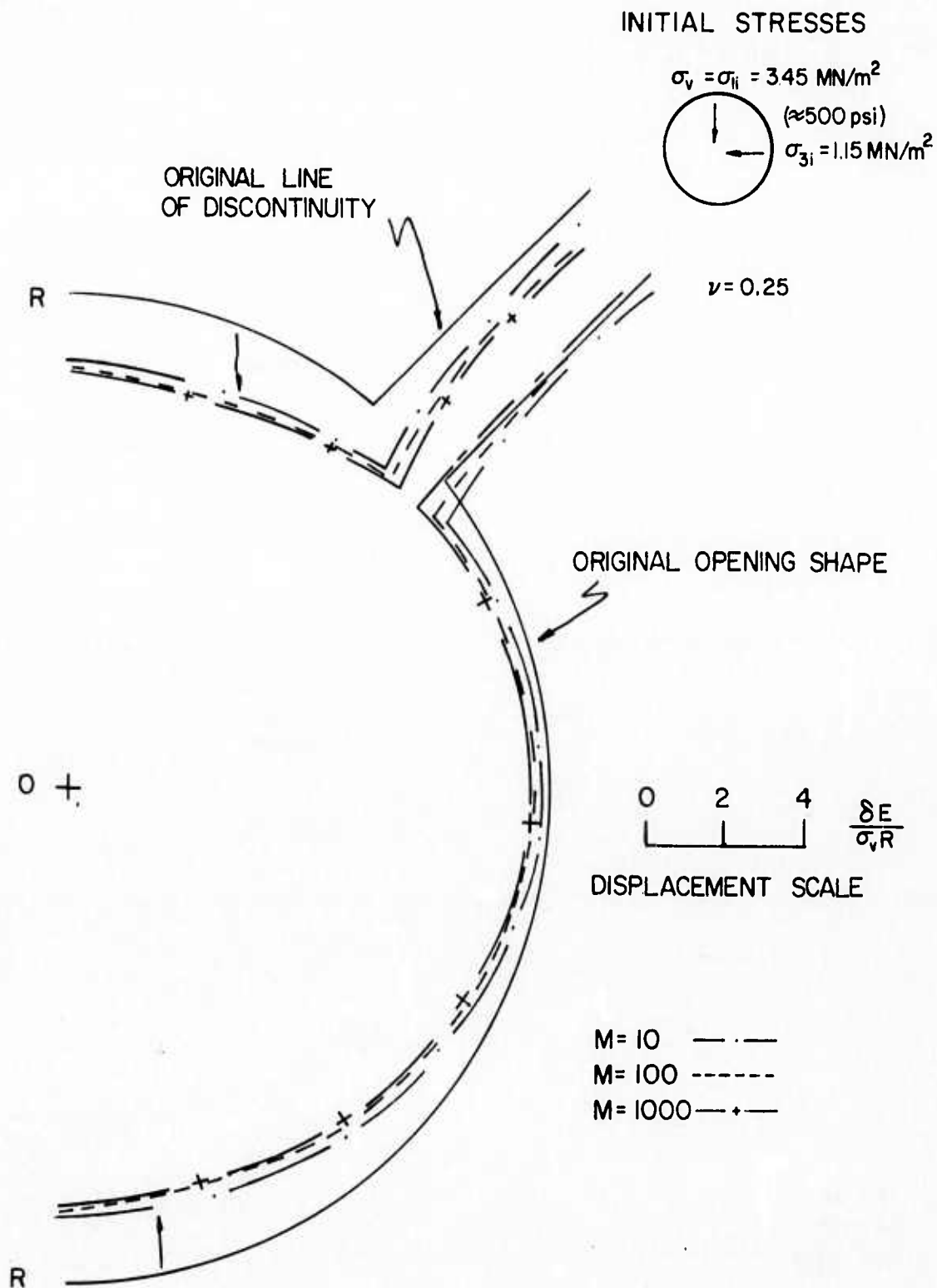


**FIG. 5-45 DISPLACEMENTS OF CIRCULAR OPENING  
IN ROCK WITH A PLANAR DISCONTINUITY  
 $K=1/3$ ,  $\theta=0^\circ$ ,  $\alpha=45^\circ$**

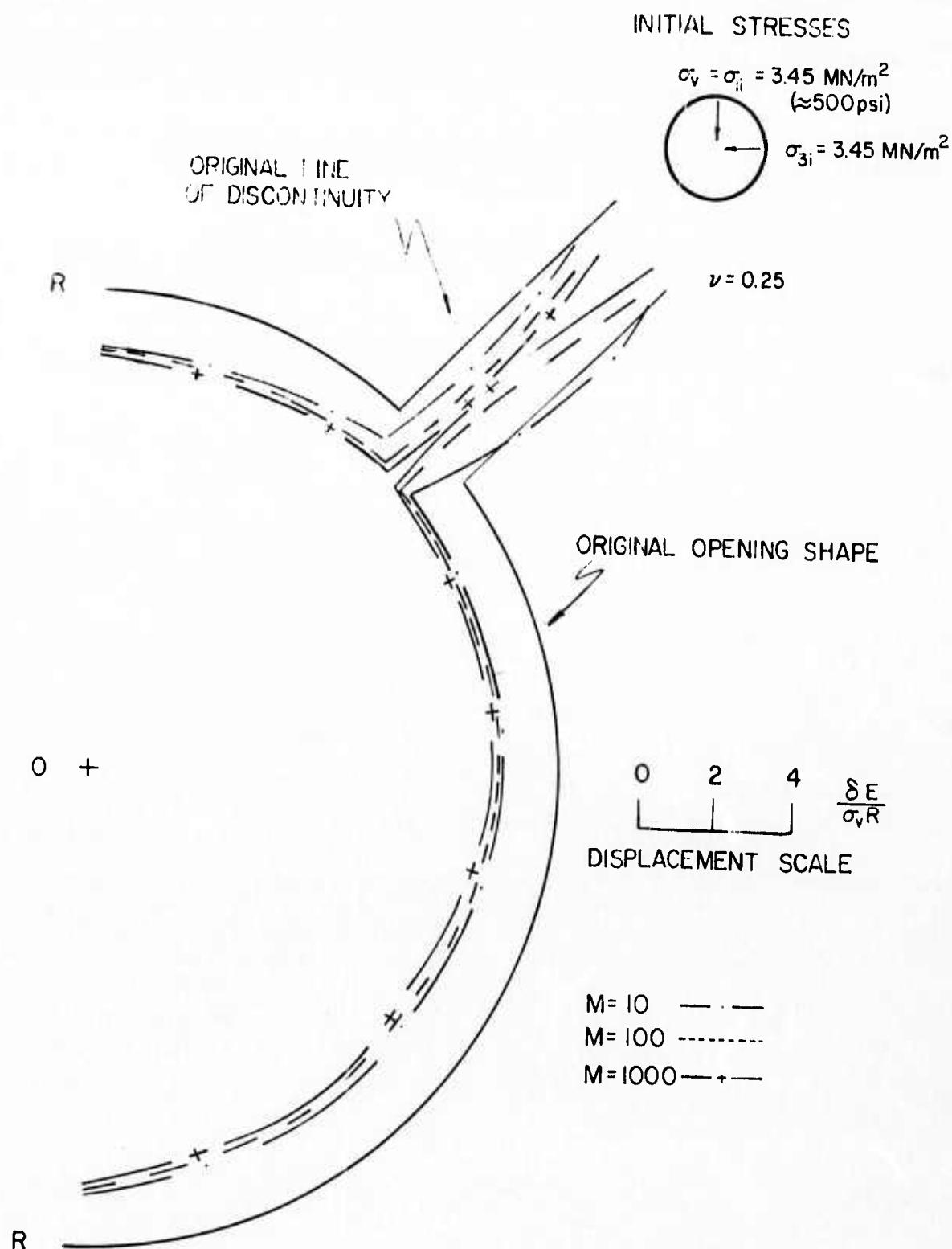


**FIG. 5-46 DISPLACEMENTS OF CIRCULAR OPENING  
IN ROCK WITH A PLANAR DISCONTINUITY  
 $K=1$ ,  $\theta=0^\circ$ ,  $\alpha=45^\circ$**

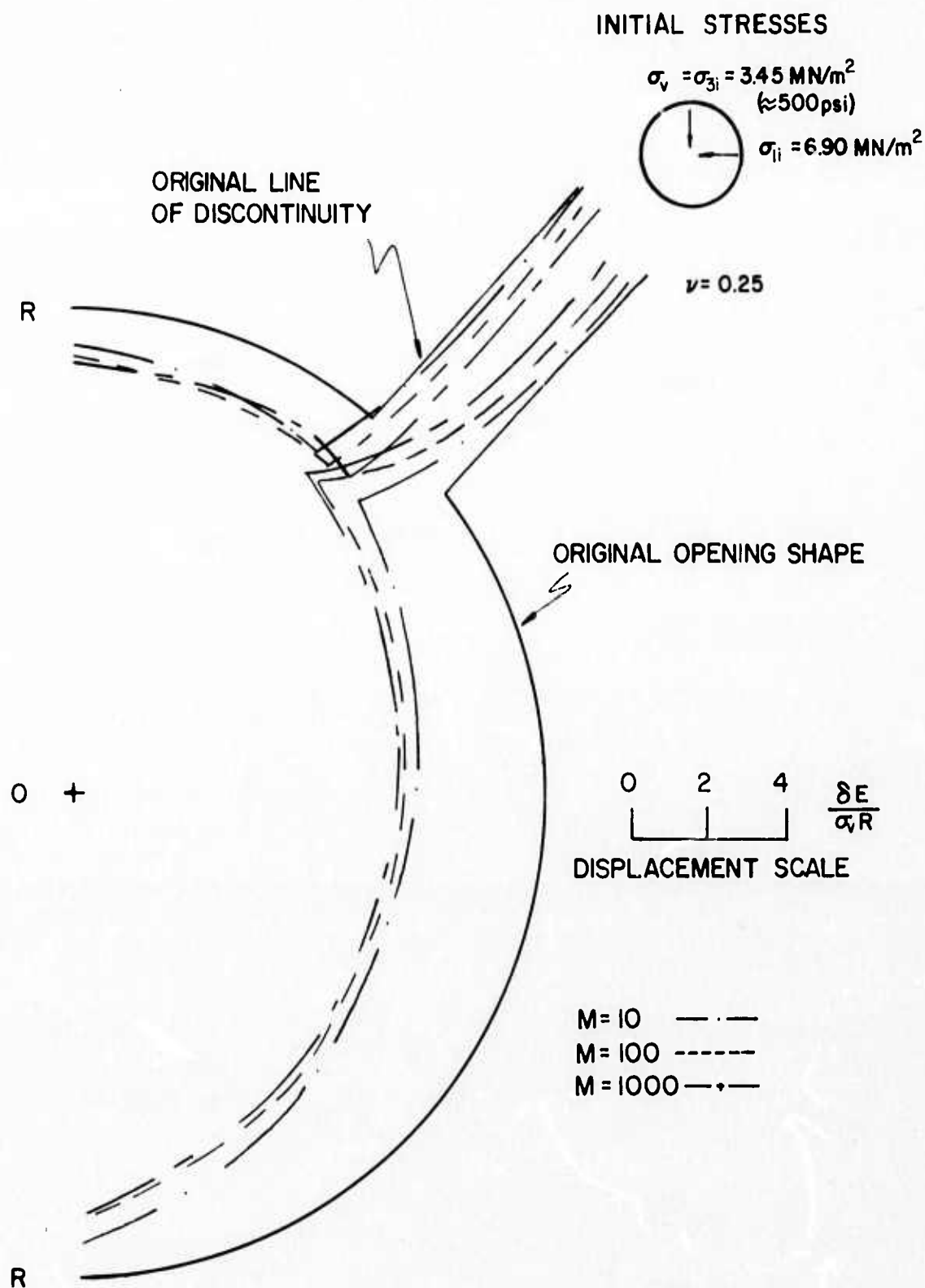


**FIG. 5-47 DISPLACEMENTS OF CIRCULAR OPENING  
 IN ROCK WITH A PLANAR DISCONTINUITY  
 $K=1/2$ ,  $\theta=90^\circ$ ,  $\alpha=45^\circ$**

### Summary

The analyses presented in this chapter were conducted to evaluate the significance of discontinuity stiffness and orientation on the resulting stresses and displacements around underground openings in rock containing a single, prominent, planar discontinuity. The results of these analyses showed that the stress changes, i.e., load transfer, become more substantial, tension zones increase, normal and shear stresses on the discontinuity decrease and displacements increase as the discontinuity becomes softer. These changes are very significant when  $M$  goes from 1 to 10, are fairly important when  $M$  goes from 10 to 100 and are small when  $M$  goes from 100 to 1000.

When the planes of the discontinuity and the minimum principal stress coincide, a substantial reduction occurs in the dimensionless  $\sigma_1$  values, the dimensionless normal stresses on the discontinuity are greatest, the discontinuity compression is greatest and the inward displacements are least.

When the planes of the discontinuity and the maximum principal stress coincide, a substantial increase occurs in the dimensionless  $\sigma_1$  values in the discontinuity with a decrease adjacent to the discontinuity, the dimensionless shear stresses on the discontinuity are greatest, the discontinuity compression is least and the inward displacements are greatest.

When the discontinuity is at  $45^\circ$  to the initial principal stresses and as the discontinuity becomes softer, the dimensionless  $\sigma_1$  values in the discontinuity become equal to one and the dimensionless  $\sigma_3$  values in the discontinuity become equal to  $K$ , the ratio of initial minimum to maximum principal stresses.

All other changes are minor.



## CHAPTER 6

### STRESS-DEFORMATION BEHAVIOR OF PLANAR DISCONTINUITIES

Rock masses normally contain natural planar discontinuities which may be joints, sheared zones, crushed zones, seams, faults, cleavage planes, bedding planes or openings along schistosity or foliation. The stress-deformation behavior of these discontinuities depends upon a number of factors including the density, porosity, structure, degree of weathering, type and quality of cementing agent, stress history, duration of loading, normal stress and shear stress. In many cases it may be possible to account for these factors by selecting specimens and test conditions which simulate the anticipated field conditions, but even when this is done, it is commonly found that the stress-deformation behavior of the discontinuity is nonlinear and dependent upon the magnitude of the normal stresses. Because of these variations, the studies described in this chapter were conducted to summarize the available data on the properties of discontinuities and to evaluate the manner in which these properties can be modeled in finite element solutions.

#### One-Dimensional Element

Goodman et al (1968) developed a one-dimensional finite element (i.e., no width) for simulating the behavior of rock discontinuities. A typical element is shown in Figure 6-1 along with its possible modes of behavior; extension, compression, shear and their combinations. The properties defining the discontinuity are the normal stiffness,  $K_n$ , and the shear stiffness,  $K_s$ , which relate the average stresses to the average displacements of the discontinuity, as shown below:

$$\sigma_j = K_n \delta_n \quad (6-1)$$

and

$$\tau_j = K_s \delta_s \quad (6-2)$$

in which  $\sigma_j$  and  $\tau_j$  are the average normal and shear stresses on the discontinuity plane and  $\delta_n$  and  $\delta_s$  are the average normal and shear displacements of the discontinuity.

The earlier analyses with this type of element assumed linear stress-displacement behavior for  $K_n$  and  $K_s$ , except when either tension or shear failure developed, at which point these parameters would be adjusted to other values. Heuze'et al (1971)

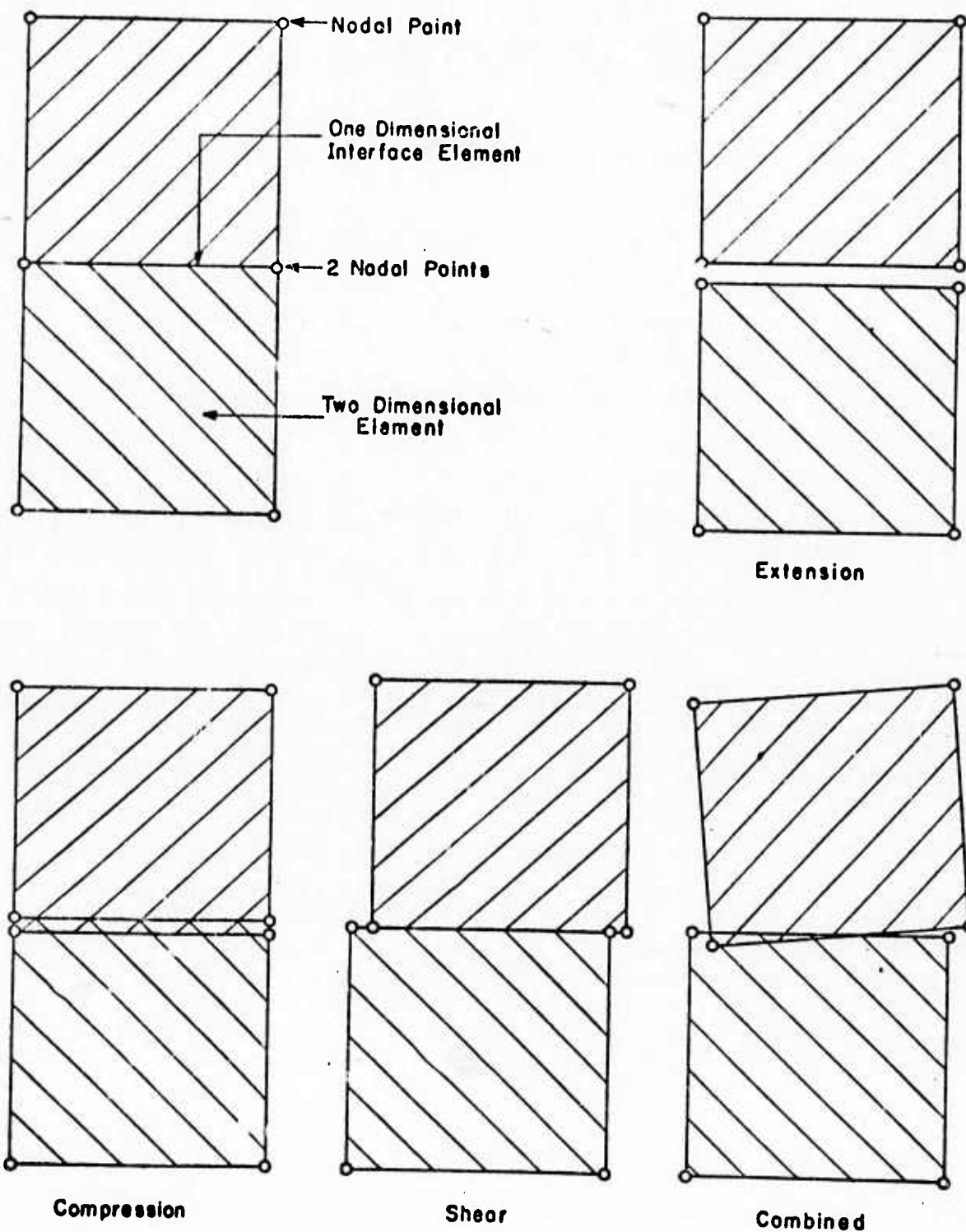


**FIG. 6-1 MODES OF BEHAVIOR OF DISCONTINUITY ELEMENT  
(FROM CLOUGH AND DUNCAN, 1969 )**

modified this approach by using an iterative "perturbation" solution in which the stiffness values would vary with the stress and displacement states. Secant stiffness were therefore used and several iterations would be required to achieve a solution.

Clough and Duncan (1969), in their studies of interface behavior between soil and concrete, developed a different approach for accommodating stiffness variations by developing a nonlinear, stress-dependent relationship which can evaluate the tangent shear stiffness for any level of shear stress up to failure and for any normal stress. The normal stiffness was assumed to be constant. Their relationship was based upon a hyperbolic relationship of the form:

$$\tau = \frac{\delta_s}{a + b \delta_s} \quad (6-3)$$

in which  $\tau$  = shear stress,  $\delta_s$  = shear displacement,  $a$  = constant (reciprocal of initial tangent shear stiffness) and  $b$  = constant (reciprocal of ultimate shear strength).

Following a development similar to that shown in Chapter 3 for the modulus and Poisson's ratio, they obtained the following equation:

$$K_{st} = K_{si} \left( 1 - \frac{\tau R_{fj}}{c_j + \sigma_n \tan \phi_j} \right)^2 \quad (6-4)$$

in which  $K_{st}$  = tangent shear stiffness,  $K_{si}$  = initial tangent shear stiffness,  $\tau$  = mobilized shear stress,  $R_{fj}$  = failure ratio similar to that described in Chapter 3,  $\sigma_n$  = discontinuity angle of friction,  $c_j$  = discontinuity cohesion and  $\phi_j$  = discontinuity angle of friction.

They further noted that  $K_{si}$  varies linearly with  $\sigma_n$  on a log-log basis and this led to the following equation:

$$K_{si} = K_j \gamma_w \left( \frac{\sigma_n}{p_a} \right)^{n_j} \quad (6-5)$$

in which  $K_j$  = stiffness number,  $n_j$  = stiffness exponent,  $p_a$  = atmospheric pressure and  $\gamma_w$  = unit weight of water. The  $\gamma_w$  and  $p_a$  terms were introduced to make the  $K_j$  term dimensionless for ease in comparison between different types of discontinuities. In an analysis, the values of  $\gamma_w$  and  $p_a$  are introduced in units consistent with those for  $\sigma_n$  and  $K_{sj}$ .

By substituting Equation (6-5) into Equation (6-4), it is found that:

$$K_{st} = K_j \gamma_w \left( \frac{\sigma_n}{p_a} \right)^{n_j} \left( 1 - \frac{\tau R_{fj}}{c_j + \sigma_n \tan \phi_j} \right)^2 \quad (6-6)$$

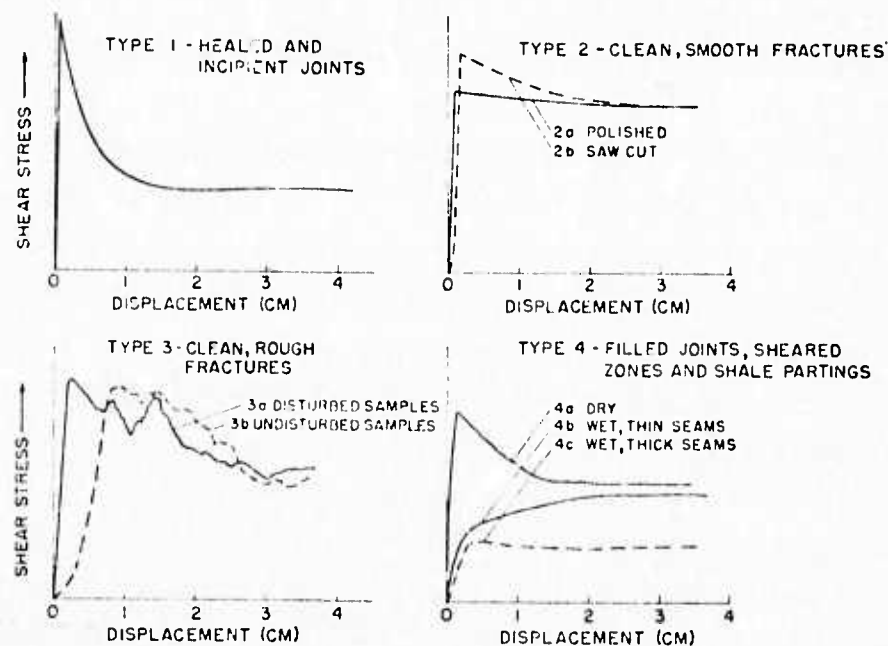
which is the final equation for tangent shear stiffness as a function of mobilized shear stress and normal stress. If the stress-deformation curve is linear,  $R_{fj}$  can be set equal to zero and if the stiffness is not stress-dependent,  $n_j$  can be set equal to zero. All of the parameters can be simply evaluated in a manner similar to that discussed in Chapter 3. The advantages of this relationship are that it is a simple, practical relationship for describing the nonlinearity and stress-dependency of the shear stiffness for a discontinuity, and that it is well-suited for excavation analyses which are made on a stage basis because the properties can be simply and accurately evaluated at each stage.

#### Properties of Discontinuities

The stiffness values can be determined from direct shear tests on rock samples containing discontinuities by applying normal and shear stresses to the discontinuity plane and measuring the corresponding displacements. The equipment to conduct these tests on natural discontinuities is rather elaborate and is discussed in some detail by Goodman (1969).

Figure 6-2 shows the typical stress-deformation behavior which has been observed for discontinuities. Types 1 and 2 display little, if any, nonlinearity while Types 3 and 4 display progressively more nonlinearity. All four types display stress-dependency to varying degrees.

A study was made of the literature to summarize the available data on the properties of discontinuities. It was found that very little data were available and that most of the data which were available had been included in a report by



Type	Type of Surfaces Typically Exhibiting Behavior in This Class
1	Healed joints and incipient joints
2	Clean, smooth fractures
	2a polished
	2b unpolished (rough saw cut)
3	Clean, rough fractures
	3a artificial extension fractures and disturbed samples
	3b undisturbed samples
4	Filled joints, sheared zones, shale partings, and smooth bedding
	4a dry or slightly moist
	4b wet; thin seam
	4c wet; thick seam

**FIG. 6-2 TYPICAL STRESS-DEFORMATION BEHAVIOR OF DISCONTINUITIES (FROM GOODMAN, 1969)**

Goodman (1968). The data were analyzed further and it was found that both the stress-dependency and nonlinearity components of Equation 6-6 reasonably well described the data. The results of this study are shown in Table 6-1, which is a compilation of the properties of discontinuities for both linear and nonlinear conditions. It can be seen that very little data were available for normal stiffnesses, but a reasonable amount of data were available for the linear secant shear stiffness,  $K_s$ , evaluated at both the yield and peak points of the stress-deformation curves. From these values it was possible to determine the stress-dependent parameters,  $K_j$  and  $n_j$ , for the yield and peak points as well as the strength parameters at the peak (maximum) and in the post-peak residual state. Since the original stress-deformation curves were not available for most of the data, the initial  $K_j$  and  $n_j$  could only be established for three data sets (DL-3,4,15) and these three showed very similar values. While the yield and peak values of  $K_j$  and  $n_j$  cannot be directly used in the nonlinear analyses, they at least serve as a reference base to establish the appropriate order of magnitude which may be expected for the initial  $K_j$  and  $n_j$  values.

#### Equivalence of One-Dimensional and Two-Dimensional Element Properties

The properties of one-dimensional and two-dimensional elements representing discontinuities may be made equivalent under certain conditions. For the one-dimensional element, the stresses are given by Equations 6-1 and 6-2. For the two-dimensional element representing a long thin discontinuity, the stresses may be given by the following expression:

$$\sigma = \frac{\delta_n E}{T} \quad (6-7)$$

and 
$$\tau = \frac{\delta_s G}{T} \quad (6-8)$$

in which  $\sigma$  and  $\tau$  are the normal and shear stresses,  $\delta_n$  and  $\delta_s$  are the normal and shear displacements,  $E$  is the elastic modulus,  $G$  is the shear modulus, and  $T$  is the thickness of the two-dimensional element representing the discontinuity. By equating the stresses in Equations 6-7 and 6-8 with those in Equations 6-1 and 6-2, it can be seen that the properties of the two types of elements representing the discontinuities can be interrelated as below:

$$K_n = \frac{E}{T} \quad (6-9)$$







and

$$K_s = \frac{G}{T} = \frac{E}{2(1+\nu)T} \quad (6-10)$$

in which  $\nu$  = Poisson's ratio. Furthermore it can be seen that, if the stiffnesses of the one-dimensional element are directly related to equivalent elastic parameters, then they must be related to each other as below:

$$K_s = \frac{K_n}{2(1+\nu)} \quad (6-11)$$

Since Poisson's ratio can range from 0.0 to 0.5, then  $K_s$  must range from 1/3 to 1/2 of the value of  $K_n$ .

However, even though it is always possible to establish equivalent discontinuity stiffnesses for two-dimensional elements, it may not be possible to establish equivalent elastic properties for one-dimensional elements since there are no restrictions on the interrelationship between  $K_n$  and  $K_s$ . A one-dimensional element may be rigid in compression and yet have a small shear resistance or vice versa. For example, the ratios of  $K_s/K_n$  for the four cases of  $K_n$  shown in Table 6-1 range from 0.04 to 1.20 which clearly shows that, even though the two types of elements may be mathematically equated, there is no restriction which can make them equivalent in many physical cases.

## CHAPTER 7

### ANALYSIS OF OPENINGS IN ROCK CONTAINING A SINGLE PLANAR ONE-DIMENSIONAL DISCONTINUITY

Rock masses frequently contain natural discontinuities which are planar features of virtually no width. These discontinuities include relatively unweathered joints and fracture surfaces, cleavage and bedding planes, and openings along schistosity or foliation. The analysis of rock masses containing these features is different from that discussed in Chapter 5, where discontinuities of finite width were considered, because the normal and shear stiffnesses of the one-dimensional discontinuities do not have to be related to each other, as discussed in Chapter 6. Since the stiffnesses may vary independently, the studies presented in this chapter were conducted to evaluate the effect of stiffness variations on the resulting stress and displacement pattern around underground openings in rock containing a single prominent discontinuity.

#### Finite Element Idealization

In this chapter, all of the analyses were conducted using a circular opening with a three meter radius and a horizontal discontinuity of zero width. The finite element mesh used is shown in Figure 7-1. The initial stresses were constant with depth in all of the analyses with the vertical stresses equal to  $3.45 \text{ MN/m}^2$  ( $\approx 500 \text{ psi}$ ) and the horizontal stresses equal to  $1.15 \text{ MN/m}^2$ . In all cases a three step horizontal excavation sequence, as shown in Figure 4-3, was followed.

The properties of the intact rock were held constant and were set equal to  $50,000 \text{ MN/m}^2$  for the modulus and 0.25 for Poisson's ratio. For the discontinuity, the normal stiffnesses,  $K_n$ , employed were 250, 2500 and  $25,000 \text{ KN/m}^3$ ; the limited data for  $K_n$  shown in Chapter 6 indicate that this range is possible. A nonlinear, stress-dependent tangent shear stiffness,  $K_{st}$ , as described in Chapter 6, was used in these analyses. The ranges in values of the parameters to evaluate  $K_{st}$  were selected to cover reasonably well the variations as summarized in Table 6-1. The values used in the analyses were: (1) 30,000 and 150,000 for the stiffness number,  $K_j$ , which is a measure of the initial stiffness, (2) 0.0 and 0.6 for the stiffness exponent,  $n_j$ , which is a measure of the stress-dependency of the stiffness, and (3) 0.0 and 0.8 for the failure ratio,  $R_{fj}$ , which is a measure of the nonlinearity.

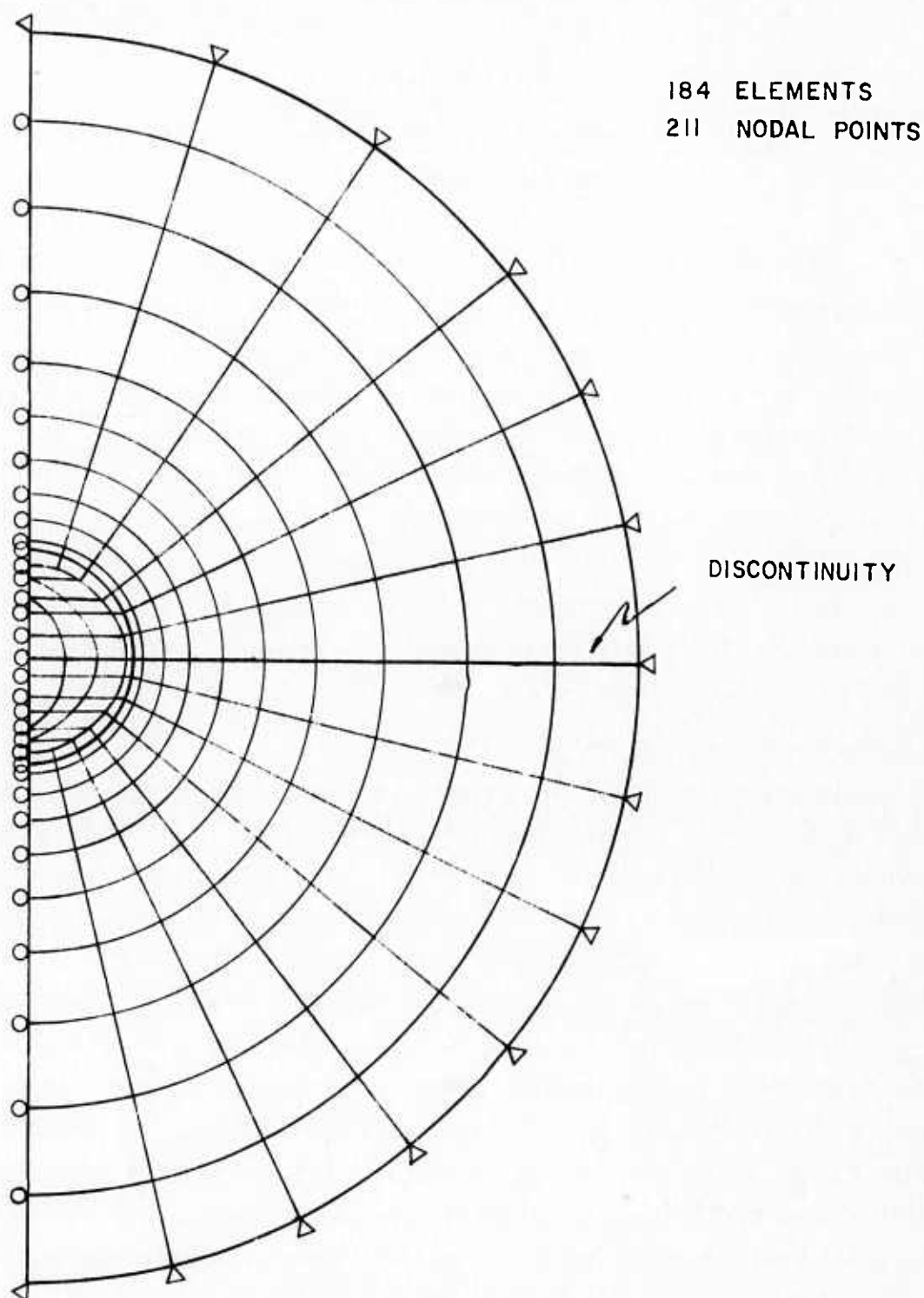


**FIG. 7-1** FINITE ELEMENT MESH FOR CIRCULAR OPENING  
IN ROCK WITH A ONE-DIMENSIONAL PLANAR  
DISCONTINUITY

The strength parameters for the discontinuity were held constant with zero cohesion and an angle of friction equal to  $40^\circ$ .

It should be noted that the shear and normal stiffnesses selected are such that, under most conditions, equivalent elastic parameters cannot be established. As shown previously with Equation 6-11,  $K_n$  must equal  $2.5 K_s$  if equivalent elastic parameters exist when Poisson's ratio is equal to 0.25. Since  $K_s = K_j \gamma_w$  for linear conditions, then  $K_n$  (in  $\text{MN/m}^3$ ) must equal  $0.0245 K_j$  for parameter equivalence. The available data discussed in Chapter 6 show that this condition frequently is not met.

#### Stresses Around Opening

Figures 7-2 and 7-3 show the dimensionless  $\sigma_1$  and  $\sigma_3$  contours for  $K_n = 2500 \text{ MN/m}^3$  and these figures are representative of all variations considered in the shear stiffness since the stresses differed by no more than 10% when  $K_j$ ,  $n_j$ , or  $R_{fj}$  was varied. Figure 7-2 shows a stress concentration in the wall of the opening above the discontinuity with stress reductions at the crown and invert, all of which are less than those which occur for homogeneous rock, shown in Figure 4-16. Figure 7-3 shows that a fairly large tension zone occurs in the wall directly above the discontinuity and that small tension zones occur at the crown and invert. Yet the dimensionless  $\sigma_3$  values increase between the crown and wall tension zones and below the discontinuity, indicating that the upper wall is moving relative to the lower wall creating different stress conditions in upper and lower wall sections. This type of behavior could not be modeled in analyses with two-dimensional discontinuities because relative movements of this type could not occur with two-dimensional elements.

Figures 7-4 and 7-5 show the dimensionless stress contours when the normal stiffness is increased to  $25,000 \text{ MN/m}^3$  while Figures 7-6 and 7-7 show the dimensionless stress contours when the normal stiffness is decreased to  $250 \text{ MN/m}^3$ . In all of these figures, for the sake of identification,  $M_j$  represents the ratio of rock modulus to unit normal stiffness. Comparing Figures 7-2 through 7-7, it can be seen that as the normal stiffness increases, the stress contours become more symmetrical about the springline elevation and more similar to the contours obtained for the homogeneous solution. As the normal stiffness decreases, the dimensionless  $\sigma_1$  values decrease and the dimensionless  $\sigma_3$  values increase below the discontinuity and both stresses increase in the wall at a short distance above the discontinuity. Immediately above the discontinuity, the tension zone increases as the normal

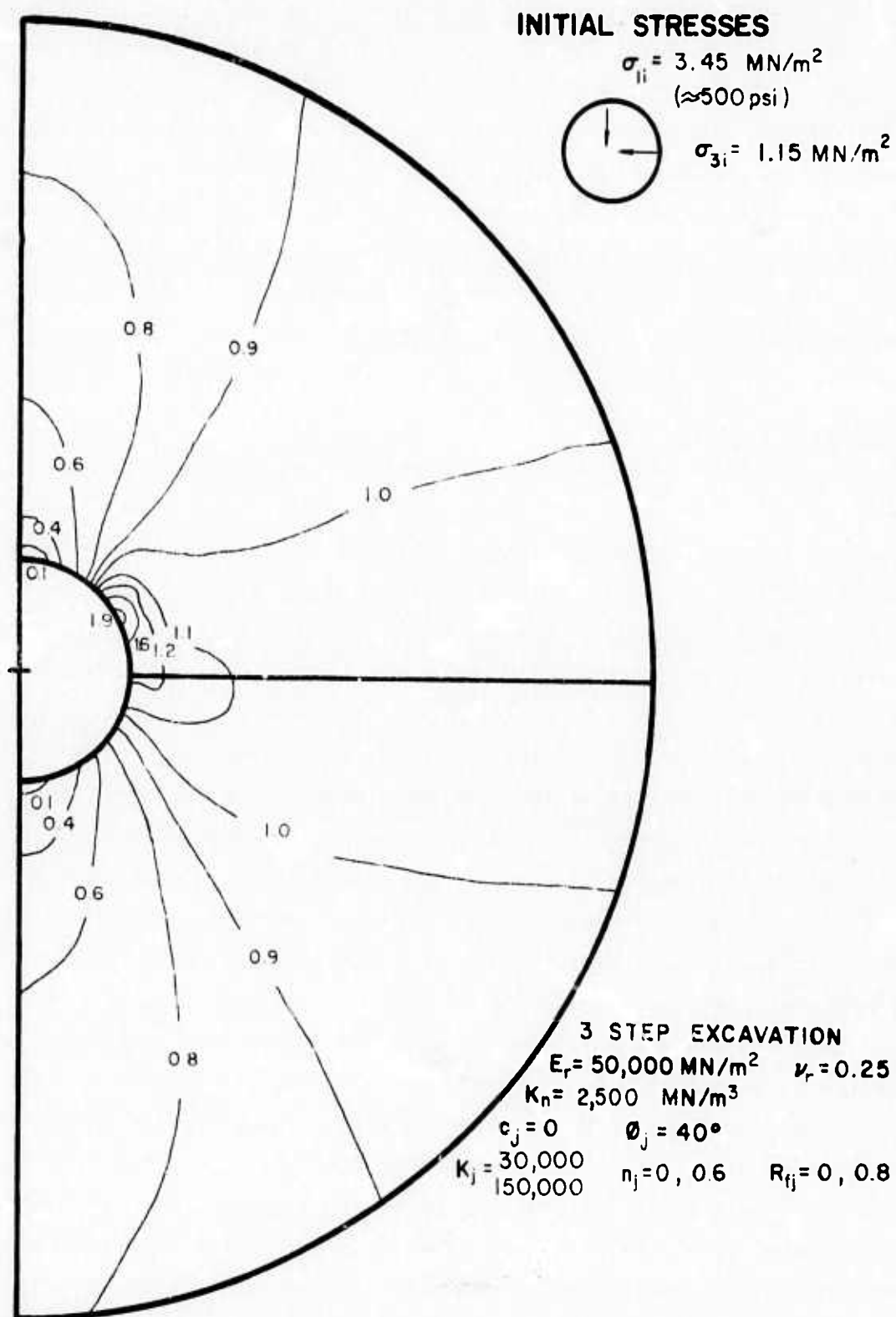


**FIG. 7-2    CONTOURS OF  $\sigma_1 / \sigma_{1i}$  FOR CIRCULAR OPENING  
IN ROCK WITH A I-D DISCONTINUITY  
 $K=1/3$  ,  $\theta=0^\circ$  ,  $\alpha=0^\circ$  ,  $M_j=20$**



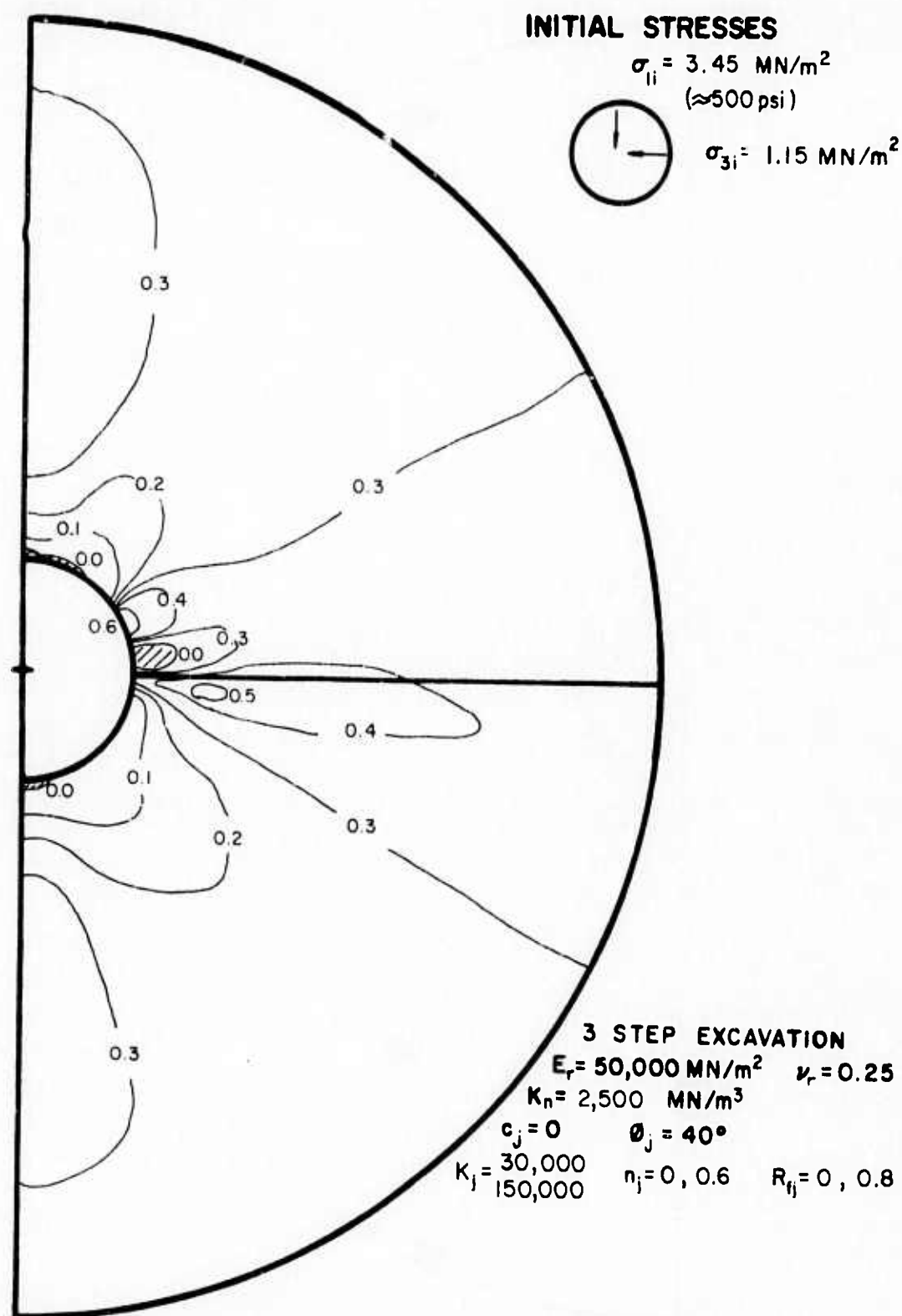


**FIG. 7-3    CONTOURS OF  $\sigma_3/\sigma_{li}$  FOR CIRCULAR OPENING  
 IN ROCK WITH A 1-D DISCONTINUITY  
 $K=1/3$  ,  $\theta=0^\circ$  ,  $\alpha=0^\circ$  ,  $M_j=20$**

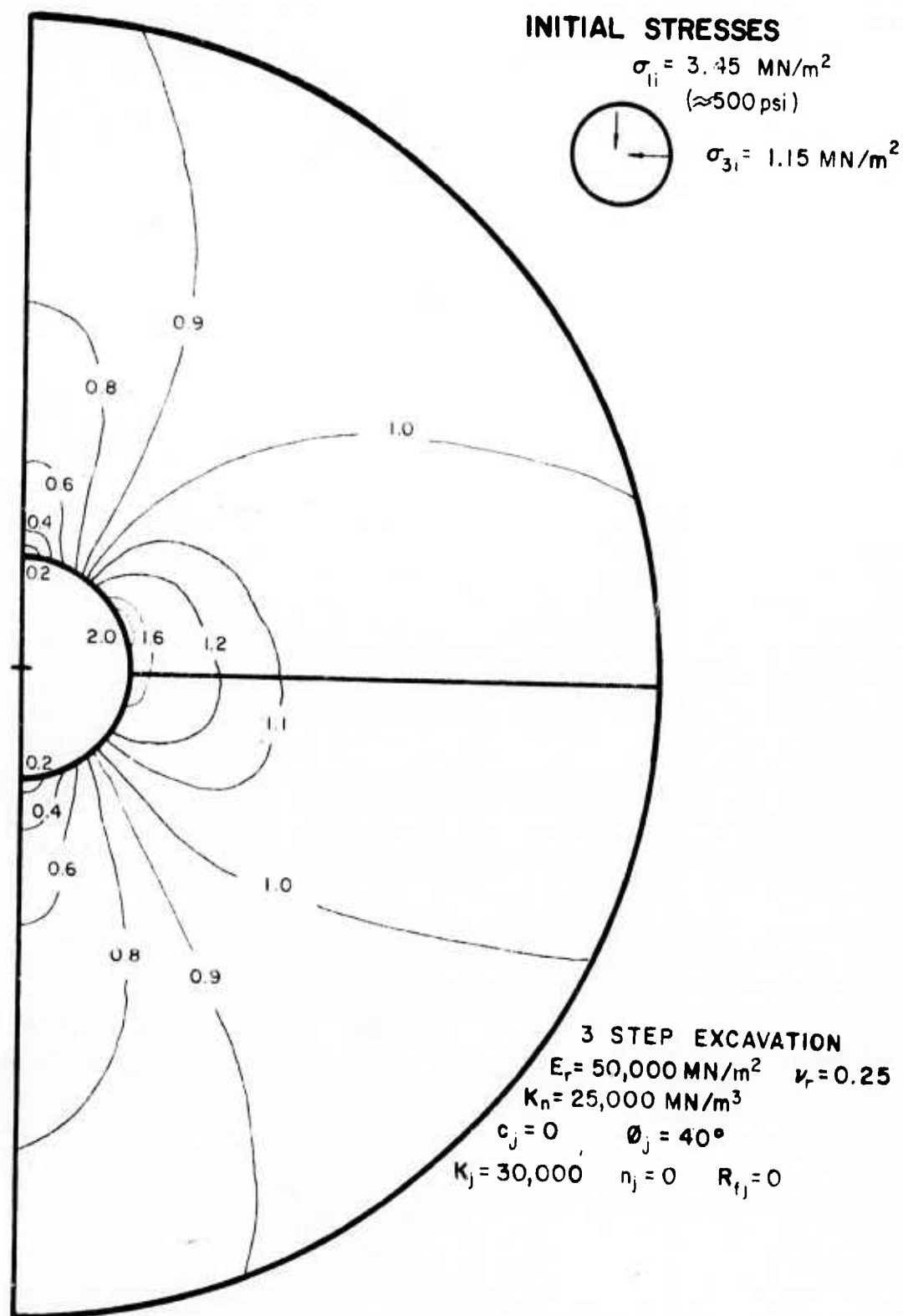


**FIG. 7-4** CONTOURS OF  $\sigma_1/\sigma_{1i}$  FOR CIRCULAR OPENING  
 IN ROCK WITH A 1-D DISCONTINUITY  
 $K=1/3$  ,  $\theta=0^\circ$  ,  $\alpha=0^\circ$  ,  $M_j=2$



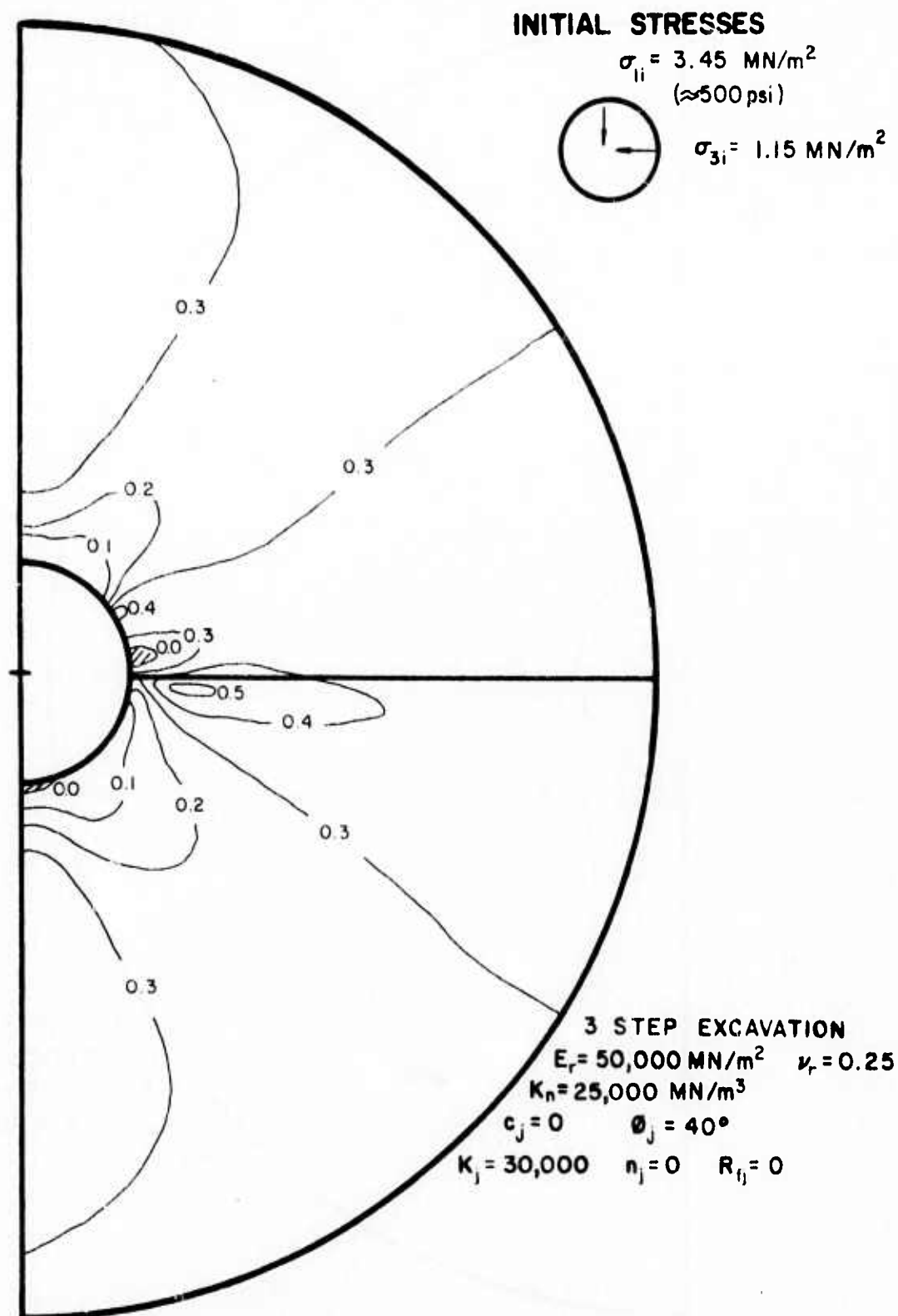


**FIG. 7-5    CONTOURS OF  $\sigma_3/\sigma_{1i}$  FOR CIRCULAR OPENING  
IN ROCK WITH A I-D DISCONTINUITY  
 $K=1/3$  ,  $\theta=0^\circ$  ,  $\alpha=0^\circ$  ,  $M_j=2$**

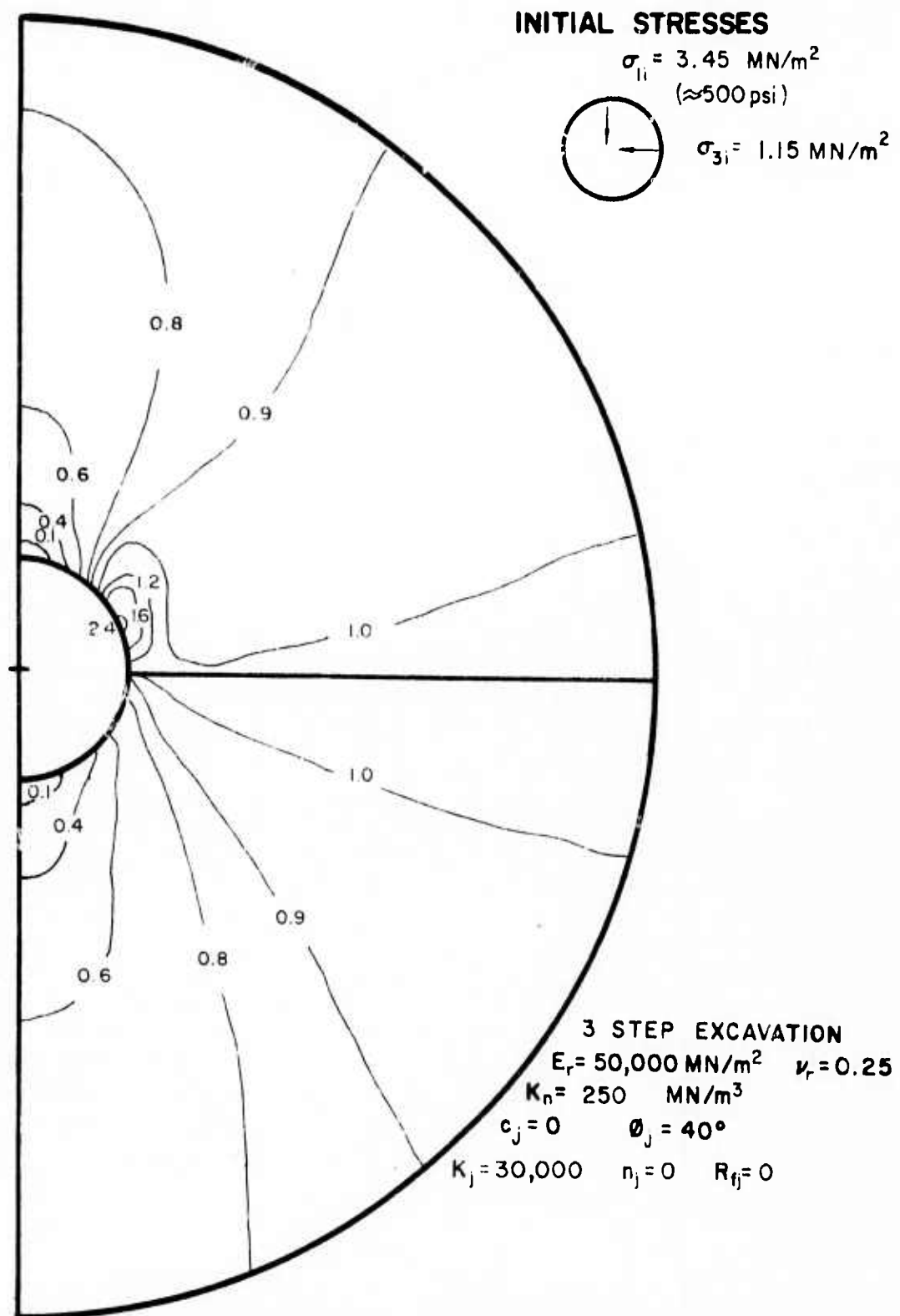


**FIG. 7-6 CONTOURS OF  $\sigma_1/\sigma_{1i}$  FOR CIRCULAR OPENING IN ROCK WITH A I-D DISCONTINUITY  $K=1/3$ ,  $\theta=0^\circ$ ,  $\alpha=0^\circ$ ,  $M_j=200$**

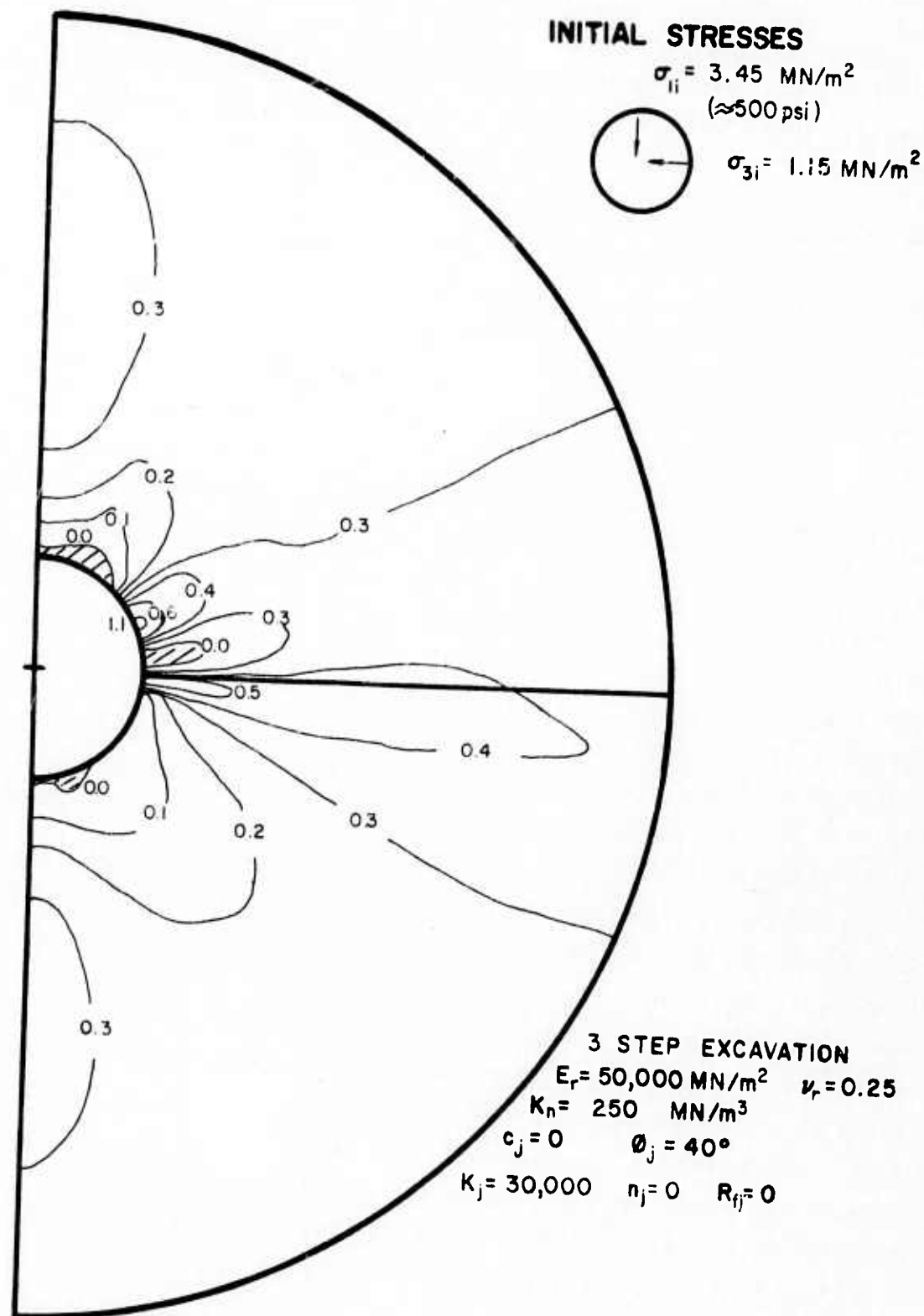


**FIG. 7-7**    **CONTOURS OF  $\sigma_3/\sigma_{ii}$  FOR CIRCULAR OPENING**  
**IN ROCK WITH A 1-D DISCONTINUITY**  
 $K=1/3$  ,  $\theta=0^\circ$  ,  $\alpha=0^\circ$  ,  $M_j=200$

stiffness decreases and tension zones increase in size in both the crown and invert. These trends are similar to those which developed for the two-dimensional discontinuity.

#### Discontinuity Stresses

The stresses which develop within the discontinuity are shown in Figure 7-8. In the top figure, the variation in the dimensionless normal stress with normal stiffness is shown for a constant shear stiffness ( $K_j = 30,000$ ,  $n_j = R_{fj} = 0.0$ ). This figure shows that as the normal stiffness increases, the normal stresses increase significantly within about three radii of the opening center, in a manner similar to that observed previously for the two-dimensional discontinuity. In addition, variations in shear stiffnesses had virtually no effect on the normal stresses because the resulting values were almost identical.

The dimensionless shear stresses which develop in the discontinuity are shown in the center and bottom of Figure 7-8, the center showing the variation with normal stiffness for a constant shear stiffness ( $K_j = 30,000$ ,  $n_j = R_{fj} = 0.0$ ) and the bottom showing the variation with shear stiffness for a constant normal stiffness ( $K_n = 2500 \text{ KN/m}^3$ ). The center shows that the shear stresses are slightly affected by normal stiffness with higher values occurring with a lower normal stiffness (i.e., softer). However, the magnitude of these stresses is very small. The bottom figure shows that the shear stresses increase substantially within one radius of the opening face, in a manner similar to that for the two-dimensional discontinuity, when the initial stiffness number,  $K_j$ , increases and when  $n_j$  increases, indicating increased stress-dependency. Increases in  $R_{fj}$ , indicating increased nonlinearity, showed virtually no differences in the resulting shear stresses, and subsequently these variations are not shown. It should be noted that in all of these cases, the mobilized strengths within the discontinuity were low indicating that no shear failure was imminent; specific values at the opening face varied with a constant normal stiffness from a high of 17.3% for  $K_j = 150,000$  and  $n_j = 0.6$  to a low of 1.7% for  $K_j = 30,000$  and  $n_j = 0.0$  and varied with a constant shear stiffness from a high of 3.2% for  $K_n = 250 \text{ MN/m}^3$  to a low of 0.8% for  $K_n = 25,000 \text{ MN/m}^3$ .

#### Opening Displacements

Figure 7-9 shows the dimensionless displacements of the opening as the shear stiffness of the discontinuity is varied when the normal stiffness is held constant.

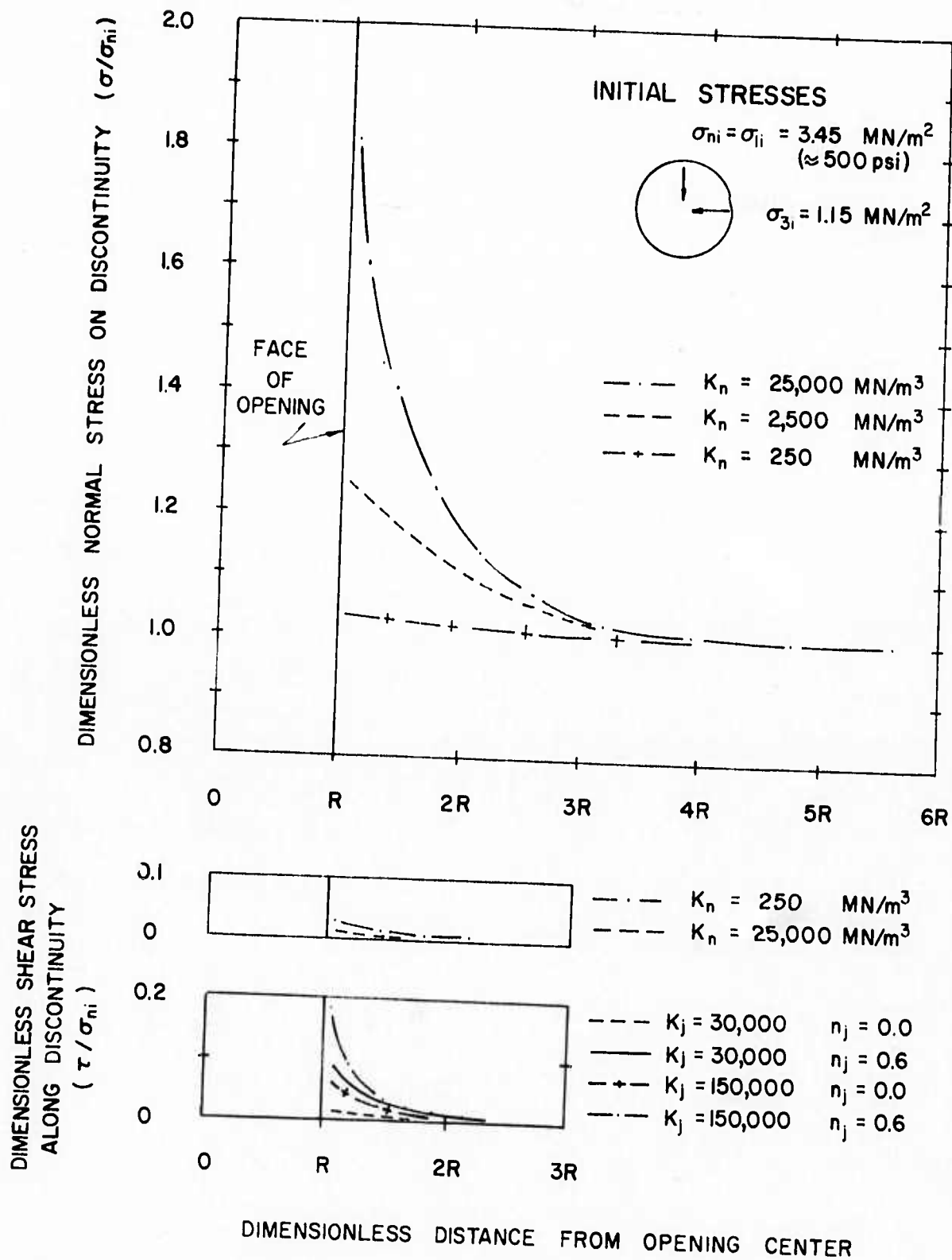


**FIG. 7-8 NORMAL AND SHEAR STRESSES ON HORIZONTAL I-D DISCONTINUITY**

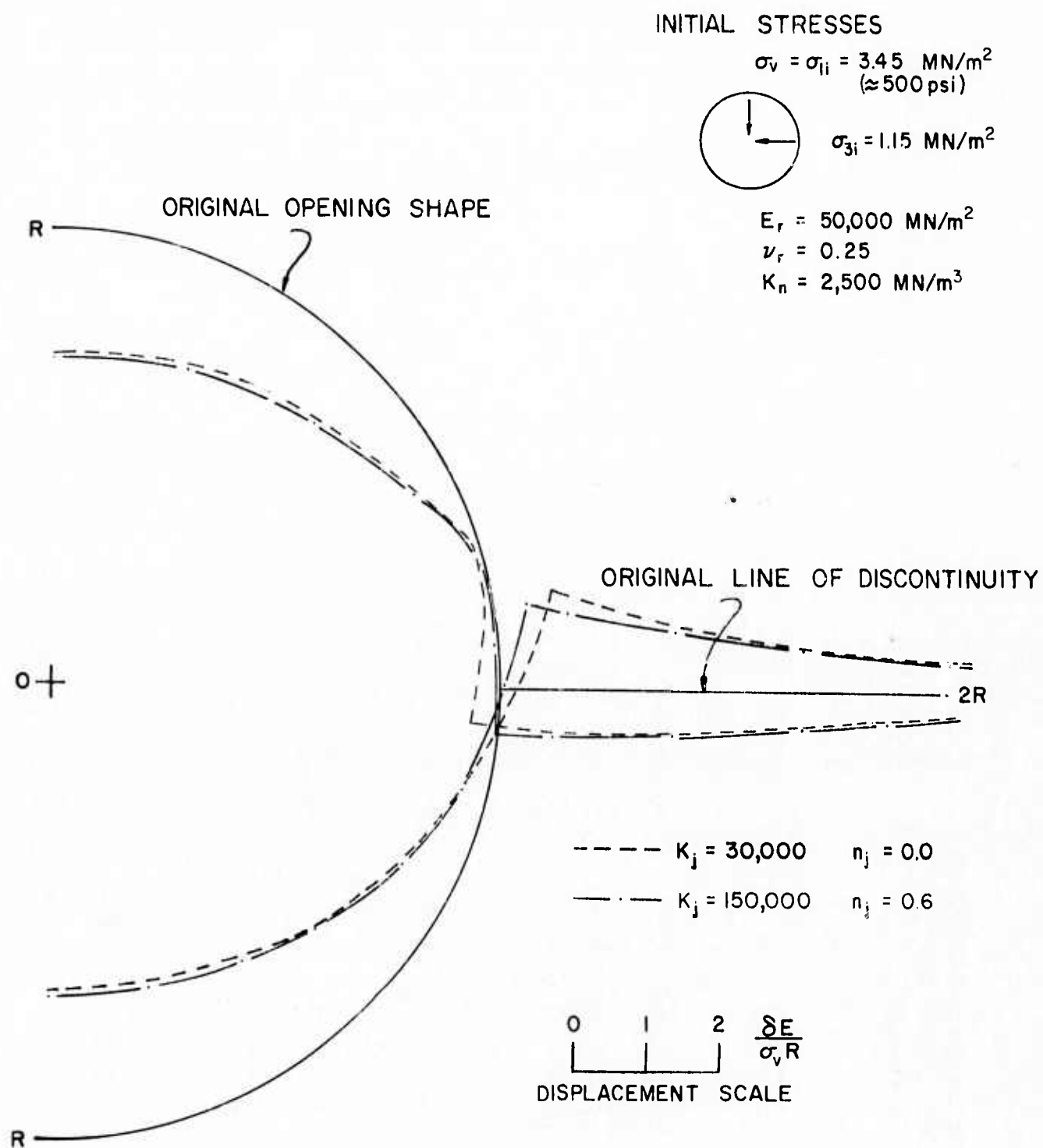


**FIG. 7-9 DISPLACEMENTS OF CIRCULAR OPENING  
IN ROCK WITH A 1-D DISCONTINUITY  
 $K = 1/3$ ,  $\theta = 0^\circ$ ,  $\alpha = 0^\circ$ ,  $K_j$  VARIABLE**

The two cases shown represent the maximum and minimum movements calculated. It can be seen that the only significant effects are near the discontinuity while the crown and invert variations are very small. The compression of the discontinuity is almost the same regardless of shear stiffness, but the inward movement of the upper wall and the outward movement of the lower wall increase as the stiffness number and exponent decrease because both parameters decrease the resulting shear stiffness. Variations because of nonlinearity were minor.

Figure 7-10 shows the dimensionless displacements of the opening as the normal stiffness of the continuity is varied when the shear stiffness is held constant. This figure shows that the displacements are greatly affected by variations in normal stiffness and that compression of the discontinuity, inward movement of the crown, invert and upper wall, and outward movement of the lower wall all increase as  $K_n$  decreases (i.e., the discontinuity becomes "softer").

#### Summary

The analyses presented in this chapter were conducted to evaluate the effect of variations in the normal and shear stiffnesses of a one-dimensional discontinuity on the resulting stresses and displacements around underground openings in rock containing a single prominent discontinuity. The results of these analyses are similar to those obtained when a two-dimensional discontinuity was analyzed in Chapter 5. These results showed that, as the discontinuity becomes softer, the stress changes (or load transfer) become more substantial, tension zones increase, normal and shear stresses on the discontinuity decrease and displacements of the opening increase.

These conclusions can be further amplified by the studies conducted in this chapter since the stiffness of the one-dimensional discontinuity is based upon independent normal and shear stiffnesses. These studies showed that the resulting stresses and displacements were affected more by the normal stiffness than by the shear stiffness, indicating that the stiffness component acting in the same direction as the initial maximum principal stress is the most important in determining the resulting behavior of the opening. These studies further showed that the nonlinearity of the shear stiffness is of minor importance but that the initial stiffness and stress-dependency is significant in determining the stresses and displacements of the opening.



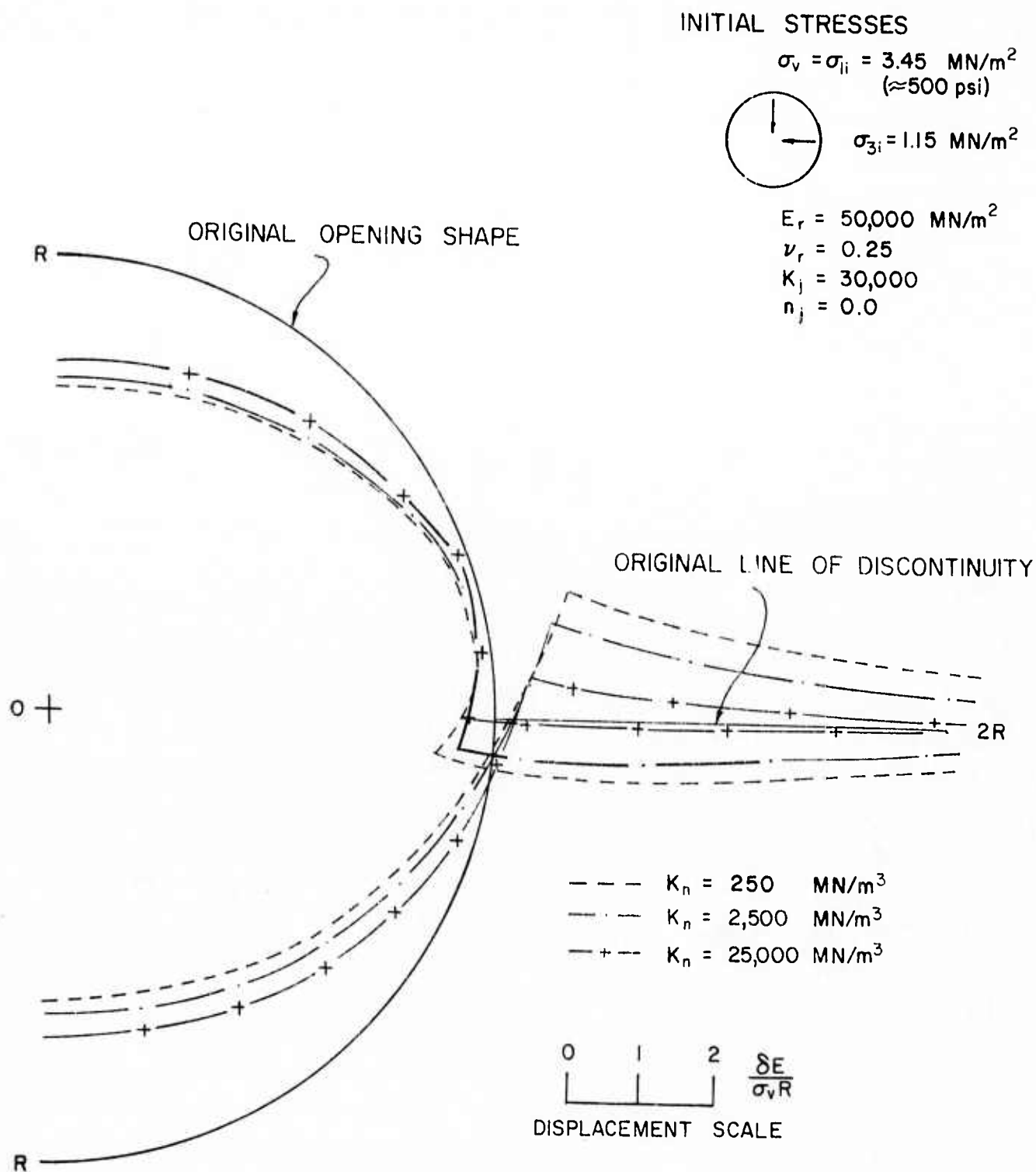


FIG. 7-10 DISPLACEMENTS OF CIRCULAR OPENING  
IN ROCK WITH A 1-D DISCONTINUITY  
 $K = 1/3$ ,  $\theta = 0^\circ$ ,  $\alpha = 0^\circ$ ,  $K_n$  VARIABLE

## CHAPTER 8

### ANALYSIS OF THE BEHAVIOR OF EDWARD HYATT POWERPLANT

The Edward Hyatt Powerplant, shown in Figure 8-1 near the completion of excavation, is a large underground powerplant situated 300 feet (91.5 m) below ground surface, in the left abutment beneath Oroville Dam. Designed and constructed by the State of California Department of Water Resources, the powerplant has been the subject of numerous technical articles related to various features of its analysis, design and construction (e.g., Gianelli, 1969; Gianelli and Jansen, 1972; Colze', 1971; Kruse, 1969, 1971; Merrill et al, 1964; Thayer et al, 1964). Because of the numerous technical accomplishments made by this project, the Oroville Dam and Edward Hyatt Powerplant were awarded the Civil Engineering Achievement of the Year Award for 1968 by the American Society of Civil Engineers. As further evidence of the accomplishments involved, the California State Water Project, in which the key units are Oroville Dam and Edward Hyatt Powerplant, was awarded the Civil Engineering Achievement of the Year Award for 1972 by the American Society of Civil Engineers.

Very detailed investigations were made at the site of the powerplant and extensive instrumentation was installed to monitor the behavior of the opening during construction. The availability of these data provided the opportunity to determine the effectiveness of the finite element analysis techniques described previously for predicting the behavior of large, irregularly shaped openings in discontinuous rock. The results of these analyses are discussed in subsequent sections of this chapter.

#### General Description of Edward Hyatt Powerplant

Oroville Dam and Edward Hyatt Powerplant are the key units in the California State Water Project which will convey water from Northern California to Southern California. The dam and powerplant are located on the Feather River in Northern California, about 150 miles northeast of San Francisco in the foothills of the Sierra Nevada. Figure 8-2 shows a plan view of the facilities, including the dam, powerplant, penstocks, tunnels and associated facilities. Figure 8-3 shows the location of the powerplant beneath the dam. Final siting was determined by hydraulic requirements, economics and the results of a comprehensive exploration program.

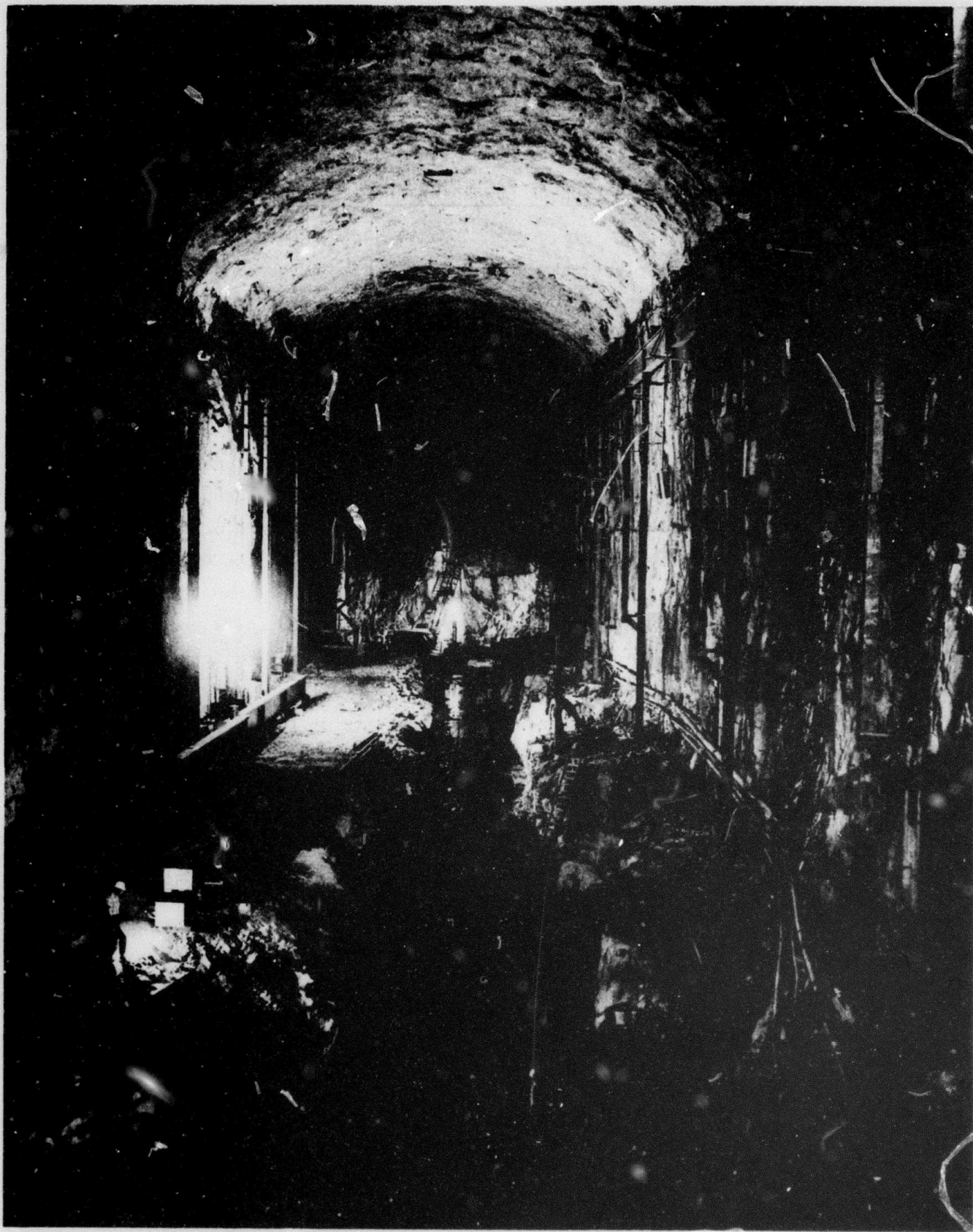


**FIG. 8-1 EDWARD HYATT POWERPLANT NEAR  
COMPLETION OF EXCAVATION (FROM KRUSE, 1971)**

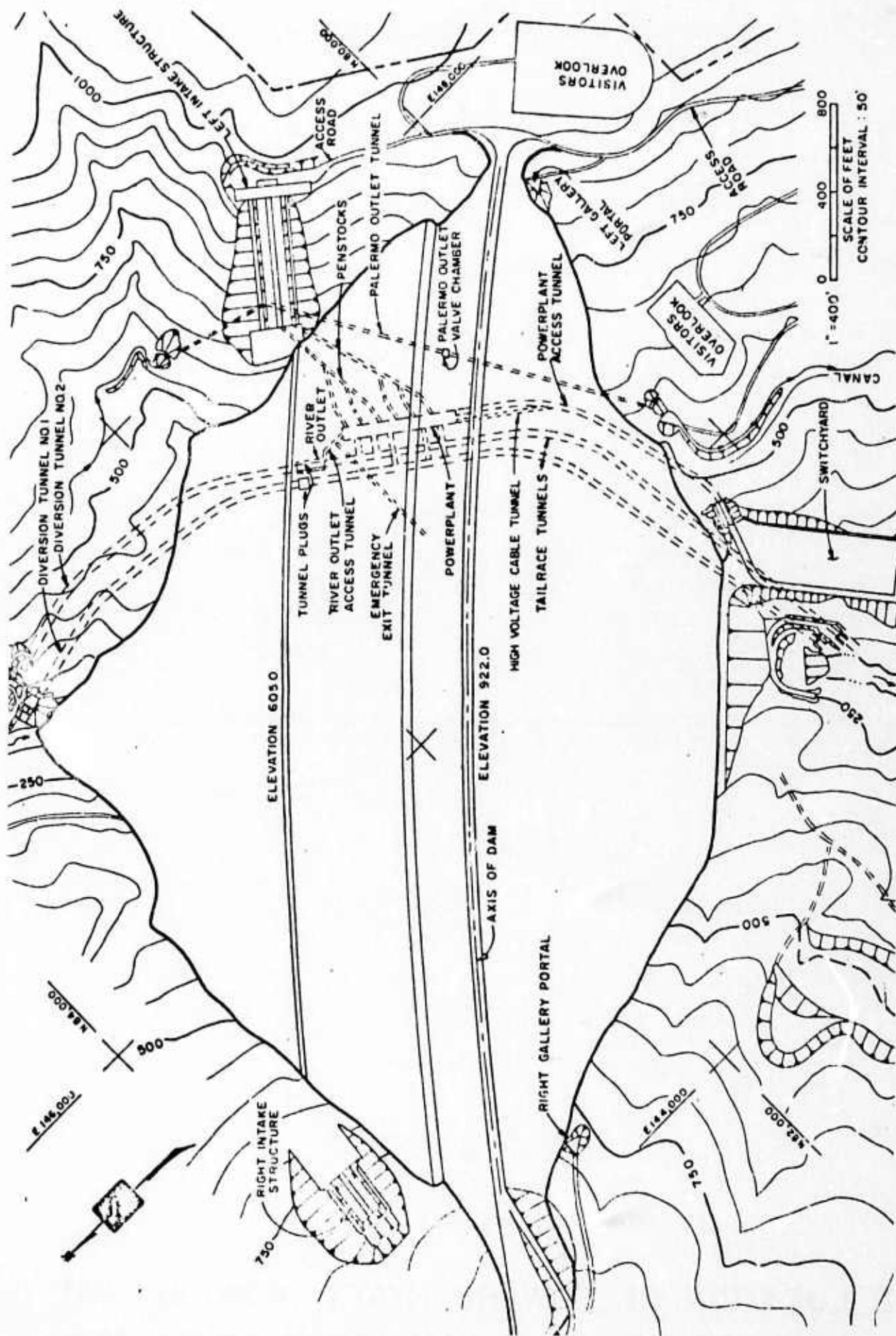
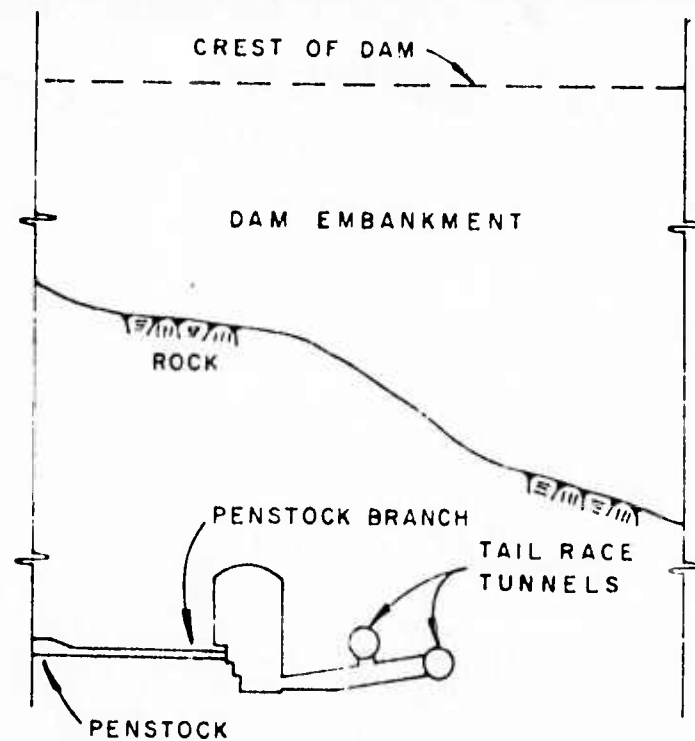
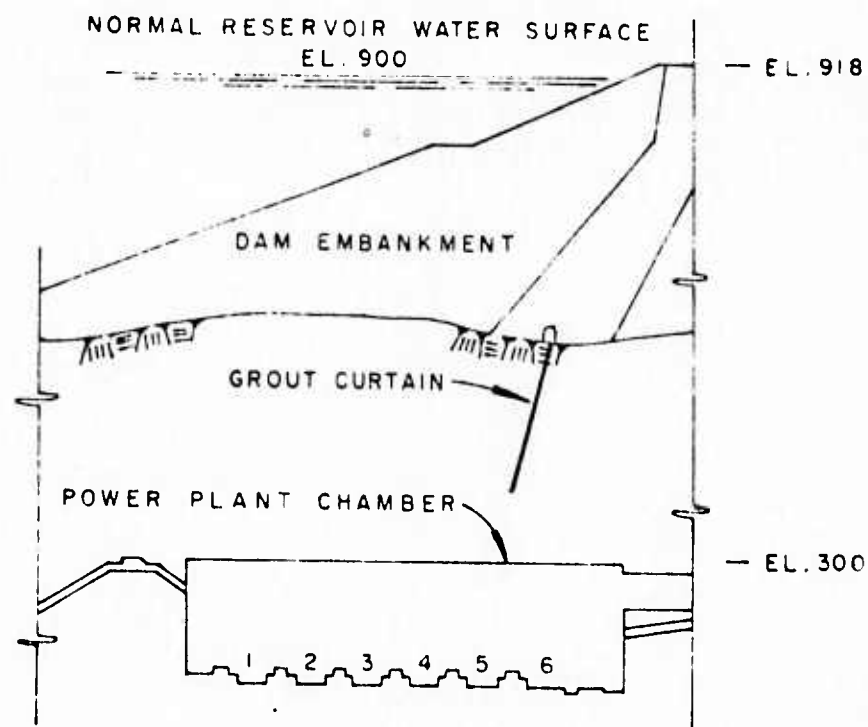


**FIG.8-2 PLAN VIEW OF OROVILLE DAM AND EDWARD HYATT POWERPLANT  
(FROM GROSS, 1968)**





TRANSVERSE SECTION



LONGITUDINAL SECTION

**FIG. 8-3 LOCATION OF EDWARD HYATT POWERPLANT  
BENEATH OROVILLE DAM (FROM KRUSE, 1971)**

The powerplant chamber is 550 feet (168 m) long, 69 feet (21 m) wide and nominally about 140 feet (42.7 m) high, but the height varies from section to section. The facility includes six turbine generators which can produce approximately 2.5 billion kilowatt-hours of electrical power per year.

The initial powerplant contract was awarded in June 1963 to the low bidder, a joint venture of McNamara Corporation Limited and George A. Fuller Company. Actual excavation of the powerplant chamber began in March 1964 and was completed in June 1966. Following the completion of Oroville Dam in 1967, the first generating unit began operation in 1968.

#### Site Geology

The powerplant site is in the western foothills of the Sierra Nevada, a large, tilted, granite fault block. Overlying the granite at the site are a series of tightly folded, steeply dipping metamorphic rocks. The powerplant is in this metamorphic series within an unnamed metavolcanic formation of predominantly amphibolite, a basic metamorphic rock, containing abundant thin veins of calcite, quartz, epidote, asbestos, palygorskite "mountain leather" and pyrite. The generally unweathered amphibolite at the powerplant is hard, dense, greenish gray to black, fine to coarse-grained and generally massive, although a slight schistosity is commonly found with an attitude striking N 12° W and dipping 77° E.

At the powerplant excavation, the rock is moderately to strongly jointed with three prominent joint sets, all generally tight, causing some blockiness in the rock. Steeply dipping, planar, shear and schistose zones strike 60° to 80° with the longitudinal axis of the powerplant and are spaced from five to twenty feet apart. Most of these discontinuities are one to six inches wide and contain crushed rock, schist and clay gouge. Ground water inflow was very small and was conducted almost exclusively along the discontinuities.

Figures 8-4 and 8-5 show the prominent discontinuities intersecting the powerplant. Considering that the powerplant is 550 feet (168 m) long, it can be seen that the site geology was generally favorable. Figure 8-6 shows a more detailed isometric view of the left or upstream wall from which it can be seen that in certain areas, the discontinuities were more closely spaced. More detailed geologic information is presented by Gross (1968).

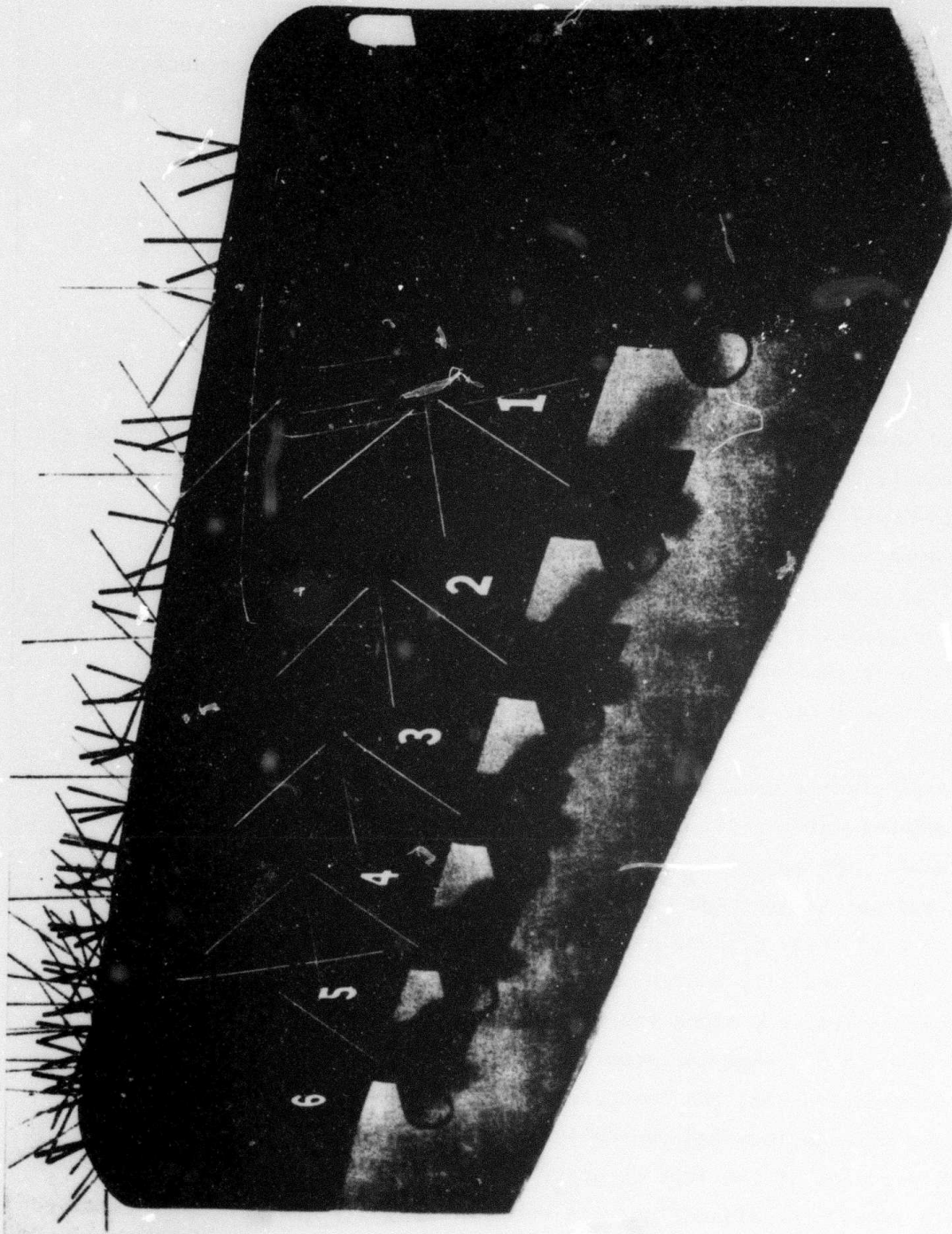
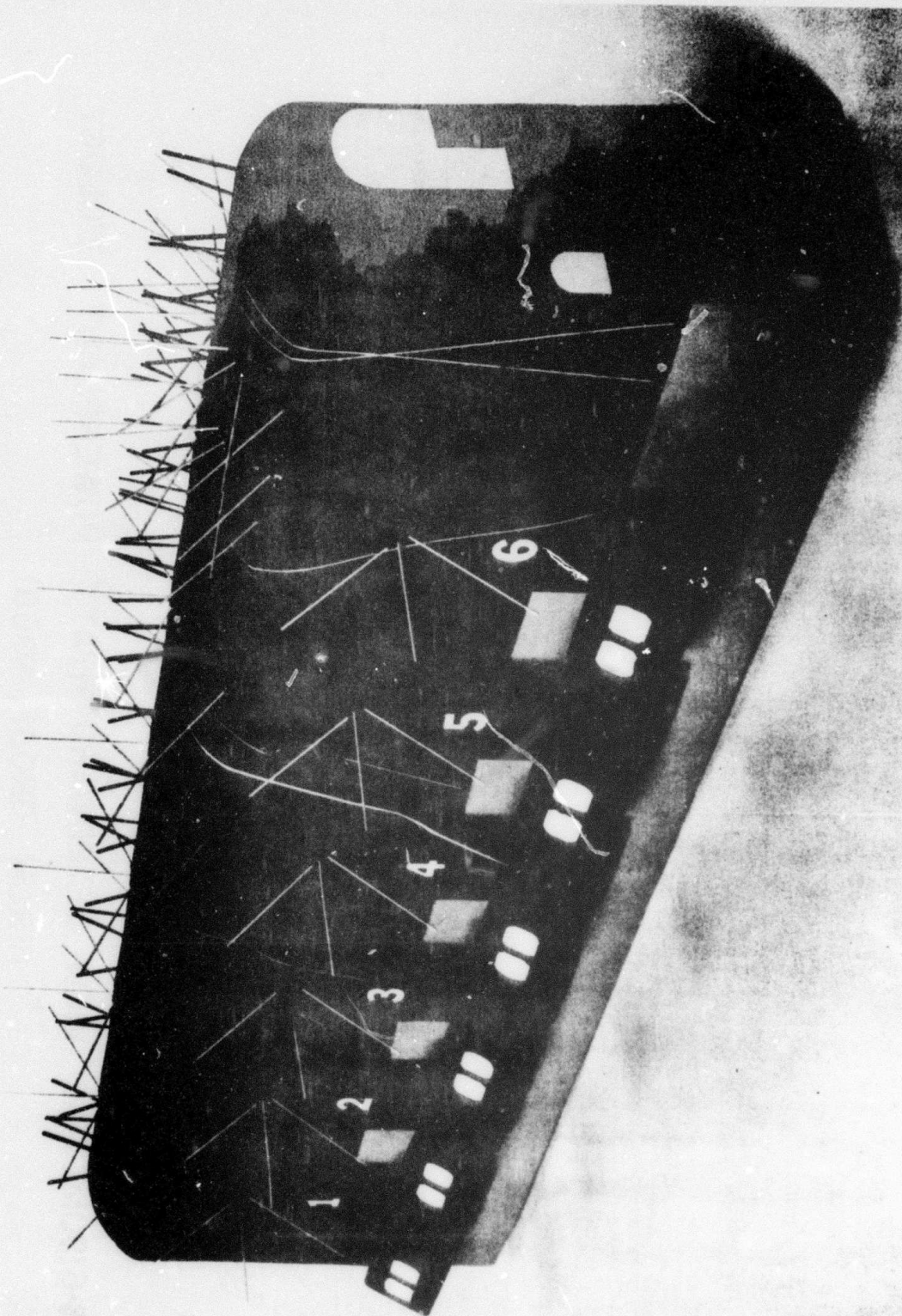
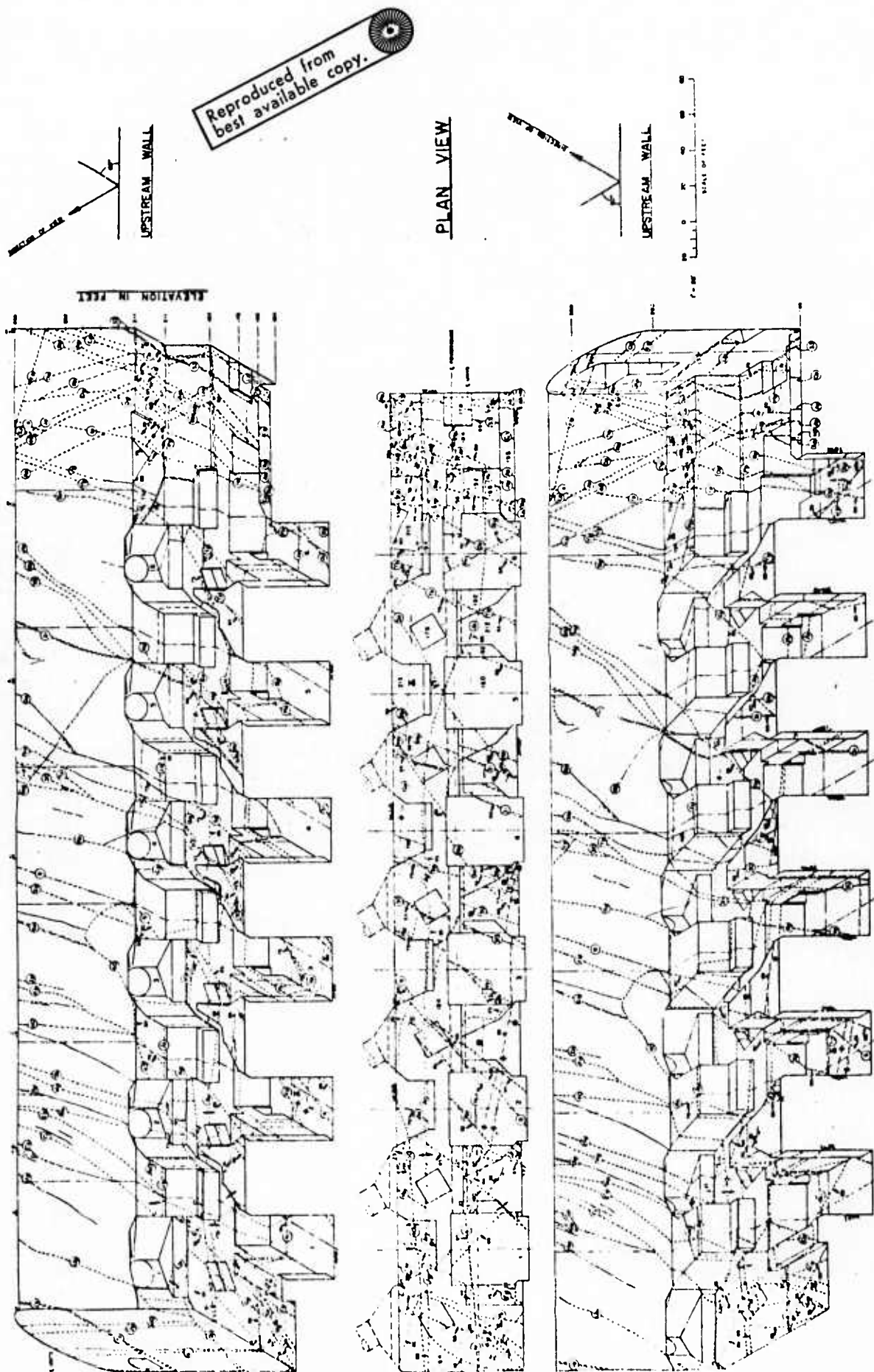


FIG. 8-4 MODEL OF EDWARD HYATT POWERPLANT, LEFT WALL  
(FROM KRUSE, 1971)





**FIG. 8-5 MODEL OF EDWARD HYATT POWERPLANT, RIGHT WALL  
(FROM KRUSE, 1971)**



**FIG.8-6 ISOMETRIC VIEW OF EDWARD HYATT POWERPLANT GEOLOGY  
(FROM GROSS, 1968)**

### Engineering Investigations

Preliminary investigations were conducted at the site by seismic refraction survey and with nine NX core borings to determine the extent of unweathered rock above the powerplant and to locate rock discontinuities in the powerplant area. After analysis of the preliminary data, the final investigations were conducted from a five foot (1.52 m) wide by seven foot (2.14 m) high unsupported exploration adit with several branches and crosscuts. Geologic details were revealed in the adit and in 33 BX core borings drilled from the adit and its branches and crosscuts.

In addition to geologic data, the adit was employed to conduct in-situ testing of the rock mass. These tests included: 1390 measurements of rock stress from 27 flatjacks installed in the walls, floor and roof of the adit, 157 borehole stress relief measurements in five overcored boreholes, plate bearing tests and rock bolt pull-out tests since it was planned to use rock bolt roof and wall support. In addition, measurements of tunnel convergence were made from thirty borehole extensometers at six sites in one of the diversion tunnels. Laboratory sonic and static uniaxial tests were also conducted on intact core specimens of the rock.

The results of the flatjack and borehole tests, although scattered, showed that the in-situ stress field was essentially isotropic with stresses approximately equal to 500 psi ( $3.4 \text{ MN/m}^2$ ). The stresses were measured approximately 350 feet (107 m) below ground surface where overburden pressure would account for about 89% of the vertical stress measurements. Tectonic effects were indicated to account for the difference, as well as for the isotropic values of the stresses.

The field and laboratory tests also provided information on the in-situ rock modulus. Table 8-1 shows the values obtained from the different tests and it can be seen that the tests on the intact cores yielded high modulus values, while the field tests which include the discontinuities present in the rock mass yielded lower modulus values. The averages ranged from 10,300 to 110,000  $\text{MN/m}^2$  ( $1.5$  to  $16.0 \times 10^6$  psi).

The laboratory uniaxial tests also showed that the average compressive strength was about 276  $\text{MN/m}^2$  (40,000 psi) while the average tensile strength was about 23.4  $\text{MN/m}^2$  (3,300 psi).

Type of Test	Number of Measurements	Rock Modulus			
		psi		MN/m <sup>2</sup>	
		Range	Average	Range	Average
Static Uniaxial Tests on Cores	21	10.8-15.2 x 10 <sup>6</sup>	12.9 x 10 <sup>6</sup>	74.4-104.6 x 10 <sup>3</sup>	88.8 x 10 <sup>3</sup>
Sonic Tests on Cores	3	14.8-17.0	16.0	101.9-117.0	110.0
Geophysical-Seismic Velocity	19	4.9-15.5	10.2	33.7-106.7	70.2
Flatjack	30	1.4-16.4	7.5	9.6-112.9	51.6
Tunnel Relaxation	22	0.6- 7.5	2.6	4.1- 51.6	17.9
Plate Bearing	5	1.2- 1.8	1.5	8.3- 12.4	10.3

TABLE 8-1 SUMMARY OF ROCK MODULI, EDWARD HYATT POWER PLANT  
(FROM KRUSE, 1969)



### Finite Element Idealization

For any finite element analyses, other than linear elastic analyses, the construction sequence employed in the field must be reasonably well modeled in the analyses for the results to be meaningful. The sequence followed in the field was first to excavate the crown and then to bench down and outwards at lower elevations. The crown sequence is shown in Figure 8-7 while the sequence employed at unit one is shown in Figure 8-8. The finite element analyses were conducted with a three step excavation sequence. The first step was the crown excavation, the second step was to an intermediate depth and the third step was to the final geometry. In all of these analyses, the simulation of embankment placement was not considered because the instrumentation results showed that it caused very little effect.

In the field, one inch (2.54 cm) diameter and twenty foot (6.1 m) long rock bolts were installed on a four foot (1.22 m) square pattern in the crown and on a six foot (1.83 m) square pattern in the walls. The rock bolts were not considered in the finite element analyses discussed in this chapter.

Four types of plane strain finite element analyses were conducted for this study. As long as the system is homogeneous and isotropic, the plane strain assumption will be accurate if the opening is long. But if discontinuities are being modeled, and they are not normal to the section being analyzed, the plane strain assumption will not be completely satisfied and the results will be slightly inaccurate because the basic assumptions are not being satisfied. Considering the complexities of the three-dimensional analyses and the high costs, it is felt that the plane strain analyses of openings similar to this powerplant will provide sufficiently accurate results for at least a preliminary design basis.

The four types of analyses conducted were: (1) linear, homogeneous, one step excavation, (2) linear, homogeneous, three step excavation, (3) nonlinear, homogeneous, three step excavation, and (4) nonlinear, jointed, three step excavation. For the first three analyses, the mesh shown in Figure 8-9 was used. This mesh contains 704 elements and 744 nodal points to provide sufficient accuracy because of the irregular geometry of the opening. The top of the mesh corresponds to the average ground surface elevation while the other three boundaries were established in accordance with criteria discussed in Chapter 2.

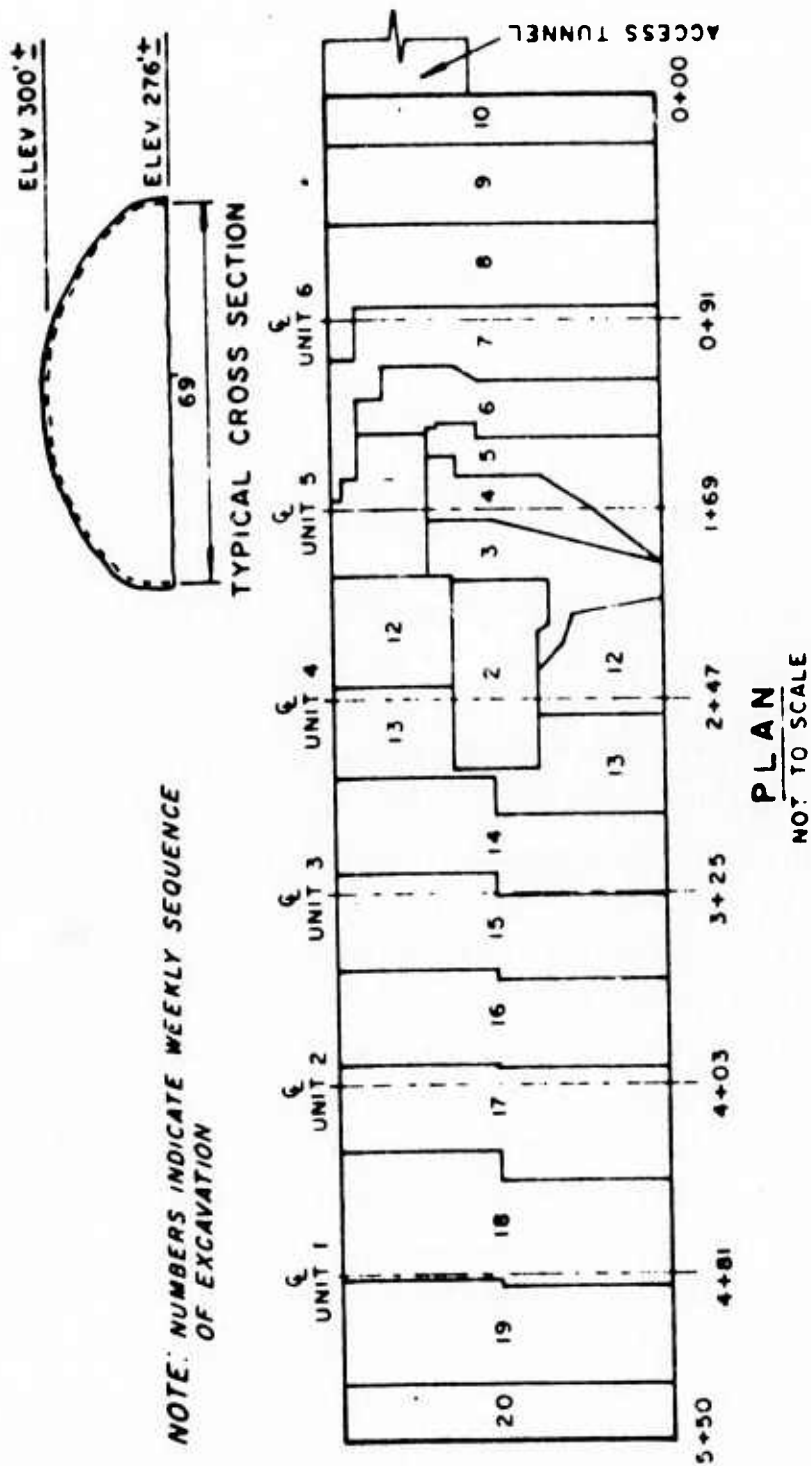


FIG.8-7 EXCAVATION SEQUENCE FOR CROWN OPENING, EDWARD  
HYATT POWERPLANT (FROM KRUSE, 1971)



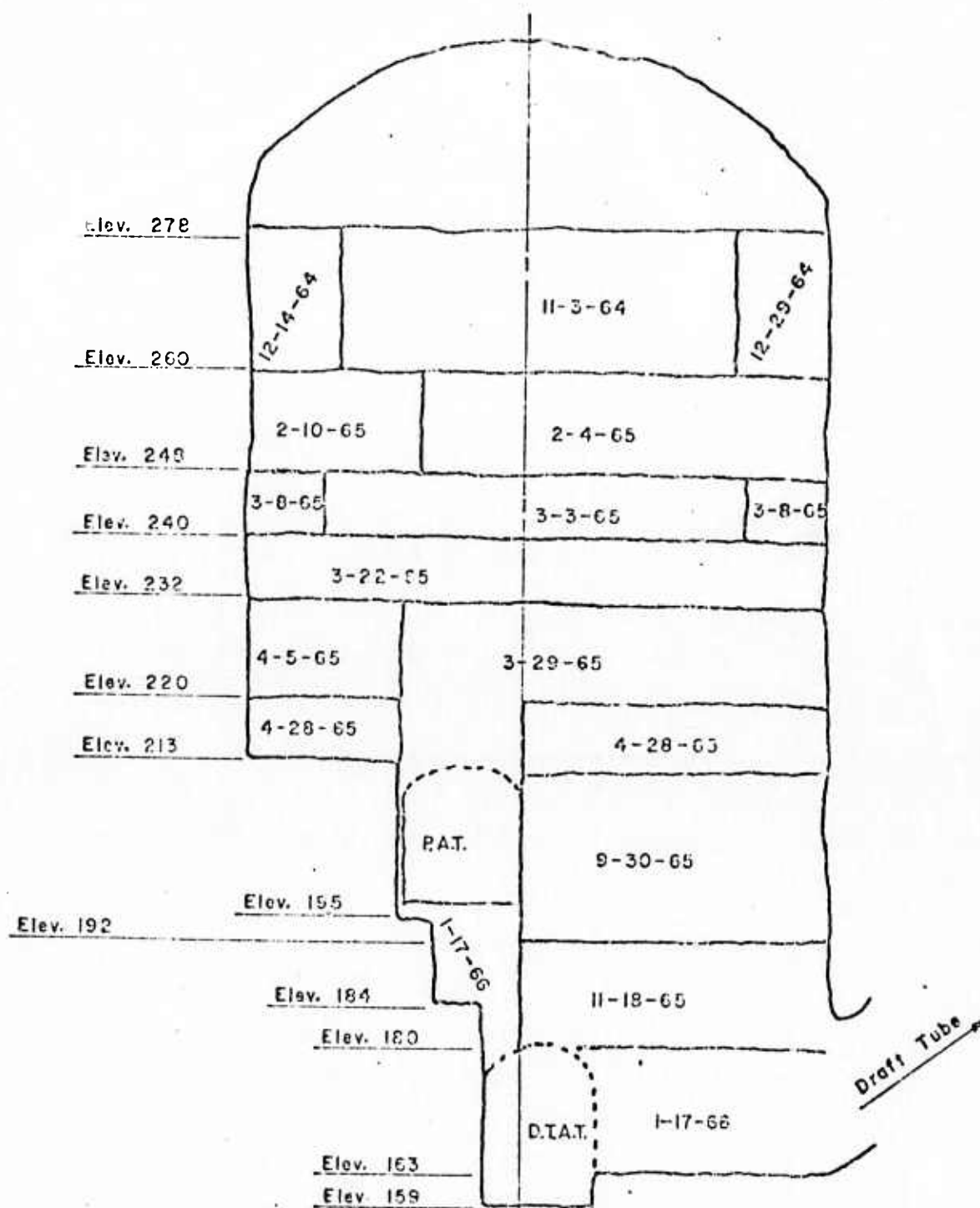
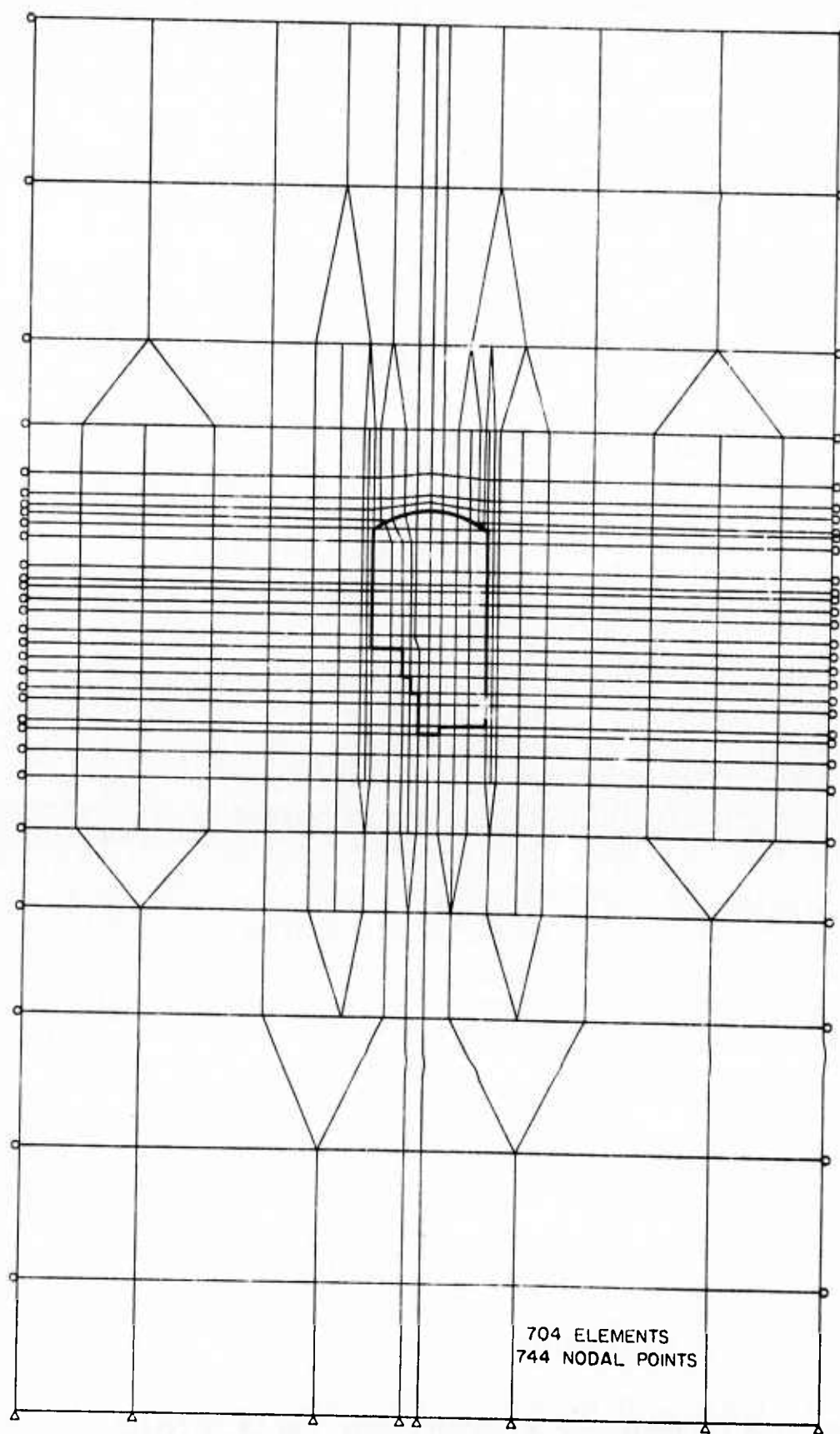


FIG. 8-8 UNIT ONE EXCAVATION SEQUENCE  
EDWARD HYATT POWERPLANT (FROM DWR, 1967)



**FIG. 8-9 MESH FOR HOMOGENEOUS ANALYSES  
OF EDWARD HYATT POWERPLANT**

For the fourth analysis, the discontinuities were taken into account by extrapolating the discontinuities to intersect the section at unit one, the section chosen for analysis. Figure 8-10 shows the resulting unit one section. Because of the large number of discontinuities involved, this section was generalized and the eleven discontinuities which were modeled are shown in Figure 8-11. The finite element mesh used for this modeled section is shown in Figure 8-12 and it contains 895 elements and 982 nodal points. It is interesting to note that the discontinuities involved are quite similar, as shown in Table 8-2, with almost all of the discontinuities being several inches of crushed rock with varying degrees of clay gouge.

The properties used in these analyses are shown in Table 8-3. For the linear analyses, a representative modulus value of  $35,000 \text{ MN/m}^2$  ( $5 \times 10^6 \text{ psi}$ ) was selected based on the field test results shown in Table 8-1. The Poisson's ratio value of 0.20 was selected on the basis of the results of tests discussed in Chapter 3. The strength parameters were obtained from the average uniaxial compressive and tensile strengths by plotting Mohr strength circles for both cases and assuming a linear variation between them. The resulting values were a cohesion of  $39.2 \text{ MN/m}^2$  (5,700 psi) and an angle of friction of  $58^\circ$ . These values were used for the rock in the subsequent analyses as well.

For the nonlinear, homogeneous analyses and for the rock in the nonlinear, jointed analyses, the value of K (modulus number) was inferred from the results of the static uniaxial tests on unjointed cores. This was done by considering that the uniaxial tests were conducted with a confining pressure of one atmosphere. For this condition, the initial tangent modulus,  $E_i$ , would be equal to  $Kp_a$ . Substituting the uniaxial modulus value for  $E_i$ , the resulting value of K is equal to 880,000. The remaining modulus and Poisson's ratio parameters were established based upon the results discussed in Chapter 3.

For the nonlinear, jointed analyses, the nonlinear properties of the rock were the same as those discussed above. For the joints, it was considered that they are very similar in character, as shown in Table 8-2. Since they are similar, the same values were used for all eleven joints modeled in the analyses and these values were adopted based upon the results presented in Chapter 6.

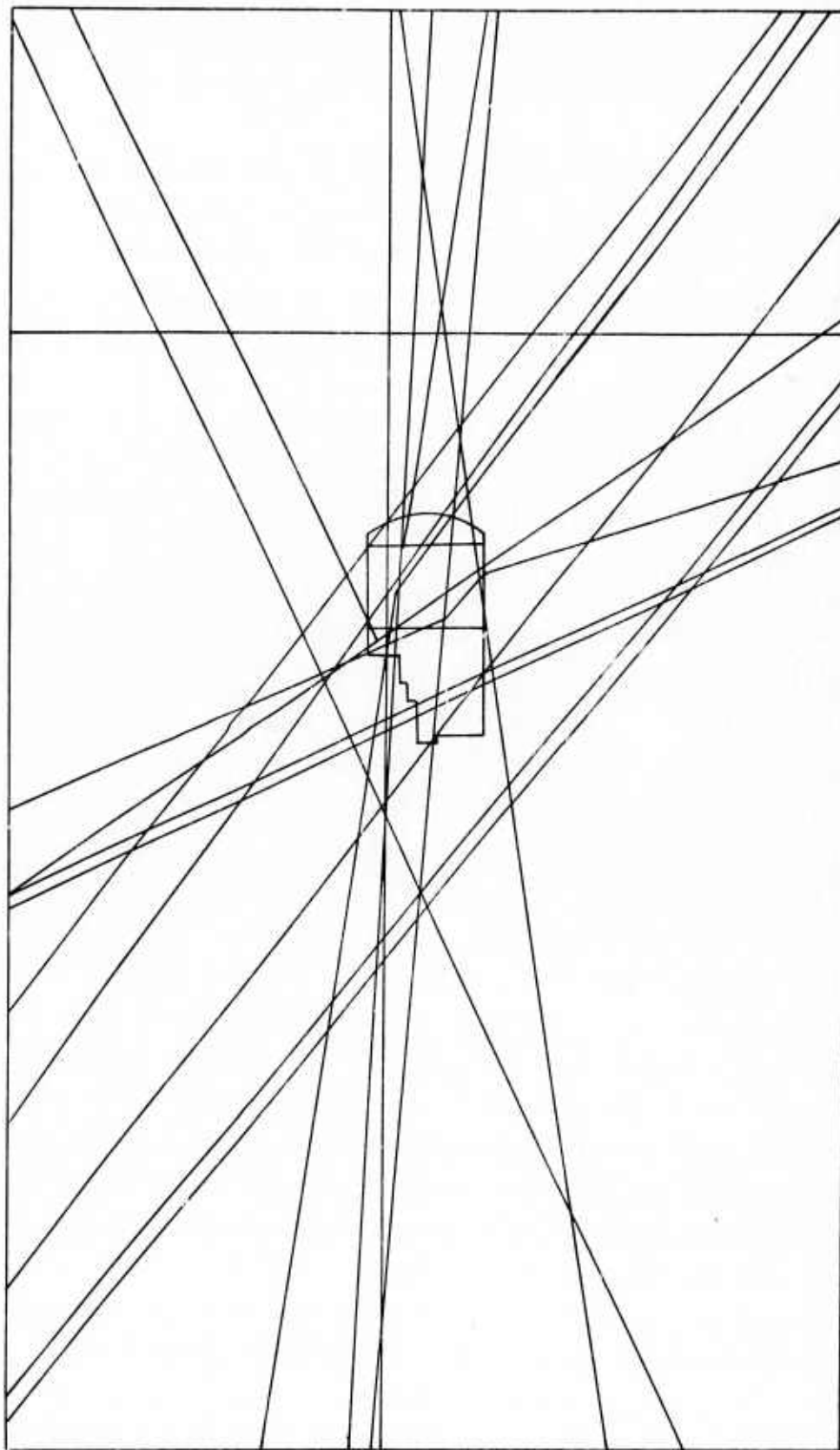


**FIG. 8-10 DISCONTINUITIES THROUGH  $\mathbb{Q}$  UNIT ONE  
EDWARD HYATT POWERPLANT**

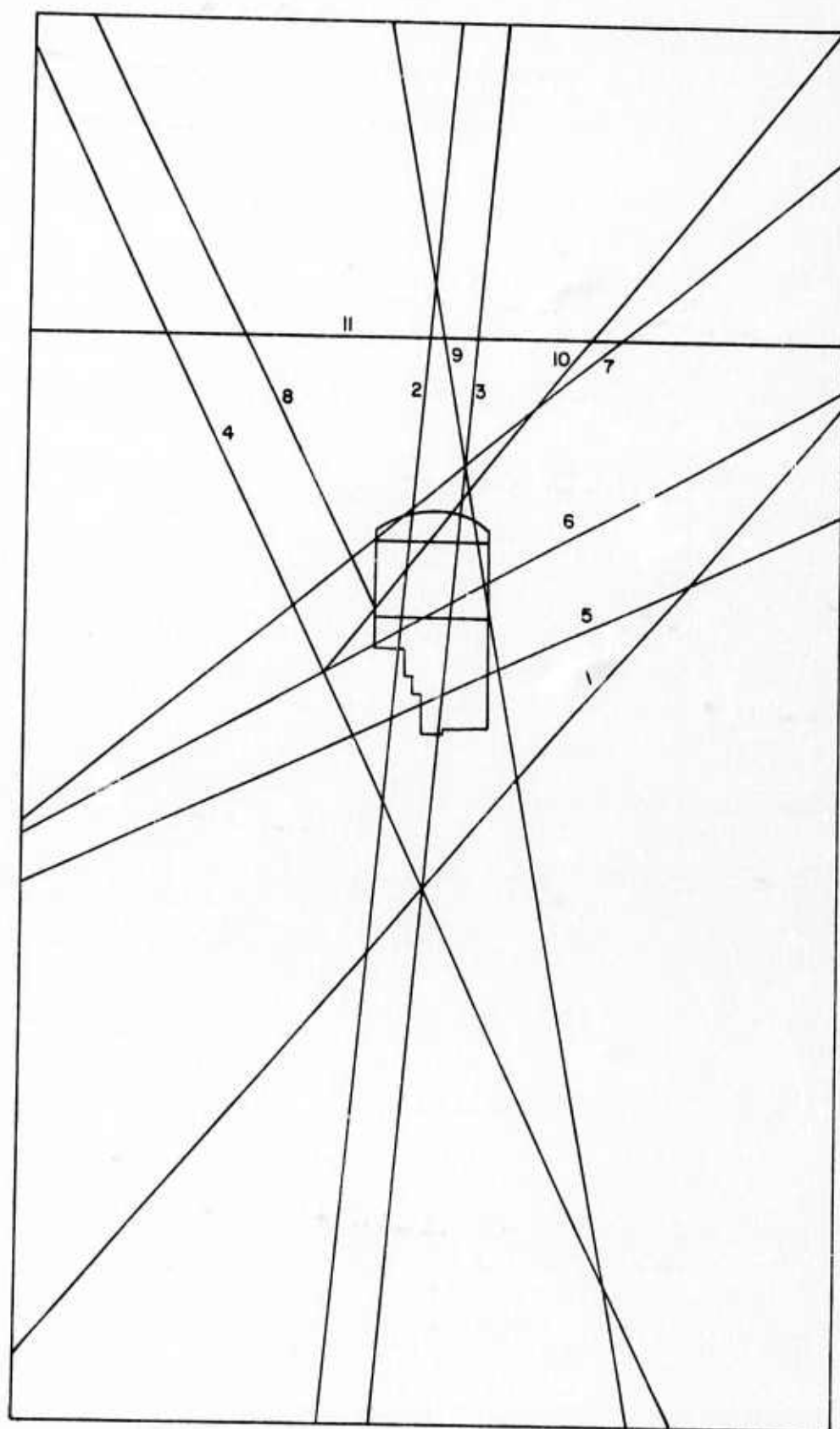


**FIG. 8-II MODELED DISCONTINUITIES THROUGH  
UNIT ONE, EDWARD HYATT POWERPLANT**

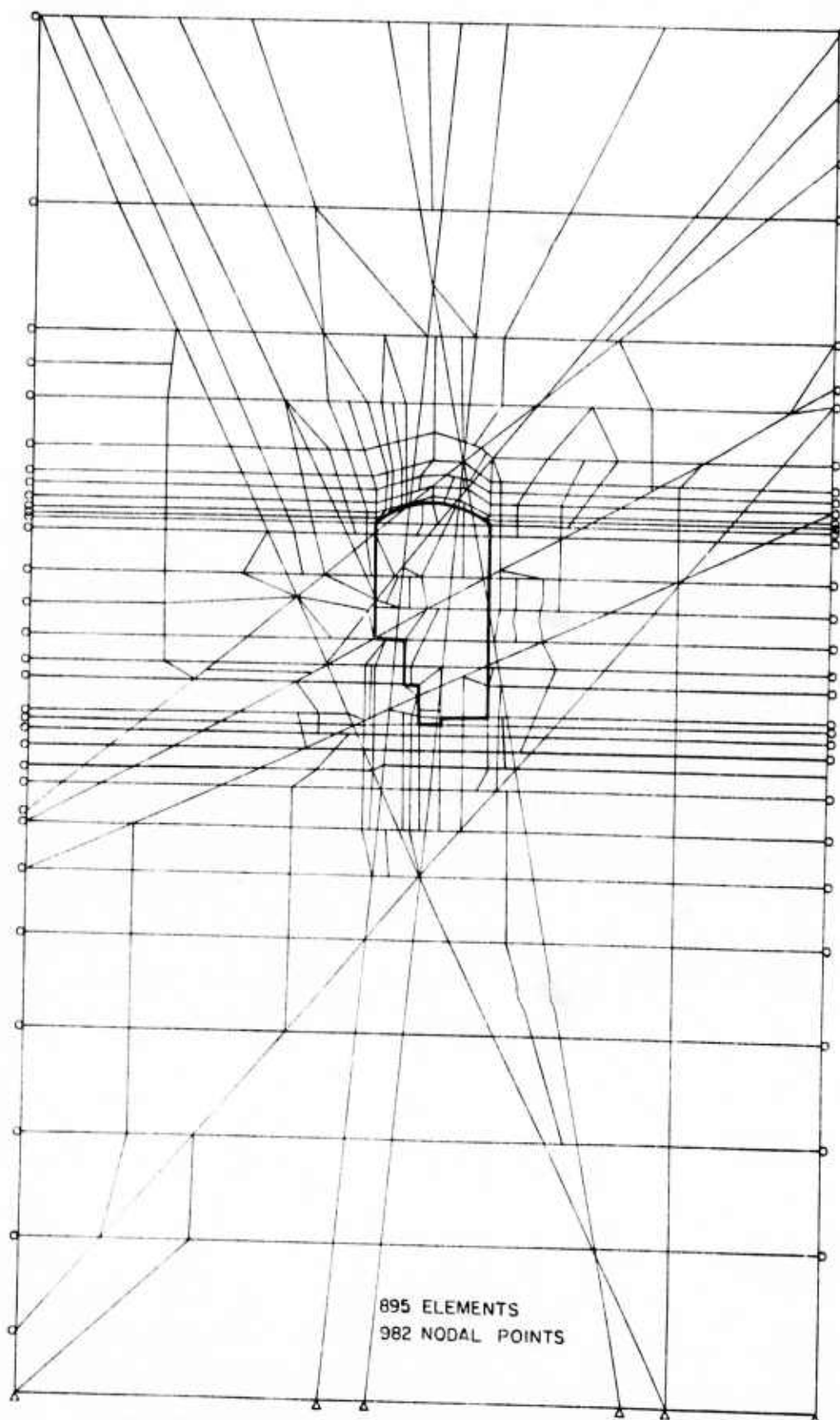


**FIG. 8-12 MESH FOR JOINTED ANALYSIS OF  
EDWARD HYATT POWERPLANT**



Joint Number	Thickness (in.)	Generalized Field Geologic Description
1	1-3	Clay Gouge and Crushed Rock
2	1-4	Clay Gouge to Crushed Rock
3	2-4	Clay Gouge and Crushed Rock
4	1/2-1	Clay Gouge and Crushed Rock
5	1-4	Tight Crushed Quartz, Calcite and Schistose Fragments with minor Clay Gouge
6	1-6	Crushed Rock with 1-2 inch Clay Gouge
7	2-6	Crushed Rock with up to 1 inch Clay Gouge - Strongly Fractured Rock with Schist and Epidote ranges from 10-30 inches wide locally along seam
8	1-2	Crushed Rock and minor Clay Gouge
9	1-3	Clay Gouge and Crushed Rock
10	---	Crushed Rock, Quartz and up to 1/2 inch Clay Gouge in 8 foot wide zone of Strongly Fractured Rock
11	6-30	Strongly Fractured Schistose Rock with up to 2 inch Clay Gouge

TABLE 8-2 DESCRIPTION OF MODELED DISCONTINUITIES  
EDWARD HYATT POWER PLANT

Analysis	Modulus or Stiffness Parameters	Poisson's Ratio Parameters	Strength Parameters
Linear-Homogeneous	$E = 35,000 \text{ MN/m}^2$ ( $\approx 5 \times 10^6 \text{ psi}$ )	$\nu = 0.20$	$c = 39.0 \text{ MN/m}^2$ $\phi = 58^\circ$ ( $\approx 5,700 \text{ psi}$ )
Nonlinear-Homogeneous	$K = 880,000$ $n = 0.10$ $R_f = 0.60$	$G = 0.20$ $F = 0.0$ $d = 115.0$	same as above
Nonlinear-Jointed a) Rock b) Joints	same as above $K_j = 50,000$ $n_j = 0.25$ $R_{fj} = 0.75$ $K_n = 1,000 \text{ MN/m}^3$ ( $\approx 3,700 \text{ psi/in}$ ) $K_j$ after shear failure = 20,000 $K_n$ and $K_s$ after tension failure = $10 \text{ MN/m}^3$	same as above	same as above $c_j = 0$ $\phi_j = 35^\circ$

TABLE 8-3 SUMMARY OF PROPERTIES USED IN ANALYSES OF EDWARD HYATT POWER PLANT

### Displacements

The displacements in the crown and walls were measured by extensometers installed in arrays during excavation. During the initial crown arch excavation, twenty foot (6.1 m) mechanical extensometers were installed to measure the arch displacements. As excavation proceeded downward after the crown was excavated, these devices were replaced by forty foot (12.2 m) extensometers with attached electrical sensors. The same type of devices were installed in the walls. The centerline of each of the six generating units was instrumented as shown in Figure 8-13 with eleven extensometers to measure the displacements at five locations and in several different directions.

It should be noted that, because of obvious physical difficulties, the extensometers cannot measure the total displacement at a point because the cut has to be made before the device can be installed and subsequently a certain amount of deformation occurs which is not measured. Furthermore, the extensometers can only measure relative displacement between the two ends of the device.

#### a) Displacements at Extensometer Locations

Table 8-4 shows the measured and computed vertical displacements for the twenty foot (6.1 m) centerline crown extensometers which developed from the crown excavation. This corresponds to step 1 in the finite element solution. These results show that the measured relative displacements ranged from 0.2 mm to 1.0 mm with an average value of 0.5 mm. The computed relative displacements were 0.5 mm for the linear analysis (the one step and three step solutions were virtually identical), 0.1 mm for the nonlinear analysis and 2.0 mm for the jointed analysis. Comparison of the measured and computed displacements shows that the linear analysis agrees well with the average measured value while the nonlinear value was one-half the minimum measured and the jointed value was twice the maximum measured. However all of the values are very small with the maximum difference between the measured and computed being only 1.0 mm. Based upon the computed results it can be seen that the relative displacements only accounted for 20% to 48% of the total displacements at the face.

Table 8-5 shows the measured relative displacements for the eleven forty foot (12.2 m) extensometers installed at the centerline of each of the six generating units. Extensometers 4 through 8 were installed after the equivalent of step 1

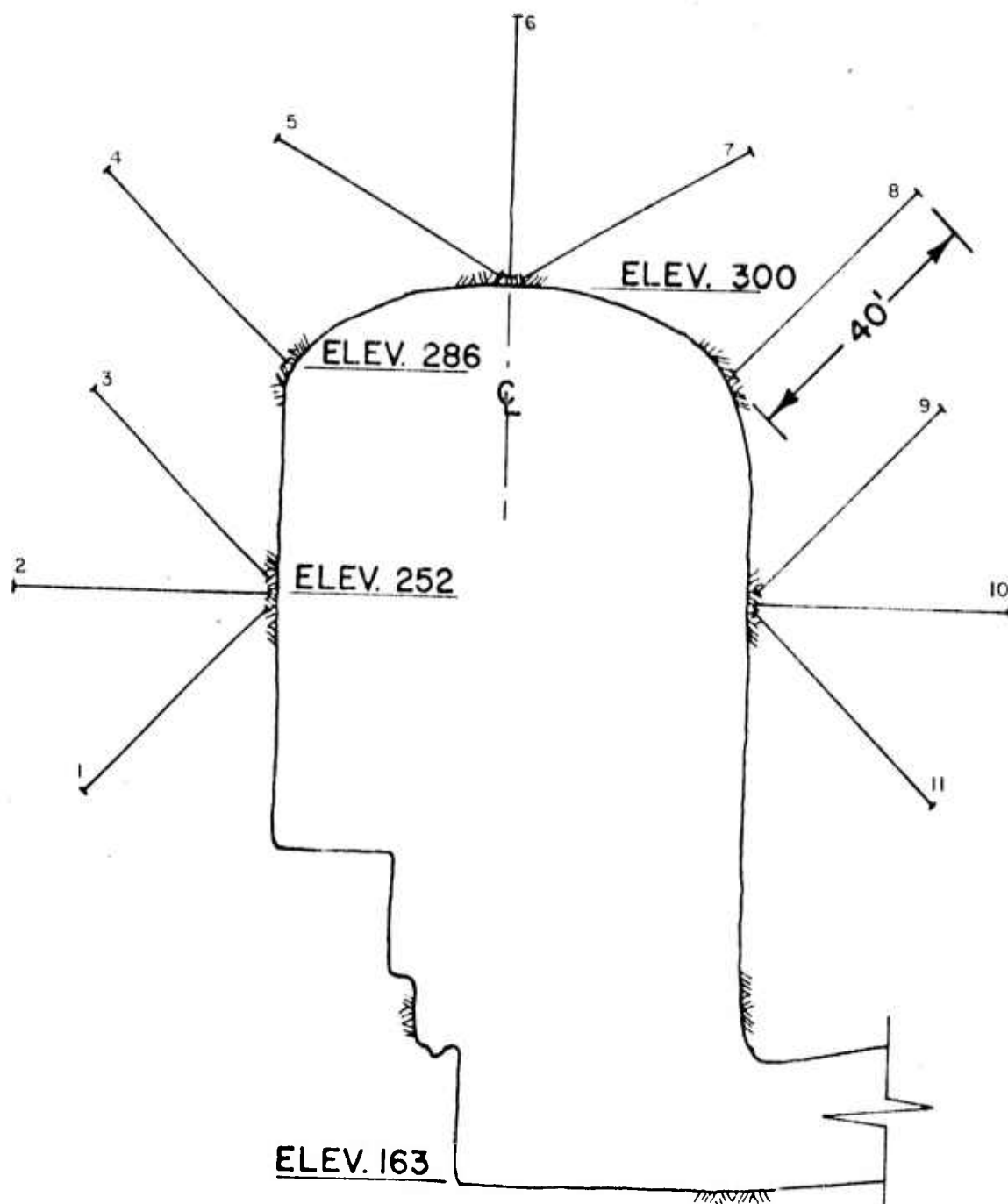


FIG.8-13 TYPICAL INSTALLATION OF BOREHOLE  
EXTENSOMETERS, EDWARD HYATT POWERPLANT  
(FROM KRUSE, 1971)

Extensometer Station (ft)	Relative Vertical Displacement (mm)
0 + 22	0.3
0 + 40	0.3
0 + 83	0.3
1 + 37	1.0
2 + 31	0.7
2 + 90	0.6
3 + 49	0.7
4 + 28	0.2
5 + 00	0.2

Method		Relative Displacement (mm)	Total Face Displacement (mm)
Measured	Maximum	1.0	---
	Minimum	0.2	---
	Average	0.5	---
Computed (Step 1)	Linear	0.5	2.0
	Nonlinear	0.1	0.5
	Jointed	2.0	4.2

TABLE 8-4 MEASURED AND COMPUTED VERTICAL DISPLACEMENTS  
FOR 20 FOOT CENTERLINE CROWN EXTENSOMETERS  
EDWARD HYATT POWERPLANT

Excav. Step	Unit and Station (ft) Extensometer	1	2	3	4	5	6
		4 + 81	4 + 03	3 + 25	2 + 47	1 + 69	0 + 91
3	1	0.2	-2.4	0.4	1.8	0.5	-1.2
	2	1.1	0.4	4.4	3.2	1.5	3.3
	3	0.5	5.1	0.6	0.9	0.9	0.2
	9	1.2	2.6	2.8	2.2	0.7	-0.1
	10	2.0	2.2	3.0	3.8	1.4	2.4
	11	0.4	2.2	0.5	1.9	0.7	1.7
2	4	-0.2	0.3	0.2	0.3	0.1	0.1
	5	0.1	-0.1	0.0	-0.1	0.2	-0.2
	6	-0.1	0.1	0.1	0.0	0.0	0.1
	7	0.2	0.2	0.1	0.0	0.5	-0.2
	8	0.1	0.7	0.1	0.1	0.0	0.1
3	4	-0.2	0.3	2.1	0.4	0.1	0.1
	5	0.0	-0.2	-0.2	0.2	0.2	-0.4
	6	-0.1	0.2	0.1	0.1	0.1	0.2
	7	0.2	0.1	0.0	0.0	0.5	-0.4
	8	0.1	1.6	-0.6	0.1	0.1	0.4

Note: Displacements are in mm with positive values indicating extensometer extension or relative movement toward the face.

TABLE 8-5 MEASURED RELATIVE DISPLACEMENTS  
FOR 40 FOOT EXTENSOMETERS  
EDWARD HYATT POWERPLANT



of the solutions so they only measure the relative displacements corresponding to steps 2 and 3. Extensometers 1 through 3 and 9 through 11 were installed after the equivalent of step 2 of the solutions so they only measure the relative displacements corresponding to step 3.

The maximum, minimum and average values measured are shown in Table 8-6 along with the computed relative values and computed total values at the face. For the wall extensometers (1 through 3 and 9 through 11) the measured relative values ranged from -2.4 mm to 6.4 mm. Most of the computed relative values fall within the measured range but typically the linear analysis values are  $1/3$  to  $1/2$  the measured while the nonlinear analysis values are  $1/4$  to  $1/3$  the linear values. The jointed analysis values typically are larger than the linear values. One interesting point to note is the relative inward wall movement. The measured values show that the horizontal extensometer 2 (left or penstock side) moves inward more than the horizontal extensometer 10 (right or draft tube side). The jointed analysis shows this same behavior while the linear and nonlinear analyses show the opposite.

For the crown extensometers (4 through 8) the measured relative values ranged from -0.6 mm to 2.1 mm with only relatively small changes from excavation step 2 to step 3. All of the computed relative values fall within the measured range with the nonlinear analysis values most closely representing the average measured values. The linear analysis values are larger than the nonlinear values while the jointed analysis values vary from greater than to less than the linear values.

Comparison of the computed relative and total displacements shows that for the linear and nonlinear analyses, the relative values vary from about  $1/5$  to  $1/2$  the total values with an average of about  $1/3$  and for the nonlinear analyses, the relative values vary from about  $1/10$  to  $3/4$  the total values with an average slightly over  $1/3$ . These values imply that extensometers can only measure a small amount of the "elastic" deformation of an opening but would be of greatest value in measuring time-dependent deformation.

Further scrutiny of the data shown in Table 8-6 would imply that, based upon the measured relative values which show greater wall than crown displacements (i.e., compare the horizontal extensometers 2 and 10 with vertical extensometer 6), either there is substantial anisotropy in the initial stresses and/or the rock or the vertical rock bolting effectiveness is far superior to the horizontal rock bolting.

Excavation Step	Extensometer	Displacement (mm)									
		Measured (Relative)			Computed (Relative)			Computed (Total Face)			
		Maximum	Minimum	Average	Linear	Nonlinear	Jointed	Linear	Nonlinear	Jointed	
3	1	1.8	-2.4	-0.1	0.4	0.1	1.6	1.3	0.4	3.0	
	2	6.4	1.1	3.3	1.1	0.3	1.8	2.5	0.7	5.5	
	3	5.1	0.2	1.4	0.6	0.2	3.0	2.3	0.6	4.8	
	9	2.8	-0.1	1.6	0.6	0.2	-0.4	2.9	0.8	1.7	
	10	3.8	1.4	2.5	1.4	0.4	1.0	2.8	0.8	2.2	
	11	2.2	0.4	1.2	0.5	0.1	4.3	1.1	0.3	5.7	
2	4	0.3	-0.2	0.1	0.4	0.1	0.2	1.4	0.4	2.2	
	5	0.2	-0.2	0.0	0.2	0.1	1.6	1.2	0.3	3.3	
	6	0.1	-0.1	0.0	0.4	0.1	0.4	2.4	0.7	4.6	
	7	0.5	-0.2	0.1	0.2	0.1	0.2	1.2	0.3	1.3	
	8	0.7	0.0	0.2	0.5	0.1	0.2	1.5	0.4	1.4	
3	4	2.1	-0.2	0.4	0.4	0.1	0.2	1.9	0.5	2.6	
	5	0.2	-0.4	-0.1	0.0	-0.1	1.4	1.2	0.3	3.4	
	6	0.2	-0.1	0.1	0.8	0.2	0.5	2.7	0.8	4.8	
	7	0.5	-0.4	0.1	0.0	0.0	-0.1	1.5	0.4	1.4	
	8	1.6	-0.6	0.3	0.5	0.1	0.2	2.3	0.6	1.8	

Note: Measured relative displacements are extensometer measurements.  
 Extensometers 4 through 8 were installed after step 1, others installed after step 2.  
 Computed relative displacements were obtained from values at face less those at anchorage, measured along the extensometer orientation.  
 Computed total face displacements are those at the face, measured along the extensometer orientation.  
 Positive values indicate extensometer extension or relative movement toward the face.

TABLE 8-6 MEASURED AND COMPUTED DISPLACEMENTS FOR 40 FOOT EXTENSOMETERS  
 EDWARD HYATT POWERPLANT

The computed relative displacements also show this effect but, when the computed total displacements are considered, it can be seen that for the linear and non-linear analyses the results are within about 10% of each other. The jointed analysis shows substantially greater differences which implies that the main reason for the differences is the presence and interaction of the discontinuities in the rock mass.

b) Computed Displacements Around the Opening

The preceding discussion is very helpful in evaluating the displacements at specific locations but the finite element solution can be used further to look at the overall displacements along the opening face. Figures 8-14 and 8-15 show the displacements of the opening face for the 1 step and 3 step linear analyses from which it can be seen that the final displacements are virtually identical. The advantage of the 3 step analysis lies in the fact that the displacements at various stages of excavation can be obtained. The maximum displacements occur at mid-height and crown and the direction of movement is always inward toward the opening center.

Figure 8-16 shows the displacements of the opening face for the nonlinear analysis. The total displacements are less than the linear analyses but, as noted previously, the relative movements are not too different from those of the linear analyses. The maximum displacements also occur at mid-height and crown while the direction of movement is always inward.

The displacements of the opening face for the jointed analysis are shown in Figure 8-17 with the discontinuities superimposed for reference. It can be seen that the discontinuities play an important role in determining the form of face movement with some rock blocks moving more than others. It may be noted that some outward movement occurred but for the most part the movement was inward toward the opening center.

A further way of using the results of the jointed analysis is to look at the relative movement of the rock blocks separated by discontinuities. The rock block movement is shown in Figures 8-18 through 8-20 with the approximate average movement of the blocks shown by vector displacement arrows. The blocks all show relative inward movement which increases as excavation proceeds. Of special interest to note is the relatively large inward movement of several of the smaller triangular blocks in the crown and walls which may have "fallen" into the excavation if rock bolting had not been employed.

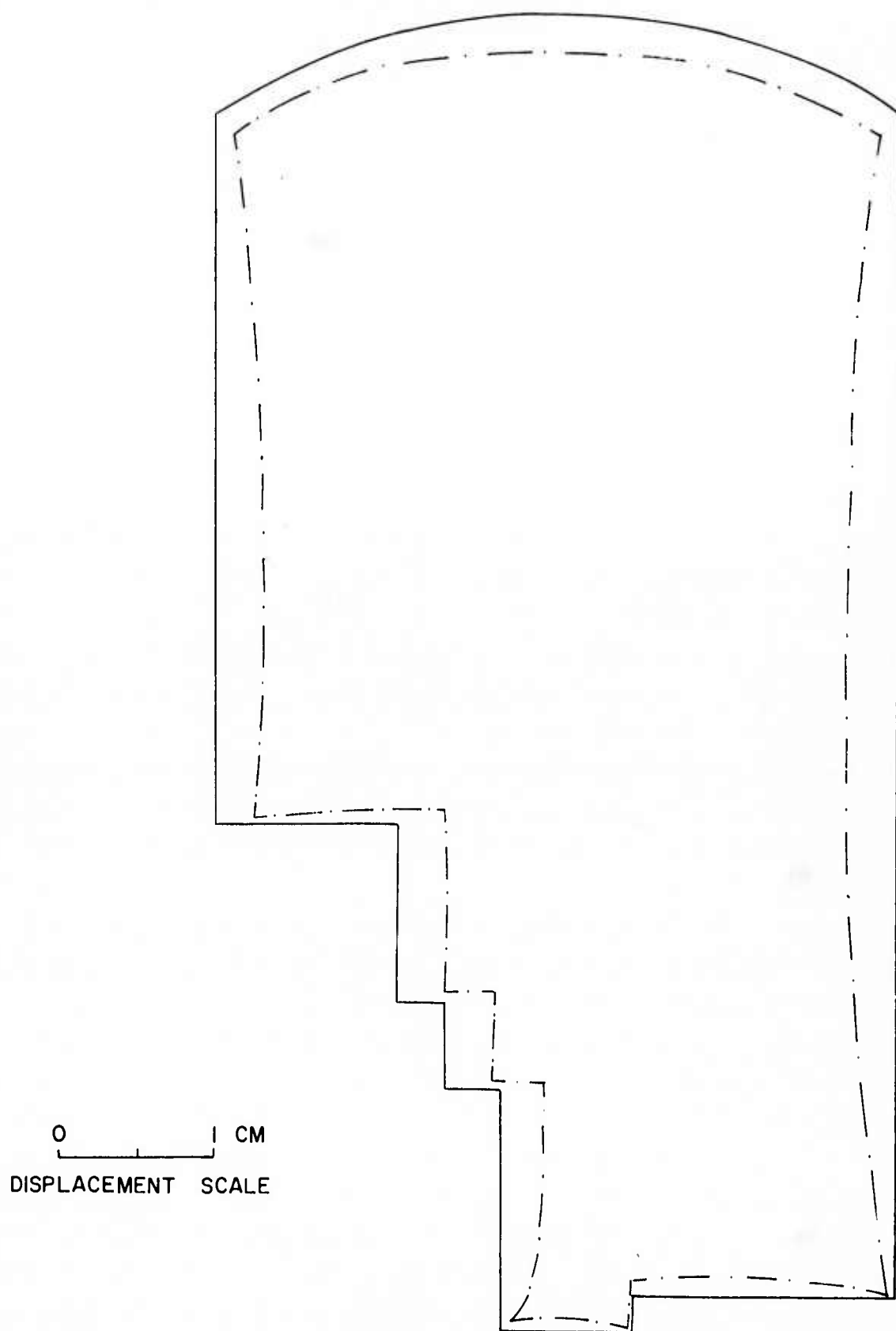


**FIG. 8-14 DISPLACEMENTS OF OPENING FACE  
EDWARD HYATT POWERPLANT  
1 STEP LINEAR ANALYSIS**

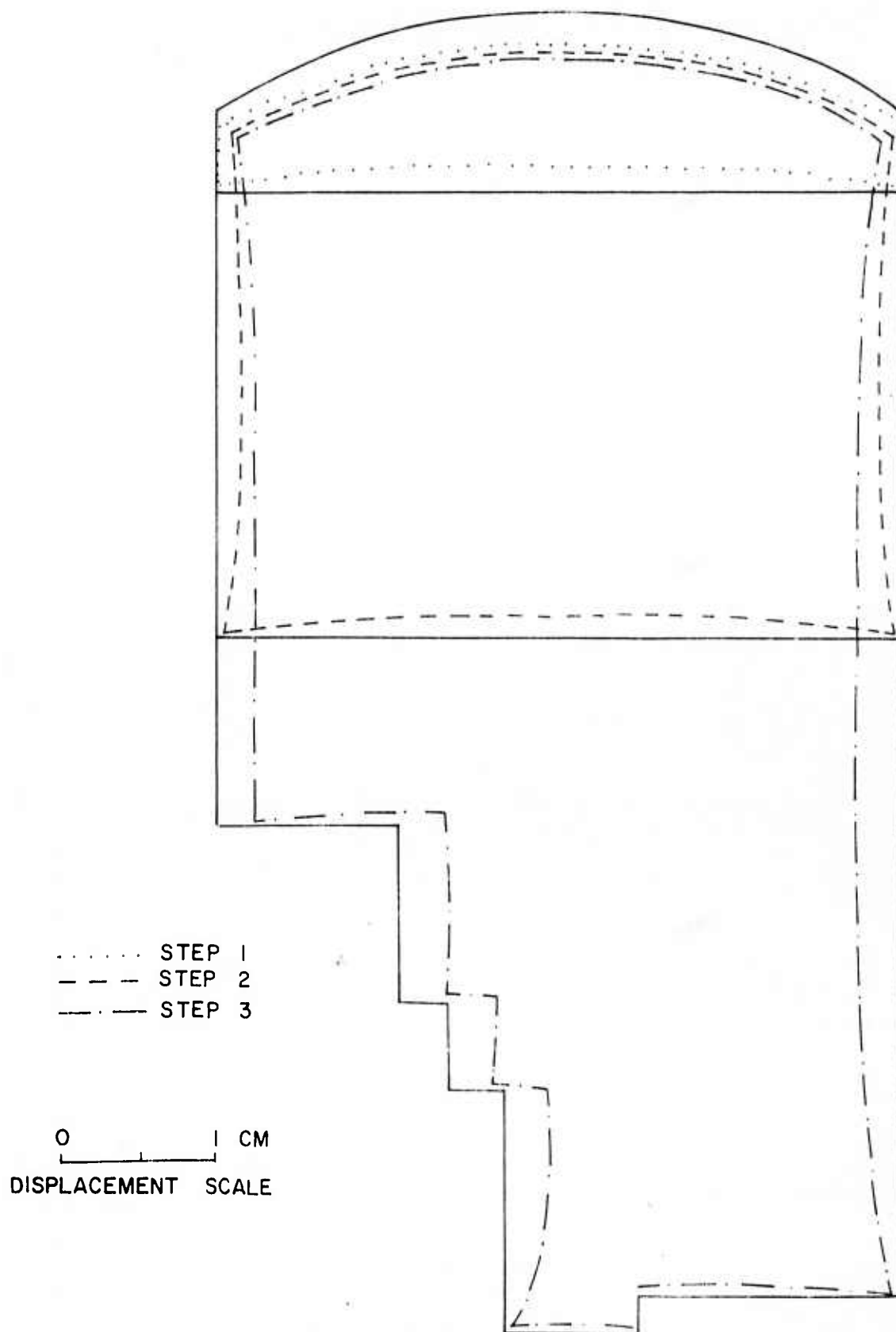


**FIG. 8-15 DISPLACEMENTS OF OPENING FACE  
EDWARD HYATT POWERPLANT  
3 STEP LINEAR ANALYSIS**

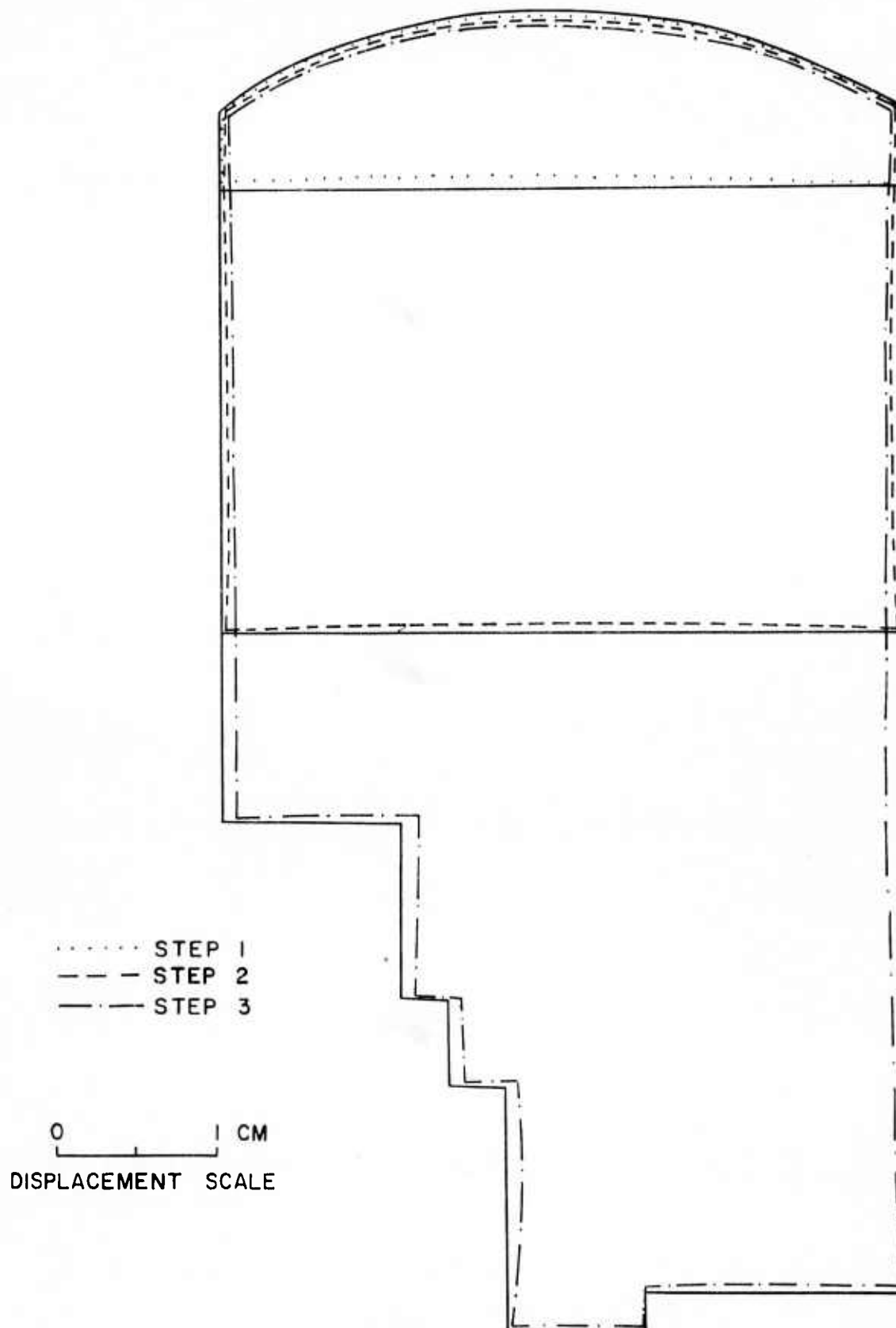


**FIG. 8-16 DISPLACEMENTS OF OPENING FACE  
EDWARD HYATT POWERPLANT  
NONLINEAR ANALYSIS**



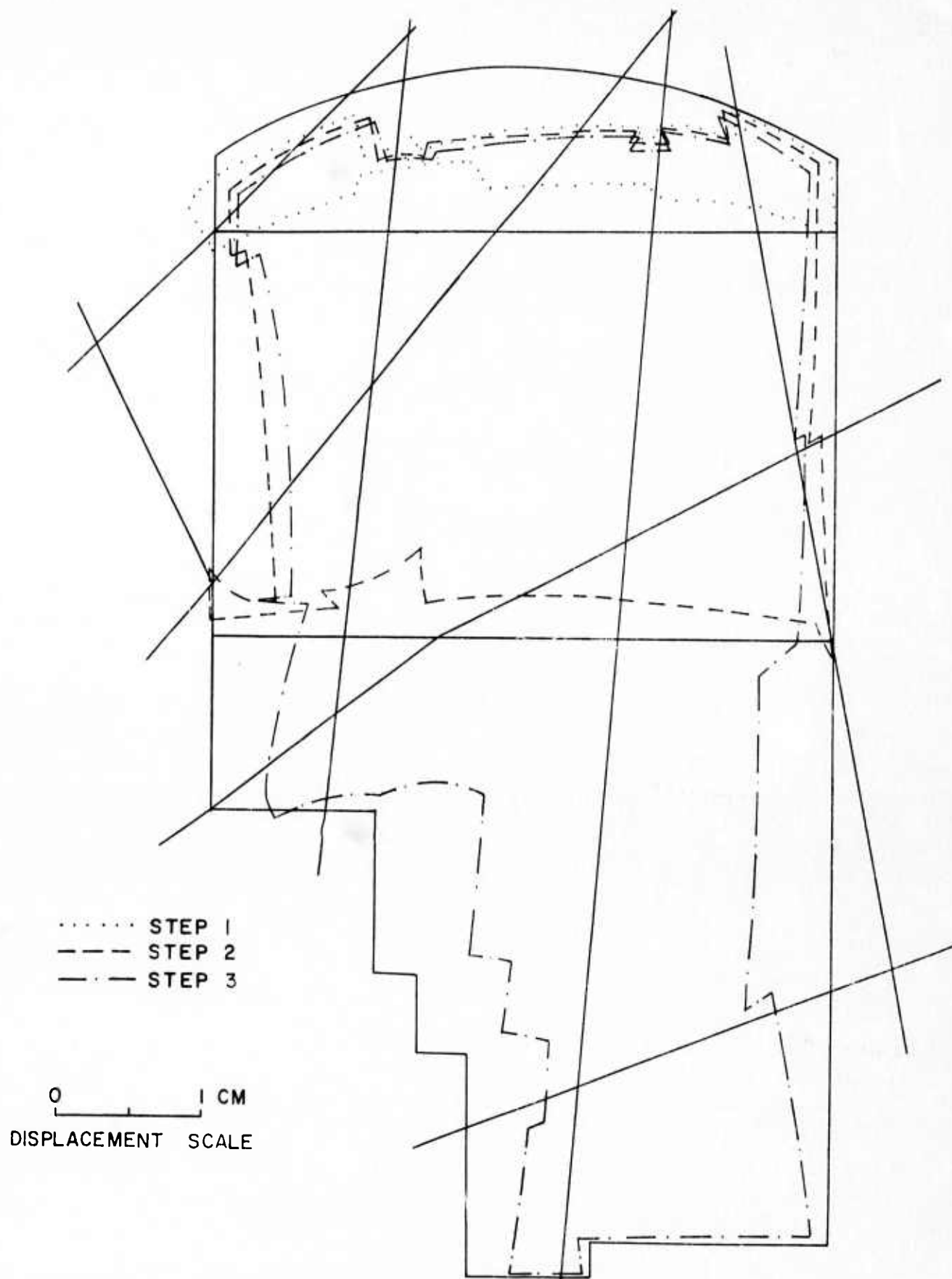


**FIG. 8-17 DISPLACEMENTS OF OPENING FACE,  
Q UNIT ONE, EDWARD HYATT  
POWERPLANT - JOINTED ANALYSIS**

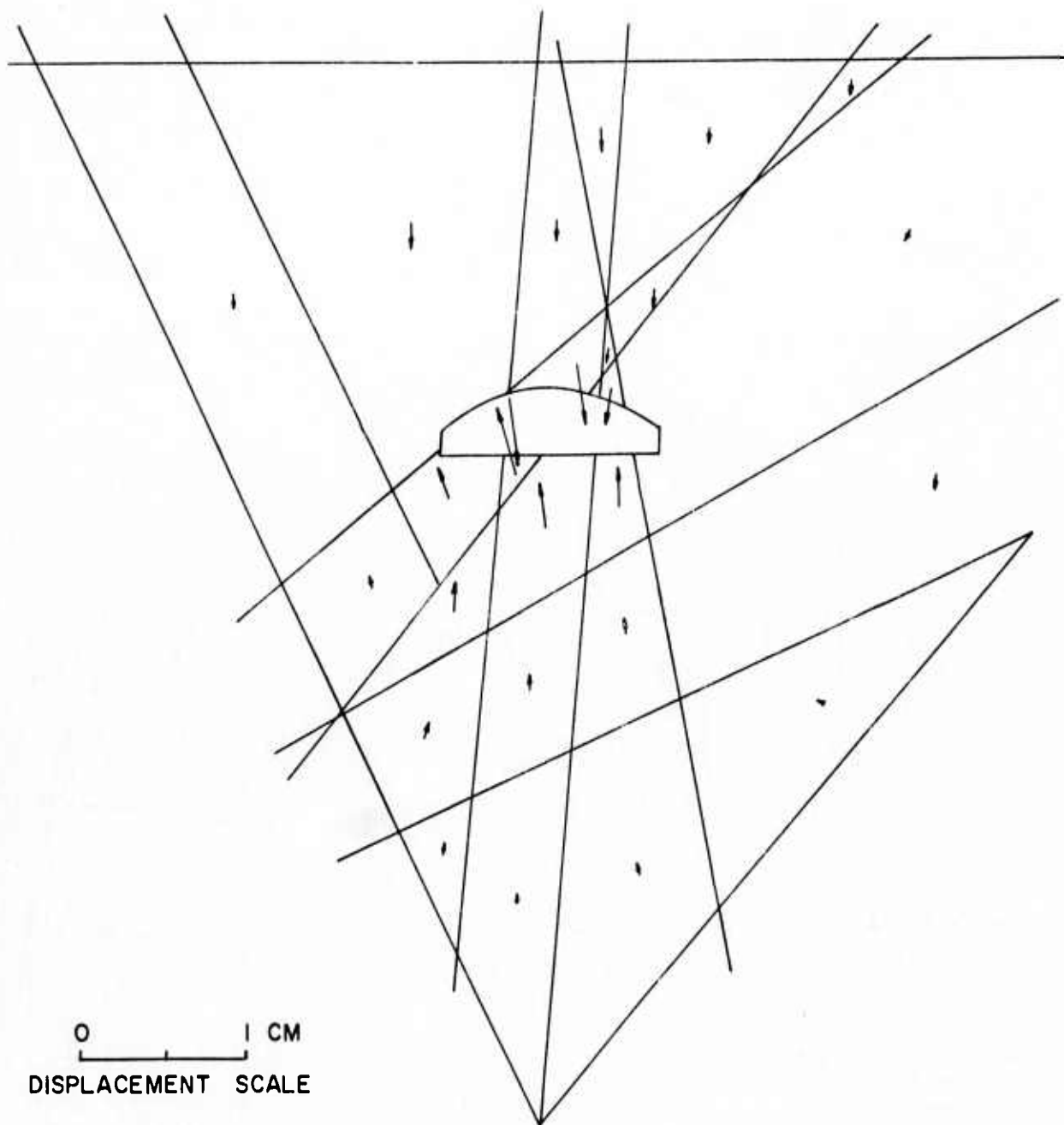


**FIG. 8-18 MOVEMENT OF ROCK BLOCKS AROUND  
EDWARD HYATT POWERPLANT - STEP 1**

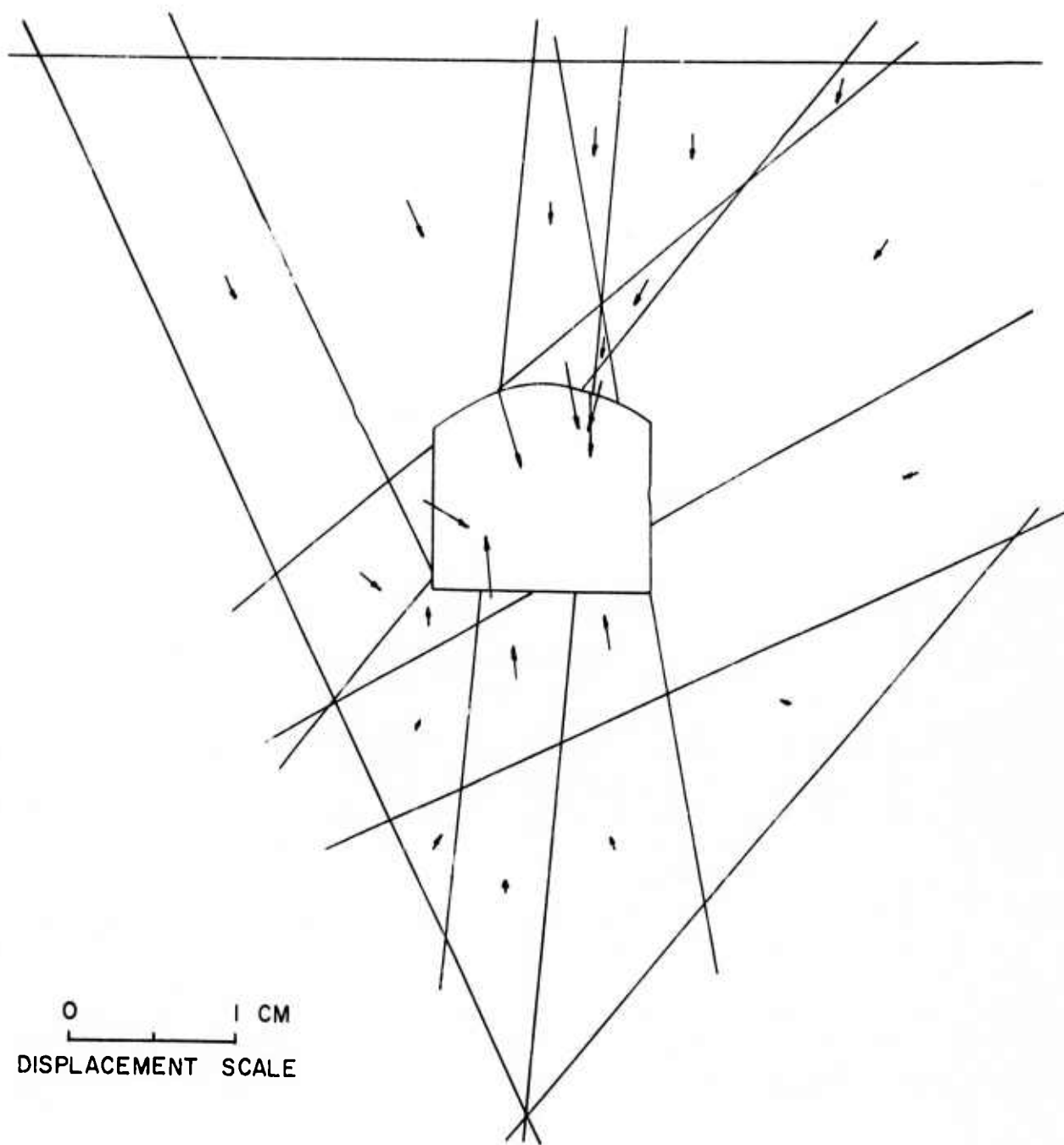


**FIG. 8-19    MOVEMENT OF ROCK BLOCKS AROUND  
EDWARD HYATT POWERPLANT - STEP 2**

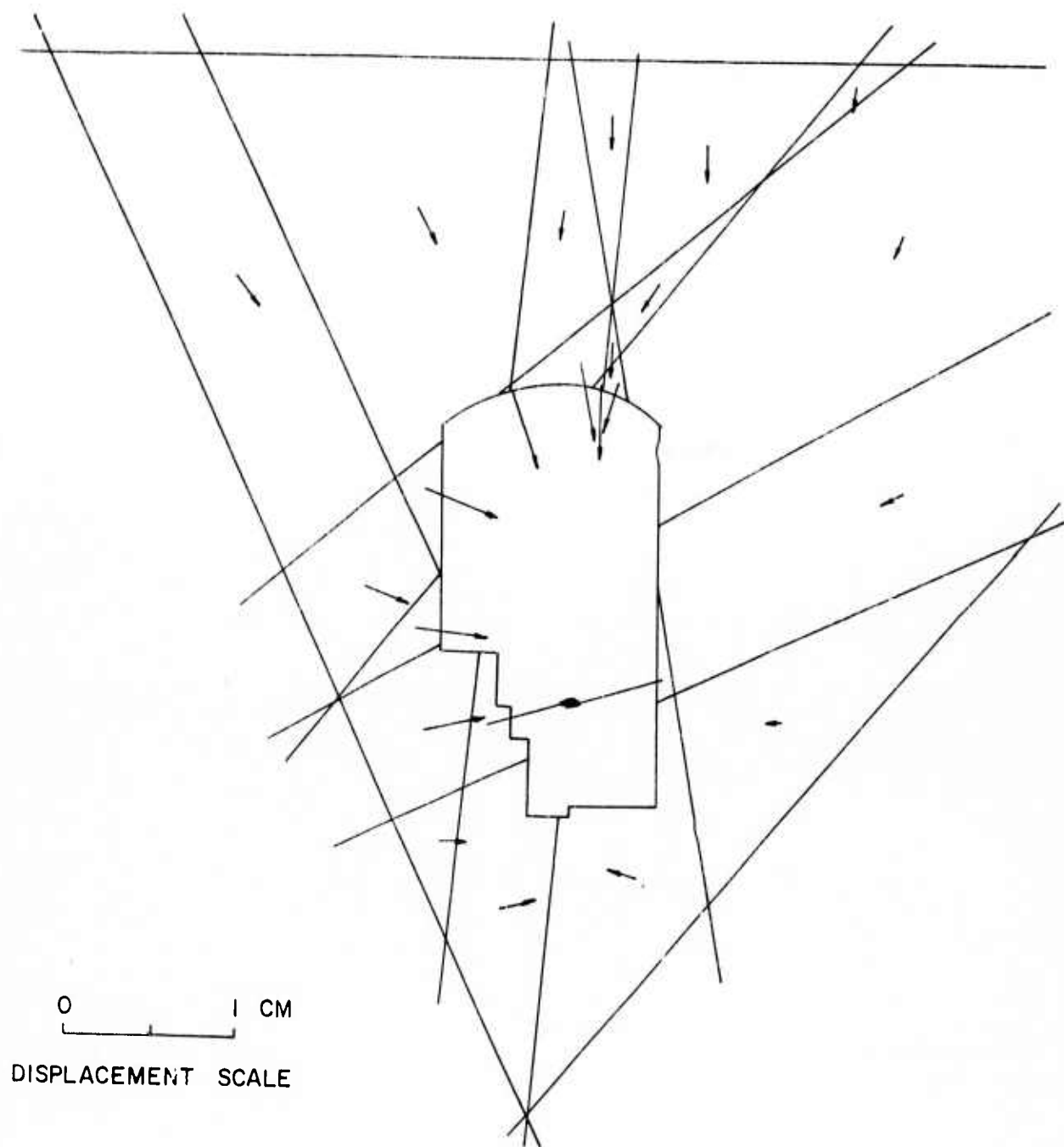


**FIG.8-20 MOVEMENT OF ROCK BLOCKS AROUND  
EDWARD HYATT POWERPLANT - STEP 3**

## Stresses

The finite element solutions further provide an overall picture of the stresses developing around the opening during construction which can be used to isolate zones of stress concentration and relief and to evaluate potential failure zones which should be supported. Figures 8-21 and 8-22 show the  $\sigma_1$  contours during excavation for the nonlinear analysis, the results of which are virtually identical to the linear analysis. It can be seen that as excavation proceeds, the crown and base stresses increase, stresses increase to a progressively greater distance from the opening and stress concentrations develop at re-entrant corners while stress relaxations occur at the benches. The greatest stress concentrations are larger than  $11 \text{ MN/m}^2$  ( $\approx 1620 \text{ psi}$ ). Figures 8-23 and 8-24 show the  $\sigma_3$  contours during excavation for the nonlinear analyses. It can be seen that as excavation proceeds, these stresses are relieved to progressively greater distances from the opening and tensile zones develop in the walls, indicating potential tensile failure. However since the tensile strength of the rock is high and since discontinuity movement would occur, the effect of these tensile zones would be minimized. The rock bolt installation would further minimize these effects.

Figures 8-25 through 8-27 show the development of the  $\sigma_1$  stress contours during excavation in the jointed analysis. These figures show that the discontinuities play a significant role in modifying the stress distribution around an opening because the stresses largely follow the discontinuities. This leads to an asymmetrical stress distribution around the opening which is a function of discontinuity orientation, frequency and stiffness. However it can be noted that the largest stress concentrations still develop at the re-entrant corners and they are nearly the same value as those developed in the linear and nonlinear analyses.

Figures 8-28 through 8-30 show the  $\sigma_3$  contours during excavation for the jointed analyses. These figures also show that the stresses are relieved to progressively greater distances as the excavation proceeds, but that tensile zones develop and these tensile zones follow along the discontinuities where the largest relative block movement occurs. Therefore it can be seen that even though relative movement occurs along the discontinuities, the rock is still in tension under the imposed stress state.

The results of these analyses can be further used to evaluate the relative stability of the rock mass surrounding the opening. This can be accomplished by

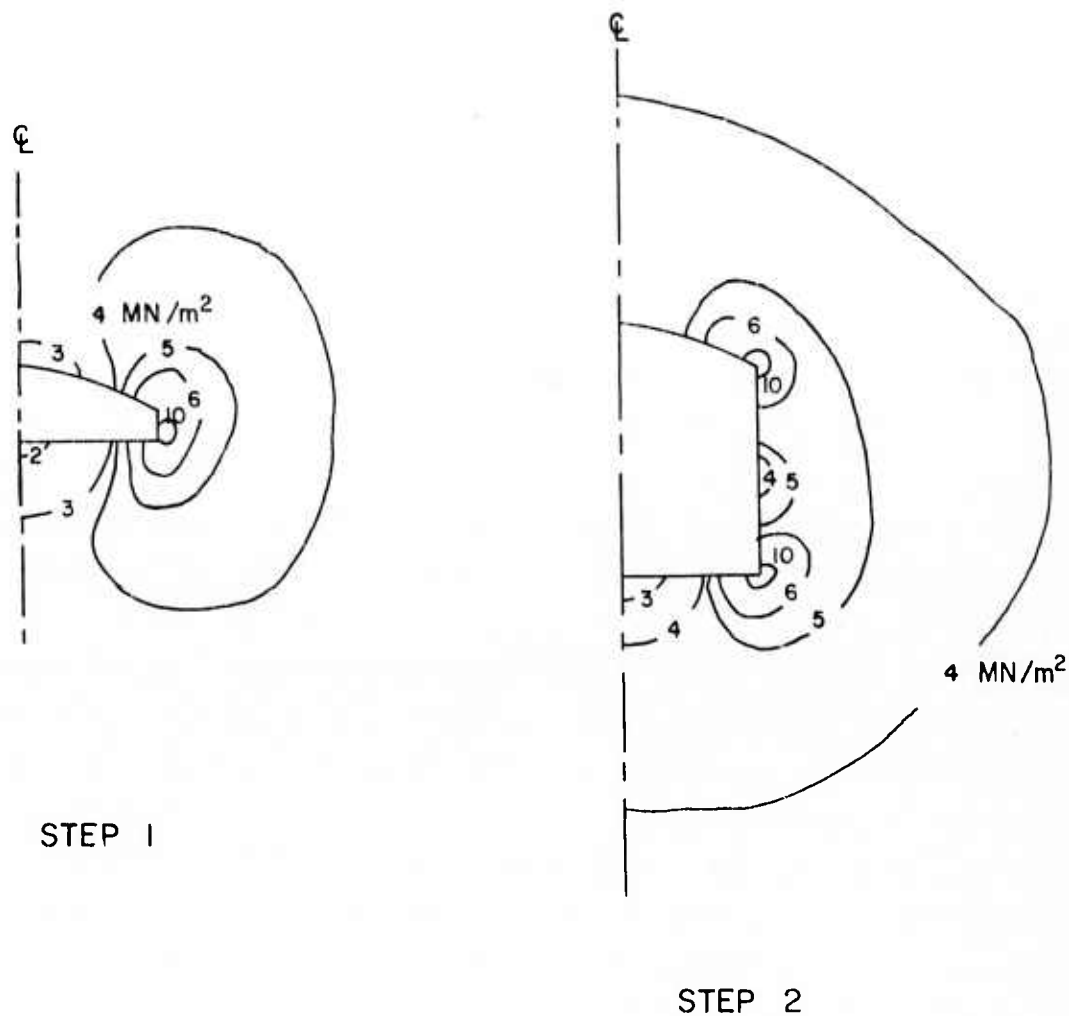


**FIG.8-21    CONTOURS OF  $\sigma_1$  FOR  $\zeta$  UNIT ONE  
EDWARD HYATT POWERPLANT  
NONLINEAR ANALYSIS - STEPS 1 AND 2**



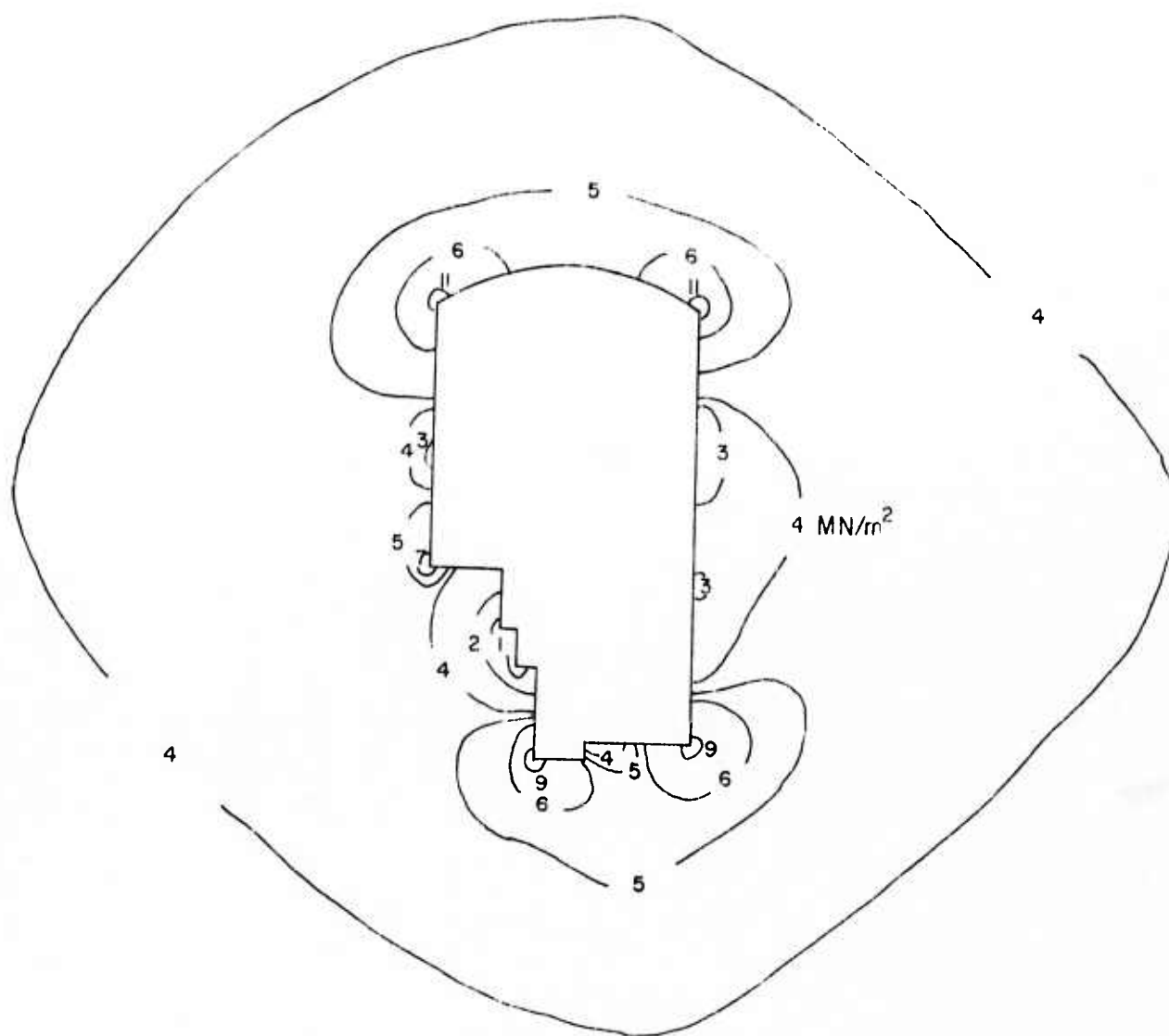
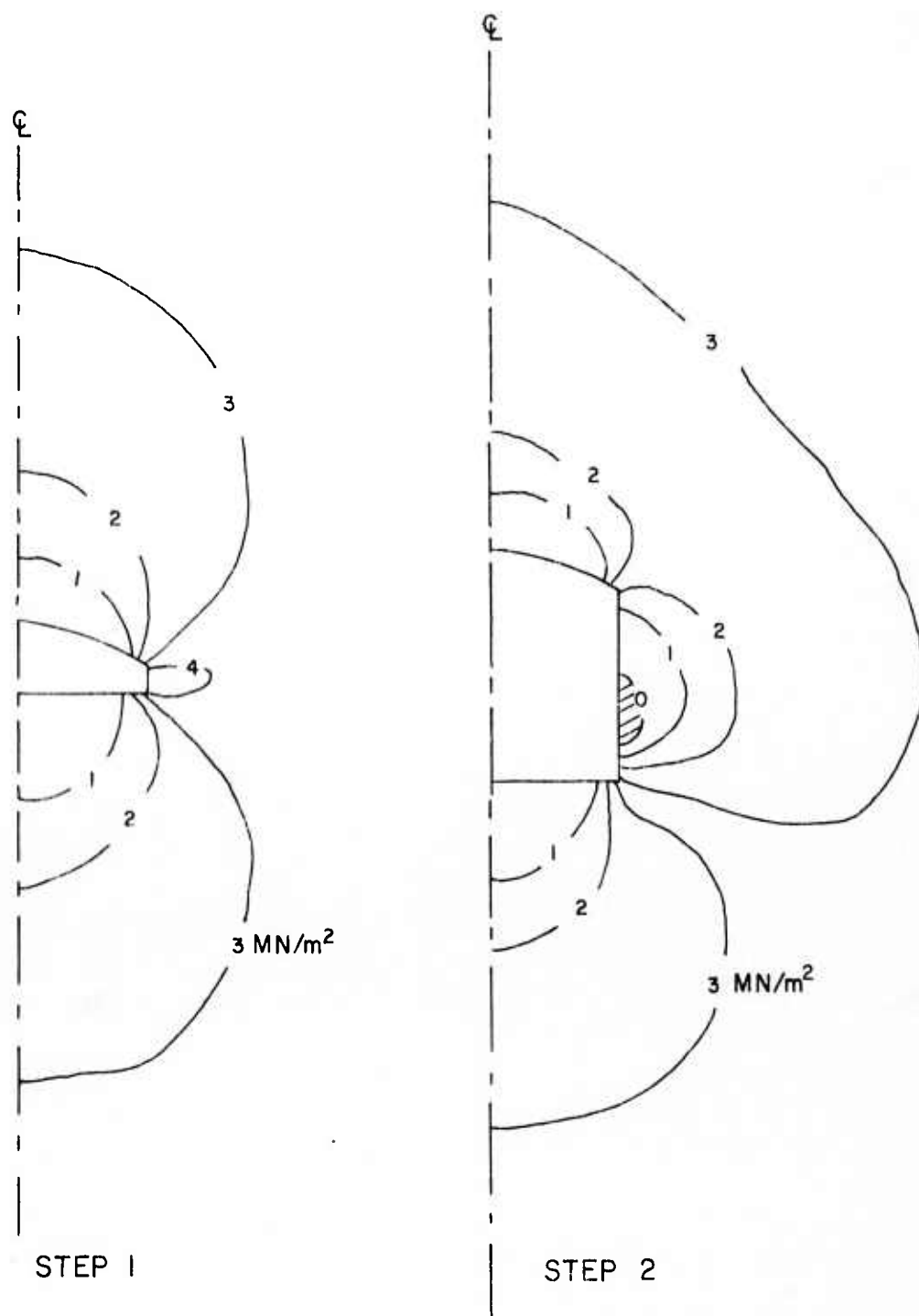


FIG. 8-22 CONTOURS OF  $\sigma_1$  FOR Q UNIT ONE  
EDWARD HYATT POWERPLANT  
NONLINEAR ANALYSIS - STEP 3



**FIG. 8-23 CONTOURS OF  $\sigma_3$  FOR Q UNIT ONE  
EDWARD HYATT POWERPLANT  
NONLINEAR ANALYSIS - STEPS 1 AND 2**

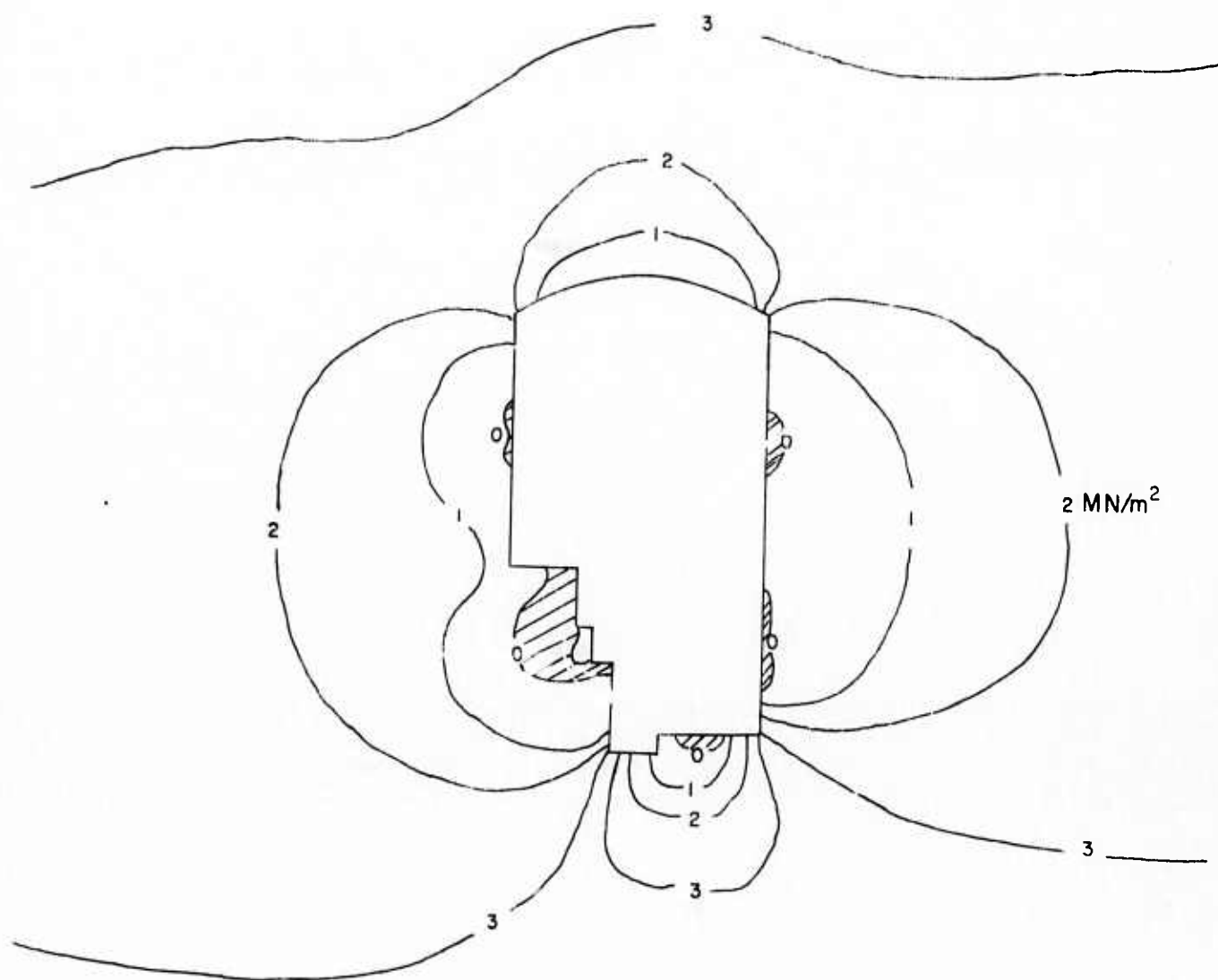


FIG. 8-24 CONTOURS OF  $\sigma_3$  FOR  $\phi$  UNIT ONE  
EDWARD HYATT POWERPLANT  
NONLINEAR ANALYSIS - STEP 3

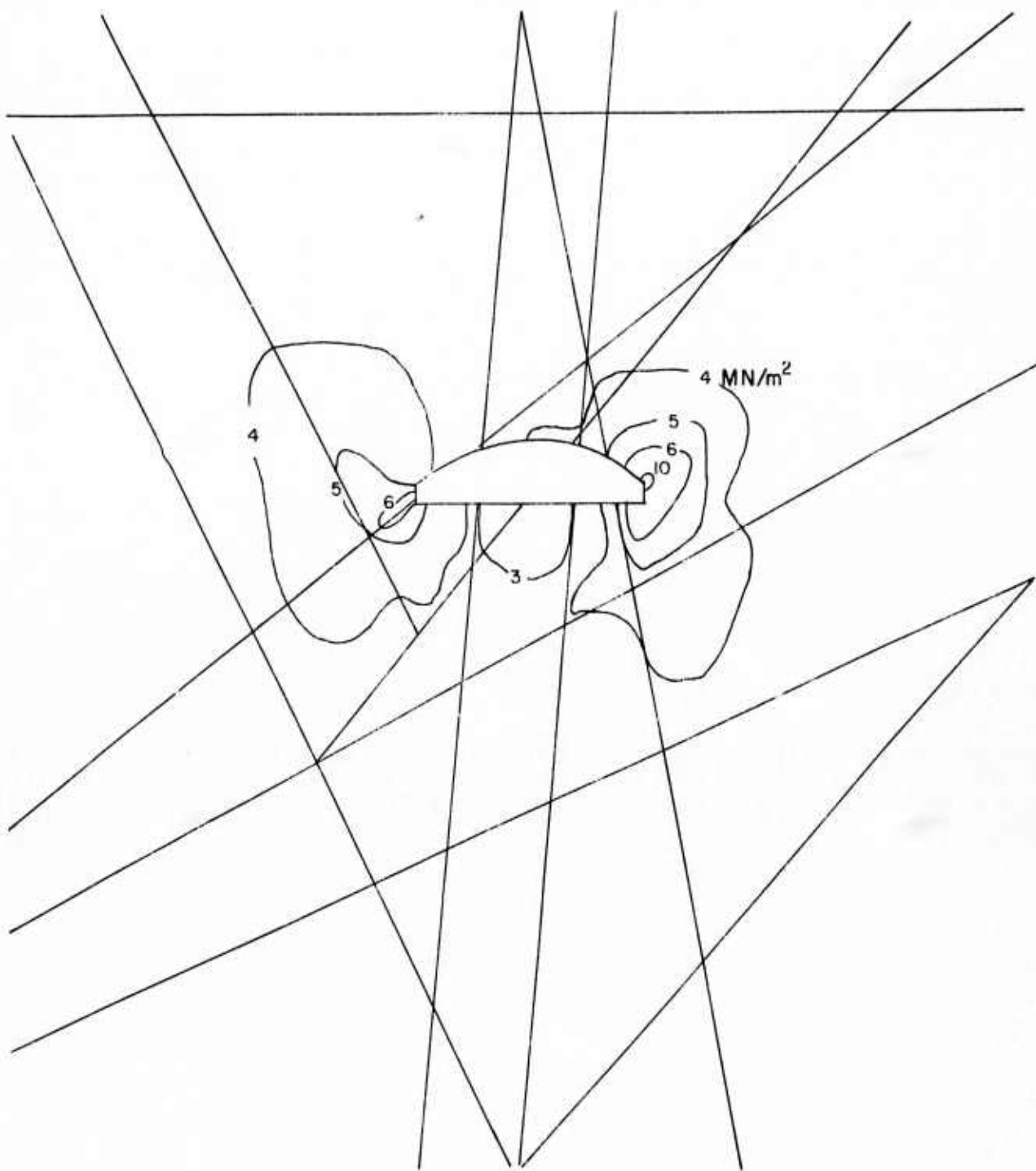


FIG. 8-25 CONTOURS OF  $\sigma_1$  FOR Q UNIT ONE  
EDWARD HYATT POWERPLANT  
JOINTED ANALYSIS - STEP 1

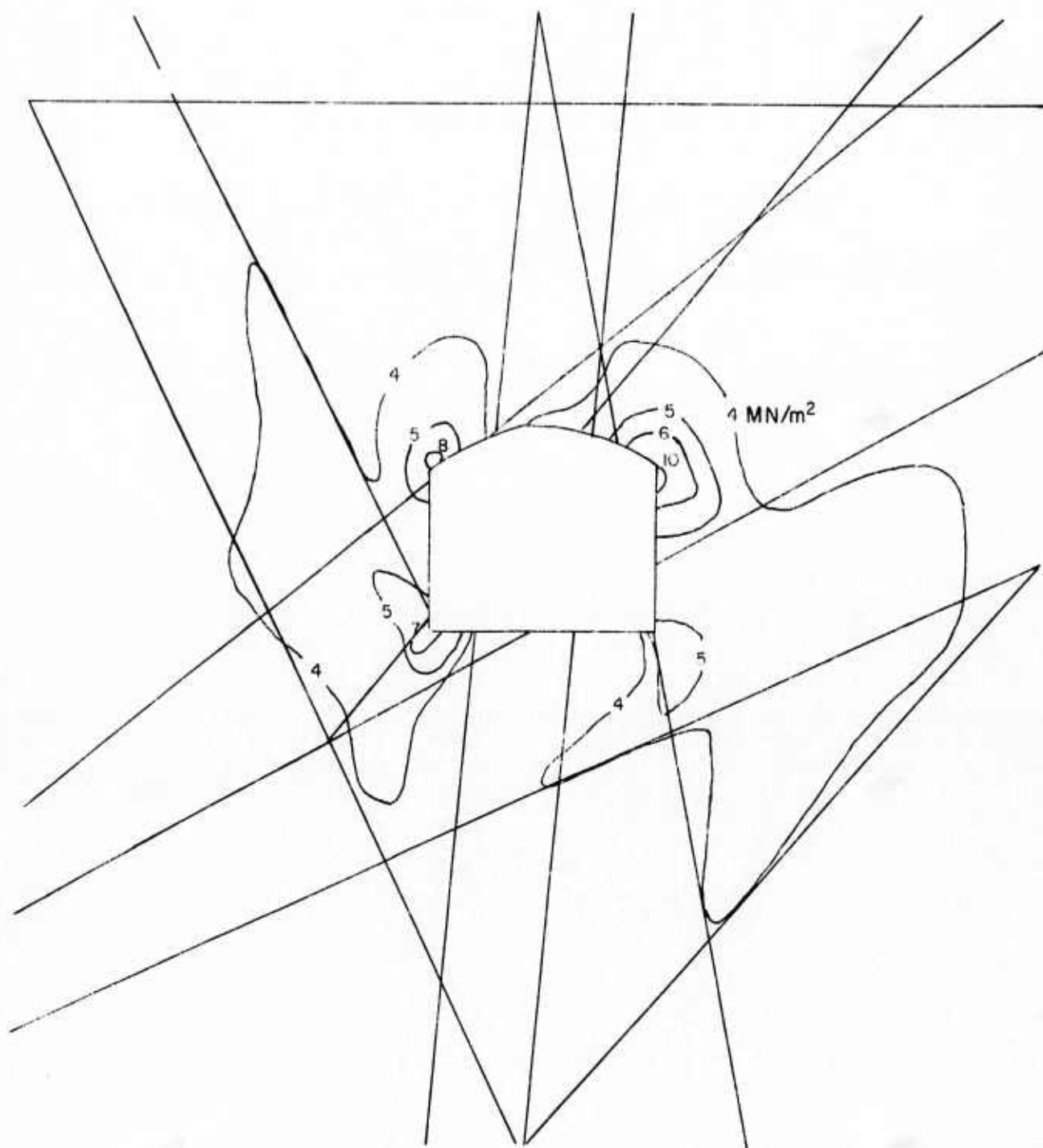


FIG. 8-26 CONTOURS OF  $\sigma_1$  FOR  $\mathcal{Q}$  UNIT ONE  
EDWARD HYATT POWERPLANT  
JOINTED ANALYSIS - STEP 2

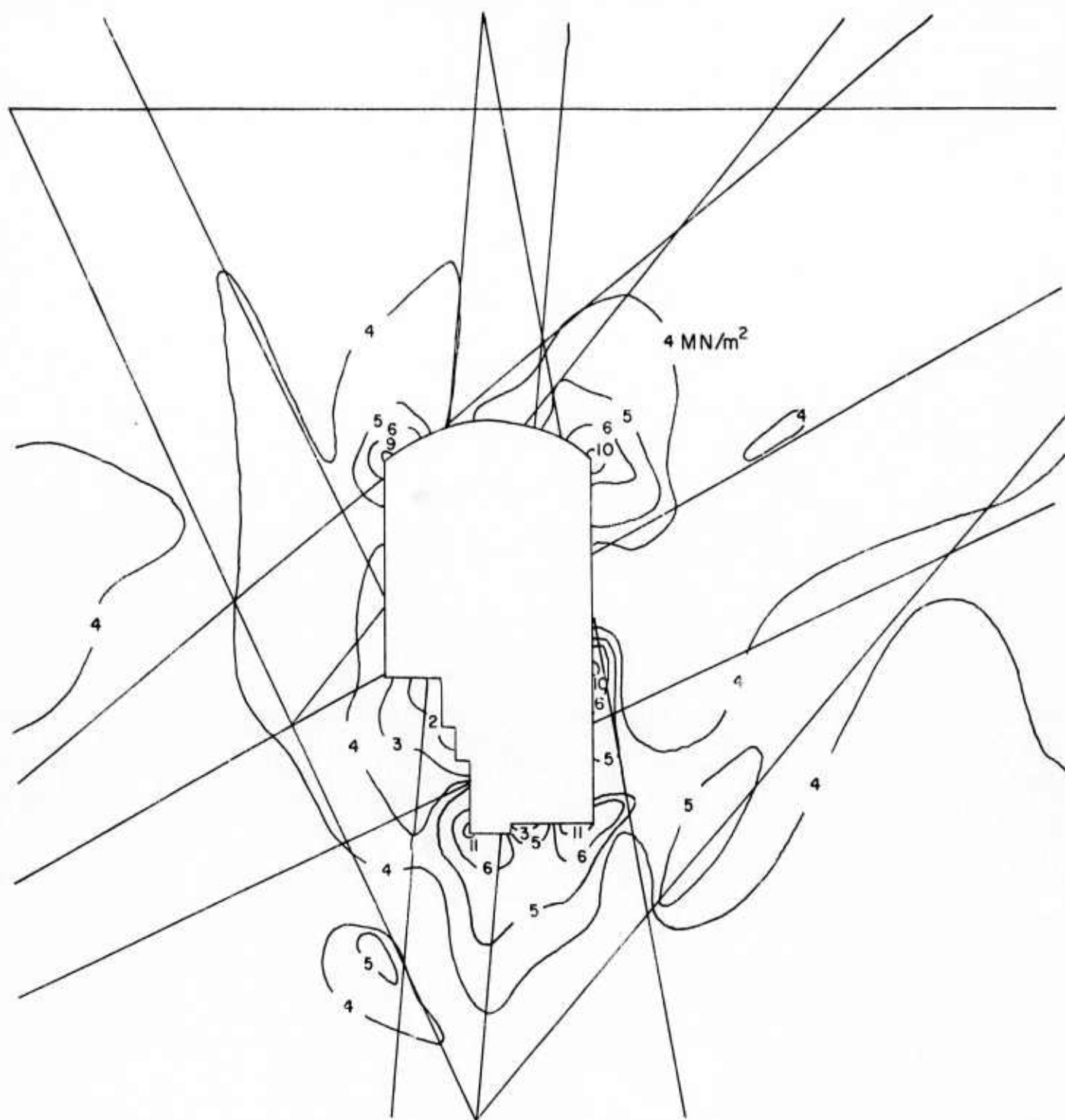


FIG. 8-27 CONTOURS OF  $\sigma_1$  FOR Q UNIT ONE  
EDWARD HYATT POWERPLANT  
JOINTED ANALYSIS - STEP 3

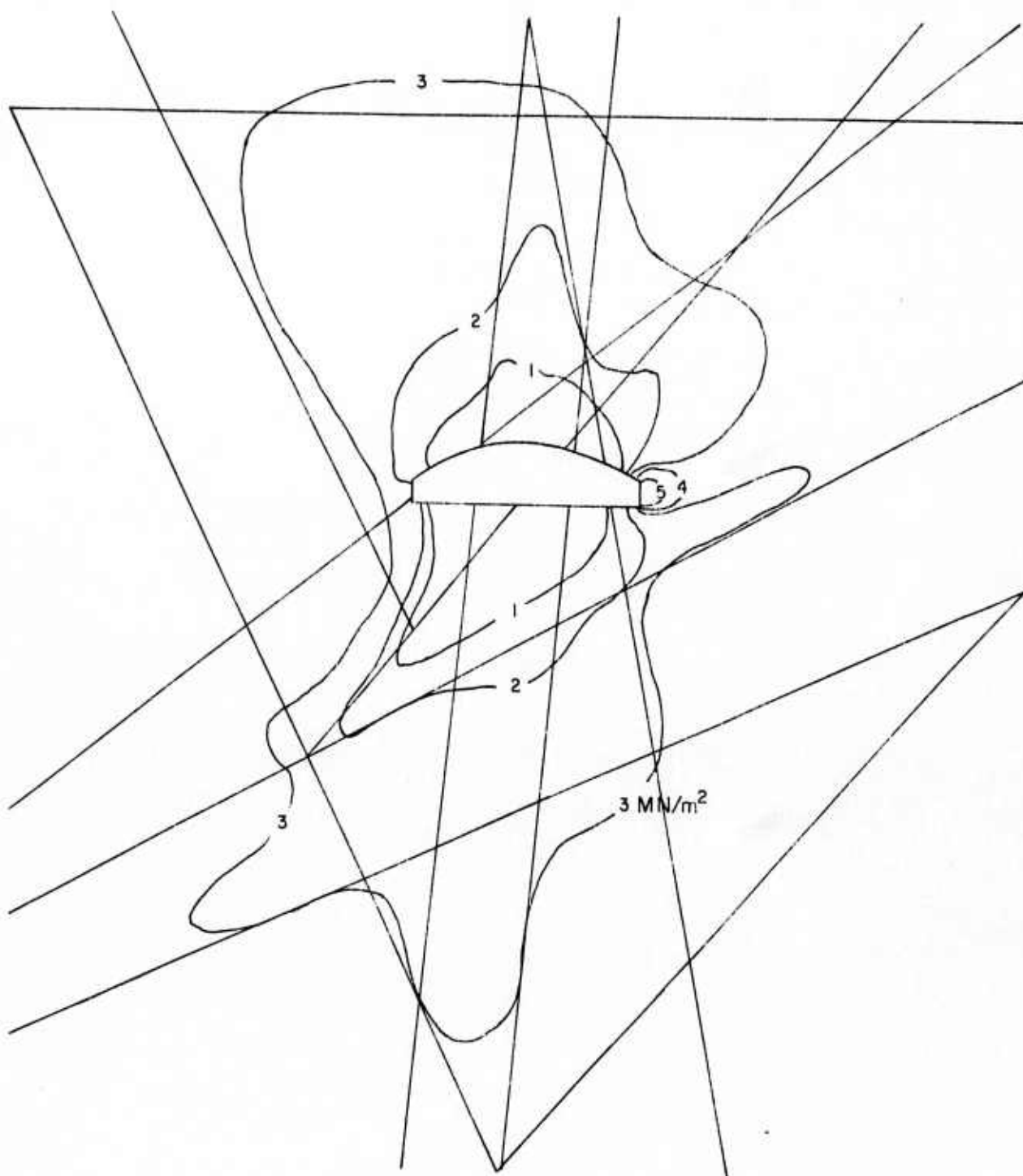


FIG. 8-28 CONTOURS OF  $\sigma_3$  FOR Q UNIT ONE  
EDWARD HYATT POWERPLANT  
JOINTED ANALYSIS - STEP I



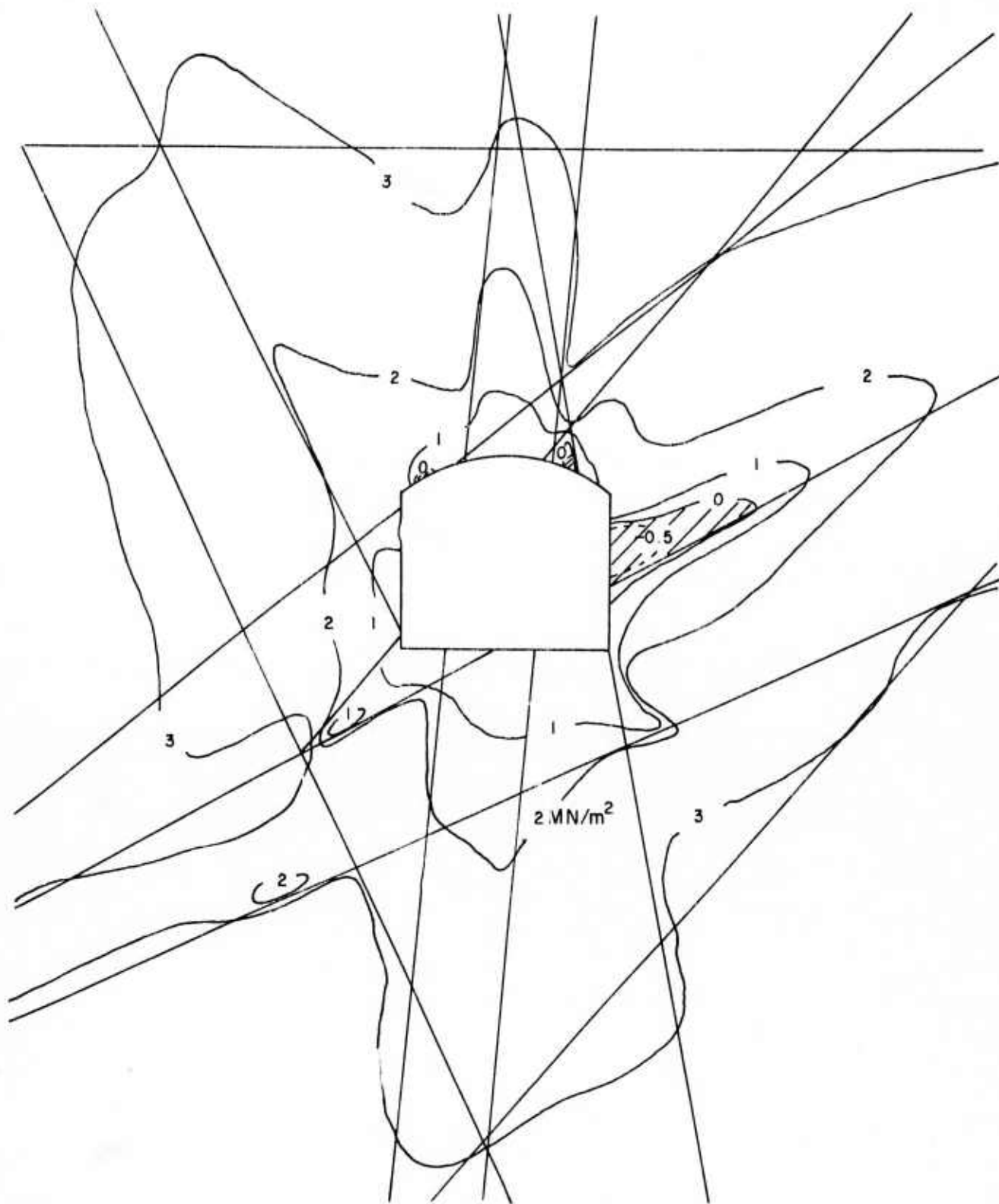


FIG. 8-29 CONTOURS OF  $\sigma_3$  FOR  $\mathbb{Q}$  UNIT ONE  
EDWARD HYATT POWERPLANT  
JOINTED ANALYSIS - STEP 2

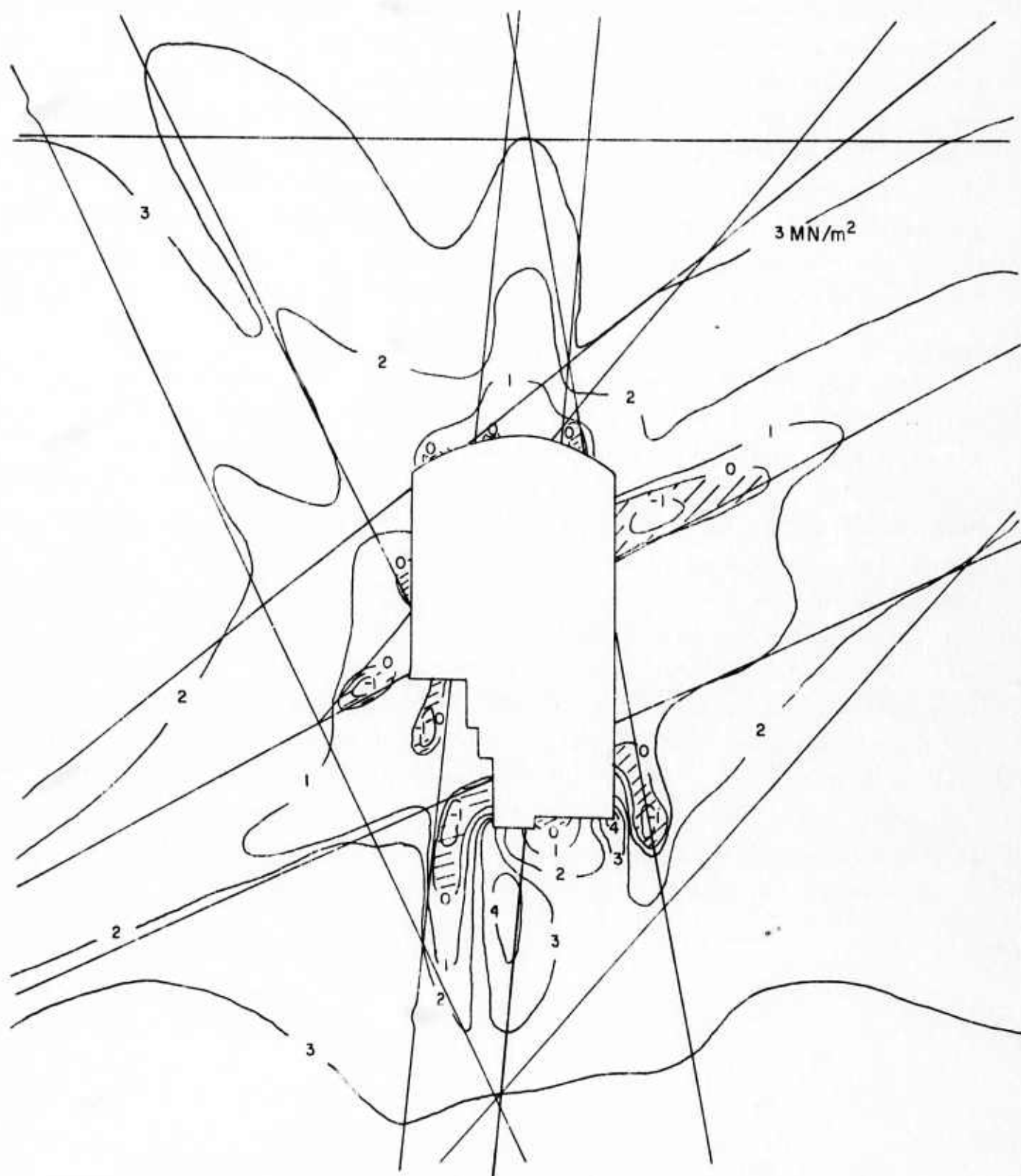
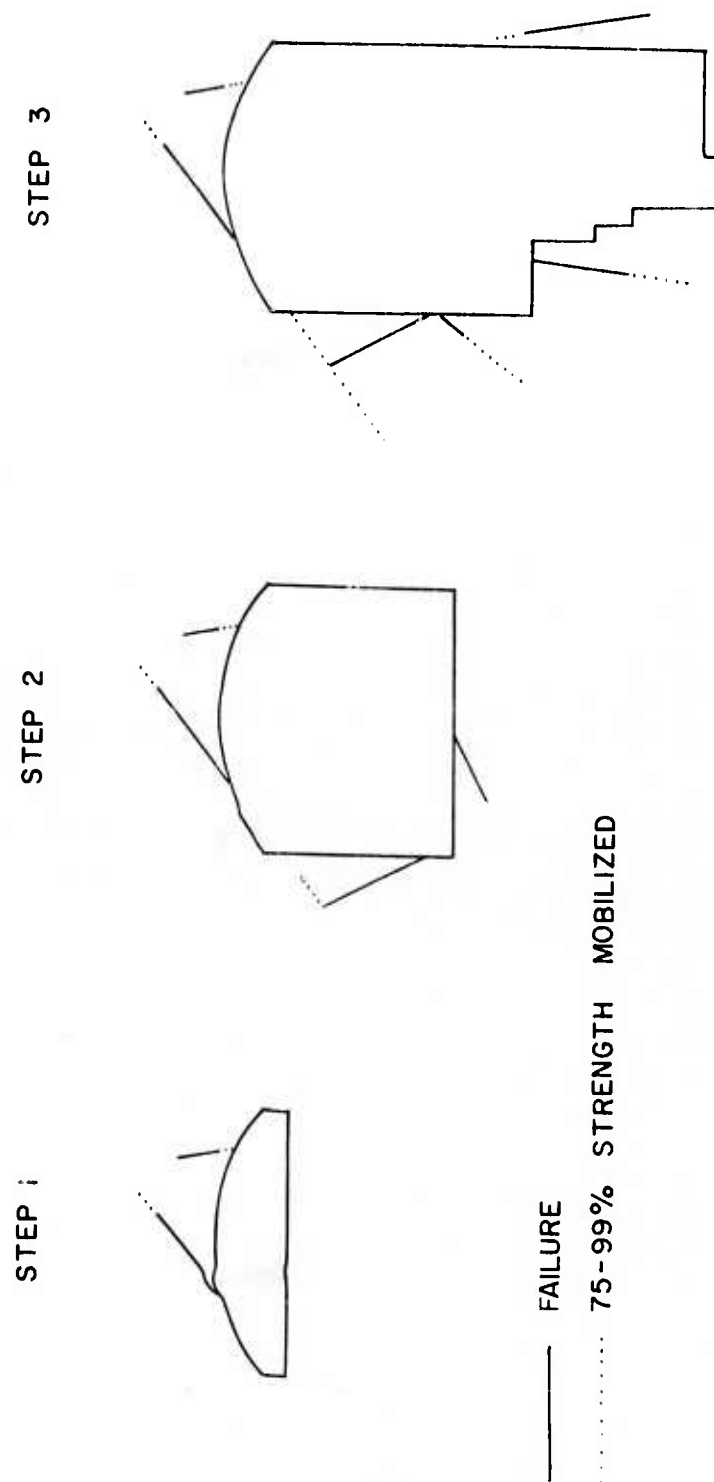


FIG. 8-30 CONTOURS OF  $\sigma_3$  FOR  $\mathcal{Q}$  UNIT ONE  
EDWARD HYATT POWERPLANT  
JOINTED ANALYSIS - STEP 3

comparing the developed stresses to the available strength. For the linear, nonlinear and jointed analyses it was found that the mobilized strength in the rock (i.e., developed stresses/available strength) was less than 5% in all cases and that tensile failure did not occur. But in the jointed analysis, as shown in Figure 8-31, several portions of the discontinuities had reached failure and stress states approaching failure. However, none of the rock blocks developed full failure conditions along the discontinuities bounding it, indicating that no major fallout would occur, even though several blocks appear to be only marginally stable based on this analysis.

#### Summary

Based upon the four types of finite element analyses presented in this chapter (1 step linear, 3 step linear, 3 step nonlinear and 3 step jointed), it can be said that all of the analyses can provide reasonable representations of the observed behavior if the material properties can be adequately defined. The 1 step linear analysis is limited because it cannot follow the excavation sequence. Both of the linear analyses are limited because the selection of material properties hinges to a large degree on the availability of a large body of field data and a broad generalization of these results. The nonlinear analysis appears to yield displacements somewhat lower than those measured but the values for analysis are easily and inexpensively obtained. The jointed analysis appears to yield the best overall method of evaluating the performance of the opening. The rock properties can be determined as easily as for the nonlinear analysis, but field data is required to define the prominent discontinuities and their properties. However, if this data is available, the resulting deformations, stresses and stability of the rock mass may be evaluated with a reasonable degree of accuracy.



**FIG. 8-31 MOBILIZED STRENGTH ALONG DISCONTINUITIES  
 AROUND EDWARD HYATT POWERPLANT**

## CHAPTER 9

### SUMMARY AND CONCLUSIONS

The studies conducted and presented in this report were oriented toward establishing a simple, practical approach for applying the finite element method to predict the behavior of underground openings in rock during excavation. The techniques presented use nonlinear, stress-dependent empirical models for the rock and discontinuity properties in analyses which can simulate the actual excavation sequences employed in the field. A wide range of generalized analyses was conducted to evaluate the relative effects of variations in opening shape, excavation sequence, initial stress values and orientations, material properties and discontinuity orientation on the resulting stresses and displacements. Finally, to check the validity and general applicability of these techniques, the results of finite element analyses using these techniques were compared to the results of instrumentation studies which had been conducted to measure the displacements within the Edward Hyatt Powerplant during excavation. Comparisons of the observed and computed behavior were excellent and showed that these techniques may be used as a powerful design tool to: (1) predict stresses and displacements around openings in rock, (2) aid in the selection of instrument locations for monitoring displacements, and (3) interpret the results obtained from instrumentation of an opening. More specific details are summarized in the following sections.

#### Finite Element Modeling Techniques

A generalized procedure for incremental excavation analysis was discussed and its general applicability was demonstrated. A number of analyses were conducted to establish minimum criteria for the design of finite element meshes and these analyses showed that, for simple structures in homogeneous rock where there is a plane of symmetry and only one-half of the system must be analyzed, a minimum of 125 to 150 elements should suffice. More will be needed for more complex shapes or rock masses. These studies also showed that to conduct analyses with a minimum of boundary interference, the boundary must be located at least six radii from the center of the opening.

#### Stress-Strain Behavior of Rock

An extensive literature survey was conducted to evaluate the properties of rock types for use in analyses and to examine the applicability for rock of simple,

practical stress-strain relationships recently proposed for soil. The results of this study showed that these relationships simulate the nonlinear, stress-dependent behavior of rock quite well. The results of the literature survey, including 163 values under uniaxial test conditions and 115 values under triaxial test conditions, were tabulated and analyzed and representative values of the parameters were discussed. It was found that for certain classes of rock, material properties varied little and that nonlinearity and/or stress-dependency was sometimes a minor factor in the behavior. Furthermore, this survey showed the degree and importance of anisotropy of the material parameters.

#### Analysis of Openings in Homogeneous Rock Masses

Analyses were conducted to investigate the importance of material properties, initial stresses, excavation operations and opening shapes on the final stresses and displacements around underground openings in homogeneous rock masses. The results of these analyses showed that opening shape, initial stress magnitude, initial stress orientation and gravity initial stresses, when shallow, effect the resulting stresses and displacements considerably, while the modulus, in a linear analysis, or the initial tangent stiffness and stress-dependency in a nonlinear analysis, greatly effect the displacements. Poisson's ratio variations cause relatively small effects on the stresses and displacements and all other parameters cause minor, if any, variations. It should be noted that in all of these analyses, representative strength parameters were used. The mobilized shear stresses which resulted were small and subsequently no shear failures occurred. Furthermore, tension zones were allowed to develop and no analysis modifications were made to account for tension failure.

#### Analysis of Openings in Rock Containing a Single Planar Two-Dimensional Discontinuity

Analyses were conducted to evaluate the significance of discontinuity stiffness and orientation on the resulting stresses and displacements around underground openings in rock containing a single, prominent, planar discontinuity. The results of these analyses showed that the stress changes, i.e., load transfer, become more substantial, tension zones increase, normal and shear stresses on the discontinuity decrease and displacements increase as the discontinuity becomes softer. These changes are very significant when  $M$  (discontinuity modulus/rock modulus) goes from 1 to 10, are fairly important when  $M$  goes from 10 to 100 and are small when  $M$  goes from 100 to 1000.

When the planes of the discontinuity and the minimum principal stress coincide, a substantial reduction occurs in the dimensionless  $\sigma_1$  values, the dimensionless normal stresses on the discontinuity are greatest, the discontinuity compression is greatest and the inward displacements are least. When the planes of the discontinuity and the maximum principal stress coincide, a substantial increase occurs in the dimensionless  $\sigma_1$  values in the discontinuity with a decrease adjacent to the discontinuity, the dimensionless shear stresses on the discontinuity are greatest, the discontinuity compression is least and the inward displacements are greatest. When the discontinuity is at  $45^\circ$  to the initial principal stresses and as the discontinuity becomes softer, the dimensionless  $\sigma_1$  values in the discontinuity become equal to one and the dimensionless  $\sigma_3$  values in the discontinuity become equal to  $K$ , the ratio of initial minor to major principal stresses. All other changes are minor.

#### Stress-Deformation Behavior of Planar Discontinuities

An extensive literature survey was conducted to evaluate the properties of discontinuities for use in analyses and to examine the applicability of a simple, practical stress-deformation relationship for rock discontinuities. The results of this study showed that these relationships simulate the behavior quite well. The results of the literature survey, including 32 different types of discontinuities, were tabulated and analyzed and representative values of the parameters were noted. It was found that many of the parameters do not vary over a very wide range.

#### Analysis of Openings in Rock Containing a Single Planar One-Dimensional Discontinuity

Analyses were conducted to evaluate the effect of variations in the normal and shear stiffnesses of a one-dimensional discontinuity on the resulting stresses and displacements around underground openings in rock containing a single prominent discontinuity. The results of these analyses are similar to those obtained when a two-dimensional discontinuity was analyzed. These results showed that, as the discontinuity becomes softer, the stress changes (or load transfer) become more substantial, tension zones increase, normal and shear stresses on the discontinuity decrease and displacements of the opening increase.

These conclusions can be further amplified since the stiffness of the one-dimensional discontinuity is based upon independent normal and shear stiffnesses. These studies showed that the resulting stresses and displacements were affected more



by the normal stiffness than by the shear stiffness, indicating that the stiffness component acting in the same direction as the initial maximum principal stress is the most important in determining the resulting behavior of the opening. These studies further showed that the nonlinearity of the shear stiffness is of minor importance but that the initial stiffness and stress-dependency is significant in determining the stresses and displacements of the opening.

#### Analysis of the Behavior of Edward Hyatt Powerplant

Based upon the four types of finite element analyses conducted for the Edward Hyatt Powerplant (1 step linear, 3 step linear, 3 step nonlinear and 3 step jointed), it can be said that all of the analyses can provide reasonable representations of the observed behavior if the material properties can be adequately defined. The 1 step linear analysis is limited because it cannot follow the excavation sequence. Both of the linear analyses are limited because the selection of material properties hinges to a large degree on the availability of a large body of field data and a broad generalization of these results. The nonlinear analysis appears to yield displacements somewhat lower than those measured but the values for analysis are easily and inexpensively obtained. The jointed analysis appears to yield the best overall method of evaluating the performance of the opening. The rock properties can be determined as easily as for the nonlinear analysis, but field data is required to define the prominent discontinuities and their properties. However, if this data is available, the resulting deformations, stresses and stability of the rock mass may be evaluated with a degree of accuracy.

#### Conclusions

The analyses presented during the course of this investigation have shown that the finite element method, coupled with the analytical techniques for simulating the excavation sequence and the nonlinear, stress-dependent behavior of the rock and the discontinuities, can predict the behavior of underground openings in rock quite well. This approach is well-suited for practical use because the material properties can be evaluated relatively easily and the field excavation sequence can be followed directly.

For preliminary design and evaluation, the generalized results presented may be used very effectively to evaluate the probable range of behavior for a proposed

opening. For final design and evaluation, the techniques presented may be used to:

- (1) predict stresses and displacements around openings in rock,
- (2) assess zones of potential instability,
- (3) aid in the selection of instrument locations, and
- (4) interpret the results obtained from field instrumentation.

#### ACKNOWLEDGMENTS

This work is supported by the U.S. Government through the Advanced Research Projects Agency and its agent the Bureau of Mines. Mr. Richard F. Flanagan and Mr. Robert L. White contributed significantly to the research reported herein. Mr. Avram Ninyo drafted the figures while Ms. Cindy Mudge and Ms. Marne Godfrey typed the text. Dr. William J. Karwoski of the Spokane Mining Research Center, Bureau of Mines, acted as Project Officer for the sponsor. In the early stages of the project, Mr. Peter Chamberlain of the Twin Cities Mining Research Center, Bureau of Mines, acted as Project Officer for the sponsor.

Special thanks is due Mr. George H. Kruse and Mr. Jack W. Marlette of the State of California Department of Water Resources who provided extensive data to the writer which resulted in the detailed studies of the behavior of the Edward Hyatt Powerplant.

## REFERENCES

- Baldovin, G. (1970), "The Shear Strength of Some Rocks by Laboratory Tests" Proceedings, 2nd Congress of the International Society for Rock Mechanics, Vol. 2, Belgrade, 1970, pp. 165-172.
- Balmer, G. G. (1953), "Physical Properties of Some Typical Foundation Rocks", Concrete Laboratory Report No. SP-39, U. S. Bureau of Reclamation, Denver, Colo., August 1953.
- Birch, F. (1966), "Compressibility: Elastic Constants", Memoir 97 - Handbook of Physical Constants (Revised Edition), Geological Society of America, 1966, pp. 97-173.
- Brown, C. B. and King, I. P. (1966), "Automatic Embankment Analysis: Equilibrium and Instability Conditions", Geotechnique, Vol. 16, No. 3, Sept. 1966, pp. 209-219.
- Chang, C.-Y. and Duncan, J. M. (1970), "Analysis of Soil Movement Around A Deep Excavation", Journal of the Soil Mechanics and Foundations Division, ASCE, Vol. 96, No. SM5, Sept. 1970, pp. 1655 - 1681.
- Clough, G. W. (1971), "Personal Communication", Dec.
- Clough, G. W. and Duncan, J. M. (1969), "Finite Element Analyses of Port Allen and Old River Locks", Contract Report S-69-6, U.S. Army Engineer Waterways Experiment Station, Vicksburg, Miss., Sept. 1969.
- Clough, R. W. (1960), "The Finite Element Method in Plane Stress Analysis", Proceedings, 2nd Conference on Electronic Computation, ASCE, Pittsburgh, 1960, pp. 345-377.
- Clough, R. W. (1965), "The Finite Element Method in Structural Mechanics", Chapter 7 in Stress Analysis, ed. by O. C. Zienkiewicz and G. S. Holister, John Wiley and Sons, New York, 1965.
- Cording, E. J. (1967), "The Stability During Construction of Three Large Underground Openings in Rock", Thesis presented to the University of Illinois at Urbana, Ill., in 1967, in partial fulfillment of the requirements for the degree of Doctor of Philosophy.
- Dayre, M., Dessenne, J. L. and Wack, B. (1970), "Local and Mean Changes of the Density of Chalk Samples Tested Under Triaxial Conditions" (In French), Proceedings, 2nd Congress of the International Society for Rock Mechanics, Vol. 1, Belgrade, 1970, pp. 373-381.
- Deklotz, E. J. and Heck, W. J. (1965), "Tests for Strength Characteristics of Rock, Piledriver Project", MRD Laboratory No. 64/474, U.S. Army Corps of Engineers, Missouri River Division, Omaha, Neb., April 1965.
- Deklotz, E. J., Brown, J. W. and Stemler, O. A. (1966), "Anisotropy of a Schistose Gneiss", Proceedings, 1st Congress of the International Society for Rock Mechanics, Vol. 1, Lisbon, 1966, pp. 465-470.



- Deklotz, E. J., Heck, W. J. and Neff, T. L. (1965), "Tests for Strength Characteristics of a Schistose Gneiss: First Interim Report, Preliminary Tests", MRD Laboratory No. 64/126, U.S. Army Corps of Engineers, Missouri River Division, Omaha, Neb., May 1965.
- Deklotz, E. J., Heck, W. J. and Neff, T. L. (1966), "Strength Parameters of Selected Intermediate Quality Rocks: First Interim Report", MRD Laboratory No. 64/493, U.S. Army Corps of Engineers, Missouri River Division, Omaha, Neb., July 1966.
- Department of Water Resources (1967), "Instrumentation Report, Oroville Power Plant (Rock Relaxations)", State of California, Jan. 1, 1967.
- Desai, C. S. and Abel, J. F. (1971), Introduction to the Finite Element Method, A Numerical Method for Engineering Analysis, Van Nostrand Reinhold, New York, 1971.
- Donath, F. A. (1970), "Some Information Squeezed out of Rock", American Scientist, Vol. 58, No. 1, Jan. - Feb. 1970, pp. 54-72.
- Duncan, J. M. and Chang, C.-Y. (1970), "Nonlinear Analysis of Stress and Strain in Soils", Journal of the Soil Mechanics and Foundations Division, ASCE, Vol. 96, No. SM5, Sept. 1970, pp. 1629 - 1653.
- Duncan, J. M. and Goodman, R. E. (1968), "Finite Element Analyses of Slopes in Jointed Rock", Contract Report S-68-3, U.S. Army Engineer Waterways Experiment Station, Vicksburg, Miss., Feb. 1968.
- Felippa, C. A. (1966), "Refined Finite Element Analysis of Linear and Nonlinear Two Dimensional Structures", Dissertation presented to the University of California, Berkeley, in 1966, in partial fulfillment of the requirements for the degree of Doctor of Philosophy.
- Geyer, R. L. and Myung, J. I. (1970), "The 3-D Velocity Log: A Tool for In-Situ Determination of the Elastic Moduli of Rocks", Proceedings, 12th Symposium on Rock Mechanics, Rolla, Mo., 1970, pp. 71-107.
- Gianelli, W. R. (1969), "Oroville Dam and Edward Hyatt Power Plant", Civil Engineering, June 1969, pp. 68-72.
- Gianelli, W. R. and Jansen, R. B. (1972), "California Water Project", Civil Engineering, June 1972, pp. 78-84.
- Golzé, A. R. (1971), "Edward Hyatt (Oroville) Underground Power Plant", Journal of the Power Division, ASCE, Vol. 97, No. P02, Mar. 1971, pp. 419-434.
- Goodman, L. E. and Brown, C. B. (1963), "Dead Load Stresses and the Instability of Slopes", Journal of the Soil Mechanics and Foundations Division, ASCE, Vol. 89, No. SM3, May 1963, pp. 103-134.

- Goodman, R. E. (1968), "Effect of Joints on the Strength of Tunnels", Technical Report No. 5, U.S. Army Corps of Engineers, Omaha District, Omaha, Nebraska, Sept. 1968.
- Goodman, R. E. (1969), "The Deformability of Joints", STP 477 - Determination of the In-Situ Modulus of Deformation of Rock, ASTM, 1969, pp. 174-196.
- Goodman, R. E., Taylor, R. L. and Brekke, T. L. (1968), "A Model for the Mechanics of Jointed Rock", Journal of the Soil Mechanics and Foundations Division, ASCE, Vol. 94, No. SM3, May 1968, pp. 637-659.
- Griggs, D. T. (1936), "Deformation of Rocks Under High Confining Pressure: I. Experiments at Room Temperature", Journal of Geology, Vol. 44, July-August 1936, pp. 541-577.
- Gross, D. J. (1968), "Final Geologic Report on Oroville Power Plant and Intakes", Project Geology Report C-24, Department of Water Resources, State of California, Feb. 1968.
- Handin, J. and Hager, R. V., Jr. (1957), "Experimental Deformation of Sedimentary Rocks Under Confining Pressure: Tests at Room Temperature on Dry Samples", Bulletin, American Association of Petroleum Geologists, Vol. 41, No. 1, Jan. 1957, pp. 1-50.
- Handin, J., Hager, R. V., Jr., Friedman, M., and Feather, J. M. (1963), "Experimental Deformation of Sedimentary Rocks Under Confining Pressure: Pore Pressure Tests", Bulletin, American Association of Petroleum Geologists, Vol. 47, No. 5, May 1963, pp. 717-755.
- Heard, H. C. (1960), "Transition from Brittle Fracture to Ductile Flow in Solenhofen Limestone as a Function of Temperature, Confining Pressure and Interstitial Fluid Pressure", Memoir 79-Rock Deformation, Geological Society of America, 1960, pp. 193-226.
- Heard, H. C. (1967), "Experimental Deformation of Rocks and the Problem of Extrapolation to Nature", NSF Advanced Science Seminar in Rock Mechanics, Boston College, 1967, published by Terrestrial Sciences Laboratory, Air Force Cambridge Research Laboratories, Bedford, Mass., pp. 439-507.
- Heuzé, F. E., Goodman, R. E., and Bornstein, A. (1971), "Numerical Analyses of Deformability Tests in Jointed Rock - 'Joint Perturbation' and 'No Tension' Finite Element Solutions", Rock Mechanics, Vol. 3, No. 1, May 1971, pp. 13-24.
- Hoshino, K. and Koide, H. (1970), "Process of Deformation of the Sedimentary Rocks", Proceedings, 2nd Congress of the International Society for Rock Mechanics, Vol. 1, Belgrade, 1970, pp. 353-359.

- Hoskins, J. R. and Horino, F. G. (1969), "Influence of Spherical Head Size and Specimen Diameters on the Uniaxial Compressive Strength of Rocks", Report of Investigations 7234, U.S. Bureau of Mines, Washington, D.C., Jan. 1969.
- Imrie, A. S. and Jory, L. T. (1968), "Behavior of the Underground Powerhouse Arch at the W.A.C. Bennett Dam During Excavation", Proceedings, 5th Canadian Rock Mechanics Symposium, Toronto, 1968, pp. 19-38.
- Jaeger, J. C. (1969), "Behavior of Closely Jointed Rock", Proceedings, 11th Symposium on Rock Mechanics, Berkeley, Calif., 1969, pp. 57-68.
- Janbu, N. (1963), "Soil Compressibility as Determined by Oedometer and Triaxial Tests", Proceedings, European Conference on Soil Mechanics and Foundation Engineering, Vol. 1, Weisbaden, 1963, pp. 19-25.
- Judd, W. R. (1969), "Statistical Methods to Compile and Correlate Rock Properties", School of Civil Engineering, Purdue University, Lafayette, Ind. Dec. 1969.
- King, M. S. (1968), "Ultrasonic Compressional and Shear Wave Velocities of Confined Rock Samples", Proceedings, 5th Canadian Rock Mechanics Symposium, Toronto, 1968, pp. 127-156.
- Kondner, R. L. (1963), "Hyperbolic Stress-Strain Response: Cohesive Soils", Journal of the Soil Mechanics and Foundations Division, ASCE, Vol. 89, No. SM1, Feb. 1963, pp. 115-143.
- Kondner, R. L. and Horner, J. M. (1965), "Triaxial Compression of a Cohesive Soil with Effective Octahedral Stress Control", Canadian Geotechnical Journal, Vol. 2, No. 1, Feb. 1965, pp. 40-52.
- Kondner, R. L. and Zelasko, J. S. (1963a), "A Hyperbolic Stress-Strain Formulation for Sands", Proceedings, 2nd Pan-American Conference on Soil Mechanics and Foundation Engineering, Vol. 1, Rio de Janeiro, 1963, pp. 289-324.
- Kondner, R. L. and Zelasko, J. S. (1963b), "Void Ratio Effects on the Hyperbolic Stress-Strain Response of a Sand", STP 361 - Laboratory Shear Testing of Soils, ASTM, 1963, pp. 250-257.
- Kruse, G. H. (1963), "Static Stress Determinations at Oroville Underground Powerhouse", Rock Mechanics Report RM-4, Department of Water Resources, State of California, Dec. 1963.
- Kruse, G. H. (1969), "Deformability of Rock Structures, California State Water Project", STP 477 - Determination of the In-Situ Modulus of Deformation of Rock, ASTM, 1969, pp. 58-68.
- Kruse, G. H. (1971), "Power Plant Chamber under Oroville Dam", Symposium on Underground Rock Chambers, ASCE, Phoenix, 1971, pp. 333-379.



- Kulhawy, F. H., Duncan, J. M. and Seed, H.B. (1969), "Finite Element Analysis of Stresses and Movements in Embankments During Construction", Contract Report S-69-8, U.S. Army Engineer Waterways Experiment Station, Vicksburg, Miss., Nov. 1969.
- Leeman, E. R. (1968), "The Determination of the Complete State of Stress in Rock in a Single Borehole -- Laboratory and Underground Measurements", International Journal of Rock Mechanics and Mining Sciences, Vol. 5, No. 1, Jan. 1968, pp. 31-56.
- Mahtab, M. A. (1970), "Three Dimensional Finite Element Analysis of Jointed Rock Slopes", Thesis presented to the University of California at Berkeley, California, in 1970, in partial fulfillment of the requirements for the degree of Doctor of Philosophy.
- McLamore, R.T. (1966), "Strength-Deformation Characteristics of Anisotropic Sedimentary Rocks" Thesis presented to the University of Texas at Austin, Texas, in 1966, in partial fulfillment of the requirements for the degree of Doctor of Philosophy.
- Merrill, R. H., Williamson, J. V., Ropchan, D. M. and Kruse, G. H. (1964), "Stress Determinations by Flatjack and Borehole Deformation Methods", Report of Investigations 6400, U.S. Bureau of Mines, Washington, DC, 1964.
- Miller, R. P. (1965), "Engineering Classification and Index Properties for Intact Rock", Thesis presented to the University of Illinois at Urbana, Ill., in 1965, in partial fulfillment of the requirements for the degree of Doctor of Philosophy.
- Mogi, K. (1964), "Deformation and Fracture of Rocks Under Confining Pressure: Compression Tests on Dry Rock Samples", Bulletin of the Earthquake Research Institute, University of Tokyo, Vol. 24, Part 3, Sept. 1964, pp. 491-514.
- Mogi, K. (1965), "Deformation and Fracture of Rocks Under Confining Pressure: Elasticity and Plasticity of Some Rocks", Bulletin of the Earthquake Research Institute, University of Tokyo, Vol. 43, Part 2, June 1965, pp. 349-379.
- Morgenstern, N. R. and Phukan, A. L. T. (1966), "Nonlinear Deformation of a Sandstone", Proceedings, 1st Congress of the International Society for Rock Mechanics, Vol. 1, Lisbon, 1966, pp. 543-547.
- Morgenstern, N. R. and Phukan, A. L. T. (1969), "Nonlinear Stress-Strain Relations For a Homogeneous Sandstone", International Journal of Rock Mechanics and Mining Sciences, Vol. 6, No. 1, Jan. 1969, pp. 127-142.
- Muir, W. G., and Cochrane, T. S. (1966), "Rock Mechanics Investigations in a Canadian Salt Mine", Proceedings, 1st Congress of the International Society for Rock Mechanics, Vol. 2, Lisbon, 1966, pp. 411-416.

- Nesbitt, J. H. (1960), "Laboratory Tests of Rock Cores From Fremont Canyon Tunnel Area -- Glendo Unit -- Missouri River Basin Project, Wyoming", Laboratory Report No. C-945, U. S. Bureau of Reclamation, Denver, Colorado, May 1960.
- Obert, L. and Duvall, W. I. (1967), Rock Mechanics and the Design of Structures in Rock, John Wiley and Sons, New York, 1967.
- Paterson, M. S. (1958), "Experimental Deformation and Faulting in Wombeyan Marble", Bulletin, Geological Society of America, Vol. 69, Apr. 1958, pp. 465-476.
- Raleigh, C. B. and Paterson, M. S. (1965), "Experimental Deformation of Serpentine and Its Tectonic Implications", Journal of Geophysical Research, Vol. 70, No. 16, Aug. 1965, pp. 3965 - 3985.
- Ruiz, M. D. (1966), "Some Technological Characteristics of 26 Brazilian Rock Types", Proceedings, 1st Congress of the International Society for Rock Mechanics, Vol. 1, Lisbon, 1966, pp. 115-117.
- Salas, J. A. J. (1968), "Mechanical Resistances", Proceedings, International Symposium on Determination of the Properties of Rock Masses in Foundations and Observation of Their Behavior, Madrid, 1968, pp. 115-129.
- Saucier, K. L. (1969), "Properties of Cedar City Tonalite", Miscellaneous Paper C-69-9, U.S. Army Corps of Engineers, Waterways Experiment Station, Vicksburg, Miss., June 1969.
- Schwartz, A. E. (1964), "Failure of Rock in the Triaxial Test", Proceedings, 6th Symposium on Rock Mechanics, Rolla, Mo., 1964, pp. 109-151.
- Sinclair, S. R. and Brooker, E. W. (1967), "The Shear Strength of Edmonton Shale", Proceedings, Conference on Shear Strength Properties of Natural Soils and Rocks, Vol. 1, Oslo, 1967, pp. 295-299.
- Stowe, R. L. (1969), "Strength and Deformation Properties of Granite, Basalt, Limestone and Tuff at Various Loading Rates", Miscellaneous Paper C-69-1, U.S. Army Corps of Engineers, Waterways Experiment Station, Vicksburg, Miss., Jan. 1969.
- Thayer, D. P., Stroppini, E. W. and Kruse, G. H. (1964), "Properties of Rock at Underground Powerhouse, Oroville Dam", Proceedings, 8th Congress on Large Dams, Edinburgh, 1964, R.3, Q.28, pp. 45-72.
- Turner, M. J., Clough, R. W., Martin, H. C. and Topp, L. J. (1956), "Stiffness and Deflection Analysis of Complex Structures", Journal of the Aeronautical Sciences, Vol. 23, No. 9, Sept. 1956, pp. 805-823.

U. S. Bureau of Reclamation (1965), "Morrow Point Dam and Power Plant Foundation Investigation", Colorado River Storage Project, U.S. Bureau of Reclamation, Denver, Colo., Oct. 1965, 190 pp.

Wilson, E. L. (1963), "Finite Element Analysis of Two-Dimensional Structures", Dissertation presented to the University of California, Berkeley, in 1963, in partial fulfillment of the requirements for the degree of Doctor of Engineering.

Zienkiewicz, O. C. and Cheung, Y. K. (1967), The Finite Element Method in Structural and Continuum Mechanics, McGraw-Hill, London, 1967.

## APPENDIX A

### SELECTED UNITS CONVERSION FACTORS

$$\begin{aligned} 1 \text{ kilonewton/square meter (KN/m}^2\text{)} &= 0.01 \text{ bar (b)} \\ &= 0.00001 \text{ kilobar (kb)} \\ &= 0.00986 \text{ atmosphere (atm)} \\ &= 0.0104 \text{ ton/square foot (tsf)} \\ &= 0.0209 \text{ kip/square foot (ksf)} \\ &= 20.9 \text{ pound/square foot (psf)} \\ &= 0.0102 \text{ kilogram/square centimeter (kg/cm}^2\text{)} \\ &= 102.0 \text{ kilogram/square meter (kg/m}^2\text{)} \\ &= 0.1452 \text{ pound/square inch (psi)} \\ &= 0.0001452 \text{ kip/square inch (ksi)} \end{aligned}$$

$$\begin{aligned} 1 \text{ kilonewton/cubic meter (KN/m}^3\text{)} &= 0.00317 \text{ ton/cubic foot (tcf)} \\ &= 0.000102 \text{ kilogram/cubic centimeter (kg/cm}^3\text{)} \\ &= 0.00369 \text{ pound/cubic inch (pci)} \end{aligned}$$

Frequently Used Constants In Units Suitable For Analyses With The Above SI Units

$$\text{Unit Weight of Rock (Typical)} = 1 \text{ psi/ft} = 144 \text{ pcf} = 22.6 \text{ KN/m}^3$$

$$\text{Unit Weight of Water} = 62.4 \text{ pcf} = 9.80 \text{ KN/m}^3$$

$$1 \text{ Atmosphere} = 101.3 \text{ KN/m}^2$$

## APPENDIX B

### COMPUTER PROGRAM USER'S GUIDE

#### Title

Finite Element Analysis for the Excavation of Underground Openings in Nonlinear, Discontinuous Rock

#### Identification

The computer program consists of a main program and nine subroutines (LAYOUT, LSSTIF, BANSOL, LSRESL, EXCAV, LSQUAD, LST8, JTSTIF, JTSTR). The program was coded by Professor F. H. Kulhawy of Syracuse University (1971-72) using the general finite element programming concepts and solution techniques developed by Professor E. L. Wilson of the University of California (1963-date). Specific formulations included are the linear strain element of Felippa (1966), the excavation simulation concepts of Clough and Duncan (1969), the nonlinear one-dimensional element of Goodman et al (1968) and Clough and Duncan (1969), and the nonlinear stress-strain relationships of Duncan and Chang (1970) and Kulhawy et al (1969).

#### Purpose

The purpose of this computer program is to calculate the stresses, strains, and displacements around underground openings in rock by simulating actual field construction sequences. The analysis is performed by finite element methods, assuming plane strain deformation and isotropic rock properties.

#### Options

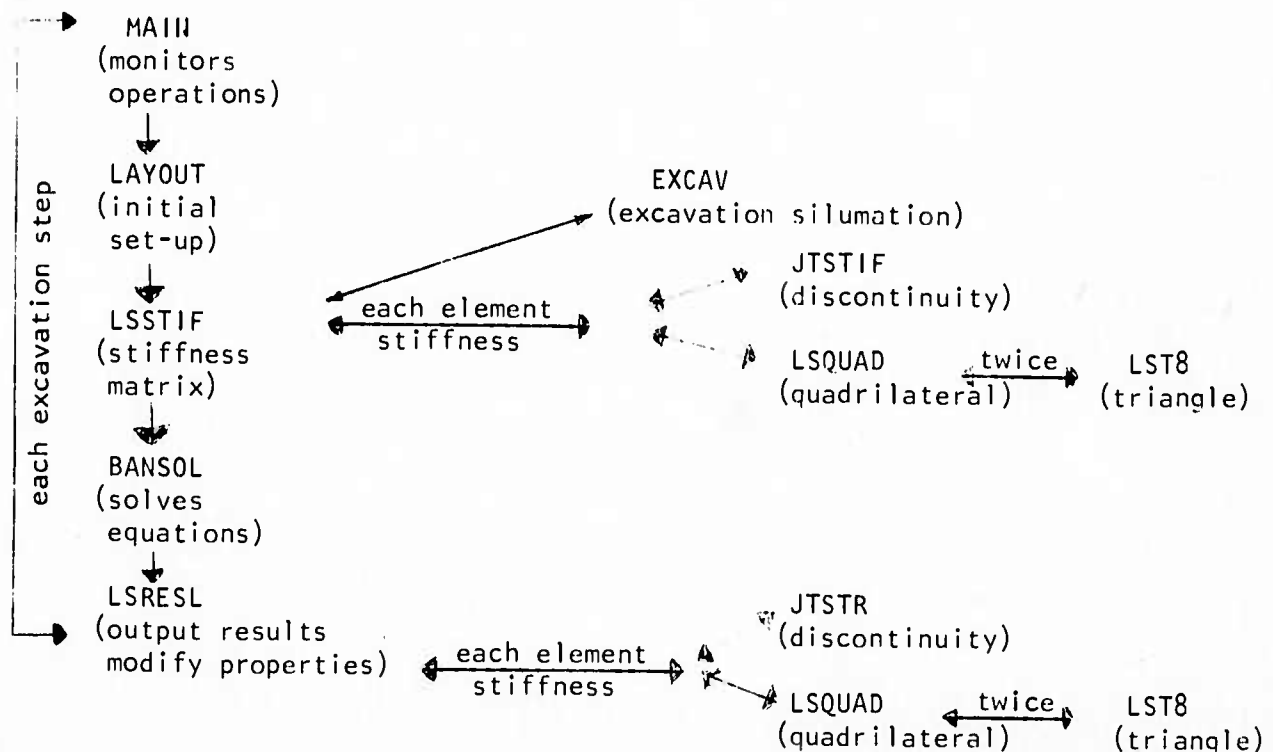
The computer program has the capability to follow nearly any single or multiple excavation sequence in rock which may have initial stresses constant with depth or increasing linearly with depth. The program also has provisions for one-dimensional and two-dimensional elements, the properties for which may be either linear or hyperbolically nonlinear and/or stress-dependent.

#### Sequence of Operations

The main program monitors all operations by calling the following subroutines (which may call further subroutines) to perform the analyses for each excavation step:

- a) LAYOUT reads and prints the input data and computes the initial element stresses and material properties.
- b) LSSTIF develops the stiffness and load matrices of the entire assemblage of elements in the system, applies the excavation boundary forces and modifies the matrices for the specified boundary constraints.

- c) BANSOL solves for the unknown nodal point displacements from the known stiffness and load matrices by a Gaussian elimination technique.
- d) LSRESL computes and prints the displacements, strains and stresses in the system at the end of each excavation step and modifies the rock and discontinuity properties for the next step.
- e) EXCAV is called by LSSTIF and evaluates the equivalent forces along an excavation boundary which are applied to simulate excavation.
- f) LSQUAD is called by LSSTIF and by LSRESL for each two-dimensional quadrilateral element and it sets up the stiffness matrix for each element. In LSSTIF this matrix is used to set up the stiffness matrix for the entire system. In LSRESL this matrix is used to compute the element strains (and subsequently the stresses) from the nodal point displacements.
- g) LST8 is called twice by LSQUAD for each quadrilateral element since LST8 sets up the stiffness matrix for each of the two linear strain triangular elements making up the quadrilateral element.
- h) JTSTIF is called by LSSTIF for each one-dimensional discontinuity element, if any are present, and sets up the stiffness matrix for each element.
- i) JTSTR is called by LSRESL for each one-dimensional discontinuity element, if any are present, and computes the displacements, strains (through the stiffness matrix) and stresses for each element. New stiffnesses are then computed for the next step. Diagrammatically, the operations can be shown as below:





## INPUT DATA PROCEDURE

### 1. CONTROL CARDS (3 cards required)

#### a) Card 1 (18A4)

2-72 HED - Title card for program identification

#### b) Card 2 (215)

1-5 NUMELT - Number of elements in mesh. (275 max)

6-10 NUMNPT - Number of nodal points in mesh. (300 max)

#### c) Card 3 (715)

1-5 NUMBC - Number of nodal points in mesh with constrained deformation -  
x fixity, y fixity, x and y fixity. (100 max)

6-10 NZONES - Number of different material types. (10 max)

11-15 NLAY - Number of excavation steps in problem. (10 max)

16-20 NUMIT - Number of solution cycles per excavation step.  
(e.g., for 1 iteration cycle per step, NUMIT = 2)  
Normally NUMIT = 1 is used

21-25 NONLIN - Code for nonlinear two-dimensional material properties.  
( 0 for all linear, 1 for some or all nonlinear )

26-30 NJOINT - Code for identifying discontinuities.  
(All material types  $\geq$  NJOINT are discontinuities.  
If no discontinuities, NJOINT = NZONES + 1)

31-35 NPUNCH - Code for punching final stresses if desired.  
(0 = no, 1 = yes)

2. ROCK PROPERTY CARDS (2\*NJOINT - 1 cards required)

a) Units Card (F10.0)

1-10 CONS - Atmospheric pressure is consistent units.

b) Stress-Strain Property Cards (14,6F10.4) (NJOINT - 1 cards required)

1-4	N	- Material type number
5-14	GAM	- Unit weight
15-24	COEF	- Modulus constants (K and n)
25-34	EXP	
35-44	DD	- Poisson's ratio constants (d,G,F)
45-54	GG	
55-64	FF	

c) Strength Property Cards (14,4F10.4) (NJOINT - 1 cards required)

1-4	N	- Material type number
5-14	CC	- Cohesion
15-24	PHI	- Angle of friction (degrees)
25-34	RF	- Failure ratio
35-44	CODE	- Code for nonlinear properties (0.0 for linear, 1.0 for nonlinear)

The use of these parameters is discussed in the main text, but the following should serve as a convenient reference base. Above all, be consistent with all units.

If NONLIN = 0 on control card 1c (all rock materials linear elastic), use the following for each rock material type:

COEF = modulus of elasticity (E)  
 GG = Poisson's ratio ( $\nu$ )  
 RF = 1.0  
 EXP = DD = FF = CODE = 0.0

If NONLIN = 1 on control card 1c (one or more rock materials nonlinear), the tangent modulus ( $E_t$ ) and the tangent Poisson's ratio ( $\nu_t$ ) are calculated after each excavation step according to the following:

$$E_t = E_i \left[ 1.0 - \frac{(CODE) (RF) (1.0 - \sin PHI) (\sigma_3 / \sigma_3)}{(2.0) (CC) (\cos PHI) + (2.0) (\sigma_3) (\sin PHI)} \right]^2$$

$$\text{in which } E_i = (COEF) (CONS) \left( \frac{\sigma_3}{CONS} \right)^{EXP}$$

$$\nu_t = \nu_i / (1.0 - (DD) (\epsilon_a))^2$$

$$\text{in which } \nu_i = GG - FF \log (\sigma_3 / CONS)$$

When NONLIN = 1 on control card 1c and it is desired to have different degrees of nonlinearity and/or stress-dependency for E or  $\nu$ , the following can be used:

modulus only nonlinear, set EXP = 0.0 and  $E_i = (COEF) (CONS)$

modulus only stress-dependent, set CODE = 0.0

Poisson's ratio only nonlinear, set FF = 0.0

Poisson's ratio only stress-dependent, set DD = 0.0

If Poisson's ratio becomes greater than 0.49 in the equations, it is automatically reset to a maximum value of 0.49.

### 3. DISCONTINUITY PROPERTY CARDS (NZONES-NJOINT + 2 cards required)

(If there are no discontinuity elements, do not include any cards for this section)

#### a) Units Card (F10.0)

1-10 GAMW - Unit weight of water in consistent units.

#### b) Property Cards (14, F10.2, 2F5.2, 4F10.2, 2F5.2) (NZONES-NJOINT + 1 cards required)

1-4	N	- Material type number
5-14	CJ	- Cohesion
15-19	PHIJ	- Angle of friction (degrees)
20-24	ANGJ	- Angle of discontinuity, counterclockwise from horizontal (degrees)
25-34	EJT1	- Normal stiffness ( $K_n$ )
35-44	EJT2	- Shear stiffness ( $K_s$ ) or Stiffness number ( $K_j$ )
45-54	EJT3	- $K_n$ and $K_s$ after tension failure
55-64	EJT4	- $K_n$ (or $K_j$ ) after shear failure
65-69	EJT5	- Stiffness exponent ( $n_j$ )
70-74	EJT6	- Failure ratio ( $F_{fj}$ )

The use of these parameters is discussed in the main text, but the following should serve as a convenient reference base. Above all, be consistent with all units.

The normal stiffness ( $K_n$ ) is treated as a constant but the tangent shear stiffness ( $K_{st}$ ) is evaluated by the following:

$$K_{st} = K_{si} \left[ 1.0 - \frac{(EJT6) (1)}{CJ + (\sigma_n) \tan PHIJ} \right]^2$$

$$\text{in which } K_{si} = (EJT2) (GAMW) \left( \frac{n}{CONS} \right)^{EJT5}$$

For different degrees of nonlinearity and/or stress-dependency, the following may be used:

stiffness only nonlinear, set  $EJT5 = 0.0$  and  $K_{si} = (EJT2) (GAMW)$

stiffness only stress-dependent, set  $EJT6 = 0.0$

stiffness only linear, set  $EJT5 = EJT6 = 0.0$ ,  $GAMW = 1.0$  and  $EJT2 = K_s$



#### 4. NODAL POINT CARDS

a) Coordinate cards (15, 2F10.2)

(Use as many cards as necessary to define the system)

1-5	MM	- Nodal point number
6-15	ORD (MM,1)	- X coordinate of MM (+ to right)
16-25	ORD (MM,2)	- Y coordinate of MM (+ up)

Use a reference system such that the point furthest to the left has  
ORD (MM,1) = 0.0 and the lowest point has ORD (MM,2) = 0.0.

If nodal points are omitted, the computer program generates the omitted points by incrementing MM in intervals of 1 and by calculating ORD (MM,1) and ORD (MM,2) at equal intervals along a straight line between the two defined nodal points. The first and last nodal points must always be given. (e.g. - MM = 1 and MM = NUMNPT) Nodal points must be read in numerical sequence.

b) Constrained deformation cards (1615)

(Use as many cards as necessary to define NUMBC nodal points)

1-5	NBC	- Number of constrained nodal point
6-10	NFIX	- Code to define the type of fixity at this nodal point (NFIX = 0 for X and Y fixity) (NFIX = 1 for X fixity only) (NFIX = 2 for Y fixity only)

Continue across the card for the constrained modal points at repeating 10 column intervals as above for a maximum of eight alternating values of NBC and NFIX per card. Omitted nodal points are free to move in both the X and Y directions.

5. ELEMENT CARDS (715) (Use as many cards as necessary to define the system)

1-5	N	- Element number
6-10	NPN (N,1)	- Number of nodal point I for this element.
11-15	NPN (N,2)	- Number of nodal point J for this element.
16-20	NPN (N,3)	- Number of nodal point K for this element.
21-25	NPN (N,4)	- Number of nodal point L for this element.
26-30	NPN (N,5)	- Material type for this element.
31-35	NPN (N,6)	- Set equal to zero.

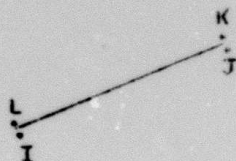
If element cards are omitted, the program generates the omitted elements by incrementing N and NPN (N, 1 through 4) in intervals of 1 while retaining the same values of NPN (N,5) and NPN (N,6). The first and last elements must always be given. (e.g. - N = 1 and N = NUMELT) Elements must be numbered consecutively, proceeding counterclockwise around the quadrilateral elements. Nodal point numbers within any given element must be  $\leq 26$ .

Triangular shaped elements may be used as long as a fourth nodal point is placed along one side of this element. Care must be exercised that the diagonal from nodal point J to nodal point L is not on a straight line including either I or K. Numbering should be done in either of the following ways:



In elements which are not square, reasonable efforts should be made to ensure that the diagonal from nodal point J to nodal point L is the shortest diagonal in the element.

For discontinuity elements, number as below:





6. INITIAL STRESS AND GEOMETRY CARD (8F10.0)

1-10	ELEV	- Surface elevation of top of mesh.
11-20	GRAD	- Initial rate of increase of vertical stress with depth. (0.0 if initial stresses constant with depth) (1.0 if rate of increase = unit weight of material type 1 per unit depth)
21-30	SIGA	- Initial maximum principal stress at top of mesh.
31-40	SIGB	- Initial minimum principal stress at top of mesh.
41-50	AKO	- Initial principal stress ratio. (If SIGA and SIGB > 0, AKO = SIGB/SIGA.) (For shallow openings, when SIGA = SIGB = 0.0, AKO is the desired initial principal stress ratio in the rock mass.)
51-60	ANGSIG	- Principal stress angle from horizontal to SIG3, measured counterclockwise.
61-70	SIGCL*	- Initial maximum principal stress at center of final opening.
71-80	RADIUS	- Radius of opening.

$$*SIGCL = SIGA + \frac{(2.0)(GRAD)(GAM(1)) (ELEV-ELEV \text{ at center})}{(1 + \frac{SIGB}{SIGA}) + (1 - \frac{SIGB}{SIGA}) (\cos (2.0)(ANGSIG))}$$

## 7. EXCAVATION SEQUENCE CARDS (Repeat the following NLAY times)

### a) Excavation step control card (515)

1-5	LN	- Number of excavation step.
6-10	NOMEL	- Number of elements excavated during this step (50 max)
11-15	NCUT	- Number of elements directly along the excavated surface
16-20	NOMNP	- Number of nodal points along the exposed excavation face after the above elements are removed, including those along the excavation surface from previous steps.
21-25	NPS	- Number of nodal points along excavated surface (NOMNP), plus all other nodal points included in the NCUT elements. (50 max)

### b) Element cards (1615)

1-5	NEL	- Number of element excavated.
-----	-----	--------------------------------

Continue across the card for each of the NOMEL elements at 5 column intervals for a maximum of 16 values per card. The NCUT elements (those directly along the excavated surface) must be read in before any of the excavated elements not touching the excavation surface.

### c) Nodal point cards (515) (Number of cards required = NPS)

1-5	NOD (J,1)	- Number of nodal point along excavation surface or in one of the NCUT elements.
6-10	NOD (J,2)	- Number of first interpolation element.
11-15	NOD (J,3)	- Number of second interpolation element.
16-20	NOD (J,4)	- Number of third interpolation element.
21-25	NOD (J,5)	- Number of fourth interpolation element.

All of the nodal points along the excavation surface must be read before any of the remaining nodal points in the NCUT elements.

The interpolation elements should be read in criss-cross fashion as below:

2 & 3 would be "NCUT" elements

A would be an excavated element not along the cut

N1, N2, N3 are nodal points along excavated surface

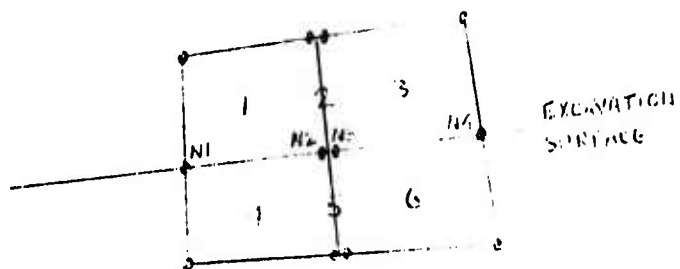
N4, N5, N6 are the other nodal points in the NCUT elements



No three of the interpolation elements can lie on a straight line.

If NOD (J,1) is along a completely excavated surface already, set the values of NOD (J,2) through NOD (J,5) equal to zero.

Do not include discontinuity elements as interpolation elements. Set up as below:



Reproduced from  
best available copy.

for N2, use 1,6,4,3

for N3, use 1,6,4,3

APPENDIX C  
FORTRAM IV COMPUTER PROGRAM LISTING

**Best  
Available  
Copy**

```

C*****
C   FEM EXCAVATION ANALYSIS - F.H. KULHAWY - 1971-1972
C   S.O. IBM 370 VERSION
C*****
COMMON /INIT/ HED(18),NMDEL,NCUT,NCMNP,NPUNCH
COMMON /NDEL/ NPM(275,6),DKD(300,2),YCP(275),YCP(275)
COMMON /EPRC/ EX(300),EY(300),RUMEC,NRC(100),NEIX(100)
COMMON /RANS/ REND,NUMBLK,R(108),A(108,54)
COMMON /CUT1/ NLAY,LN,NMDEL,NCUT,NCMNP,NPS,NMDEL,IT
COMMON /CUT2/ NEL(58),NM(50,5)
COMMON /MAT1/ RULK(275),SHEAR(275),PITS(275),GAP(10),HINLIN
COMMON /MAT2/ CONS,CHEF(10),EXP(10),DD(10),GG(10),FE(10),N7DNE5
COMMON /MAT3/ CC(10),PHI(10),RF(10),DEV1(10),DEV2(10),CODE(10)
COMMON /STRS/ STRESS(275,3),SIGCL,RADIUS
C*****
C   PROCESS INPUT AND INITIALIZE - THEN ANALYZE EACH EXCAVATION STEP
C*****
100 CALL LAYOUT
200 PRINT 2000, HED
   READ 1000, LN,NMDEL,NCUT,NCMNP,NPS
   PRINT 2010, LN,NMDEL,NCUT,NCMNP,NPS
   READ 1000, (NEL(I),I=1,NMDEL)
   PRINT 2020, (NEL(I),I=1,NMDEL)
   PRINT 2030, (NEL(I),I=1,NCUT)
   READ 1010, ((NM(I,J,N),N=1,5),J=1,NPS)
   PRINT 2040, ((NM(I,J,N),N=1,5),J=1,NCMNP)
   NPA=NCMNP+1
   PRINT 2050, ((NM(I,J,N),N=1,5),J=NPA,NPS)
   DO 400 IT=1,NMDEL
   CALL TIME (2,JT1)
C
C   DEVELOP STIFFNESS MATRIX, SOLVE EQUATIONS, EVALUATE RESULTS
C
   CALL LSSTIF
   CALL RANSIL
   CALL LSRESL
   CALL TIME (2,JT2)
   SEC=(JT2-JT1)/100
400 PRINT 2060, LN,IT,SEC
   IF (LN,LT,NLAY) GO TO 200
   GO TO 100
C*****
1000 FORMAT (16I5)
1010 FORMAT (5I5)
2000 FORMAT (1H1 // 18A4 //)
2010 FORMAT (29H0 EXCAVATION STEP NO. = 16 /
1      29H TOTAL NO. ELEMENTS REMOVED = 16 /
2      29H NO. ELEMENTS ALONG CUT = 16 /
3      29H NO. NODAL POINTS ALONG CUT = 16 /
4      29H NO. CUT AND AUXILIARY N.P. = 16 /)
2020 FORMAT (33H0 ELEMENTS REMOVED THRU THIS STEP (16I5) )
2030 FORMAT (25H0 ELEMENTS ALONG THIS CUT / (16I5) )
2040 FORMAT (39H0 N.P. ALONG CUT-INTERPOLATION ELEMENTS/(110,113,3I5))
2050 FORMAT (39H0 AUXILIARY N.P.-INTERPOLATION ELEMENTS/(110,113,3I5))
2060 FORMAT (7H0LAYER=13.5X,11H ITERATION=12.5X,15H TIME(SECONDS)=49.3)
C*****
END

```



# SUBROUTINE LAYOUT

```

C*****
COMMON /INIT/ HED(18),NUMELT,NUMNPT,NJOINT,NPLINCH
COMMON /NPEL/ NPN(275,6),ORD(300,2),XCP(275),YCP(275)
COMMON /NPHC/ FX(300),FY(300),NUMBC,NBC(100),NFIIX(100)
COMMON /RANS/ MRAND,NUMBLK,B(108),A(108,54)
COMMON /CHIT1/ NLAY,LN,NUMEL,NCHIT,NUMBP,NPS,NUMIT,IT
COMMON /MAT1/ BULK(275),SHEAR(275),POIS(275),GAM(10),NONLIN
COMMON /MAT2/ CONS,COFF(10),EXP(10),DD(10),GG(10),FF(10),NZONES
COMMON /MAT3/ CC(10),PHI(10),RF(10),DEV1(10),DEV2(10),CODE(10)
COMMON /MAT4/ CJ(10),PHIJ(10),ANGJ(10),EJT(10,6),NJT,GAMW
COMMON /STRS/ STRESS(275,3),SIGCL,RADIUS
C*****
C READ AND PRINT CONTROL DATA
C*****
READ (1,1000,END=999) HED
READ 1005, NUMELT,NUMNPT
READ 1005, NUMBC,NZONES,NLAY,NUMIT,NONLIN,NJOINT,NPLINCH
PRINT 2000, HED
PRINT 2005, NUMELT,NUMNPT
PRINT 2010, NUMBC,NZONES,NLAY,NUMIT,NONLIN,NJOINT,NPLINCH
C*****
C READ AND PRINT MATERIAL PROPERTY DATA
C*****
NJT=NJOINT-1
READ 1010, CONS
READ 1015, (N,GAM(N),COFF(N),EXP(N),DD(N),GG(N),FF(N),N=1,NJT)
READ 1020, (N,CC(N),PHI(N),RF(N),CODE(N),N=1,NJT)
PRINT 2025, CONS
PRINT 2030
PRINT 1015, (N,GAM(N),COFF(N),EXP(N),DD(N),GG(N),FF(N),N=1,NJT)
PRINT 2035
PRINT 1020, (N,CC(N),PHI(N),RF(N),CODE(N),N=1,NJT)
IF (NJOINT.GT. NZONES) GO TO 100
READ 1010, GAMW
READ 1022, (N,CJ(N),PHIJ(N),ANGJ(N),(EJT(N,I),I=1,6),N=NJOINT,
1 NZONES)
PRINT 2036, GAMW
PRINT 2037, (N,CJ(N),PHIJ(N),ANGJ(N),(EJT(N,I),I=1,6),N=NJOINT,
1 NZONES)
C*****
C READ AND PRINT NODAL POINT ARRAY
C*****
100 LL=0
105 READ 1025, MM,(ORD(M,M),M=1,2)
DELT=MM-LL
DX=(ORD(MM,1)-ORD(LL,1))/DELT
DY=(ORD(MM,2)-ORD(LL,2))/DELT
110 LL=LL+1
IF (MM-LL) 140,130,120
120 ORD(LL,1)=ORD(LL-1,1)+DX
ORD(LL,2)=ORD(LL-1,2)+DY
GO TO 110
130 IF (NUMNPT-MM) 140,150,105
140 PRINT 5000, MM
CALL EXIT
150 PRINT 2040
PRINT 1025, (M,(ORD(M,M),M=1,2),N=1,NUMNPT)
C
READ 1005, (NBC(K),NFIIX(K),K=1,NUMBC)

```

Reproduced from  
best available copy.

```

PRINT 2045
DO 180 K=1,NUMRC
IF (NFIX(K) .EQ. 0) PRINT 2050,NUMC(K)
IF (NFIX(K) .EQ. 1) PRINT 2055,NUMC(K)
IF (NFIX(K) .EQ. 2) PRINT 2060,NUMC(K)
180 CONTINUE
C*****
C READ AND PRINT ELEMENT ARRAY. COMPUTE PT. FOR STRESSES
C*****
NN=0
200 READ 1005, N, (NPN(N,M), M=1,6)
210 NN=NN+1
IF (N .LE. NN) GO TO 230
DO 220 K=1,4
220 NPN(NN,K)=NPN(NN-1,K)+1
NPN(NN,5)=NPN(NN-1,5)
NPN(NN,6)=0
230 IF (N .GT. NN) GO TO 210
IF (NUMELT .GT. NN) GO TO 200
C
PRINT 2065
DO 250 N=1,NUMELT
J=NPN(N,2)
L=NPN(N,4)
XCP(N)=0.5*(ORD(J,1)+ORD(L,1))
YCP(N)=0.5*(ORD(J,2)+ORD(L,2))
250 PRINT 2070, N, (NPN(N,M), M=1,5), XCP(N), YCP(N)
C*****
C DETERMINE BAND WIDTH OF STIFFNESS MATRIX, ABORT IF TOO LARGE
C*****
500 MBRAND=0
DO 510 N=1,NUMELT
II=MAX0(NPN(N,1),NPN(N,2),NPN(N,3),NPN(N,4))
JJ=MIN0(NPN(N,1),NPN(N,2),NPN(N,3),NPN(N,4))
KK=2*(II-JJ+1)
IF (KK .GT. MBRAND) MBRAND=KK
IF (MBRAND .LE. 54) GO TO 510
PRINT 5005, N
GO TO 999
510 CONTINUE
C*****
C INITIALIZE VALUES IN MESH
C*****
READ 1010, ELEV,GRAD,SIGA,SIGR,AKO,ANGSIG,SIGCL,RADIUS
RATE=GRAD*GAFF(1)
PRINT 2085, ELEV,SIGA,SIGR,AKO,ANGSIG,RATE,SIGCL,RADIUS
PRINT 2090
C*****
C 1. CALCULATE INITIAL STRESSES
C*****
DO 530 N=1,NUMT
PHI(N)=PHI(N)/57.29577451
CONST=2.0/(RF(N)*(1.0-SIN(PHI(N))))
DEV1(N)=CONST*CC(N)*COS(PHI(N))
530 DEV2(N)=CONST*SIN(PHI(N))
ANG=ANGSIG/57.29578
ANGC=COS(2.0*ANG)
ANGS=SIN(2.0*ANG)
C
DO 750 N=1,NUMELT

```

```

      DO 550 M=1,3
550 STRESS(N,M)=0.0
      MTYPE=MPN(N,5)
      DSIG=RATF*(ELEV-YCP(N))
      DSIG1=2.0*DSIG/((1.0+AK0)+(1.0-AK0)*ANGC)
      SIG1=SIGA+DSIG1
      SIG3=SIGH+DSIG1*AK0
      CTR=(SIG1+SIG3)/2.0
      RAD=(SIG1-SIG3)/2.0
      STRESS(N,1)=CTR-RAD*ANGC
      STRESS(N,2)=CTR+RAD*ANGC
      STRESS(N,3)=-RAD*ANGS
      IF (MTYPE.LT.NJOINT) GO TO 570
      PRINT 2092, N,XCP(N),YCP(N),(STRESS(N,M),M=1,3),SIG1,SIG3
      GO TO 750
C*****
C      2. CALCULATE INITIAL E AND NU VALUES
C*****
570 IF (MINLIN.EQ.1) GO TO 700
      POIS(N)=GG(MTYPE)
      EMOD=COFF(MTYPE)
      SHEAR(N)=EMOD/(2.0*(1.0+POIS(N)))
      BULK(N)=SHEAR(N)/(1.0-2.0*POIS(N))
      GO TO 740
C
700 DEVSTR=SIG1-SIG3
      DEVEH=DEV1(MTYPE)+DEV2(MTYPE)*SIG3
      EI=COFF(MTYPE)*CONS*((SIG3/CONS)**EXP(MTYPE))
      EPS=DEVSTR/(EI*(1.0-(DEVSTR/DEVEH)))
      POISI=GG(MTYPE)-FE(MTYPE)*ALOG10(SIG3/CONS)
      POIS(N)=POISI/((1.0-ID(MTYPE)*EPS)**2.0)
      IF (POIS(N).GT.0.490) POIS(N)=0.490
      EMOD=EI*((1.0-(COFF(MTYPE)*DEVSTR/DEVEH)**2.0))
      SHEAR(N)=EMOD/(2.0*(1.0+POIS(N)))
      BULK(N)=SHEAR(N)/(1.0-2.0*POIS(N))
740 PRINT 2095, N,XCP(N),YCP(N),EMOD,BULK(N),SHEAR(N),POIS(N),
      1 (STRESS(N,M),M=1,3),SIG1,SIG3
750 CONTINUE
C*****
C      3. CALCULATE INITIAL DISCONTINUITY STRESSES AND STIFFNESSES
C*****
      IF (NJOINT.GT.NZONES) RETURN
      PRINT 3000
      DO 800 M=1,NJ=ELT
      MTYPE=MPN(N,5)
      IF (MTYPE.LT.NJOINT) GO TO 800
      ALF=ANGJ(MTYPE)/57.29578
      ALJ=PHIJ(MTYPE)/57.29578
      SXX=STRESS(N,1)
      SYY=STRESS(N,2)
      SXY=STRESS(N,3)
      STRESS(N,1)=SYY*(COS(ALF)**2)+SXX*(SIN(ALF)**2)+SXY*SIN(2.0*ALF)
      STRESS(N,2)=0.5*(SYY-SXX)*SIN(2.0*ALF)-SXY*COS(2.0*ALF)
      STRESS(N,3)=0.0
      BULK(N)=EJT(MTYPE,1)
      SHEAR1=EJT(MTYPE,2)*GAMW*((STRESS(N,1)/CONS)**EJT(MTYPE,5))
      STRJ=ABS(STRESS(N,2))/(CJ(MTYPE)+STRESS(N,1)*SIN(ALJ)/COS(ALJ))
      SHEAR(N)=SHEAR1*((1.0-EJT(MTYPE,4)*STRJ)**2.0)
      POIS(N)=0.0
      PRINT 3010, N,XCP(N),YCP(N),ANGJ(MTYPE),(STRESS(N,M),M=1,2),

```

```

1          BULK (N), SHEAR (N)
800 CONTINUE
      RETURN
C*****
1000 FORMAT (18A4)
1005 FORMAT (16I5)
1010 FORMAT (8F10.0)
1015 FORMAT (14,F10.4,F10.0,4F10.4)
1020 FORMAT (14.4F10.4)
1022 FORMAT (14,F10.2,2F5.2,4F10.2,2F5.2)
1025 FORMAT (15.2F10.2)
2000 FORMAT (1H) //// 18A4)
2005 FORMAT (21H) TOTAL NO. ELEMENTS = I4 / 21H TOTAL NO. NODES      = I4 /
2010 FORMAT (27H) NO. RESTRAINED NODES      = I4 /
      1      27H NO. DIFFERENT MATERIALS      = I4 /
      2      27H NO. CONSTRUCTION LAYERS      = I4 /
      3      27H NO. ITERATIONS PER LAYER      = I4 //
      4      49H NONLINEAR CODE (0=LINEAR, 1=NONLINEAR)----- I4 /
      5      49H MATERIALS THIS CODE OR OVER ARE DISCONTINUITIES- I4 /
      6      49H CODE FOR PUNCHING FINAL STRESSES (0=NO,1=YES)--- I4 //
2025 FORMAT (23H) MATERIAL PROPERTY DATA // 17H UNITS CONSTANT = F8.4 //
2030 FORMAT (21X,8H MODULUS,13X,14H POISSON RATIO /
      1      39H MATL UNIT WT CONSTANT EXPONENT      D,9X,1HG,9X,1HF //
2035 FORMAT (48H) MATL C      PHI      FAIL.RATIO NONLIN(1=YES) //
2036 FORMAT (19H) DISCONTINUITY DATA // 16H UNIT WT WATER = F8.4 //
      1      5H MATL,6X,2H C,7X,33H PHI JT. ANGLE      INTACT KN      ,
      2      51H INTACT KS TENS.FAIL.KN+KS SHEAR FAIL. KS EXPONENT,
      3      11H FAIL.RATIO //
2037 FORMAT (15,3F10.2,4F15.2,2F10.2)
2040 FORMAT (19H) NODAL POINT ARRAY // 25H NP      X-ORD      Y-ORD //
2045 FORMAT (39H) NODAL POINTS WITH GEOMETRIC RESTRAINTS //
2050 FORMAT (12H NODAL POINT, I4 ,13H CAN NOT MOVE)
2055 FORMAT (12H NODAL POINT, I4 ,33H CAN MOVE ONLY IN THE Y-DIRECTION)
2060 FORMAT (12H NODAL POINT, I4 ,33H CAN MOVE ONLY IN THE X-DIRECTION)
2065 FORMAT (50H) ELEMENT ARRAY + PT. WHERE STRESSES ARE EVALUATED //
      1      50H ELE      I      J      K      L MATL      X-ORD      Y-ORD //
2070 FORMAT (6I5,2F10.3)
2085 FORMAT (33H) SURFACE ELEVATION OF MESH = F10.2 /
      1      33H INIT. SIG-1 STRESS AT SURFACE = F10.2 /
      2      33H INIT. SIG-3 STRESS AT SURFACE = F10.2 /
      3      33H INIT. PRINCIPAL STRESS RATIO = F10.2 /
      4      33H INIT. PRIM. STR. ANGLE (DEG.) = F10.2 /
      5      33H RATE OF STRESS INCR. W. DEPTH = F10.2 /
      6      33H INIT. SIG-1 IN OPENING CENTER = F10.2 /
      7      33H RADIUS OF OPENING      = F10.2 //
2090 FORMAT (28H) INITIAL VALUES IN ELEMENTS //
      1      45H ELE      X-ORD      Y-ORD ELAS MOD BULK MOD,
      2      50H SHEAR MOD POISSON      SIG-X      SIG-Y      TAU-XY,
      3      20H      SIG-1      SIG-3 //
2092 FORMAT (15.2F10.3,7X,26H 1-D DISCONTINUITY ELEMENT,7X,5F10.3)
2095 FORMAT (15.2F10.3,3F10.1,6F10.3)
3000 FORMAT (34H) DISCONTINUITY ELEMENT INITIAL VALUES //
      1      51H ELE      X-ORD      Y-ORD      ANGLE      SIGMA      .
      2      24H TAU      KN      KS //
3010 FORMAT (15.5F10.3,2F10.1)
5000 FORMAT (17H N.O. FORMER , N = I4)
5005 FORMAT (32H RANG WIDTH TOO LARGE AT ELEMENT I4)
C*****
999 STOP
      END

```

# SUBROUTINE LSS11F

```

C*****
COMMON /INIT/ HFD(18),NUMFLT,NUMNPT,NJOINT,NPUNCH
COMMON /NPFL/ NPN(275,6),ORD(300,2),XCP(275),YCP(275)
COMMON /NPRC/ FX(300),FY(300),NUMBC,NBC(100),NFI(100)
COMMON /RANS/ MRAND,NUMBLK,R(108),A(108,54)
COMMON /CUT1/ NLAY,LN,NOMEL,NCHT,NOMNP,NPS,NUMIT,IT
COMMON /CUT2/ NFL(58),NOD(50,5)
COMMON /MAT1/ BULK(275),SHEAR(275),POIS(275),GAM(10),NONLIN
COMMON /MAT4/ CJ(10),PHIJ(10),ANGJ(10),EJT(10,6),NJT,GAMW
COMMON /STRS/ STRESS(275,3),SIGCL,RADIUS
COMMON /LST1/ S(10,10),ST(3,10),C(3,3),P(10),NP(4),VOL,I,J,K
C*****
C REVERSE BOUNDARY STRESSES
C*****
IF (IT .GT. 1) GO TO 200
CALL EXCAV
C*****
C INITIALIZE BLOCK CONSTANTS AND STIFFNESS ARRAY
C*****
200 REWIND 9
NR=27
NI=2*NR
ND2=2*NI
NUMBLK=0
DO 210 N=1,NI2
R(N)=0.0
DO 210 M=1,MRAND
210 A(N,M)=0.0
C*****
C FORM STIFFNESS MATRIX IN BLOCKS
C*****
300 NUMBLK=NUMBLK+1
NH=NR*(NUMBLK+1)
NM=NH-NR
NNL=NM-NR+1
KSHIFT=2*NNL-2
C
DO 440 M=1,NUMFLT
KMIN=MIND(NPN(N,1),NPN(N,2),NPN(N,3),NPN(N,4))
IF (KMIN .LT. NNL .OR. KMIN .GT. NM) GO TO 440
IF (NPN(N,5) .LT. NJOINT) CALL LSQUAD(M)
IF (NPN(N,5) .GE. NJOINT) CALL JTSTIF(M)
C*****
C 1. ADD ELEMENT STIFFNESS TO TOTAL STIFFNESS
C*****
DO 440 I=1,4
DO 440 K=1,2
II=2*NPN(N,I)-2+K-KSHIFT
KK=2*I-2+K
R(II)=R(II)+P(KK)
DO 440 J=1,4
DO 440 L=1,2
JJ=2*NPN(N,J)-2+L-II+1-KSHIFT
LL=2*J-2+L
IF (JJ .LE. 0) GO TO 430
IF (NM .GE. JJ) GO TO 420
PRINT 1000, MRAND,N
CALL EXIT
420 A(II,JJ)=A(II,JJ)+S(KK,LL)

```



```

430 CONTINUE
440 CONTINUE
C*****
C 2. ADD CONC. FORCES IN EACH BLOCK, ELIMINATE RESIDUALS
C*****
      DO 500 N=NNL,NM
      K=2*N-KSHIFT
      FORX=ABS(FX(N))
      FORY=ABS(FY(N))
      IF (FORY .GT. (1000.*FORX)) FX(N)=0.0
      IF (FORX .GT. (1000.*FORY)) FY(N)=0.0
      R(K)=R(K)+FY(N)
500 R(K-1)=R(K-1)+FX(N)
C*****
C 3. MODIFY STIFFNESS EQUATIONS FOR BOUNDARY CONSTRAINTS
C*****
      DO 650 M=1,NUMBC
      IF (NRC(M) .LT.>NNL) GO TO 650
      IF (NRC(M) .GT. NM) GO TO 650
      N=2*NRC(M)-1-KSHIFT
      IF (NFIX(M) .EQ. 0 .OR. NFIX(M) .EQ. 1) GO TO 620
610 IF (NFIX(M) .EQ. 0 .OR. NFIX(M) .EQ. 2) N=N+1
620 DO 640 MM=2,MBAND
      KK=N-MM+1
      IF (KK .LE. 0) GO TO 630
      A(KK,MM)=0.0
630 KK=N+MM-1
      IF (ND2 .LT. KK) GO TO 640
      A(N,MM)=0.0
640 CONTINUE
      A(N,1)=1.0
      R(N)=0.0
      IF (NFIX(M) .EQ. 0 .AND. N .EQ. (2*NRC(M)-1-KSHIFT)) GO TO 610
650 CONTINUE
C*****
C 4. WRITE BLOCK ON TAPE, MOVE UP LOWER BLOCK, CHECK FOR LAST BLOCK
C*****
700 WRITE (9) (R(N), (A(N,M), M=1, MBAND), N=1, ND)
      DO 710 N=1, ND
      K=N+ND
      R(N)=R(K)
      R(K)=0.0
      DO 710 M=1, MBAND
      A(N,M)=A(K,M)
710 A(K,M)=0.0
      IF (NM .LT. NUMBPT) GO TO 300
      RETURN
C*****
1000 FORMAT (13H BAND WIDTH = 14, 20H EXCEEDED AT ELEMENT 14)
C*****
      END

```



```

      SUBROUTINE JTSIF(N)
C*****
      COMMON /MPFL/ NPN(275,6),ORD(300,2),XCP(275),YCP(275)
      COMMON /CUT1/ NLAY,LN,NMEL,NCUT,NOMNP,NPS,NIMJT,IT
      COMMON /CUT2/ NEL(58),MOD(50,5)
      COMMON /MAT1/ BULK(275),SHEAR(275),POIS(275),GAM(10),NONLIN
      COMMON /LST1/ S(10,10),ST(3,10),C(3,3),P(10),NP(4),VOL,1,J,K
      DIMENSION AA(4,4),TR(2,2)
      DATA AA/2..1..-1..-2..1..2..-2..-1..-1..-2..2..1..-2..-1..1..2./
C*****
C      INITIALIZE GEOMETRY AND PROPERTIES
C*****
      I=NPN(N,1)
      J=NPN(N,2)
      DX=ORD(J,1)-ORD(I,1)
      DY=ORD(J,2)-ORD(I,2)
      DL=SQRT(DX*DX+DY*DY)
C*****
C      SET UP STIFFNESS IN LOCAL COORDINATE SYSTEM
C*****
      DO 100 II=1,8
        P(II)=0.0
      DO 100 JJ=1,8
        S(II,JJ)=0.0
100
      IF (NPN(N,6) .NE. 0) GO TO 150
      DO 120 MN=1,NMEL
        IF (M .EQ. NEL(MN)) GO TO 130
120 CONTINUE
      GO TO 150
130 NPN(N,6)=LN
      SHEAR(N)=0.000001
      BULK(N)=0.000001
150 CKS=SHEAR(N)*DL/6.0
      CKB=BULK(N)*DL/6.0
C
      DO 200 II=1,4
        IS=2*II-1
        IN=2*II
      DO 200 JJ=1,4
        JS=2*JJ-1
        JN=2*JJ
        S(IS,JS)=CKS*AA(II,JS)
200 S(IN,JN)=CKB*AA(II,JJ)
      IF (DY .EQ. 0.0) RETURN
C*****
C      ROTATE STIFFNESS TO GLOBAL COORDINATE SYSTEM
C*****
      TR(1,1)=DX/DL
      TR(1,2)=DY/DL
      TR(2,1)=-DY/DL
      TR(2,2)=DX/DL
      DO 450 MN=1,4
      DO 410 II=1,8
        JJ=2*MN-1
        TEMP=S(II,JJ)
      DO 410 KK=1,2
        S(II,JJ)=TEMP*TR(1,KK)+S(II,2*MN)*TR(2,KK)
410 JJ=JJ+1
      DO 420 II=1,8

```

JJ=2\*NM-1

TEMP=S(JJ,11)

DO 420 KK=1,2

S(JJ,11)=TEMP\*TR(1,KK)+S(2\*NM,11)\*TR(2,KK)

420 JJ=JJ+1

450 CONTINUE

RETURN

C\*\*\*\*\*  
END

# SUBROUTINE EXCAV

```

C*****
COMMON /INIT/ NFEL(18),NUMEEL,NUMNPT,M,INT,NUMCH
COMMON /NPFL/ NPN(275,6),ORD(300,2),XCP(275),YCP(275)
COMMON /NPRC/ FX(300),FY(300),NUMRC,MRC(100),NFI(100)
COMMON /CUT1/ NLAY,LM,NOMEL,NCUT,NOMMP,NPS,NUMIT,IT
COMMON /CUT2/ FEL(58),NTH(50,5)
COMMON /STRS/ STRESS(275,3),SIGCL,RADIUS
DIMENSION NI(4),CF(4,4),AB(3,4),SM(3,50),XY(2,4),F(2,4),Z(3,4)
C*****
C      INITIALIZE, SELECT N.P. + CORRESPONDING INTERPOLATION ELEMENTS
C*****
      DO 100 NP=1,NUMNPT
        FX(NP)=0.0
      100 FY(NP)=0.0
C
      DO 350 JMP=1,NPS
        MP=NTH(JMP,1)
        NI(1)=NTH(JMP,2)
        IF (NI(1).EQ.0) GO TO 350
        NI(2)=NTH(JMP,3)
        NI(3)=NTH(JMP,4)
        NI(4)=NTH(JMP,5)
C*****
C      SET ELEMENT COORD. MATRIX, THEN INVERT
C*****
      DO 200 NM=1,4
        MM=NI(NM)
        CF(NM,1)=1.0
        CF(NM,2)=XCP(MP)
        CF(NM,3)=YCP(MP)
      200 CF(NM,4)=XCP(MP)*YCP(MP)
C
      DO 280 N=1,4
        D=CF(N,N)
        IF (D.EQ.0.0) PRINT 4000, NP
      220 DO 240 J=1,4
        CE(N,J)=-CF(N,J)/D
      260 DO 240 I=1,4
        IF (N.EQ.I) GO TO 260
      240 DO 240 J=1,4
        IF (N.EQ.J) GO TO 240
        CE(I,J)=CE(I,J)+CF(I,N)*CF(N,J)
      240 CONTINUE
      260 CE(I,N)=CE(I,N)/D
      280 CE(N,N)=1.0/D
C*****
C      COMPUTE INTERP COEF MATRIX, THEN MODAL STRESS MATRIX FOR NP
C*****
      DO 300 KK=1,3
        DO 300 J,I=1,4
          AB(KK,J,I)=0.0
        DO 300 II=1,4
          NM=NI(II)
      300 AB(KK,J,I)=AB(KK,J,I)+CF(J,I,II)*STRESS(NM,KK)
C
      DO 320 J,I=1,3
        XX=ORD(NP,1)
        YY=ORD(NP,2)
      320 SM(J,I,JMP)=AB(J,I,1)+AB(J,I,2)*XX+AB(J,I,3)*YY+AB(J,I,4)*XX*YY

```

350 CONTINUE

C\*\*\*\*\*  
C SET GEOM OF EXC ELE, THEN COMPUTE EQUIV NP FORCES

C\*\*\*\*\*

PRINT 1005

DO 450 JFL=1,NCJT

NN=NFL(JFL)

C

DO 410 N=1,4

I=NPN(MN,N)

NN=N+I

IF (MM.EQ.5) MM=1

J=NPN(MN,MM)

XY(1,N)=ORD(J,1)-ORD(I,1)

XY(2,N)=ORD(I,2)-ORD(J,2)

DO 400 JNP=1,NPS

NP=NOD(JNP,1)

IF (NP.EQ.1) GO TO 405

400 CONTINUE

PRINT 5000

CALL EXIT

405 DO 410 JJ=1,3

410 Z(JJ,N)=SM(JJ,JNP)

C

DO 420 J=1,2

L=4

DO 420 I=1,4

K=I+1

IF (I.EQ.4) K=1

F(J,I)=( XY(3-J,L)\*Z(J,L) + 2.0\*Z(J,I)\*(XY(3-J,L)+XY(3-J,I))  
1 + XY(3-J,I)\*Z(J,K) )/6.0 + ( XY(J,L)\*Z(3,L)  
2 + 2.0\*Z(3,I)\*(XY(J,L)+XY(J,I)) + XY(J,I)\*Z(3,K) )/6.0  
L=I

420 CONTINUE

C

DO 430 I=1,4

IM=NPN(MN,I)

DO 430 N=1,NIMP

NP=NOD(N,1)

IF (IM.NE.NP) GO TO 430

FX(IM)=FX(IM)+F(1,I)

FY(IM)=FY(IM)+F(2,I)

PRINT 1010, MN,IM,(Z(JJ,I),JJ=1,3),F(1,I),F(2,I)

430 CONTINUE

450 CONTINUE

C\*\*\*\*\*  
C ERASE FORCES PLACED AT BOUNDARY POINTS

C\*\*\*\*\*

DO 500 NPP=1,NIMBC

DO 500 N=1,NIMP

NP=NOD(N,1)

IF (NP.NE.NBC(NPP)) GO TO 500

IF (NFI(NPP).EQ.0) FX(NP)=0.0

IF (NFI(NPP).EQ.0) FY(NP)=0.0

IF (NFI(NPP).EQ.1) FX(NP)=0.0

IF (NFI(NPP).EQ.2) FY(NP)=0.0

500 CONTINUE

RETURN

C\*\*\*\*\*

1005 FORMAT (54H1INTERPOLATED N.P. STRESSES AND RESULTANT FORCES ALONG,

1 16H EXCAVATION FACE // 28H ELF HP SIG-X  
2 42H SIG-Y TAU-XY X-FORCE Y-FORCE /)  
1010 FORMAT (2I5,5F12.4)  
4000 FORMAT (49H07ER0 DETERMINANT IN EXCAV - CHECK DATA FOR N.P. 14)  
5000 FORMAT (48H ABORT IN EXCAV - PROBABLY EXCAVATION INPUT DATA )  
C\*\*\*\*\*  
END

# SUBROUTINE LSQUAD(N)

```

C*****
COMMON /INIT/ HED(18),NUMELT,NUMMPT,NJOINT,NPINCH
COMMON /NPFL/ NPN(275,6),ORD(300,2),XCP(275),YCP(275)
COMMON /CUT1/ NLAY,LN,MMEL,NCUT,NOMNP,NPS,NUMIT,IT
COMMON /CUT2/ MEL(58),MID(50,5)
COMMON /MAT1/ BULK(275),SHEAR(275),POIS(275),GAM(101,NONLIN)
COMMON /LST1/ S(10,10),ST(3,10),C(3,3),P(10),NP(4),VOL,1,J,K
COMMON /STRS/ STRESS(275,3),SIGCL,RADIUS
C*****
C    INITIALIZE AND FORM STRESS-STRAIN MATRIX
C*****
      DO 100 II=1,10
        P(II)=0.0
      DO 100 JJ=1,10
100    S(II,JJ)=0.0
        VOL=0.0

C
      IF (NPN(N,6) .NE. 0) GO TO 150
      DO 120 NN=1,MMEL
        IF (N .EQ. MEL(NN)) GO TO 130
120    CONTINUE
      GO TO 150
130    NPN(N,6)=LN
        BULK(N)=BULK(N)*0.000001
        SHEAR(N)=SHEAR(N)*0.000001

C
150    DO 160 IC=1,3
      DO 160 JC=1,3
160    C(IC,JC)=0.0
        C(1,1)=BULK(N)+SHEAR(N)
        C(1,2)=BULK(N)-SHEAR(N)
        C(2,1)=C(1,2)
        C(2,2)=C(1,1)
        C(3,3)=SHEAR(N)

C*****
C    FORM 10*10 QUAD. STIFFNESS, REDUCE TO 8*8, CALCULATE GRAVITY LOADS
C*****
      I=NPN(N,1)
      J=NPN(N,2)
      K=NPN(N,4)
      CALL LSTR(1,3,7)
      I=NPN(N,3)
      J=NPN(N,4)
      K=NPN(N,2)
      CALL LSTR(5,7,3)
      IF (VOL .GT. 0.0) GO TO 200
      PRINT 1000, N
      CALL EXIT
200    DO 300 K=1,2
      IH=10-K
      ID=IH+1
      DO 300 I=1,IH
        S(ID,I)=S(ID,I)/S(ID,ID)
      DO 300 J=1,IH
300    S(J,I)=S(J,I)-S(J,ID)*S(ID,I)
      RETURN
C*****
1000  FORMAT (34H ZERO OR NEGATIVE AREA AT ELEMENT 14)
C*****
      END

```



```
C*****
C *****
      CUMMIL /MPFL/ MPN(275,6),ORD(300,2),XCP(275),YCP(275)
      CUMMIL /LST1/ S(10,10),ST(3,10),C(3,3),P(10),NP(4),VOL,I,J,K
      DIMENSION RA(3,2),U(3,4),V(3,4),UV(3,4,2)
      EQUIVALENCE (UV(1,1)),(UV(13),V)
C *****
C   • DEFINE TRIANGULAR ELEMENT NODAL POINTS, GEOMETRY, AND AREA
C *****
      NP(1)=1
      NP(2)=2
      NP(3)=3
      NP(4)=4
      RA(1,1)=(ORD(J,2)-ORD(K,2))
      RA(2,1)=(ORD(K,2)-ORD(I,2))
      RA(3,1)=(ORD(I,2)-ORD(J,2))
      RA(1,2)=(ORD(K,1)-ORD(J,1))
      RA(2,2)=(ORD(I,1)-ORD(K,1))
      RA(3,2)=(ORD(J,1)-ORD(I,1))
      ARFA=((ORD(J,1)*RA(2,1)+ORD(I,1)*RA(1,1)+ORD(K,1)*RA(3,1))/2.0
      IF (ARFA .LE. 0.0) GO TO 400
      VOL=VOL+ARFA
C *****
C   SET UP TERMS FOR STRESS-STRAIN AND STRAIN-DISPLACEMENT MATRICES
C *****
      ARFA48=48.0*ARFA
      C11=C(1,1)/ARFA48
      C12=C(1,2)/ARFA48
      C13=C(1,3)/ARFA48
      C22=C(2,2)/ARFA48
      C23=C(2,3)/ARFA48
      C33=C(3,3)/ARFA48

      DO 200 M=1,2
        UV(1,1,M)= RA(1,M)
        UV(2,1,M)= RA(1,M)
        UV(3,1,M)= RA(1,M)
        UV(1,2,M)= RA(2,M)
        UV(2,2,M)= RA(2,M)-2.0*RA(3,M)
        UV(3,2,M)= -RA(2,M)
        UV(1,3,M)= RA(3,M)
        UV(2,3,M)= -RA(3,M)
        UV(3,3,M)= RA(3,M)-2.0*RA(2,M)
        UV(1,4,M)= 0.0
        UV(2,4,M)= RA(3,M)*4.0
200    UV(3,4,M)= RA(2,M)*4.0
C *****
C   DEVELOP CENTER N.P. STRAIN-DISP. MATRIX AND TRIANGLE STIFFNESS
C *****
      ARFAR=8.0*ARFA
      DO 300 I=1,4
        II=NP(I)
        S1(1,II)=ST(1,II)+(U(2,I)+U(3,I))/ARFAR
        S1(2,II+1)=ST(2,II+1)+(V(2,I)+V(3,I))/ARFAR
        S1(3,II)=ST(3,II)+(V(2,I)+V(3,I))/ARFAR
        S1(3,II+1)=ST(3,II+1)+(U(2,I)+U(3,I))/ARFAR

        SUMU=U(1,I)+U(2,I)+U(3,I)
        SUMV=SUMU+U(1,I)
```

```

SUM2=SUM1+U(2,I)
SUM3=SUM1+U(3,I)
SUMV=V(1,I)+V(2,I)+V(3,I)
SVM1=SUMV+V(1,I)
SVM2=SUMV+V(2,I)
SVM3=SUMV+V(3,I)

```

C

```

DO 300 J=1,4
JJ=NP(J)
UQU=U(1,J)*SUM1 + U(2,J)*SUM2 + U(3,J)*SUM3
VQU=V(1,J)*SUM1 + V(2,J)*SUM2 + V(3,J)*SUM3
VOV=V(1,J)*SVM1 + V(2,J)*SVM2 + V(3,J)*SVM3
UQV=U(1,J)*SVM1 + U(2,J)*SVM2 + U(3,J)*SVM3

```

C

```

S(II ,JJ )=S(II ,JJ ) + C11*UQU + C13*(VQU+UQV) + C33*VOV
S(II+1,JJ+1)=S(II+1,JJ+1) + C22*VOV + C23*(VQU+UQV) + C33*UQU
S(II ,JJ+1)=S(II ,JJ+1) + C21*VOV + C13*UQU + C12*VQU + C33*UQV
300 S(JJ+1,II )=S(II ,JJ+1)
400 RETURN

```

```

C*****
END

```

# SUBROUTINE RANSOL

```

C*****
C      COMMON /RANS/  MRAND,NUMBLK,9(108),A(108,54)
C*****
C      INITIALIZE
C*****
      F01=54
      N1=NR+1
      NL=F01+NR
      REV(100)=
      REV(100)=9
      NR=0
      GO TO 120
C*****
C      1. SHIFT BLOCK OF EQUATIONS AND READ NEXT BLOCK INTO CODE
C*****
      DO 100 NR=NR+1
        DO 110 M=1,MRAND
          NM=NR+M
          R(N)=R(NM)
          R(NM)=0.0
          DO 110 M=1,MRAND
            A(N,M)=A(NM,M)
          110 A(NM,M)=0.0
C
      IF (NUMBLK.EQ.NR) GO TO 200
      120 READ (9) (R(N),(A(N,M),M=1,MRAND),N=NL,NH)
      IF (NR.EQ.0) GO TO 100
C*****
C      2. REDUCE BLOCK OF EQUATIONS, THEN WRITE THEM ON TAPE 1
C*****
      200 DO 220 N=1,NH
        IF (A(N,1).EQ.0.0) GO TO 230
        R(N)=R(N)/A(N,1)
        DO 220 L=2,MRAND
          IF (A(N,L).EQ.0.0) GO TO 220
          C=A(N,L)/A(N,1)
          I=N+L-1
          J=0
          DO 210 K=L,MRAND
            J=J+1
            210 A(I,J)=A(I,J)-C*A(N,K)
            R(I)=R(I)-A(I,L)*R(L)
            A(I,L)=C
        220 CONTINUE
        230 CONTINUE
C
      IF (NUMBLK.EQ.NR) GO TO 300
      WRITE (8) (R(N),(A(N,M),M=2,MRAND),N=1,NH)
      GO TO 100
C*****
C      BACK-SUBSTITUTION
C*****
      300 DO 320 N=1,NH
        N=NH+1-N
        DO 310 K=2,MRAND
          L=N+K-1
          310 R(N)=R(N)-A(N,K)*R(L)
        NM=N+NR
        R(NM)=R(N)

```



```

320 A(NM,NR)=R(N)
NR=NR-1
IF (NR.EQ. 0) GO TO 400
BACKSPACE R
READ (R) (R(N), (A(N,M), M=2, NR AND), N=1, NM)
BACKSPACE R
GO TO 300
C*****
C ORDER JUNKIES IN R ARRAY
C*****
400 K=0
DO 410 IK=1,NUMBERK
DO 410 I=1,NM
NM=N+NM
K=K+1
410 R(K)=A(NM,NR)
RETURN
C*****
END

```

# SUBROUTINE LSRESL

```

C*****
COMMON /INIT/ HED(18),NUMELT,NUMNPT,NJOINT,NPUNCH
COMMON /MPFL/ MPN(275,6),ORD(300,2),XCP(275),YCP(275)
COMMON /MPRC/ FX(300),FY(300),NUMRC,NRC(100),NPIX(100)
COMMON /RANS/ MBAND,MINRBLK,R(108),A(108,54)
COMMON /CUT1/ NLAY,LN,NUMEL,NCUT,MOAMP,NPS,NUMIT,IT
COMMON /CUT2/ MFL(58),MID(50,5)
COMMON /MAT1/ BULK(275),SHEAR(275),PHIS(275),GAM(10),MINLIN
COMMON /MAT2/ CONS,COFF(10),EXP(10),DD(10),GG(10),FF(10),N7DNFS
COMMON /MAT3/ CC(10),PHI(10),RF(10),DEV1(10),DEV2(10),CODE(10)
COMMON /MAT4/ CJ(10),PHIJ(10),ANGJ(10),EJT(10,6),NJIT,GAMW
COMMON /LST1/ S(10,10),ST(3,10),C(3,3),P(10),NP(4),VOL,I,J,K
COMMON /STRS/ STRESS(275,3),SIGCL,RADIUS
DIMENSION
    SIG(3),EPS(3),O(5),OO(4)
DIMENSION
    SIGIT(275,3),EPSIT(275,3),DISPIT(300,2)
DIMENSION
    STRAIN(275,3),DISP(300,2)
EQUIVALENCE
    (STRAIN,A(1000)),(DISP,A(2000))
EQUIVALENCE
    (SIGIT,A(3000)),(EPSIT,A(4000)),(DISPIT,A(5000))
C*****
C    INITIALIZE
C*****
    IF (LN .GT. 1 .OR. IT .GT. 1) GO TO 120
    DO 100 N=1,NUMNPT
    DO 100 M=1,2
100 DISP(N,M)=0.0
    DO 110 N=1,NUMELT
    DO 110 M=1,3
110 STRAIN(N,M)=0.0
120 IF (LN .EQ. 1) GO TO 140
    REWIND 4
    READ (4) ((STRAIN(N,M),M=1,3),N=1,NUMELT)
    READ (4) ((DISP(N,M),M=1,2),N=1,NUMNPT)
140 IF (IT .GT. 1) GO TO 300
    DO 150 N=1,NUMELT
    DO 150 M=1,3
    SIGIT(N,M)=0.0
    EPSIT(N,M)=0.0
    SIGIT(N,M)=STRESS(N,M)
150 EPSIT(N,M)=STRAIN(N,M)
    DO 200 N=1,NUMNPT
    DO 200 M=1,2
    DISPIT(N,M)=0.0
200 DISPIT(N,M)=DISP(N,M)
C*****
C    CALCULATE THE DISPLACEMENTS
C*****
    IF (MINLIN .EQ. 0) CONST=COFF(1)/(SIGCL*RADIUS)
    IF (NONLIN .EQ. 1) CONST=(COFF(1)*CONS)/(SIGCL*RADIUS)
300 DO 340 N=1,NUMNPT
    IF (IT .LT. NUMIT) GO TO 310
    XN=N
    XXN=XN/50
    IF (XXN .EQ. (XN/50.0) .OR. N .EQ. 1) PRINT 1000
310 DX=B(2*N-1)
    DY=B(2*N)
    DISP(N,1)=DISP(N,1)+DX
    DISP(N,2)=DISP(N,2)+DY
    IF (IT .EQ. NUMIT) DISP(N,1)=DISPIT(N,1)+DX

```

```

      IF (II .EQ. NUNIT) DISP(N,2)=DISP(1,N,2)+DY
      TD=SQRT(DISP(N,1)**2+DISP(N,2)**2)
      IF (II .LT. NUNIT) GO TO 340
      DIMX=DISP(N,1)*CONST
      DIMY=DISP(N,2)*CONST
      PRINT 1005, N, (DISP(N,M), M=1,2), DIMX, DIMY, DX, DY, TD, FX(N), FY(N), M
340 CONTINUE
C*****
C      CALCULATE THE STRESSES AND STRAINS, PRINT STRAINS
C*****
      DO 450 N=1, NUNIT
      IF (II .LT. NUNIT) GO TO 390
      YN=N
      YYN=N/50
      IF (YYN .EQ. (YN/50.0) .OR. N .EQ. 1) PRINT 1010
390 MTYPE=IPN(N,5)
      EMOD=2.0*BULK(M)*(1.0+POIS(N))*(1.0-2.0*POIS(N))
395 DO 400 I=1,3
      SIG(I)=0.0
      EPS(I)=0.0
      DO 400 J=1,10
400 ST(I,J)=0.0
      IF (MTYPE .GE. NJOINT) GO TO 449
      IF (NPN(N,6) .NE. 0) GO TO 446
C
      CALL LSQUAD(N)
C
      DO 410 I=1,4
      II=2*I
      JJ=2*NPN(N,I)
      P(II-1)=R(JJ-1)
410 P(II)=R(JJ)
      DO 420 I=9,10
      P(I)=0.0
      KK=I-1
      DO 420 K=1, KK
420 P(I)=P(I)-S(I,K)*P(K)
C
      DO 430 I=1,3
      DO 430 K=1,10
430 EPS(I)=EPS(I)+ST(I,K)*P(K)
      DO 440 I=1,3
      DO 440 K=1,3
440 SIG(I)=SIG(I)+C(I,K)*EPS(K)
      DO 445 I=1,3
      IF (II .LT. NUNIT) STRESS(N,I)=STRESS(N,I)-SIG(I)*0.5
      IF (II .EQ. NUNIT) STRESS(N,I)=SIG(I)
      IF (II .LT. NUNIT) STRAIN(N,I)=STRAIN(N,I)-EPS(I)*100.0
      IF (II .EQ. NUNIT) STRAIN(N,I)=EPS(I)*100.0
445 CONTINUE
      GO TO 448
446 DO 447 I=1,3
      STRESS(N,I)=0.0
447 STRAIN(N,I)=0.0
C
448 F=(STRAIN(N,2)+STRAIN(N,1))/2.0
      F=(STRAIN(N,2)-STRAIN(N,1))/2.0
      G=SQRT((STRAIN(N,3)/2.0)**2+F**2)
      DO(1)=F+G
      DO(2)=F-G

```



```

      O(3)=2.0*G
      IF (IT.LT. NIMIT) GO TO 450
      PRINT 1015, N, EMO, BULK(N), SHEAR(N), POIS(N), (STRAIN(N,M), M=1,3),
1      (O(L), L=1,3), N
      GO TO 450
449 PRINT 1017, N
450 CONTINUE
C*****
C      CALCULATE PRINCIPAL STRESSES AND PRINT, CALCULATE MEAN AND DEV
C*****
      DO 470 M=1, NTYPE
      MTYPE=MPH(M,5)
      IF (IT.LT. NIMIT) GO TO 455
      ZN=N
      ZZ=N/50
      IF (ZZN.EQ. (ZN/50.0).OR. M.EQ. 1) PRINT 1025
455 IF (MTYPE.GE. NIMIT) GO TO 449
      CT=(STRESS(N,2)+STRESS(N,1))/2.0
      D=(STRESS(N,2)-STRESS(N,1))/2.0
      O(3)=SQRT(STRESS(N,3)**2 + D**2)
      O(1)=CT+O(3)
      O(2)=CT-O(3)
      O(4)=0.0
      IF (STRESS(N,3).EQ. 0.0.AND. D.EQ. 0.0) GO TO 456
      O(4)=90.0/3.14159265*ATAN2(-STRESS(N,3),D)
456 DEVSTR=O(1)-O(2)
      DEVFH=DEV1(MTYPE)+DEV2(MTYPE)*O(2)
      IF (DEVFH.GT. 0.0) GO TO 457
      STRLEV=0.0
      DEVLEV=0.0
      GO TO 458
457 DEVLEV=DEVSTR/DEVFH
      STRLEV=DEVLEV/RH(MTYPE)
C
458 IF (IT.LT. NIMIT) GO TO 460
      IF (O(2).EQ. 0.0) O(5)=999.999
      IF (O(2).NE. 0.0) O(5)=O(1)/O(2)
      G1=O(1)/SIGCL
      G2=O(2)/SIGCL
      G3=O(3)/SIGCL
      PRINT 1030, N, (STRESS(N,M), M=1,3), (O(L), L=1,5), STRLEV, G1, G2, G3, N
C
460 IF (MOBLIM.EQ. 0) GO TO 470
      IF (O(5).EQ. 999.999) GO TO 470
461 IF (STRLEV.LT. 1.0.AND. SHEAR(N).GT. 0.0) GO TO 465
462 SHEAR(N)=0.0
      GO TO 470
465 IF (O(2).GE. CIMS) GO TO 467
      FINIT=CIMS*COEF(MTYPE)
      POISI=GG(MTYPE)
      GO TO 468
467 FINIT=CIMS*COEF(MTYPE)*((O(2)/CIMS)**EXP(MTYPE))
      POISI=GG(MTYPE)-FF(MTYPE)*ALOG(O(2)/CIMS)
468 EMO=EINIT*((1.0-DEVLEV*COEF(MTYPE))**2.0)
      EPSAX=DEVSTR/(FINIT*(1.0-DEVLEV))
      POIS(N)=POISI/((1.0-EMO(MTYPE)*EPSAX)**2.0)
      IF (POIS(N).GT. 0.490) POIS(N)=0.490
      SHEAR(N)=EMO/(2.0*(1.0+POIS(N)))
      BULK(N)=SHEAR(N)/(1.0-2.0*POIS(N))
      GO TO 470

```

```

469 PRINT 1017, N
470 CONTINUE
C
      IF (NJOINT .LE. N7JMES) CALL JTSTR
C
600 REWIND 4
      WRITE (4) ((STRAIN(N,M),M=1,3),N=1,NUMELT)
      WRITE (4) ((DISP (N,M),M=1,2),N=1,NUMNPT)
      IF (LN .NE. NLAY .OR. IT .NE. NUNIT .OR. NPUNCH .NE. 1) RETURN
      PUNCH 1035. (N,XCP(N),YCP(N),(STRESS(N,M),M=1,3),N=1,NUMELT)
      PUNCH 1035. (N,XCP(N),YCP(N),(STRAIN(N,M),M=1,3),N=1,NUMELT)
      PUNCH 1035. (N,XCP(N),YCP(N),BULK(N),SHEAR(N),POIS(N),N=1,NUMELT)
      PUNCH 1040. (N,(DRD(N,M),M=1,2),(DISP(N,M),M=1,2),N=1,NUMNPT)
      RETURN
C*****
1000 FORMAT (4F11.4,1P X-DISP Y-DISP DIM X-DISP DIM Y-DISP,
1          43H DELTA-X DELTA-Y TOTAL X-FORCE ,
2          14H Y-FORCE NP /)
1005 FORMAT (I4,1P9E11.3,I4)
1010 FORMAT (50H1ELE ELAS MOD BULK MOD SHEAR MOD NU EPS-X ,
1          54H EPS-Y GAM-XY EPS-1 EPS-3 GAMMAX ELE/
2          58X,23H STRAINS ARE IN PERCENT /)
1015 FORMAT (I4,3E10.3,F6.3,1P6E10.2,I4)
1017 FORMAT (I4,26H 1-D DISCONTINUITY ELEMENT)
1025 FORMAT (54H1ELE SIG-X SIG-Y TAU-XY SIG-1 SIG-3,
1          50H TAU-MAX THETA SIG1/3 LEVEL SIG1/CL SIG3/CL,
2          12H TAUH/CL ELE /)
1030 FORMAT (I4,1P6E10.2,OP6E8.3,I4)
1035 FORMAT (I10,5E10.3)
1040 FORMAT (I10,4E10.4)
C*****
      END

```

# SUBROUTINE JTSTR

```

C*****
COMMON /INIT/ HED(18),NUMELT,NUMNPT,NJOINT,NPUNCH
COMMON /NPFL/ NPN(275,6),ORD(300,2),XCP(275),YCP(275)
COMMON /RANS/ RAND,NUMBLK,R(108),A(108,54)
COMMON /MAT1/ BULK(275),SHEAR(275),POIS(275),GAM(10),NONLIN
COMMON /MAT2/ CIPS,COFF(10),EXP(10),DD(10),GG(10),FF(10),N2ONES
COMMON /MAT4/ CJ(10),PHIJ(10),ANGJ(10),EJT(10,6),NJT,GAMW
COMMON /STRS/ STRESS(275,3),SIGCL,PADJIS
DIMENSION H(4),V(4)
C*****
C    CALCULATE NORMAL(V) + TANGENTIAL(U) DISPLACEMENTS
C*****
PRINT 1000
DO 500 N=1,NUMELT
  MTYPE=NPN(N,5)
  IF (MTYPE.LT. NJOINT) GO TO 500
  IF (NPN(N,6).EQ. 0) GO TO 100
  PRINT 1010, N,BULK(N),SHEAR(N)
  GO TO 500
100 I=NPN(N,1)
  J=NPN(N,2)
  DX=ORD(J,1)-ORD(I,1)
  DY=ORD(J,2)-ORD(I,2)
  DL=SQRT(DX*DX+DY*DY)
  DX=DX/DL
  DY=DY/DL
  DO 120 I=1,4
    K=NPN(N,I)
    V(I)=-R(2*K-1)*DY+R(2*K)*DX
  120 U(I)= R(2*K-1)*DX+R(2*K)*DY
C*****
C    CALC. STRAINS + STRESSES, CHECK FAILURE, CALC. NEW STIFFNESSES
C*****
EPS=0.5*(U(4)-U(1)+U(3)-U(2))
EPN=0.5*(V(4)-V(1)+V(3)-V(2))
STRESS(N,1)=STRESS(N,1)-EPN*BULK(N)
STRESS(N,2)=STRESS(N,2)-EPS*SHEAR(N)
C
  ANG=PHIJ(MTYPE)/57.29578
  STREM=CJ(MTYPE)+STRESS(N,1)*SIN(ANG)/COS(ANG)
  STRLEV=ABS(STRESS(N,2))/STREM
  IF (STRESS(N,1).GT. 0.0) GO TO 200
  POIS(N)=1.0
  GO TO 220
200 IF (STRLEV.LT. 1.0) GO TO 220
  POIS(N)=2.0
220 PRINT 1020, N,BULK(N),SHEAR(N),POIS(N),EPN,EPS,STRESS(N,1),
  1      STRESS(N,2),STRLEV,N
C
250 IF (POIS(N)=1.0) 400,300,310
300 BULK(N)=EJT(MTYPE,3)
  SHEAR(N)=EJT(MTYPE,3)
  GO TO 500
310 SHEAR(N)=EJT(MTYPE,4)
  GO TO 500
400 SHEAR1=EJT(MTYPE,2)*GAMW*((STRESS(N,1)/COS(ANG))*EJT(MTYPE,5))
  SHEAR(N)=SHEAR1*(1.0-EJT(MTYPE,6)*STRLEV)**2.0
500 CONTINUE
RETURN

```

```

C*****
1000 FORMAT (54H)ELE      KN      KS FAIL CODE      EPS-N      EPS-S,
      1      34H      SIG-M      TAU      LEVEL ELE / 4X, 11H (FAIL CODE,
      2      53H =0.0-INTACT, =1.0-TENS. FAILURE, =2.0-SHEAR FAILURE)/)
1010 FORMAT (14,1P2E10.3,13H EXCAVATED ELEMENT )
1020 FORMAT (14,1P2E10.3,0P1E10.1,1P4E10.2,0P1E10.3,14)
C*****
      END

```